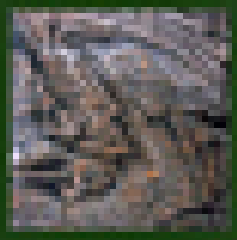

Structural Geology

HAAKON FOSSEN

CAMBRIDGE www.cambridge.org/9780521516648

This page intentionally left blank

Structural Geology

Lavishly illustrated in color, this textbook takes an applied approach to introduce undergraduate students to the basic principles of structural geology. The book provides unique links to industry applications in the upper crust, including petroleum and groundwater geology, which highlight the importance of structural geology in exploration and exploitation of petroleum and water resources. Topics range from faults and fractures forming near the surface to shear zones and folds of the deep crust. Students are engaged through examples and parallels drawn from practical everyday situations, enabling them to connect theory with practice. Containing numerous end-of-chapter problems, e-learning modules, and with stunning field photos and illustrations, this book provides the ultimate learning experience for all students of structural geology.

Haakon Fossen is Professor of Structural Geology at the University of Bergen, Norway, where he is affiliated with the Department of Earth Science, the Natural History Collections, and the Centre for Integrated Petroleum Research (CIPR). His professional career has also involved work as an exploration and production geologist/geophysicist for Statoil and periods of geologic mapping and mineral exploration in Norway. His research ranges from hard to soft rocks and includes studies of folds, shear zones, formation and collapse of the Caledonian Orogen, numerical modeling of deformation (transpression), the evolution of the North Sea rift, and studies of deformed sandstones in the western United States. He has conducted extensive field work in various parts of the world, notably Norway, Utah/Colorado and Sinai, and his research is based on field mapping, microscopy, physical and numerical modeling, geochronology and seismic interpretation. Professor Fossen has been involved in editing several international geology journals, has authored over 90 scientific publications, and has written two books and several book chapters. He has taught undergraduate structural geology courses for over ten years and has a keen interest in developing electronic teaching resources to aid student visualization and understanding of geologic structures.

Structural Geology

Haakon Fossen

UNIVERSITY OF BERGEN, NORWAY

CAMBRIDGE UNIVERSITY PRESS

CAMBRIDGE UNIVERSITY PRESS
Cambridge, New York, Melbourne, Madrid, Cape Town, Singapore,
São Paulo, Delhi, Dubai, Tokyo

Cambridge University Press
The Edinburgh Building, Cambridge CB2 8RU, UK

Published in the United States of America by Cambridge University Press, New York

www.cambridge.org
Information on this title: www.cambridge.org/9780521516648

First published in print format 2010

ISBN-13 978-0-511-77282-5 eBook (Dawsonera)

ISBN-13 978-0-521-51664-8 Hardback

Contents

HOW TO USE THIS BOOK

Each chapter starts with a general **introduction**, which presents a context for the topic within structural geology as a whole. These introductions provide a roadmap for the chapter and will help you to navigate through the book.

BOX 4.2 | VECTORS, MATRICES AND TEN

A scalar is a real number, reflecting temperature, mass
no direction. A vector has both magnitude (length) ar
or velocity. A matrix is a two-dimensional array of nu
meaning that they have 9 or 4 components). Matrice

The term tensor is, in rock mechanics, applied to v
scalars as tensors of order zero, vectors as first-orde
Hence, for our purposes, the terms matrix and seco
cases where numbers are arranged in matrices that

The main text contains **highlighted terms** and **key expressions** that you will need to understand and become familiar with. Many of these terms are listed in the **Glossary** at the back of the book. The Glossary allows you to easily look up terms whenever needed and can also be used to review important topics and key facts. Each chapter also contains a series of **highlighted statements** to encourage you to pause and review your understanding of what you have read.

Most chapters have one or more **boxes** containing in-depth information about a particular subject, helpful examples or relevant background information. Other important points are brought together in the **chapter summaries. Review questions** should be used to test your understanding of the chapter before moving on to the next topic. **Answers** to these questions are given on the book's web-page.

Review questions

1. When is it appropriate to use the term pressure in geology?
2. How can we graphically visualize the state of stress in two and th
3. Where could we expect to find tensile stress in the crust?
4. How will the shape and orientation of the stress ellipsoid change
   system?
5. Will the stress tensor (matrix) look different if we choose a differ
6. A diagonal tensor has numbers on the diagonal running from the
   with all other entries being zero. What does a diagonal stress tens

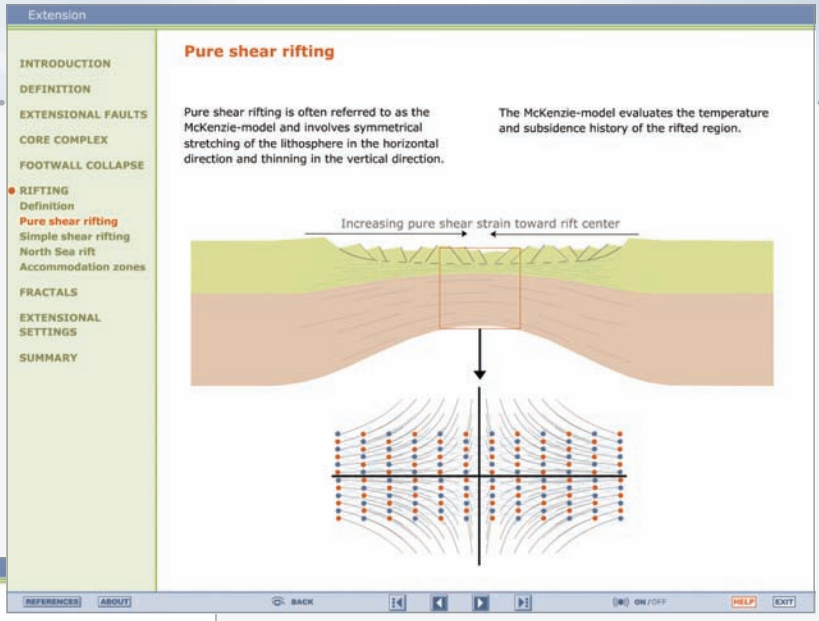

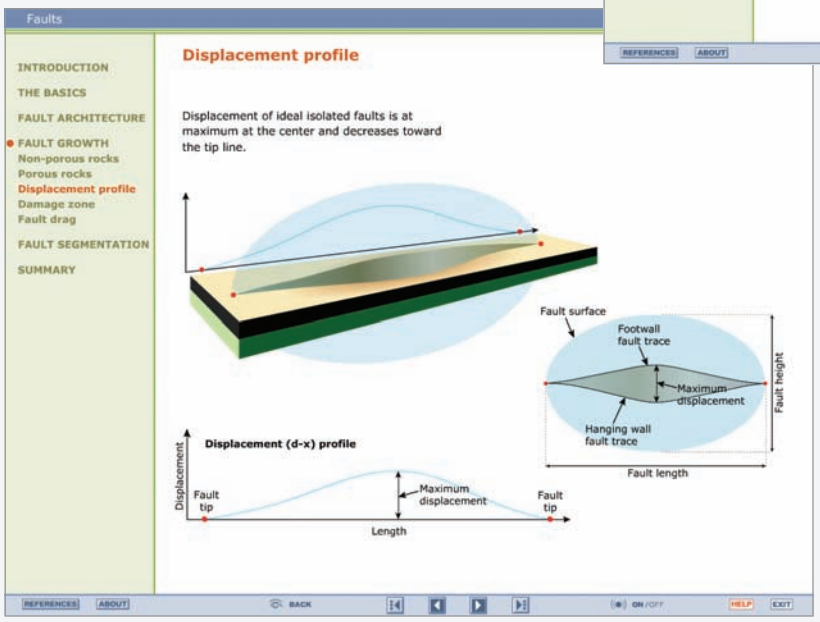

Further reading sections provide references to selected papers and books for those interested in more detailed or advanced information. In addition, there are links to web-based **e-learning modules** at the end of the chapters. Using these modules is highly recommended after reading the chapter as part of review and exam preparation. The modules provide supplementary information that complements the main text.

Web-based resources

Specially prepared resources, unique to this book, are available from the book's web-page: www.cambridge.org/fossen. These are:

- Flash based e-learning modules that combine animations, text, illustrations and photographs. These present key aspects of structural geology in a highly visual and interactive environment.
- All of the figures for each chapter as jpeg files for use by instructors and readers.
- Supplementary figures illustrating additional geologic structures and field examples.
- Answers to the review questions presented at the end of each chapter.
- Additional exercises and solutions.
- A repository for further images, animations, videos, exercises and other resources provided by readers and instructors as a community resource.

Preface

This textbook is written to introduce undergraduate students, and others with a general geologic background, to basic principles, aspects and methods of structural geology. It is mainly concerned with the structural geology of the crust, although the processes and structures described are relevant also for deformation that occurs at deeper levels within our planet. Further, remote data from Mars and other planets indicate that many aspects of terrestrial structural geology are relevant also beyond our own planet.

The field of structural geology is very broad, and the content of this book presents a selection of important subjects within this field. Making the selection has not been easy, knowing that lecturers tend to prefer their own favorite aspects of, and approaches to, structural geology, or make selections according to their local departmental course curriculum. Existing textbooks in structural geology tend to emphasize the ductile or plastic deformation that occurs in the middle and lower crust. In this book I have tried to treat the frictional regime in the upper crust more extensively so that it better balances that of the deeper parts of the crust, which makes some chapters particularly relevant to courses where petroleum geology and brittle deformation in general are emphasized.

Obtaining this balance was one of several motivating factors for writing this book, and is perhaps related to my mixed petroleum geology and hard-rock structural geology experience. Other motivating factors include the desire to make a book where I could draw or redraw all of the illustrations and be able to present the first full-color book in structural geology. I also thought that a fundamental structural geology text of the twenty-first century should come with specially prepared e-learning resources, so the package of e-learning material that is presented with this book should be regarded as part of the present book concept.

Book structure

The structure of the book is in many ways traditional, going from strain (Chapters 2 and 3) to stress (Chapters 4 and 5) and via rheology (Chapter 6) to brittle deformation (Chapters 7 and 8). Of these, Chapter 2 contains material that would be too detailed and advanced for some students and classes, but selective reading is possible. Then, after a short introduction to the microscale structures and processes that distinguish crystal-plastic from brittle deformation (Chapter 10), ductile deformation structures such as folding, boudinage, foliations and shear zones are discussed (Chapters 11–15). Three consecutive chapters then follow that are founded on the three principal tectonic regimes (Chapters 16–18) before salt tectonics and restoration principles are presented (Chapters 19 and 20). A final chapter, where links to metamorphic petrology as well as stratigraphy are drawn, rounds off the book, and suggests that structural geology and tectonics largely rely on other disciplines. The chapters do not have to be read in numerical order, and most chapters can be used individually.

Emphasis and examples

The book seeks to cover a wide ground within the field of structural geology, and examples presented in the text are from different parts of the world. However, pictures and illustrations from a few geographic areas reappear. One of those is the North Sea rift system, notably the Gullfaks oil field, which I know quite well from my years with the Norwegian oil company Statoil. Another is the Colorado Plateau (mostly Utah), which over the last two decades has become one of my favorite places to do field work. A third, and much wetter and greener one, is the Scandinavian Caledonides. From this ancient orogen I have chosen a number of examples to illustrate structures typical of the plastic regime.

Acknowledgments

During the writing of this textbook I have built on experience and knowledge achieved through my entire career, from early days as a student, via various industrial and academic positions, to the time I have spent writing the manuscript. In this respect I want to thank fellow students, geologists and professors with whom I have interacted during my time at the Universities of Bergen, Oslo, Minnesota and Utah, at Utah State University, in Statoil and at the Geological Survey of Norway. In particular, my advisers and friends Tim Holst, Peter Hudleston and Christian Teyssier deserve thanks for sharing their knowledge during my three years in Minnesota, and among the many fellow PhD students there special thanks are due to Jim Dunlap, Eric Heatherington, David Kirschner, Labao Lan and, particularly, Basil Tikoff for valuable discussions and exchange of ideas as we were exploring various aspects of structural geology. Among coworkers and colleagues I wish to extend special thanks to Roy Gabrielsen, who contributed to the Norwegian book on which this book builds, Jonny Hesthammer for good company in Statoil and intense field discussions, Egil Rundhovde for co-leading multiple field trips to the Colorado Plateau, and to Rich Schultz who is always keen on intricate discussions on fracture mechanics and deformation bands in Utah and elsewhere.

Special thanks also go to Wallace Bothner, Rob Butler, Nestor Cardozo, Declan DePaor, Jim Evans, James Kirkpatrick, Stephen Lippard, Christophe Pascal, Atle Rotevatn, Zoe Shipton, Holger Stunitz and Bruce Trudgill for reading and commenting on earlier versions of the text. I am also thankful to colleagues and companies who assisted in finding appropriate figures and seismic examples of structures, each of which is acknowledged in connection with the appearance of the illustration in the book, and to readers who will send their comments to me so that improvements can be made for the next edition.

Symbols

a	long axis of ellipse representing a microcrack
A	area; empirically determined constant in flow laws
c	short axis of ellipse representing a microcrack
C	cohesion or cohesional strength of a rock
C_f	cohesive strength of a fault
d	offset
d_{cl}	thickness of clay layer
D	displacement; fractal dimension
D_{max}	maximum displacement along a fault trace or on a fault surface
$\mathbf{D}$	deformation (gradient) matrix
$e = \varepsilon$	elongation
$\dot{e} = \dot{\varepsilon}$	elongation rate (de/dt)
$\dot{e}_x$ and $\dot{e}_y$	elongation rates in the x and y directions (s^{-1})
$\mathbf{e}_1$, $\mathbf{e}_2$ and $\mathbf{e}_3$	eigenvectors of deformation matrix, identical to the three axes of strain ellipsoid
$\bar{e}$	logarithmic (natural) elongation
$\bar{e}_s$	natural octahedral unit shear
E	Young's modulus; activation energy for migration of vacancies through a crystal ($J\,mol^{-1}\,K^{-1}$)
E^*	activation energy
$\mathbf{F}$	force vector ($kg\,m\,s^{-2}$, N)
F_n	normal component of the force vector
F_s	shear component of the force vector
g	acceleration due to gravity (m/s^2)
h	layer thickness
h_0	initial layer thickness
h_T	layer thickness at onset of folding (buckling)
ISA_{1-3}	instantaneous stretching axes
K	bulk modulus
K_i	stress intensity factor
K_c	fracture toughness
k	parameter describing the shape of the strain ellipsoid (lines in the Flinn diagram)
k_x and k_y	pure shear components, diagonal elements in the pure shear and simple shear matrices
l	line length (m)

l_0	line length prior to deformation (m)
$\mathbf{L}$	velocity tensor (matrix)
L	fault length; wavelength
L_d	dominant wavelength
L_T	actual length of a folded layer over the distance of one wavelength
n	exponent of displacement-length scaling law
p_f	fluid pressure
P	pressure (Pa)
Q	activation energy
R	ellipticity or aspect ratio of ellipse (long over short axis); gas constant ($J\,kg^{-1}\,K^{-1}$)
R_f	final ellipticity of an object that was non-circular prior to deformation
R_i	initial ellipticity of an object (prior to deformation)
R_s	same as R, used in connection with the R_f/ϕ-method to distinguish it from R_f
R_{xy}	X/Y
R_{yz}	Y/Z
s	stretching
$\dot{\mathbf{S}}$	stretching tensor, symmetric part of $\mathbf{L}$
t	time (s)
T	temperature (K or °C); uniaxial tensile strength (bar); local displacement or throw of a fault when calculating SGR and SSF
$\mathbf{v}$	velocity vector (m/s)
V	volume (m^3)
V_0	volume prior to deformation
V_p	velocity of P-waves
V_s	velocity of S-waves
$\mathbf{w}$	vorticity vector
w	vorticity
$\mathbf{W}$	vorticity (or spin) tensor, which is the skew-symmetric component of $\mathbf{L}$
W_k	kinematic vorticity number
$\mathbf{x}$	vector or point in a coordinate system prior to deformation
$\mathbf{x}'$	vector or point in a coordinate system after deformation
x, y, z	coordinate axes, z being vertical
X, Y, Z	principal strain axes; $X \geq Y \geq Z$
Z	crustal depth (m)
α	thermal expansion factor (K^{-1}); Biot poroelastic parameter; angle between passive marker and shear direction at onset of non-coaxial deformation (Chapter 15); angle between flow apophyses (Chapter 2)
α'	angle between passive marker and shear direction after a non-coaxial deformation
β	stretching factor, equal to s
Δ	volume change factor
$\Delta\sigma$	change in stress

γ	shear strain
$\bar{\gamma}_{oct}$	octahedral shear strain
$\dot{\gamma}$	shear strain rate
Γ	non-diagonal entry in deformation matrix for subsimple shear
η	viscosity constant ($N\,s\,m^{-2}$)
λ	quadratic elongation
λ_1, λ_2 and λ_3	eigenvalues of deformation matrix
$\sqrt{\lambda_1}$, $\sqrt{\lambda_2}$ and $\sqrt{\lambda_3}$	length of strain ellipse axes
μ	shear modulus; viscosity
μ_f	coefficient of sliding friction
μ_L	viscosity of buckling competent layer
μ_M	viscosity of matrix to buckling competent layer
ν	Poisson's ratio; Lode's parameter
θ	angle between the normal to a fracture and σ_1; angle between ISA_1 and the shear plane
θ'	angle between X and the shear plane
ρ	density (g/cm^3)
σ	stress ($\Delta F/\Delta A$) (bar: 1 bar = 1.0197 $kg/cm^2 = 10^5$ Pa= 10^6 $dyne/cm^2$)
$\boldsymbol{\sigma}$	stress vector (traction vector)
$\sigma_1 > \sigma_2 > \sigma_3$	principal stresses
$\bar{\sigma}$	effective stress
σ_a	axial stress
σ_{dev}	deviatoric stress
σ_{diff}	differential stress ($\sigma_1 - \sigma_3$)
σ_H	max horizontal stress
σ_h	min horizontal stress
σ_h^*	average horizontal stress in thinned part of the lithosphere (constant-horizontal-stress model)
σ_m	mean stress $(\sigma_1 + \sigma_2 + \sigma_3)/3$
σ_n	normal stress
σ_r	remote stress
σ_s	shear stress
σ_t	tectonic stress
σ_{tip}	stress at tip of fracture or point of max curvature along pore margin
σ_{tot}	total stress ($\sigma_m + \sigma_{dev}$)
σ_v	vertical stress
σ_n^g	normal stress at grain–grain or grain–wall contact areas in porous medium
σ_n^w	average normal stress exerted on wall by grains in porous medium
ϕ	internal friction (rock mechanics); angle between X and a reference line at onset of deformation (R_f/ϕ-method)
ϕ'	angle between X and a reference line after a deformation (R_f/ϕ-method)
Φ	porosity
ψ	angular shear
$\boldsymbol{\omega}$	angular velocity vector

Chapter 1

Structural geology and structural analysis

Structural geology is about folds, faults and other deformation structures in the lithosphere – how they appear and how and why they formed. Ranging from features hundreds of kilometers long down to microscopic details, structures occur in many different settings and have experienced exciting changes in stress and strain – information that can be ours if we learn how to read the code. The story told by structures in rocks is beautiful, fascinating and interesting, and it can also be very useful to society. Exploration, mapping and exploitation of resources such as slate and schist (building stone), ores, groundwater, and oil and gas depend on structural geologists who understand what they observe so that they can present reasonable interpretations and predictions. In this first chapter we will set the stage for the following chapters by defining and discussing fundamental concepts and some of the different data sets and methods that structural geology and structural analysis rely on. Depending on your background in structural geology, it may be useful to return to this chapter after going through other chapters in this book.

1.1 Approaching structural geology

For us to understand structural geology we need to observe deformed rocks and find an explanation for how and why they ended up in their present state. Our main methods are field observations, laboratory experiments and numerical modeling. All of these methods have advantages and challenges. Field examples portray the final results of deformation processes, while the actual deformation history may be unknown. Progressive deformation can be observed in laboratory experiments, but how representative are such hour- or perhaps week-long observations of geologic histories that span thousands to millions of years in nature? Numerical modeling, where we use computers and mathematical equations to model deformation, is hampered by simplifications necessary for the models to be runable with today's codes and computers. However, by combining different approaches we are able to obtain realistic models of how structures form and what they mean. Field studies will always be important, as any modeling, numerical or physical, must be based directly or indirectly on accurate and objective field observations and descriptions. Objectivity during fieldwork is both important and challenging, and field studies in one form or another are the main reason why many geologists chose to become geoscientists!

1.2 Structural geology and tectonics

The word **structure** is derived from the Latin word *struere*, to build, and we could say:

A geologic structure is a geometric configuration of rocks, and structural geology deals with the geometry, distribution and formation of structures.

It should be added that **structural geology** only deals with structures created during rock deformation, not with primary structures formed by sedimentary or magmatic processes. However, deformation structures can form through the modification of primary structures, such as folding of bedding in a sedimentary rock.

The closely related word **tectonics** comes from the Greek word *tektos*, and both structural geology and tectonics relate to the building and resulting structure of the Earth's lithosphere, and to the motions that change and shape the outer parts of our planet. We could say that tectonics is more closely connected to the underlying processes that cause structures to form:

Tectonics is connected with external and often regional processes that generate a characteristic set of structures in an area or a region.

By external we mean external to the rock volume that we study. External processes or causes are in many cases plate motions, but can also be such things as forceful intrusion of magma, gravity-driven salt or mud diapirs, flowing glaciers and meteor impacts. Each of these "causes" can create characteristic structures that define a **tectonic style**, and the related tectonics can be given special names. **Plate tectonics** is the large-scale part of tectonics that directly involves the movement and interaction of lithospheric plates. Within the realm of plate tectonics, expressions such as subduction tectonics, collision tectonics and rift tectonics are applied for more specific purposes.

Glaciotectonics is the deformation of sediments and bedrock (generally sedimentary rocks) at the toe of an advancing ice sheet. In this case it is the pushing of the ice that creates the deformation, particularly where the base of the glacier is cold (frozen to the substrate).

Salt tectonics deals with the deformation caused by the (mostly) vertical movement of salt through its overburden (see Chapter 19). Both glaciotectonics and salt tectonics are primarily driven by gravity, although salt tectonics can also be closely related to plate tectonics. For example, tectonic strain can create fractures that enable salt to gravitationally penetrate its cover, as discussed in Chapter 19. The term **gravity tectonics** is generally restricted to the downward sliding of large portions of rocks and sediments, notably of continental margin deposits resting on weak salt or overpressured shale layers. Raft tectonics is a type of gravity tectonics occurring in such environments, as mentioned in Chapter 19. Smaller landslides and their structures are also considered examples of gravity tectonics by some, while others regard such surficial processes as **non-tectonic**. Typical non-tectonic deformation is the simple compaction of sediments and sedimentary rocks due to loading by younger sedimentary strata.

Neotectonics is concerned with recent and ongoing crustal motions and the contemporaneous stress field. Neotectonic structures are the surface expression of faults in the form of fault scarps, and important data sets stem from seismic information from earthquakes (such as focal mechanisms, Box 9.1) and changes in elevation of regions detected by repeated satellite measurements.

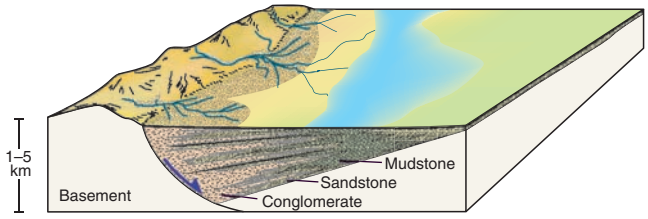

Figure 1.1 Illustration of the close relationship between sedimentary facies, layer thickness variations and syndepositional faulting (growth fault) along the margin of a sedimentary basin.

At smaller scales, **microtectonics** describes microscale deformation and deformation structures visible under the microscope.

Structural geology typically pertains to the observation, description and interpretation of structures that can be mapped in the field. How do we recognize deformation or **strain** in a rock? "Strained" means that something primary or preexisting has been geometrically modified, be it cross stratification, pebble shape, a primary magmatic texture or a preexisting deformation structure. Hence strain can be defined as a change in length or shape, and recognizing strain and deformation structures actually requires solid knowledge of undeformed rocks and their primary structures.

Being able to recognize tectonic deformation depends on our knowledge of primary structures.

The resulting deformation structure also depends on the initial material and its texture and structure. Deforming sandstone, clay, limestone or granite results in significantly different structures because they respond differently. Furthermore, there is often a close relationship between tectonics and the formation of rocks and their primary structures. Sedimentologists experience this as they study variations in thickness and grain size in the hanging wall (down-thrown side) of syndepositional faults. This is illustrated in Figure 1.1, where the gradual rotation and subsidence of the down-faulted block gives space for thicker strata near the fault than farther away, resulting in wedge-shaped strata and progressively steeper dips down section. There is also a facies variation, with the coarsest-grained deposits forming near the fault, which can be attributed to the fault-induced topography seen in Figure 1.1.

Another close relationship between tectonics and rock forming processes is shown in Figure 1.2, where forceful rising and perhaps inflating of magma deforms the outer and oldest part of the pluton and its country rock.

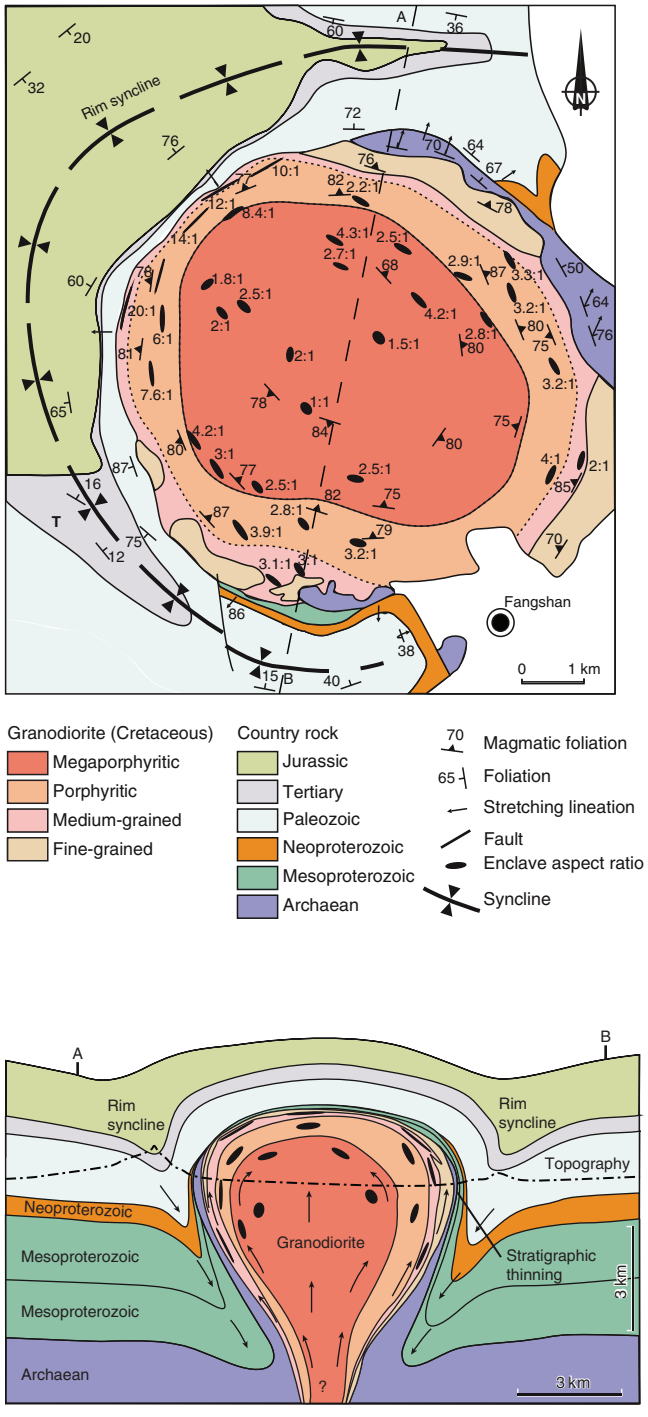

Figure 1.2 Structural geology can be linked to processes and mechanisms other than plate stresses. This map and profile from a granodioritic pluton southwest of Beijing, China, portray close connection between forceful intrusion of magma, strain and folds in the country rock. Black ellipses indicate strain, as discussed in Chapters 2 and 3. The strain (deformation) pattern within and around the pluton can be explained in terms of diapirism, where the intrusion ascends and squeezes and shears its outer part and the surrounding country rock to create space. Based on He *et al.* (2009).

Forceful intrusion of magma into the crust is characterized by deformation near the margin of the pluton, manifested by folding and shearing of the layers in Figure 1.2. Ellipses in this figure illustrate the shape of enclaves (inclusions), and it is clear that they become more and more elongated as we approach the margin of the pluton. Hence, the outer part of the pluton has been flattened during a forceful intrusion history.

Metamorphic growth of minerals before, during, and after deformation may also provide important information about the pressure–temperature conditions during deformation, and may contain textures and structures reflecting kinematics and deformation history. Hence, sedimentary, magmatic and metamorphic processes may all be closely associated with the structural geology of a locality or region.

These examples relate to strain, but structural geologists, especially those dealing with brittle structures of the upper crust, are also concerned with **stress**. Stress is a somewhat diffuse and abstract concept to most of us, since it is invisible. Nevertheless, there will be no strain without a stress field that exceeds the rock's resistance against deformation. We can create a stress by applying a force on a surface, but at a point in the lithosphere stress is felt from all directions, and a full description of such a state of stress considers stress from all directions and is therefore three-dimensional. There is always a relationship between stress and strain, and while it may be easy to establish from controlled laboratory experiments it may be difficult to extract from naturally formed deformation structures.

Structural geology covers deformation structures formed at or near the Earth's surface, in the cool, upper part of the crust where rocks have a tendency to fracture, in the hotter, lower crust where the deformation tends to be ductile, and in the underlying mantle. It embraces structures at the scale of hundreds of kilometers down to micro- or atomic-scale structures, structures that form almost instantaneously, and structures that form over tens of millions of years.

A large number of subdisciplines, approaches and methods therefore exist within the field of structural geology. The oil exploration geologist may be considering trap-forming structures formed during rifting or salt tectonics, while the production geologist worries about subseismic sealing faults (faults that stop fluid flow in porous reservoirs; Section 8.7). The engineering geologist may consider fracture orientations and densities in relation to a tunnel project, while the university professor uses structural mapping, physical modeling or computer modeling to understand mountain-building processes. The methods and approaches are many, but they serve to understand the structural or tectonic development of a region or to predict the structural pattern in an area. In most cases structural geology is founded on data and observations that must be analyzed and interpreted. Structural analysis is therefore an important part of the field of structural geology.

Structural data are analyzed in ways that lead to a tectonic model for an area. By **tectonic model** we mean a model that explains the structural observations and puts them into context with respect to a larger-scale process, such as rifting or salt movements. For example, if we map out a series of normal faults indicating E–W extension in an orogenic belt, we have to look for a model that can explain this extension. This could be a rift model, or it could be extensional collapse during the orogeny, or gravity-driven collapse after the orogeny. Age relations between structures and additional information (radiometric dating, evidence for magmatism, relative age relations and more) would be important to select a model that best fits the data. It may be that several models can explain a given data set, and we should always look for and critically evaluate alternative models. In general, a simple model is more attractive than a complicated one.

1.3 Structural data sets

Planet Earth represents an incredibly complex physical system, and the structures that result from natural deformation reflect this fact through their multitude of expressions and histories. There is thus a need to simplify and identify the one or few most important factors that describe or lead to the recognition of deformation structures that can be seen or mapped in naturally deformed rocks. **Field observations** of deformed rocks and their structures represent the most direct and important source of information on how rocks deform, and objective observations and careful descriptions of naturally deformed rocks are the key to understanding natural deformation. Indirect observations of geologic structures by means of various **remote sensing methods**, including satellite data and seismic surveying, are becoming increasingly important in our mapping and description of structures and tectonic deformation. **Experiments** performed in the laboratory give us valuable knowledge of how various physical conditions, including stress field, boundary condition, temperature or the physical properties of the deforming material, relate to deformation. **Numerical models**, where rock deformation is simulated on a computer, are also useful as they allow us to control the various parameters and properties that influence deformation.

Experiments and numerical models not only help us understand how external and internal physical conditions control or predict the deformation structures that form, but also give information on how deformation structures evolve, i.e. they provide insights into the deformation history. In contrast, naturally deformed rocks represent end-results of natural deformation histories, and the history may be difficult to read out of the rocks themselves. Numerical and experimental models allow one to control rock properties and boundary conditions and explore their effect on deformation and deformation history. Nevertheless, any deformed rock contains some information about the history of deformation. The challenge is to know what to look for and to interpret this information. Numerical and experimental work aids in completing this task, together with objective and accurate field observations.

Numerical, experimental and remotely acquired data sets are important, but should always be based on field observations.

1.4 Field data

It is hard to overemphasize the importance of traditional field observations of deformed rocks and their structures. Rocks contain more information than we will ever be able to extract from them, and the success of any physical or numerical model relies on the accuracy of observation of rock structures in the field. Direct contact with rocks and structures that have not been filtered or interpreted by people or computers is invaluable.

Unfortunately, our ability to make objective observations is limited. What we have learned and seen in the past strongly influences our visual impressions of deformed rocks. Any student of deformed rocks should therefore train himself or herself to be objective. Only then can we expect to discover the unexpected and make new interpretations that may contribute to our understanding of the structural development of a region and to the field of structural geology in general. Many structures are overlooked until the day that someone points out their existence and meaning, upon which they all of a sudden appear "everywhere". Shear bands in strongly deformed ductile rocks (mylonites) are one such example (Figure 15.25). They were either overlooked or considered as cleavage until the late 1970s, when they were properly described and interpreted. Since then, they have been described from almost every major shear zone or mylonite zone in the world.

Traditional fieldwork involves the use of simple tools such as a hammer, measuring device, topomaps, a hand lens and a compass, and the data collected are mainly structural orientations and samples for thin section studies. This type of data collection is still important, and is aided by modern global positioning system (GPS) units and high-resolution aerial and satellite photos. More advanced and detailed work may involve the use of a portable laser-scanning unit, where pulses of laser light strike the surface of the Earth and the time of return is recorded. This information can be used to build a detailed topographic or geometrical model of the outcrop, onto which one or more high-resolution field photographs can be draped. An example of such a model is shown in Figure 1.3, although the advantage of virtually moving around in the model cannot be demonstrated by a flat picture. Geologic observations such as the orientation of layering or fold axes can then be made on a computer.

In many cases, the most important way of recording field data is by use of careful field sketches, aided by photographs, orientation measurements and other measurements that can be related to the sketch. Sketching also forces the field geologist to observe features and details that may otherwise be overlooked. At the same time, sketches can be made so as to emphasize relevant information and neglect irrelevant details. Field sketching is, largely, a matter of practice.

1.5 Remote sensing and geodesy

Satellite images, such as those shown in Figure 1.4a, c, are now available at increasingly high resolutions and are a valuable tool for the mapping of map-scale structures. An increasing amount of such data is available on the World Wide Web, and may be combined with digital elevation data to create three-dimensional models. Orthorectified **aerial photos** (orthophotos) may give more or other details (Figure 1.4b), with resolutions down to a few tens of centimeters in some cases. Both ductile structures, such as folds and foliations, and brittle faults and fractures are mappable from satellite images and aerial photos.

In the field of neotectonics, **InSAR** (Interferometric Synthetic Aperture Radar) is a useful remote sensing technique that uses radar satellite images. Beams of radar waves are constantly sent toward the Earth, and an image is generated based on the returned information. The intensity of the reflected information reflects the composition of the ground, but the phase of the wave as it hits and becomes reflected is also recorded. Comparing phases enables us to monitor millimeter-scale changes in elevation and geometry of the surface, which may reflect active tectonic

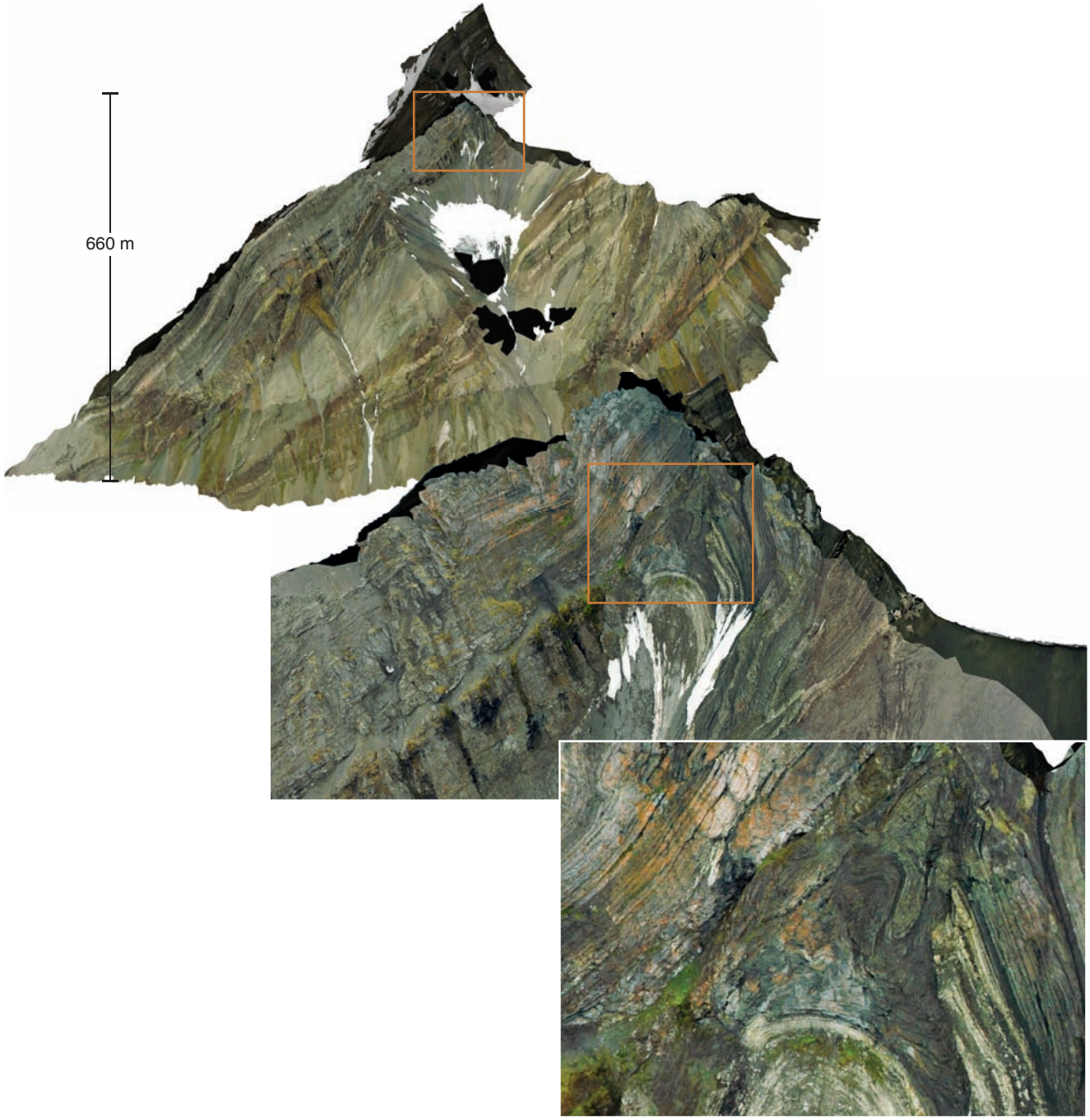

Figure 1.3 Mediumfjellet, Svalbard, based on LIDAR (LIght Detection And Ranging) data (laser scanning from helicopter) and photos. This type of model, which actually is three dimensional, allows for geometric analysis on a computer and provides access to otherwise unreachable exposures. The lower figures are more detailed views. Modeling by Simon Buckley.

movements related to earthquakes. In addition, accurate digital elevation models (see next section) and topographic maps can be constructed from this type of data.

GPS data in general are an important source of data that can be retrieved from GPS satellites to measure plate movements (Figure 1.5). Such data can also be collected on the ground by means of stationary GPS units with down to millimeter-scale accuracy.

1.6 DEM, GIS and Google Earth

Conventional paper maps are still useful for many field mapping purposes, but rugged laptops, tablets and handheld devices now allow for direct digitizing of structural features on digital maps and images and are becoming more and more important. Field data in digital form can be combined with elevation data and other data by

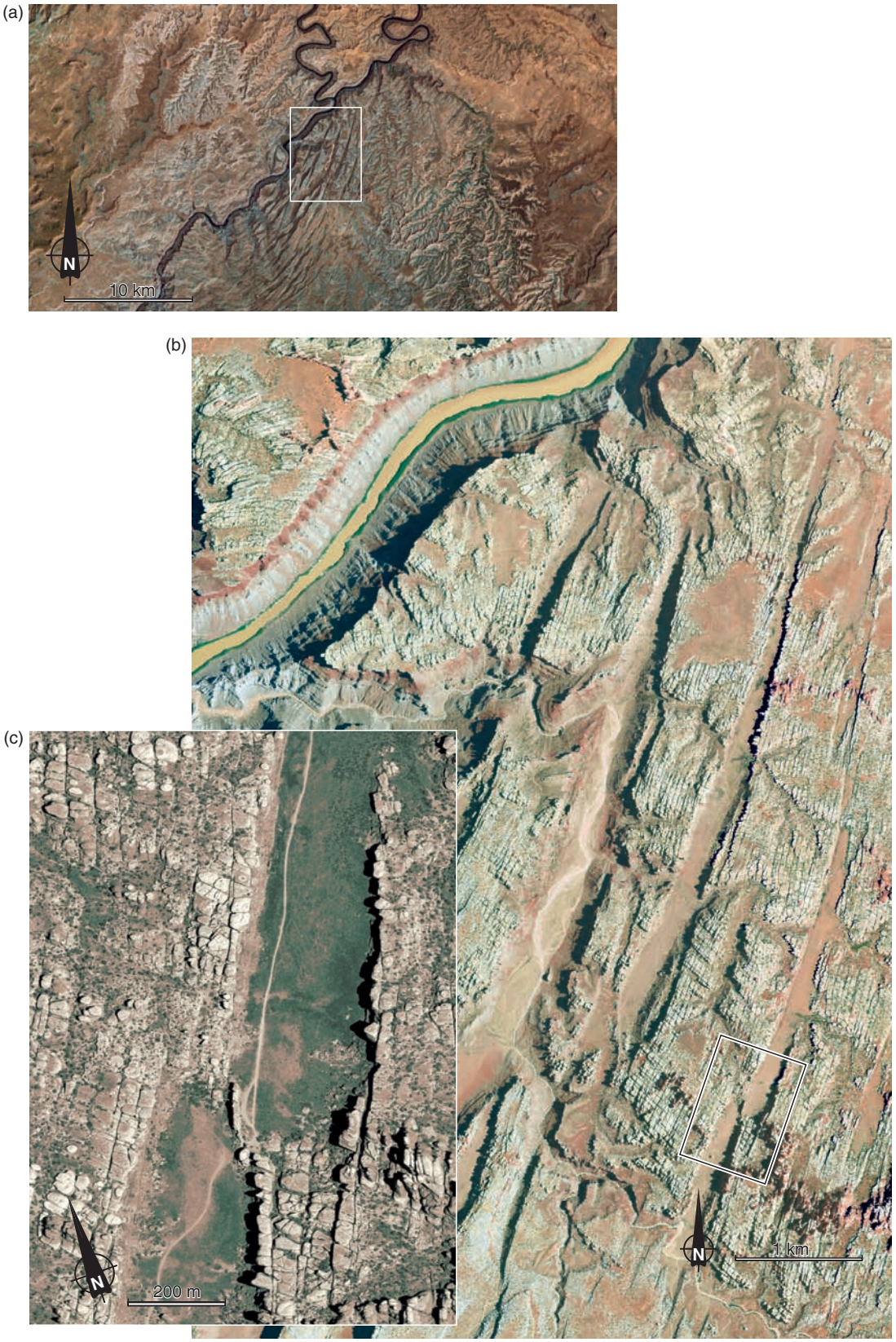

Figure 1.4 (a) Satellite image of the Canyonlands National Park area, Utah. The image reveals graben systems on the east side of the Colorado River. An orthophoto (b) reveals that the grabens run parallel to fractures, and a high-resolution satellite image (c) shows an example of a graben stepover structure. *Source*: Utah AGRC.

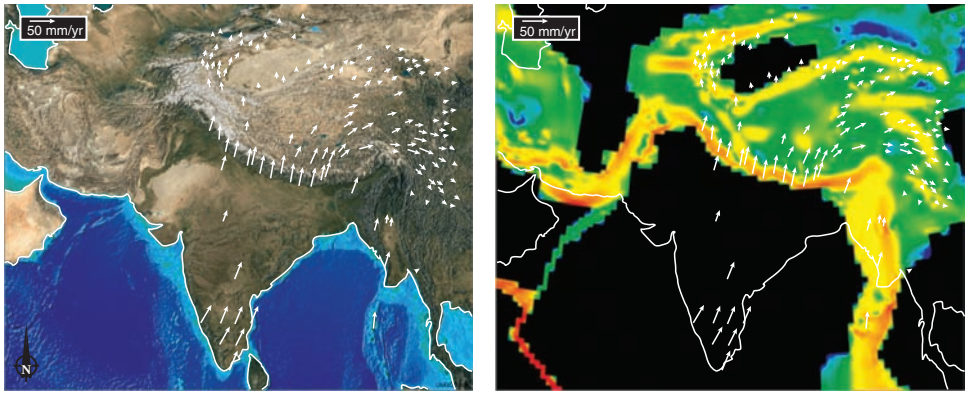

Figure 1.5 Use of GPS data from stationary GPS stations worldwide over time can be used to map relative plate motions and strain rates. (Left) White arrows (velocity vectors) indicating motions relative to Europe. The vectors clearly show how India is moving into Eurasia, causing deformation in the Himalaya–Tibetan Plateau region. (Right) Strain rate map based on GPS data. Calculated strain rates are generally less than 3×10^{-6} y^{-1} or 10^{-13} s^{-1}. Warm colors indicate high strain rates. Similar use of GPS data can be applied to much smaller areas where differential movements occur, for example across fault zones. From the project The Global Strain Rate Map (http://jules.unavco.org). See Kreemer *et al.* (2003) for more information.

means of a Geographical Information System (GIS). By means of GIS we can combine field observations, various geologic maps, aerial photos, satellite images, gravity data, magnetic data, typically together with a digital elevation model, and perform a variety of mathematical and statistical calculations. A **digital elevation model (DEM)** is a digital representation of the topography or shape of a surface, typically the surface of the Earth, but a DEM can be made for any geologic surface or interface that can be mapped in three dimensions. Surfaces mapped from cubes of seismic data are now routinely presented as DEMs and can easily be analyzed in terms of geometry and orientations.

Inexpensive or free access to geographic information exists, and this type of data was revolutionized by the development of Google Earth in the first decade of this century. The detailed data available from Google Earth and related sources of digital data have taken the mapping of faults, lithologic contacts, foliations and more to a new level, both in terms of efficiency and accuracy. Because of the rapid evolution of this field, further information and resources will be posted at the webpage of this book.

1.7 Seismic data

In the mapping of subsurface structures, seismic data are invaluable and since the 1960s have revolutionized our understanding of fault and fold geometry. Some seismic data are collected for purely academic purposes, but the vast majority of seismic data acquisition is motivated by exploration for petroleum and gas. Most seismic data are thus from rift basins and continental margins.

Acquisition of seismic data is, by its nature, a special type of remote sensing (acoustic), although always treated separately in the geo-community. Marine seismic reflection data (Figure 1.6) are collected by boat, where a sound source (air gun) generates sound waves that penetrate the crustal layers under the sea bottom. Microphones can also be put on the sea floor. This method is more cumbersome, but enables both seismic S- and P-waves to be recorded (S-waves do not travel through water). Seismic data can also be collected onshore, putting the sound source and microphones (geophones) on the ground. The onshore sound source would usually be an explosive device or a vibrating truck, but even a sledgehammer or specially designed gun can be used for very shallow and local targets.

The sound waves are reflected from layer boundaries where there is an increase in acoustic impedance, i.e. where there is an abrupt change in density and/or the velocity with which sound waves travel in the rock. A long line of microphones, onshore called geophones and offshore referred to as hydrophones, record the reflected sound signals and the time they appear at the surface. These data are collected in digital form and processed by computers to generate a seismic image of the underground.

Seismic data can be processed in a number of ways, depending on the focus of the study. Standard reflection seismic lines are displayed with two-way travel time as the vertical axis. Depth conversion is therefore necessary to create an ordinary geologic profile from those data. Depth conversion is done using a velocity model that depends on the lithology (sound moves faster in sandstone than in shale, and yet faster in limestone) and burial depth (lithification

BOX 1.1 MARINE SEISMIC ACQUISITION

Offshore collection of seismic data is done by a vessel that travels at about 5 knots while towing arrays of air guns and streamers containing hydrophones a few meters below the surface of the water. The tail buoy helps the crew locate the end of the streamers. The air guns are activated periodically, such as every 25 m (about every 10 seconds), and the resulting sound wave that travels into the Earth is reflected back by the underlying rock layers to hydrophones on the streamer and then relayed to the recording vessel for further processing.

The few sound traces shown on the figure indicate how the sound waves are both refracted across and reflected from the interfaces between the water and Layer 1, between Layer 1 and 2, and between Layer 2 and 3. Reflection occurs if there is an increase in the product between velocity and density from one layer to the next. Such interfaces are called reflectors. Reflectors from a seismic line image the upper stratigraphy of the North Sea Basin (right). Note the upper, horizontal sea bed reflector, horizontal Quaternary reflectors and dipping Tertiary layers. Unconformities like this one typically indicate a tectonic event. Note that most seismic sections have seconds (two-way time) as vertical scale.

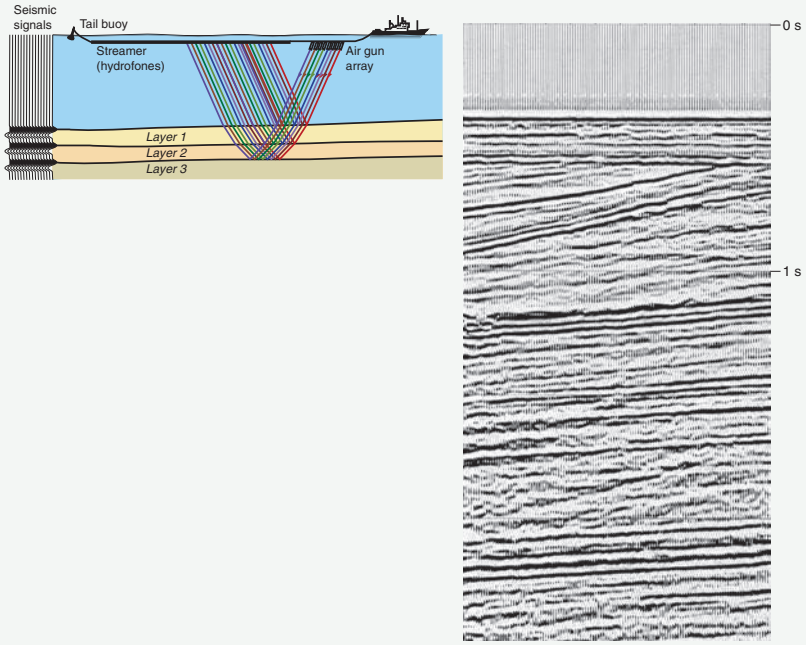

leads to increased velocity). In general it is the interpretation that is depth converted. However, the seismic data themselves can also be depth migrated, in which case the vertical axis of the seismic sections is depth, not time. This provides more realistic displays of faults and layers, and takes into account lateral changes in rock velocity that may cause visual or geometrical challenges to the interpreter when dealing with a time-migrated section. The accuracy of the depth-migrated data does however rely on the velocity model.

Deep seismic lines can be collected where the energy emitted is sufficiently high to penetrate deep parts of the crust and even the upper mantle. Such lines are useful for exploring the large-scale structure of the lithosphere. While widely spaced deep seismic lines and regional seismic lines are called two-dimensional (2-D) seismic data, more and more commercial (petroleum company) data are collected as a three-dimensional (3-D) cube where line spacing is close enough (*c.* 25 m) that the data can be processed in three dimensions, and where sections through the cube can be made in any direction. The lines parallel to the direction of collection are sometimes called **inlines**, those orthogonal to inlines are referred to as **crosslines**, while other vertical lines are **random lines**. Horizontal sections are called **time slices**, and can be useful during fault interpretation.

Three-dimensional seismic data provide unique opportunities for 3-D mapping of faults and folds in the subsurface. However, seismic data are restricted by **seismic resolution**, which means that one can only distinguish

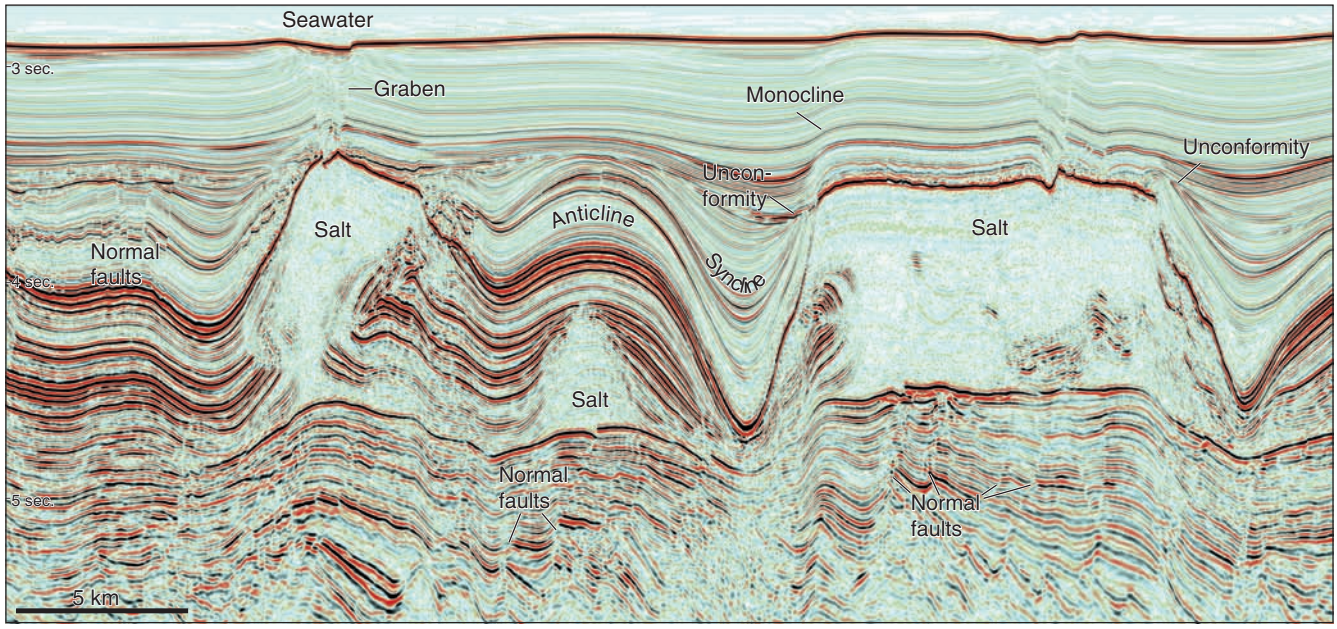

Figure 1.6 Seismic 2-D line from the Santos Basin offshore Brazil, illustrating how important structural aspects of the subsurface geology can be imaged by means of seismic exploration. Note that the vertical scale is in seconds. Some basic structures returned to in later chapters are indicated. Seismic data courtesy of CGGVeritas.

layers that are a certain distance apart (typically around 5–10m), and only faults with a certain minimum offset can be imaged and interpreted. The quality and resolution of 3-D data are generally better than those of 2-D lines because the reflected energy is restored more precisely through 3-D migration. The seismic resolution of high-quality 3-D data depends on depth, acoustic impedance of the layer interfaces, data collection method and noise, but would typically be at around 15–20 m for identification of fault throw.

Sophisticated methods of data analysis and visualization are now available for 3-D seismic data sets, helpful for identifying faults and other structures that are underground. Petroleum exploration and exploitation usually rely on seismic 3-D data sets interpreted on computers by geophysicists and structural geologists. The interpretation makes it possible to generate structural contour maps and geologic cross-sections that can be analyzed structurally in various ways, e.g. by structural restoration (Chapter 20).

3-D seismic data form the foundation of our structural understanding of hydrocarbon fields.

Other types of seismic data are also of interest to structural geologists, particularly seismic information from earthquakes. This information gives us important information about current fault motions and tectonic regime, which in simple terms means whether an area is undergoing shortening, extension or strike-slip deformation.

1.8 Experimental data

Physical modeling of folding and faulting have been performed since the earliest days of structural geology (Figure 1.7), and since the middle part of the twentieth century such modeling has been carried out in a more systematic way. Buckle folding, shear folding, reverse, normal and strike-slip faulting, fault populations, fault reactivation, porphyroclast rotation, diapirism and boudinage are only some of the processes and structures that have been modeled in the laboratory. The traditional way of modeling geologic structures is by filling a box with clay, sand, plaster, silicone putty, honey and other media and applying extension, contraction, simple shear or some other deformation. A ring shear apparatus is used when large amounts of shear are required. In this setup, the outer part of the disk-shaped volume is rotated relative to the inner part. Many models can be filmed and photographed during the deformation history or scanned using computer tomography. Another tool is the centrifuge, where material is deformed under the influence of the centrifugal force. Here the centrifugal force plays the same role in the models as the force of gravity does in geologic processes.

Ideally we wish to construct a **scale model**, where not only the size and geometry of the natural object or structure that it refers to are shrunk, but where also physical properties are scaled proportionally. Hence we

Figure 1.7 Experimental work in 1887, carried out by means of clay and a simple contractional device. This and similar models were made by H. M. Cadell to illustrate the structures of the northwest Scottish Highlands. With permission of the Geological Survey of Britain.

need a geometrically similar model where its lengths are proportional to the natural example and where equality of angles is preserved. We also need kinematic similarity, with comparability of changes in shape and position and proportionality of time. Dynamic similarity requires proportional values of cohesion or viscosity contrast and similar angles of internal friction.

In practice, it is impossible to scale down every aspect or property of a deformed part of the Earth's crust. Sand has grains that, when scaled up to natural size, may be as large as huge boulders, preventing the replication of small-scale structures. The grain size of clay may be more appropriate, but we may find that the fine grain size of clay makes it too cohesive. Plaster has properties that change during the course of the experiment and are thus difficult to describe accurately. Obviously, physical models have their limitations, but observations of progressive deformation under known boundary conditions still provide important information that can help us to understand natural structures.

For a small physical model to realistically reproduce a natural example, we must proportionally scale down physical proportions and properties as best we can.

Experimental deformation of rocks and soils in a deformation rig under the influence of an applied pressure (stress) is used to explore how materials react to various stress fields and strain rates. The samples can be

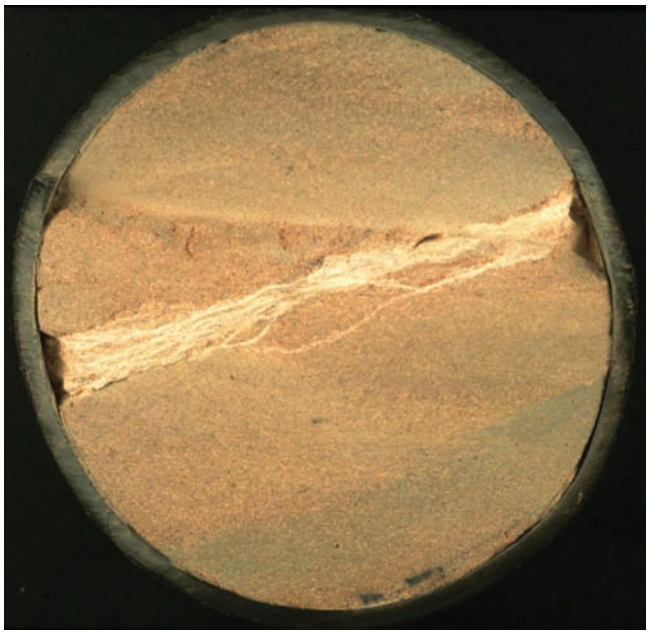

Figure 1.8 Section through a sandstone sample deformed in a triaxial deformation rig. The light bands are called deformation bands (see Chapter 7), the sandstone is the Scottish Locharbrigg Sandstone and the diameter of the cylindrical sample is 10 cm. You can read about these experiments in Mair *et al.* (2000). Photo: Karen Mair.

a few tens of cubic centimeters in size (Figure 1.8), and are exposed to uniaxial compression or tension (uniaxial means that a force is applied in only one direction) with a fluid-controlled confining pressure that relates to the crustal depth of interest. Triaxial tests are also performed, and the resulting

deformation may be both plastic and brittle. For plastic deformation we run into problems with strain rate. Natural plastic strains accumulate over thousands or millions of years, so we have to apply higher temperatures to our laboratory samples to produce plastic structures at laboratory strain rates. We are thus back to the challenge of scaling, this time in terms of temperature, time and strain rate.

1.9 Numerical modeling

Numerical modeling of geologic processes has become increasingly simple with the development of increasingly faster computers. Simple modeling can be performed using mathematical tools such as spreadsheets or Matlab™. Other modeling requires more sophisticated and expensive software, often building on finite element and finite difference methods. The models may range from microscale, for instance dealing with mineral grain deformation, to the deformation of the entire lithosphere. We can model such things as stress field changes during faulting and fault interaction, fracture formation in rocks, fold formation in various settings and conditions, and microscale diffusion processes during plastic deformation. However, nature is complex, and when the degree of complexity is increased, even the fastest supercomputer at some point reaches its physical limitations. Nor can every aspect of natural deformation be described by today's numerical theory. Hence, we have to consider our simplifications very carefully and use field and experimental data both during the planning of the modeling and during the evaluation of the results. Therefore there is a need for geologists who can combine field experience with a certain insight into numerical methodology, with all of its advantages and limitations.

1.10 Other data sources

There is a long list of other data sources that can be of use in structural analysis. **Gravimetric** and **magnetic data** (Figure 1.9) can be used to map large-scale faults and fault patterns in sedimentary basins, covered crust and subsea oceanic crust. Magnetic anisotropy as measured from oriented hand samples can be related to finite strain. Thin section studies and electron microscope images reveal structural information on the microscale. Earthquake data and focal mechanism solutions give valuable information about intraplate stresses and neotectonism and may be linked with *in situ* stress measurements by means of strain gauges, borehole breakouts, hydraulic fracturing, overcoring etc. Radiometric data can be used to date tectonic events. Sedimentological data and results of basin analysis are closely related to fault activity in sedimentary basins (Figure 1.1). Dike intrusions and their orientations are related to the stress field and preexisting weaknesses, and geomorphologic features can reveal important structures in the underground. The list can be made longer, illustrating how the different geologic disciplines rely on each other and should be used in concert to solve geologic problems.

1.11 Organizing the data

Once collected, geologic data need to be analyzed. Structural field data represent a special source of data because they directly relate to the product of natural deformation in all its purity and complexity. Because of the vastness of information contained in a field area or outcrop, the field geologist is faced with the challenge of sorting out the information that is relevant to the problem in question. Collecting too much data slows down both collection and analyses of the data. At the same time an incomplete data set prevents the geologist from reaching sound and statistically significant conclusions.

There are several examples where general structural mapping was done and large databases were constructed for future unknown purposes and needs. However, later problems and studies commonly require one or more key parameters that are missing or not ideally recorded in preexisting data sets. Consequently, new and specifically planned fieldwork commonly has to be carried out to obtain the type, quality and consistency of data that are required in each case.

Always have a clear objective during data sampling.

Collecting the wrong type of data is of course not very useful, and the quality of the data must be acceptable for further use. The quality of the analysis is limited by the quality of the data upon which it is based. It is therefore essential to have a clear and well-defined objective during data collection. The same is the case for other data types, such as those gathered by seismic methods or remote sensing.

Once collected, data must be grouped and sorted in a reasonable way for further analysis. In some cases field data are spatially homogeneous, and they can all be represented in a single plot (Figure 1.10a). In other cases data show some type of heterogeneity (Figure 1.10b–e), in

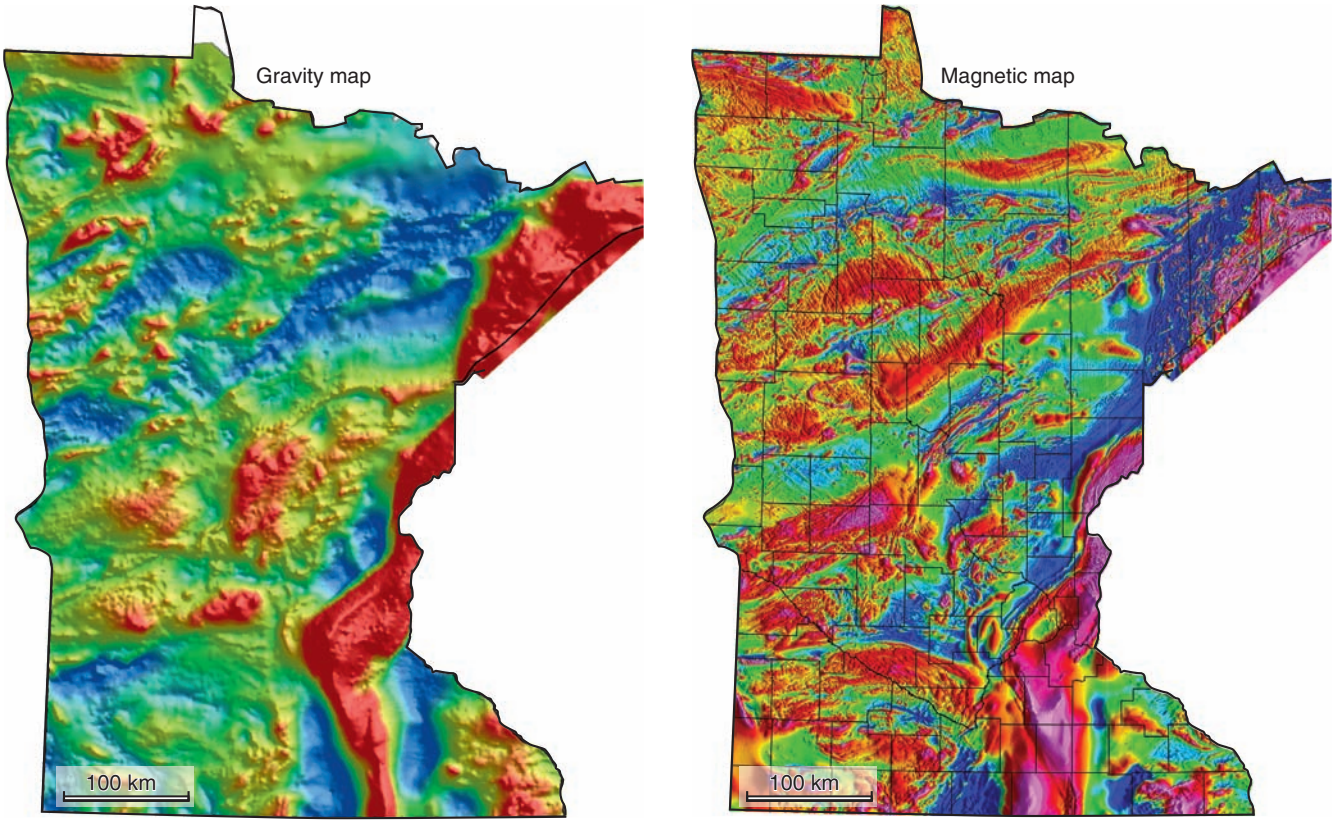

Figure 1.9 Gravity and magnetic maps of the state of Minnesota, where most of the bedrock and its structures are covered by glacial deposits. Modern structural mapping of the bedrock in this state has therefore involved extensive use of gravity and magnetic data. Warm (reddish) colors indicate high density (left) or high magnetic intensity (right). Maps reproduced courtesy of Minnesota Geological Survey.

which case it may be useful to subdivide the data set into subsets or **subpopulations**.

It is sometimes useful to subdivide data into subsets based on geographic occurrence or distribution. A **structural subarea** is a geographic area within which the structural data set is approximately homogeneous (Figure 1.10a) or where it shows a systematic change (Figure 1.10b–e). Completely non-systematic or chaotic structural data are very unusual; there is usually some fabric or systematic orientation of minerals or fractures resulting from rock deformation.

As an example, Figure 1.11 shows the overall pattern of lineations in a part of the Caledonian orogenic wedge in Scandinavia. Each lineation arrow represents the local average orientation of many field measurements. The lineation pattern is far from homogeneous, so the region should be subdivided into subareas of more homogeneous character, as shown in Figure 1.11c. We can then study each subarea individually, and the variation within each subarea can be displayed by means of stereographic presentation of individual measurements (Figure 1.12). We could also distinguish between different types of lineations, as discussed in Chapter 13. Figure 1.12 illustrates the distribution of observations as well as the mean orientation of lineations by means of individual poles (points). In addition, rose diagrams (yellow) are presented that reflect the trend of the observations. In this example lineations are thought to reflect the motion of Caledonian thrust nappes, and the plots can be used to say something about movement patterns within the lower parts of an orogenic belt. As usual in structural geology, there are different ways of interpreting the data.

A second example is taken from the petroleum province of the North Sea (Figure 1.13). It shows how fault populations look different at different scales and must therefore be treated at the scale suitable to serve the purpose of the study. The Gullfaks oil field itself (Figure 1.13b) is dominated by N–S oriented faults with 100–300 m offset. This is a bit different from the regional NNE–SSE trend seen from Figure 1.13a. It is also different from the large range in orientations shown by small-scale faults within the Gullfaks oil field. These small faults can be subdivided based on orientation, as shown in Figures 1.13c–g. At this point each

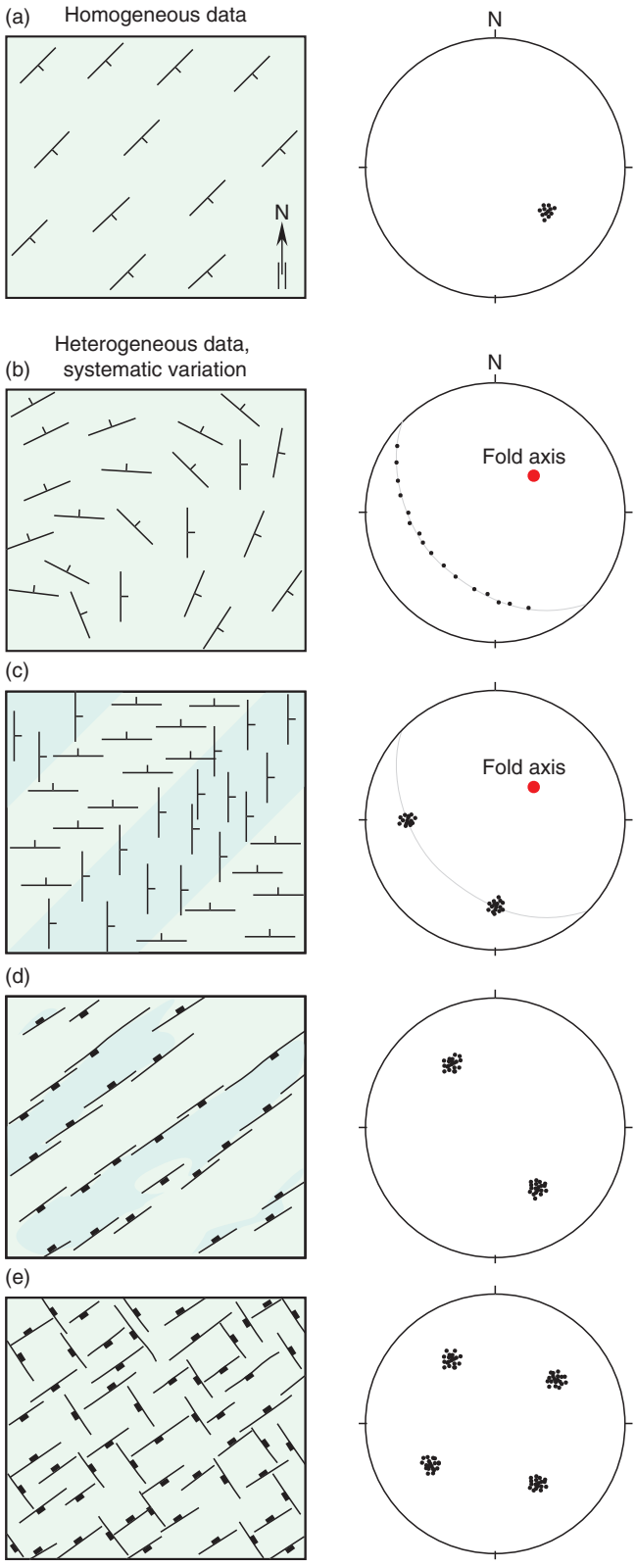

Figure 1.10 Synthetic structural data sets showing different degree of homogeneity. (a) Synthetic homogeneous set of strike and dip measurements. (b) Systematic variation in layer orientation measurements. (c) Homogeneous subareas due to kink or chevron folding. (d, e) Systematic fracture systems. Note how the systematics is reflected in the stereonets.

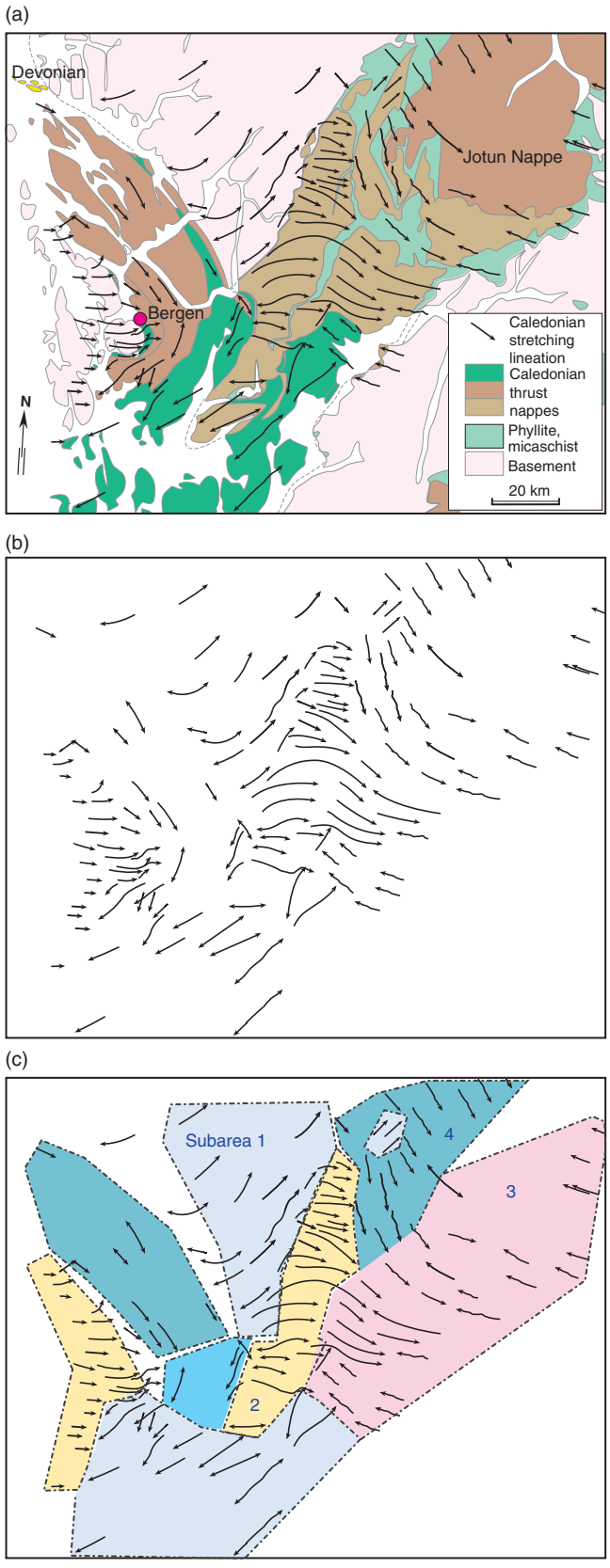

Figure 1.11 (a, b) Caledonian lineation pattern in the Scandinavian Caledonides east of Bergen, Norway. To analyze this pattern, subareas of approximately uniform orientation are defined (c).

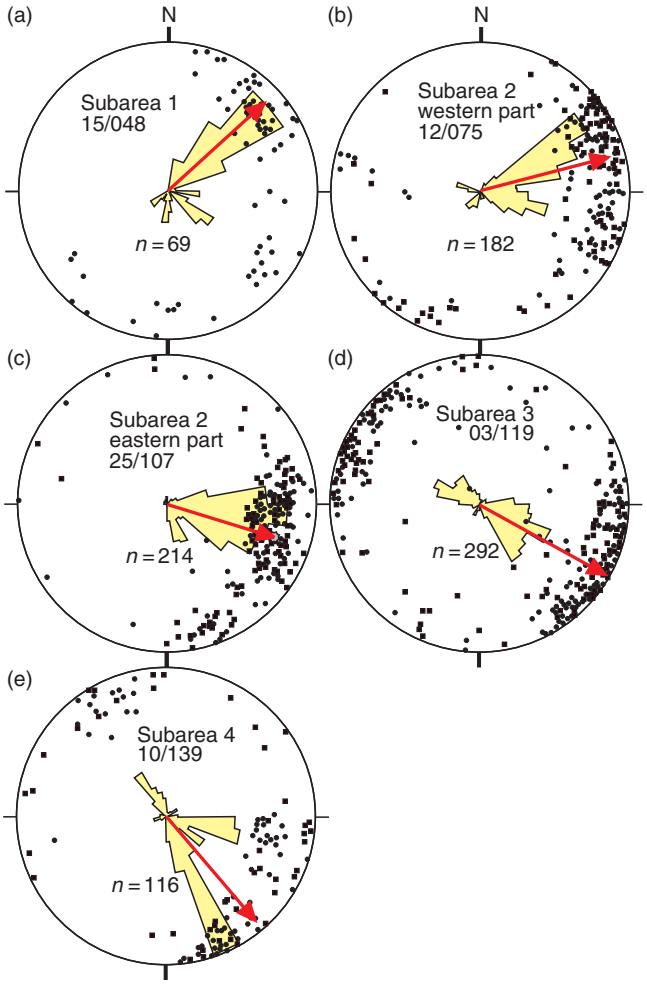

Figure 1.12 Lineation data from subareas defined in the previous figure. The plots show the variations within each subarea, portrayed by means of poles, rose diagrams, and an arrow indicating the average orientation. The number of data within each subarea is indicated by "*n*". From Fossen (1993).

subgroup can be individually analyzed with respect to orientation (stereo plots), displacement, sealing properties, or other factors, depending on the purpose of the study.

1.12 Structural analysis

Many structural processes span thousands to millions of years, and most structural data describe the final product of a long deformation history. The history itself can only be revealed through careful analysis of the data. When looking at a fold, it may not be obvious whether it formed by layer parallel shortening, shearing or passive bending (see Chapter 11). The same thing applies to a fault. What part of the fault formed first? Did it form by linking of individual segments, or did it grow from a single point outward, and if so, was this point in the central part of the present fault surface? It may not always be easy to answer such questions, but the approach should always be to analyze the field information and compare with experimental and/or numerical models.

Geometric analysis

The analysis of the geometry of structures is referred to as geometric analysis. This includes the shape, geographic orientation, size and geometric relation between the main (first-order) structure and related smaller-scale (second-order) structures. The last point emphasizes the fact that most structures are composite and appear in certain **structural associations** at various scales. Hence, various methods are needed to measure and describe structures and structural associations.

Geometric analysis is the classic descriptive approach to structural geology that most secondary structural geologic analytical methods build on.

Shape is the spatial description of open or closed surfaces such as folded layer interfaces or fault surfaces. The shape of folded layers may give information about the fold-forming process or the mechanical properties of the folded layer (Chapter 11), while fault curvature may have implications for hanging-wall deformation (Figure 20.6) or could give information about the slip direction (Figure 8.3).

Orientations of linear and planar structures are perhaps the most common type of structural data. Shapes and geometric features may be described by mathematical functions, for instance by use of vector functions. In most cases, however, natural surfaces are too irregular to be described accurately by simple vector functions, or it may be impossible to map faults or folded layers to the extent required for mathematical description. Nevertheless, it may be necessary to make geometric interpretations of partly exposed structures. Our data will always be incomplete at some level, and our minds tend to search for geometric models when analyzing geologic information. For example, when the Alps were mapped in great detail early in the twentieth century, their major fold structures were generally considered to be cylindrical, which means that fold axes were considered to be straight lines. This model made it possible to project folds onto cross-sections, and impressive sections or geometric models were created. At a later stage it became clear that the folds were in fact non-cylindrical, with curved hinge lines, requiring modification of earlier models.

In geometric analysis it is very useful to represent orientation data (e.g. Figures 1.10 and 1.12) by means

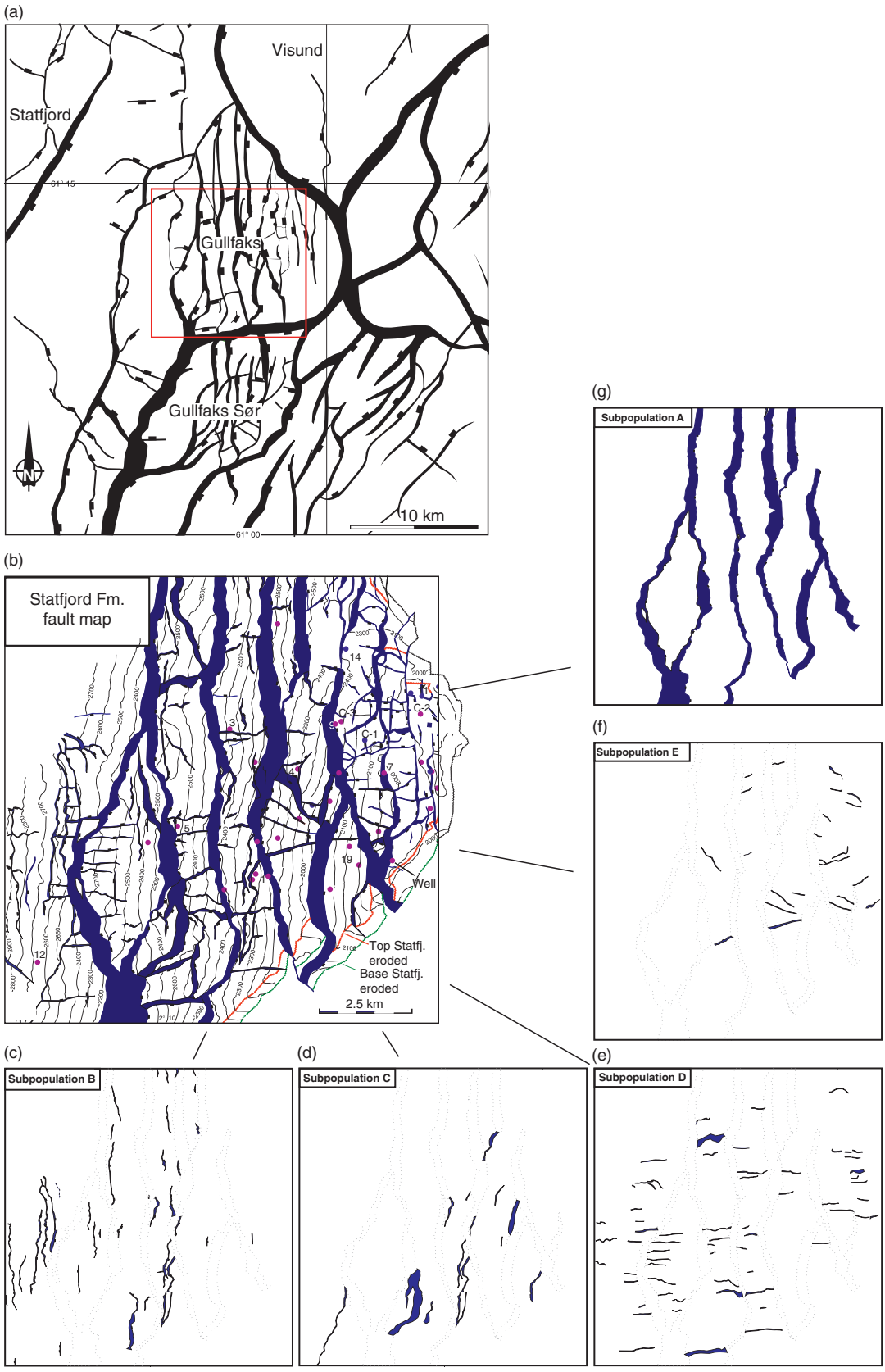

Figure 1.13 This set of figures from the northern North Sea Gullfaks oil field area illustrates how fault patterns may change from one scale to another. Note the contrast between the N–S faults dominating the Gullfaks area and the different orientations of small (<100 m displacement) faults in lower panels. They should be separated as shown for further analysis. See Fossen and Rørnes (1997) for more details.

of **stereographic projection** (see Appendix B). Stereographic projection is used to show or interpret both the orientation and geometry of structures. The method is quick and efficient, and the most widely used tool for presenting and interpreting spatial data. In general, geometry may be presented in the form of maps, profiles, stereographic projections, rose diagrams or three-dimensional models based on observations made in the field, from geophysical data, satellite information or laser scanning equipment. Any serious structural geologist needs to be familiar with the stereographic projection method.

Strain and kinematic analysis

Geometric description and analysis may form the basis for strain quantification or strain analysis. Such quantification is useful in many contexts, e.g. in the restoration of geologic sections through deformed regions. Strain analysis commonly involves **finite strain analysis**, which concerns changes in shape from the initial state to the very end result of the deformation. Structural geologists are also concerned with the deformation history, which can be explored by **incremental strain analysis**. In this case only a portion of the deformation history is considered, and a sequence of increments describes the deformation history.

By definition, strain applies to **ductile deformation**, i.e. deformation where originally continuous structures such as bedding or dikes remain continuous after the deformation. Ductile deformation occurs when rocks **flow** (without fracture) under the influence of stress. The opposite, **brittle deformation**, occurs when rocks break or **fracture**. However, modern geologists do not restrict the use of strain to ductile deformation. In cases where fractures occur in a high number and on a scale that is significantly smaller than the discontinuity each of them causes, the discontinuities are overlooked and the term **brittle strain** is used. It is a simplification that allows us to perform strain analysis on brittle structures such as fault populations.

Geometric description also forms the foundation of **kinematic analysis**, which concerns how rock particles have moved during deformation (the Greek word *kinema* means movement). Striations on fault surfaces (Figure 1.14) and deflection of layering along faults and in shear zones are among the structures that are useful in kinematic analysis.

To illustrate the connection between kinematic analysis and geometric analysis, consider the fault depicted in Figure 1.15a. We cannot correlate the layers from one side to the other, and we do not know whether this is a normal or reverse fault. However, if we find a deflection of the layering along the fault, we can use that geometry to interpret the sense of movement on the fault. Figure 1.15b, c shows the different geometries that we would expect for normal and reverse movements. In other words, a field-based kinematic analysis relies on geometric analysis. More examples of kinematic analysis are given in Chapters 9 and 15, while strain analysis is dealt with in Chapters 3 and 20.

Figure 1.14 Abrasive marks (slickenlines) on fault slip surfaces give local kinematic information. Seismically active fault in the Gulf of Corinth.

Dynamic analysis

Dynamics is the study of forces that cause motion of particles (kinematics). Forces acting on a body generate **stress**, and if the level of stress becomes high enough, rocks start to move. Hence dynamics in the context of structural geology is about the interplay between stress and kinematics. When some particles start to move relative to other particles we get deformation, and we may be able to see changes in shape and the formation of new structures.

Dynamic analysis explores the stresses or forces that cause structures to form and strain to accumulate.

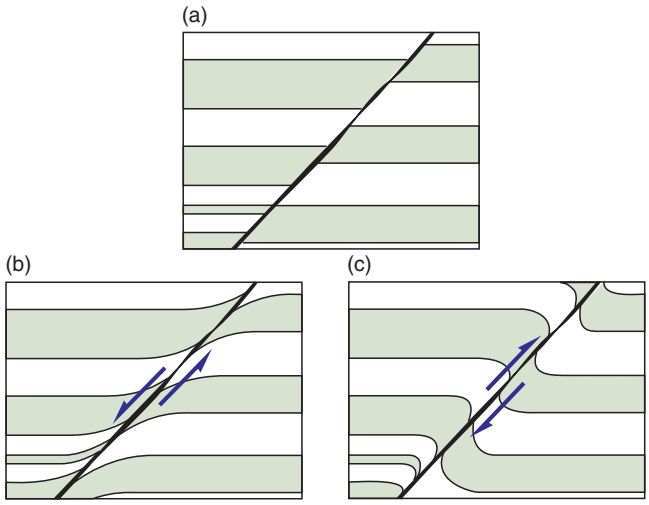

Figure 1.15 An example of how geometric analysis can lead to a kinematic model, in this case of sense of movement on a fault. (a) A fault where stratigraphy cannot be correlated across the fault. (b, c) Relative movement can be determined if layer rotation can be observed close to the fault. The geometry shown in (b) supports a normal fault movement, while (c) illustrates the geometry expected along a reverse fault.

In most cases dynamic analysis seeks to reconstruct the orientation and magnitude of the stress field by studying a set of structures, typically faults and fractures. Returning to the example shown in Figure 1.15, it may be assumed that a strong force or stress acted in the vertical direction in case (b), and in the horizontal direction in case (c). In practice, the exact orientations of forces and stress axes (see Chapters 4 and 5) are difficult or impossible to estimate from a single fault structure, but can be estimated for populations of faults forming in a uniform stress field. This is dealt with in Chapter 9, where it becomes clear that several assumptions have to be made to relate stress and kinematics.

Applying stress to syrup gives a different result than stressing a cold chocolate bar: the syrup will flow, while the chocolate bar will break. We are still dealing with dynamic analyses, but the part of dynamics related to the flow of rocks is referred to as **rheologic analysis**. Similarly, the study of how rocks (or sugar) break or fracture is the field of **mechanical analysis**. In general, rocks flow when they are warm enough, which usually means when they are buried deep enough. "Deep enough" means little more than surface temperatures for salt, around 300 °C for a quartz-rich rock, perhaps closer to 550 °C for a feldspathic rock, and even more for olivine-rich rocks. Pressure also plays an important role, as does water content and strain rate. It is important to realize that different rocks behave differently under any given conditions, but also that the same rock reacts differently to stress under different physical conditions.

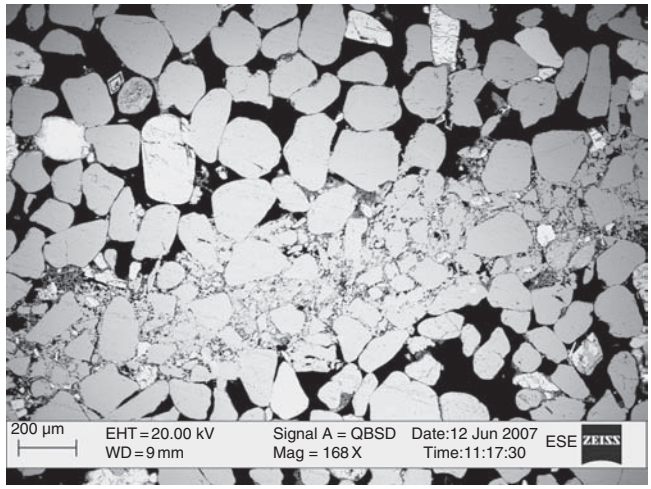

Figure 1.16 Scanning electron microphotograph of a millimeter-thin zone of grain deformation (deformation band) in the Entrada Sandstone near Goblin Valley State Park, Utah. Photo: Anita Torabi.

Rheological testing is done in the laboratory in order to understand how different rocks flow in the lithosphere.

Tectonic analysis

Tectonic analysis involves dynamic, kinematic and geometric analysis at the scale of a basin or orogenic belt. This kind of analysis may therefore involve additional elements of sedimentology, paleontology, petrology, geophysics and other subdisciplines of geoscience. Structural geologists involved in tectonic analysis are sometimes referred to as **tectonicists**. On the opposite end of the scale range, some structural geologists analyze the structures and textures that can only be studied through the microscope. This is the study of how deformation occurs between and within individual mineral grains and is referred to as **microstructural analysis** or **microtectonics**. Both the optical microscope and the scanning electron microscope (SEM) (Figure 1.16) are useful tools in microstructural analysis.

1.13 Concluding remarks

Structural geology has changed from being a descriptive discipline to one where analytical methods and physical and numerical modeling are increasingly important. Many new data types and methods have been applied over the last few decades, and more new methods will probably appear in this field in the years to come. Nevertheless, it is hard to overemphasize the importance of field studies even where the most sophisticated numerical algorithms are being used or where the best 3-D seismic data set is available. The connection between field observations and modeling must be tight. It is the lithosphere and the processes acting in it

that we seek to understand. It is the rocks themselves that contain the information that can reveal their structural or tectonic history. Numerical and physical modeling help us create simple models that capture the main features of a deformed region or a structural problem. Models can also help us understand what is a likely and what is an unlikely or impossible interpretation. However, they must always comply with the information retrievable from the rocks.

Review questions

1. What is structural geology all about?
2. Name the four principal ways a structural geologist can learn about structural geology and rock deformation. How would you rank them?
3. How can we collect structural data sets? Name important data types that can be used for structural analysis.
4. What are the advantages and disadvantages of seismic reflection data sets?
5. What is a scale model?
6. What is kinematic analysis?

E-MODULE

The e-learning module called *Stereographic projection, Structural geology* and Appendix B are recommended for this chapter.

FURTHER READING

Traditional field methods

Lisle, R. J., 2003, Geological Structures and Maps: A Practical Guide. Amsterdam: Elsevier.

McClay, K., 1987, *The Mapping of Geological Structures.* New York: John Wiley and Sons.

Modern field methods

Jones, R. R., McCaffrey, K. J. W., Clegg, P., Wilson, R. W. and Holliman, N. S., 2009, Integration of regional to outcrop digital data: 3D visualisation of multi-scale geological models. *Computers and Geosciences* **35**: 4–18.

McCaffrey, K., Jones, R. R., Holdsworth, R. E., Wilson, R. W., Clegg, P., Imber, J., Hollinman, N. and Trinks, I., 2005, Unlocking the spatial dimension: digital technologies and the future of geoscience fieldwork. *Journal of the Geological Society* **162**: 927–938.

Remote sensing

Hollenstein, M. D., Müller, A. and Geiger, H. -G. K., 2008, Crustal motion and deformation in Greece from a decade of GPS measurements, 1993–2003. *Tectonophysics* **449**: 17–40.

Kreemer, C., Holt, W. E. and Haines, A. J., 2003, An integrated global model of present-day plate motions and plate boundary deformation. *Geophysical Journal International* **154**: 8–34.

Zhang, P.-Z. et al., 2004, Continuous deformation of the Tibetan Plateau from global positioning system data. *Geology* **32**: 809–812.

Physical and numerical modeling

Hubbert, M. K., 1937, Theory of scale models as applied to the study of geologic structures. *Bulletin of the Geological Society of America* **48**: 1459–1520.

Huismans, R. S. and Beaumont, C., 2003, Symmetric and asymmetric lithospheric extension: Relative effects of frictional-plastic and viscous strain softening. *Journal of Geophysical Research* **108**: doi:10.1029/2002JB002026.

Maerten, L. and Maerten, F., 2006, Chronologic modeling of faulted and fractured reservoirs using geomechanically based restoration: Technique and industry applications. *American Association of Petroleum Geologists Bulletin* **90**, 1201–1226.

Chapter 2

Deformation

Deformed rocks and their structures and fabrics can be studied and mapped, and we had a glimpse of some methods and techniques in the previous chapter. Each structure reflects a change in shape and perhaps transport within a given reference frame. We generally refer to these changes as deformation, and as we inspect deformed rocks we automatically start to imagine what the rock could have looked like before the deformation started and what it has gone through. If we want to understand the structures we need to understand the fundamentals of deformation, including some useful definitions and mathematical descriptions. That is the topic of this chapter.

2.1 What is deformation?

The term **deformation** is, like several other structural geology terms, used in different ways by different people and under different circumstances. In most cases, particularly in the field, the term refers to the distortion (strain) that is expressed in a (deformed) rock. This is also what the word literally means: a change in form or shape. However, rock masses can be translated or rotated as rigid units during deformation, without any internal change in shape. For instance, fault blocks can move during deformation without accumulating any internal distortion. Many structural geologists want to include such rigid displacements in the term deformation, and we refer to them as **rigid body deformation**, as opposed to **non-rigid body deformation** (strain or distortion).

Deformation is the transformation from an initial to a final geometry by means of rigid body translation, rigid body rotation, strain (distortion) and/or volume change.

It is useful to think of a rock or rock unit in terms of a continuum of particles. Deformation relates the positions of particles before and after the deformation history, and the positions of points before and after deformation can be connected with vectors. These vectors are called **displacement vectors**, and a field of

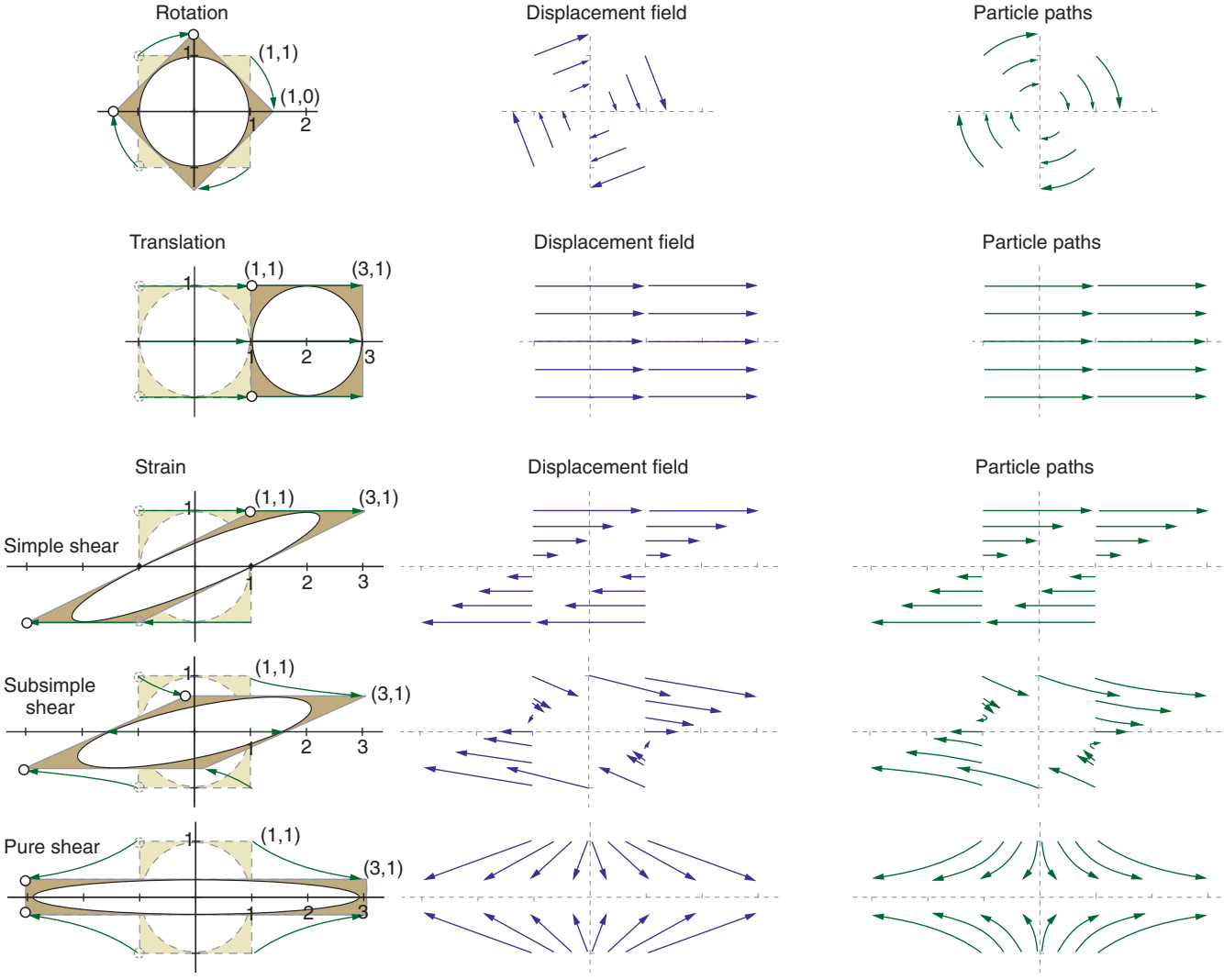

Figure 2.1 Displacement field and particle paths for rigid translation and rotation, and strain resulting from simple shear, subsimple shear and pure shear (explained later in this chapter). Particle paths trace the actual motion of individual particles in the deforming rock, while displacement vectors simply connect the initial and final positions. Hence, displacement vectors can be constructed from particle paths, but not the other way around.

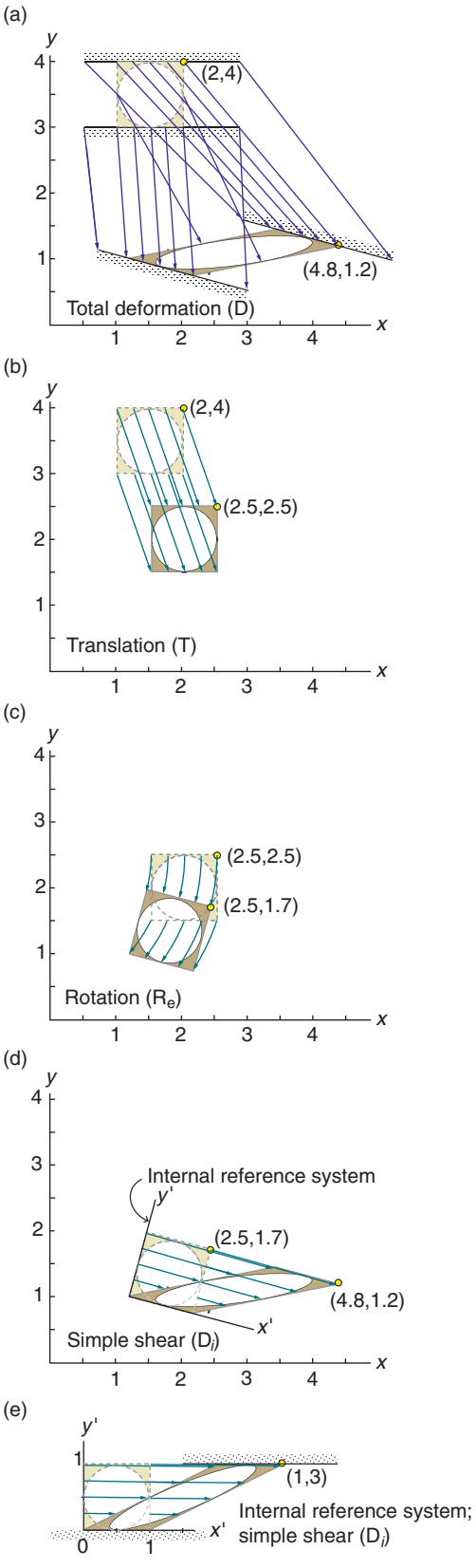

Figure 2.2 (a) The total deformation of an object (square with an internal circle). Arrows in (a) are displacement vectors connecting initial and final particle positions. Arrows in (b)–(e) are particle paths. (b, c) Translation and rotation components of the deformation shown in (a). (d) The strain component. A new coordinate system (x', y') is introduced (d). This internal system eliminates the translation and rotation (b, c) and makes it easier to reveal the strain component, which is here produced by a simple shear (e).

such vectors is referred to as the **displacement field**. Displacement vectors, such as those displayed in the central column of Figure 2.1, do not tell us *how* the particles moved during the deformation history – they merely link the undeformed and deformed states. The actual path that each particle follows during the deformation history is referred to as a **particle path**, and for the deformations shown in Figure 2.1 the paths are shown in the right column (green arrows). When specifically referring to the progressive changes that take place during deformation, terms such as **deformation history** or **progressive deformation** should be used.

2.2 Components of deformation

The displacement field can be decomposed into various components, depending on the purpose of the decomposition. The classic way of decomposing it is by separating rigid body deformation in the form of rigid translation and rotation from change in shape and volume. In Figure 2.2 the translation component is shown in (b), the rotation component in (c) and the rest (the strain) in (d). Let us have a closer look at these expressions.

Translation

Translation moves every particle in the rock in the same direction and the same distance, and its displacement field consists of parallel vectors of equal length. Translations can be considerable, for instance where thrust nappes (detached slices of rocks) have been transported several tens or hundreds of kilometers. The Jotun Nappe (Figure 2.3) is an example from the Scandinavian Caledonides. In this case most of the deformation is rigid translation. We do not know the exact orientation of this nappe prior to the onset of deformation, so we cannot estimate the rigid rotation (see below), but field observations reveal that the change in shape, or strain, is largely confined to the lower parts. The total deformation thus consists of a huge translation component, an unknown but possibly small rigid rotation component and a strain component localized to the base of the nappe.

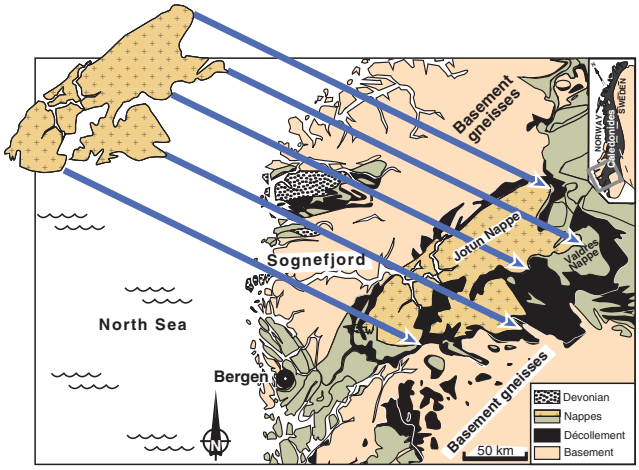

Figure 2.3 The Jotun Nappe in the Scandinavian Caledonides seems to have been transported more than 300 km to the southeast, based on restoration and the orientation of lineations. The displacement vectors are indicated, but the amount of rigid rotation around the vertical axis is unknown. The amount of strain is generally concentrated to the base.

On a smaller scale, rock components (mineral grains, layers or fault blocks) may be translated along slip planes or planar faults without any internal change in shape. One model where there is only translation and rigid rotation is the classic domino fault model, which we will explore in Chapter 17.

Rotation

Rotation is here taken to mean rigid rotation of the entire deformed rock volume that is being studied. It should not be confused with the rotation of the (imaginary) axes of the strain ellipse during progressive deformation, as discussed in Section 2.25. Rigid rotation involves a uniform physical rotation of a rock volume (such as a shear zone) relative to an external coordinate system.

Large-scale rotations of a major thrust nappe or entire tectonic plate typically occur about vertical axes. Fault blocks in extensional settings, on the other hand, may rotate around horizontal axes, and small-scale rotations may occur about any axis.

Strain

Strain or distortion is non-rigid deformation and relatively simple to define:

Any change in shape, with or without change in volume, is referred to as strain, and it implies that particles in a rock have changed positions relative to each other.

A rock volume can be transported (translated) and rotated rigidly in any way and sequence, but we will never be able to tell just from looking at the rock itself. All we can see in the field or in samples is strain, and perhaps the way that strain has accumulated. Consider your lunch bag. You can bring it to school or work, which involves a lot of rotation and translation, but you cannot see this deformation directly. It could be that your lunch bag has been squeezed on your way to school – you can tell by comparing it with what it looked like before you left home. If someone else prepared your lunch and put it in your bag, you would use your knowledge of how a lunch bag should be shaped to estimate the strain (change in shape) involved.

The last point is very relevant, because with very few exceptions, we have not seen the deformed rock in its undeformed state. We then have to use our knowledge of what such rocks typically look like when unstrained. For example, if we find strained ooliths or reduction spots in the rock, we may expect them to have been spherical (circular in cross-section) in the undeformed state.

Volume change

Even if the shape of a rock volume is unchanged, it may have shrunk or expanded. We therefore have to add volume change (area change in two dimensions) for a complete description of deformation. Volume change, also referred to as dilation, is commonly considered to be a special type of strain, called **volumetric strain**. However, it is useful to keep this type of deformation separate if possible.

2.3 System of reference

For studies of deformation, a reference or coordinate system must be chosen. Standing on a dock watching a big ship entering or departing can give the impression that the dock, not the ship, is moving. Unconsciously, the reference system gets fixed to the ship, and the rest of the world moves by translation relative to the ship. While this is fascinating, it is not a very useful choice of reference. Rock deformation must also be considered in the frame of some reference coordinate system, and it must be chosen with care to keep the level of complexity down.

We always need a reference frame when dealing with displacements and kinematics.

It is often useful to orient the coordinate system along important geologic structures. This could be the base of a thrust nappe, a plate boundary or a local shear zone

(see Chapter 15). In many cases we want to eliminate translation and rigid rotation. In the case of shear zones we normally place two axes parallel to the shear zone with the third being perpendicular to the zone. If we are interested in the deformation in the shear zone as a whole, the origin could be fixed to the margin of the zone. If we are interested in what is going on around any given particle in the zone we can "glue" the origin to a particle within the zone (still parallel/perpendicular to the shear zone boundaries). In both cases translation and rigid rotation of the shear zone are eliminated, because the coordinate system rotates and translates along with the shear zone. There is nothing wrong with a coordinate system that is oblique to the shear zone boundaries, but visually and mathematically it makes things more complicated.

2.4 Deformation: detached from history

Deformation is the difference between the deformed and undeformed states. It tells us nothing about what actually happened during the deformation history.

A given strain may have accumulated in an infinite number of ways.

Imagine a tired student (or professor for that matter) who falls asleep in a boat while fishing on the sea or a lake. The student knows where he or she was when falling asleep, and soon figures out the new location when waking up, but the exact path that currents and winds have taken the boat is unknown. The student only knows the position of the boat before and after the nap, and can evaluate the strain (change in shape) of the boat (hopefully zero). One can map the deformation, but not the deformation history.

Let us also consider **particle flow**: Students walking from one lecture hall to another may follow infinitely many paths (the different paths may take longer or shorter time, but deformation itself does not involve time). All the lecturer knows, busy between classes, is that the students have moved from one lecture hall to the other. Their history is unknown to the lecturer (although he or she may have some theories based on cups of hot coffee etc.). In a similar way, rock particles may move along a variety of paths from the undeformed to the deformed state. One difference between rock particles and individual students is of course that students are free to move on an individual basis, while rock particles, such as mineral grains in a rock, are "glued" to one another in a solid continuum and cannot operate freely.

2.5 Homogeneous and heterogeneous deformation

Where the deformation applied to a rock volume is identical throughout that volume, the deformation is homogeneous. Rigid rotation and translation by definition are homogenous, so it is always strain and volume or area change that can be heterogeneous. Thus **homogeneous deformation** and **homogeneous strain** are equivalent expressions.

For homogeneous deformation, originally straight and parallel lines will be straight and parallel also after the deformation, as demonstrated in Figure 2.4. Further, the strain and volume/area change will be constant throughout the volume of rock under consideration. If not, then the deformation is **heterogeneous** (inhomogeneous). This means that two objects with identical initial shape and orientation will end up having identical shape and orientation after the deformation. Note, however, that the initial shape and orientation in general will differ from the final shape and orientation. If two objects have identical shapes but different orientations before deformation, then they will generally have different shapes after deformation even if the deformation is homogeneous. An example is the deformed brachiopods in Figure 2.4. The difference reflects the strain imposed on the rock.

Homogeneous deformation: Straight lines remain straight, parallel lines remain parallel, and identically shaped and oriented objects will also be identically shaped and oriented after the deformation.

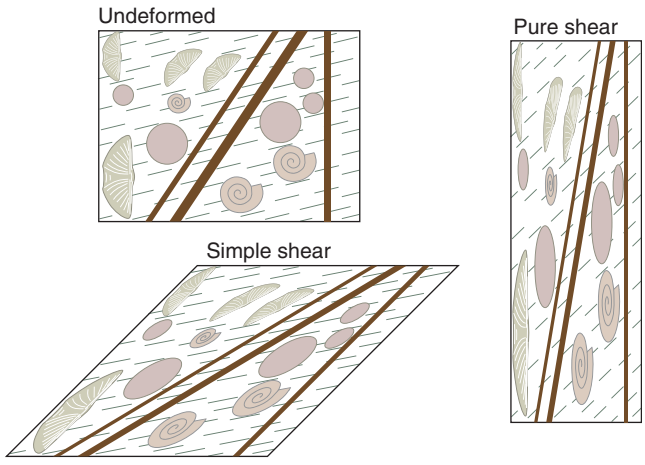

Figure 2.4 Homogeneous deformations of a rock with brachiopods, reduction spots, ammonites and dikes. Two different deformations are shown (pure and simple shear). Note that the brachiopods that are differently oriented before deformation obtain different shapes.

A circle will be converted into an ellipse during homogeneous deformation, where the **ellipticity** (ratio between the long and short axes of the ellipse) will depend on the type and intensity of the deformation. Mathematically, this is identical to saying that homogeneous deformation is a linear transformation. Homogeneous deformation can therefore be described by a set of first-order equations (three in three dimensions) or, more simply, by a transformation matrix referred to as the deformation matrix.

Before looking at the deformation matrix, the point made in Figure 2.5 must be emphasized:

A deformation that is homogeneous on one scale may be considered heterogeneous on a different scale.

A classic example is the increase in strain typically seen from the margin toward the center of a shear zone. The strain is heterogeneous on this scale, but can be subdivided into thinner elements or zones in which strain is approximately homogeneous. Another example is shown in Figure 2.6, where a rock volume is penetrated by faults. On a large scale, the deformation may be considered homogeneous because the discontinuities represented by the faults are relatively small. On a smaller scale, however, those discontinuities become more apparent, and the deformation must be considered heterogeneous.

2.6 Mathematical description of deformation

Deformation is conveniently and accurately described and modeled by means of elementary linear algebra. Let us use a local coordinate system, such as one attached to a shear zone, to look at some fundamental deformation types. We will think in terms of particle positions (or vectors) and see how particles change positions during deformation. If (x, y) is the original position of a particle, then the new position will be denoted (x', y'). For homogeneous deformation in two dimensions (i.e. in a section) we have that

$$\begin{aligned} x' &= D_{11}x + D_{12}y \\ y' &= D_{21}x + D_{22}y \end{aligned} \tag{2.1}$$

These equations can be written in terms of matrices and position vectors as

$$\begin{bmatrix} x' \\ y' \end{bmatrix} = \begin{bmatrix} D_{11} & D_{12} \\ D_{21} & D_{22} \end{bmatrix} \begin{bmatrix} x \\ y \end{bmatrix} \tag{2.2}$$

which can be written

$$\mathbf{x}' = \mathbf{D}\mathbf{x} \tag{2.3}$$

The matrix **D** is called the deformation matrix or the position gradient tensor, and the equation describes a linear transformation or a homogeneous deformation.

There is a corresponding or inverse matrix $\mathbf{D}^{-1}$ (where the matrix product $\mathbf{D}\mathbf{D}^{-1} = \mathbf{I}$ and **I** is the identity matrix) that represents the **reciprocal** or **inverse deformation**. $\mathbf{D}^{-1}$ reverses the deformation imposed by **D**:

$$\mathbf{x} = \mathbf{D}^{-1}\mathbf{x}' \tag{2.4}$$

The reciprocal or inverse deformation takes the deformed rock back to its undeformed state.

The deformation matrix **D** is very useful if one wants to model deformation using a computer. Once the deformation matrix is defined, any aspect of the deformation itself can be found. Once again, it tells us nothing about the deformation history, nor does it reveal how a given deforming medium responds to such a deformation. For more information about matrix algebra, see Box 2.1.

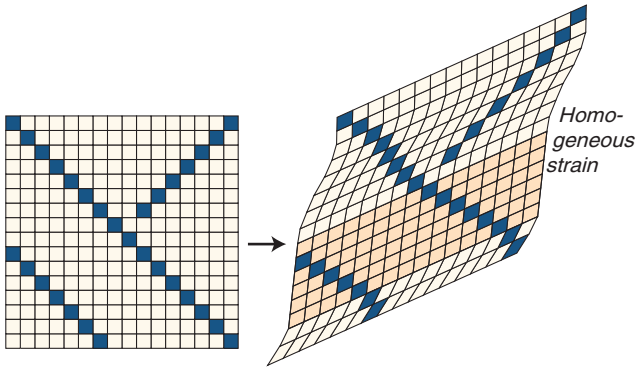

Figure 2.5 A regular grid in undeformed and deformed state. The overall strain is heterogeneous, so that some of the straight lines have become curved. However, in a restricted portion of the grid, the strain is homogeneous. In this case the strain is also homogeneous at the scale of a grid cell.

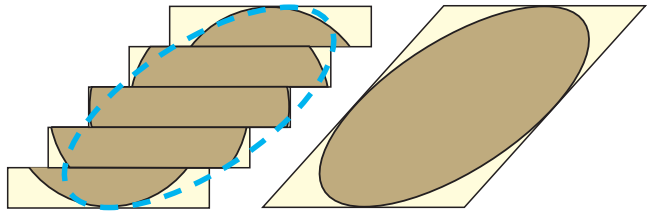

Figure 2.6 Discrete or discontinuous deformation can be approximated as continuous and even homogeneous in some cases. In this sense the concept of strain can also be applied to brittle deformation (brittle strain). The success of doing so depends on the scale of observation.

BOX 2.1 MATRIX ALGEBRA

Matrices contain coefficients of systems of equations that represent linear transformations. In two dimensions this means that the system of equations shown in Equation 2.1 can be expressed by the matrix of Equation 2.2. A linear transformation implies a homogeneous deformation. The matrix describes the shape and orientation of the strain ellipse or ellipsoid, and the transformation is a change from a unit circle, or a unit sphere in three dimensions.

Matrices are simpler to handle than sets of equations, particularly when applied in computer programs. The most important matrix operations in structural geology are multiplications and finding eigenvectors and eigenvalues:

Matrix multiplied by a vector:

$$\begin{bmatrix} D_{11} & D_{12} \\ D_{21} & D_{22} \end{bmatrix} \begin{bmatrix} x \\ y \end{bmatrix} = \begin{bmatrix} D_{11}x + D_{12}y \\ D_{21}x + D_{22}y \end{bmatrix}$$

Matrix–matrix multiplication:

$$\begin{bmatrix} D_{11} & D_{12} \\ D_{21} & D_{22} \end{bmatrix} \begin{bmatrix} d_{11} & d_{12} \\ d_{21} & d_{22} \end{bmatrix} = \begin{bmatrix} D_{11}d_{11} + D_{12}d_{21} & D_{11}d_{12} + D_{12}d_{22} \\ D_{21}d_{11} + D_{22}d_{21} & D_{21}d_{12} + D_{22}d_{22} \end{bmatrix}$$

Transposition, meaning shifting of columns and rows in a matrix:

$$\begin{bmatrix} D_{11} & D_{12} \\ D_{21} & D_{22} \end{bmatrix}^{\mathrm{T}} = \begin{bmatrix} D_{11} & D_{21} \\ D_{12} & D_{22} \end{bmatrix}$$

The inverse of a matrix $\mathbf{D}$ is denoted $\mathbf{D}^{-1}$ and is the matrix that gives the identity matrix $\mathbf{I}$ when multiplied by $\mathbf{D}$:

$$\begin{bmatrix} D_{11} & D_{12} \\ D_{21} & D_{22} \end{bmatrix}^{-1} \begin{bmatrix} D_{11} & D_{12} \\ D_{21} & D_{22} \end{bmatrix} = \begin{bmatrix} 1 & 0 \\ 0 & 1 \end{bmatrix} = \mathbf{I}$$

Matrix multiplication is non-commutative:

$$\mathbf{D}_1\mathbf{D}_2 \neq \mathbf{D}_2\mathbf{D}_1$$

The determinant of a matrix $\mathbf{D}$ is

$$\det \mathbf{D} = \begin{vmatrix} \mathrm{D}_{11} & \mathrm{D}_{12} \\ \mathrm{D}_{21} & \mathrm{D}_{22} \end{vmatrix} = \mathbf{D}_{11}\mathbf{D}_{22} - \mathbf{D}_{21}\mathbf{D}_{12}$$

The determinant describes the area or volume change: If $\det \mathbf{D} = 1$ then there is no area or volume change involved for the transformation (deformation) represented by $\mathbf{D}$.

Eigenvectors (x) and eigenvalues (λ) of a matrix $\mathbf{A}$ are the vectors and values that fulfill

$$\mathbf{A}x = \lambda x$$

If $\mathbf{A} = \mathbf{D}\mathbf{D}^{\mathrm{T}}$, then the deformation matrix has two eigenvectors for two dimensions and three for three dimensions. The eigenvectors describe the orientation of the ellipsoid (ellipse), and the eigenvalues describe its shape (length of its principal axes) (see Appendix A). Eigenvalues and eigenvectors are easily found by means of a spreadsheet or computer program such as MatLab™.

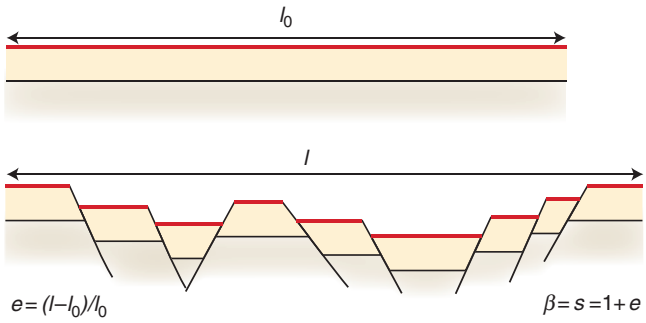

Figure 2.7 Extension of layers by faulting. The red layer has an original (l_0) and a new length, and the extension e is found by comparing the two. The beta-factor (β) is commonly used to quantify extension across extensional basins.

2.7 One-dimensional strain

In one dimension (a single direction), strain is about stretching and shortening (negative stretching) of lines or approximately linear (straight) objects. One might say that one-dimensional strain makes no sense, since an extending straight line does not change shape, just length. On the other hand, a change in shape, such as a circle changing into an ellipse, can be described by the change in length of lines of different orientations. It is therefore convenient to include change of line lengths in the concept of strain.

There are special terms in use, such as elongation, extension, stretching, contraction, shortening, and, as any other strain quantity, they are dimensionless.

Elongation (e or ε) of a line is defined as $e=(l-l_0)/l_0$, where l_0 and l are the lengths of the line before and after deformation, respectively (Figure 2.7). The line may represent a horizontal line or bedding trace in a cross-section, the long axis of a belemnite or some other fossil on which a line can be defined, the vertical direction in a rock mechanics experiment, and many other things. The logarithmic or **natural elongation** $\bar{e}=\ln(e)$ is also in use.

Extension of a line is identical to elongation (e) and is used in the analysis of extensional basins where the elongation of a horizontal line in the extension direction indicates the extension. Negative extension is called **contraction** (the related terms compression and tension are reserved for stress).

Stretching of a line is designated $s=1+e$, where s is called the stretch. Hence, $s=l/l_0$. **Stretching factors** are commonly referred to in structural analysis of rifts and extensional basins. These are sometimes called β-factors, but are identical to s.

Quadratic elongation, $\lambda=s^2$, is identical to the eigenvalues of the deformation matrix **D**. Quadratic stretch would be a better name, because we are looking at the square value of the stretch, not of the elongation. Nevertheless, quadratic elongation is the term in common use.

Natural strain, $\bar{e}$, is simply $\ln(s)$ or $\ln(1+e)$.

2.8 Strain in two dimensions

Observations of strain in planes or sections are described by the following dimensionless quantities:

Angular shear, ψ, which describes the change in angle between two originally perpendicular lines in a deformed medium (Figures 2.8 and 2.9).

Shear strain, $\gamma=\tan\psi$, where ψ is the angular shear (Figure 2.8). The shear strain can be found where objects of known initial angular relations occur. Where a number of such objects occur within a homogeneously strained area, the strain ellipse can be found.

The **strain ellipse** is the ellipse that describes the amount of elongation in any direction in a plane of homogeneous deformation (Box 2.2). It represents the deformed shape of an imaginary circle on the undeformed section. The strain ellipse is conveniently described by a long (X) and a short (Y) axis. The two

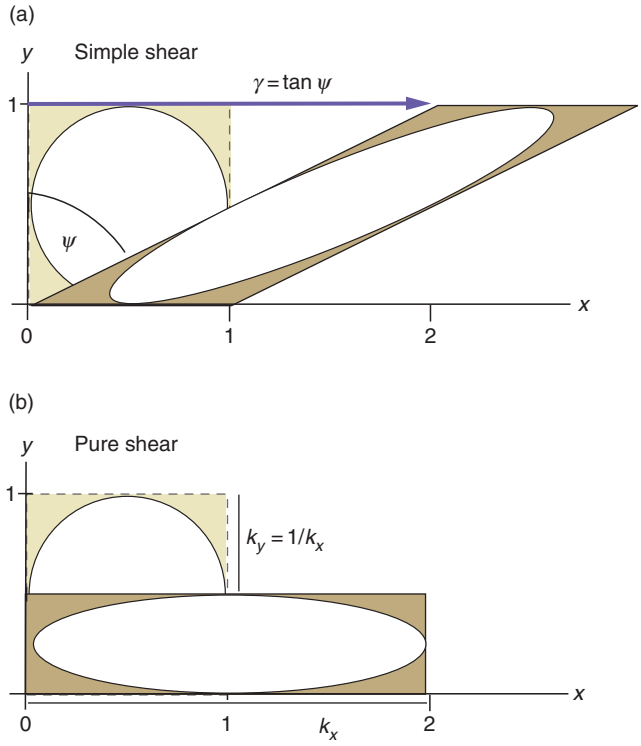

Figure 2.8 Simple and pure shear.

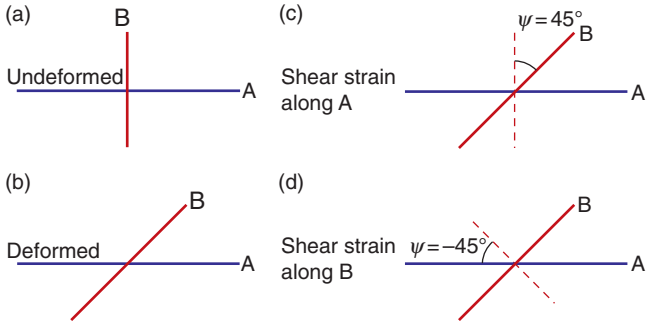

Figure 2.9 Angular shear strain is the change in angle between two initially perpendicular lines, and is positive for clockwise rotations and negative for anti-clockwise rotations. In this example the angular shear strain is 45° along line A and −45° along line B.

BOX 2.2 THE SECTIONAL STRAIN ELLIPSE

X, *Y* and *Z* are the three principal strains or strain axes in three-dimensional strain analysis. However, when considering a section, *X* and *Y* are commonly used regardless of the orientation of the section relative to the strain ellipsoid. It would perhaps be better to name them *X*′ and *Y*′ or something similar, and reserve the designations *X*, *Y* and *Z* for the true principal strains in three dimensions. An arbitrary section through a deformed rock contains a strain ellipse that is called a **sectional strain ellipse**. It is important to specify which section we are describing at any time.

axes have lengths $1 + e_1$ and $1 + e_2$, and the ratio $R = X/Y$ or $(1 + e_1)/(1 + e_2)$ describes the ellipticity or eccentricity of the ellipse and thus the strain that it represents. For a circle (no strain), $R = 1$.

Area change: For area change without any strain, $R = X/Y = 1$. A circle drawn on the initial section remains a circle after a pure area change, albeit with a smaller or larger radius. In a simple diagram where *X* is plotted against *Y*, **isochoric** deformations will plot along the main diagonal (Figure 2.10). The same diagram illustrates strain fields characteristic for different combinations of area change and strain. We will later look at the different types of structures formed in these different fields.

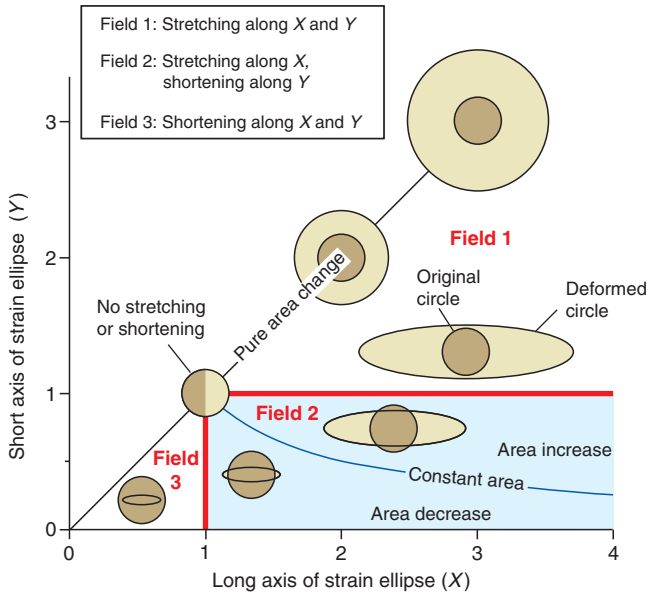

Figure 2.10 Classification of strain ellipses. Only the lower part of the diagram is in use because $X \geq Y$. Note that Field 2 is divided in two by the constant area line. The plot is called an *X*–*Y* plot, but we could also call it an *X*–*Z* plot if we plot the largest and smallest principal strains. Based on Ramsay and Huber (1983).

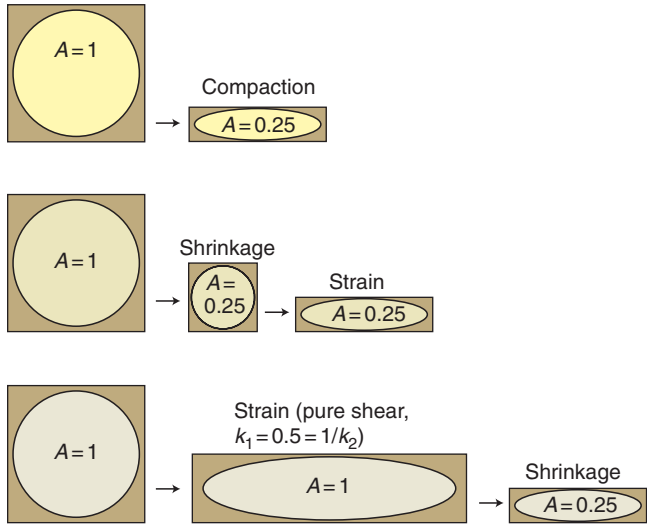

Figure 2.11 Compaction involves strain. The deformation can be considered as a combination of uniform shrinking and strain (middle drawings). The lower drawings illustrate that the order (strain versus dilation) is irrelevant (only true for coaxial deformations): the final strain ellipses are identical for the three cases.

It will always be possible to decompose a deformation into some combination of area change and strain, i.e. to isolate the strain and area change components. Figure 2.11 shows how compaction can be decomposed into a strain and an area change.

2.9 Three-dimensional strain

The spectrum of possible states of strain widens significantly if we allow for stretching and contraction in three dimensions. Classic reference situations are known as uniform extension, uniform flattening and plane strain, as illustrated in Figure 2.12. **Uniform extension**, also referred to as axially symmetric extension, is a state of strain where stretching in X is compensated for by equal shortening in the plane orthogonal to X. **Uniform flattening** (axially symmetric flattening) is the opposite, with shortening in a direction Z compensated for by identical stretching in all directions perpendicular to Z. These two reference states are end-members in a continuous spectrum of deformation types. Between uniform flattening and extension lies **plane strain**, where stretching in one direction is perfectly compensated by shortening in a single perpendicular direction. The strain is "plane" or two-dimensional because there is no stretching or shortening in the third principal direction, i.e. along the Y-axis.

Strain is said to be plane (two-dimensional) where there is no length change along the *Y*-axis, while three-dimensional strain implies a length change along *X*, *Y* and *Z*.

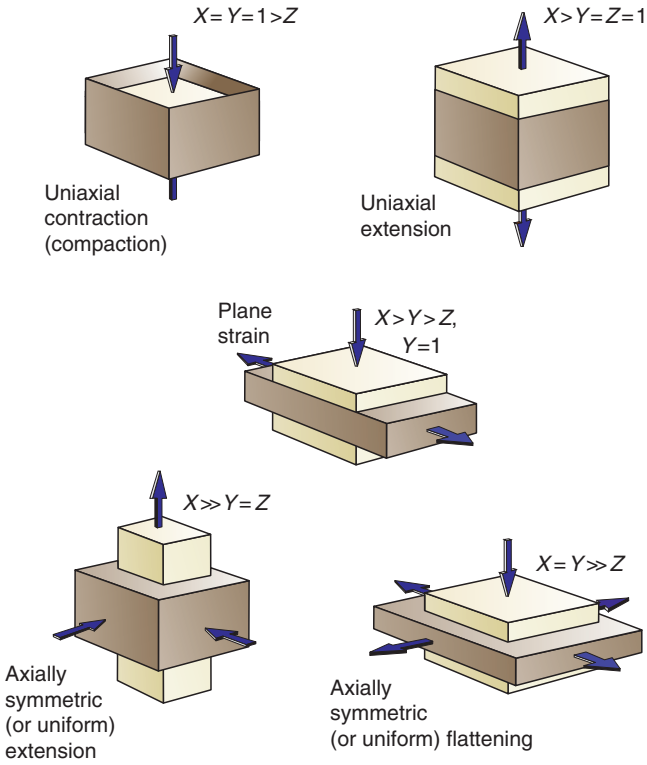

Figure 2.12 Some reference states of strain. The conditions are uniaxial (top), planar (middle) and three-dimensional (bottom).

2.10 The strain ellipsoid

The finite spatial change in shape that is connected with deformation is completely described by the **strain ellipsoid**. The strain ellipsoid is the deformed shape of an imaginary sphere with unit radius that is deformed along with the rock volume under consideration.

The strain ellipsoid has three mutually orthogonal planes of symmetry, the **principal planes of strain**, which intersect along three orthogonal axes that are referred to as the **principal strain axes**. Their lengths (values) are called the **principal stretches**. These axes are commonly designated X, Y and Z, but the designations $\sqrt{\lambda_1}$, $\sqrt{\lambda_2}$ and $\sqrt{\lambda_3}$, S_1, S_2 and S_3 as well as ε_1, ε_2 and ε_3 are also used. We will use X, Y and Z in this book, where X represents the longest, Z the shortest and Y the intermediate axis:

$$X > Y > Z$$

When the ellipsoid is fixed in space, the axes may be considered vectors of given lengths and orientations. Knowledge of these vectors thus means knowledge of both the shape and orientation of the ellipsoid. The vectors are named $\mathbf{e}_1$, $\mathbf{e}_2$ and $\mathbf{e}_3$, where $\mathbf{e}_1$ is the longest and $\mathbf{e}_3$ the shortest, as shown in Figure 2.13.

If we place a coordinate system with axes x, y and z along the principal strain axes X, Y and Z, we can write the equation for the strain ellipse as

$$\frac{x^2}{\lambda_1^2} + \frac{y^2}{\lambda_2^2} + \frac{z^2}{\lambda_3^2} = 1 \qquad (2.4)$$

It can be shown that λ_1, λ_2 and λ_3 are the eigenvalues of the matrix product $\mathbf{DD}^{\mathrm{T}}$, and that $\mathbf{e}_1$, $\mathbf{e}_2$ and $\mathbf{e}_3$ are the corresponding eigenvectors (see Appendix A). So if $\mathbf{D}$ is known, one can easily calculate the orientation and shape of the strain ellipsoid or vice versa. A deformation matrix would look different depending on the choice of coordinate system. However, the eigenvectors and eigenvalues will always be identical for any given state of strain. Another way of saying the same thing is that they are **strain invariants**. Shear strain, volumetric strain and the kinematic vorticity number (W_k) are other examples of strain invariants. Here is another characteristic related to the strain ellipsoid:

Lines that are parallel with the principal strain axes are orthogonal, and were also orthogonal in the undeformed state.

This means that they have experienced no finite shear strain. No other set of lines has this property. Thus,

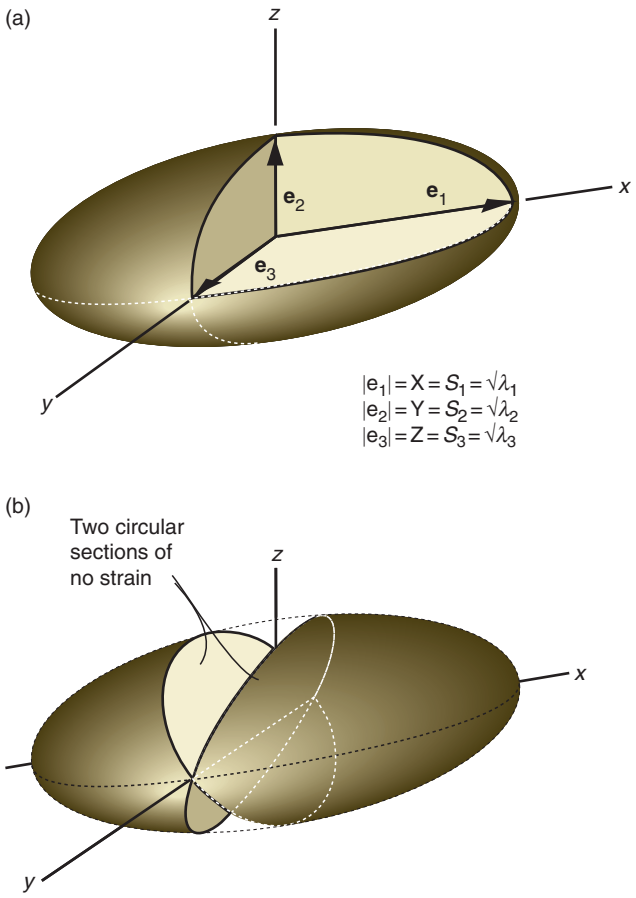

Figure 2.13 (a) The strain ellipsoid is an imaginary sphere that has been deformed along with the rock. It depends on homogeneous deformation and is described by three vectors, $\mathbf{e}_1$, $\mathbf{e}_2$ and $\mathbf{e}_3$, defining the principal axes of strain (X, Y and Z) and the orientation of the ellipsoid. The length of the vectors thus describes the shape of the ellipsoid, which is independent of choice of coordinate system. (b) The ellipsoid for plane strain, showing the two sections through the ellipsoid that display no strain.

estimating shear strain from sets of originally orthogonal lines gives information about the orientation of X, Y and Z (see next chapter). This goes for two- as well as three-dimensional strain considerations.

2.11 More about the strain ellipsoid

Any strain ellipsoid contains two **surfaces of no finite strain**. For constant volume deformations, known as **isochoric deformations**, these surfaces are found by connecting points along the lines of intersection between the ellipsoid and the unit sphere it was deformed from. For plane strain, where the intermediate principal strain axis has unit length, these surfaces happen to be planar (Figure 2.13b). In general, when strain is three-dimensional, the surfaces of no finite strain are non-planar. Lines contained in these surfaces have the same length as in the undeformed state for constant volume deformations, or are stretched an equal amount if a volume change is involved. This means that:

A plane strain deformation produces two planes in which the rock appears unstrained.

It also means that physical lines and particles move through these theoretical planes during progressive deformation.

The shape of the strain ellipsoid can be visualized by plotting the axial ratios X/Y and Y/Z as coordinate axes. As shown in Figure 2.14a, logarithmic axes are commonly used for such diagrams. This widely used diagram is called the **Flinn diagram**, after the British geologist Derek Flinn who first published it in 1962. The diagonal of the diagram describes strains where $X/Y = Y/Z$, i.e. planar strain. It separates **prolate** geometries or cigar shapes of the upper half of the field from **oblate** geometries or pancake shapes of the lower half. The actual shape of the ellipsoid is characterized by the Flinn k-value: $k = (R_{XY} - 1)/(R_{YZ} - 1)$, where $R_{XY} = X/Y$ and $R_{YZ} = Y/Z$.

The horizontal and vertical axes in the Flinn diagram represent axially symmetric flattening and extension, respectively. Any point in the diagram represents a unique combination of strain magnitude and three-dimensional shape or **strain geometry**, i.e. a strain ellipsoid with a unique Flinn k-value. However, different types of deformations may in some cases produce ellipsoids with the same k-value, in which case other criteria are needed for separation. An example is pure shear and simple shear (see below), which both plot along the diagonal of the Flinn diagram ($k = 1$). The orientation of the strain ellipse is different for simple and pure shear, but this is not reflected in the Flinn diagram. Thus, the diagram is useful within its limitations.

In the Flinn diagram, strain magnitude generally increases away from the origin. Direct comparison of strain magnitude in the various parts of the diagram is, however, not trivial. How does one compare pancake-shaped and cigar-shaped ellipsoids? Which one is more strained? We can use the radius (distance from the origin; dashed lines in Figure 2.14), although there is no good mathematical or physical reason why this would be an accurate measure of strain magnitude. An alternative parameter is given by the formula

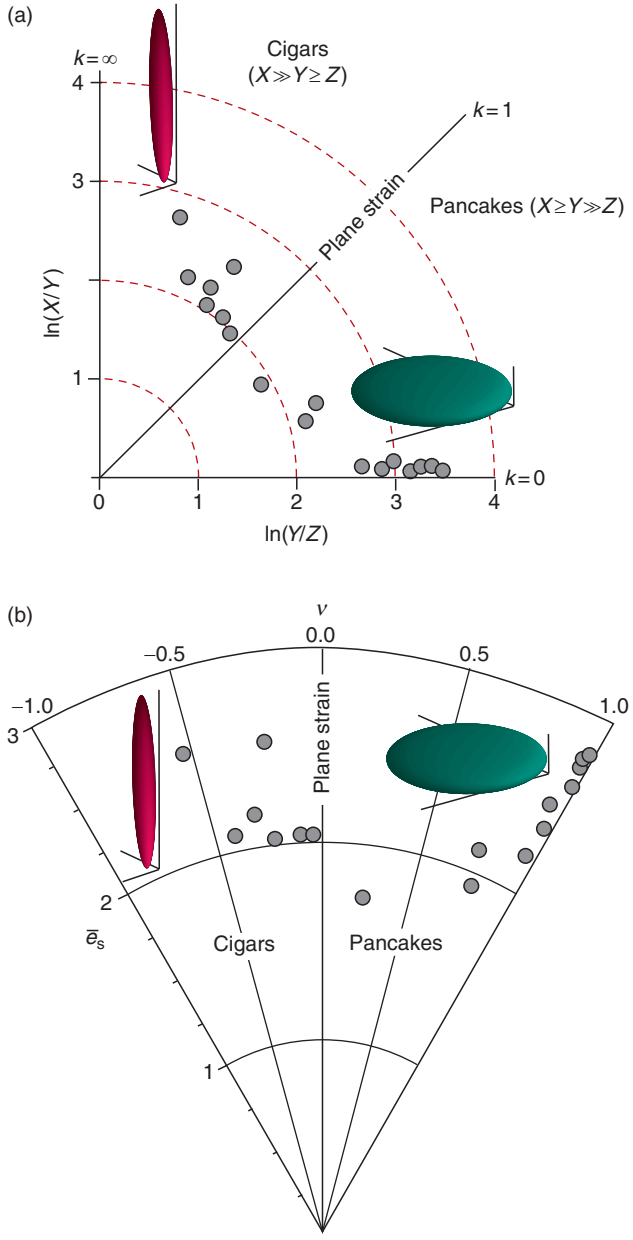

Figure 2.14 Strain data can be represented in (a) the Flinn diagram (linear or logarithmic axes) or (b) the Hsü diagram. The same data are plotted in the two diagrams for comparison. Data from Holst and Fossen (1987).

$$\bar{e}_s = \frac{\sqrt{3}}{2}\bar{\gamma}_{oct} \tag{2.5}$$

The variable $\bar{e}_s$ is called the natural octahedral unit shear, and

$$\bar{\gamma}_{oct} = \frac{2}{3}\sqrt{(\bar{e}_1 - \bar{e}_2)^2 + (\bar{e}_2 - \bar{e}_3)^2 + (\bar{e}_3 - \bar{e}_1)^2} \tag{2.6}$$

where the $\bar{e}$'s are the natural principal strains. This unit shear is directly related to the mechanical work that is performed during the deformation history. It does however not take into consideration the rotation of the strain ellipse that occurs for non-coaxial deformations (see Section 2.12) and is therefore best suited for coaxial deformations.

An alternative strain diagram can be defined by means of $\bar{\gamma}_{oct}$, where the natural octahedral unit shear is plotted against a parameter v called the Lode parameter, where

$$v = \frac{2\bar{e}_2 - \bar{e}_1 - \bar{e}_3}{\bar{e}_1 - \bar{e}_3} \tag{2.7}$$

This diagram is shown in Figure 2.14b, and is known as the **Hsü diagram**. The radial lines in this diagram indicate equal amounts of strain, based on the natural octahedral unit shear.

2.12 Volume change

A pure volume change or **volumetric strain** of an object is given by $\Delta = (V - V_0)/V_0$, where V_0 and V are volumes of the object before and after the deformation, respectively. The volume factor Δ is thus negative for volume decrease and positive for volume increase. The deformation matrix that describes general volume change is

$$\begin{bmatrix} D_{11} & 0 & 0 \\ 0 & D_{22} & 0 \\ 0 & 0 & D_{33} \end{bmatrix} = \begin{bmatrix} 1+\Delta_1 & 0 & 0 \\ 0 & 1+\Delta_2 & 0 \\ 0 & 0 & 1+\Delta_3 \end{bmatrix} \tag{2.8}$$

The product $D_{11}D_{22}D_{33}$, which is identical to the determinant of the matrix in Equation 2.8 (see Box 2.3), is always different from 1. This goes for any deformation that involves a change in volume (or area in two dimensions). The closer $\det \mathbf{D}$ is to 1, the smaller the volume (area) change. Volume and area changes do not involve any internal rotation, meaning that lines parallel to the principal strain axes have the same orientations that they had in the undeformed state. Such deformation is called **coaxial**.

A distinction is sometimes drawn between isotropic and anisotropic volume change. **Isotropic volume change** (Figure 2.15) is real volume change where the object is equally shortened or extended in all directions, i.e. the diagonal elements in Equation 2.8 are equal and $\det \mathbf{D} \neq 1$. This means that any marker object has decreased or increased in size, but retained its shape. So, strictly speaking, there is no change in shape involved in isotropic volume change, and the only strain involved is a volumetric strain. In two dimensions, there is

BOX 2.3 THE DETERMINANT OF THE DEFORMATION MATRIX D

The determinant of a matrix **D** is generally found by the following formula:

$$\det\begin{bmatrix} D_{11} & D_{12} & D_{13} \\ D_{21} & D_{22} & D_{23} \\ D_{31} & D_{32} & D_{33} \end{bmatrix} = D_{11}(D_{22}D_{33} - D_{23}D_{32}) - D_{12}(D_{21}D_{33} - D_{23}D_{31}) + D_{13}(D_{21}D_{32} - D_{22}D_{31})$$

If the matrix is diagonal, meaning that it has non-zero values along the diagonal only, then det **D** is the product of the diagonal entries of **D**. Fortunately, this is also the case for triangular matrices, i.e. matrices that have only zeros below (or above) the diagonal:

$$\det\begin{bmatrix} D_{11} & D_{12} & D_{13} \\ 0 & D_{22} & D_{23} \\ 0 & 0 & D_{33} \end{bmatrix} = D_{11}D_{22}D_{33}$$

The deformation matrices for volume change and pure shear are both examples of diagonal matrices, and those for simple and subsimple shear are triangular matrices. When det $\mathbf{D} = 1$, then the deformation represented by the matrix is isochoric, i.e. it involves no change in volume.

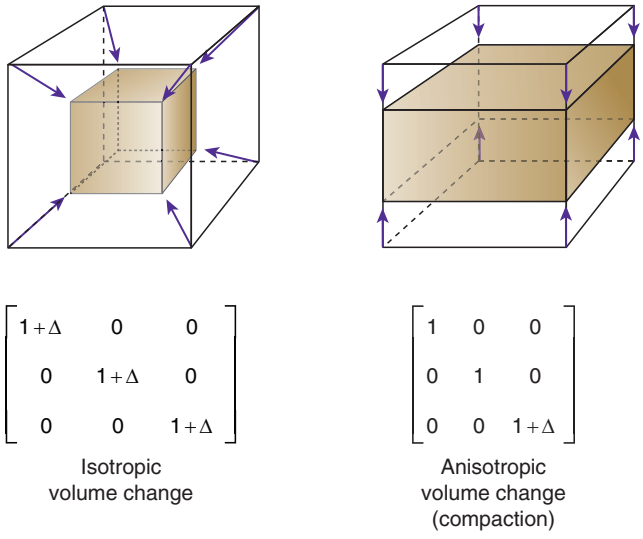

Figure 2.15 The difference between isotropic volume change, which involves no strain, and anisotropic volume change represented by uniaxial shortening (compaction).

isotropic area change in which an initial circle remains a circle, albeit with a different radius.

Isotropic volume increase: $X = Y = Z > 1$
Isotropic volume decrease: $X = Y = Z < 1$

Anisotropic volume change involves not only a volume (area) change but also a change in shape because its effect on the rock is different in different directions. The most obvious examples are compaction or uniaxial contraction and uniaxial extension, as shown in Figure 2.11 and discussed in the next section.

One may argue that anisotropic volume change is a redundant term, because any anisotropic strain can be decomposed into a combination of (isotropic) volume change and change in shape. The fact that deformation is not concerned with the deformation history makes any decomposition of the deformation into such components mathematically correct, even though they have nothing to do with the actual process of deformation in question. However, if we think about how compaction of sediments and sedimentary rocks comes about, it makes sense to consider it as an anisotropic volume change rather than a combination of isotropic volume change and a strain. Sediments compact by vertical shortening (Figure 2.11, top), not discretely by shrinking and then straining (Figure 2.11, middle). As geologists, we are concerned with reality and retain the term anisotropic volume change where we find it useful.

Anisotropic volume increase: $XYZ \neq 1$, where two or all of X, Y and Z are different.

2.13 Uniaxial strain (compaction)

Uniaxial strain is contraction or extension along one of the principal strain axes without any change in length along the other two. Such strain requires a reorganization,

addition or removal of rock volume. If volume is lost, we have **uniaxial contraction** and volume reduction. This happens through grain reorganization during physical compaction of porous sediments and tuffs near the surface, leading to a denser packing of grains. Only water, oil or gas that filled the pore space leaves the rock volume, not the rock minerals themselves.

In calcareous rocks and deeply buried siliciclastic sedimentary rocks, uniaxial strain can be accommodated by (pressure) solution, also referred to as chemical compaction. In this case, minerals are dissolved and transported out of the rock volume by fluids. Removal of minerals by diffusion can also occur under metamorphic conditions in the middle and lower crust. This can result in cleavage formation or can lead to compaction across shear zones. **Uniaxial extension** implies expansion in one direction. This may occur by the formation of tensile fractures or veins or during metamorphic reactions.

Uniaxial contraction: $X = Y > Z$, $X = 1$
Uniaxial extension: $X > Y = Z$, $Z = 1$

Uniaxial strain may occur in isolation, such as during compaction of sediments, or in concert with other deformation types such as simple shear. It has been found useful to consider many shear zones as zones of simple shear with an additional uniaxial shortening across the zone.

Uniaxial shortening or compaction is such an important and common deformation that it needs some further attention. The deformation matrix for uniaxial strain is

$$\begin{bmatrix} 1 & 0 & 0 \\ 0 & 1 & 0 \\ 0 & 0 & 1+\Delta \end{bmatrix} \tag{2.9}$$

where Δ is the elongation in the vertical direction (negative for compaction) and $1+\Delta$ is the vertical stretch (Figure 2.16). The fact that only the third diagonal element is different from unity implies that elongation or shortening only occurs in one direction. The matrix gives the strain ellipsoid, which is oblate or pancake-shaped for compaction. It can also be used to calculate how planar features, such as faults and bedding, are affected by compaction (Figure 2.16).

If we can estimate the present and initial porosity Φ_0 of a compacted sediment or sedimentary rock, then we can use the equation

$$\Phi = \Phi_0 e^{-CZ} \tag{2.10}$$

to find $1+\Delta$, where Z is the burial depth and C is a constant that typically is about 0.29 for sand, 0.38 for silt and 0.42 for shale; e is now the exponential function, not the extension factor. Equation 2.10 tells us that the porosity Φ changes with depth Z, and we are looking at a matrix of the form

$$\begin{bmatrix} 1 & 0 & 0 \\ 0 & 1 & 0 \\ 0 & 0 & 1+f(Z) \end{bmatrix} \tag{2.11}$$

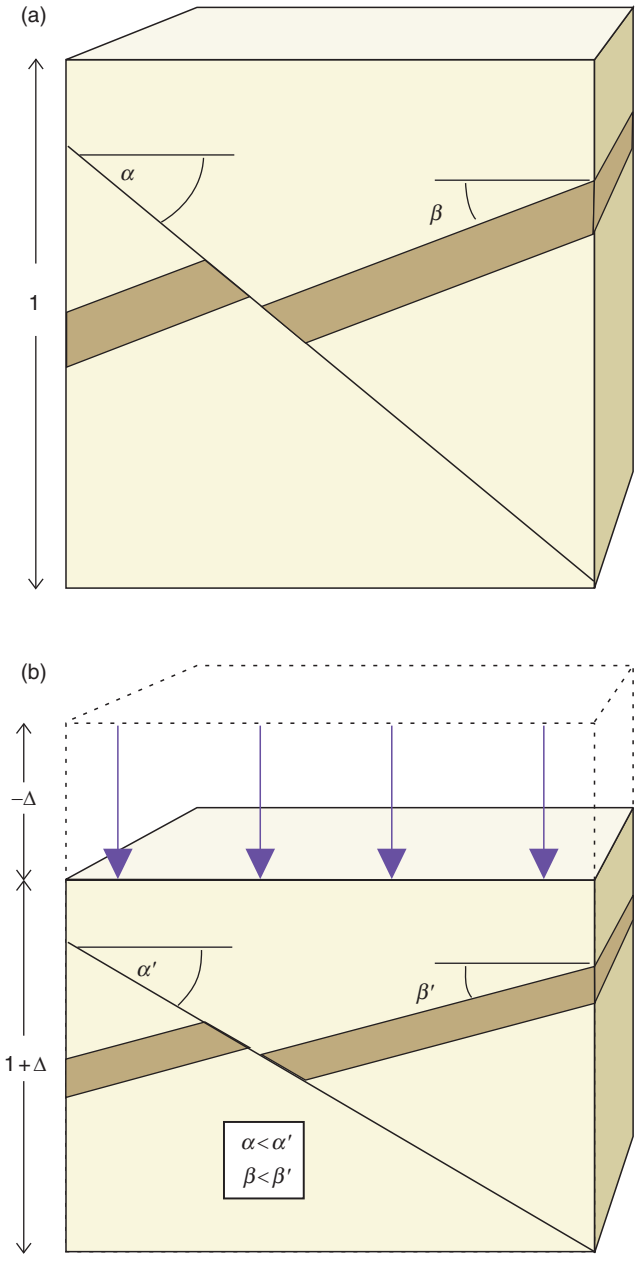

Figure 2.16 Compaction reduces the dips of both layers and faults. The effect depends on the amount of post-faulting compaction and can be estimated using the deformation matrix for compaction (Equation 2.9).

It can be shown that $\Delta = (1 - \Phi_0)/(1 - \Phi_0\, e^{-CZ})$, and the deformation matrix then becomes

$$\begin{bmatrix} 1 & 0 & 0 \\ 0 & 1 & 0 \\ 0 & 0 & 1 + (1 - \Phi_0)/(1 - \Phi_0 e^{-CZ}) \end{bmatrix} \tag{2.12}$$

Matrix (2.12) helps us predict the compaction at any point in a sedimentary basin, and it also predicts how structures such as folds and faults are modified by compaction. A relationship that can be found from matrix (2.12) relates the original dip (α) to the new dip (α') after the compaction:

$$\alpha' = \tan^{-1}[(1 + \Delta)\tan\alpha] \tag{2.13}$$

In metamorphic rocks, uniaxial shortening or compaction can be estimated by comparing portions of the rock affected by compaction with those believed to be unaffected. If the concentration of an immobile mineral, such as mica or an opaque phase, is C in the compacted part of the rock, and is believed to have been C_0 before compaction, then the compaction factor is given by the relationship

$$1 + \Delta = \frac{C_0}{C}\begin{bmatrix} k_x & 0 \\ 0 & k_y \end{bmatrix} \tag{2.14}$$

C_0 is found outside of the deformation zone, which could be a millimeter-thick cleavage-related microlithon, as discussed in Chapter 12 on cleavages and foliations. The deformation zone could also be a mesoscopic shear zone, where the wall rock is assumed to be unaffected by both shearing and compaction. As we will see in Chapter 15 on shear zones, ideal shear zones can only accommodate compaction in addition to simple shear.

2.14 Pure shear and coaxial deformations

Pure shear (Figure 2.8b) is a perfect **coaxial deformation**. This means that a marker that is parallel to one of the principal axes has not rotated away from its initial position. Uniaxial strain, where the rock shortens or extends in one direction, is another example of coaxial deformation.

Coaxial deformation implies that lines along the principal strain axes have the same orientation as they had in the undeformed state.

Pure shear is here considered a plane (two-dimensional) strain with no volume change, although some geologists also apply the term to three-dimensional coaxial deformations. Pure shear is identical to balance shortening in one direction with extension in the other, as expressed by its deformation matrix:

$$\begin{bmatrix} k_x & 0 \\ 0 & k_y \end{bmatrix} \tag{2.15}$$

where k_x and k_y are the stretch and shortening along the x and y coordinate axes, respectively. Since pure shear preserves area (volume) we have that $k_y = 1/k_x$.

2.15 Simple shear

Simple shear (Figure 2.8) is a special type of constant-volume plane strain deformation. There is no stretching or shortening of lines or movement of particles in the third direction. Unlike pure shear, it is a **non-coaxial deformation**, meaning that lines parallel to the principal strain axes have rotated away from their initial positions. This **internal rotation** component of the strain has caused several geologists to refer to simple shear and other non-coaxial deformations as **rotational deformations**. By internal rotation we here mean the difference between the orientation of a line along the longest finite strain axis and the orientation of this material line prior to deformation. While pure shear has no internal rotation component, the internal rotation component of a simple shear strain depends on the amount of strain.

Another characteristic of non-coaxial deformations relates the orientation of the strain ellipsoid and the amount of strain:

For non-coaxial deformations, the orientations of the principal strain axes are different for different amounts of strain, while for coaxial deformations they always point in the same directions (same orientation, different lengths).

As for any plane strain deformation type, the strain ellipsoid produced by simple shear has two circular sections (Figure 2.13b). One of them is parallel to the shear plane, regardless of the amount of strain involved. By **shear plane** we mean the plane on which shear occurs, as shown in Figure 2.17. The shear plane is similar to the slip plane for faults, and for simple shear it is a plane of no strain.

The consideration of coaxiality and internal rotations is easier to discuss in terms of progressive deformation (below). For now, we will look at the deformation matrix for simple shear:

$$\begin{bmatrix} 1 & \gamma \\ 0 & 1 \end{bmatrix} \tag{2.16}$$

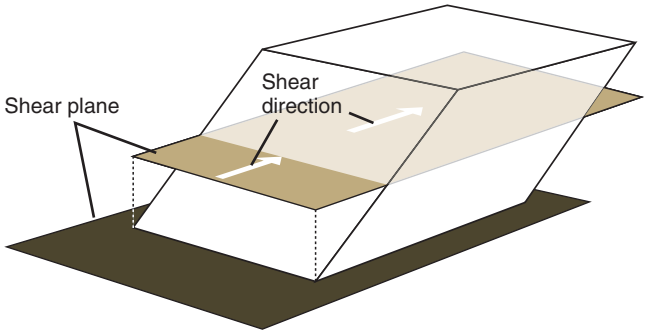

Figure 2.17 Illustration of the meaning of the terms shear plane and shear direction, by means of a deformed cube. The terms relate to simple shear or the simple shear component of a more general deformation type, such as subsimple shear.

The factor γ is called the shear strain and $\gamma = \tan\psi$, where ψ is the angle of rotation of a line that was perpendicular to the shear plane in the undeformed state (Figure 2.8). Lines and planes that lie within (parallel to) the shear plane do not change orientation or length during simple shear. Lines and planes with any other orientation do. It is noteworthy that deformation matrices describing coaxial deformations are symmetric, while those describing non-coaxial deformations are asymmetric.

2.16 Subsimple shear

Between pure shear and simple shear is a spectrum of planar deformations, commonly referred to as **subsimple shear** (also referred to as general shear, although these deformations are just a subset of planar deformations and thus not very general). Subsimple shear can be considered as a mix of pure and simple shear because the internal rotation involved is less than for simple shear. Mathematically we have to combine the deformation matrices for simple and pure shear, which is not as trivial as it may sound. It turns out that the matrix can be written as

$$\begin{bmatrix} k_x & \Gamma \\ 0 & k_y \end{bmatrix} \qquad (2.17)$$

where $\Gamma = \gamma[(k_x - k_y)] \,/\, [\lambda_n(k_x - k_y)]$. If there is no area change in addition to the pure and simple shear components, then $k_y = 1/k_x$ and $\Gamma = \gamma(k_x - 1/k_x)/2\ln(k_x)$. An example of subsimple shear and its displacement field and particle paths is shown in Figure 2.1.

2.17 Progressive deformation and flow parameters

Simple shear, pure shear, volume change and any other deformation type relate the undeformed to the deformed state only. The history that takes place between the two states is a different matter, and is the focus of the study of **flow** and **progressive deformation of rocks**.

It is useful to consider individual particles in the rock or sediment when discussing progressive deformation. If we keep track of a single particle during the deformation history, we can get a picture of a single **particle path**. If we map the motion of a number of such particles we get an impression of the **flow pattern**.

The flow pattern is the sum of particle paths in a deforming medium.

Particle paths can be recorded directly in experiments where individual particles or (colored) grains can be traced throughout the deformation history. The particle paths shown in Figure 2.18 are not quite complete, because they are based on points of intersection between faults and markers. The flow pattern is also affected by faults, which are displacement discontinuities (see Chapter 8), but the overall pattern can be seen to be close to that of pure shear. Filming an ongoing experiment enables the scientist to reconstruct the flow pattern during the experiment. In the field, things are different and we can only see the final stage of the deformation, i.e. the last picture of the film roll.

Let us imagine that we can photograph a deformation from the start to the end. Then the difference between any two adjacent pictures represents a small interval of the total deformation. Based on the differences between the two pictures we may be able to find the size and orientation of the **incremental strain ellipsoid** for this interval and describe this increment of the deformation history. When such an interval becomes very small, we get the **infinitesimal** or **instantaneous deformation parameters**. Parameters that act instantaneously during the deformation history are called **flow parameters**. As indicated by Figure 2.19, the flow parameters include the infinitesimal or instantaneous stretching axes, the flow apophyses, vorticity and the velocity field, all of which deserve some extra attention.

The Instantaneous Stretching Axes (ISA) are the three perpendicular axes (two for plane deformations) that describe the directions of maximum and minimum stretching at any time during deformation. They are all called instantaneous stretching axes although the minimum stretching axis (ISA_3) is the direction of maximum shortening, or negative stretching. Lines along the longest axis (ISA_1) are stretching faster than any other line orientation. Similarly, no line is stretching slower

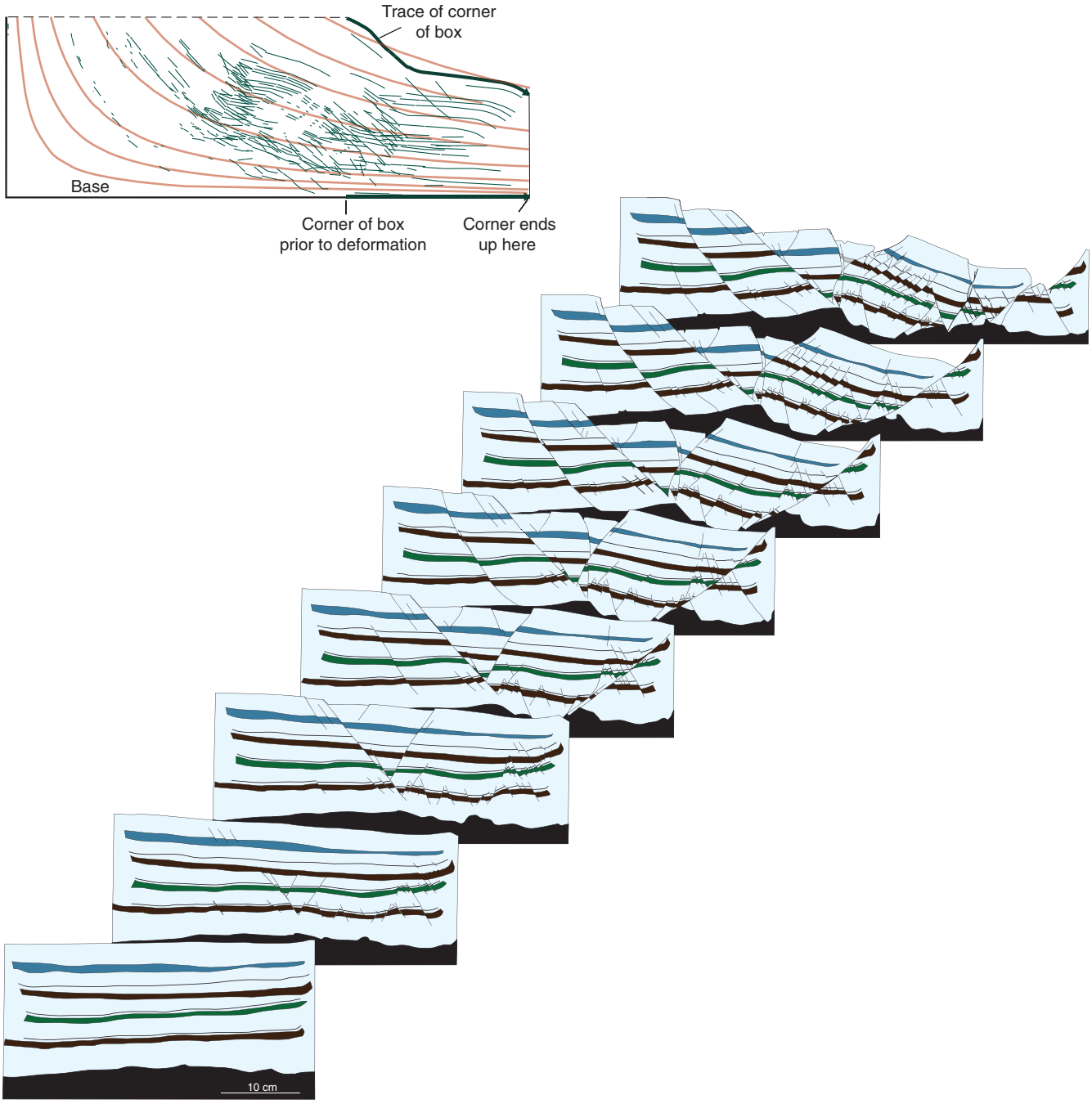

Figure 2.18 Particle path for plaster experiment, with theoretical pure-shear pattern (in red) shown for comparison. Drawings of pictures taken during the experiment are also shown. Particle paths are found by connecting corner points and points where faults intersect bedding. In this case the deformation is heterogeneous and brittle, but can be compared to homogeneous flow (pure shear) because the discontinuities are many and distributed. The experiment is described in Fossen and Gabrielsen (1996).

(or shortening faster) than those along the shortest instantaneous stretching axis (ISA_3).

Flow apophyses separate different domains of particle paths (AP in Figure 2.19). Particles located along the apophyses rest or move along the straight apophyses. Other particle paths are curved. No particle can cross a flow apophysis unless the conditions change during the deformation history.

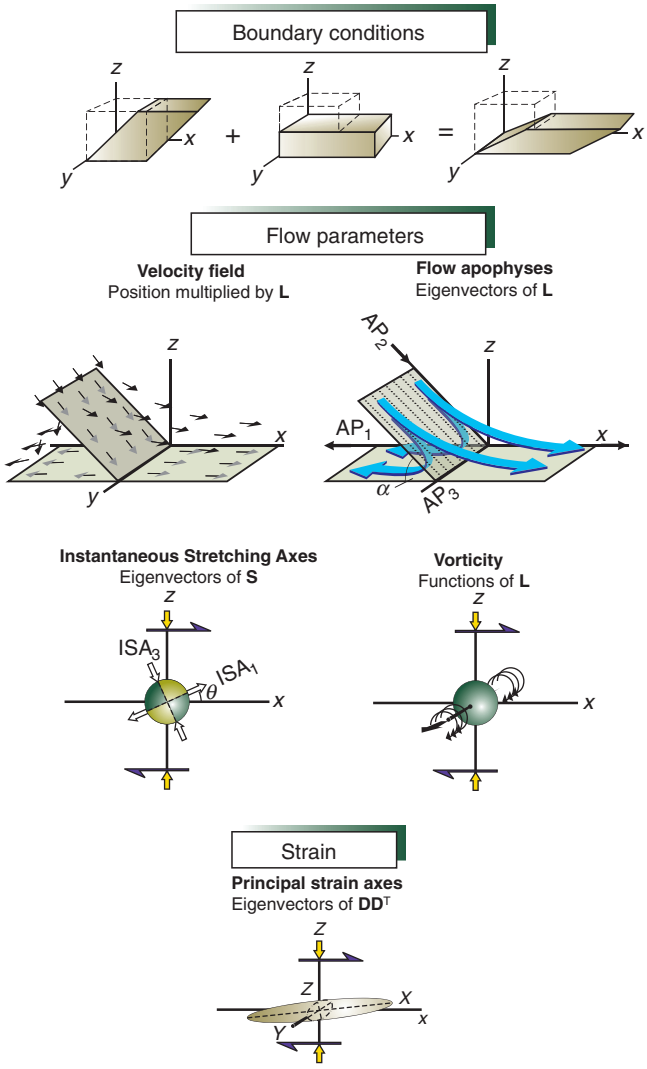

Figure 2.19 The most important deformation parameters. Boundary conditions control the flow parameters, which over time produce strain. Modified from Fossen and Tikoff (1997).

Vorticity describes how fast a particle rotates in a soft medium during the deformation (Section 2.20). A related quantity is the **kinematic vorticity number** (W_k), which is 1 for simple shear and 0 for pure shear and somewhere between the two for subsimple shear.

The **velocity field** describes the velocity of the particles at any instance during the deformation history. Let us have a closer look.

2.18 Velocity field

The velocity (gradient) matrix (or tensor) **L** describes the velocity of the particles at any instant during the deformation. In three dimensions the velocity field is described by the equations

$$
\begin{aligned}
v_1 &= L_{11}x + L_{12}y + L_{13}z \\
v_2 &= L_{21}x + L_{22}y + L_{23}z \\
v_3 &= L_{31}x + L_{32}y + L_{33}z
\end{aligned}
$$

which in matrix notation become

$$
\begin{bmatrix} v_1 \\ v_2 \\ v_3 \end{bmatrix} = \begin{bmatrix} L_{11} & L_{12} & L_{13} \\ L_{21} & L_{22} & L_{23} \\ L_{31} & L_{32} & L_{33} \end{bmatrix} \begin{bmatrix} x \\ y \\ z \end{bmatrix} \tag{2.18}
$$

or

$$\mathbf{v} = \mathbf{L}\mathbf{x}$$

Here, the vector **v** describes the velocity field and the vector **x** gives the particle positions.

If we consider flow with a 3-D coaxial component, such as axially symmetric flattening or extension (Figure 2.12) in combination with a progressive simple shear whose shear plane is the *x*–*y* plane, then we have the following velocity matrix:

$$
\mathbf{L} = \begin{bmatrix} \dot{e}_x & \dot{\gamma} & 0 \\ 0 & \dot{e}_y & 0 \\ 0 & 0 & \dot{e}_z \end{bmatrix} \tag{2.19}
$$

In this matrix, $\dot{e}_x$, $\dot{e}_y$ and $\dot{e}_z$ are the elongation rates in the *x*, *y* and *z* directions, respectively, and $\dot{\gamma}$ is the shear strain rate (all with dimension s^{-1}). These strain rates are related to the particle velocities and thereby to the velocity field. Inserting Equation 2.19 into 2.18 gives the following velocity field:

$$
\begin{aligned}
v_1 &= \dot{e}_x x + \dot{\gamma} y \\
v_2 &= \dot{e}_y y \\
v_3 &= \dot{e}_z z
\end{aligned} \tag{2.20}
$$

The matrix **L** is composed of time-dependent deformation rate components, while the deformation matrix has spatial components that do not involve time or history. The matrix **L** for progressive subsimple shear now becomes

$$
\begin{aligned}
\mathbf{L} &= \begin{bmatrix} \dot{e}_x & 0 \\ 0 & \dot{e}_y \end{bmatrix} + \begin{bmatrix} 0 & \dot{\gamma} \\ 0 & 0 \end{bmatrix} \\
&= \begin{bmatrix} 0 & \dot{\gamma} \\ 0 & 0 \end{bmatrix} + \begin{bmatrix} \dot{e}_x & 0 \\ 0 & \dot{e}_y \end{bmatrix} = \begin{bmatrix} \dot{e}_x & \dot{\gamma} \\ 0 & \dot{e}_y \end{bmatrix}
\end{aligned} \tag{2.21}
$$

This equation illustrates a significant difference between deformation rate matrices and ordinary deformation matrices: while deformation matrices are noncommutative, strain rate matrices can be added in any order without changing the result. The disadvantage is

that information about the strain ellipse is more cumbersome to extract from deformation rate matrices, since we then need to integrate with respect to time over the interval in question.

L can be decomposed into a symmetric matrix $\dot{\mathbf{S}}$ and a so-called skew-symmetric matrix **W**:

$$\mathbf{L} = \dot{\mathbf{S}} + \mathbf{W} \tag{2.22}$$

$\dot{\mathbf{S}}$ is the stretching matrix (or tensor) and describes the portion of the deformation that over time produces strain. **W** is known as the vorticity or spin matrix (tensor) and contains information about the internal rotation during the deformation. For progressive subsimple shear the decomposition becomes

$$\mathbf{L} = \mathbf{S} + \mathbf{W} = \begin{bmatrix} \dot{\varepsilon}_x & \frac{1}{2}\dot{\gamma} \\ \frac{1}{2}\dot{\gamma} & \dot{\varepsilon}_y \end{bmatrix} + \begin{bmatrix} 0 & \frac{1}{2}\dot{\gamma} \\ -\frac{1}{2}\dot{\gamma} & 0 \end{bmatrix} \tag{2.23}$$

The eigenvectors and eigenvalues to $\dot{\mathbf{S}}$ give the orientations and lengths of the ISA (instantaneous stretching axes). The eigenvectors of **L** describe the flow apophyses, which are discussed in the next section. Whether one wants to work with strain rates or simple deformation parameters such as k and γ is a matter of personal preference in many cases. Both are in use, and both have their advantages and disadvantages.

2.19 Flow apophyses

Flow apophyses, shown as blue lines along with green particle paths in Figure 2.20, are **theoretical lines** (meaning that they are invisible "ghost lines" that are free to rotate independently of material lines) that separate different fields of the flow. Particles cannot cross an apophysis, but they can move along them or rest on them. For the case of simple shearing (progressive simple shear), the particles will always move straight along the shear direction. This occurs because there is no shortening or extension perpendicular to the shear plane, and it tells us that one of the apophyses is parallel to the shear direction (Figure 2.20, simple shear). As we will see, there is only this one apophysis for simple shear. For pure shear there are two orthogonal apophyses along which particles move straight toward or away from the origin. Subsimple shear has two oblique apophyses; one parallel to the shear direction and one at an angle α to the first one. The angle α between the two apophyses varies from 90° for pure shear to 0° for simple shear.

For simple shear, pure shear and subsimple shear, the apophyses occur in the plane perpendicular to the shear plane and parallel to the shear direction, which means

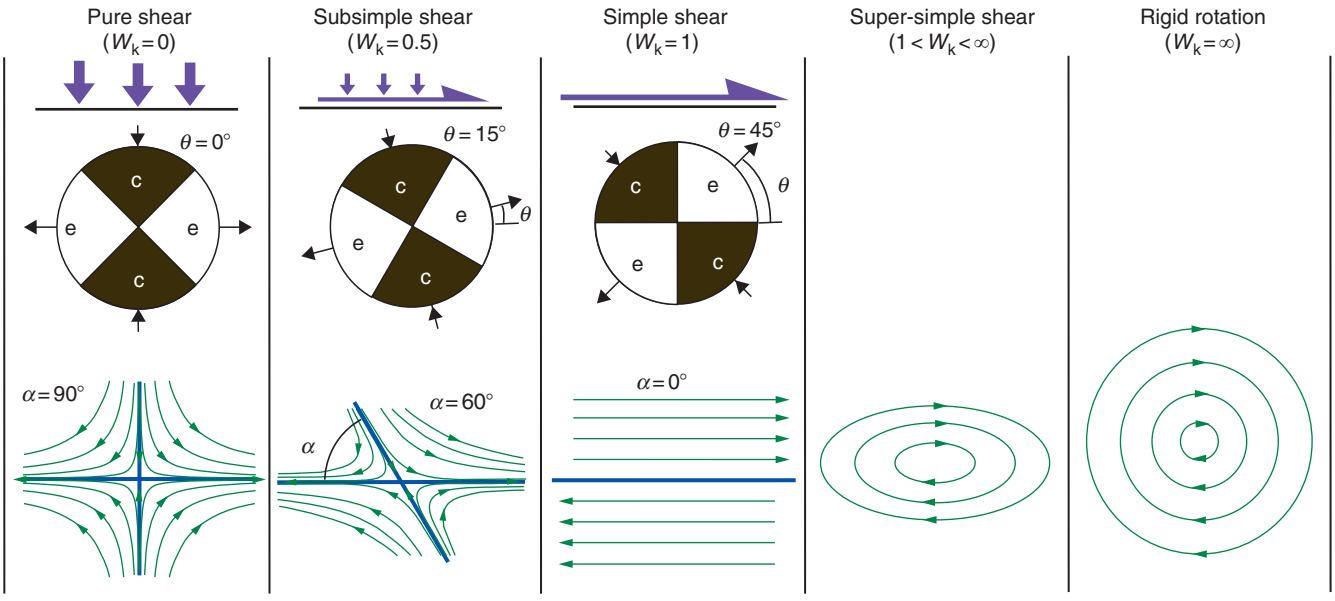

Figure 2.20 Particle paths (green) and flow apophyses (blue) for planar deformations. The two flow apophyses, which describe the flow pattern, are orthogonal for pure shear, oblique for subsimple shear and coincident for simple shear. For deformations with more internal rotation, particles move along elliptical paths. The end-member is rigid rotation, where particles move along perfect circles. Rigid rotation involves perfect rotation without strain, while pure shear is simply strain with no rotation. Note that ISA are generally oblique to the flow apophyses for $W_k > 0$.

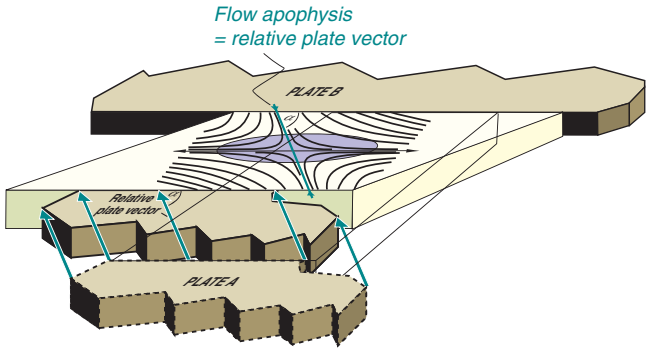

Figure 2.21 Two rigid plates (A and B) and an intermediate deforming zone (yellow). Standing on plate B, we will observe plate A moving obliquely towards us. If this shortening is compensated by lateral extension, then the oblique flow apophysis is parallel to the plate vector and the particle path is known. W_k can be found from Figure 2.24. Modified from Fossen and Tikoff (1998).

that we can express the vectors in two dimensions if we wish:

$$\begin{bmatrix} 1 \\ 0 \end{bmatrix}, \begin{bmatrix} \frac{-\gamma}{\ln(k_x/k_y)} \\ 1 \end{bmatrix} \tag{2.24}$$

The first of these vectors or apophyses is the one that is parallel to the shear direction (here chosen to be along the x-axis of our coordinate system), while the other one is oblique. The angle α between the apophyses is directly related to how close to simple shear or pure shear the deformation is. α is zero for simple shear and 90° for pure shear, and W_k thus depends on α:

$$W_k = \cos(\alpha) \tag{2.25}$$

To illustrate how flow apophyses can be useful in tectonics, consider the convergent motion of one tectonic plate relative to another. It actually turns out that the oblique apophysis is parallel to the convergence vector, which becomes apparent if we recall that straight particle motion can only occur in the direction of the apophyses. In other words, for oblique plate convergence (transpression, see Chapter 18) α describes the angle of convergence and is 90° for head-on collision and 0° for perfect strike-slip. Head-on collision is thus a pure shear on a large scale, while strike-slip or conservative boundaries deform by overall simple shear. Figure 2.21 illustrates a theoretical example of oblique convergence, and if we know the plate motion vector of one of the plates relative to the other, we can, at least in principle, estimate the average orientations of the oblique flow apophysis, because the two will be parallel. Once we know the flow apophysis, we also know W_k (from Equation 2.25) and we can use this information to model or evaluate deformation structures along the plate boundary. Or we can analyze old structures along a (former) plate boundary and say something about the paleo-convergence angle. Hence, matrix calculus and field geology meet along plate boundaries, among other places, in very useful ways.

2.20 Vorticity and W_k

We separate **non-coaxial deformation histories**, where material lines (imaginary lines drawn on a section through the deforming rock) that in one instance are parallel to ISA and in the next instance have rotated away from them, and **coaxial deformation histories**, where the material lines along ISA remain along these axes for the entire deformation history. The degree of (internal) rotation or coaxiality is denoted by the kinematic vorticity number W_k. This number is 0 for perfectly coaxial deformation histories, 1 for progressive simple shear, and between 0 and 1 for subsimple shear. Values between 1 and ∞ are deformation histories where the principal strain axes rotate continuously around the clock. $W_k > 1$ deformations are therefore sometimes termed spinning deformations, and the result of such deformations is that the strain ellipsoid records a cyclic history of being successively strained and unstrained.

To get a better understanding of what W_k actually means, we need to explore the concept of vorticity. **Vorticity** is a measure of the internal rotation during the deformation. The term comes from the field of fluid dynamics, and the classic analogy is a paddle wheel moving along with the flow, which we can imagine is the case with the paddle wheel shown in Figure 2.22. If the paddle wheel does not turn, then there is no vorticity. However, if it does turn around, there is a vorticity, and the vector that describes the velocity of rotation, the angular velocity vector $\boldsymbol{\omega}$, is closely associated with the vorticity vector $\mathbf{w}$:

$$\mathbf{w} = 2\omega = \text{curl } \mathbf{v} \tag{2.26}$$

where $\mathbf{v}$ is the velocity field.

Another illustration that may help is one where a spherical volume of the fluid freezes, as in Figure 2.23. If the sphere is infinitely small, then the vorticity vector $\mathbf{w}$ will represent the axis of rotation of the sphere, and its length will be proportional to the speed of the rotation.

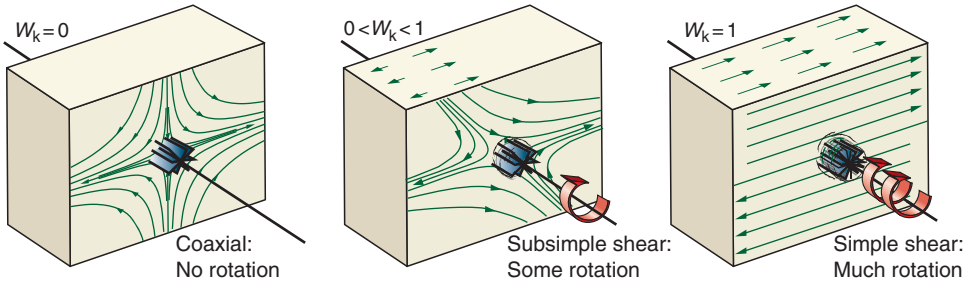

Figure 2.22 The paddle-wheel interpretation of flow. The axis of the paddle wheel is parallel to the vorticity vector and is not rotating for coaxial deformation ($W_k = 0$) and shows an increasing tendency to rotate for increasing W_k.

The vorticity vector can be interpreted as: (1) the average rotation of all lines in the plane perpendicular to **w** relative to the ISA; (2) the speed of rotation of a set of physical lines that are parallel to the ISA; (3) the average speed of rotation of two orthogonal physical lines in the plane perpendicular to **w**; or (4) half the speed of rotation of a rigid spherical inclusion in a ductile matrix where there is no slip along the edge of the sphere and where the viscosity contrast is infinitely high.

As an example, let us put a rigid sphere in a deformation box filled with a softer material that contains strain markers. If we apply a coaxial deformation by squeezing the box in one direction and letting it extend in the other (s), the sphere will not rotate and the vorticity is 0. However, if we add a simple shear to the content of the box, the sphere will rotate, and we will observe that there is a relationship between the strain and the rotation, regardless of how fast we perform the experiment: the more strain, the more rotation. This relation between strain and (internal) rotation is the kinematic vorticity number W_k. For a simultaneous combination of pure shear and simple shear, i.e. subsimple shear, there is less rotation of the sphere for a certain strain accumulation than for simple shear. Therefore W_k is less than 1 by an amount that depends on the relative amount of simple versus pure shear.

W_k is a measure of the relation between the vorticity (internal rotation) and how fast strain accumulates during the deformation.

Mathematically, the kinematic vorticity number is defined as

$$W_k = \frac{w}{\sqrt{2(s_x^2 + s_y^2 + s_z^2)}} \tag{2.27}$$

where s_n are the principal strain rates, i.e. the strain rates along the ISA. This equation can be rewritten in terms of pure and simple shear components if we assume steady flow (see next section) during the deformation:

$$W_k = \frac{\gamma}{\sqrt{2\left[(\ln k_x)^2 + (\ln k_y)^2\right] + (\gamma)^2}} \tag{2.28}$$

which for constant area becomes

$$W_k = \cos[\arctan(2 \ln k/\gamma)] \tag{2.29}$$

This expression is equivalent to the simpler equation $W_k = \cos(\alpha)$ (Equation 2.25), where α and α' are the acute and obtuse angles between the two flow apophyses, respectively, and k and γ are the pure shear and simple shear components, as above. The relation between W_k and α is shown graphically in Figure 2.24, where also the corresponding relation between W_k and ISA_1 is shown.

2.21 Steady-state deformation

If the flow pattern and the flow parameters remain constant throughout the deformation history, then we have **steady-state flow** or deformation. If, on the other hand, the ISA rotate, W_k changes value or the particle paths

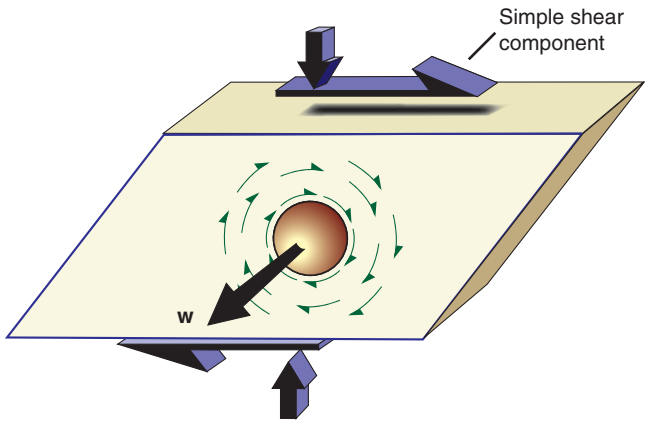

Figure 2.23 The vorticity vector (**w**) in progressive subsimple shear.

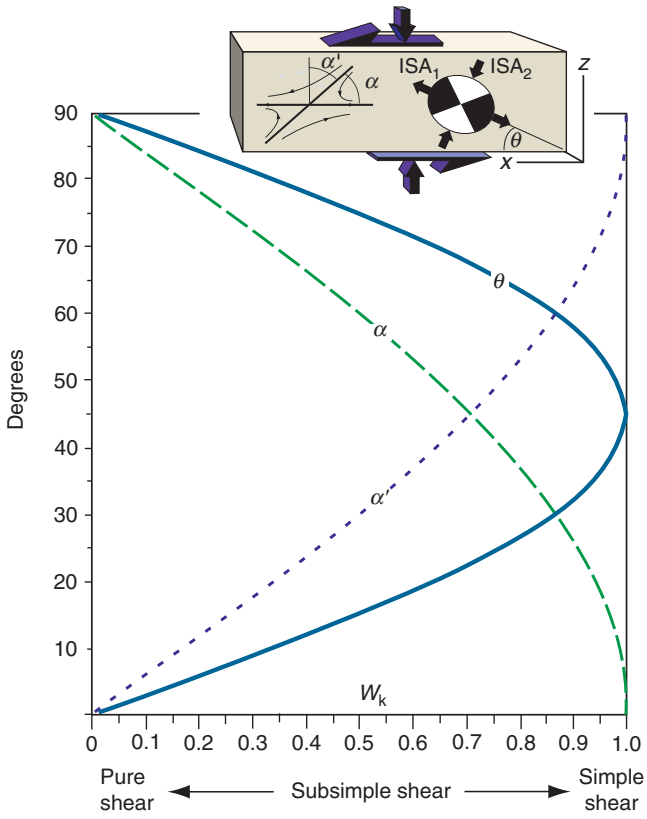

Figure 2.24 The relationship between W_k, α, α' and θ.

change during the course of deformation, then we have a non-steady-state flow.

During steady-state deformation the ISA and flow apophyses retain their initial orientation throughout the deformation history, and W_k is constant.

An example of non-steady deformation is a subsimple shear that moves from being close to simple shearing towards a more pure shear dominated flow. For practical reasons, and because non-steady-state deformations are difficult to identify in may cases, steady-state flow is assumed. In nature, however, non-steady-state deformation is probably quite common.

2.22 Incremental deformation

The theory around the deformation matrix can be used to model progressive deformation in a discrete way. We make a distinction between **finite deformation** or **finite strain** on one hand, which is the result of the entire deformation history, and **incremental deformation** or **incremental strain** on the other, which concerns only a portion of the deformation history. When using an incremental approach, each deformation increment is represented by an **incremental deformation matrix**, and the product of all of the incremental deformation matrices equals the finite deformation matrix.

There is an important thing about matrix multiplication that we should be aware of: The order by which we multiply matrices (apply deformations) is not arbitrary. For example, a pure shear followed by a simple shear does not result in the same deformation as a simple shear followed by a pure shear:

$$\begin{bmatrix} k_x & 0 \\ 0 & k_y \end{bmatrix} \begin{bmatrix} 1 & \gamma \\ 0 & 1 \end{bmatrix} \neq \begin{bmatrix} 1 & \gamma \\ 0 & 1 \end{bmatrix} \begin{bmatrix} k_x & 0 \\ 0 & k_y \end{bmatrix} \tag{2.30}$$

Interestingly, the matrix representing the first deformation or deformation increment is the last of the matrices to be multiplied. For example, if a deformation is represented by three increments, D_1 representing the first part of the history and D_3 the last part, then the matrix representing the total deformation is the product $D_{tot} = D_3 D_2 D_1$.

Another point to note is that since we are here operating in terms of kinematics only (not time), it does not make any difference whether D_1, D_2 and D_3 represent different deformation phases or increments of the same progressive history.

One can define as many increments as one needs to model progressive deformation. When the incremental matrices represent very small strain increments, the principal strain axes of the matrices approximate the ISA and other flow parameters can be calculated for each increment and compared. Modeling progressive deformation numerically can provide useful information about the deformation history. It may be difficult, however, to extract information from naturally deformed rocks that reveal the actual deformation history. For this reason, steady-state deformations represent useful reference deformations, although natural deformations are not restricted by the limitations of steady-state flow.

2.23 Strain compatibility and boundary conditions

If we deform a chunk of soft clay between our hands, there will be free surfaces where the clay can extrude. The situation is quite different for a volume of rock undergoing natural deformation in the crust. Most deformation happens at depth where the rock volume is surrounded by other rock and under considerable pressure. The resulting

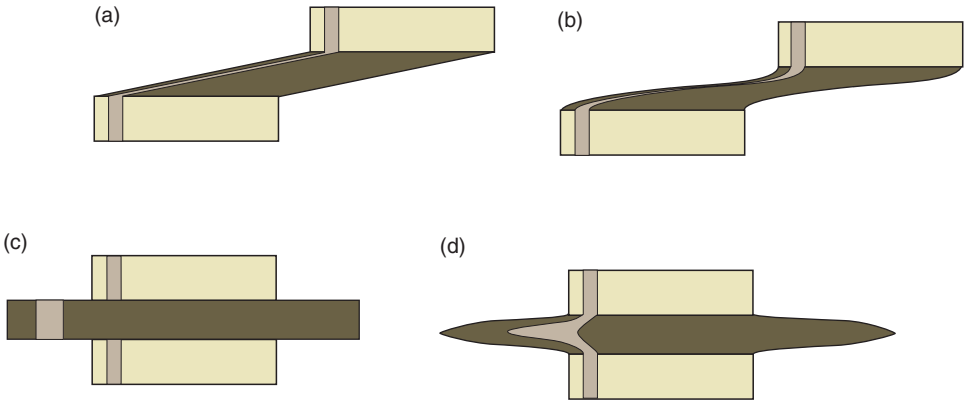

Figure 2.25 Homogeneous (a) and heterogeneous (b) simple shear create no compatibility problems between the deformed and undeformed rocks. Homogeneous pure shear (c) does, because lateral extrusion of material creates discontinuities. The space problem is also apparent for heterogeneous pure shear (d), but the discontinuities can be eliminated.

strain will depend on the anisotropy of the rocks. Anisotropy, such as a weak layer or foliation, may control the deformation just as much as the stress field.

Let us illustrate this by a ductile shear zone with straight and parallel margins and undeformed walls, as shown in Figure 2.25a, b. In principle, simple shearing can continue "forever" in such a zone without creating any problem with the wall rock (challenges may arise around shear zone termination points, but we will neglect those here).

Adding shortening across the shear zone as a result of anisotropic volume change is also easy to accommodate. However, adding a pure shear means that the shear zone will have to extrude laterally while the wall rock remains undeformed (Figure 2.25c, d). This causes a classic **strain compatibility problem** since the continuity across the shear zone boundaries is lost. The strain in the shear zone is no longer compatible with the undeformed walls.

For the state of strain in two adjacent layers to be compatible, the section through their respective strain ellipsoids parallel to their interface must be identical.

For our shear zone example, the rock on one side is undeformed, and the section must be circular, which it is for simple shear with or without shear zone perpendicular compaction (Figure 2.26). However, if a pure shear component is involved, compatibility between the deformed and undeformed volumes is not maintained.

A practical solution to this problem is to introduce a discontinuity (slip surface or fault) between the zone and each of the walls. The shear zone material can then be squeezed sideways in the direction of the shear zone. The problem is that it has nowhere to go, since the neighboring part of a parallel-sided shear zone will try to do exactly the same thing. We can therefore conclude that a shear zone with parallel boundaries is not compatible with (cannot accommodate) pure shear. Besides, strain compatibility as a concept requires that the deformed volume is coherent and without discontinuities, overlaps or holes. Discontinuities and non-parallel shear zones are, as we know, common in many deformed rocks. The requirement of continuity in strain compatibility is thus negotiable.

2.24 Deformation history from deformed rocks

It is sometimes possible to extract information about the deformation history from naturally deformed rocks. The key is to find structures that developed during a limited part of the total deformation history only. In some cases the deformation has moved from one part of the deformed rock volume to another, leaving behind deformed rock that has recorded the conditions during earlier increments of the deformation. For example, strain may after some time localize to the central part of the shear zone. Thus the margins bear a record of the first increment of the deformation. But shear zones can

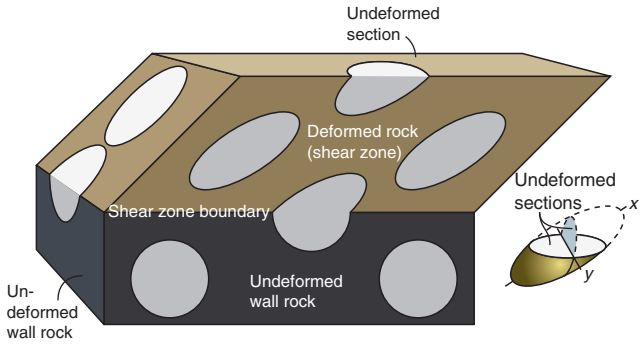

Figure 2.26 The compatibility between undeformed wall rock and a simple shear zone. Any section parallel to the shear zone wall will appear undeformed.

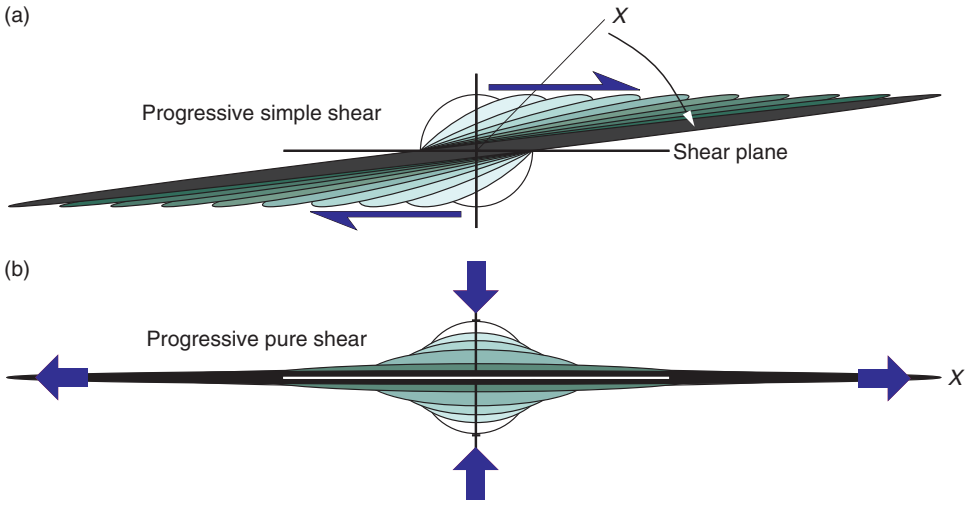

Figure 2.27 The evolution of strain during progressive simple and pure shear.

also initiate as narrow zones and widen over time. In this case the outer portion of the shear zone records the last increments of deformation. The search for deformation history is not necessarily an easy task!

In some cases there is evidence for mineral fiber growth at various stages or veins forming successively during deformation. The orientation of fibers and veins reflects the orientation of ISA and thus gives information about the flow parameters.

If the metamorphic conditions change during the course of deformation, structures that carry information about incremental deformation may be separated by means of metamorphic mineralogy.

2.25 Coaxiality and progressive simple shear

Earlier in this chapter we defined certain reference deformation types such as simple shear, pure shear, subsimple shear and volume change. The same deformations define progressive deformation if every increment, large or small, represents the same deformation type as the total one. Hence, a deformation that not only ends up as simple shear, but where any interval of the deformation history is also a simple shear is a progressive simple shear or **simple shearing**. Similarly we have progressive pure shear or **pure shearing**, progressive subsimple shear or **subsimple shearing**, and progressive volume change or **dilating**.

A given simple shear does not have to be produced by progressive simple shear, but may for example be a pure shear followed by rigid rotation. The rigid rotation must then be exactly $\arctan(1/2 \tan \psi)$.

Progressive deformations are separated into coaxial and non-coaxial ones. A **non-coaxial deformation history** implies that the orientation of the progressive strain ellipsoid is different at any two points in time during the deformation, as clearly is the case in Figure 2.27a where X rotates progressively. Another characteristic feature is that lines that are parallel to ISA or the principal strain axes rotate during deformation. These rotational features allow us to call them rotational deformation histories. During a **coaxial deformation history** the orientation of the strain ellipsoid is constant throughout the course of the deformation and lines parallel to ISA do not rotate. Coaxial deformation histories, such as the pure shearing shown in Figure 2.27b, are therefore referred to as non-rotational.

Simple shearing involves no stretching, shortening or rotation of lines or planar structures parallel to the shear plane. Other lines will rotate towards the shear direction as they change length, and planes will rotate toward the shear plane. The long axis of the strain ellipse also rotates toward the shear direction during the shearing history, although it will never reach this direction.

In order to improve our understanding of simple shearing we will study a circle with six physical lines numbered from 1 to 6 (Figure 2.28). We will study what happens to three orthogonal pairs of lines, numbered 1 and 4, 2 and 5, and 3 and 6, at various stages during the shearing. At the moment the shearing starts, the rock (and circle) is stretched fastest in the direction of ISA_1 and slowest along ISA_3 (negative stretching, which actually means shortening along ISA_3). The ISA are constant during the entire history of deformation, since we are considering a steady-state deformation. Two important

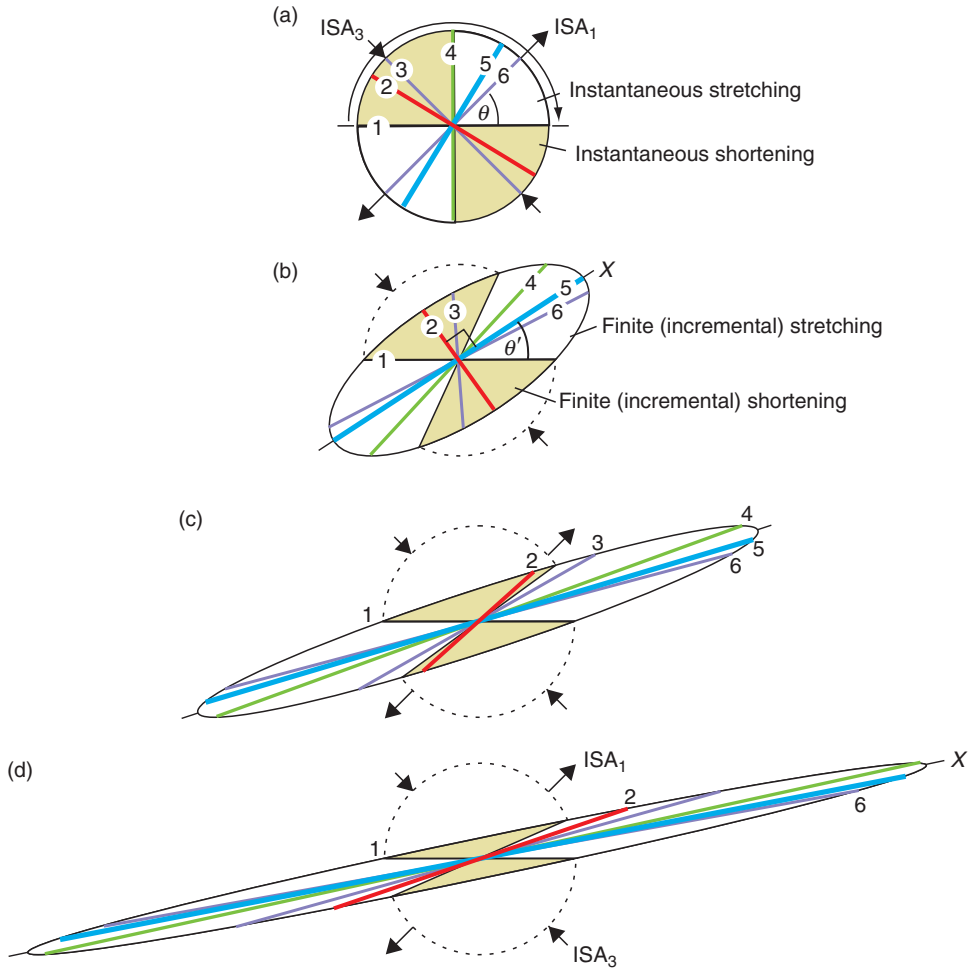

Figure 2.28 Simple shearing of a circle and three sets of orthogonal lines (1–6). The arrow along the circle in (a) indicates the rotation direction for lines during the deformation.

pairs of fields occur in Figure 2.28a. In the two white fields, lines are continuously being stretched, and we can call them the **fields of instantaneous stretching**. Similarly, lines in the two yellow fields continuously experience shortening and we call them the **fields of instantaneous shortening**. The borderlines between these fields are the **lines of no stretching or shortening**. In three dimensions the fields become volumes and the borderlines become surfaces of no stretching or shortening. These fields remain constant during the deformation history while lines may rotate from one field to the next.

Lines 1 and 4 start out parallel to the boundary between active stretching and shortening. Line 1 lies in the shear plane and maintains its original orientation and length, i.e. remains undeformed. Line 4 quickly rotates into the stretching field toward ISA_1 (Figure 2.28b). In Figure 2.28c, line 4 has rotated through ISA_1 and will also pass the long axis X of the strain ellipse if the deformation keeps going.

Lines 2 and 5 are located in the fields of shortening and stretching, respectively. In Figure 2.28b, line 2 is shortened and line 5 extended, but the two lines are orthogonal at this point. They were orthogonal also before the deformation started, which means that the angular shear along these two directions is now zero. This also means that lines 2 and 5 are parallel to the strain axes at this point. They do, however, rotate faster than the deformation ellipse, and in Figure 2.28c line 5 has passed X and line 2 has passed the shortest axis of the strain ellipse. In fact, line 2 is now parallel with ISA_1 and has passed the boundary between the fields of instantaneous shortening and stretching. This means that the line has gone from a history of shortening to one of stretching. The total shortening still exceeds the total stretching, which is why this line is still in the contractional field of the cumulative strain ellipsoid. On the way toward the last stage (Figure 2.28d), line 2 passes ISA_1 as well as the borderline between total stretching and shortening.

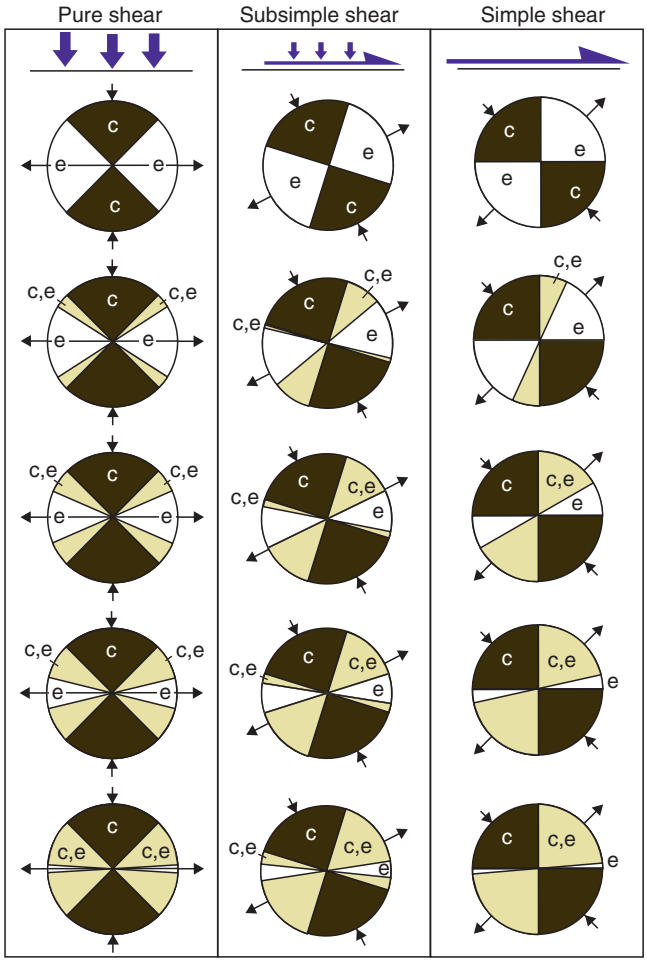

Figure 2.29 The development of sectors where lines experience a qualitatively common history: c, contractional field; e, extension field. c, e indicate that lines in this field were first shortened and then extended. Note the symmetric picture produced by pure shear and the asymmetry created by non-coaxial deformation histories. Field observations of deformed dikes and veins can sometimes be used to construct the sectors and thus the degree of coaxiality.

The last pair of lines (3 and 6) start out parallel with ISA_3 and ISA_1, respectively. Both lines immediately rotate away from the principal stretching directions because of the rotational or non-coaxial nature of simple shearing. Line 3 experiences shortening until stage (b). Soon thereafter it is stretched and its original length is restored as it passes through the borderline between the fields of instantaneous stretching and shortening (between stages b and c). It keeps stretching as it rotates toward the shear direction. Line 6 experiences stretching during the entire deformation history, but less and less so as it rotates toward the shear direction and away from ISA_1. Clearly, line 6 rotates faster than X, with which it was parallel at the onset of deformation.

The deformation history can also be represented in terms of sectors, in which lines share a common history of contraction, extension or contraction followed by extension (Figure 2.29). If we start out with a randomly oriented set of lines, we will soon see a field containing lines that first shortened, then stretched (yellow fields in Figure 2.29). This field increases in size and will cover more and more of the field of instantaneous stretching. Note that the fields are asymmetric for simple shearing and other non-coaxial deformations, but symmetric for coaxial deformations such as pure shearing (left column in Figure 2.29).

Even though the line rotations discussed here were in a plane perpendicular to the shear plane, simple shearing can cause lines and planes to rotate along many other paths. Figure 2.30 shows how lines (or particles) move along great circles when exposed to simple shearing. This is yet another characteristic feature of simple shearing that may help in separating it from other deformations.

Based on these observations we can list the following characteristics of simple shearing:

Lines along the shear plane do not deform or rotate.
Physical (material) lines rotate faster than the axes of the strain ellipse (generally true).
The sense of line (and plane) rotation is the same for any line orientation.
Lines that are parallel with the ISA rotate (generally true for non-coaxial progressive deformations).
Lines can rotate from the field of instantaneous shortening to that of instantaneous stretching (to produce boudinaged folds) but never the other way (never folded boudins) for steady-state simple shearing.
In the Schmidt net, lines rotate along great circles toward the shearing direction.

2.26 Progressive pure shear

Progressive pure shear or pure shearing is a two-dimensional coaxial deformation, i.e. the strain ellipsoid does not rotate and is fixed with respect to the ISA throughout the deformation (Figures 2.27b and 2.29). Coaxial deformation histories result in coaxial (finite) deformations, which are characterized by symmetric deformation matrices.

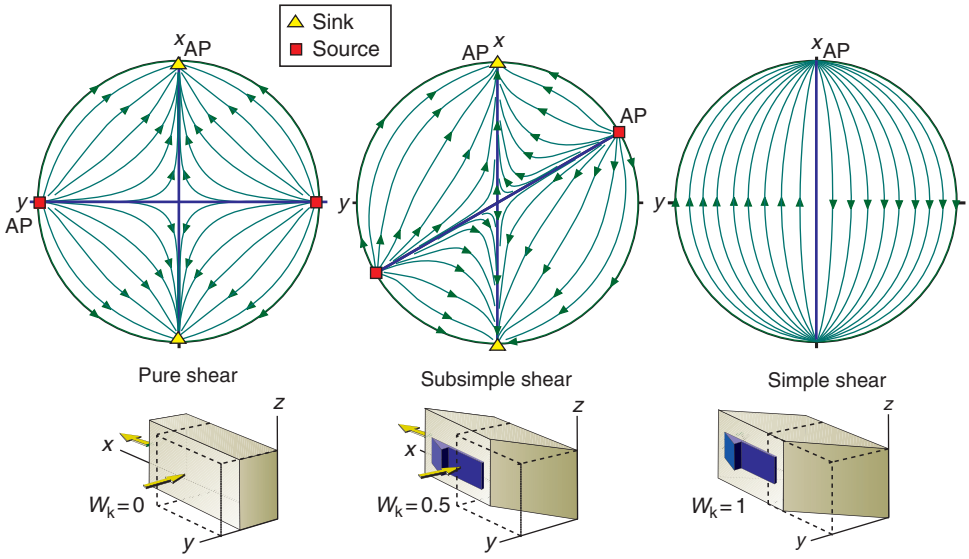

Figure 2.30 Stereographic representation of line rotation during pure shearing, subsimple shearing and simple shearing. AP are flow apophyses, where one is an attractor (sink) and the other is a repeller (source).

For pure shearing the ISA and the fields of instantaneous stretching and shortening are symmetrically arranged with respect to the principal strain axes (axes of the strain ellipse). The following characteristics of pure shearing can be found by studying the different stages shown in Figure 2.31:

The greatest principal strain axis (X) does not rotate and is always parallel with ISA_1.
Lines that are parallel with the ISA do not rotate during the deformation.
Any other line rotates toward X and ISA_1.
The lines rotate both clockwise and anti-clockwise in a symmetric pattern about the ISA.
Lines that are parallel with ISA do not rotate (generally true for coaxial deformation histories).
Lines can rotate from the shortening field and into the stretching field, but not the other way.

2.27 Progressive subsimple shear

Progressive subsimple shear or **subsimple shearing** can be described as a simultaneous combination of simple and pure shearing, and the component of simple shearing gives it a non-coaxial nature.

The same sets of orthogonal lines that were discussed for simple and pure shearing can also be deformed under subsimple shearing. We have chosen a subsimple shearing where $W_k = 0.82$ in Figure 2.32, which means that it has a substantial component of simple shearing. An important difference from simple shearing is that lines in the sector approximately between lines 1 and 2 rotate against the shearing direction. The size of this sector is identical to the angle between the flow apophyses (α) and depends on W_k and θ (see Figure 2.24). The smaller the pure shearing component, the larger the sector of back-rotation. For pure shearing ($W_k = 0$) the two sectors of oppositely rotating lines are of equal size (Figure 2.31a), while for simple shearing one of them has vanished.

Line 1 is parallel to the shear plane and does not rotate, but in contrast to the case of simple shearing it is stretched in the shearing direction. Line 4 rotates clockwise and demonstrates the high degree of non-coaxiality of this version of subsimple shearing. Line 4 rotates from the instantaneous shortening field into that of stretching, where it retains its original length at stage (b). From this point line 4 grows longer while it, together with all the other lines, rotates toward the horizontal apophysis, which is the shearing direction of the simple shearing component.

Line 2 rotates counterclockwise as it shortens, while lines 5 and 6 are stretched on their way toward the horizontal apophysis. At stage (e), line 6 has rotated through the theoretical X-axis, while line 5 has not quite reached that point.

Line 3 is in the field of instantaneous shortening. At stage (c) it parallels ISA_3 and rotates through this axis due to the non-coaxial nature of this deformation. From this point it follows the path already taken by line 4.

These are some of the characteristic features of subsimple shearing:

Lines of any orientation rotate toward a flow apophysis (the shear direction).

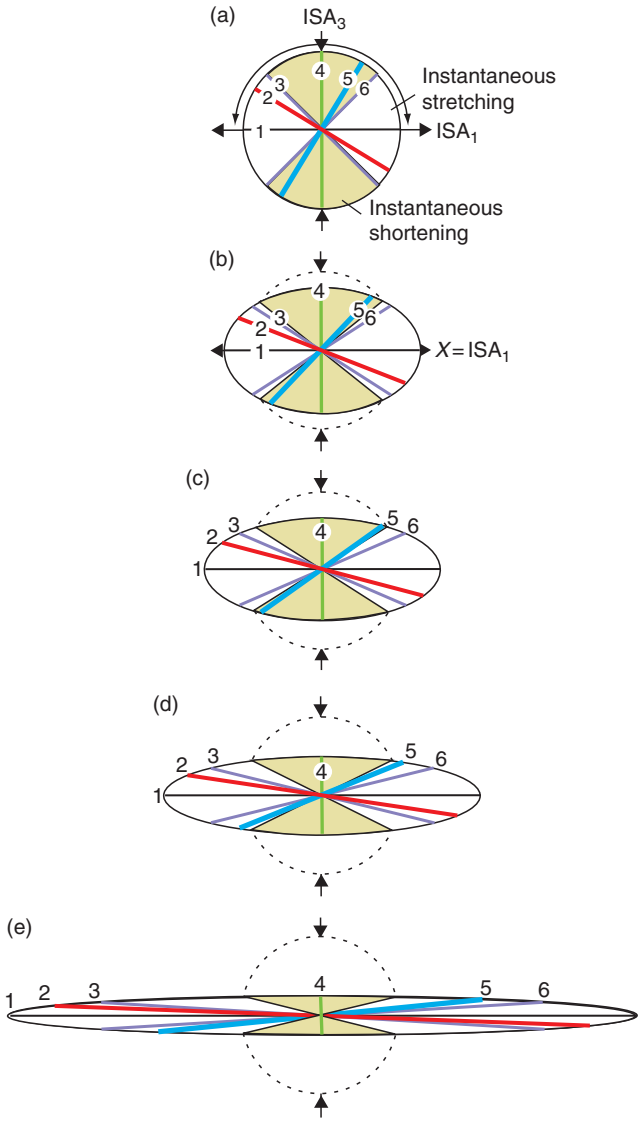

Figure 2.31 Pure shearing of a circle and three sets of orthogonal lines (1–6). The arrows along the circle in (a) indicate the rotation directions for lines during the deformation.

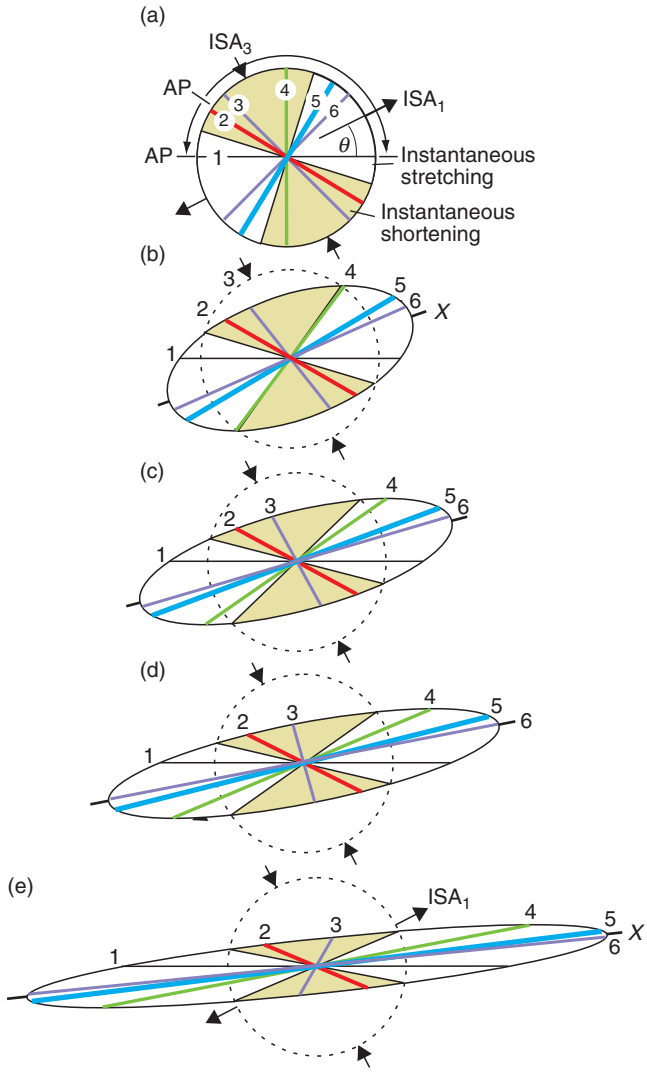

Figure 2.32 Subsimple shearing of a circle and three sets of orthogonal lines (1–6). The arrows along the circle in (a) indicate the rotation directions for lines during the deformation. AP: flow apophysis.

There are two sectors of opposite line rotation. The size and asymmetry of the fields is controlled by the flow apophyses and indicate W_k and one of the flow apophyses (shear direction).

Lines of any orientation are being stretched or shortened during subsimple shearing.

Lines parallel with ISA rotate. Only those parallel with the shear plane do not rotate.

The long axis X of the strain ellipsoid rotates, but slower than for simple shearing.

Lines rotate from the field of instantaneous shortening into that of instantaneous stretching, but never the other way.

2.28 Simple and pure shear and their scale dependence

Simple and pure shear(ing) have been defined mathematically in this chapter. The practical use of these terms depends on the choice of coordinate system and scale. As an example, consider a simple shear zone in the crust that is 50 m thick and 5 km long. If we want to study this zone it would be natural to place a coordinate system with the x-axis in the shear direction and another axis perpendicular to the zone. We could then study or model the effect of simple shear in this zone. Now, if there should be some tens of such shear zones on a bigger scale dipping in opposite directions, then it would be

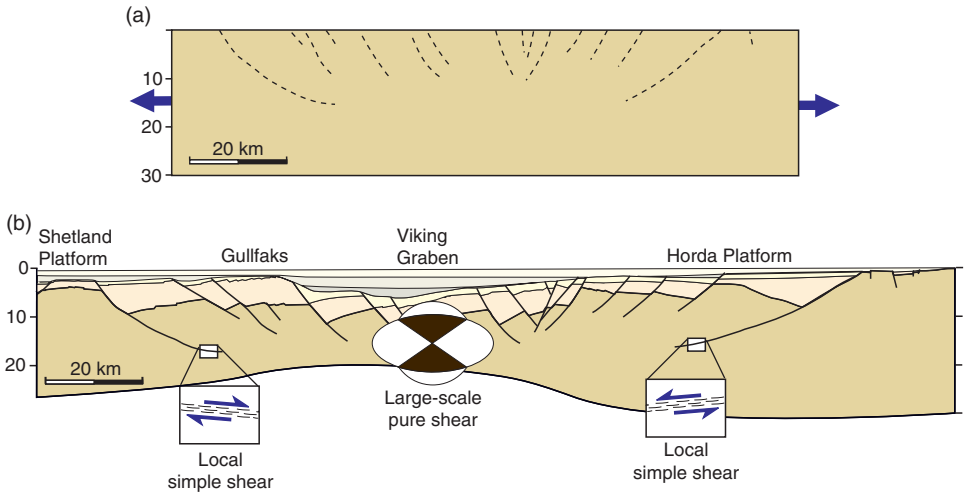

Figure 2.33 Profile across the northern North Sea rift (restored and current). Locally the deformation is simple shear, but is better treated as pure shear on a larger scale.

better to orient the *x*-axis horizontally, which is parallel to the surface (or base) of the crust. In this case the deformation is closer to pure shear, although it contains simple shear zones and perhaps discrete faults on a smaller scale. This can be applied to a profile across a rift, such as the North Sea in Figure 2.33, where the total assemblage of faults and shear zones generates an overall strain that is close to pure shear.

This example illustrates how deformation can be considered as simple shear on one scale and as pure shear on a larger scale. The opposite can also be the case, where there is a partitioning of simple shear on a smaller scale. Some shear zones contain small-scale domains of different deformation types that together constitute an overall simple shear. Hence, pure and simple shear are scale-dependent concepts.

2.29 General three-dimensional deformation

Strain measurements in deformed rocks typically indicate that strain is three-dimensional, i.e. they plot off the diagonal in the Flinn diagram (Figure 2.14). Three-dimensional deformation theory tends to be considerably more complex than that of plane deformation. Pure shear, which is a two-dimensional coaxial deformation, is replaced by a wealth of coaxial deformations, where uniform extension and uniform flattening are end-members (Figure 2.34). Furthermore, there is room for several simple shear components in different directions, all of which can be combined with coaxial strain.

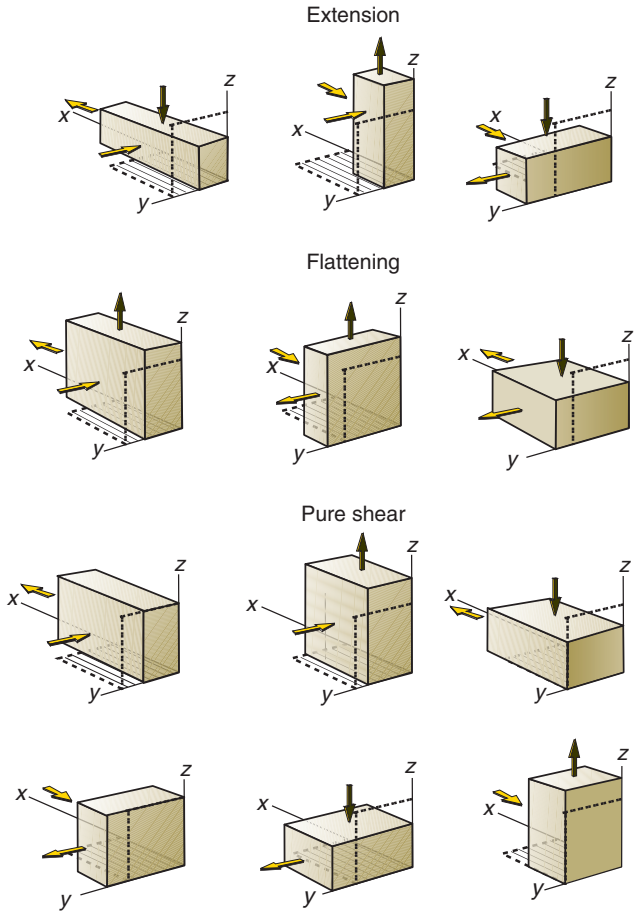

Figure 2.34 Types of coaxial strain.

It is therefore useful to define a few simple three-dimensional deformation types, where two of the principal strain axes of the coaxial strain coincide with the shear plane(s) involved. Figure 2.35 shows a spectrum of three-dimensional deformations that arises

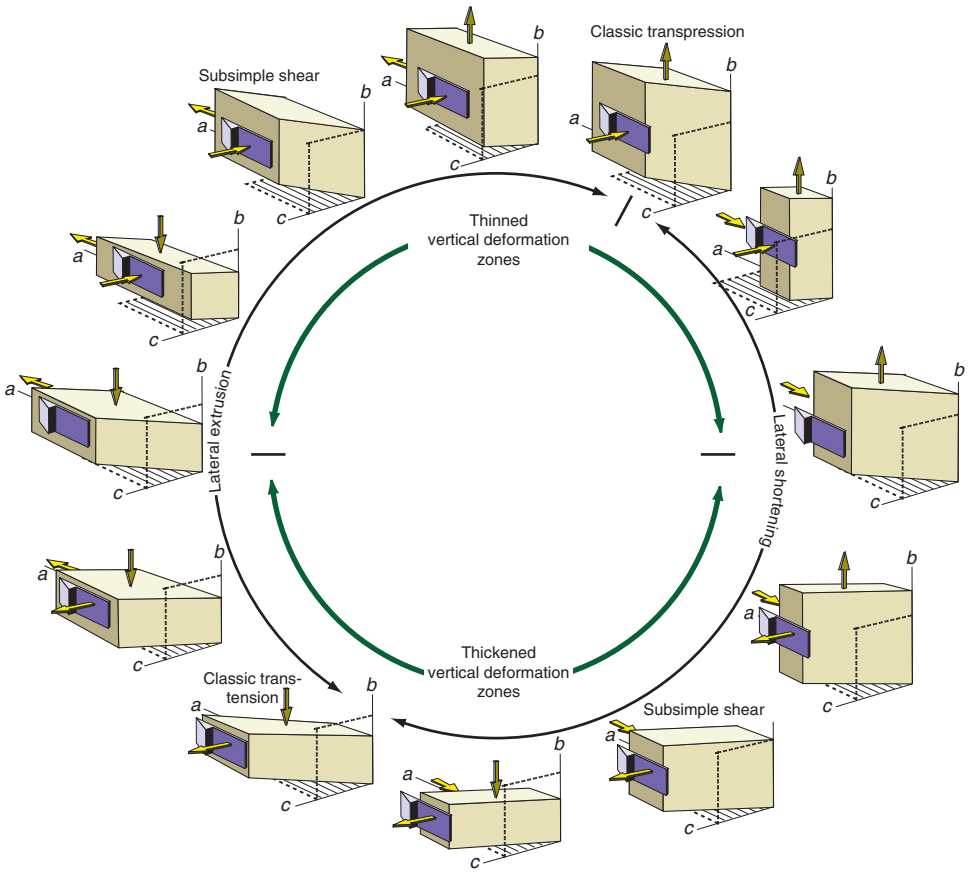

Figure 2.35 Spectrum of deformations based on combinations of a single simple shear (violet arrows) and orthogonal coaxial deformations (yellow). Thinning shear zones occur in the upper half and thickening zones in the lower half of the circle. Based on Tikoff and Fossen (1999).

from a combination of coaxial deformations shown in Figure 2.34 with a simple shear. Transpression and transtension are some of the deformations found in this spectrum and will be discussed later in this book (Chapter 18). Also note that subsimple shear separates different types of three-dimensional deformations in Figure 2.35.

2.30 Stress versus strain

One would perhaps think that the deformation type (pure shear, simple shear, general flattening etc.) is given when the magnitudes and orientations of the three principal stresses are known. This is not so, and strain information combined with observable structures in deformed rocks usually gives more information about the deformation type than does stress information alone.

As an illustration, consider a homogeneous medium that is exposed to linear-viscous (Newtonian) deformation (Chapter 6). In such an idealized medium there will be a simple relationship between stress and strain, and the ISA will parallel the principal stresses (this is the case for any isotropic medium that deforms according to a so-called power-law stress–strain rate).

Natural rocks are rarely (if ever) homogeneous, and linear-viscous deformation is an idealization of natural flow in rocks. Thus, even if we constrain our considerations to planar deformations, the orientation of the principal stresses does not predict the type of plane strain caused by the stresses in a heterogeneous rock. For a given state of stress, the deformation may be pure shear, simple shear or subsimple shear, depending on boundary conditions or heterogeneities of the deforming material. Figure 2.36 shows how the introduction of a rigid wall rock completely changes the way the rock deforms. In this case the boundary between the rigid rock and the weak, deforming rock is important. A related example is the deformation that can occur along plate boundaries. There will usually be a weak zone between the two plates along which most strain is accommodated, and the orientation of the plate boundaries will be important in addition to their relative motions. Further, the weak, deforming

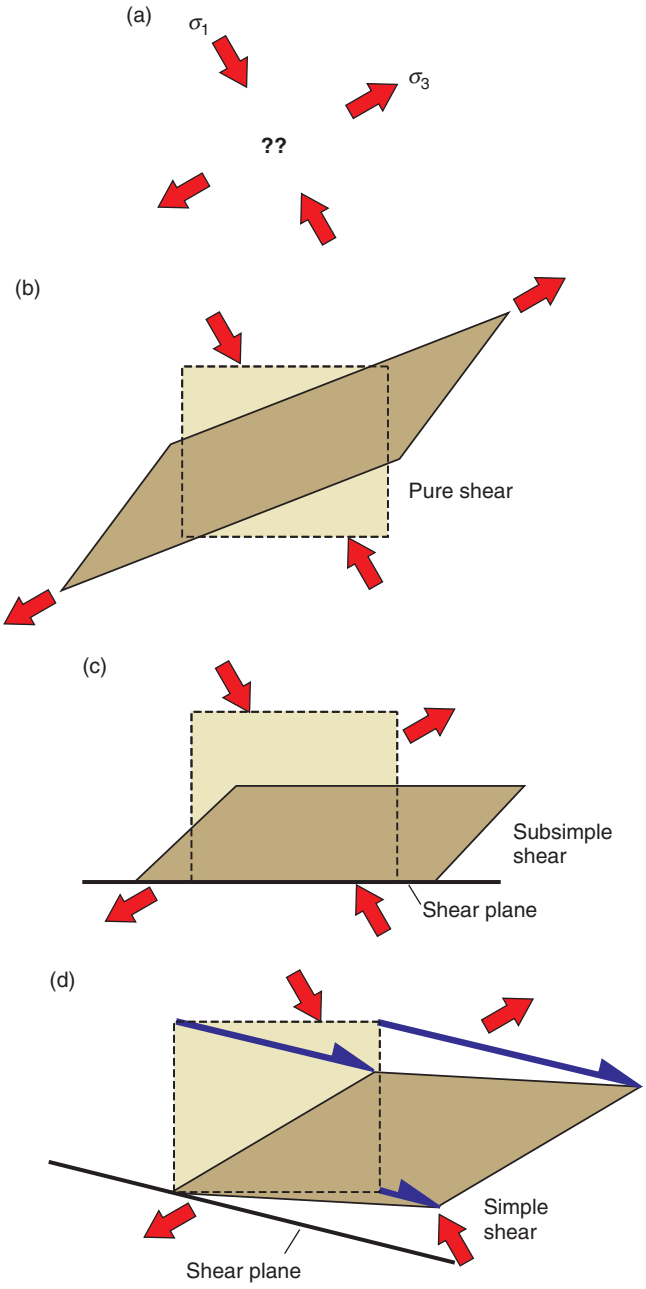

Figure 2.36 Knowledge about the orientations of the principal stresses (a) is not sufficient to predict the resulting deformation. In a perfectly isotropic medium the deformation will be a pure shear as shown in (b). However, if our boundary conditions involve a plane of weakness (potential shear plane), then we could have a subsimple (c) shear. In the special case where the angle between σ_1 and the weak plane is 45° a simple shear could result.

zone may contain faults, soft layers or other heterogeneities that may cause the deformation to partition into domains dominated by coaxial and non-coaxial strains.

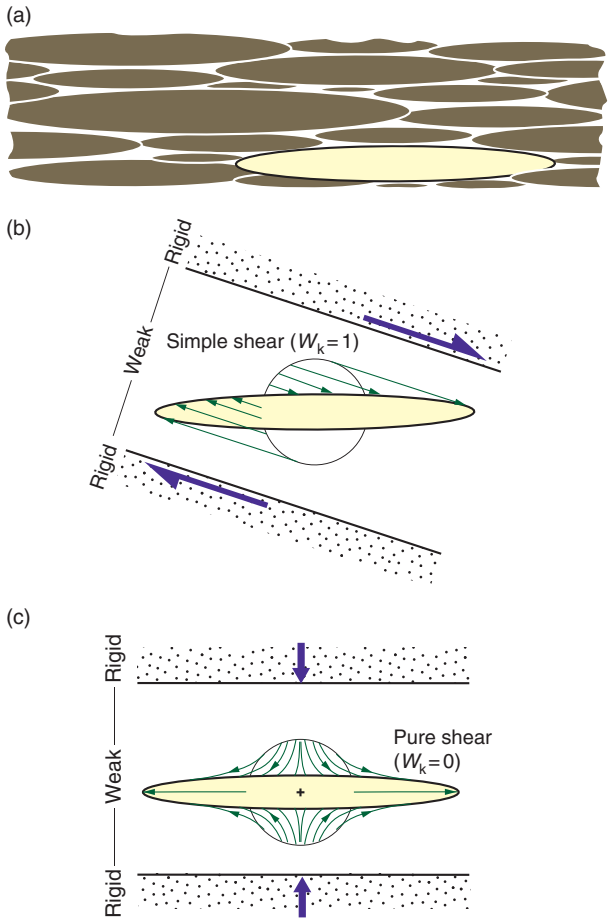

Figure 2.37 Deformed markers (a) such as strained pebbles or ooids give no information about the type of deformation. It could represent simple shear (b), pure shear (c) or any other type of deformation. Knowledge of the orientation of shear zone boundaries or lithologic layering could however give us the necessary information. The yellow ellipses in the three illustrations are identical.

If it is difficult or impossible to predict strain from stress alone, can we more easily go from strain to stress? If we know only the shape and orientation of the strain ellipse (ellipsoid in three dimensions), then Figure 2.37 reveals that we have no clue about even the deformation type. However, if we can relate the strain to such things as shear zone boundaries, then we can find the orientation of the ISA (if we assume steady-state deformation). The question then is whether the ISA correspond to the principal stresses. Paleostress analyses rely on the assumption that they are equal, which is not necessarily quite true. We will return to this topic in Chapter 9.

Summary

In this chapter we have covered the basic theory of deformation and strain. Make sure you understand that strain is the difference between undeformed and deformed states, that flow parameters describe any instant during a deformation history and that they relate to strain only when the flow that they describe is considered over a specified time period. The deformation theory of this chapter forms the foundation for most of the later chapters, where structures resulting from strain are treated. Concepts such as pure and simple shear, ISA and coaxiality will reappear throughout the text, and the next chapter gives some ideas about how to retrieve information about strain from deformed rocks. Before that, we review some of the many important points from this chapter:

- Deformation is strictly the sum of strain, rigid rotation and translation.
- Each of these components results in a change in position of particles in a deforming body.
- Mathematically, homogeneous deformation is a linear transformation and can be represented by a deformation (or transformation) matrix that connects the deformed and undeformed states.
- Deformation history deals with the evolution from the undeformed to the deformed state.
- Strain alone tells us nothing about the deformation history (the way that strain accumulated over time).
- Flow parameters describe the situation or flow at any instant during the deformation history. If these parameters stay fixed during deformation we have steady-state deformation.
- Flow apophyses separate different fields of flow, or different domains of particle paths. They are orthogonal for coaxial strain, parallel for simple shear and oblique for subsimple shear.
- The fastest and slowest stretching directions (ISA_1 and ISA_3) are fixed at 45° to the shear plane for progressive simple shear. They bisect the fields of instantaneous stretching and shortening.
- The instantaneous stretching axes (ISA) are not necessarily equal to principal stress axes, but describe how strain accumulates at a given instance during the deformation history.
- The deformation history can be described by intervals, each with its own incremental deformation matrix and strain ellipsoid.
- Flow parameters describe deformation at an instant, while strain accumulates over time and is directly related to flow parameters only if the latter remain constant during the deformation history.

Review questions

1. List and explain the flow parameters discussed in this chapter.
2. What is the deformation called if flow parameters are constant throughout the deformation history?
3. Are ISA equal to stress axes?
4. What is the difference between angular shear and shear strain?
5. What is plane strain and where does it plot in the Flinn diagram?
6. Give examples of plane strain.

7. What is meant by particle paths?
8. What happens to the principal strain axes during pure shearing?
9. What is meant by the expression non-coaxial deformation history?
10. What is the kinematic vorticity number?
11. What set of material lines do not rotate or change length during simple shear?

E-MODULE

The first part of the e-learning module called *Deformation* is recommended for this chapter. Also see Appendix A for more details about the deformation matrix.

FURTHER READING

General deformation theory

Means, W. D., 1976, *Stress and Strain: Basic Concepts of Continuum Mechanics for Geologists*. New York: Springer-Verlag.

Means, W. D., 1990, Kinematics, stress, deformation and material behavior. *Journal of Structural Geology* **12**: 953–971.

Ramsay, J. G., 1980, Shear zone geometry: a review. *Journal of Structural Geology* **2**: 83–99.

Tikoff, B. and Fossen, H., 1999, Three-dimensional reference deformations and strain facies. *Journal of Structural Geology* **21**: 1497–1512.

The deformation matrix

Flinn, D., 1979, The deformation matrix and the deformation ellipsoid. *Journal of Structural Geology* **1**: 299–307.

Fossen, H. and Tikoff, B., 1993, The deformation matrix for simultaneous simple shearing, pure shearing, and volume change, and its application to transpression/transtension tectonics. *Journal of Structural Geology* **15**: 413–422.

Ramberg, H., 1975, Particle paths, displacement and progressive strain applicable to rocks. *Tectonophysics* **28**: 1–37.

Sanderson, D. J., 1976, The superposition of compaction and plane strain. *Tectonophysics* **30**: 35–54.

Sanderson, D. J., 1982, Models of strain variations in nappes and thrust sheets: a review. *Tectonophysics* **88**: 201–233.

The strain ellipse

Flinn, D., 1963, On the symmetry principle and the deformation ellipsoid. *Geological Magazine* **102**: 36–45.

Treagus, S. H. and Lisle, R. J., 1997, Do principal surfaces of stress and strain always exist? *Journal of Structural Geology* **19**: 997–1010.

The Mohr circle for strain

Passchier, C. W., 1988, The use of Mohr circles to describe non-coaxial progressive deformation. *Tectonophysics* **149**: 323–338.

Volumetric strain

Passchier, C. W., 1991, The classification of dilatant flow types. *Journal of Structural Geology* **13**: 101–104.

Xiao, H. B., and Suppe, J., 1989, Role of compaction in listric shape of growth normal faults. *American Association of Petroleum Geologists Bulletin* **73**: 777–786.

Vorticity and deformation history

Elliott, D., 1972, Deformation paths in structural geology. *Geological Society of America Bulletin* **83**: 2621–2638.

Ghosh, S. K., 1987. Measure of non-coaxiality. *Journal of Structural Geology* **9**: 111–113.

Jiang, D., 1994, Vorticity determination, distribution, partitioning and the heterogeneity and non-steadiness of natural deformations. *Journal of Structural Geology* **16**: 121–130.

Passchier, C. W., 1990, Reconstruction of deformation and flow parameters from deformed vein sets. *Tectonophysics* **180**: 185–199.

Talbot, C. J., 1970, The minimum strain ellipsoid using deformed quartz veins. *Tectonophysics* **9**: 47–76.

Tikoff, B. and Fossen, H., 1995, The limitations of three-dimensional kinematic vorticity analysis. *Journal of Structural Geology* **17**: 1771–1784.

Truesdell, C., 1953, Two measures of vorticity. *Journal of Rational Mechanics and Analysis* **2**: 173–217.

Wallis, S. R., 1992, Vorticity analysis in a metachert from the Sanbagawa Belt, SW Japan. *Journal of Structural Geology* **12**: 271–280.

The stress–strain relationship

Tikoff, B. and Wojtal, S. F., 1999, Displacement control of geologic structures. *Journal of Structural Geology* **21**: 959–967.

Chapter 3

Strain in rocks

Strain can be retrieved from rocks through a range of different methods. Much attention has been paid to one-, two- and three-dimensional strain analyses in ductilely deformed rocks, particularly during the last half of the twentieth century, when a large portion of the structural geology community had their focus on ductile deformation. Strain data were collected or calculated in order to understand such things as thrusting in orogenic belts and the mechanisms involved during folding of rock layers. The focus of structural geology has changed and the field has broadened during the last couple of decades. Today strain analysis is at least as common in faulted areas and rift basins as in orogenic belts. While we will return to strain in the brittle regime in Chapter 20, we will here concentrate on classic aspects of how strain is measured and quantified in the ductile regime

3.1 Why perform strain analysis?

It can be important to retrieve information about strain from deformed rocks. First of all, strain analysis gives us an opportunity to explore the state of strain in a rock and to map out strain variations in a sample, an outcrop or a region. Strain data are important in the mapping and understanding of shear zones in orogenic belts. Strain measurements can also be used to estimate the amount of offset across a shear zone. As will be discussed in Chapter 15, it is possible to extract important information from shear zones if strain is known.

In many cases it is useful to know if the strain is planar or three dimensional. If planar, an important criterion for section balancing is fulfilled, be it across orogenic zones or extensional basins. The shape of the strain ellipsoid may also contain information about how the deformation occurred. Oblate (pancake-shaped) strain in an orogenic setting may, for example, indicate flattening strain related to gravity-driven collapse rather than classic push-from-behind thrusting.

The orientation of the strain ellipsoid is also important, particularly in relation to rock structures. In a shear zone setting, it may tell us if the deformation was simple shear or not (Chapter 15). Strain in folded layers helps us to understand fold-forming mechanism(s) (Chapter 11). Studies of deformed reduction spots in slates give good estimates on how much shortening has occurred across the foliation in such rocks (Chapter 12), and strain markers in sedimentary rocks can sometimes allow for reconstruction of original sedimentary thickness. Strain will follow us through most of this book.

3.2 Strain in one dimension

One-dimensional strain analyses are concerned with changes in length and therefore the simplest form of strain analysis we have. If we can reconstruct the original length of an object or linear structure we can also calculate the amount of stretching or shortening in that direction. Objects revealing the state of strain in a deformed rock are known as **strain markers**. Examples of strain markers indicating change in length are boudinaged dikes or layers, and minerals or linear fossils such as belemnites or graptolites that have been elongated, such as the stretched Swiss belemnites shown in Figure 3.1. Or it could be a layer shortened by folding. It could even be a faulted reference horizon on a geologic or seismic profile, as will be discussed in Chapter 20. The horizon

Figure 3.1 Two elongated belemnites in Jurassic limestone in the Swiss Alps. The different ways that the two belemnites have been stretched give us some two-dimensional information about the strain field: the upper belemnite has experienced sinistral shear strain while the lower one has not and must be close to the maximum stretching direction.

may be stretched by normal faults or shortened by reverse faults, and the overall strain is referred to as **brittle strain**. One-dimensional strain is revealed when the horizon, fossil, mineral or dike is restored to its pre-deformational state.

3.3 Strain in two dimensions

In **two-dimensional strain analyses** we look for sections that have objects of known initial shape or contain linear markers with a variety of orientations (Figure 3.1). Strained reduction spots of the type shown in Figure 3.2 are perfect, because they tend to have spherical shapes where they are undeformed. There are also many other types of objects that can be used, such as sections through conglomerates, breccias, corals, reduction spots, oolites, vesicles, pillow lavas (Figure 3.3), columnar basalt, plutons and so on. Two-dimensional strain can also be calculated from one-dimensional data that represent different directions in the same section. A typical example would be dikes with different orientations that show different amounts of extension.

Strain extracted from sections is the most common type of strain data, and sectional data can be combine to estimate the three-dimensional strain ellipsoid.

Changes in angles

Strain can be found if we know the original angle between sets of lines. The original angular relations between structures such as dikes, foliations and bedding

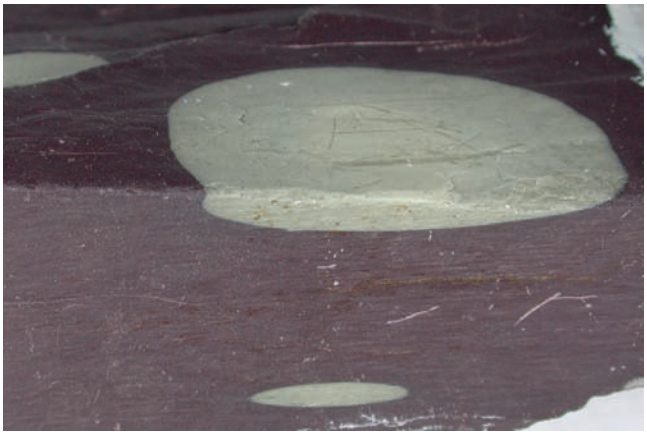

Figure 3.2 Reduction spots in Welsh slate. The light spots formed as spherical volumes of bleached (chemically reduced) rock. Their new shapes are elliptical in cross-section and oblate (pancake-shaped) in three dimensions, reflecting the tectonic strain in these slates.

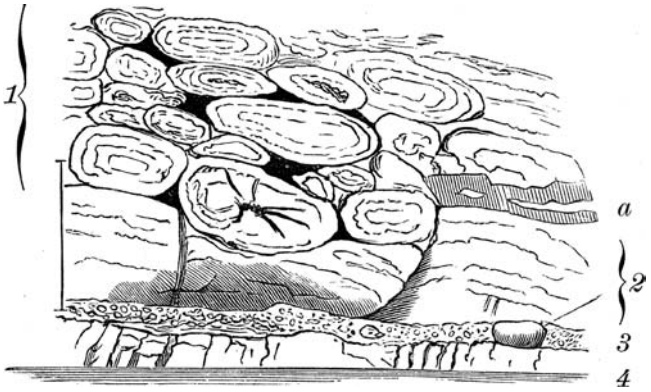

Figure 3.3 Section through a deformed Ordovician pahoe-hoe lava. The elliptical shapes were originally more circular, and Hans Reusch, who made the sketch in the 1880s, understood that they had been flattened during deformation. The R_f/ϕ, center-to-center, and Fry methods would all be worth trying in this case.

are sometimes found in both undeformed and deformed states, i.e. outside and inside a deformation zone. We can then see how the strain has affected the angular relationships and use this information to estimate strain. In other cases orthogonal lines of symmetry found in undeformed fossils such as trilobites, brachiopods and worm burrows (angle with layering) can be used to determine the angular shear in some deformed sedimentary rocks. In general, all we need to know is the change in angle between sets of lines and that there is no strain partitioning due to contrasting mechanical properties of the objects with respect to the enclosing rock.

If the angle was 90° in the undeformed state, the change in angle is the local angular shear ψ (Section 2.8). If, as we recall from the previous chapter, the two originally orthogonal lines remain orthogonal after the deformation, then they must represent the principal strains and thus the orientation of the strain ellipsoid. Observations of variously oriented line sets thus give information about the strain ellipse or ellipsoid. All we need is a useful method. Two of the most common methods used to find strain from initially orthogonal lines are known as the Wellman and Breddin methods, and are presented in the following sections.

The Wellman method

This method dates back to 1962 and is a geometric construction for finding strain in two dimensions (in a section). It is typically demonstrated on fossils with orthogonal lines of symmetry in the undeformed state. In Figure 3.4a we use the hinge and symmetry lines of brachiopods. A line of reference must be drawn (with arbitrary orientation) and pairs of lines that were orthogonal in the unstrained state are identified. The reference line must have two defined endpoints, named A and B in Figure 3.4b. A pair of lines is then drawn parallel to both the hinge line and symmetry line for each fossil, so that they intersect at the endpoints of the reference line. The other points of intersection are marked (numbered 1–6 in Figure 3.4b, c). If the rock is unstrained, the lines will define rectangles. If there is a strain involved, they will define parallelograms. To find the strain ellipse, simply fit an ellipse to the numbered corners of the parallelograms (Figure 3.4c). If no ellipse can be fitted to the corner points of the rectangles the strain is heterogeneous or, alternatively, the measurement or assumption of initial orthogonality is false. The challenge with this method is, of course, to find enough fossils or other features with initially orthogonal lines – typically 6–10 are needed.

The Breddin graph

We have already stated that the angular shear depends on the orientation of the principal strains: the closer the deformed orthogonal lines are to the principal strains, the lower the angular shear. This fact is utilized in a method first published by Hans Breddin in 1956 in German (with some errors). It is based on the graph shown in Figure 3.5, where the angular shear changes with orientation and strain magnitude R. Input are the

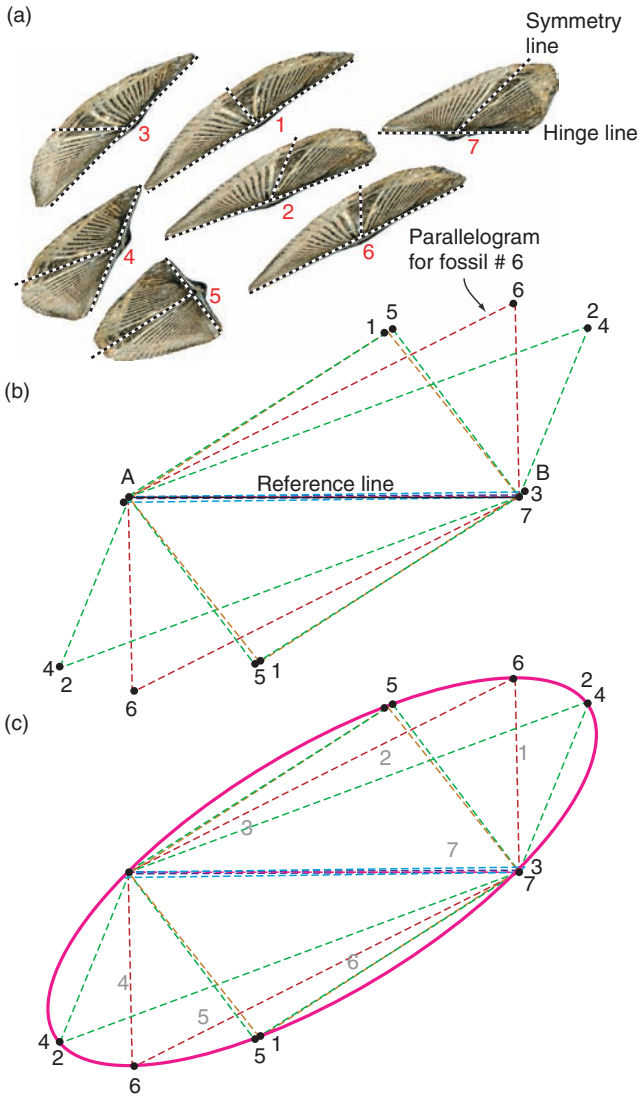

Figure 3.4 Wellman's method involves construction of the strain ellipse by drawing parallelograms based on the orientation of originally orthogonal pairs of lines. The deformation was produced on a computer and is a homogeneous simple shear of $\gamma = 1$. However, the strain ellipse itself tells us nothing about the degree of coaxiality: the same result could have been attained by pure shear.

angular shears and the orientations of the sheared line pairs with respect to the principal strains. These data are plotted in the so-called Breddin graph and the *R*-value (ellipticity of the strain ellipse) is found by inspection (Figure 3.5). This method may work even for only one or two observations.

In many cases the orientation of the principal axes is unknown. In such cases the data are plotted with respect to an arbitrarily drawn reference line. The data are then moved horizontally on the graph until they fit one of

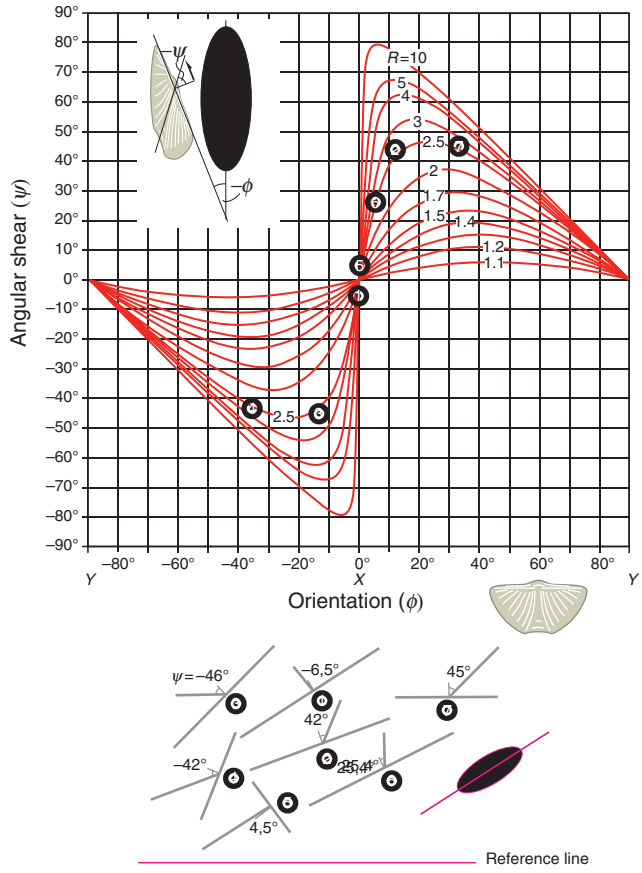

Figure 3.5 The data from the previous figure plotted in a Breddin graph. The data points are close to the curve for $R = 2.5$.

the curves, and the orientations of the strain axes are then found at the intersections with the horizontal axis (Figure 3.5). In this case a larger number of data are needed for good results.

Elliptical objects and the R_f/ϕ-method

Objects with initial circular (in sections) or spherical (in three dimensions) geometry are relatively uncommon, but do occur. Reduction spots and ooliths perhaps form the most perfect spherical shapes in sedimentary rocks. When deformed homogeneously, they are transformed into ellipses and ellipsoids that reflect the local finite strain. Conglomerates are perhaps more common and contain clasts that reflect the finite strain. In contrast to oolites and reduction spots, few pebbles or cobbles in a conglomerate are spherical in the undeformed state. This will of course influence their shape in the deformed state and causes a challenge in strain analyses. However, the clasts tend to have their long axes in a spectrum of orientations in the undeformed state, in which case

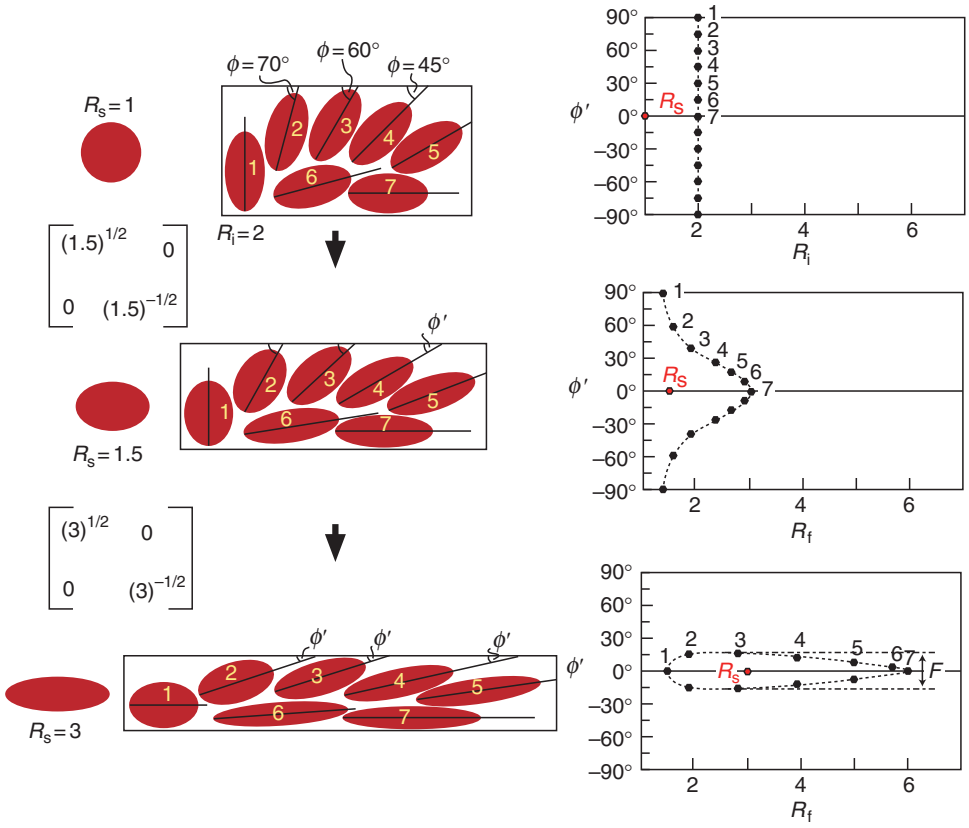

Figure 3.6 The R_f/ϕ method illustrated. The ellipses have the same ellipticity (R_i) before the deformation starts. The R_f–ϕ diagram to the right indicates that $R_i = 2$. A pure shear is then added with $R_s = 1.5$ followed by a pure shear strain of $R_s = 3$. The deformation matrices for these two deformations are shown. Note the change in the distribution of points in the diagrams to the right. R_s in the diagrams is the actual strain that is added. Modified from Ramsay and Huber (1983).

methods such as the R_f/ϕ-method may be able to take the initial shape factor into account.

The R_f/ϕ-method was first introduced by John Ramsay in his well-known 1967 textbook and was later improved. The method is illustrated in Figure 3.6. The markers are assumed to have approximately elliptical shapes in the deformed (and undeformed) state, and they must show a significant variation in orientations for the method to work.

The R_f/ϕ-method handles initially non-spherical markers, but the method requires a significant variation in the orientations of their long axes.

The ellipticity (X/Y) in the undeformed (initial) state is called R_i. In our example (Figure 3.6) $R_i = 2$. After a strain R_s the markers exhibit new shapes. The new shapes are different and depend on the initial orientation of the elliptical markers. The new (final) ellipticity for each deformation marker is called R_f and the spectrum of R_f-values is plotted against their orientations, or more specifically against the angle ϕ' between the long axis of the ellipse and a reference line (horizontal in Figure 3.6). In our example we have applied two increments of pure shear to a series of ellipses with different orientations. All the ellipses have the same initial shape $R_i = 2$, and they plot along a vertical line in the upper right diagram in Figure 3.6. Ellipse 1 is oriented with its long axis along the minimum principal strain axis, and it is converted into an ellipse that shows less strain (lower R_f-value) than the true strain ellipse (R_s). Ellipse 7, on the other hand, is oriented with its long axis parallel to the long axis of the strain ellipse, and the two ellipticities are added. This leads to an ellipticity that is higher than R_s. When $R_s = 3$, the true strain R_s is located somewhere between the shape represented by ellipses 1 and 7, as seen in Figure 3.6 (lower right diagram).

For $R_s = 1.5$ we still have ellipses with the full spectrum of orientations (−90° to 90°; see middle diagram in Figure 3.6), while for $R_s = 3$ there is a much more limited spectrum of orientations (lower graph in Figure 3.6). The scatter in orientation is called the fluctuation F. An important change happens when ellipse 1, which has its long axis along the Z-axis of the strain ellipsoid, passes the shape of a circle ($R_s = R_i$,) and starts to develop an ellipse whose long axis is parallel to X. This happens when $R_s = 2$, and for larger strains the data points define

a circular shape. Inside this shape is the strain R_s that we are interested in. But where exactly is R_s? A simple average of the maximum and minimum R_f-values would depend on the original distribution of orientations. Even if the initial distribution is random, the average R-value would be too high, as high values tend to be overrepresented (Figure 3.6, lower graph).

To find R_s we have to treat the cases where $R_s > R_i$ and $R_s < R_i$ separately. In the latter case, which is represented by the middle graph in Figure 3.6, we have the following expressions for the maximum and minimum value for R_f:

$$R_{fmax} = R_s R_i$$

$$R_{fmin} = R_i / R_s$$

Solving for R_i and R_s gives

$$R_s = (R_{fmax}/R_{fmin})^{1/2}$$

$$R_i = (R_{fmax} R_{fmin})^{1/2}$$

which represent expressions for both the strain related to the deformation and the initial ellipticity.

For higher-strain cases, where $R_s < R_i$, we obtain

$$R_{fmax} = R_s R_i$$

$$R_{fmin} = R_s / R_i$$

Solving for R_s gives

$$R_s = (R_{fmax} R_{fmin})^{1/2}$$

$$R_i = (R_{fmax}/R_{fmin})^{1/2}$$

In both cases the orientation of the long (X) axis of the strain ellipse is given by the location of the maximum R_f-values. Strain could also be found by fitting the data to pre-calculated curves for various values for R_i and R_s. In practice, such operations are most efficiently done by means of computer programs.

The example shown in Figure 3.6 and discussed above is idealized in the sense that all the undeformed elliptical markers have identical ellipticity. What if this were not the case, i.e. some markers were more elliptical than others? Then the data would not have defined a nice curve but a cloud of points in the R_f/ϕ-diagram. Maximum and minimum R_f-values could still be found and strain could be calculated using the equations above. The only change in the equation is that R_i now represents the maximum ellipticity present in the undeformed state.

Another complication that may arise is that the initial markers may have had a restricted range of orientations. Ideally, the R_f/ϕ-method requires the elliptical objects to be more or less randomly oriented prior to deformation. Conglomerates, to which this method commonly is applied, tend to have clasts with a preferred orientation. This may result in an R_f–ϕ plot in which only a part of the curve or cloud is represented. In this case the maximum and minimum R_f-values may not be representative, and the formulas above may not give the correct answer and must be replaced by a computer-based iterative retrodeformation method where X is input. However, many conglomerates have a few clasts with initially anomalous orientations that allow the use of R_f/ϕ analysis.

Center-to-center method

This method, here demonstrated in Figure 3.7, is based on the assumption that circular objects have a more or less statistically uniform distribution in our section(s). This means that the distances between neighboring particle centers were fairly constant before deformation. The particles could represent sand grains in well-sorted sandstone, pebbles, ooids, mud crack centers, pillow-lava or pahoe-hoe lava centers, pluton centers or other objects that are of similar size and where the centers are easily definable. If you are uncertain about how closely your section complies with this criterion, try anyway. If the method yields a reasonably well-defined ellipse, then the method works.

The method itself is simple and is illustrated in Figure 3.7: Measure the distance and direction from the center of an ellipse to those of its neighbors. Repeat this for all ellipses and graph the distance d' between the centers and the angles α' between the center tie lines and a reference line. A straight line occurs if the section is unstrained, while a deformed section yields a curve with maximum (d'_{max}) and minimum values (d'_{min}). The ellipticity of the strain ellipse is then given by the ratio: $R_s = (d'_{max})/(d'_{min})$.

The Fry method

A quicker and visually more attractive method for finding two-dimensional strain was developed by Norman Fry at the end of the 1970s. This method, illustrated in Figure 3.8, is based on the center-to-center method and

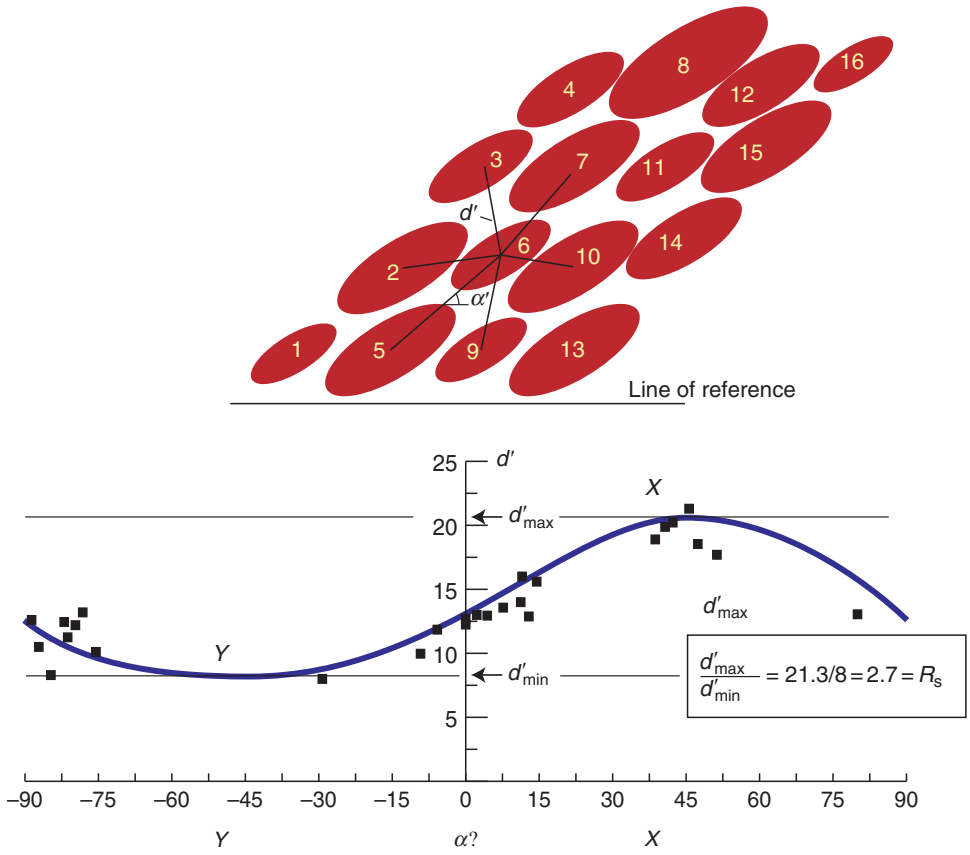

Figure 3.7 The center-to-center method. Straight lines are drawn between neighboring object centers. The length of each line (d') and the angle (α') that they make with a reference line are plotted in the diagram. The data define a curve that has a maximum at X and a minimum at the Y-value of the strain ellipse, and where $R_s = X/Y$.

is most easily dealt with using one of several available computer programs. It can be done manually by placing a tracing overlay with a coordinate origin and pair of reference axes on top of a sketch or picture of the section. The origin is placed on a particle center and the centers of all other particles (not just the neighbors) are marked on the tracing paper. The tracing paper is then moved, without rotating the paper with respect to the section, so that the origin covers a second particle center, and the centers of all other particles are again marked on the tracing paper. This procedure is repeated until the area of interest has been covered. For objects with a more or less uniform distribution the result will be a visual representation of the strain ellipse. The ellipse is the void area in the middle, defined by the point cloud around it (Figure 3.8c).

The Fry method, as well as the other methods presented in this section, outputs two-dimensional strain. Three-dimensional strain is found by combining strain estimates from two or more sections through the deformed rock volume. If sections can be found that each contain two of the principal strain axes, then two sections are sufficient. In other cases three or more sections are needed, and the three-dimensional strain must be calculated by use of a computer.

3.4 Strain in three dimensions

A complete strain analysis is **three-dimensional**. Three-dimensional strain data are presented in the Flinn diagram or similar diagrams that describe the shape of the strain ellipsoid, also known as the **strain geometry**. In addition, the orientation of the principal strains can be presented by means of stereographic nets. Direct field observations of three-dimensional strain are rare. In almost all cases, analysis is based on two-dimensional strain observations from two or more sections at the same locality (Figure 3.9). A well-known example of three-dimensional strain analysis from deformed conglomerates is presented in Box 3.1.

In order to quantify ductile strain, be it in two or three dimensions, the following conditions need to be met:

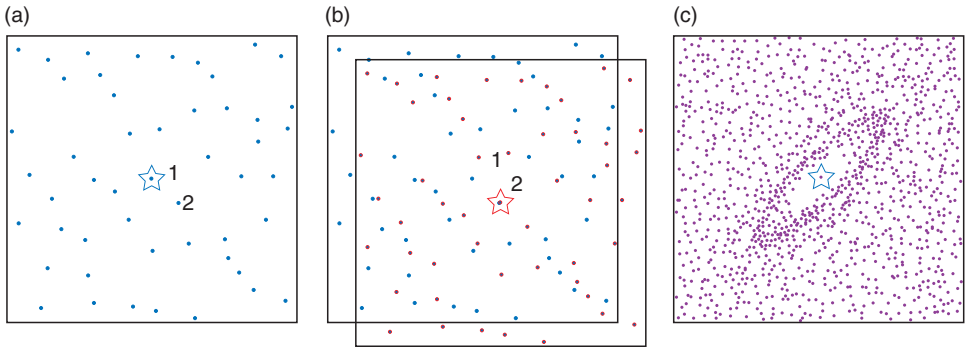

Figure 3.8 The Fry method performed manually. (a) The centerpoints for the deformed objects are transferred to a transparent overlay. A central point (1 on the figure) is defined. (b) The transparent paper is then moved to another of the points (point 2) and the centerpoints are again transferred onto the paper (the overlay must not be rotated). The procedure is repeated for all of the points, and the result (c) is an image of the strain ellipsoid (shape and orientation). Based on Ramsay and Huber (1983).

The strain must be homogeneous at the scale of observation, the mechanical properties of the objects must have been similar to those of their host rock during the deformation, and we must have a reasonably good knowledge about the original shape of strain markers.

The first point is obvious. If the strain is heterogeneous we have to look at another scale, either a larger one where the heterogeneities vanish, or subareas where strain can be considered to be approximately homogeneous. The latter was done in the example in Box 3.2, where a strain pattern was mapped out that could be related to a larger structure. This example shows how mapping of the state of strain can help us to understand the formation of larger-scale structures, in this case the history of folding.

The second point is an important one. For ductile rocks it means that the object and its surroundings must have had the same competence or viscosity (see Chapter 5). Otherwise the strain recorded by the object would be different from that of its surroundings. This effect is one of several types of **strain partitioning**, where the overall strain is distributed unevenly in terms of intensity and/or geometry in a rock volume. As an example, we mark a perfect circle on a piece of clay before flattening it between two walls. The circle transforms passively into an ellipse that reveals the two-dimensional strain if the deformation is homogeneous. If we embed a colored sphere of the same clay, then it would again deform along with the rest of the clay, revealing the three-dimensional strain involved. However, if we put a stiff marble in the clay the result is quite different. The marble remains unstrained while the clay around it becomes more intensely and heterogeneously strained than in the previous case. In fact, it causes a more heterogeneous strain pattern to appear. Strain markers with the same mechanical properties as the surroundings are called **passive strain markers** because they deform passively along with their surroundings. Those that have anomalous mechanical properties respond differently than the surrounding medium to the overall deformation, and such markers are called **active strain markers**.

An example of data from active strain markers is shown in Figure 3.10. These data were collected from a deformed polymictic conglomerate where three-dimensional strain has been estimated from different clast types in the same rock and at the same locality. Clearly, the different clast types

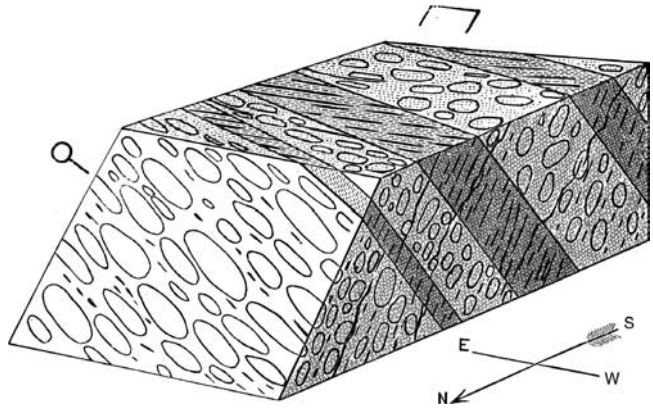

Figure 3.9 Three-dimensional strain expressed as ellipses on different sections through a conglomerate. The foliation (*XY*-plane) and the lineation (*X*-axis) are annotated. This illustration was published in 1888, but what are now routine strain methods were not developed until the 1960s.

BOX 3.1 DEFORMED QUARTZITE CONGLOMERATES

Quartz or quartzite conglomerates with a quartzite matrix are commonly used for strain analyses. The more similar the mineralogy and grain size of the matrix and the pebbles, the less deformation partitioning and the better the strain estimates. A classic study of deformed quartzite conglomerates is Jake Hossack's study of the Norwegian Bygdin conglomerate, published in 1968. Hossack was fortunate – he found natural sections along the principal planes of the strain ellipsoid at each locality. Putting the sectional data together gave the three-dimensional state of strain (strain ellipsoid) for each locality. Hossack found that strain geometry and intensity varies within his field area. He related the strain pattern to static flattening under the weight of the overlying Caledonian Jotun Nappe. Although details of his interpretation may be challenged, his work demonstrates how conglomerates can reveal a complicated strain pattern that otherwise would have been impossible to map.

Hossack noted the following sources of error:

- Inaccuracy connected with data collection (sections not being perfectly parallel to the principal planes of strain and measuring errors).
- Variations in pebble composition.
- The pre-deformational shape and orientation of the pebbles.
- Viscosity contrasts between clasts and matrix.
- Volume changes related to the deformation (pressure solution).
- The possibility of multiple deformation events.

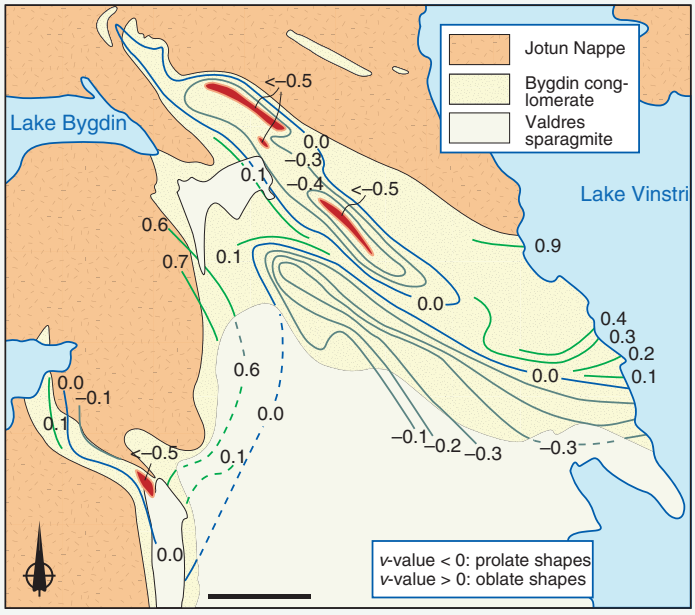

Hossack's strain map from the Bygdin area, Norway.

The Bygdin conglomerate.

BOX 3.2 STRAIN AROUND A FOLD

Deformed conglomerates are an important source of strain data in deformed rocks because conglomerates are relatively common and contain large numbers of objects (clasts). An example is shown where strain was evaluated at several stations around a folded conglomerate layer, deformed under greenschist facies conditions. It was found that the long limbs were totally dominated by flattening strain (oblate strain geometry) while there was a change toward constrictional strain in the hinge and short limb area. This information would have been difficult to achieve without mesoscopic strain markers, because the rock is recrystallized so that the original sand grain boundaries are obliterated.

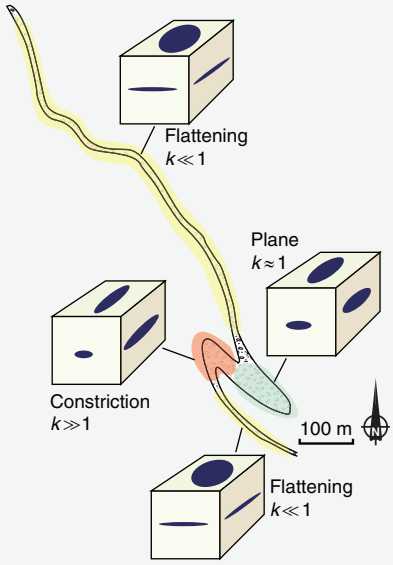

Map of the conglomerate layer. Note the thickened short fold limb.

The conglomerate in a constrictional state of strain.

The strain distribution then had to be explained, and was found to fit a model where an already flattened conglomerate layer is rotated into the field of shortening during shearing. A dextral shear rotates the foliation and the oblate clasts into the shortening field, which makes the *Y*-axis shrink. This takes the strain ellipsoid across the plane strain diagonal of the Flinn diagram and into the constrictional field ($k > 1$). At this point we are on the inverted limb or at the lower fold hinge. The process continues, and the strain ellipse again becomes flattened. This model explains strain data by means of a particular deformation history, defining a certain strain path, which in this case is flattening to constriction and then back to flattening strain again.

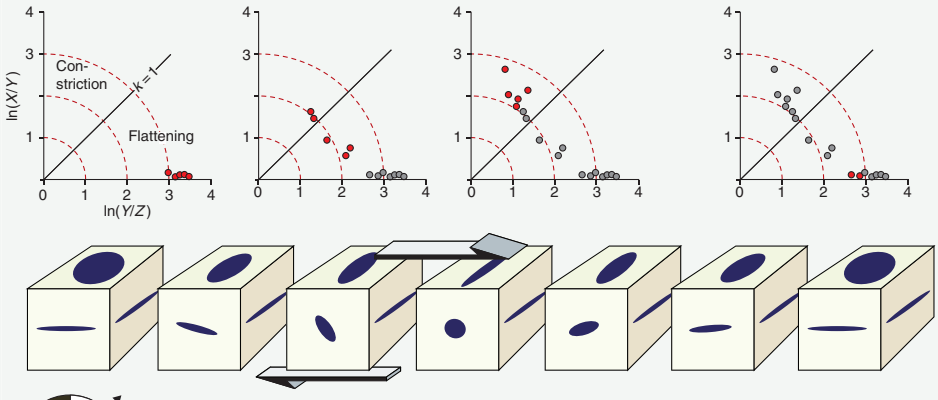

Illustration of the strain history in terms of block diagrams showing sections through the strain ellipsoid and strain data plotted in Flinn diagrams. The positions of the Flinn diagrams approximately correspond to those of the block diagrams below. Also shown is the direction of the instantaneous stretching axes and fields of instantaneous contraction (black) and extension for dextral simple shear.

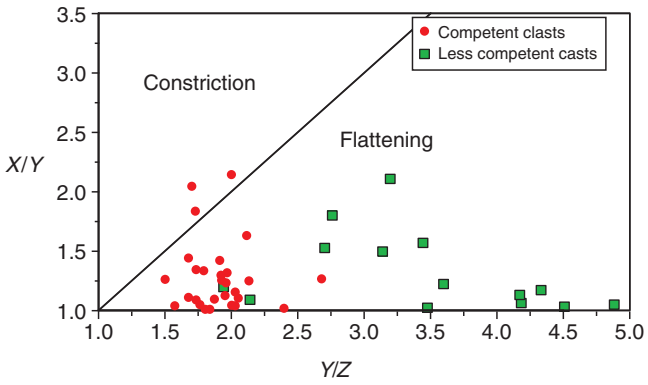

Figure 3.10 Strain obtained from deformed conglomerates, plotted in the Flinn diagram. Different pebble types show different shapes and finite strains. Polymict conglomerate of the Utslettefjell Formation, Stord, southwest Norway. Data collected by D. Kirschner, R. Malt and the author.

have recorded different amounts of strain. Competent (stiff) granitic clasts are less strained than less competent greenstone clasts. This is seen using the fact that strain intensity generally increases with increasing distance from the origin in Flinn space. But there is another interesting thing to note from this figure: It seems that competent clasts plot higher in the Flinn diagram (Figure. 3.10) than incompetent ("soft") clasts, meaning that competent clasts take on a more prolate shape. Hence, not only strain intensity but also strain geometry may vary according to the mechanical properties of strain markers.

The way that the different markers behave depends on factors such as their mineralogy, preexisting fabric, grain size, water content and temperature–pressure conditions at the time of deformation. In the case of Figure 3.10, the temperature–pressure regime is that of lower to middle greenschist facies. At higher temperatures, quartz-rich rocks are more likely to behave as "soft" objects, and the relative positions of clast types in Flinn space are expected to change.

The last point above also requires attention: the initial shape of a deformed object clearly influences its post-deformational shape. If we consider two-dimensional objects such as sections through oolitic rocks, sandstones or conglomerates, the R_f/ϕ method discussed above can handle this type of uncertainty. It is better to measure up two or more sections through a deformed rock using this method than dig out an object and measure its three-dimensional shape. The single object could have an unexpected initial shape (conglomerate clasts are seldom perfectly spherical or elliptical), but by combining numerous measurements in several sections we get a statistical variation that can solve or reduce this problem.

Three-dimensional strain is usually found by combining two-dimensional data from several differently oriented sections.

There are now computer programs that can be used to extract three-dimensional strain from sectional data. If the sections each contain two of the principal strain axes everything becomes easy, and only two are strictly needed (although three would still be good). Otherwise, strain data from at least three sections are required.

Summary

Strain markers in deformed rocks reveal how much the rock has been strained, and information about the nature of the deformation (e.g. flattening versus constriction, and the direction of strain axes) can be obtained. This is very useful when trying to understand what has happened to a deformed region, and when searching for a model for the deformation. The way that rocks accumulate strain depends on the stress field, boundary conditions, physical properties of the rock as well as external factors such as temperature, pressure and state of stress. In the next few chapters we will explore some of these relationships. Some key points to review and questions to address:

- Strain is only revealed by means of new deformation structures (cleavage, shear zones, fractures) or by means of preexisting markers that have changed shape during deformation.
- Strain analysis requires knowledge about the shape or geometry of strain markers before the deformation initiated.

- Objects that were circular or spherical before deformation are ideal, but non-spherical objects with a spread in initial orientations can also be used.
- Several techniques and computer codes exist that can help us extract strain from deformed rocks.
- Always look for objects, layers or linear features that can reveal strain in deformed rocks.

Review questions

1. What is meant by the term "strain marker"? Give examples.
2. What information can we obtain from linear or planar strain markers?
3. What is the effect of a viscosity (competence) difference between strain markers and the matrix?
4. How can we deal with pre-deformational fabrics, for example in conglomerate pebbles?
5. What is needed to find shear strain in a rock?
6. Give some serious concerns (pitfalls) regarding strain analysis.
7. How can we find three-dimensional strain from a deformed conglomerate?
8. Shear zones are expression of heterogeneous strain. How can we perform strain analyses in shear zones?
9. What are meant by passive and active strain markers?
10. What is meant by strain partitioning in this context?

E-MODULE

The e-learning module called *Strain in rocks* is recommended for this chapter.

FURTHER READING

Strain techniques in more detail

Lisle, R., 1985, *Geological Strain Analysis*. Amsterdam: Elsevier.

Ramsay, J. G. and Huber, M. I., 1983, *The Techniques of Modern Structural Geology. Vol. 1: Strain Analysis*. London: Academic Press.

Strain ellipsoid from sectional data

De Paor, D. G., 1990, Determination of the strain ellipsoid from sectional data. *Journal of Structural Geology* **12**: 131–137.

Erslev, E. A., 1988. Normalized center-to-center strain analysis of packed aggregates. *Journal of Structural Geology* **10**: 201–209.

Three-dimensional strain

Bhattacharyya, P. and Hudleston, P., 2001, Strain in ductile shear zones in the Caledonides of northern Sweden: a three-dimensional puzzle. *Journal of Structural Geology* **23**: 1549–1565.

Holst, T. B. and Fossen, H., 1987, Strain distribution in a fold in the West Norwegian Caledonides. *Journal of Structural Geology* **9**: 915–924.

Hossack, J., 1968, Pebble deformation and thrusting in the Bygdin area (Southern Norway). *Tectonophysics* **5**: 315–339.

Strine, M. and Wojtal, S. F. 2004, Evidence for non-plane strain flattening along the Moine thrust, Loch Srath nan Aisinnin, North-West Scotland. *Journal of Structural Geology* **26**, 1755–1772.

Strain associated with cleavage

Goldstein, A., Knight, J. and Kimball, K., 1999, Deformed graptolites, finite strain and volume loss during cleavage formation in rocks of the taconic slate belt, New York and Vermont, U.S.A. *Journal of Structural Geology* **20**: 1769–1782.

Chapter 4

Stress

In the previous chapter we looked at how strain can be observed and measured in deformed rocks. The closely related concept of stress is a much more abstract concept, as it can never be observed directly. We have to use observations of strain (preferentially very small strains) to say something about stress. In other words, the deformation structures that we can observe tell us something about the stress field that the rock experienced. The relation is not straightforward, and not even the most precise knowledge of the state of stress can predict the resulting deformation structures unless additional information, such as mechanical or physical properties of the rock, temperature, pressure and physical boundary conditions, is added. The most basic concepts of stress are presented here, before looking at stress in the lithosphere and the relations between stress, strain and physical properties in the following two chapters.

4.1 Definitions, magnitudes and units

The terms pressure and stress are often used interchangeably, but as structural geologists we need to use these terms more carefully. In geology, use of the term **pressure** (p) is generally limited to media with no or very low shear resistance (fluids), while **stress** (σ) is used when dealing with media with a minimum of shear resistance (rocks). To check if a medium has a **shear resistance**, put some of it between your hands and move them in parallel but opposite directions. The resistance you feel reflects the shear resistance. Water will have no shear resistance (repeat the above exercise in a swimming pool, with just water between your hands), while clay and loose sand will resist shearing.

In a buried porous sandstone layer we can talk about both pressure and stress: it has a certain **pore pressure** and it is in a certain state of **stress**. They are both related to the external forces that affect the rock volume.

There are two different types of forces. One type affects the entire volume of a rock, the outside as well as the inside, and is known as **body forces**. Body forces define three-dimensional fields. The most important type of body force in structural geology is gravity. Another example is magnetic forces.

The other type of force acts on surfaces only and is referred to as **surface forces**. Surface forces originate when one body pushes or pulls another body. The force that acts across the contact area between the two bodies is a surface force. Surface forces are of great importance during deformation of rocks. In a similar way we can talk about stress on a surface and state of stress at a point. Stress on a plane is a vector quantity, while stress at a point is a second-order tensor.

Stress on a surface is a vector (first-order tensor), while state of stress at a point is a second-order tensor.

Engineers and rock mechanics-oriented geologists may refer to stress on a surface as **traction** and reserve the term stress to mean the state of stress at a point in a body. Also, as geologists we need to be aware of these two different uses and avoid confusion between those two meanings of stress.

4.2 Stress on a surface

The **stress on a surface** such as a fracture or a grain–grain contact is a vector ($\boldsymbol{\sigma}$) that can be defined as the ratio between a force (F) and the area (A) across which the force acts. The stress that acts on a point on the surface can be formulated as

$$\bar{\sigma} = \lim_{\Delta A \to 0} (\Delta F / \Delta A) \tag{4.1}$$

This formulation indicates that the stress value may change from place to place on a surface. The SI unit for force (F) is the **newton** (N) = m kg/s^2: 1 N is the force at the surface of the Earth that is created by a mass of 102 g. Some geologists use the unit dyne, where 1 dyne (g cm/s^2) = 10^{-5} N. Differential stress or pressure is given in **megapascals** (MPa), where

1 Pa = 1N/m^2 = 1 kg/(m s^2)

1 MPa = 10 bar = 10.197 kp/cm^2 = 145 lb/in^2

100 MPa = 1 kbar

Compressive stresses are normally considered positive in the geologic literature, while tension is regarded as negative (see Box 4.1). In material science the definition is reversed, so that tension becomes positive. This is related to the fact that the tensile strength of a material is lower than its compressional strength. Tensile strength thus becomes more important during the evaluation of constructions such as bridges and buildings. The crust, on the other hand, is dominated by compression. Remember the difference between stress and strain: Both extension and contraction can result from a stress field where all stress axes are compressional.

Stresses in the lithosphere are almost everywhere compressional, even in rifts and other areas undergoing extension.

Normal stress and shear stress

A stress vector oriented perpendicular to a surface is called the **normal stress** on that surface, while a stress vector that acts parallel to a surface is referred to as the **shear stress**. In general, stress vectors act obliquely on planes. The stress vector can then be resolved into normal and shear stress components. It is emphasized that the concept of normal and shear stress has a meaning only when related to a specific surface.

While the decomposition of forces is quite simple, the decomposition of stress vectors is slightly more complicated. The complications relate to the fact that stress depends on the area across which it acts while forces do not. Therefore, simple vector addition does not work for stress vectors. As shown in Figure 4.1 we have the relationships

BOX 4.1 SIGN CONVENTIONS

Compressive normal forces are always positive in geology, while tensile ones are negative (in engineering geology the sign convention is opposite). Geologists like this convention because stresses tend to be compressive in the crust. Note, however, that shear stresses are subjected to at least two conventions. For the Mohr circle construction, we have the following convention: Shear stresses consistent with clockwise rotation are negative. For tensor notation the sign convention is different for the shear stresses (absolute values are identical): If the shear components on the negative (hidden) sides of the cube shown in the figures act in the positive directions of the coordinate axes, then the sign is positive and vice versa. This may be confusing, so always check if the sign of an output of a calculation makes sense.

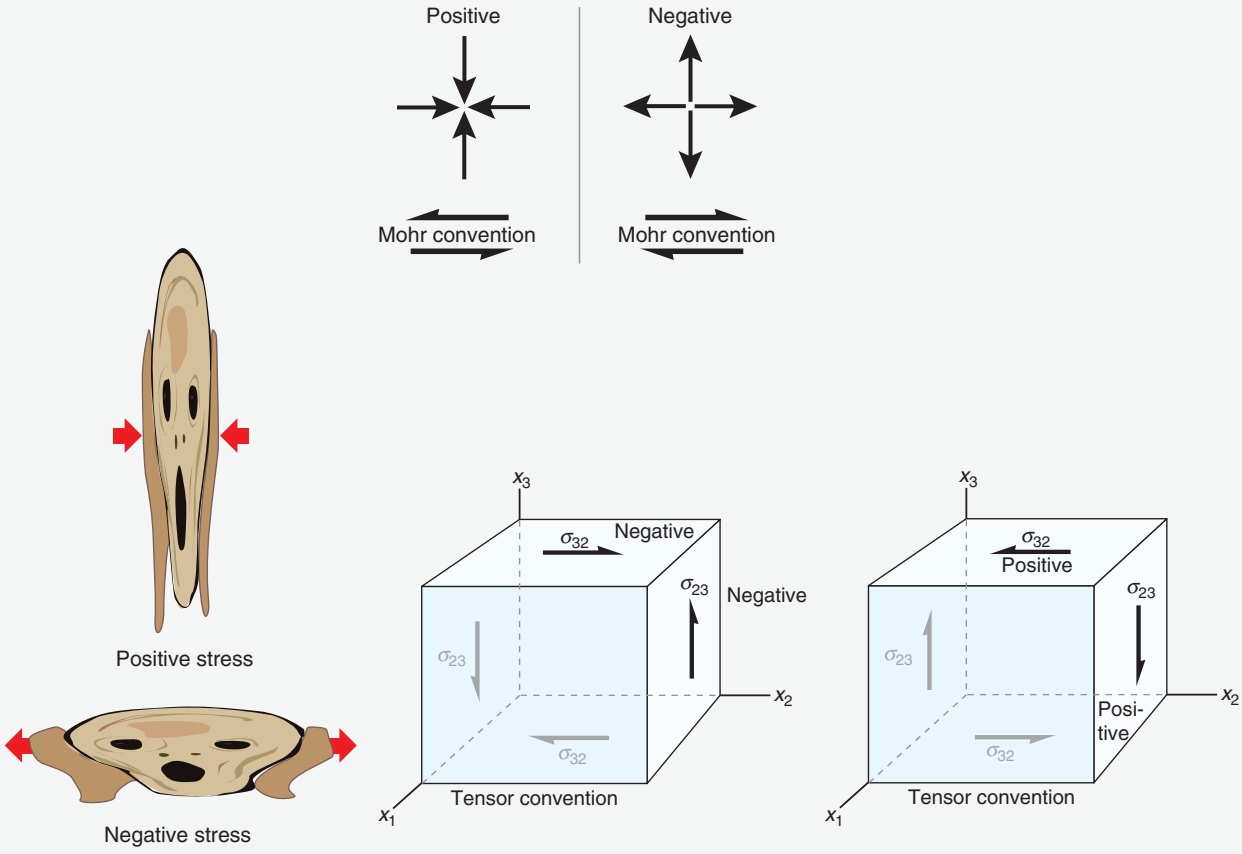

$$\sigma_n = \sigma \cos^2 \theta, \quad \sigma_s = (\sigma \sin 2\theta)/2 \tag{4.2}$$

where θ is the angle between the stress vector and the surface in question, or the dip of the surface if the stress vector is vertical. For comparison, decomposition of the force vector into normal and shear force vectors (Figure 4.1) gives

$$F_n = F \cos \theta, \quad F_s = F \sin \theta \tag{4.3}$$

These four functions are illustrated graphically in Figure 4.2.

4.3 Stress at a point

We leave the concept of stress on a single plane to consider the state of stress at a given point in a rock, for example a point within a mineral grain. We may imagine that there are planes in an infinite number of orientations through this point. Perpendicularly across each of the planes there are two oppositely directed and equally long traction or stress vectors. Different pairs of

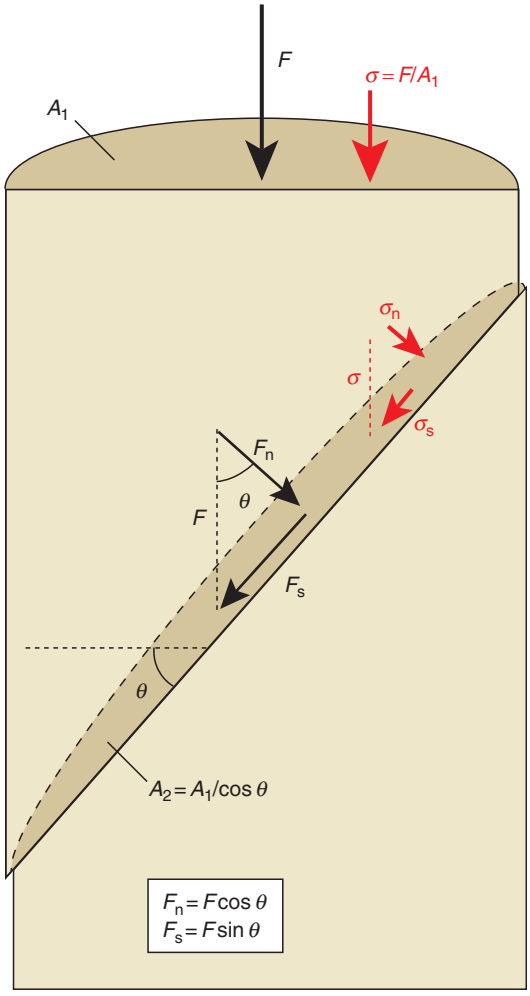

$\sigma_n = F_n/A_2 = F\cos\theta/A_2 = F\cos^2\theta/A_1 = \sigma\cos^2\theta$
$\sigma_s = F_s/A_2 = F\sin\theta/(A_1/\cos\theta)$
$= F\sin\theta\cos\theta/A_1 = \sigma\sin\theta\cos\theta = \sigma 1/2\sin 2\theta$

Figure 4.1 A force vector **F** acting on a surface can be decomposed into a normal (F_n) and a shear (F_s) component by simple vector addition. The stress vector σ cannot be decomposed in this way, because it depends on the area across which the force acts. Trigonometric expressions for the components σ_n and σ_s are derived.

stress vectors may be of different lengths, and when a representative family of such vectors is drawn about the point an ellipse emerges in two dimensions (Figure 4.3), and an ellipsoid is defined in three dimensions (Figure 4.4). An obvious requirement for expressing stress as an ellipse (ellipsoid) is that there is not a combination of positive and negative tractions. The ellipse is called the **stress ellipse**, and the ellipsoid is the **stress ellipsoid**.

The stress ellipsoid and its orientation tell us everything about the state of stress at a given point in a rock, or in a rock volume in which stress is homogeneous.

The stress ellipsoid has three axes, denoted σ_1, σ_2 and σ_3. The longest (σ_1) is the direction of maximum stress while the shortest is normal to the (imaginary) plane across which there is less traction than across any other plane through the point. The axes are called the **principal stresses** and are the poles to the **principal planes of stress**. These are the only planes where the shear stress is zero.

4.4 Stress components

The state of stress at a point is also defined by the stress components that act on each of the three orthogonal surfaces in an infinitesimal cube. Each of the surfaces has a normal stress vector (σ_n) and a shear stress vector (σ_s) along each of its two edges, as illustrated in Figure 4.5. In total, this gives three normal stress vectors and six shear stress vectors. If the cube is at rest and stable the forces that act in opposite directions are of equal

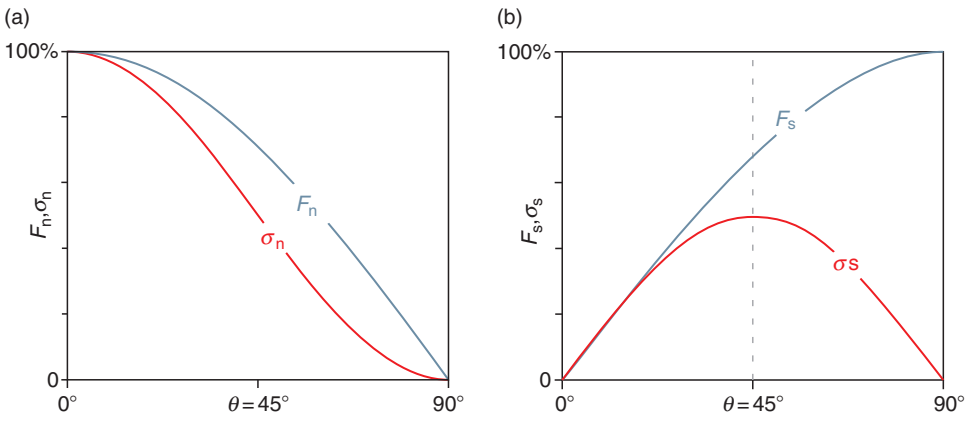

Figure 4.2 (a) The normal components of the force (F_n) and stress (σ_n) vectors acting on a surface, plotted as a function of the orientation of the vectors relative to the surface (θ, see Figure 4.1). Note the difference between the two. (b) The same for the shear components. Note that the shear stress is at its maximum at 45° to the surface while maximum shear force is obtained parallel to the surface.

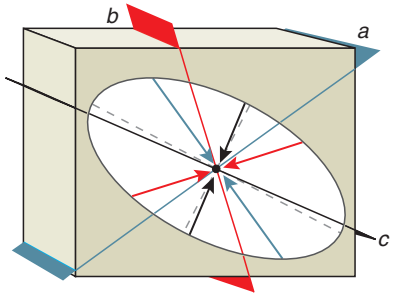

Figure 4.3 Two-dimensional illustration of stress at a point. Three planes (a, b and c) are oriented perpendicular to the section in question, and their normal stresses are represented in the form of vectors (corresponding colors). The stress vectors define an ellipse, whose ellipticity depends on the state of stress.

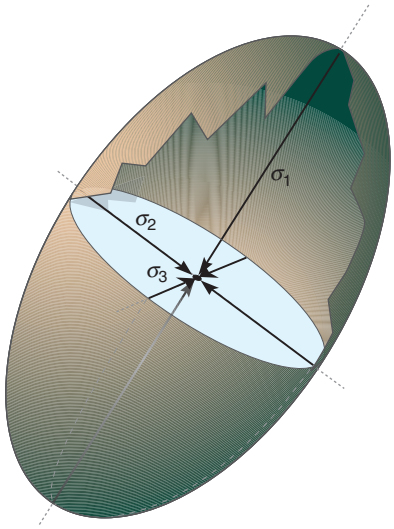

Figure 4.4 The stress ellipsoid.

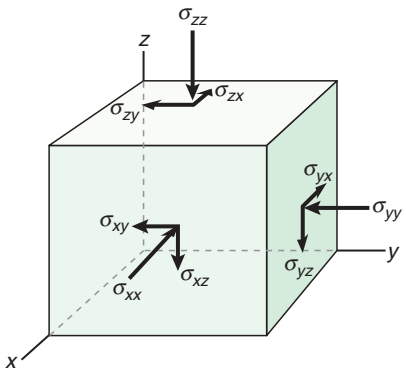

Figure 4.5 The stress components acting on the faces of a small cube. Positive stress components are shown – corresponding stress components exist on the negative and hidden faces of the cube. σ_{xx}, σ_{yy} and σ_{zz} are normal stresses, the others are shear stresses and are parallel to the edges of the cube.

magnitude and hence cancel each other out. This implies that

$$\sigma_{xy} = -\sigma_{yx}, \sigma_{yz} = -\sigma_{zy} \quad \text{and} \quad \sigma_{xz} = -\sigma_{zx} \tag{4.4}$$

and we are left with six independent stress components.

The cube can be oriented so that all of the shear stresses are zero, in which case the only non-zero components are the three normal stress vectors. In this situation these vectors represent the principal stress directions and are the **principal stresses** or **principal axes of the stress ellipsoid**. The three surfaces that define the cube are the **principal planes of stress** that divide the stress ellipsoid into three.

4.5 The stress tensor (matrix)

It is useful to put the nine components of stress into a matrix (second-order tensor) known as the **stress tensor** or **stress matrix** (Box 4.2):

$$\begin{bmatrix} \sigma_{11} & \sigma_{12} & \sigma_{13} \\ \sigma_{21} & \sigma_{22} & \sigma_{23} \\ \sigma_{31} & \sigma_{32} & \sigma_{33} \end{bmatrix} \tag{4.5}$$

The normal stresses σ_{11}, σ_{22} and σ_{33} occupy the diagonal while the off-diagonal terms represent the shear stresses. We have that $|\sigma_{11}| = |\sigma_{xx}|$, $|\sigma_{12}| = |\sigma_{xy}|$, $|\sigma_{13}| = |\sigma_{xz}|$ etc., but they may have different signs because of different conventions used for tensor components. In the stable situation where forces are balanced we have $\sigma_{12} = \sigma_{21}$, $\sigma_{31} = \sigma_{13}$ and $\sigma_{23} = \sigma_{32}$, and the stress tensor can be written as

$$\begin{bmatrix} \sigma_{11} & \sigma_{12} & \sigma_{13} \\ \sigma_{12} & \sigma_{22} & \sigma_{23} \\ \sigma_{13} & \sigma_{23} & \sigma_{33} \end{bmatrix} \tag{4.6}$$

This is now a symmetric matrix (a matrix where changing columns to rows does not change anything), but the values will change with choice of coordinate system or how we orient our little cube from Figure 4.5. If we are lucky or orient our little cube (coordinate system) with care, we have the principal stresses along the edges of the box, in which case the matrix becomes

$$\begin{bmatrix} \sigma_{11} & 0 & 0 \\ 0 & \sigma_{22} & 0 \\ 0 & 0 & \sigma_{33} \end{bmatrix} = \begin{bmatrix} \sigma_1 & 0 & 0 \\ 0 & \sigma_2 & 0 \\ 0 & 0 & \sigma_3 \end{bmatrix} \tag{4.7}$$

BOX 4.2 VECTORS, MATRICES AND TENSORS

A **scalar** is a real number, reflecting temperature, mass, density, speed or any other physical magnitude that has no direction. A **vector** has both magnitude (length) and direction, such as force, traction (stress vector) or velocity. A **matrix** is a two-dimensional array of numbers (3×3 or 2×2 in most geologic applications, meaning that they have 9 or 4 components). Matrices can represent the state of stress or strain in a medium.

The term **tensor** is, in rock mechanics, applied to vectors and particularly matrices. We can consider scalars as tensors of order zero, vectors as first-order tensors and matrices as second-order tensors. Hence, for our purposes, the terms matrix and second-order tensor are identical. However, there are other cases where numbers are arranged in matrices that are not tensors, such as in the field of economics.

An important tensor property is that they are independent of any chosen frame of reference, meaning that the "quantity" represented by the tensor (such as the state of stress or strain at any point in a volume) remains the same regardless of the choice of coordinate system. Hence a vector will be of the same length and of the same magnitude in two different coordinate systems, even though it is represented by different numbers.

A tensor may be defined at a single point or collection of isolated points, or it may be defined over a continuum of points and thus form a field (scalar field, vector field etc.). In the latter case, the elements of the tensor are functions of position and the tensor forms what is called a **tensor field**. This simply means that the tensor is defined at every point within a region of space (or space-time), rather than just at a point or collection of isolated points.

Being the only non-zero entries, the principal stresses can now readily be extracted from the matrix. The three principal stress vectors are the three columns $(\sigma_{11}, 0, 0)$, $(0, \sigma_{22}, 0)$ and $(0, 0, \sigma_{33})$. In other words:

The stress tensor is composed of the three principal stress vectors.

In other cases we have to find the eigenvectors and eigenvalues of the matrix, which are the principal stress vectors and principal stresses, respectively. This is easily done by means of readily available computer programs. It is important to know that even if the elements of the stress tensor vary for different choices of coordinate system, the eigenvalues and eigenvectors of the tensor remain the same – they are **invariant**.

Stress tensors represent the same state of stress (same shape and orientation of the stress ellipsoid) regardless of our choice of coordinate system.

Since the state of stress will vary from point to point in the lithosphere, so will the stress ellipsoid and the stress tensor. This leads us into the concept of tensor fields. Hence, a complete description of the state of stress in a volume of rock is given by a tensor field.

4.6 Deviatoric stress and mean stress

Any stress tensor can be split into two symmetric matrices, where the first part represents the mean stress and the second is called the deviatoric stress. This is not just another boring mathematical exercise, but a very useful decomposition that allows us to distinguish two very important components of stress, which we also can denote as the isotropic and anisotropic components. The decomposition is

$$\begin{bmatrix} \sigma_{11} & \sigma_{12} & \sigma_{13} \\ \sigma_{12} & \sigma_{22} & \sigma_{23} \\ \sigma_{13} & \sigma_{23} & \sigma_{33} \end{bmatrix} =$$

total stress tensor

$$\begin{bmatrix} \sigma_m & 0 & 0 \\ 0 & \sigma_m & 0 \\ 0 & 0 & \sigma_m \end{bmatrix} + \begin{bmatrix} \sigma_{11} - \sigma_m & \sigma_{12} & \sigma_{13} \\ \sigma_{12} & \sigma_{22} - \sigma_m & \sigma_{23} \\ \sigma_{13} & \sigma_{23} & \sigma_{33} - \sigma_m \end{bmatrix} \quad (4.8)$$

isotropic component + anisotropic component

(mean stress tensor) (deviatoric stress tensor)

The σ_m in this decomposition is called the **mean stress** and is simply the arithmetic mean of the three principal stresses. Thus, $\sigma_m = (\sigma_1 + \sigma_2 + \sigma_3)/3$ gives an average measure of stress.

If there is no deviatoric stress so that the anisotropic component is zero (in which case the deviatoric stress

tensor becomes the identity matrix), then the stress or traction is identical on any plane through the point, regardless of the orientation of the plane. Furthermore, the stress ellipsoid is a perfect sphere, $\sigma_1 = \sigma_2 = \sigma_3$, there is no shear stress "anywhere" and there is no off-diagonal stress in the total stress tensor. Such a condition is commonly referred to as **hydrostatic stress** or **hydrostatic pressure**, and represents an isotropic state of stress. In the lithosphere, the mean stress is closely related to **lithostatic pressure**, which is controlled by burial depth and the density of the overlying rock column. We will return to this discussion in Chapter 5.

Deviatoric stress is the difference between the mean stress and the total stress: $\sigma_{dev} = \sigma_{tot} - \sigma_m$, or $\sigma_{tot} = \sigma_m + \sigma_{dev}$. The deviatoric stress tensor represents the **anisotropic** component of the total stress and the deviatoric stress is generally considerably smaller than the isotropic mean stress, but of greater significance when it comes to the formation of geologic structures in most settings. While isotropic stress results in dilation (inflation or deflation), only the anisotropic component results in strain. The relationship between its principal stresses influences what type of structures are formed.

4.7 Mohr circle and diagram

Before looking at stress states in the crust in the next chapter we will consider a practical graphical way of presenting and dealing with stress that is based on a diagram referred to as the **Mohr diagram**. In the nineteenth century, the German engineer Otto Mohr found a particularly useful way of dealing with stress. He constructed the diagram shown in Figure 4.6, now known as the Mohr diagram, where the horizontal and vertical axes represent the normal (σ_n) and shear (σ_s) stresses that act on a plane through a point. The value of the maximum and minimum principal stresses (σ_1 and σ_3, also denoted σ_1 and σ_2 for two dimensional cases) are plotted on the horizontal axis, and the distance between σ_1 and σ_3 defines the diameter of a circle centered at $((\sigma_1 + \sigma_3)/2, 0)$. This circle is called the **Mohr circle**,

The Mohr circle describes the normal and shear stress acting on planes of all possible orientations through a point in the rock.

More specifically, for any given point on the circle a normal stress and a shear stress value can be read off the axes of the diagram. These are the normal and shear stresses acting on the plane represented by that point.

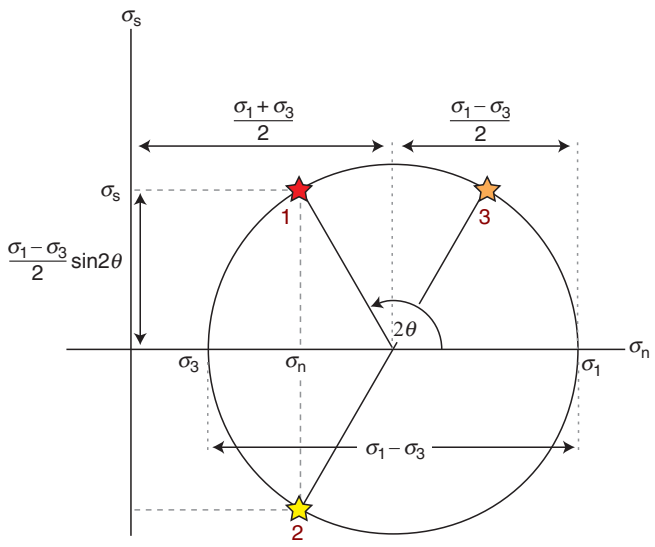

Figure 4.6 The Mohr circle. θ is the angle between the largest stress and a given plane. Note the use of double angles.

How do we know the orientation of the plane represented by a given point on the Mohr circle? In two dimensions and with σ_1 and σ_3 plotted on the horizontal axis, the planes represented on the circle contain σ_2. If θ is the angle between the normal to the plane and σ_1, as shown in Figure 4.1, then the angle between the radius to the point on the circle and the horizontal axis is 2θ.

The difference between the maximum and minimum principal stresses $(\sigma_1 - \sigma_3)$ is the diameter of the circle. This difference is called **differential stress** and is important in fracture mechanics. In general, great differential stress promotes rock fracturing.

Angle θ and other angles are measured in the same sense on the Mohr diagram as in physical space, but the angles are doubled in Mohr space. Two points representing perpendicular planes are thus separated by 180° in the Mohr diagram. This is why the two principal stresses both plot on the horizontal axis. Another reason is that principal planes have no shear stress, which is fulfilled only along the horizontal axis. This illustrates how the Mohr space is different from physical space, and it is important to understand the connection between the two. Let us explore some more. The doubling of angles in Mohr space means that any plane, such as that indicated by point 1 in Figure 4.6, has a complementary plane (point 3 in the same figure) with identical shear stress and different normal stress. Point 1 in Figure 4.6 also has another complementary plane (point 2) of identical normal stress and a shear stress that differs by sign only. Maximum shear stress occurs for planes where $2\theta = \pm 90°$, or where

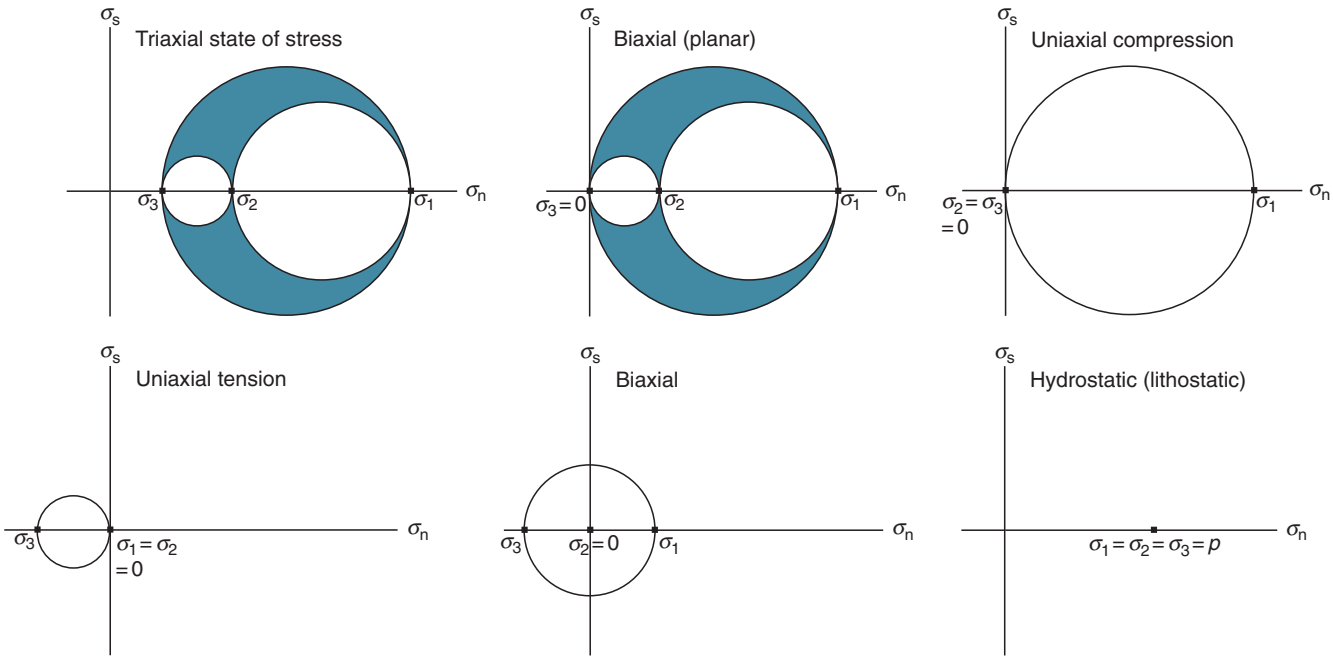

Figure 4.7 Characteristic states of stress are illustrated in the Mohr diagram for 3-D stress. The 3-D state of stress is illustrated by means of three circles connecting the three principal stresses. The largest circle contains σ_1 and σ_3. The three circles reduce to two or one for special states of stress.

the angle to σ_1 is 45° (Figure 4.2b). The Mohr diagram used in geologic applications is generally constructed so that compression is positive and tension is negative, while the opposite convention is common in the engineering literature. In most cases all principal stresses are positive in the lithosphere, but not always. For tensile stress, the Mohr circle is moved to the left of the origin into the tensile field. If all principal stresses are tensile (a most unusual case in geology), then the entire circle is located to the left of the origin.

The Mohr diagram can also be used in three dimensions, where all three principal stresses are plotted along the horizontal axis. In this way we can represent three Mohr circles in a single Mohr diagram. A number of important states of stress can be represented in the three-dimensional Mohr diagram, as shown in Figure 4.7.

Summary

In this chapter we have looked at the fundamentals of stress. It is important to understand the difference between forces, stress on a plane (both vector quantities) and stress at a point (second-order tensor). Stress at a point and the stress ellipsoid are in many ways similar to strain and the strain ellipsoid. The principal stresses correspond in a similar way to the principal strains. But despite the similarities it is important to understand that stress is something that may or may not lead to strain, and if it does, it cannot be expected to produce a strain ellipsoid of similar shape and orientation. At this point we should be able to understand and answer the following statements and questions:

- The term stress can be used for stress on a plane or stress at a point (local state of stress).
- Stress acting on a plane (surface) is a vector determined by the applied force and the area that it acts on. An oblique vector decomposes into a normal and a shear stress component.
- Stress at a point (state of stress) describes the total state of stress at that point and is a second-order tensor (3×3 matrix in three dimensions).

- A complete description of the state of stress in a body is given by the stress tensor field, which describes how the three-dimensional state of stress varies in the body (rock).
- Stress cannot be decomposed in the same way as force, because stress also depends on area.

Review questions

1. When is it appropriate to use the term pressure in geology?
2. How can we graphically visualize the state of stress in two and three dimensions?
3. Where could we expect to find tensile stress in the crust?
4. How will the shape and orientation of the stress ellipsoid change if we define a different coordinate system?
5. Will the stress tensor (matrix) look different if we choose a different coordinate system?
6. A diagonal tensor has numbers on the diagonal running from the upper left to the lower right corner, with all other entries being zero. What does a diagonal stress tensor imply?
7. If the diagonal entries in a diagonal stress matrix are equal, what does the stress ellipsoid look like, and what do we call this state of stress?
8. If we apply a stress vector at various angles to a given surface, at what angle is the shear stress at its maximum? How does that compare to applying a force (also a vector) to the same surface, i.e. at what orientation would the shear component of the force be maximized?

E-MODULE

The first part of the e-learning module called *Stress* is recommended for this chapter.

FURTHER READING

Means, W. D., 1976, *Stress and Strain: Basic Concepts of Continuum Mechanics for Geologists*. New York: Springer-Verlag.

Oertel, G. F., 1996, *Stress and Deformation: A Handbook on Tensors in Geology*. Oxford: Oxford University Press.

Price, N. J. and Cosgrove, J. W., 1990, *Analysis of Geological Structures*. Cambridge: Cambridge University Press.

Turcotte, D. L. and Schubert, G., 2002, *Geodynamics*. Cambridge: Cambridge University Press.

Twiss, R. J. and Moores, E. M., 2007, *Structural Geology*, 2nd edition. New York: H.W. Freeman and Company.

Chapter 5

Stress in the lithosphere

With a basic understanding of the nature of stress, we will now look at how we get information about stress in the crust and how to understand it. A large number of stress measurements have been performed globally over the last few decades. These measurements indicate that the stress conditions in the crust are complex, partly because of geologic heterogeneities (faults, fracture zones and compositional contrasts), and partly because many areas have been exposed to multiple phases of deformation, each associated with different stress fields. The latter is of importance because the crust has the ability to "freeze in" a state of stress and preserve remnants of it over geologic time. Knowledge of the local and regional stress fields has a number of practical applications, including evaluation of tunneling operations, drilling and stimulation of petroleum and water wells. Besides, knowledge of the present and past states of stress provides important information about tectonic processes, then and now.

5.1 Importance of stress measurements

Knowledge of stress is important for many purposes, for instance during drilling and blasting in highly stressed rock during underground construction, tunneling, quarrying and mining operations. In these cases, high stresses may cause pieces of rock to literally shoot off the walls or the roof, obviously a serious safety issue. As we will see, there is always a stress concentration associated with underground openings. Such concentrations may result in roof closure, sidewall movement and ground subsidence. Unlined pressure tunnels and shafts used in hydroelectric and water supply systems may leak (by hydrofracture) if the internal water pressure exceeds the minimum *in situ* principal stress in the surrounding rock mass. High rock stresses counteract the water pressure and help keep fractures closed. Hence, in this case, high stresses are advantageous.

At greater depths, in oil fields for example, the *in situ* stress field helps steer the drill head in the desired direction during well drilling, prevents sand production and maintains borehole stability. Stresses around wells must also be monitored during production because pore pressure reduction may reduce horizontal stresses by a factor large enough to cause formations to collapse and the seafloor to subside. Hydrofracturing of reservoirs in order to increase permeability around producing wells also requires information about the stress field.

At any level in the crust, stresses are related to the formation and orientation of geologic structures, i.e. the accumulation of strain. Any deformation can be related to some stress field that deviates from the "normal" stress situation. In the deeper portions of the crust, stress cannot be measured or estimated, except for the information obtained from focal mechanisms. There are, however, ways to estimate paleostress in rocks that have been exhumed and exposed at the surface.

5.2 Stress measurements

A challenging aspect of stress is that it cannot be observed directly. Only the effect of stress in the form of elastic or permanent strain, if any, can be observed. Obviously, different media (rock types) react differently to stress (Chapter 6), and if the medium is anisotropic the relations tend to be complex. However, because the strains typically involved in measurements of current stress fields are very small, the connection between the two is close, and useful estimates of stress can be obtained.

A series of different methods are applied, depending on where stress data are to be collected. Some are applied in boreholes (borehole breakouts and hydraulic fracturing), some are more commonly used at the surface or in tunnels (overcoring), and one is related to the first motion generated by stress release during the rupture of faults (focal mechanisms). In addition, neotectonic or recent geologic structures affecting the surface can give useful information about the present state of stress in an area.

Borehole breakouts are zones of failure of the wall of a well that give the borehole an irregular and typically elongated shape, as illustrated in Figure 5.1a. It is assumed that the spalling of fragments from the wellbore occurs preferentially parallel to the minimum horizontal stress (σ_h) and orthogonal to the maximum horizontal stress (σ_H).

The ellipticity of the hole indicates the local orientation of the horizontal stress axes in the wellbore.

Information about the shape of the hole is obtained by **dipmeter tools** or **well imaging tools**. These are tools with arms that are pressed against the borehole wall as the tool is moved along the wellbore. The tool thus records the geometry of the hole, and the orientation of the tool is also recorded. Hence, in addition to the measurements of the orientation of planar structures intersecting the wellbore (the primary purpose of a dipmeter tool), a record of the shape of the borehole is produced, yielding information about the horizontal stresses.

Borehole breakout data are primarily collected in wells drilled for petroleum exploration and production. The shapes of holes drilled for road and tunnel blasting operations have also been used for stress analyses, although this method is not regarded as very reliable. Even in tubular tunnels, preferred spalling of fragments sometimes indicates the orientation of the stress field (Figure 5.2). The principle is the same for all cases: the borehole takes on an "elliptical" shape where the elongated direction is assumed to parallel σ_h.

Overcoring (Figure 5.1b) is a strain relaxation method where, in principle, a sample (core or block) is extracted from a rock unit, measured, and then released so that it can freely expand. The change in shape that occurs reflects the compressive stresses that have been released, but also depends on the rock's elasticity. In general, maximum expansion occurs in the direction of σ_h.

Overcoring is done to map the state of stress at or near the surface. Less commonly, it is done by bringing a sample from a deep bore hole in a confined condition to the surface, and measuring the three-dimensional expansion as the sample is unconfined. Surface or

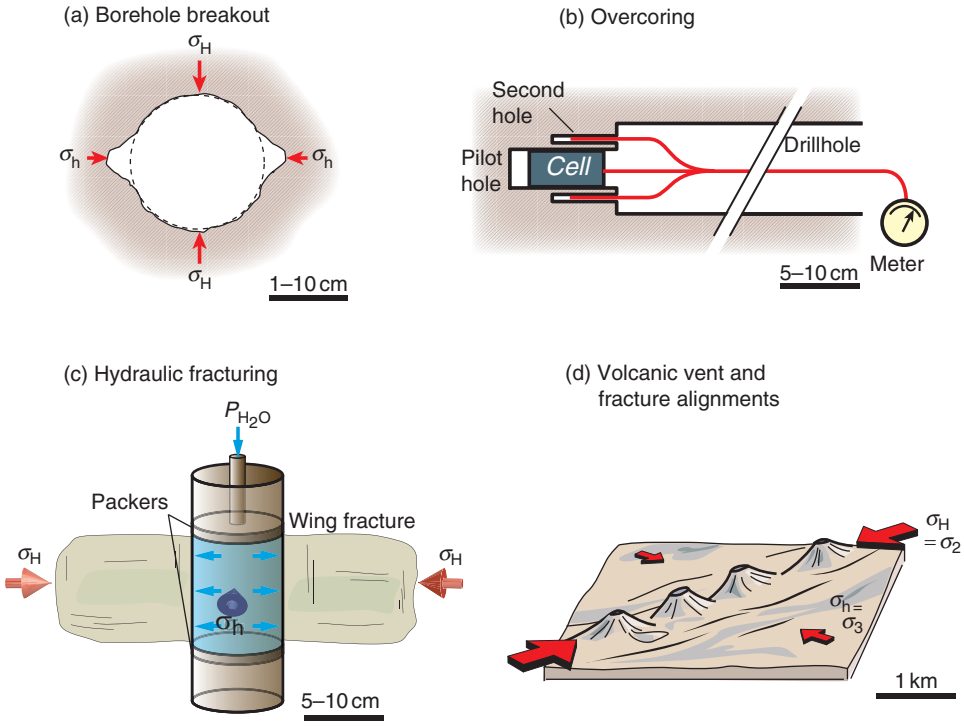

Figure 5.1 Examples of stress determination. (a) Borehole breakouts as illustrated by a horizontal section through a vertical wellbore. Maximum and minimum horizontal stresses σ_H and σ_h are generally equal to or close to two of the principal stresses. (b) The overcoring method. A pilot hole is drilled at the end of the main hole into which stress meters or a strain cell is placed. A wider core is cut outside the cell, and strain is calculated by comparing measurements before and after the drilling. Strain is related to stress by means of elastic theory, and the state of stress is found. (c) Hydraulic fracturing. (d) Recent surface structures related to the current stress field.

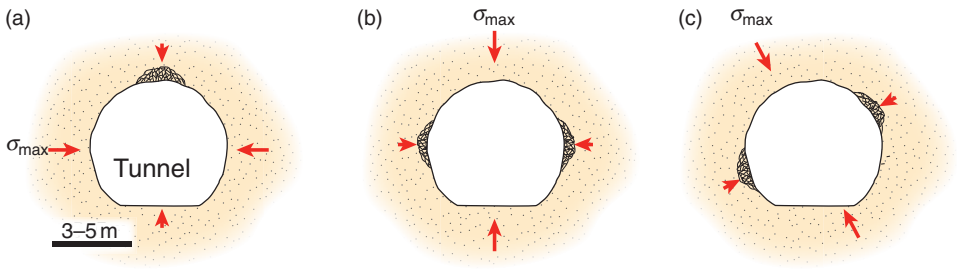

Figure 5.2 Spalling of rock fragments in certain parts of a tunnel gives information about the orientation of the principal stresses and the differential stress.

near-surface overcoring is done by drilling a hole (typically 76 mm in diameter) into the rock and adding a small (36 mm) pilot hole at the end of the main hole. Stressmeters or a strain cell are placed in the pilot hole before it is overcored using a larger coring bit, which relieves the stress in the overcored hollow core. This stress release causes elastic deformation that is recorded by the stressmeters or strain cell. The fact that the unit of microstrain ($\mu e = 10^{-6} e$) is used indicates that the strains involved are minute. At least six stressmeters are required in the hole to completely record the three-dimensional stress field. Calculation of the stress tensor is based on elasticity theory. Elasticity is about how a rock responds to stress below the limit where strain becomes permanent, and elasticity theory is applied to calculate the orientations and magnitudes of the principal stresses. To do this, the elastic properties known as Young's modulus (E) and Poisson's ratio (ν) are measured in the laboratory.

In short, Young's modulus describes the relationship between stress and strain ($E = \sigma/e$) while Poisson's ratio characterizes how much an object that is shortening extends perpendicular to the direction of shortening (or how much it shortens perpendicular to the direction of extension if we extend the object). We will deal with these elastic properties and elasticity more closely in the next chapter.

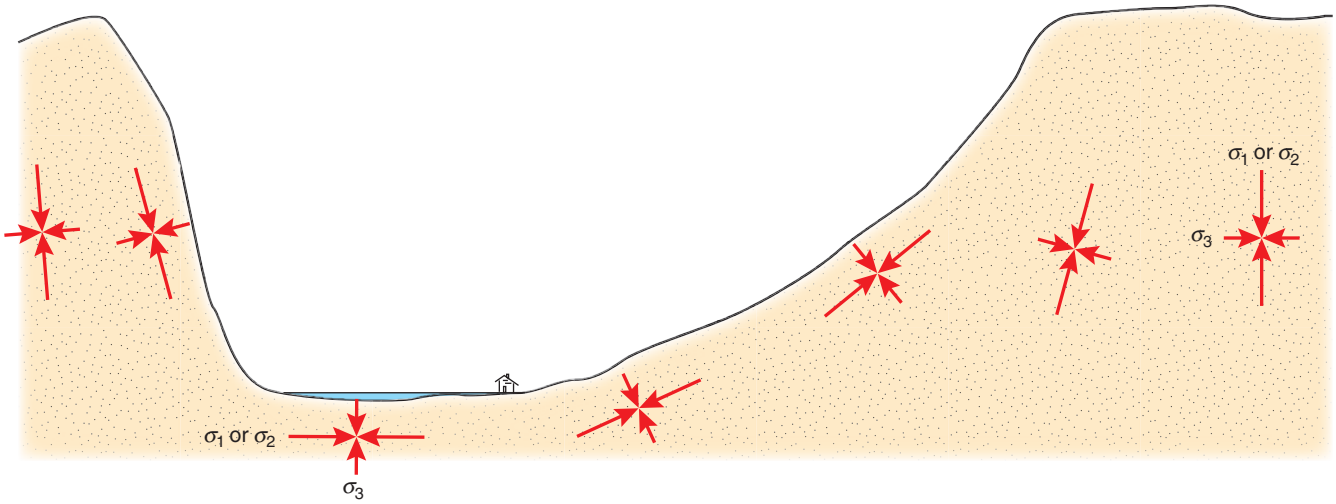

Figure 5.3 State of stress around a valley or fjord. One of the principal stresses will always be perpendicular to the free surface of the Earth, because the shear stress is zero along any free surface. Thus, a non-planar surface causes the orientation of the stresses to rotate as shown on the figure. Note that these deviations occur near the surface only, but must be considered when stress is measured at or near the surface or other free surfaces (tunnel walls, etc.).

At the surface, topography creates local stresses that must be accounted for. Mountains and valleys create stress effects near the surface that influence regional stress patterns, as shown in Figure 5.3. In tunnels and rock chambers, the effect of free space in the rock on the stress field must be taken into consideration, or holes must be drilled far enough away from the tunnel that this effect is negligible. Even the perturbation of the stress field by the drill hole itself must be corrected for, although such a correction is easily done using modern equipment. Weak faults and fracture zones, weathering, and contacts between rocks of contrasting physical properties are examples of geologic structures that are likely to distort the stress field locally. The effect is shown schematically in Figure 5.4: σ_3 will try to orient itself parallel to the weak structure.

Hydraulic fracturing (hydrofracturing, "hydrofracking"; Figure 5.1c) means increasing the fluid pressure until the rock fractures. The technique is frequently applied to petroleum reservoirs to increase the near-well permeability. In this case the interval of the wellbore that is to be fractured is sealed off and pressure is pumped up until tensile fractures form. The pressure that is just enough to keep the fracture(s) open equals σ_h in the formation. Knowing the tensile strength of the rock, it is possible to calculate σ_H. Furthermore, the vertical stress is assumed to be a principal stress and equal to ρgz. Petroleum engineers use knowledge of the stress field to plan hydrofracturing of reservoir units to take advantage of the predicted direction of fracture propagation.

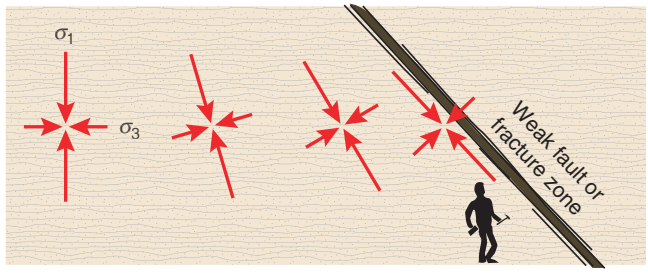

Figure 5.4 Deflection of the stress field near a fault or fracture zone. The structure is weaker than the surrounding rock and can support lower shear stresses than its surroundings. The situation is similar to that where an open surface exists, e.g. the free surface of the Earth (see Figure 5.3).

Earthquake focal mechanisms (Box 9.1) give information about the Earth's immediate response to stress release along new or preexisting fractures. They provide information about the stress regime (Section 5.6) as well as the relative magnitude of the principal stresses. The main problem with this method is that the *P*- and *T*-axes do not necessarily parallel principal stress axes. Combining focal mechanisms of faults of different orientation helps reduce this problem.

Geologic structures formed by active tectonic processes also give reliable indications of certain aspects of the present day stress field. The orientation and pattern of recent fault scarps, fold traces, tensile fractures (Figure 5.5) and volcanic vent alignments (Figure 5.1d) all indicate the orientation of the principal stresses.

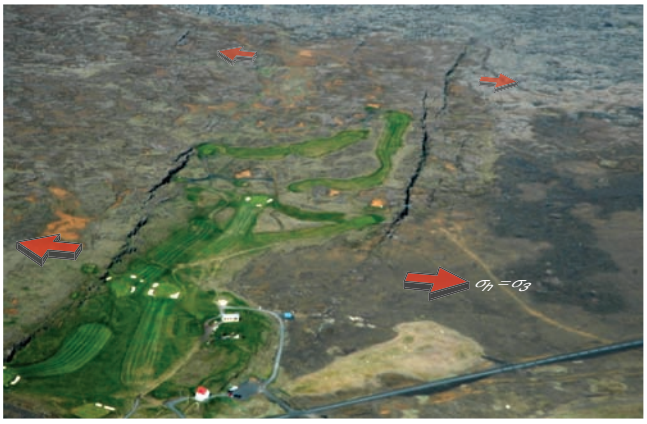

Figure 5.5 Active vertical fractures on the surface of Holocene lava flows in southeast Iceland indicate the orientation of σ_h. Because the fractures occur at the surface, $\sigma_h = \sigma_3$, and σ_1 must be vertical. A historic basalt flow in the background is less influenced by the fractures.

We have now seen how stress can be measured *in situ* from rocks in the upper crust, i.e. without taking samples away to a laboratory for stress determinations. The deepest reliable stress measurement reported so far was made at a depth of about 9 km in the German Continental Deep Drilling Project (hydrofracturing). Information about the stress conditions deeper in the crust can only be inferred from focal mechanisms, theoretical considerations, and through the use of paleostress methods, which will be treated in Chapter 9.

Our information about the current stress field below a few (4–5) kilometers depth is indirect, inaccurate and incomplete.

5.3 Reference states of stress

Various theoretical models exist that describe how the state of stress changes through the crust, and three of them are presented below. Such models are referred to as reference models or **reference states of stress**. They assume a planet with only one lithospheric shell, without the complications of plate tectonics. In fact, no tectonic forces are included in the reference states of stress. Thus, to find tectonic stress we need to look at deviations from the reference models.

Reference states of stress define idealized states of stress in the crust as if the crust were a static planet with no tectonic processes.

Lithostatic/hydrostatic reference state

The **lithostatic reference state** is the simplest general stress model for the interior of the Earth. It is based on an idealized situation where the rock has no shear strength ($\sigma_s = 0$). A rock volume with this condition cannot support differential stress over geologic time ($\sigma_1 - \sigma_3 = 0$), which means that its state of stress is described as a point on the horizontal axis of the Mohr diagram (Figure 4.7, hydrostatic/lithostatic). This means that stress is independent of direction:

$$\sigma_1 = \sigma_2 = \sigma_3 = \rho g z \qquad (5.1)$$

The lithostatic reference state is an isotropic state of stress, where the vertical and horizontal stresses are equal.

The stress is, according to this model, completely controlled by the height and density of the overlying rock column. For continental rocks, which have an average density of ~2.7 g/cm^3, this means a vertical stress gradient of 26.5 MPa/km, which fits the data shown in Figure 5.6 (blue symbols) quite well. Porous rocks have lower density (2.1–2.5 g/cm^3) depending on porosity and mineralogy, and the gradient becomes somewhat lower in sedimentary basins.

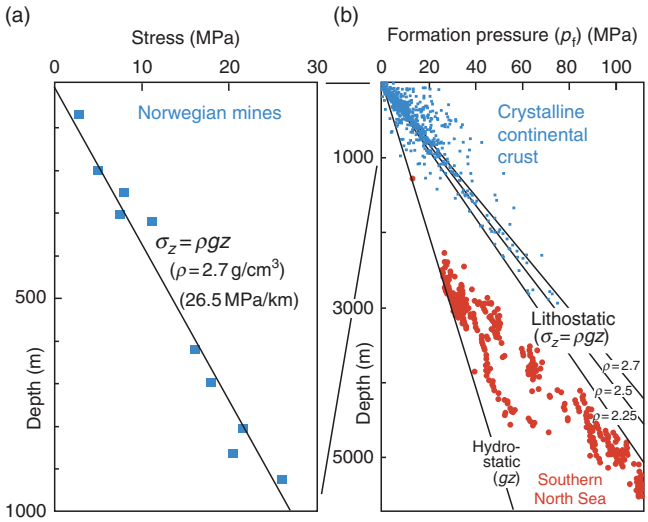

Figure 5.6 (a) Vertical stress measurements compared to the theoretical curve for lithostatic stress ($\rho g z$) in Norwegian mines down to 1 km depth (crystalline rocks). (b) Pressure data from crystalline rocks worldwide and North Sea sedimentary rocks. The North Sea data plot between the gradients for hydrostatic and lithostatic pressure. Individual linear trends are seen, indicating overpressured formations and multiple pressure regimes. Note that these pressure data are for formation pressures, meaning fluid pressures. Data in (a) from Myrvang (2001), in (b) from Darby *et al.* (1996) (North Sea) and many other sources.

BOX 5.1 PRESSURE AND METAMORPHISM

Metamorphic petrologists tend to talk about pressure rather than stress (commonly in terms of kilobars, where 1 kbar = 100 MPa), while structural geologists reserve the term pressure for fluids. Any rock in the lithosphere has a shear strength even over geologic time: rocks can sustain anisotropic stress as long as the melting point is not reached. Metamorphic petrologists use the term pressure to discuss phase transitions and stability of metamorphic minerals, such as the Al_2SiO_5 system or the transformation of graphite into diamond. This use closely matches our lithostatic reference state. They can do this because they operate at relatively large depths, where anisotropic (tectonic) stresses do not make a big difference when, for example, andalusite changes into kyanite or graphite becomes diamond. Anisotropic stresses do however determine the tectonic regime and the structures formed.

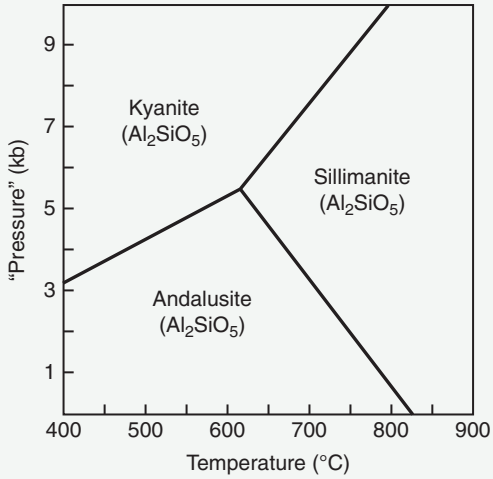

Field of stability for the Al_2SiO_5-system.

Some similar numbers: Common stress gradient, 27 MPa/km; common temperature gradient, 27 °C/km; common rock density, 2.7 g/cm^3.

No real, solid rock experiences a perfectly lithostatic reference state. Only magma and other fluids do, in which case the term **hydrostatic pressure** is more appropriate (also see Box 5.1). This is also relevant in sedimentary basins where the formation fluid is generally water. The density contrast between water and rock forces us to operate with two different stress situations. One is the hydrostatic pressure, which is $P_{H_2O} = \rho gz = gz$ (using a water density of 1 g/cm^3). The other is the lithostatic stress, which is larger by a factor of around 2.7 (using 2.7 g/cm^3 for rock density). If the rock contains oil and/or gas, the densities of hydrocarbons must also be considered.

In a rock column where the rock is porous, the lithostatic stress is distributed over the grain contact area, and this stress is called the **effective stress** $\bar{\sigma}$. In addition we have the pore pressure of the water p_f (or perhaps hydrocarbons) in the pore volume. Hence, we have to operate with two different stress systems in porous media, and the sum of the two is the vertical stress at any given depth:

$$\sigma_v = \bar{\sigma} + p_f \tag{5.2}$$

Pore fluid pressure reduces the effective stress, which is the stress at grain contacts in porous rocks.

If the fluid pressure p_f, often referred to as the formation pressure, equals the hydrostatic pressure ρgz, then the fluid pressure is normal or hydrostatic. In this case pores are interconnected all the way to the surface, and the pore fluid forms a continuous column. This is not always the situation, and deviations from hydrostatic pressure are common. The pore fluid pressure p_f is routinely measured in oil fields and exploration wells, and many reservoir formations are found to be overpressured.

Overpressure forms when formation fluid in porous formations is trapped between non-permeable layers. Sandstones sandwiched between shale layers typically become overpressured during burial because the pore fluid is trapped at the same time as the sandstone carries an increasingly heavy load. The deeper the burial, the larger the deviation between the actual pore pressure and the (theoretical) hydrostatic pressure. This explains the deviations from hydrostatic pressure shown by the red data points in Figure 5.6b (North Sea data). This figure shows evidence of several pressure regimes in southern North Sea reservoirs, each with their own trends between the hydrostatic and lithostatic gradients.

Deviation from hydrostatic pore pressure is important. A high deviation (overpressure) may indicate that the sandstone is poorly compacted, which could mean sand production (sand flowing into the well together with oil during production) and unstable well conditions. This may occur because, during overpressure, p_f in Equation 5.2 increases, and the effective stress across the grain contact points decreases. Where the pore

pressure approaches lithostatic pressure, very loose sand (stone) may be expected even at several kilometers depth.

Anomalously high pore pressure can have consequences for deformation. Overpressured layers are weak and may act as detachments during deformation. Thrust faults in foreland settings or accretionary prisms preferentially form in overpressured formations, and extensional detachments are known to develop along such zones. On a smaller scale, grain reorganization rather than cataclasis is promoted by overpressure during deformation of sandstones and other porous rocks.

Artificial overpressure in a formation can be created by increasing the mud weight (hydrostatic pressure) in a chosen interval of a wellbore. The rock responds by fracturing at some critical pressure level, and the operation is known as hydraulic fracturing (Figure 5.1c).

Uniaxial-strain reference state

The lithostatic state of stress is easy and convenient, but not necessarily realistic. A somewhat related model is called the **uniaxial-strain reference state**. This reference state is based on the boundary condition that no elongation (positive or negative) occurs in the horizontal directions (Figure 5.7). Strain only occurs in the vertical direction (strain is uniaxial), and the stress has to comply with this condition. Make sure you do not confuse uniaxial strain with uniaxial stress, which was defined in Figure 4.7. The uniaxial strain model discussed here results in a triaxial stress. It is interesting to note that stress in this case is prescribed by strain (boundary conditions), whereas often we are inclined to think of strain being the product of stress. Is this really realistic?

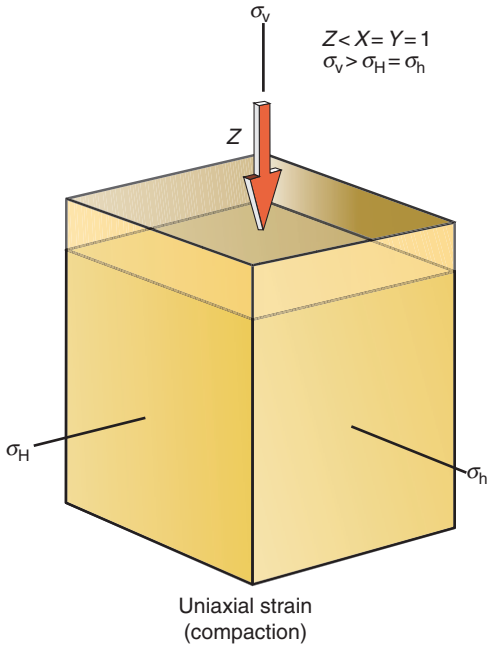

Figure 5.7 Uniaxial-strain reference state of lithostatic stress. Note the difference between the principal stresses (σ_v, σ_H and σ_h) and principal strains (X, Y and Z). The strain is uniaxial (one component different from zero), while stress is not. In this model the vertical stress comes from overburden while the horizontal one is influenced by the uniaxial-strain boundary condition. The model fits well the effect of compaction in sedimentary basins.

The answer is, as you may suspect, yes. This is related to the fact that there is a free surface at the top of any rock column, i.e. the surface of the Earth. In the upper part of the crust this is important, because it is possible to lift or lower this free surface. Lowering is perhaps easier than lifting, and compaction is a deformation that conforms to this uniaxial strain field. Hence, a rock or rock column can shorten (compact) in the vertical direction, but not in the horizontal plane.

Uniaxial strain is characteristic of compaction of sediments where tectonic stresses are absent or negligible. During burial, the horizontal stresses are equal ($\sigma_H = \sigma_h$) and will increase as a function of increasing burial depth or σ_v, but, as shown in Section 6.3, the vertical stress will increase faster than the horizontal stress if the crust is modeled as a linearly elastic medium.

The vertical stress is identical to that predicted by the lithostatic reference state, i.e. $\sigma_v = \rho g z = \sigma_1$, and the horizontal stress $\sigma_H = \sigma_h = \sigma_2 = \sigma_3$ is given by the expression

$$\sigma_H = \frac{\nu}{1-\nu}\sigma_v = \frac{\nu}{1-\nu}\rho g z \qquad (5.3)$$

where ν is Poisson's ratio (see Section 6.3 for derivation). In contrast to the lithostatic model, the horizontal stress depends on the physical properties of the rock.

Let us explore Equation 5.3 in more detail. Rocks typically have ν-values in the range 0.25–0.33. For $\nu = 0.25$ the equation gives $\sigma_H = (1/3)\sigma_v$ and, for $\nu = 0.33$, $\sigma_H = (1/2)\sigma_v$. In other words, the horizontal stress is predicted to be between half and one-third of the vertical stress, i.e. considerably less than what is predicted by the lithostatic reference state. The two models are identical ($\sigma_H = \sigma_h = \sigma_v$) only if the lithosphere is completely incompressible, i.e. if $\nu = 0.5$. As stated in Chapter 6, rocks do not even come close to incompressible, but for a sediment that progressively becomes more and more cemented and lithified, its elastic property changes (ν increases) and the uniaxial-strain model approaches the lithostatic one.

The uniaxial-strain reference state predicts that the vertical stress is considerably larger than the horizontal stress.

This fact predicts a state of stress characteristic of extensional regimes ($\sigma_v > \sigma_H > \sigma_h$). However, stress regimes where $\sigma_H > \sigma_h > \sigma_v$ are very common even in the upper crust, so the uniaxial-strain reference state alone does not sufficiently explain the state of stress in many cases. Besides, it predicts somewhat unrealistically large changes in σ_H during thermal changes and uplift events in the lithosphere. A third model has thus been proposed, called the constant-horizontal-stress reference state.

Constant-horizontal-stress reference state

The **constant-horizontal-stress reference state** is based on the assumption that the average stress in the lithosphere is everywhere the same to the depth of isostatic compensation under the thickest lithosphere (z_1 in Figure 5.8). Below z_1, the Earth is assumed to behave like a fluid ($\sigma_H = \sigma_h = \sigma_v = \sigma_m$ in Figure 5.8), where the lithostatic stress σ_m is generated by the overburden. This is a plane strain model with strain in the vertical and one horizontal direction only. In general, this model is probably the most realistic one for a lithosphere unaffected by tectonic forces.

The constant horizontal stress requirement is maintained by isostatic equilibrium. After erosion, but before isostatic reequilibration, the average horizontal stress (σ_h^*) in the thinner portion of the lithosphere must be higher than that in the thicker portion (σ_h) if the horizontal forces are balanced. The depth of isostatic compensation is z_1, and it is assumed that the mantle below has no shear strength over geologic time. Hence, the state of stress is lithostatic below z_1. The average horizontal stress σ_h^* can then be expressed by the equation:

$$\sigma_h^* = \sigma_h[z_1/(z_1 - z)] - \rho_1 g z(\rho_1/\rho_m)[(z_1 - z/2)/(z_1 - z)] \quad (5.4)$$

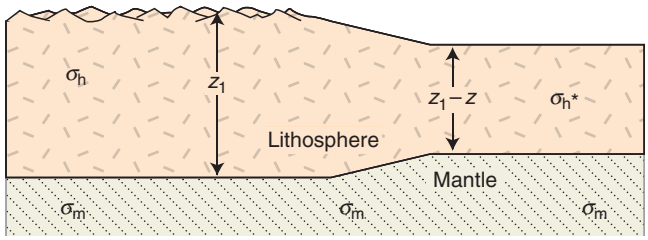

Figure 5.8 Schematic illustration of the relationship between erosion, isostasy and stress for a constant-horizontal-stress reference state, as indicated in Equation 5.4. Erosion of the right-hand side caused upward movement of the base of the lithosphere until isostatic equilibrium was reached. The mantle is considered as a fluid where $\sigma_H = \sigma_h = \sigma_v = \sigma_m$. Based on Engelder (1993).

where $\sigma_h z_1/(z_1 - z)$ describes the horizontal stress increase resulting from lithospheric thinning (horizontal forces must balance, and stress increases as the force acts across a smaller area), and $\rho_1 g z(\rho_1/\rho_m)[(z_1 - z/2)/(z_1 - z)]$ expresses the stress reduction caused by isostasy. Lithospheric thickening can be considered by making $z_1 > z$.

Calculations indicate that the constant-horizontal-stress model predicts lower stress changes during uplift related to lithospheric thinning than the uniaxial-strain model.

5.4 The thermal effect on horizontal stress

Temperature changes occur as rocks are buried, uplifted or exposed to local heat sources (intrusions and lavas) and must be added to the three reference states of stress discussed above. The effect of temperature changes on horizontal stress can be significant, and can be calculated using the following equation for uniaxial strain behavior:

$$\Delta\sigma_h^T = \frac{E\alpha_T(\Delta T)}{1 - \nu} \quad (5.5)$$

where E is Young's modulus, α_T is the linear thermal expansion coefficient, ΔT is the temperature change and ν is Poisson's ratio. As an example, a temperature change of 100 °C on a rock with $\nu = 0.25$, $E = 100$ and $\alpha_T = 7 \times 10^{-6}\,°C^{-1}$ results in a reduction of the horizontal stress of 93 MPa. Cooling during uplift thus has the potential to cause extension fractures in rocks and may in part explain why many uplifted rocks tend to be extensively jointed. Joints are particularly common in competent layers in uplifted sedimentary sequences, such as the sandstones of the Colorado Plateau (Figure 5.9). Let us explore this feature in terms of non-tectonic horizontal stress variations before turning to tectonic stress.

Stress variations during burial and uplift

Rocks that are buried and later uplifted go through a stress history that can be explored by considering the thermal effect, the Poisson effect (the horizontal stress generated due to a change in the overburden, see Section 6.3) and the effect of overburden. Modifying the horizontal stress from Equation 5.3 and adding the thermal effect from Equation 5.5 gives the following equation for a change in depth (change in vertical stress and temperature):

$$\sigma_H = \sigma_h = \left(\frac{\nu}{1 - \nu}\right)\Delta\sigma_v + \left(\frac{E}{1 - \nu}\right)\alpha\Delta T \quad (5.6)$$

where $\Delta\sigma_v$ is the change in vertical stress.

Figure 5.9 Densely jointed Permian sandstones of the Colorado Plateau, exposed by the Colorado River. Such joints would not occur in a reservoir sandstone unless it was uplifted and cooled substantially.

Equation 5.6 can be used to estimate changes in horizontal stress as a rock moves from one crustal depth to another. The result depends on the mechanical properties of the rock (E and ν), which means that adjacent sandstone and shale layers will develop different stress histories during burial and uplift. To simplify the calculations, we use one set of mechanical properties during burial and another during uplift, assuming that lithification occurs at the deepest point of the burial curve. In other words, sand and clay layers go down, and sandstone and shale layers come back up. The result is illustrated in Figure 5.10, which indicates that the clay/shale is always in the compressional regime while the sandstone is predicted to enter the tensional regime during uplift. The exact path depends on the elastic properties, and the effect of pore pressure is not considered. Furthermore, tensile stresses are rarely recorded in the crust, but in spite of the simplistic aspect of this model it illustrates how adjacent layers may develop different states of stress and therefore different fracture patterns during uplift.

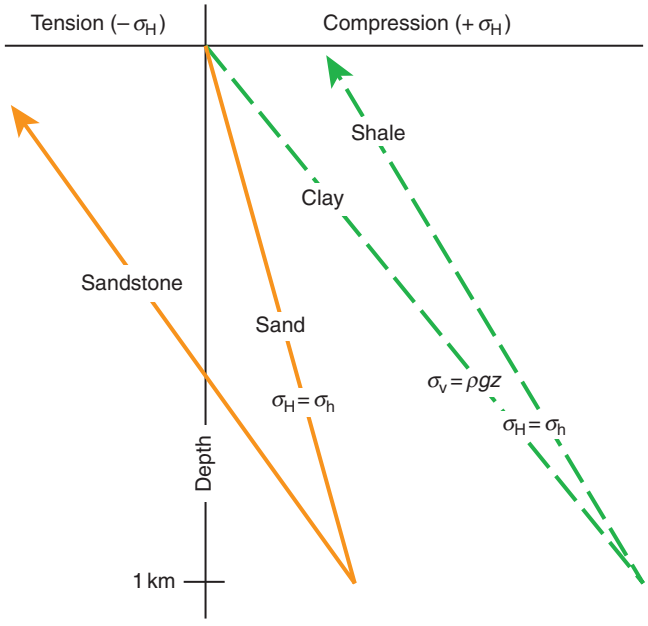

Figure 5.10 Simple modeling of stress variations during burial and uplift for sand(stone) and clay (shale). Lithification is assumed to occur instantaneously at maximum burial depth. Based on Engelder (1985).

Tensile fractures or joints are more likely to develop in rock layers with the highest Young's modulus and the lowest Poisson's ratio, which in simple terms means that stiff and competent layers (e.g. sandstones and limestones) build up more differential stress than surrounding layers.

Joints are more likely to initiate in sandstones than in shale during uplift of clastic sedimentary rocks.

This can be important to geologists exploring petroleum reservoirs in uplifted areas, where vertical tensile fractures that may cause leakage of oil traps are more likely. It also means that a smaller overpressure is needed to produce fractures in sandstone than in claystone (Figure 5.11), which is why hydrofractures tend to be confined to sandstone layers rather than adjacent claystones or shales.

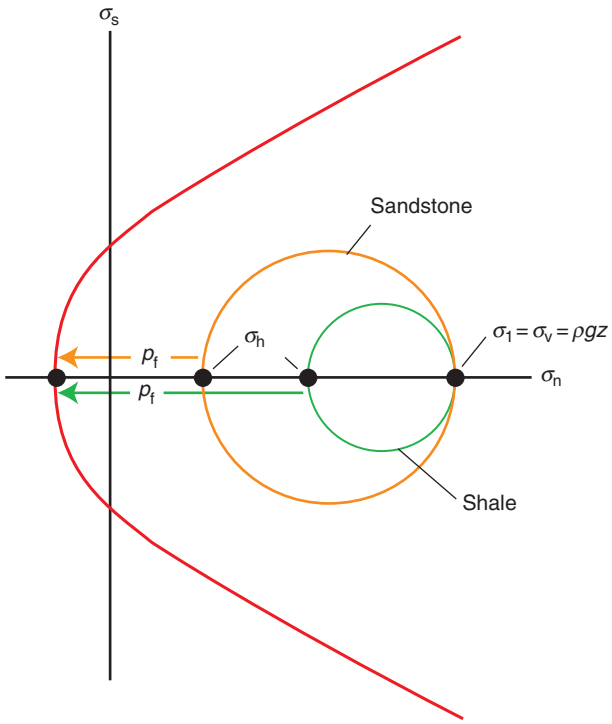

Figure 5.11 Stresses in alternating shale–sandstone layers. Sandstone is stronger and can sustain a higher differential stress than shale. The critical pore pressure needed to generate tensile fractures in the sandstone is less than for shale, since the vertical stress is the same for the layers. The red curve defines the fracture criterion that describes the conditions at which the rocks fracture. Fracturing happens when the circle for sandstone or shale touches the red curve. This can happen due to increased pore fluid pressure (see next chapter) or due to uplift. In either case, the sandstone first touches the red line, and it happens at the tensile side of the normal stress axis, meaning that tensile fractures form. Fracture criteria are treated in Chapter 7 (Section 7.3).

5.5 Residual stress

Stress can be locked in and preserved after the external force or stress field has been changed or removed, and is then referred to as **residual stress**. In principle, any kind of stress can be locked into a rock if, for some reason, elastic strain remains after the external stress field is removed. The causes for the external stress may be overburden, tectonic stress or thermal effects.

Let us look at how residual stress can form in sandstone during compaction, cementation and uplift. During burial and physical loading, stress builds up across grain contact areas. Assume that cementation occurs prior to removal of the external stress field or the overburden. If uplift and erosion later exposes the sandstone at the surface and thereby causes a stress decrease, then the elastic deformation of the grains caused by the now removed overburden will start to relax. However, relaxation is partly prevented by the cement. Hence, some of the stress is transferred to the cement while the rest remains in the sand grains as locked-in stress. In this way, stress that was imposed on the sand during burial thus remains locked in as residual stress.

Residual stress may also be caused by metamorphic transformations that involve volumetric changes, by intrusions where magma cooling sets up stresses that are locked into the crust, by changes in temperature and/or pressure, or by past tectonic episodes. There is therefore a close connection between residual stress, thermal stress and tectonic stress, which we will look at next.

5.6 Tectonic stress

The reference states of stress discussed above relate to natural factors such as rock density, boundary conditions (uniaxial versus plane strain), thermal effects and the physical properties of rock. Natural deviations from a reference state are generally caused by **tectonic stress**. On a large scale, tectonic stress in many cases means stress related to plate movements and plate tectonics. Locally, however, tectonic stresses may be influenced by such things as bending of layers, e.g. ahead of a propagating fault, fault interference and other local effects. Hence, local tectonic stress may be quite variable with respect to orientation, while regional tectonic stress patterns are often found to be consistent over large areas.

Tectonic stresses are those parts of the local stress state that deviate from the reference state of stress as a consequence of tectonic processes.

Somewhat simplified, tectonic stress is the deviation from any chosen reference state of stress. There are also other components of stress, including thermal and residual stress, that we may want to distinguish from present tectonic stress.

Although individual components may be difficult to separate, the total state of stress in any given point in the lithosphere can be separated into a reference state of stress, residual stress, thermal stress, tectonic stress and terrestrial stress (stress related to seasonal and daily temperature changes, earth tide etc.):

Current tectonic stress = Total stress – (reference state of stress + non-tectonic residual stress + thermal stress + terrestrial stress).

If we are close to the surface, we should also eliminate the effect of topography shown in Figure 5.3.

It is seldom easy to separate the tectonic component of stress from the other contributions. Again we turn to ideal models, and we will start by looking at Anderson's classic classification of tectonic stress before looking at actual data.

Anderson's classification of tectonic stress

The traditional classification of tectonic stress regimes into normal, thrust and strike-slip regimes was coined in Anderson's famous 1951 publication. Anderson made the assumption that, since there is no shear stress at the Earth's surface (shear stress cannot occur in fluids), one of the principal stresses has to be vertical, implying that the other two are horizontal. Depending on which of the three principal stresses is the vertical one, Anderson defined three regimes, as illustrated in Figure 5.12:

$\sigma_v = \sigma_1$; normal-fault regime
$\sigma_v = \sigma_2$; strike-slip fault regime
$\sigma_v = \sigma_3$; thrust-fault regime

Anderson's classification is strictly valid only in coaxial deformational regimes, where lines parallel to ISA and principal strain axes do not rotate. Furthermore, the deforming rock must be isotropic. The vertical stress can be related to the weight and density of the overlying rock column:

$$\sigma_v = \rho g z. \tag{5.7}$$

One of the reference states of stress must be chosen to calculate the horizontal stresses. Let us use the thrust-fault regime as an example. A horizontal tectonic stress acts in this regime, which we will call σ_t^*. This stress adds to that specified by the reference state of stress (Equation 5.7). For a lithostatic state of stress, σ_H thus becomes

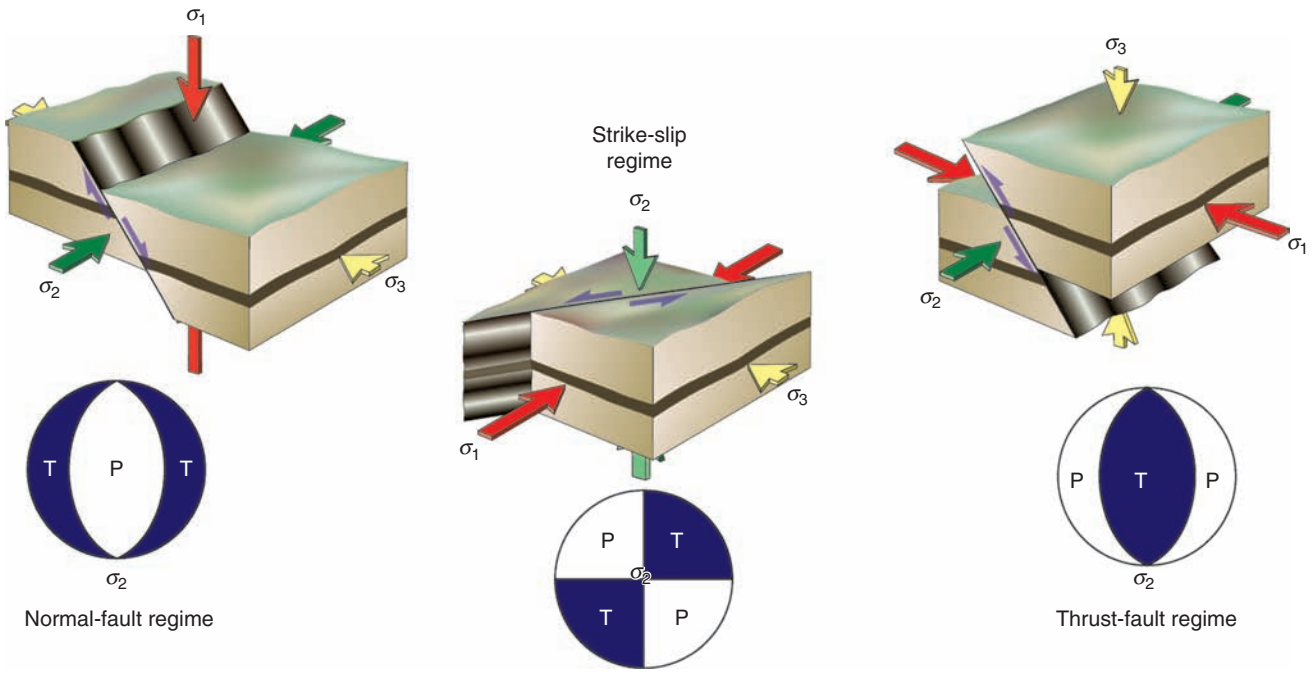

Figure 5.12 Relationships between the orientation of the principal stresses (stress regimes) and tectonic regimes according to Anderson (1951). Stereonets show fields of compression (P) and tension (T).

$$\sigma_H = \rho g z + \sigma_t^* \quad (5.8)$$

If instead we consider the uniaxial-strain reference state of stress, then we implicitly assume that the stress condition also depends on the physical properties of the rock. In this case (excluding any thermal effect) we use the designation σ_t for horizontal tectonic stress, and by adding this tectonic stress to the uniaxial-strain reference state (Equation 5.3) we have

$$\sigma_H = [\nu/(1-\nu)]\rho g z + \sigma_t \quad (5.9)$$

It follows by comparing the two expressions that, since $[\nu/(1-\nu)] < 0$, $\sigma_t > \sigma_t^*$. This means that the magnitude of the tectonic stress depends on our choice of reference state of stress. Note that when ν approaches 0.5, Equation 5.8 approaches Equation 5.9, i.e. σ_t approaches σ_t^*. These considerations also hold for the normal-fault regime, except that σ_t^* is tensional and thus becomes negative (σ_t is only negative or tensional in areas of very active normal faulting).

The examples illustrate that the definition of tectonic stress is dependent on the choice of reference state of stress. Hence, the absolute value of tectonic stress is not always easy to estimate.

5.7 Global stress patterns

Stress is estimated around the world in mines, during construction and tunneling work, during onshore and offshore drilling operations, and in relation to earthquake monitoring. Together, these data are evaluated, compiled in **The World Stress Map Project**, and are available on the World Wide Web (Figure 5.13).

In order to compile a worldwide stress map, several different sources of information are used. They are grouped into (1) earthquake focal mechanisms, (2) borehole breakouts and drilling-induced fractures, (3) *in situ* stress measurements (overcoring, hydraulic fracturing) and (4) neotectonic geologic structural data (from fault-slip analysis and volcanic vent alignments). The data are ranked according to reliability, and it is assumed that one principal stress is vertical and the other two horizontal. Focal mechanism data completely dominate the data set, particularly the deeper (4–20 km) portion of the data, and are most frequent where earthquakes are common, i.e. along plate boundaries. At shallower levels there is a dominance of data from breakouts, hydrofractures and overcoring.

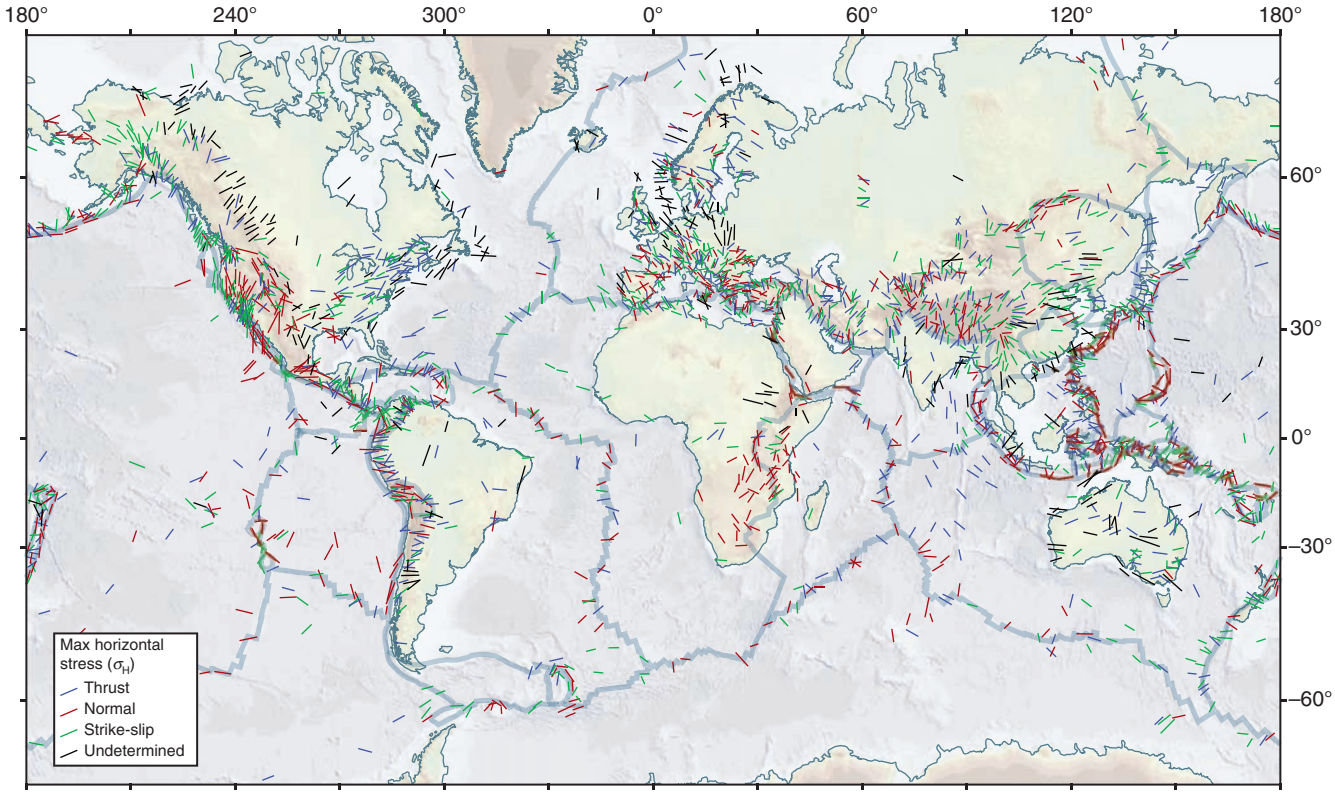

Figure 5.13 World Stress Map, based on stress measurements from around the world. Lines indicate the orientation of σ_H, and line colors indicate tectonic regime (normal-fault, strike-slip, thrust-fault regimes shown in Figure 5.12). Based on data from www.world-stress-map.org.

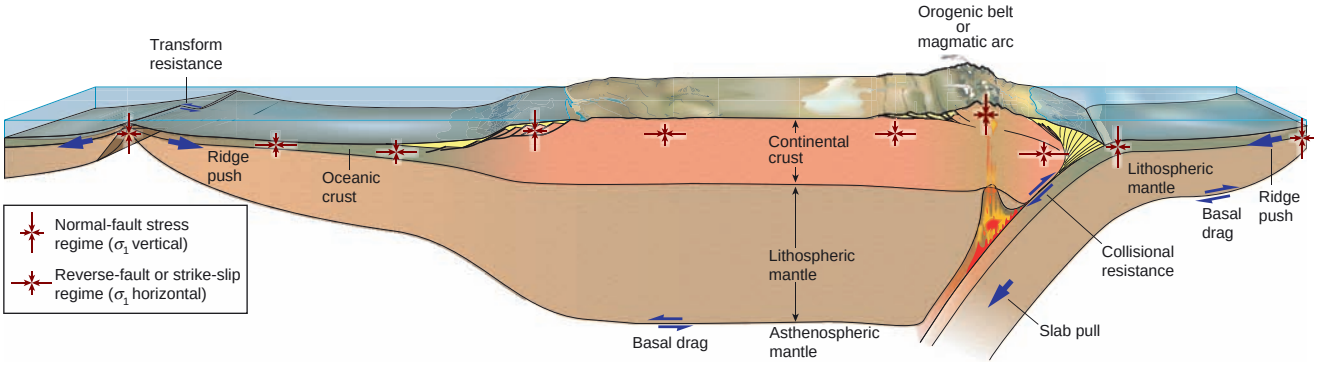

Figure 5.14 Forces related to plate tectonics (blue arrows) and stress regimes expected from these forces. The maximum stress axis in continental plates is expected to be horizontal except for the upper part of rift zones (continental rift not shown), passive margins and elevated parts of orogenic belts.

Figure 5.13 shows that there are large areas of little or no stress information, onshore as well as offshore. The correlation between the orientation of σ_H and plate motion is also obvious many places, but with many deviations that tell us that the current stress field is influenced by many different mechanisms and sources of stress. Regardless, tectonic processes at plate margins are thought to have a significant influence on the regional stress pattern, and the main sources are thought to be slab pull, ridge push, collisional resistance and basal drag (frictional drag along the base of the lithosphere) (Figure 5.14). **Slab pull** is the gravitational pull exerted by the sinking slab on the rest of the plate. It is largest for old and cold, dense oceanic lithosphere, and negative if light and buoyant continental crust is subducted. **Ridge push** is simply the push from the topographically high oceanic ridge that marks divergent plate boundaries. This ridge rises several kilometers from the ocean floor and thus produces a significant lateral force. The related stress regime promoted by ridge push is one of normal faulting in the elevated ridge area, and reverse faulting farther away. These are probably the two most important sources of plate tectonic forces and thus the most important factors in the shaping of the global-scale stress pattern. The effect of **basal drag**, which is the frictional resistance or shear force acting at the base of the lithosphere, is uncertain. This force could drive or resist plate motions, depending on plate kinematics relative to the behavior of local mantle convection cells. A similar force acts on top of the subducting slab. The effect of the **collisional resistance** depends on the strength of the coupling between the two colliding plates, but is greatest for continent–continent collision zones.

Plate tectonic processes are responsible for a global stress pattern that is locally modified by gravity-controlled second-order sources of stress.

So-called second-order sources of stress are continental margins influenced by sediment loading, areas of glacial rebound, areas of thin crust and upwelling hot mantle material, ocean–continent transitions, orogenic belts and large, weak faults such as the San Andreas Fault that can deflect the stress field (Figure 5.4). The many sources of stress may be difficult to identify from the present world stress database, but a combination of new stress data and modeling results may improve our understanding of stress in the lithosphere in the years to come.

A characteristic feature of the stress data shown in Figure 5.13 is that the orientation of σ_H is fairly consistent within broad regions. Consistent patterns can exist within continents, far from plate boundaries. One such area is the North American continent east of the Rockies, which is dominated by a NE–SW oriented σ_H. Another is Northern Europe and Scandinavia, where σ_H is oriented NW–SE. The orientation of the latter can perhaps be explained by ridge push from the North Atlantic mid-ocean ridge, while the more oblique (with respect to the ridge axis) orientation of the North American stress field may be influenced by other effects, perhaps basal drag. Even if we cannot fully explain intraplate stress orientation patterns yet, the consistent orientation of σ_H over large areas suggests that plate tectonic forces play an important role.

If we go closer to the plate boundaries, we see at least some consistency between orientations of the boundaries and that of σ_H, for example along the convergent plate boundary along the western coast of South America,

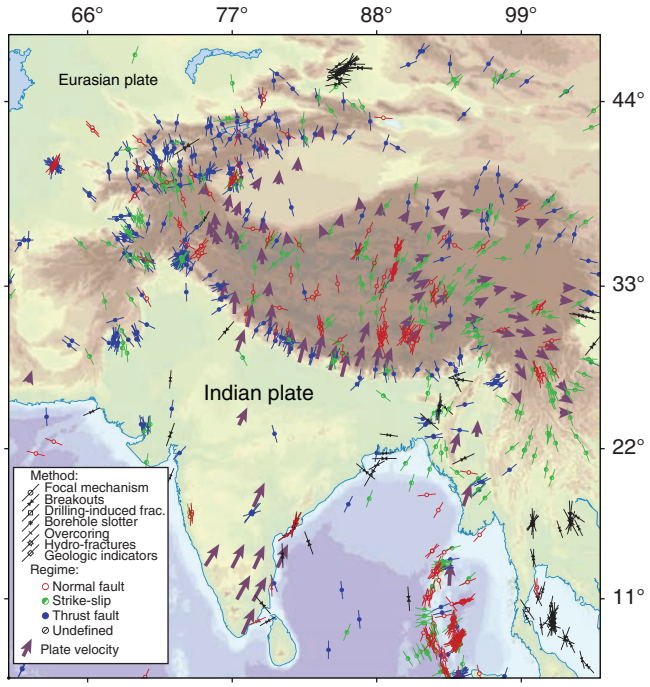

Figure 5.15 Stress data from the Himalaya area – the collision zone between the Eurasian and Indian plates, together with plate velocity vectors determined from GPS measurements. Note the close connection between kinematics and σ_H, and the occurrence of all three tectonic regimes in the collision zone. Data from www.world-stress-map.org and http://jules.unavco.org/Voyager/ILP_GSRM.

where σ_H makes a high angle to the plate boundary (Figure 5.13). In contrast, σ_H is much more oblique in the dextral strike-slip dominated San Andreas Fault area in California, an obliquity that fits with dextral sense of shear. Also in the Himalaya, where the Indian plate moves northward into the Eurasian plate, there is a good correlation between plate motions and σ_H (Figure 5.15).

When we look at the global distribution of the three different fault regimes (normal, strike-slip and thrust regimes) the pattern may seem quite complex, with two or even three of the regimes occurring in the same region. However, there are some general features that explain important aspects of this pattern. An important observation is that the maximum principal stress is horizontal ($\sigma_H = \sigma_1$), implying a thrust or strike-slip regime within large parts of continents such as eastern North America, South America and Scandinavia/Northern Europe. We could say that, in general, $\sigma_H = \sigma_1$ in large parts of the continents, if not the entire brittle upper crust. As mentioned above, we could credit or blame plate tectonics and the forces that come with it for this situation. Within this pattern, we find the **strike-slip stress regime** represented in several places, but primarily in areas of significant strike-slip faulting, such as the San Andreas Fault in California and the Dead Sea transform fault in the Middle East.

The **thrust-fault stress regime** is expected to be particularly common along convergent plate boundaries and major active orogenic zones. Examples are the Himalayan orogenic belt and the Andes, where geologic evidence of thrust tectonics is widespread. These zones also have significant elements of strike-slip and even normal-fault regimes, and there are a couple of basic explanations for this. One is the concept called strain (or stress) partitioning, which in simple terms means that the perpendicular component goes into thrusting and other contractional deformation and the boundary-parallel component is taken out by strike-slip motion and related states of stress (see Chapter 18). Another is the fact that elevated areas of the crust, such as the high Andes or the Tibetan Plateau, develop a vertical σ_1 and even tend to expand laterally due to gravity. Consequently, the high portions of an orogenic belt can extend while the deeper part is shortening, as discussed in Chapter 16.

As an example, the stress situation in and around the Himalayan orogen shows the presence of all three regimes (Figure 5.15). The thrust-fault regime dominates the lower parts along the plate boundary (southern foothills), while the normal-fault regime characterizes the high Tibetan Plateau. The strike-slip regime is particularly common in the eastern part, where crust is being squeezed sideways as India intrudes into Eurasia (see Chapter 18). Hence, relative plate motion (India moving into Eurasia), gravitational potential of overthickened crust (Tibetan Plateau) and boundary conditions (stiff Indian plate forced into heated and thus softened material immediately north of the Indian and Eurasian plate boundary) are three factors that help explain the occurrence and distribution of the different stress regimes in the Himalayan collision zone.

Stress fields consistent with Anderson's **normal-fault regime stresses** are found along divergent plate boundaries, but are more pronounced in areas of active continental rifting and extension. The East African rift zone, the Aegean area and the Basin and Range province of the western USA are obvious examples, but also elevated areas in convergent settings, such as the Tibetan Plateau, the high Andes, and the western US Cordillera, tend to be under extension. One of the most popular models for the extension in these areas is related to gravitational collapse of topographically high areas, which we will return to in Chapter 17.

5.8 Differential stress, deviatoric stress and some implications

The amount of stress increases downwards from the surface into the lithosphere. How much stress can a rock withstand before deformation occurs? The reference states predict an increase in stress all the way to the center of the Earth. Rock-forming minerals undergo phase changes and metamorphic reactions in response to this increase, and it takes a deviation from the reference state for rocks to deform by fracturing or shearing. Anderson gave us an idea of how the relative orientation of the tectonic stresses influences the style of faulting (close to the surface). We also want to know how faulting occurs in the lithosphere. Here it is not the absolute level of stress, but rather the difference between the maximum and minimum principal stresses that causes the rock to fracture or flow. This difference is called the **differential stress**:

$$\sigma_{\text{diff}} = \sigma_1 - \sigma_3 \tag{5.10}$$

For **lithostatic stress** (Figure 5.7) the principal stresses are all equal, and we have

$$\sigma_{\text{diff}} = 0 \tag{5.11}$$

Hence, the lithostatic model itself provides no differential stress to the lithosphere, regardless of depth of burial.

For a **uniaxial-strain reference state** of stress the situation is

$$\sigma_H = \sigma_h < \sigma_v \tag{5.12}$$

and the differential stress becomes

$$\sigma_{\text{diff}} = \sigma_1 - \sigma_3 = \sigma_v - \sigma_h = \sigma_v[(1-2\nu)/(1-\nu)] \tag{5.13}$$

For a rock with $\nu = 0.3$, $\sigma_{\text{diff}} = 0.57\sigma_v$ and σ_{diff} increases with depth at a rate of ~13 MPa/km for continental crust. While the uniaxial-strain reference state of stress may be reasonably realistic in sedimentary basins, it may not be very realistic deep in the lithosphere. Again we see that our choice of reference model has significant implications.

Regardless of the choice of reference state of stress, tectonic stress adds to the total differential stress in a rock. The amount of differential stress that can exist in the lithosphere is, however, limited by the strength of the rock itself. When a rock deforms by brittle fracturing, its strength changes and σ_{diff} is reduced. Hence, while the vertical stress in the lithosphere is governed by the weight of the overburden, the horizontal stresses are limited by the local rock strength.

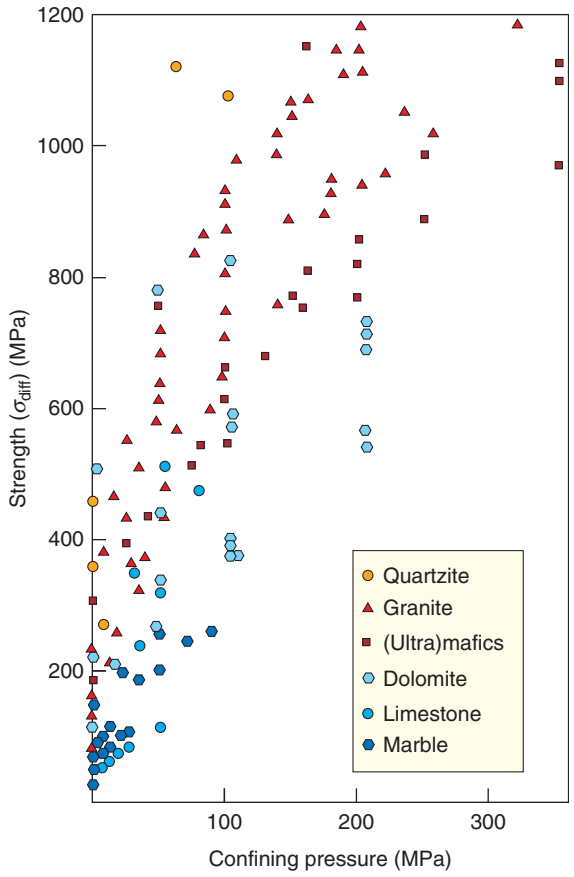

Figure 5.16 The strength of various rock types, plotted against confining pressure (burial depth). The data indicate that the strength of the brittle crust increases with depth, and that the absolute strength depends on lithology (mineralogy). Data compiled from a range of sources.

Differential stress at any given point in the Earth is limited by the strength of the rock itself. Any attempt to increase the differential stress above the ultimate rock strength will lead to deformation.

This does not mean that differential stress is independent of overburden. In fact, there is a very important positive relationship in the upper part of the crust between the amount of overburden and the differential stress that any given rock can support, as reflected by the experimental data shown in Figure 5.16. Thus, the strength increases from the surface and down toward the depth at which the rock starts to flow plastically. For granitic rocks this generally means mid-crustal depths (10–15 km). This transition is controlled by temperature rather than σ_v, and is related to the brittle–plastic transition in the crust (Section 6.9).

The strength of rocks in the crust is in practice controlled by anisotropic features, particularly weak fractures and shear zones. We will return to crustal strength

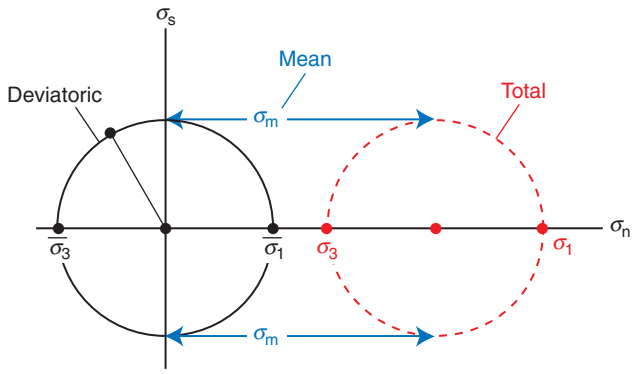

Figure 5.17 The total state of stress can be considered as consisting of an isotropic component, the mean normal stress, and an anisotropic component, the deviatoric stress. The center of the Mohr circle is moved to the origin when the mean stress is subtracted.

toward the end of the next chapter. We will conclude the present chapter by looking at deviatoric stress.

Deviatoric stress (σ_{dev}) was defined in Chapter 4 as the difference between the total stress tensor and the mean stress tensor:

$$\sigma_{diff} = \sigma_{tot} - \sigma_m \tag{5.14}$$

where

$$\sigma_m = (\sigma_1 + \sigma_2 + \sigma_3)/3 \tag{5.15}$$

In three dimensions deviatoric stress is thus defined as

$$\begin{bmatrix} \sigma_{11dev} & \sigma_{12dev} & \sigma_{13dev} \\ \sigma_{21dev} & \sigma_{22dev} & \sigma_{23dev} \\ \sigma_{31dev} & \sigma_{32dev} & \sigma_{33dev} \end{bmatrix} = \begin{bmatrix} \sigma_{11} & \sigma_{12} & \sigma_{13} \\ \sigma_{21} & \sigma_{22} & \sigma_{23} \\ \sigma_{31} & \sigma_{32} & \sigma_{33} \end{bmatrix} - \begin{bmatrix} \sigma_m & 0 & 0 \\ 0 & \sigma_m & 0 \\ 0 & 0 & \sigma_m \end{bmatrix}$$

$$= \begin{bmatrix} \sigma_{11} - \sigma_m & \sigma_{12} & \sigma_{13} \\ \sigma_{21} & \sigma_{22} - \sigma_m & \sigma_{23} \\ \sigma_{31} & \sigma_{32} & \sigma_{33} - \sigma_m \end{bmatrix} \tag{5.16}$$

Or, if the principal stresses are oriented along the coordinate axes of our reference system:

$$\begin{bmatrix} \sigma_{1dev} & 0 & 0 \\ 0 & \sigma_{2dev} & 0 \\ 0 & 0 & \sigma_{3dev} \end{bmatrix} = \begin{bmatrix} \sigma_1 & 0 & 0 \\ 0 & \sigma_2 & 0 \\ 0 & 0 & \sigma_3 \end{bmatrix} - \begin{bmatrix} \sigma_m & 0 & 0 \\ 0 & \sigma_m & 0 \\ 0 & 0 & \sigma_m \end{bmatrix}$$

$$= \begin{bmatrix} \sigma_1 - \sigma_m & 0 & 0 \\ 0 & \sigma_2 - \sigma_m & 0 \\ 0 & 0 & \sigma_3 - \sigma_m \end{bmatrix} \tag{5.17}$$

This implies that the mean stress by definition is the *isotropic* component of the total stress, while the deviatoric stress is the *anisotropic* component at the same point. This becomes clearer if we rearrange the above equation (also see Equation 4.8):

$$\begin{bmatrix} \sigma_1 & 0 & 0 \\ 0 & \sigma_2 & 0 \\ 0 & 0 & \sigma_3 \end{bmatrix} = \begin{bmatrix} \sigma_m & 0 & 0 \\ 0 & \sigma_m & 0 \\ 0 & 0 & \sigma_m \end{bmatrix} + \begin{bmatrix} \sigma_{1dev} & 0 & 0 \\ 0 & \sigma_{2dev} & 0 \\ 0 & 0 & \sigma_{3dev} \end{bmatrix} \tag{5.18}$$

Total stress = Isotropic + Anisotropic part

Deviatoric stress in two dimensions is visualized in Mohr space in Figure 5.17. The distance from the center of the Mohr circle to the origin is the mean stress. The two deviatoric stresses are positive ($\sigma_1 - \sigma_m$) and negative ($\sigma_3 - \sigma_m$), respectively, and their directions indicate the tectonic regime (normal, thrust or strike-slip). Note that even though one of the anisotropic stresses is negative or tensional ($\sigma_3 - \sigma_m < 0$), the isotropic component is generally large enough in the lithosphere that all principal stresses of the total state of stress become positive (compressive).

Summary

It is both challenging and interesting to try to measure and understand the present stress pattern in the crust. It is clear that we need more measurements and a better understanding of how stresses originate and accumulate in rocks. Nevertheless, the models and concepts presented should form a useful fundament for dealing with stress. Here are some important points to remember:

- Stress is not directly observable, but is revealed by strain in one way or another.
- Reference states of stress in the crust are very generalized models that can be used to detect anomalies.
- Anomalies could be due to local conditions, such as overpressured units (in sedimentary basins), thermal effects, stress refraction near mechanically weak zones (e.g. fracture zones), residual stress or the effect of topography near the surface.

- When these factors are accounted for, the remaining deviation from the general reference state of stress is likely to be tectonic stress.
- Tectonic stress is ideally classified by three end-member states or regimes: the normal (σ_1 vertical), strike-slip (σ_2 vertical) and thrust (σ_3 vertical) regimes.
- For deformation to occur in any of these regimes requires the differential stress to exceed the strength of the rock.
- The amount of differential stress a rock can support increases downward through the brittle upper crust.

Review questions

1. How can we get information about the stress field near the surface? Some kilometers down? Even deeper down?
2. Which of the three reference states of stress are, by nature, isotropic?
3. Is the uniaxial-strain reference state a stress or strain state? How are stress and strain related in this model?
4. What physical factors control the state of stress in a rock that is being uplifted through the upper crust?
5. Why does sandstone fracture more easily than shale when uplifted?
6. How can we define tectonic stress?
7. What conditions must apply for Anderson's classification of tectonic stress to be strictly valid?
8. What is the differential stress at 5 km depth for continental crust if we have a perfect lithostatic state of stress?
9. What forces related to plate tectonics can cause tectonic stress?
10. Why do we find evidence of strike-slip and normal-fault stress regimes in addition to the thrust-fault regime in active (contractional) orogens such as the Himalaya and Andes?
11. What stress regime(s) would we expect along strike-slip faults such as the San Andreas Fault?
12. Why does the differential stress increase downwards in the brittle crust?
13. If we increase the fluid pressure in a sandstone unit, will the effective stress increase or decrease?

E-MODULE

The second part of the e-learning module called *Stress* is recommended for this chapter.

FURTHER READING

Amadei, B and Stephansson, O., 1997, *Rock Stress and its Measurement*. London: Chapman & Hall.

Engelder, J. T., 1993, *Stress Regimes in the Lithosphere*. Princeton: Princeton University Press.

Fjær, E., Holt, R. M., Horsrud, P., Raaen, A. M. and Risnes, R., 1992, *Petroleum Related Rock Mechanics*. Amsterdam: Elsevier.

Turcotte, D. L. and Schubert, G., 2002, *Geodynamics*. Cambridge: Cambridge University Press.

Chapter 6

Rheology

Stress and strain are related, but the relationship depends on the properties of the deforming rock, which themselves depend on physical conditions such as state of stress, temperature and strain rate. A rock that fractures at low temperatures may flow like syrup at higher temperatures, and a rock that fractures when hit by a hammer may flow nicely at low strain rates. When discussing rock behavior it is useful to look to material science, where ideal behaviors or materials (elastic, Newtonian and perfectly plastic) are defined. These reference materials are commonly used when modeling natural deformation. This is what we will do in this chapter, and we will focus on a very useful arena for exploring related rock deformation, which is the rock deformation laboratory. Experimenting with different media has greatly increased our knowledge about rock deformation and rheology.

6.1 Rheology and continuum mechanics

Rheology is the study of the mechanical properties of solid materials as well as fluids and gases. The name derives from the Greek word "rheo", which means "to flow". But what have flow and fluids got to do with solid rocks? In answering this question, it is interesting to consider the Greek philosopher Heraclitus' aphorism "Panta Rhei", meaning "everything flows". He argued that everything is in constant change, which is easier to accept if geologic time is involved.

It is not only water that flows, but also oil, syrup, asphalt, ice, glass and rocks. The flow of oil and syrup can be studied over time spans of minutes, while it takes days, months or years to study the flow of ice (Figure 6.1) and salt glaciers, which again flow considerably faster than glass. While glass flows too slowly to produce observable changes in shape even over a few centuries, glass clearly flows fairly quickly when heated by a glass-maker. Temperature influences most solids, including rock.

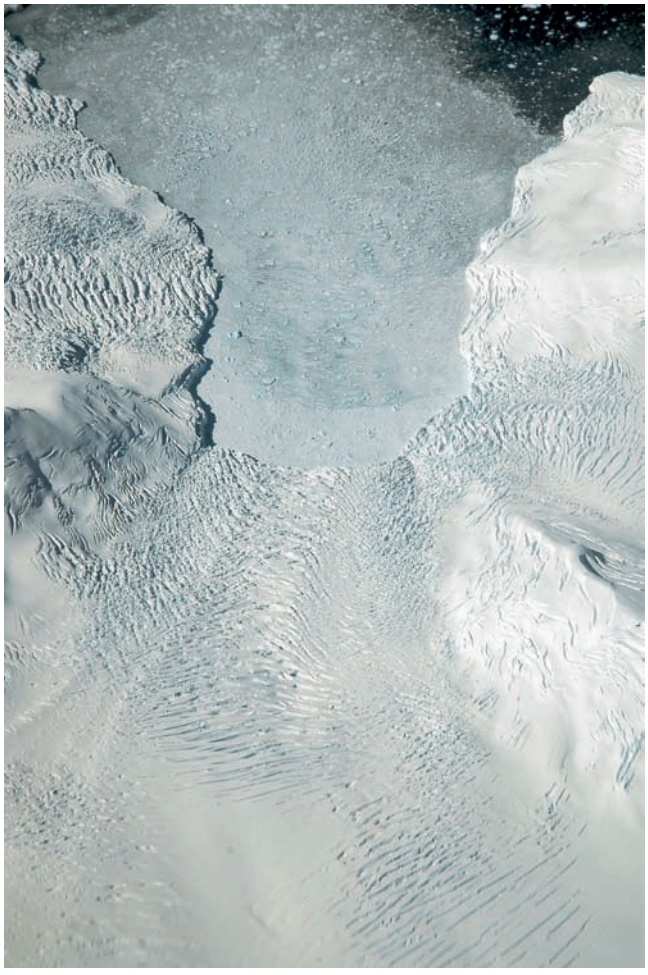

Figure 6.1 Ice in glaciers flows similarly to a viscous fluid, but the many fractures at the surface of glaciers tell us that this may not be a perfect model for its uppermost part. Southeast Greenland.

When hot rocks flow, they accumulate strain gradually, like a very slow-moving glacier or cake of syrup, without the formation of fractures or other discontinuities.

The effect of temperature is the main reason why flow mostly occurs in the middle and lower crust rather than in the cool upper crust. The upper crust tends to fracture, a behavior that strictly speaking falls outside of the field of rheology but still within the realm of **rock mechanics**. In addition to external factors, such as stress, temperature, pressure and the presence of fluids, the properties of the rock itself are of course important. There are many different types of rocks and minerals, and the upper crust tends to fracture only because that is the way common upper-crustal minerals such as quartz and feldspar react to stress under upper-crustal conditions. However, at any depth where we have thick salt layers, these layers will flow rather than fracture, as we will see in Chapter 20. Even clay or sand layers may flow, particularly when the pore pressure becomes high, so flow is not completely restricted to the lower part of the crust. However, deep earthquakes and field evidence may indicate that dry lower-crustal rocks can also fracture under certain conditions, particularly in "dry" rocks more or less devoid of fluids.

If we consider rock as a continuous medium, neglecting heterogeneities such as microfractures, mineral grain boundaries and pore space, and consider physical properties to be constant or evenly changing through the rock volume, simple mathematics and physics can be used to describe and analyze rock deformation in the framework of **continuum mechanics**. Equations that mathematically describe the relationship between stress and strain or strain rate will be important in this chapter. Such equations are called **constitutive laws** or **constitutive equations**. The term *constitutive* emphasizes the importance of the constitution or composition of the material.

Rheology and continuum mechanics deal with the flow of rocks, while rock mechanics primarily deals with the way rocks respond to stress by brittle faulting and fracturing.

6.2 Idealized conditions

In a simple and idealized continuum mechanics context, materials can be said to react to stress in three fundamentally different ways: by elastic, plastic and viscous deformation. In addition there is brittle deformation and cataclastic flow, but these are beyond the field of continuum mechanics. As the physical conditions change during the deformation history, a given material can deform according to each of these types of flow, and eventually enter the field of brittle deformation.

Deformations are commonly analyzed by plotting a stress–strain or stress–strain rate curve, where strain or strain rate is plotted along the horizontal axis and stress along the vertical axis, as shown in Figure 6.2. Time-dependent deformations are described by means of stress–time and strain–time graphs, where time is plotted along the horizontal axis. Several curves can be plotted for different external conditions or for different materials. Each curve can also be subdivided into stages, where each stage has its own slope. We will start by looking at the elastic response to stress and then move to permanent non-brittle deformation or flow.

It is always useful to start out simple, so let us consider a perfectly **isotropic medium** (rock). By isotropic we mean a medium that has the same mechanical properties in all directions, so that it reacts identically to stress regardless of its orientation. Many of the strains we will consider in this chapter are small, less than a few percent for elastic deformation. This contrasts to strains that we often face when studying rocks in the field. The advantage is that a simple relationship occurs between stress and strain for small strains in such an ideal medium. In particular, the instantaneous stretching axes (ISA) will coincide with the principal stresses, as will be assumed throughout this chapter.

6.3 Elastic materials

An **elastic material** resists a change in shape, but strains as more stress is applied. Ideally, it returns to its original shape once the applied stress (force) is removed.

Elastic strain is recoverable because it involves stretching rather than breaking of atomic bonds.

Most rubber bands fit this definition very well: more stretching requires more force, and the band recovers its original shape once the force is removed. Rubber is, however, not a linear elastic material.

Linear elasticity and Hooke's law

A **linear elastic material** shows a linear relationship between stress (or force) and strain. This means that if it flattens twice as much under two tons weight as under one, it will flatten four times as much under four tons weight. An analogy is often made with a simple spring (Figure 6.2a): If the weight on the spring is doubled then the change in length also doubles and so on. In other words, the elongation of the spring is proportional to the force applied, and the spring will return to its original

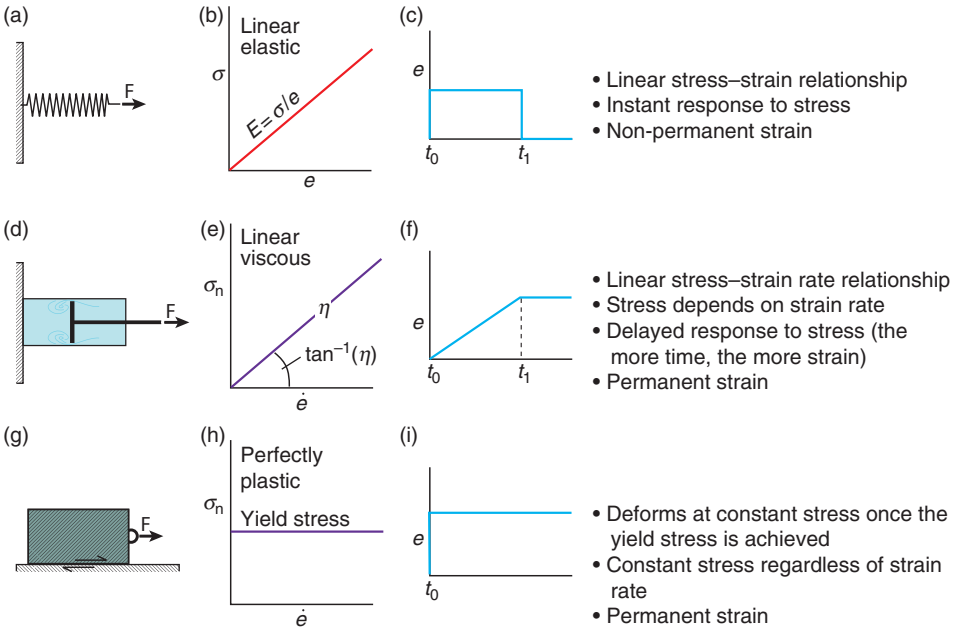

Figure 6.2 Elastic, viscous and plastic deformation illustrated by mechanical analogs, stress–strain (rate) curves (center) and strain history curves (right).

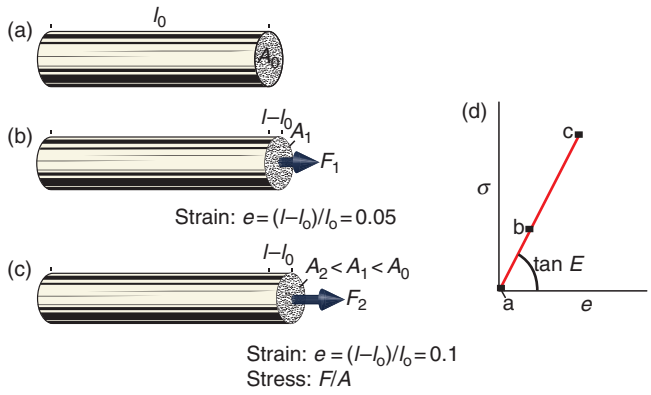

Figure 6.3 Elastic deformation illustrated (a–c) by uniaxial extension of a rod. The stronger the force F that acts on the end area A, the longer the rod (length l). If the material is linear elastic, then the relationship between the extension e and σ ($= F/A$) is linear and forms a line in e–σ-space (d). The gradient of the line is E (Young's modulus). When the force is relaxed, the material returns to its original length (the origin).

length once the force is removed. A similar example is shown in Figure 6.3, where a rod of some elastic material is pulled. Such a linear relationship between stress and strain is expressed by **Hooke's law**:

$$\sigma = Ee \tag{6.1}$$

where σ = stress, e = extension (i.e. one-dimensional strain), and E = **Young's modulus** or the **elastic modulus** (also denoted Y) or, less formally, the **stiffness** of a material. Hooke's law is a constitutive equation for elastic materials.

Young's modulus can also be viewed as the stress/strain ratio:

$$E = \sigma/e \tag{6.2}$$

and is closely related to the **shear modulus** μ (also denoted G and called the rigidity modulus, not to be confused with the friction coefficient introduced in Chapter 2). For uniaxial strain the relationship is simple:

$$E = 2\mu \tag{6.3}$$

The shear modulus μ is related to the shear strain γ, and Hooke's law can be written:

$$\sigma_s = \mu\gamma \tag{6.4}$$

or

$$\sigma = 2\mu e \tag{6.5}$$

Young's modulus E expresses the ratio between the normal stress and the related elastic extension or shortening in the same direction, and describes how hard it is to deform a certain elastic material or rock. Similarly, μ quantifies how hard it is to deform a rock elastically under simple shear (for very small finite strains).

Table 6.1 Representative values of Young's modulus (E) and Poisson's ratio (v) for some rocks, minerals and familiar media

Medium	E (GPa)	v (Poisson's ratio)
Iron	196	0.29
Rubber	0.01–0.1	almost 0.5
Quartz	72	0.16
Salt	40	~0.38
Diamond	1050–1200	0.2
Limestone	80	0.15–0.3
Sandstone	10–20	0.21–0.38
Shale	5–70	0.03–0.4
Gabbro	50–100	0.2–0.4
Granite	~50	0.1–0.25
Amphibolite	50–110	0.1–0.33
Marble	50–70	0.06–0.25

A rock with a low E-value is mechanically weak, as its resistance to deformation is small. Since strain is dimensionless, Young's modulus has the same dimension as stress, and is typically given in GPa (10^9 Pa). Young's modulus for diamond is more than 1000 GPa (very hard to strain), and for iron it is 196 GPa (under axial tension). It takes less force to squeeze aluminum (E = 69 GPa), and rubber is really easy to stretch elastically with typical values of E in the range 0.01–0.1 GPa. Table 6.1 gives some examples of experimentally determined strengths and their characteristic values of E.

Non-linear elasticity

Several minerals are linearly elastic, and we can see from Figure 6.4 that quartz and dolomite are two of them. Even some granites and dolomites obey Hookean elasticity for small strains, but most elastic materials do not, meaning that the line in σ–e-space is not straight. This implies that there is no constant stress–strain relationship, no single Young's modulus. The curves defined during straining (loading) and unstraining (unloading) may still be identical, in which case the material is **perfect elastic** (Figure 6.5b). In this case, the word *perfect* relates to the fact that the material perfectly recovers to its original shape. In many cases of experimental rock deformation, the stress–strain curves during elastic loading and unloading differ, and the material is said to be **elastic with hysteresis** (Figure 6.5c).

Elastic deformation and Poisson's ratio

Before looking at permanent deformation, let us return to our example of the elastically extended rod in Figure 6.3. Here, the axial stretching is accompanied by thinning of the rod. Therefore the area A_0 in Figure 6.3 shrinks as the rod extends. The same effect can be seen when pulling a rubber band: the more it is stretched, the thinner it gets. This effect is known as the **Poisson effect**.

If we consider an isotropic material, the shortening will be the same in any direction perpendicular to the elongation direction (long axis of the rod). If we put our rod in a coordinate system with the long axis along z and assume that volume is preserved, then the elongation along z is balanced by the elongations in the directions represented by the x- and y-axes (remember that negative elongations imply shortening):

$$e_z = -(e_x + e_y) \tag{6.6}$$

where e_z is the elongation parallel to the long axis of the rod and e_x is the perpendicular elongation. Since $e_x = e_y$ (assuming isotropy) we can write the equation as

$$e_z = -2e_x \tag{6.7}$$

or

$$0.5\, e_z = -e_x \tag{6.8}$$

In our example e_x becomes negative, because the rod gets thinner during stretching. We could of course shorten the rod in Figure 6.3. In this case the shortening causes the sample to expand in the perpendicular direction.

Equation 6.8 tells us that shortening in one direction is perfectly balanced by elongation in the plane perpendicular to the shortening direction. This holds true only for perfectly **incompressible materials**, i.e. materials that do not change volume during deformation. Rubber is a familiar material that is almost incompressible. In low-strain rock deformation there is always some volume change involved, and the 0.5 in Equation 6.8 must be replaced by a constant ν that relates the axial and perpendicular extensions. This constant is known as

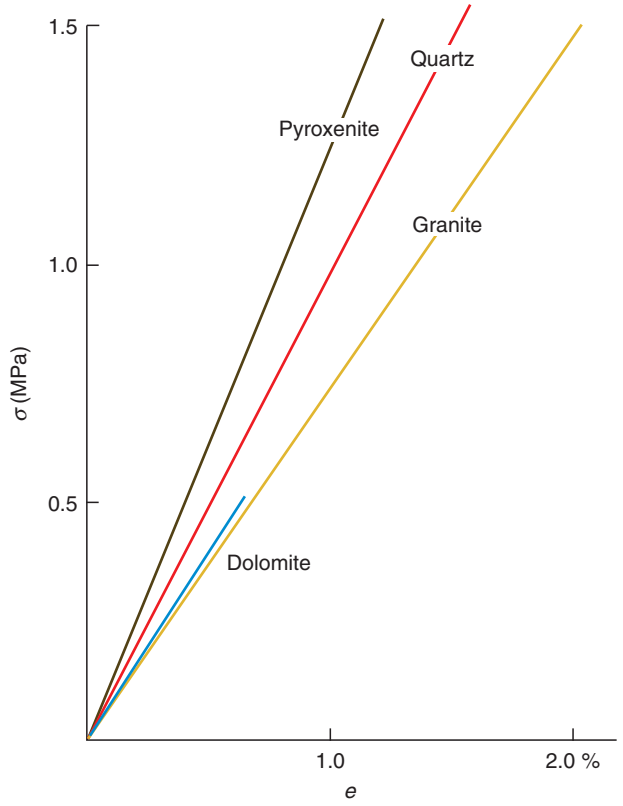

Figure 6.4 Some minerals and rocks show linear elasticity, which means that they follow the same linear path in stress–strain space during stress build-up as during unloading. Data from Griggs and Handin (1960) and Hobbs *et al.* (1972).

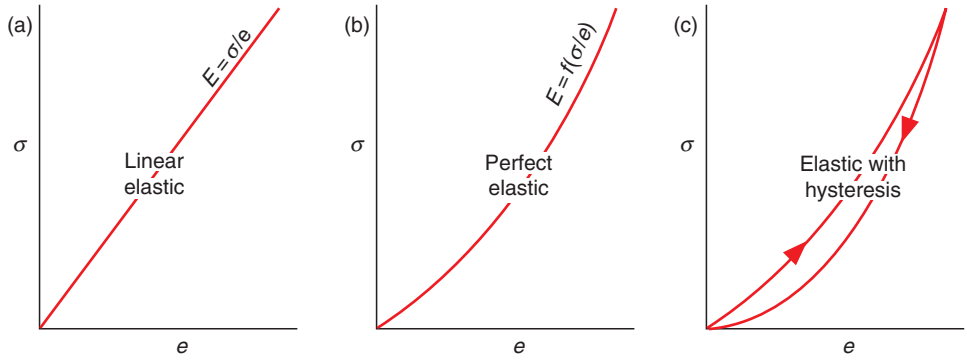

Figure 6.5 The three types of elasticity. (a) Linear elasticity where the loading (straining) and unloading (unstraining) paths are both linear and identical and where the gradient is described by Young's modulus. (b) Perfect elastic deformation follows the same non-linear path during loading and unloading. (c) Elasticity with hysteresis is where the path is non-linear and different during loading and unloading.

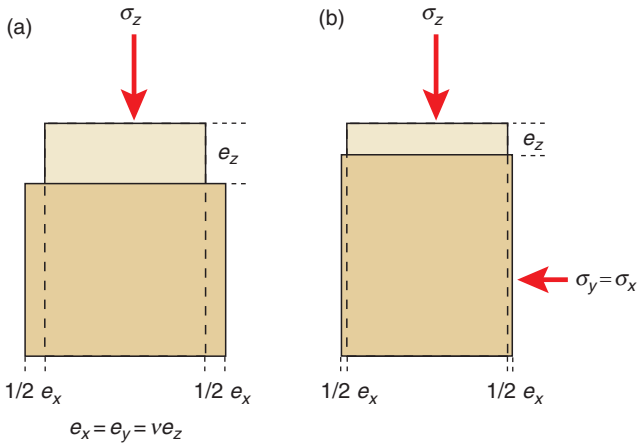

Figure 6.6 (a) A vertical stress (σ_z) applied to an unconstrained rod (unconstrained uniaxial compression). The dashed rectangle indicates the shape of the material prior to the uniaxial deformation. The horizontal elongation e_x is directly related to the vertical shortening through Poisson's ratio. (b) Adding a confining pressure gives a more realistic situation where horizontal stresses arise that counteract the effect of the vertical stress.

Poisson's ratio, which gives the ratio between the extensions normal and parallel to the stress vector σ_z in Figure 6.6:

$$\nu = -e_x/e_z \tag{6.9}$$

The minus is commonly omitted when referring to Poisson's ratio for rocks. The closer the Poisson's ratio gets to 0.5, the less compressible the material. Even steel changes volume during elastic deformation, and most steels have ν-values around 0.3, meaning that a contraction in one direction is not fully compensated for by perpendicular elongation. Most rocks have ν-values between 0.2 and 0.33. For comparison, ν for cork is close to 0, meaning that it hardly expands or shortens perpendicular to an applied stress. Curiously enough, some materials, such as polymer foams, have a negative Poisson's ratio; if these materials are stretched in one direction, they become thicker in perpendicular directions, i.e. a quite unusual scenario for a rock. Some ν-values for rocks and familiar media are given in Table 6.1.

In the crust, rocks are confined, and this puts restrictions on how much a rock volume can extend or shorten, particularly in the horizontal direction. For instance, a volume of sediment or sedimentary rock under burial would experience a vertical shortening that only to a small extent could be compensated for by horizontal extension. We could simulate this situation in the laboratory by confining our sample, and we would see that horizontal stresses arise that counteract the axial shortening e_z.

We now have the following expression for the component of vertical strain resulting from the vertical stress:

$$e_{z'} = \sigma_z/E \tag{6.10}$$

The horizontal stresses will give rise to vertical strains that counteract the effect of Equation 6.10:

$$e_{z''} = \nu\sigma_x/E \tag{6.11}$$

and

$$e_{z'''} = \nu\sigma_y/E \tag{6.12}$$

Thus, the total axial strain is

$$e_z = e_{z'} - e_{z''} - e_{z'''} \tag{6.13}$$

By substituting Equations 6.10, 6.11 and 6.12 into Equation 6.13 we obtain the following expression for the axial strain:

$$\begin{aligned} e_z &= (\sigma_z/E) - (\nu\sigma_x/E) - (\nu\sigma_y/E) \\ &= \frac{1}{E}\left[\sigma_z - \nu(\sigma_x + \sigma_y)\right] \end{aligned} \tag{6.14}$$

Similar expressions can be found for the horizontal stresses:

$$e_y = \frac{1}{E}\left[\sigma_y - \nu(\sigma_z + \sigma_x)\right] \tag{6.15}$$

and

$$e_x = \frac{1}{E}\left[\sigma_x - \nu(\sigma_z + \sigma_y)\right] \tag{6.16}$$

The generation of stresses perpendicular to the loading direction is an effect that is very relevant to rocks in the crust, and contributes to the state of stress in buried rocks. A consequence of confinement is that there will be no or very little horizontal strain ($e_x = e_y \approx 0$), which reduces the vertical shortening e_z. In fact, e_z will depend on both ν and σ_z. To find the vertical stress e_z we apply the boundary condition $e_x = 0$ to Equation 6.16 and obtain:

$$\frac{1}{E}\left[\sigma_x - \nu(\sigma_z + \sigma_y)\right] = 0 \tag{6.17}$$

Multiplying by E on each side gives:

$$\sigma_x - \nu(\sigma_z + \sigma_y) = 0 \tag{6.18}$$

Rearranging and using $\sigma_x = \sigma_y$ gives

$$\sigma_x = \sigma_y = \frac{\nu}{1-\nu}\sigma_z \tag{6.19}$$

Note that we have already seen this equation in the previous chapter during our discussion of the uniaxial-strain reference state (Equation 5.3). Also note that it is possible

BOX 6.1 POISSON'S RATIO AND SOUND WAVES

Poisson's ratio, named after the French mathematician Simeon Poisson (1781–1840), is a measure of a medium's compressibility perpendicular to an applied stress and can be expressed in terms of velocities of P-waves (V_P) and S-waves (V_S). P-waves or compressional waves are waves of elastic deformation or energy in which particles oscillate in the direction of wave propagation. Conventional seismic sections are based on P-waves. S-waves or shear waves are elastic body waves where particles oscillate perpendicular to the propagation direction. These are different ways of elastic deformation and their relation to Poisson's ratio is:

$$\nu = (V_P^2 - 2V_S^2)/2(V_P^2 - V_S^2)$$

Hence, if V_P and V_S can be measured, Poisson's ratio can be calculated. The ratio is useful in estimating rock and fluid properties in a petroleum reservoir. For example, if $V_S = 0$, then $\nu = 0.5$, indicating either a fluid (shear waves do not pass through fluids) or an incompressible material (which as already stated is not found in the crust). V_S approaching zero is characteristic of a gas reservoir.

to estimate Poisson's ratio from sound waves, as discussed in Box 6.1.

If pressure changes cause elastic deformation rather than directed force, then the **bulk modulus** K relates the pressure change Δp to volume change (volumetric strain):

$$K = \frac{\Delta p}{\Delta V / V_0} \tag{6.20}$$

The bulk modulus is the inverse of the compressibility of a medium, which is a measure of the relative volume change (volumetric strain) of a fluid or solid as a response to a pressure or mean stress change. The higher the value of bulk modulus, the more pressure is needed for the material to compress. Equation 6.20 is a specific form of Hooke's law and K is related to Young's modulus (E) and to the shear modulus (μ) by

$$K = \frac{E}{3(1-2\nu)} = \frac{2(1+\nu)}{3(1-2\nu)}\mu \tag{6.21}$$

Even though many low-strain or incipient deformation structures actually represent permanent or inelastic strain that forms beyond the stage of elasticity (see next section), elastic theory is commonly applied when, for example, fracture initiation and growth are modeled. This is to some extent justified when strain is small (a few percent or less), in which case the deviations from elasticity generally are small enough that elastic theory can successfully be used. In particular, **linear elastic fracture mechanics** is used as a simple way to explore and model the state of stress around fractures. It describes stress orientations and stress concentrations based on the geometry of the object (fracture) and the overall (remote) state of stress. However, we will not go deeper into this field here, but continue by looking at deformation beyond elasticity.

6.4 Plasticity and flow: permanent deformation

While elastic theory may work well for very small strains in the upper crust, heated rocks tend to flow and accumulate permanent deformation, and sometimes very large permanent strains. In this context it is useful to consider how fluids respond to stress. Rocks can never quite become fluids unless they melt, but at high temperatures and over geologic time they may get fairly close in terms of rheology.

Viscous materials (fluids)

The ease with which fluids flow is described in terms of their **viscosity** η. Viscosity and laminar flowing fluids were first explored quantitatively by Sir Isaac Newton. He found that the shear stress and shear strain rate are closely related:

$$\sigma_s = \eta\dot{\gamma} \tag{6.22}$$

where η is the viscosity constant, and $\dot{\gamma}$ is the shear strain rate, as indicated in Figure 6.7. A material that deforms according to this equation is a **Newtonian fluid** or a **linear** or **perfectly viscous material**. The constitutive equation for viscous materials can also be expressed in terms of normal stress and elongation rate:

$$\sigma_n = \eta\dot{e} \tag{6.23}$$

Viscous deformation implies dependence of stress on strain rate: higher stress means faster flow or more rapid strain accumulation.

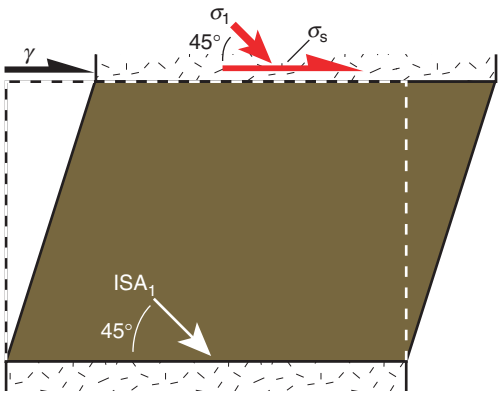

Figure 6.7 Shearing of a medium (fluid) implies that the maximum principal stress is acting at 45° to the surface. For small strains this is equal to the orientation of ISA_1. Increasing the stress results in faster shearing if the material is viscous. The relation between the two is determined by the viscosity of the material.

These two equations state that there is a simple, linear relationship between stress and strain rate (not strain): the higher the stress, the faster the flow. So, while stress was proportional to strain for elastic deformation, it is proportional to strain rate for viscous media. Viscous deformation can therefore be said to be **time-dependent deformation**; strain is not instant but accumulates over time, at rates discussed in Box 6.2.

A perfectly viscous material flows like a fluid when influenced by an external force. This means that there is no elastic deformation involved. Hence, when the force is removed, a viscous material does not recover to its original shape. Viscous deformation is therefore said to be **irreversible** and creates **permanent strain**.

A physical analogy to a perfectly viscous material is an oil-filled cylinder with a perforated piston (Figure 6.2d). When the piston is pulled, it moves through the oil at a constant speed that is proportional to the stress (Figure 6.2e). When the force is removed, the piston stops and remains where it is. If the oil is replaced by a

BOX 6.2 HOW QUICKLY DO ROCKS DEFORM?

Strain rate is a measure of how fast a rock object changes length or shape. Since strain is dimensionless, strain rate has the somewhat peculiar dimension s^{-1} (per second). There are generally two different types of strain rate that we must consider. The simplest is the **rate of elongation** and is denoted $\dot{\varepsilon}$ or $\dot{e}$. This is elongation per unit time (second):

$$\dot{e} = \frac{e}{t} = \left(\frac{l - l_0}{t l_0}\right)$$

We can also call this the extension rate or contraction rate. In experiments this is closely related to the speed at which we squeeze a sample. For an axial compression test that lasts for one hour, where the sample is shortened at 10%, the elongation rate becomes

$$\dot{e} = \frac{-0.1}{3600\ \text{s}} = -2.778 \cdot 10^{-5}\ \text{s}^{-1}$$

In some geologic settings the **shear strain rate** may be more appropriate. Here the change in shear strain over time is considered, and this is denoted $\dot{\gamma}$. Its dimension (s^{-1}) is the same as for elongation rate, and they are clearly related, since shear deformation also results in elongation. The two are, however, not linearly related, and it is important to clearly distinguish between the two.

Typical natural geologic strain rates are 10^{-14}–$10^{-15}\ s^{-1}$ and thus much slower than the ones we observe in the rock deformation laboratory ($10^{-7}\ s^{-1}$ or faster). Clearly, this is a challenge when applying experimental results to naturally deformed rocks. In many cases temperature is increased in the laboratory to "speed up" plastic deformation mechanisms and thus increase strain rates. Experimental strain rates must then be scaled down together with temperature before they can be compared to natural rock deformation. Alternatively, the processes must be studied at smaller length scales.

more viscous fluid, such as syrup or warm asphalt, then the force must be increased for strain rate to be maintained. Otherwise, the piston will move at a lower speed. If the oil is heated, viscosity goes down and the force must be decreased to keep the strain rate constant. Thus, temperature is an important variable when viscosity is considered.

In layered rocks the **relative viscosity** is also of great interest, as the most viscous (stiff) layers tend to boudinage/fracture or buckle under layer-parallel extension or shortening. Relative viscosity is related to **competency**, where a competent layer is stiffer or more viscous than its surroundings.

Competency is resistance of layers or objects to flow. The term is qualitative and relative to that of its neighboring layers or matrix.

Only fluids are truly viscous, so that in geology only magma, salt and perhaps overpressured (fluidized) mud can be modeled as truly viscous media. However, viscosity is a useful reference when dealing with certain aspects of plastic deformation. We will therefore return to viscosity in a discussion of folding and boudinage in later chapters. Note that **non-linear viscous behavior** has been recorded experimentally for deforming hot rocks and is perhaps more applicable to rocks than linear viscosity. Non-linear behavior in this context simply means that the viscosity changes with strain rate, as illustrated in Figure 6.8. For numerical modeling of folds, both linear and non-linear viscosity is assumed, while theoretical modeling of boudins require non-linear viscosity.

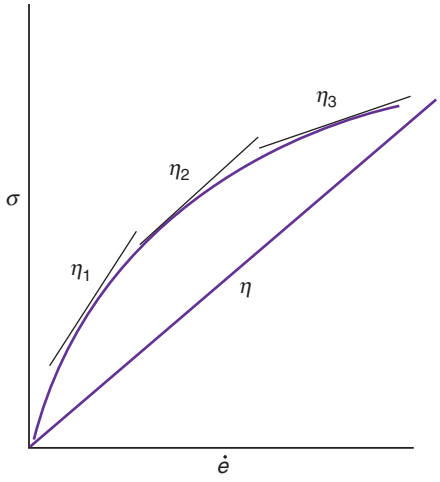

Figure 6.8 Linear (straight line) and non-linear viscous rheology in stress–strain rate space. The slope of the straight line is the viscosity (stress over strain). The non-linear curve has a gradually changing gradient, which is called the effective viscosity. The steepest gradient implies the highest viscosity, which means that it deforms relatively slowly for any given stress condition.

Viscosity is stress divided by strain rate, and is thus measured in the unit of stress multiplied by time, represented by Pa s or $kg\,m^{-1}\,s^{-1}$ in the SI system. The unit poise was used in the past, where 1 poise = 0.1 Pa s. While the viscosity of water is around 10^{-3} Pa s, that of a glacier (ice) is about 10^{11}–10^{12} Pa s. Glass flows very slowly at room temperature, with a viscosity of 10^{14} Pa s. Viscosity estimates of rocks are greatly variable, but are generally many orders of magnitude larger. Even salt, with a viscosity of $\sim 10^{17}$ Pa s (grain-size dependent) as it flows to form salt diapirs and other salt structures discussed in Chapter 19, is 1000 times more viscous than glass. The mantle underneath the lithosphere is considered as a fluid in many calculations, and it can be estimated to have a viscosity of $\sim 10^{21}$ Pa s on average, increasing downward.

Plastic deformation (flow of solid rock)

Ideally, viscous materials (fluids) react to stress according to Equations 6.22 and 6.23 no matter how small the stress may be. Under most realistic conditions a certain amount of stress is required for permanent strain to accumulate. In fact, the most important difference between fluids and solids is that solids can sustain shear stresses while fluids cannot. For rocks and other solids, elastic deformation occurs for strains up to a few percent.

Beyond the **elastic limit** or the **yield stress**, permanent strain is added to the elastic strain (Figure 6.9). If permanent strain keeps accumulating under a constant stress condition, then we have perfect **plastic deformation** (Figure 6.2g–i). When the stress is removed after a history of elastic–plastic deformation only the plastic strain will remain (the elastic component is by definition non-permanent). Another requirement for a deformation (strain) to be called plastic is that of continuity or coherency, i.e. the material must not fracture at the scale of observation.

Plastic strain is the permanent change in shape or size of a body without fracture, accumulated over time by a sustained stress beyond the elastic limit (yield point) of the material.

Plastic strain is associated with microscale deformation mechanisms such as dislocation movements, diffusion or twinning (Chapter 10). Because of the many mechanisms involved at the atomic level, plastic flow

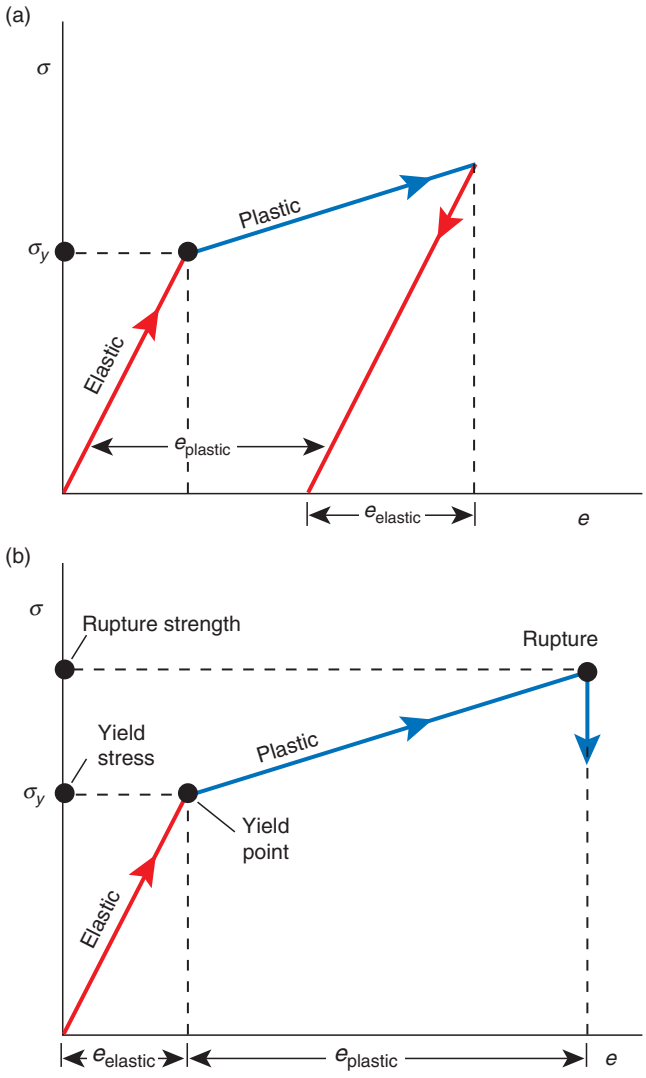

Figure 6.9 Stress–strain curve for elastic–plastic deformation. (a) Elastic strain is replaced by plastic strain as the yield stress (σ_y) is reached. When stress is removed the elastic strain is released, and the plastic or permanent strain remains. (b) In this case the stress is increased to the point where brittle rupture occurs.

does not lend itself to simple physical parameters the way elastic and viscous deformations do. Instead, there are different equations or **flow laws** for different plastic flow mechanisms. A general example is the power-law equation on the form

$$\dot{e} = A\sigma^n \exp(-Q/RT) \qquad (6.24)$$

where A is a constant, R is the gas constant, and T and Q are the absolute temperature and activation energy, respectively. For $n = 1$ the material flows as a perfectly viscous fluid, and the flow is linear. For rocks this is approximated at high temperatures. We will return to flow laws and their underlying deformation mechanisms in Chapter 10.

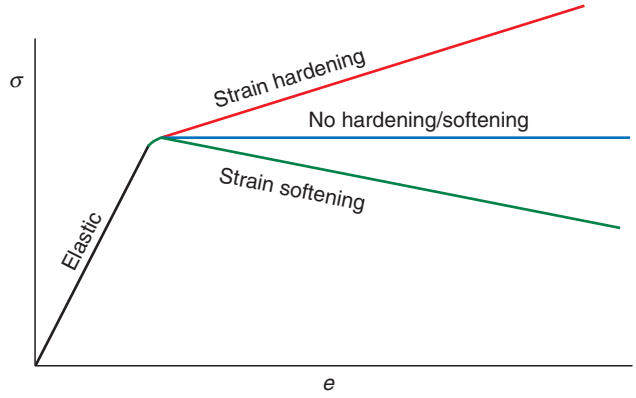

Figure 6.10 Stress–strain curve for elastic–plastic material with hardening, softening, and no hardening/softening properties.

Perfectly plastic materials

A **perfectly plastic material**, or **Saint Venant material**, is one where the stress cannot rise above the yield stress and strain can continue to accumulate without any change in the stress level (Figure 6.2h). The strength is not strain rate sensitive: it does not matter how fast you force the material to flow – the stress–strain curve will not change. A perfectly plastic material is also incompressible. Where there is an additional component of elastic deformation, then the material is called **elastic perfect plastic** (such as the blue middle curve in Figure 6.10). A mechanical analog to perfect plastic deformation is a rigid object resting on a friction surface. Force is increased without any deformation until the frictional resistance between the object and the surface (corresponding to the yield strength) is exceeded (Figure 6.2g). From this point on, the force cannot exceed the frictional resistance except during acceleration, regardless of the velocity.

Strain hardening and softening

Rocks do not generally behave as perfectly plastic materials during plastic deformation. Strain rate is likely to have an effect, and the stress level is likely to change during the deformation history. If we have to increase the applied stress for additional strain to accumulate (Figure 6.10, red curve), then we are dealing with a material science phenomenon called **work hardening** or **strain hardening**.

Strain hardening means that the stress necessary to deform the rock must be increased for strain to accumulate, because the rock becomes stronger and harder to deform.

Strain hardening is particularly apparent in metals, which can be made harder or more resistant through plastic deformation. Just bend a metal wire, and then try to bend it exactly back to its original shape. It will be difficult, because the bent part of the metal has hardened: it takes more stress to retrodeform the bend than it takes to deform an adjacent area. If you are stubborn and keep bending the wire back and forth, the hardening is going to be more and more pronounced until the wire eventually breaks: strain hardening can result in a transition from plastic to brittle deformation if the level of stress is increased. In geology, strain will try to relocalize to an adjacent zone, which may explain why many shear zones get wider as strain accumulates (see Chapter 15).

Strain hardening (during plastic deformation) is related to deformation at the atomic scale. During deformation, atomic-scale defects known as **dislocations** (see Chapter 10) form and move. These dislocations intertangle, which makes it harder to accumulate strain. Hence, more stress is needed to drive deformation, and we have strain hardening. Elevated temperature eases the motion of dislocations and thus reduces the effect of strain hardening. In other words, heating the bent wire makes rebending easier.

If there is no strain hardening and the material keeps deforming without any increase in the applied force or stress, then the process is called **creep**. If, in addition, the strain rate

$$\dot{e} = \frac{\mathrm{d}e}{\mathrm{d}t} \tag{6.25}$$

is constant, then we have **steady-state flow**. Steady-state flow may imply that dislocation movements are quick enough that strain can accumulate at a constant rate for any given stress level. The speed at which dislocations can move around in a crystal depends on differential stress, temperature, and the activation energy that it takes to break atomic bonds. The relationship between dislocation-related strain and these variables can therefore be expressed in a flow law of the type portrayed in Equation 6.24 (see Chapter 10).

Work softening or **strain softening** is the case when less stress is required to keep the deformation going. A geologic example is the effect of grain size reduction during plastic deformation (mylonitization). Grain size reduction makes deformation mechanisms such as grain boundary sliding more effective because of the increase in grain surface area. Other factors that can lead to softening are the recrystallization into new and weaker minerals, the introduction of fluid(s) and, as already mentioned, an increase in temperature.

The terms strain hardening/softening are also used in connection with the growth of brittle deformation structures, such as deformation bands, although originally defined within the context of plastic deformation. Strain hardening can, for instance, occur during deformation of unconsolidated sand or soil, where interlocking of grains may lead to strain hardening.

6.5 Combined models

Rocks and other natural materials are rheologically complex and generally do not behave as perfect elastic, viscous or plastic materials. It may therefore be useful to combine these three types of deformations in order to describe natural rock deformation. Such combinations are commonly illustrated by means of a spring (elastic), a dashpot (viscous) and a rigid block that will not slide until some critical stress is exceeded (plastic) (Figure 6.2a, d, g).

We have already briefly touched upon one combined model, which is the combination of elastic and plastic deformation. This is the situation where stress and elastic strain increase until the yield point is reached, beyond which the deformation is plastic. A material that responds in this way is **elastic–plastic** or a **Prandtl material**. The typical mechanical analog is shown in Figure 6.11a. The elastic–plastic model is commonly applied to large-scale deformation of the entire crust and the mantle.

A **viscoplastic** or **Bingham material** is one that flows as a perfectly viscous material, but only above a certain yield stress (a characteristic of plastic behavior). Below this yield stress there is no deformation at all. Both rheological experiments on lava and the actual morphology of real lava flows suggest that, over a significant range of temperatures, (liquid) silicic lava behaves like a viscoplastic fluid; that is, due to its crystal content, lava has a yield stress. Paint is a more common fluid that shows viscoplastic behavior: It takes a certain yield stress for it to flow, which prevents thin layers from running off a newly painted wall. The classic mechanical analog is a serial combination of the dashpot (a perforated piston inside a fluid-filled cylinder) and a rigid object resting on a friction surface (Figure 6.11d).

Viscoelastic models combine viscous and elastic behavior. **Kelvin viscoelastic behavior** is where the deformation process is reversible but both the accumulation and recovery of strain are delayed. Viscoelastic materials can be viewed as intermediate states between

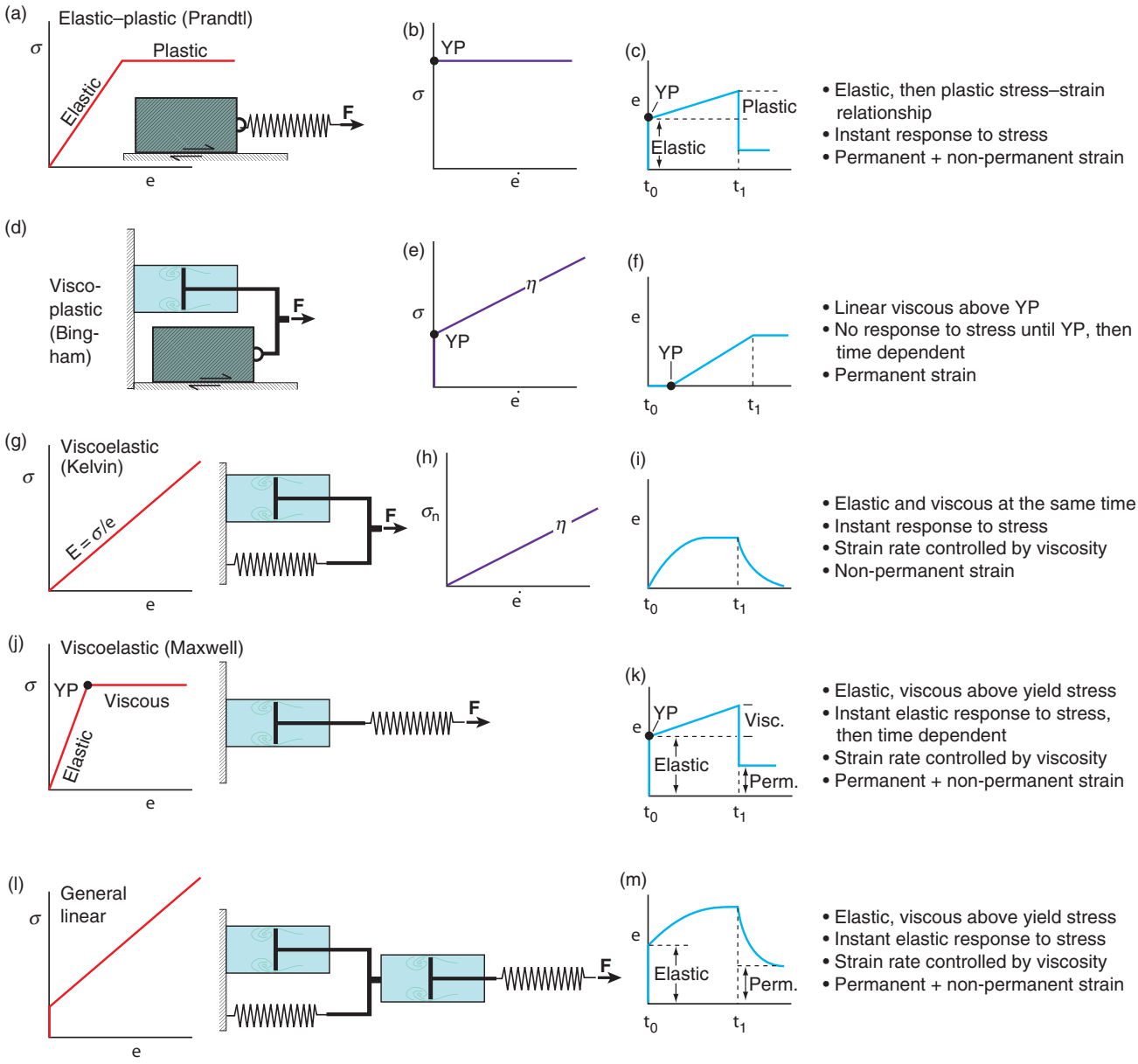

Figure 6.11 Combinations of elastic, viscous and plastic deformation illustrated by mechanical analogs (left), stress–strain (rate) curves and strain history curves (right). Perfect elastic deformation is represented by a spring, while a box with basal friction represents perfect plastic deformation. Perfect viscous deformation is represented by a dashpot. YP, yield point; t_1, time of stress removal.

fluids and solids where both the flow of a fluid and the elastic response of a solid are present. A physical model of a Kelvin viscoelastic material would be a parallel arrangement of a spring and a dashpot (Figure 6.11g). Both systems move simultaneously under the influence of stress, but the dashpot retards the extension of the spring. When the stress is released the spring will return to its original position, but again the dashpot will retard the movement. Such deformation is therefore referred to as **time dependent**.

The constitutive equation for the Kelvin viscoelastic behavior reflects the combination of viscosity and elasticity:

$$\sigma = Ee + \eta\dot{e} \tag{6.26}$$

A related viscoelastic model is the **Maxwell model**. A Maxwell viscoelastic material accumulates strain from the moment a stress is applied, first elastically and thereafter in a gradually more viscous manner. In other words, its short-term reaction to stress is elastic while its long-

term response is viscous, i.e. the strain becomes permanent. This model fits the mantle quite well: It deforms elastically during seismic wave propagation and viscously during mantle convection or flow related to lithospheric loading (e.g. glacial loading). The mechanical analog now consists of a serial arrangement of a dashpot and a spring (Figure 6.11j). A familiar example is the stirring of bread dough. Just a little push creates elastic deformation, while more serious stirring creates permanent deformation. When the stirring is stopped, the dough gradually comes to rest after rotating slightly in the opposite direction due to the release of the elastic component. The constitutive equation for Maxwell viscoelastic deformation is

$$\dot{e} = \sigma/E + \sigma/\eta \tag{6.27}$$

Viscoelastic models are useful in large-scale modeling of the crust, where the elastic deformation describes its short-term response to stress and the viscous part takes care of the long-term flow.

General linear behavior is a model that more closely approximates the response of natural rocks to stress. Its mechanical analog is shown in Figure 6.11l, where the two viscoelastic models are placed in series. The first application of stress accumulates in the elastic part of the Maxwell model. Continued stress is accommodated within the rest of the model. With the removal of stress the elastic strain is recovered first, followed by the viscoelastic component. However, some strain (from the Maxwell model) is permanent.

While most of these combined idealized models predict a linear stress–strain (rate) relationship, there is no reason to assume that plastically deforming rocks follow such simple relationships during natural deformations. In fact, experimental results indicate that they do not, and a power-law (i.e. non-linear) relationship between stress and strain rate of the form indicated in Equation 6.24 with $n > 1$ exists (curved line in Figure 6.8). This relationship characterizes **non-linear material behavior**. Nevertheless, the idealized models are useful reference models, just as deformations such as simple shear and pure shear are useful reference deformations in strain analysis.

6.6 Experiments

Experiments form the basis for much of our understanding of flow in rock. In the laboratory we can choose the medium and control physical variables such as temperature, pressure, stress conditions and strain rate. An obvious disadvantage is that we do not have enough time to apply geologic strain rates, which makes it challenging to compare laboratory results to naturally deformed rocks.

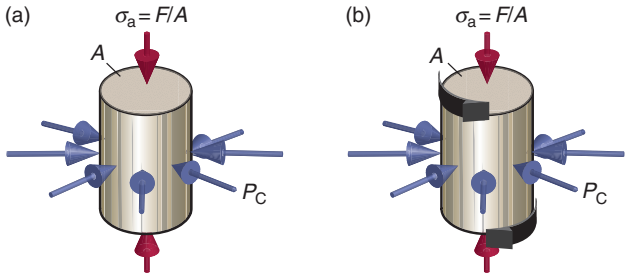

Figure 6.12 (a) The standard loading configuration in triaxial rigs. The axial load σ_a and the confining pressure (P_c) are controlled independently. (b) A configuration where a torsion is added to the axial compression and the confining pressure. This configuration allows for large shear strains to accumulate.

There are many different experimental setups, depending on the property one wants to explore and the physical conditions one wants to impose. The most common one is the triaxial deformation rig where cylindrical samples are exposed to a confining pressure and a principal axial stress (P_c and σ_a in Figure 6.12a). All stresses are compressive, and the sample is shortened when the confining pressure is smaller than the axial compressive stress. If the confining pressure is larger, then the sample extends axially.

There are thus two aspects of stress in this setup. One is the axial or directed stress (anisotropic component), which is the applied force divided by the cross-sectional area of the cylindrical sample. The other is confining pressure (isotropic component), which is created by pumping up the pressure in a confining fluid or soft material. Confining pressures up to 1 GPa are typical, while temperatures may be up to 1400 °C and strain rates 10^{-3} to 10^{-8} s^{-1}. The stress referred to is then typically differential stress (Section 5.8). A furnace around the sample chamber is used to control the temperature of the sample during the deformation.

Besides uniaxial or pure shear deformation, some deformation rigs can impose a rotary shear motion (shear strain) on the sample (Figure 6.12b). Most samples that have been deformed experimentally are monomineralic, such as quartzite or calcite. It is frequently assumed that the properties of single minerals such as quartz (upper crust), feldspar (crust) or olivine

(mantle) control the rheological properties of various parts of the lithosphere. More data from deformation of polycrystalline samples are therefore needed.

Constant stress (creep) experiments

Experiments can be sorted into those where strain rate is held constant and those where a constant stress field is maintained throughout the course of the experiment. The latter are referred to as creep experiments and involve the phenomenon called **creep**. Creep is a fairly general term used for low-strain-rate deformations. Hence, it is used in geology for anything from slow down-slope movement of soil, via slow accumulation of displacement along faults (brittle creep), to the slow yielding of solids under the influence of stress (ductile or plastic creep). Plastic creep is what we are interested in here, and in the current context it is defined as follows:

Creep is the plastic deformation of a material that is subjected to a persistent and constant stress when that material is at a high homologous temperature.

Homologous temperature T_H is the ratio of a material's temperature T to its melting temperature T_m using the Kelvin scale:

$$T_H = \frac{T}{T_m} \tag{6.28}$$

For water, with $T_m = 273$ K, the homologous temperature at 0 K is $0/273 = 0$, $273/273 = 1$ at 273 K (0 °C), and $137/273 = 0.5$ at 137 K (−100 °C). The homologous temperatures involved in creep processes are greater than 0.5, and creep processes become more active as T_H approaches 1. This is why glaciers can flow: ice deforms by creep at the high homologous temperatures of natural glaciers. The use of homologous temperature makes it possible to compare solids with different melting points. For instance, it turns out that ice and olivine behave fairly similarly at a homologous temperature of 0.95, which corresponds to −14 °C for ice and 1744 °C for olivine.

Figure 6.13 shows a generalized strain–time diagram for a creep experiment. Stress is rapidly increased to a fixed level and, after accumulation of elastic strain, creep occurs at a decreasing strain rate. This first stage of creep is called **primary** or **transient creep**. After some time, strain accumulates more steadily and the region of **secondary** or **steady-state creep is reached**. Then the **tertiary creep** stage is entered where microfracturing or recrystallization causes an increase in strain rate. This stage is terminated when a macroscopic fracture develops.

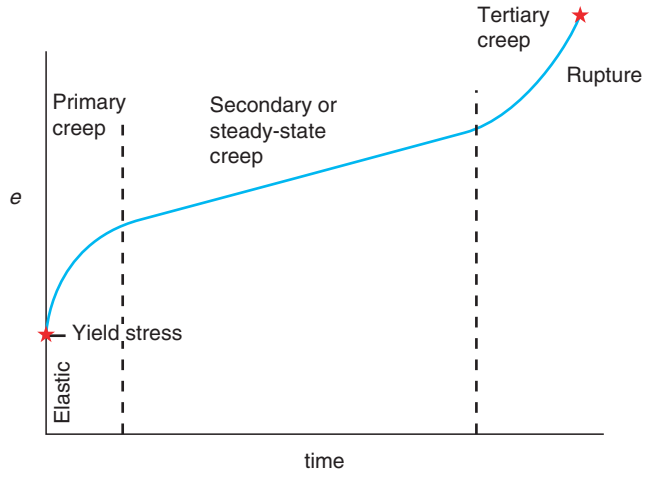

Figure 6.13 Strain–time curve for creep experiment. After initial elastic deformation, three types of creep can be defined. See text for discussion.

Steady-state creep is perhaps the most interesting one to structural geologists, because it appears that rocks can deform more or less steadily for extended periods of time. The constitutive equation during steady-state creep is the power law shown in Equation 6.24.

Constant strain rate experiments

During experiments where the strain rate is fixed, the sample first deforms elastically before accumulating permanent strain, i.e. the general behavior of rocks below the level of fracturing. An increase in stress is required at low temperatures in order to maintain a constant strain rate, consistent with the definition of strain hardening. For higher temperatures or low strain rates, strain does not harden and the deformation is close to steady state. A constitutive law in the form of Equation 6.24 is then in effect.

6.7 The role of temperature, water etc.

An increase in **temperature** lowers the yield stress or weakens the rock. We can see this from Figure 6.14 (a and b), where warmer-colored curves shows that marble can sustain less differential stress if temperature goes up. Think of a spring of the type shown in Figure 6.2a. We may be able to pull it quite hard at room temperature, but if we heat it up, we cannot pull it as hard before plastic (permanent deformation) occurs. In both examples, the temperature increase activates microscale crystal-plastic processes such as dislocation movements and diffusion (Chapter 10).

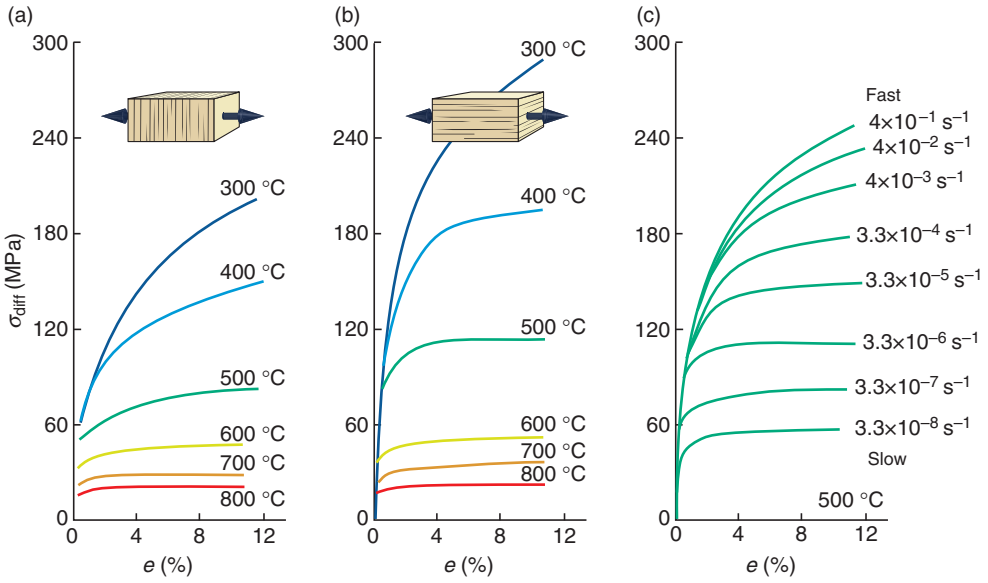

Figure 6.14 Stress–strain curves for Yule marble extended (a) normal and (b) parallel to the foliation. Data from Heard and Raleigh (1972). (c) Stress–strain curves for Yule marble at 500 °C for a variety of strain rates. From Heard (1960).

It also lowers the ultimate rock strength, which is the (differential) stress at which the rock fractures.

Increasing the **strain rate** means increasing the flow stress level, and this is clearly seen from the curves in Figure 6.14c. Since laboratory strain rates must be considerably lower than natural strain rates in most cases, this means that we must apply higher stresses to deform a rock in the laboratory, even if the temperature is the same in the laboratory experiment as in the natural setting we want to explore. As we learned from Figure 6.14a, b, increasing temperature weakens the rock and therefore counteracts this effect. An increased strain rate may also mean that less plastic strain accumulates because the rock may fracture at an earlier stage. Just think about glaciers that consist of slowly flowing ice that can be shattered by a swift hammer stroke. Parts of the Earth behave in a viscous manner because of low strain rates. Increasing the strain rate also makes the rock stronger. Conversely, rocks are weaker at lower strain rates because crystal-plastic processes can then more easily keep up with the applied stress.

Increased **presence of fluids** tends to weaken rocks, lower the yield stress and enhance crystal-plastic deformation. Fluid composition may however also influence rock rheological properties.

Increasing the **confining pressure** allows for larger finite strain to accumulate before failure and thus favors crystal-plastic deformation mechanisms. In simple terms, this is related to the difficulties involved in opening fractures at high confining pressure. The effect of increased confining pressure is counteracted by any increase in pore pressure (for porous rocks), which reduces the effective stress.

The presence of **fluids** (water) in the crystal lattice(s) may lower the strength or yield point significantly. Because of the increasing solubility of water with increasing pressure for many silicates, the effect is pressure dependent.

Non-isotropic features (Box 6.3) such as a preexisting foliation must always be considered. Figure 6.14a, b illustrates how a weak foliation in marble makes foliation-parallel extension more difficult (it takes a higher differential stress to obtain the same amount of strain). Note that the effect decreases with increasing temperature.

Even for monomineralic rocks, **grain size** and **crystallographic fabric** (preferred crystallographic orientation of minerals) may cause the rock to react differently, depending on the orientation of the applied forces. The anisotropy of olivine crystals is illustrated in Figure 6.15. The reaction to stress depends on the orientation of the applied forces relative to the dominant slip systems in olivine. Penetrative crystallographic fabrics may exist in the mantle, which may give the mantle a significant mechanical anisotropy that can influence location of rifting, strike-slip zones and orogeny. The effect of grain size itself depends on the microscale deformation mechanism during deformation, but in the plastic regime where dislocation creep (see Chapter 10) occurs, grain size reduction tends to imply strain weakening. In contrast, grain size reduction in the frictional (brittle) regime almost always implies strain hardening because of interlocking of grains.

Increasing the temperature, increasing the amount of fluid, lowering the strain rate and, in plastically deforming rocks, reducing the grain size all tend to cause strain weakening.

BOX 6.3 ISOTROPIC OR HOMOGENEOUS?

These are two related terms, but with a significant difference. **Homogeneous** means being similar or uniform, while **isotropic** means having properties that do not vary with direction. They are used in various aspects of structural geology, for instance about strain. **Homogeneous strain** means that the state of strain is identical in any one piece of the area or volume in question. It tells us nothing about the relative magnitudes of the principal strains. An **isotropic strain** means that the volume has been shortened or extended by the same amount in every direction. It involves no change in shape, only a change in volume. This is the **isotropic volume change** or volumetric strain from Chapter 3. Recall that volume can change by an equal change of length in all directions (isotropic) or preferentially in one direction (anisotropic).

Isotropic stress is a state where all three principal stresses are of equal magnitude. If they are not, stress can still be homogeneous if the state of stress is the same in every part of the rock.

A **fabric** (penetrative foliation and/or lineation) can be uniform throughout a sample, in which case the rock is homogeneous. However, a fabric represents an anisotropy because it causes the physical properties to be different in different directions. One could envisage that sliding preferentially takes place along the foliation, or that the stress–strain relationship is different in a sample when loaded parallel and perpendicular to the foliation (Figure 6.14a, b). Even a single, perfect crystal, which represents a homogeneous volume, can be anisotropic. This is the case with olivine, which has different mechanical properties along different crystallographic axes.

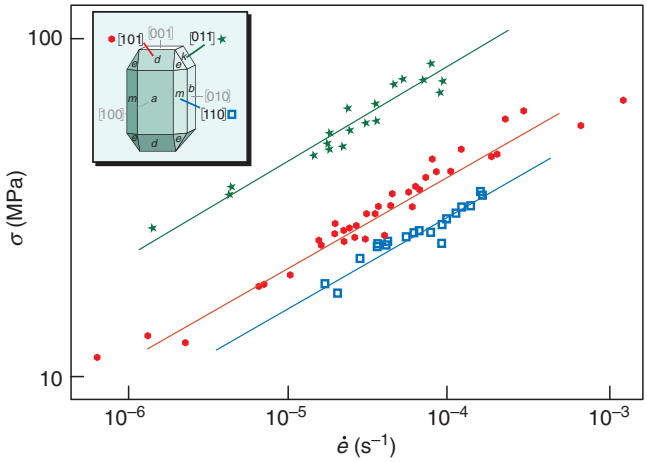

Figure 6.15 Stress–strain rate curves for dry olivine single crystals compressed in three different crystallographic directions. At any strain rate, deformation is easier for crystals shortened in the [110] direction, due to the lower strength of the (010)[100] slip system (see Chapter 10). Data from Durham and Goetze (1977).

6.8 Definition of plastic, ductile and brittle deformation

Ductile and brittle are two of the most commonly used terms in structural geology, both within and outside of the fields of rheology and rock mechanics. Again we have the challenge that these terms are given different meanings by different geologists in different contexts.

In the field of rheology and rock mechanics, a **ductile material** is one that accumulates permanent strain (flows) without macroscopically visible fracturing, at least until a certain point where its ultimate strength is exceeded. On the contrary, a **brittle material** is one that deforms by fracturing when subjected to stress beyond the yield point. To a rock-mechanics-oriented geologist, ductile materials show classic stress–strain curves such as the ones shown in Figure 6.9.

Ductile structures are well represented in metamorphic rocks, i.e. rocks that have been deformed in the middle and lower part of the crust. Ductile deformation also occurs in soils and unconsolidated to poorly consolidated sediments where distributed deformation rather than discrete fracturing occurs, even though the **deformation mechanisms** responsible for the ductile deformation in these cases are quite different. Hence, ductile deformation is, as illustrated in Figure 6.16, a scale-dependent structural style and not related to microscale deformation processes:

Ductile deformation preserves continuity of originally continuous structures and layers, and describes a scale-dependent deformation style that can form by a range of deformation mechanisms.

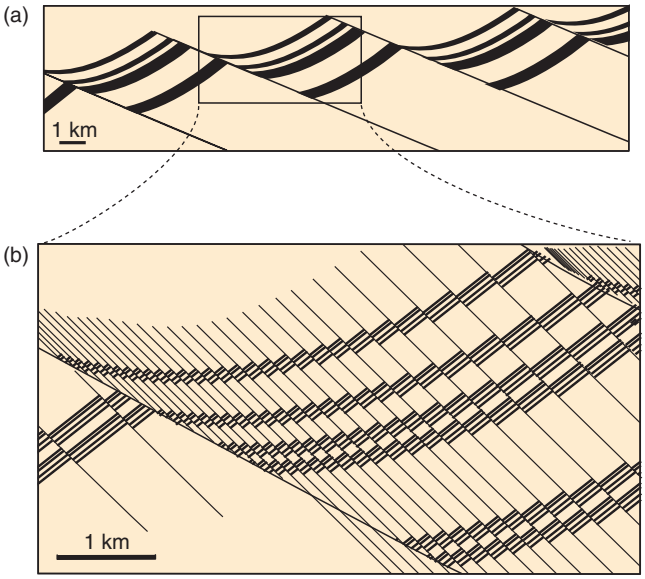

Figure 6.16 The scale-dependent nature of the ductile deformation style illustrated by a regional profile (top), where layers look continuous (ductile deformation style), and close-up (bottom), where it becomes apparent that the deformation is by multiple small faults. This example is directly relevant to seismic versus subseismic deformation.

Hence, a deformed area or volume can be ductile at the seismic or mesoscopic scale and brittle at the subseismic or microscopic scale (Figure 6.16).

In the search for a term that can be used specifically about the ductile deformation that occurs in the middle and lower crust, we turn to the term **plasticity**. The overall physical use of this term is as follows:

Plastic deformation is generally defined as the permanent change in shape or size of a body without fracture, produced by a sustained stress beyond the elastic limit of the material due to dislocation movement.

The discovery that plasticity can be explained in terms of the theory of dislocations (Chapter 10) was made in the 1930s and the theory implies that plasticity initiates where the mineralogy starts to deform by means of dislocation motion, which in general means 10–15 km depth. When needed, the term **crystal-plasticity** or **crystal-plastic deformation** can be used to distinguish this type of plasticity from that used in soil mechanics about water-rich soil. In this text we will restrict the term plasticity to intracrystalline deformation mechanisms other than brittle fracturing, rolling and frictional sliding of grains.

The latter microscale deformation mechanisms are referred to as brittle deformation mechanisms, indicating that the term brittle can be used about both deformation style and microscale deformation mechanisms. We can therefore talk about brittle deformation mechanisms, implying frictional deformation at the microscale, and about the **brittle regime**, where such mechanisms dominate. If we want to use an expression that is not also used about deformation style we can apply the term **frictional deformation** or **frictional regime**.

Plastic or crystal-plastic mechanisms occur at the atomic scale without breaking of atomic bonds by means of creep processes such as dislocation migration. The term plastic is here used in a broad sense. In a strict sense it should be distinguished from diffusion and dissolution, which also are non-brittle (non-frictional) deformation mechanisms. So, if we want to be very specific, there are brittle or frictional deformation mechanisms on one side and plastic, diffusion and dissolution mechanisms on the other.

Figure 6.17 summarizes how the term ductile refers to deformation style while the term brittle can refer to both style and microscale mechanism, and how plasticity and frictional deformation are directly related to microscale mechanism.

6.9 Rheology of the lithosphere

Rocks and minerals react differently to stress and depend on crystallographic anisotropy, temperature, presence of fluids, strain rate and pressure. Three minerals are particularly common in the lithosphere and therefore of particular interest. These are quartz and feldspar, which dominate the crust, and olivine, which controls the rheology of the upper mantle.

Quartz deforms by brittle mechanisms up to about 300–350 °C, which for typical continental temperature gradients corresponds to crustal depths of around 10–12 km. At greater depths, crystal-plastic mechanisms (creep mechanisms) and diffusion dominate. Feldspar, with its well-developed cleavages, is different because of the ease of cleavage-parallel cracking and the difficulty of dislocation glide and climb (crystal-plastic deformation mechanisms). It thus deforms in a brittle manner up to ~500 °C and depths of 20–30 km. However, olivine is brittle down to ~50 km depth.

A simple model subdivides the crust into an upper part dominated by brittle deformation mechanisms and a lower part where plastic flow dominates. The transition

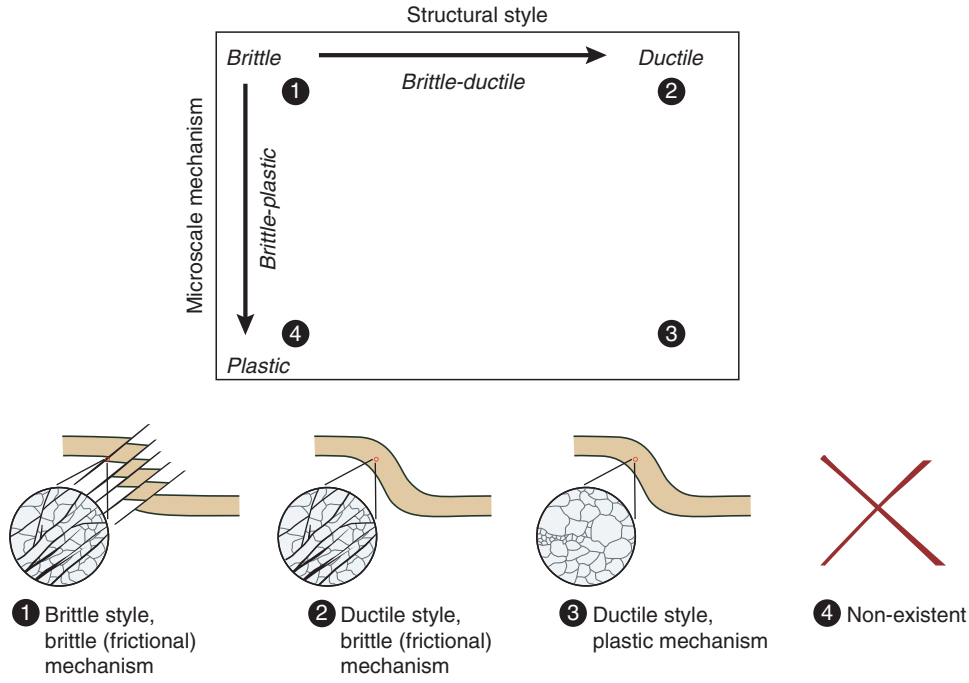

Figure 6.17 Illustration of the relationship between ductile and brittle deformation styles and plastic and brittle (frictional) microscale mechanisms. Example 4 is impossible because we cannot form a brittle deformation style by means of 100% plastic mechanisms.

is referred to as **the brittle–plastic transition** (brittle–ductile transition in some texts). For a theoretical uniform monolithologic crust with a gradual downward increase in temperature, we would expect a single brittle–plastic transitional zone at the depth where temperature-activated flow becomes important. The strength of the lower crust will then follow the constitutive equation shown in Equation 6.24, while the brittle (frictional) upper crust will follow another law known as Byerlee's law. Byerlee's law is based on frictional sliding experiments in the laboratory, since the brittle or frictional strength of the crust is governed by preexisting faults and fractures. Two different strength curves (brittle and plastic laws) can therefore be drawn, based on experimental data. We will return to this subject in Chapter 7.

In Figure 6.18 the plastic curve is based on laboratory experiments on quartz, while the brittle strength turns out to be more or less independent of mineralogy (with the exception of clay minerals). However, the stress required for thrusting is significantly larger than that required for normal faulting, so different curves are indicated in Figure 6.18 for Anderson's three different stress regimes. These curves also depend on the pore fluid pressure, because pore fluid pressure reduces friction.

The crust is not monomineralic, but it is generally assumed that there is enough quartz in the continental crust to control its rheology. This means that even if feldspar is still brittle at 15–20 km, quartz is sufficiently represented and distributed that the crust is

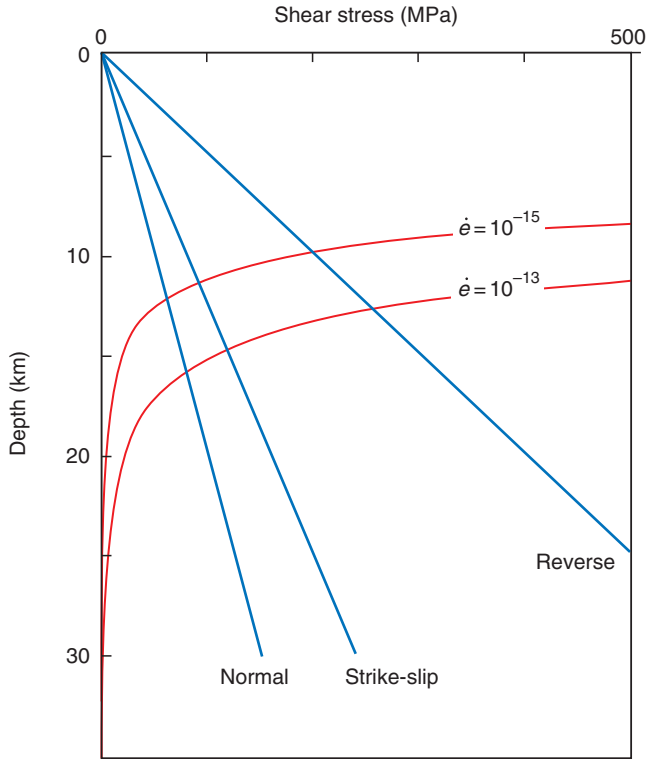

Figure 6.18 Strength (shear resistance) increases downwards through the brittle crust, until the temperature is high enough to activate plastic flow. Brittle and plastic deformation have two different strength profiles, and the intersection between the two defines the brittle–plastic transition. The plastic strength obeys a flow law as shown in Equation 6.24, which depends on strain rate. The plastic flow laws are derived from experimental deformation of quartzite (Gleason and Tullis 1995). Shear resistance for the three different stress regimes is shown.

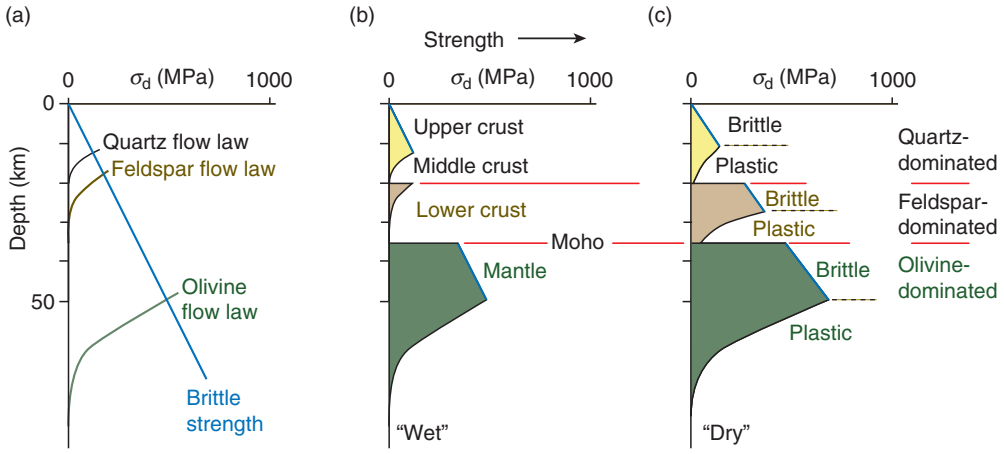

Figure 6.19 Rheologic stratification of continental lithosphere based on a combination of the brittle friction law and the plastic flow law derived experimentally for quartz (quartzite), feldspar (diabase) and olivine (dunite). Brittle–plastic transitions occur where the brittle (frictional) and plastic flow laws intersect. The strength profile depends on mineralogy and lithologic stratification. By choosing a quartz–feldspar–olivine stratification we get three brittle–plastic transitions. Note that dry rocks (c) are considerably stronger (can sustain higher differential stress) than wet rocks (b).

predominantly deforming plastically even at 10–12 km. However, if the stronger mineral feldspar becomes rheologically dominant at some depth, the flow law for feldspar becomes important (Figure 6.19a). In the olivine-dominated mantle, olivine is even stronger and defines a new intercept with the brittle strength curve. Hence, varying mineralogical composition through the lithosphere can lead to several layers of alternating brittle and plastic rheologies, known as **rheologic stratification** (Figure 6.19b, c).

The brittle–plastic transition is generally gradual or recurring over a wide zone in the continental crust.

The transition is also influenced by the presence of fluids, and the fact that "dry" rocks are more resistant to deformation is illustrated in Figure 6.19. Furthermore, strain rate shifts the plastic flow laws (and thus the brittle–plastic transition) vertically, as seen in Figure 6.18.

Because the crust is layered it is important to obtain as much information as possible about composition in order to predict the strength profile or rheological stratigraphy of the crust. Such information goes into the modeling of crustal-scale deformation, such as rifting and orogeny.

Summary

Rheology and its implications for how rocks deform are important to keep in mind when we are studying deformation structures in naturally deformed rocks. A fundamental distinction must be made between elasticity and related laws and moduli on one side, and permanent deformation and plasticity on the other. It is quite useful and fun to explore the concepts presented in this chapter during everyday activities, using rubber, plastics, modeling putty, clay, springs, plaster and many other things. The kitchen, where different types of food (syrup, honey, chocolate, dough, pudding, jelly and more) make a great selection of materials at different temperatures, can also be of good use. Before exploring and eating, here are some important points and review questions that should be familiar by now:

- Elastic theory is used for relatively small strains, from the millimeter scale to lithospheric scale. An example of the latter is the elastic subsidence of the lithosphere caused by ice sheets up to several kilometers thick during regional glaciations. The fact that the lithosphere rebounds when the ice melts tells us that it can be modeled as an elastic plate, and the rate at which it rebounds tells us something about the mantle viscosity and elastic properties of the lithosphere.

- Stress and elastic strain are related through Young's modulus: A low Young's modulus means little resistance to deformation.
- Poisson's ratio describes how much a material that is shortened in one direction expands in the two other directions, or how much a material that is stretched in one direction contracts in the plane perpendicular to the stretching direction.
- Elastic deformation of rocks reaches a critical stress or strain level (yield point) where permanent deformation starts to accumulate.
- Mechanically, plastic deformation occurs when permanent strain keeps accumulating under a constant stress level. More generally, plastic deformation is the deformation of rock by intracrystalline (non-cataclastic) flow.
- For plastic deformation, strain rate is related to stress through a non-linear (power-law) relationship called a flow law.
- Strain hardening and softening mean that the properties of the deforming rock change during deformation.
- The simple model of a predominantly plastically flowing lower crust overlain by a strong, brittle upper crust and underlain by a stronger upper mantle is a simple but useful first approximation to the large-scale rheological stratification of the crust.
- The idealized conditions in models and the laboratory are seldom met in nature, so models such as linear elasticity, viscosity etc. must be used with care.

Review questions

1. What is the difference between rheology and rock mechanics?
2. What is a constitutive law or equation?
3. What does isotropic mean?
4. What is an elastic material?
5. What is an incompressible medium, and what is its Poisson's ratio?
6. Some media are easier to elastically bend, stretch or shorten than others – we could say that there is a difference in stiffness. What constants describe the stiffness of an elastic material or its resistance to elastic deformation?
7. What is the yield stress and what happens if it is exceeded?
8. What is the difference between linear elastic and linear viscous?
9. What types of materials are truly viscous? What parts of the Earth can be modeled as being viscous?
10. What does it mean that a rock layer is more competent than its neighboring layers?
11. What could cause strain softening and strain hardening in a deforming rock?
12. What is the difference between plastic deformation and creep?
13. What controls the locations of brittle–plastic transitions in the lithosphere?

E-MODULE

The e-learning module called *Rheology* is recommended for this chapter.

FURTHER READING

General

Jaeger, C., 2009, *Rock Mechanics and Engineering*. Cambridge: Cambridge University Press.

Jaeger, J. C. and Cook, N. G. W., 1976, *Fundamentals of Rock Mechanics*. London: Chapman & Hall.

Karato, S. and Toriumi, M. (Eds.), 1989, *Rheology of Solids and of the Earth*. New York: Oxford University Press.

Ranalli, G., 1987, *Rheology of the Earth*. Boston: Allen & Unwin.

Turcotte, D. L. and Schubert, G., 2002, *Geodynamics*. Cambridge: Cambridge University Press.

Strain rates

Pfiffner, O. A. and Ramsay, J. G., 1982, Constraints on geological strain rates: arguments from finite strain states of naturally deformed rocks. *Journal of Geophysical Research* **87**: 311–321.

Chapter 7

Fracture and brittle deformation

Brittle structures such as joints and faults are found almost everywhere at the surface of the solid Earth. In fact, brittle deformation is the trademark of deformation in the upper crust, forming in areas where stress builds up to levels that exceed the local rupture strength of the crust. Brittle structures can form rather gently in rocks undergoing exhumation and cooling, or more violently during earthquakes. In either case, brittle deformation by means of fracturing implies instantaneous breakage of crystal lattices at the atomic scale, and this type of deformation tends to be not only faster, but also more localized than its plastic counterpart. Brittle structures are relatively easily explored in the laboratory, and the coupling of experiments with field and thin-section observations forms the basis of our current understanding of brittle deformation. In this chapter we will look at the formation of various small-scale brittle structures and the conditions under which they form.

7.1 Brittle deformation mechanisms

Once the differential stress in an unfractured rock exceeds a certain limit, the rock may accumulate permanent strain by plastic flow, as discussed in Chapter 6. In the **frictional regime** or **brittle regime**, however, the rock will deform by fracturing once its rupture strength is reached. During brittle fracturing, grains are crushed and reorganized and strain (displacement) becomes more localized.

The brittle regime is where the physical conditions promote brittle deformation mechanisms such as frictional sliding along grain contacts, grain rotation and grain fracture.

In some cases it is important to characterize the amount of fracture in a deformed rock, and a distinction is made between brittle deformation that does and does not involve fracture. Frictional deformation without the generation of fractures typically occurs in relatively poorly consolidated porous rocks and sediments (soils). In such rocks and sediments, frictional slip occurs along existing grain boundaries, and pore space enables grains to move relative to their neighboring grains, as shown in Figure 7.1a. Thus, the grains translate and rotate to accommodate frictional grain boundary slip, and the whole process is called **particulate flow** or **granular flow**. As always in the brittle regime, grain boundary sliding is influenced by friction, and the mechanism is therefore called **frictional sliding**. This means that a certain friction-controlled resistance against sliding must be overcome for frictional sliding to occur. Do not confuse this with the non-frictional grain boundary sliding that takes place in the plastic regime (Chapter 10).

The angle of repose in loose sand is controlled by the friction between individual sand grains. The higher the friction between the grains, the higher the angle of repose. In this case gravity exerts a vertical force on grain contact areas, and the shear stress will depend on the orientation of the surfaces, as discussed in Chapter 4.

Frictional sliding of grains may be widely distributed throughout a rock volume, but can also be localized to millimeter- to decimeter-wide zones or bands. Granular flow results in a ductile shear zone where lamination can be traced continuously from one side of the zone to the other. This is a type of ductile shear zone that is governed by brittle deformation mechanisms.

In other cases new fractures form during deformation. This always happens during brittle permanent deformation of non-porous rocks, but can also occur in porous rocks if the stress on grain contact areas becomes high enough. In the case of porous rocks we often identify **intragranular fractures**, which are fractures restricted to single grains (Figure 7.2a). **Intergranular fractures** are fractures that extend across a number of grains (Figure 7.2b), and characterize brittlely deformed low-porosity or non-porous rocks. The fracture and crushing of grains, coupled with frictional sliding along grain contacts and grain rotation, is called **cataclasis**. Intense cataclasis occurs in thin zones along slip or fault surfaces where extreme grain size reduction goes on. More moderate cataclastic deformation can occur in somewhat wider brittle or cataclastic shear zones. In this case the fragments resulting from grain crushing flow during shearing. This process is referred to as **cataclastic flow** (Figure 7.1b).

Particulate flow involves grain rotation and frictional sliding between grains, while cataclastic flow also involves grain fracturing or cataclasis. Both can give rise to structures that appear ductile at the mesoscopic scale.

Strong grain crushing without evidence of shear offset has also been observed and is called **pulverization**. The process of pulverization is not well understood, but

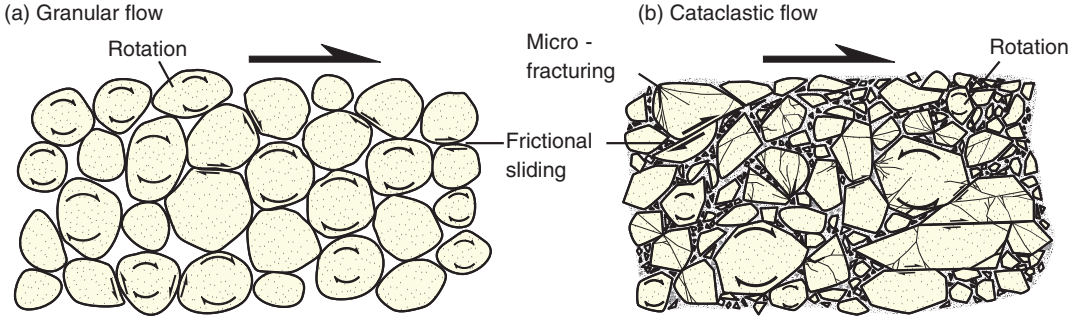

Figure 7.1 Brittle deformation mechanisms. Granular flow is common during shallow deformation of porous rocks and sediments, while cataclastic flow occurs during deformation of well-consolidated sedimentary rocks and non-porous rocks.

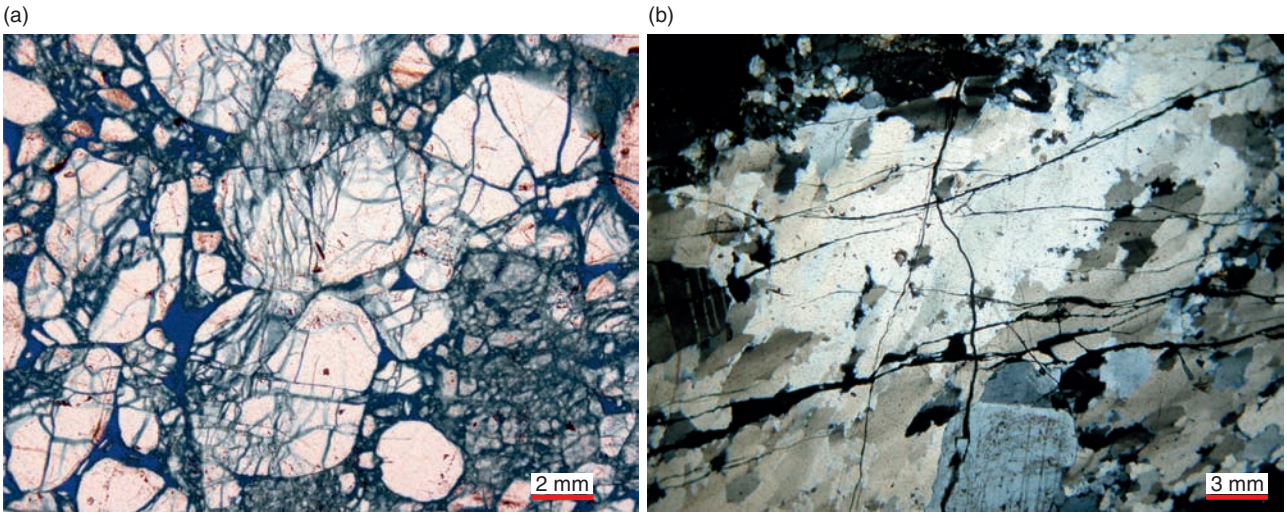

Figure 7.2 (a) Intragranular fractures in cataclastically deformed porous sandstone (Mesa Verde Group, Salina, Utah). Dark blue color is epoxy-filled pore space. (b) Intergranular fractures in metamorphic rock.

seems to be related to very high strain rates (>100 s^{-1}) and may be related to large earthquake events producing very high rupture rates.

7.2 Types of fractures

What is a fracture?

Strictly speaking, a fracture is any planar or subplanar discontinuity that is very narrow in one dimension compared to the other two and forms as a result of external (e.g. tectonic) or internal (thermal or residual) stress. Fractures are discontinuities in displacement and mechanical properties where rocks or minerals are broken, and reduction or loss of cohesion characterizes most fractures. They are often described as surfaces, but at some scale there is always a thickness involved. Fractures can be separated into shear fractures (slip surfaces) and opening or extension fractures (joints, fissures and veins), as illustrated in Figures 7.3 and 7.4. In addition, closing or contraction fractures can be defined.

Fractures are very narrow zones, often thought of as surfaces, associated with discontinuities in displacement and mechanical properties (strength or stiffness).

A **shear fracture** or **slip surface** is a fracture along which the relative movement is parallel to the fracture. The term shear fracture is used for fractures with small (mm- to dm-scale) displacements, while the term **fault** is more commonly restricted to discontinuities with larger offset. The term slip surface is used for fractures with fracture-parallel movements regardless of the amount of displacement and is consistent with the traditional use of the term fault. Fractures are commonly referred to as cracks in material science and rock mechanics oriented literature.

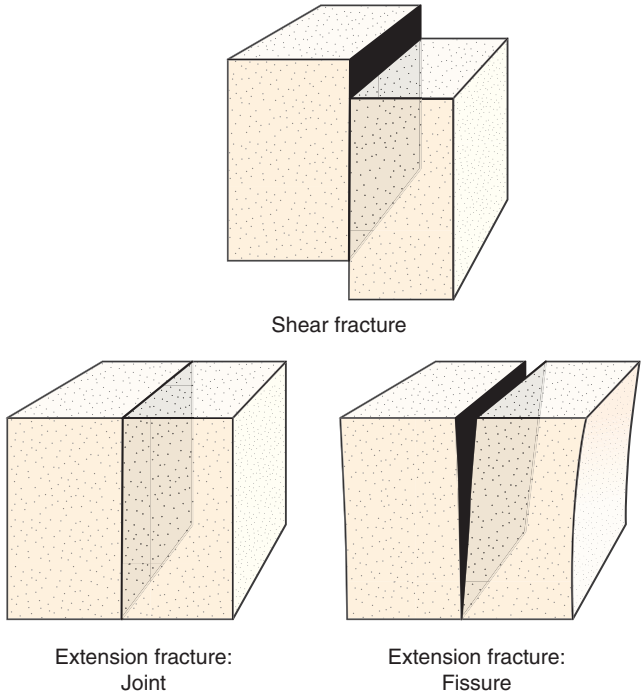

Figure 7.3 Three types of fracture.

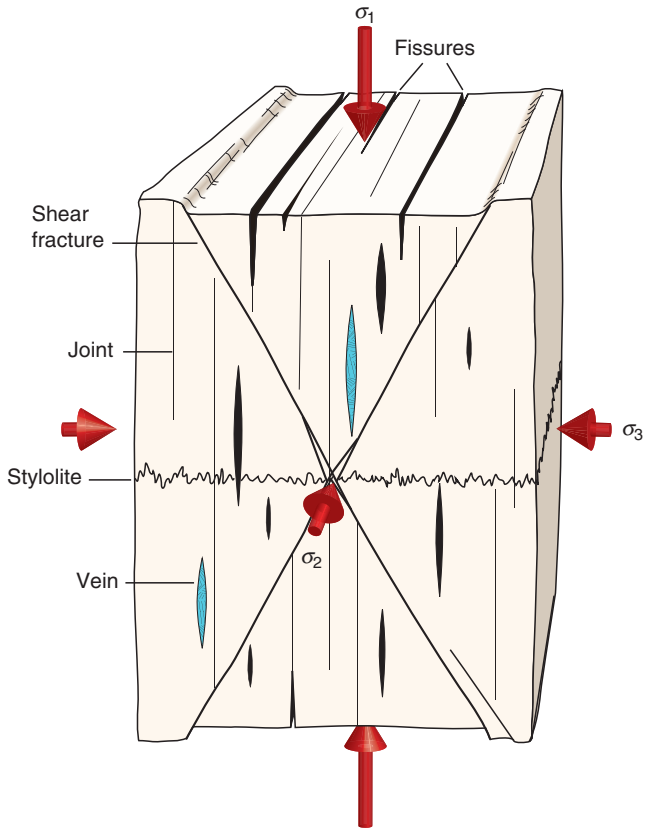

Figure 7.4 The orientation of various fracture types with respect to the principal stresses.

Extension fractures are fractures that show extension perpendicular to the walls. **Joints** have little or no macroscopically detectable displacement, but close examination reveals that most joints have a minute extensional displacement across the joint surfaces, and therefore they are classified as true extension fractures. Extension fractures are filled with gas, fluids, magma or minerals. When filled with air or fluid we use the term **fissure**. Mineral-filled extension fractures are called **veins**, while magma-filled fractures are classified as **dikes**. Joints, veins and fissures are all referred to as extension fractures.

Contractional planar features (anticracks) have contractional displacements across them and are filled with immobile residue from the host rock. Stylolites are compactional structures characterized by very irregular, rather than planar, surfaces. Some geologists now regard stylolites as **contraction fractures** or **closing fractures**, as they nicely define one of three end-members in a complete kinematic fracture framework together with shear and extension fractures. Such structures are known as **anticracks** in the engineering-oriented literature.

Rock mechanics experiments carried out at various differential stresses and confining pressures set a convenient stage for studying aspects of fracture formation (Figure 7.5), and we will refer to experimental rock deformation on several occasions in this chapter (also

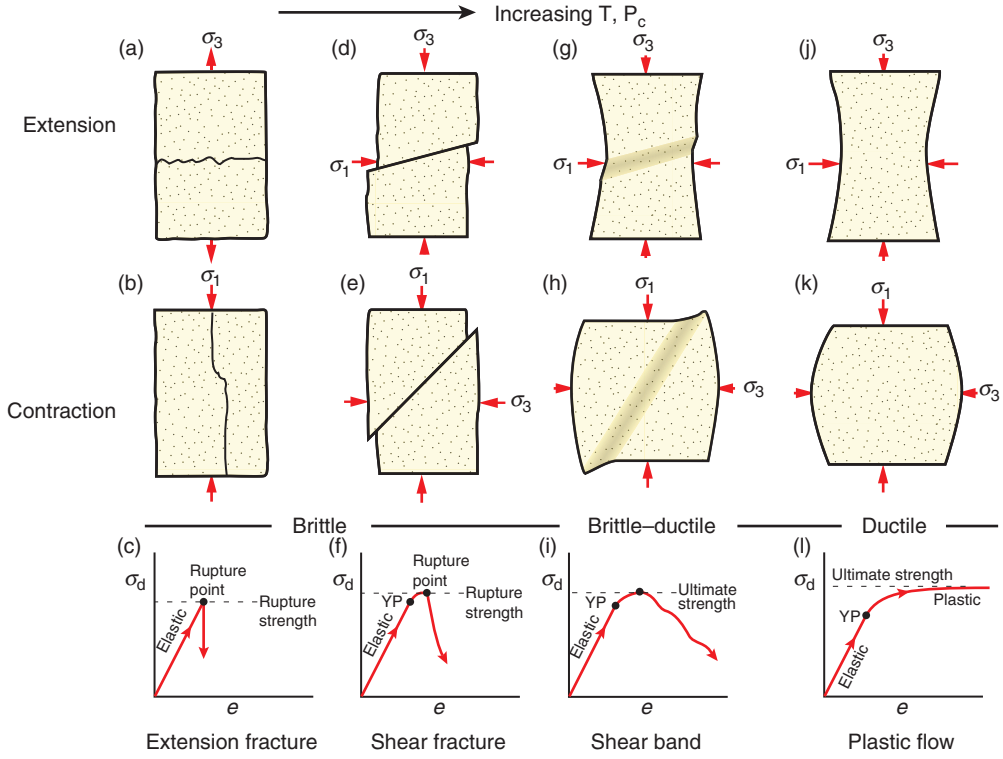

Figure 7.5 Experimental deformation structures that develop under extension and contraction. Initial elastic deformation is seen for all cases, while ductility increases with temperature (T) and confining pressure (P_c). YP, yield point.

BOX 7.1 DEFORMING ROCKS IN THE LABORATORY

The mechanical properties of rocks are explored in rock mechanics laboratories, where samples are exposed to various stress fields that relate to different depths and stress regimes in the crust. **Uniaxial** rigs can be used to test the uniaxial compressive or tensile strength of rocks. **Triaxial** tests, where $\sigma_1 > \sigma_2 = \sigma_3$, are more common, where rock cylinders are loaded in the axial direction while the sample is confined in fluid that can be pumped up to a certain confining pressure. A typical triaxial rig can build up an axial stress of 2–300 MPa and a confining pressure of up to 50–100 MPa or more. Sample and fluid are commonly separated by a membrane to avoid the fluid entering the sample and changing its mechanical properties. For porous rocks or sediments it may be possible to control the pore pressure (e.g. up to 50 MPa). The distance between the pistons is monitored together with axial loading and confining pressure. The **ringshear** apparatus is used to explore the effect of large shear strain under vertical compression of up to about 25 MPa.

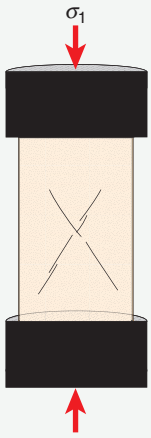

Uniaxial deformation rig, used to find the uniaxial strength of rocks. Experiments show that, in general, fine-grained rocks are stronger than coarse-grained ones, and the presence of phyllosilicates lowers the strength.

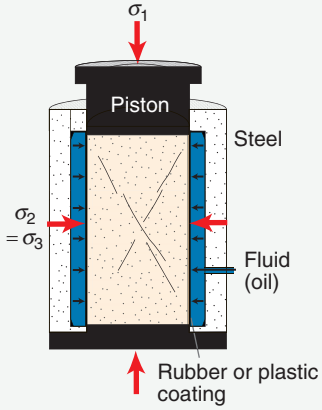

Triaxial rig. Oil pressure is pumped up in a chamber around the sample to increase the confining pressure.

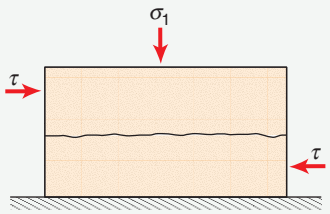

Shearbox experiment where the resistance against shear is explored. The higher the normal stress, the higher the shear stress necessary to activate the fracture. The roughness of the fracture is also important.

Ringshear apparatus, where the amount of shear strain that can be imposed on the sample is unlimited. Loose sediment is added and processes such as clay smear and cataclasis can be studied.

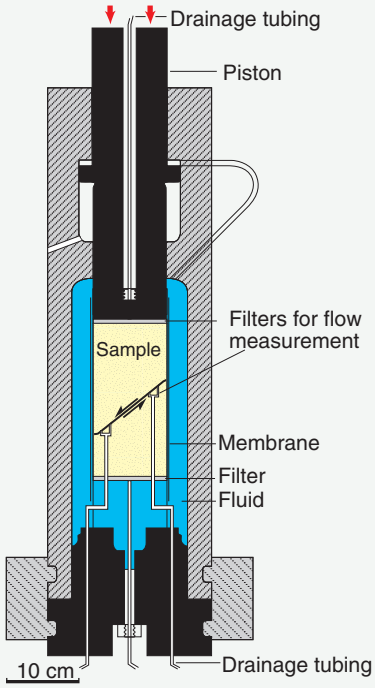

A triaxial rig where fluid (oil or water) can be pumped in and influence the behavior of an existing fracture.

see Box 7.1). Similarly, numerical modeling has added greatly to our understanding of fracture growth, particularly the field called **linear elastic fracture mechanics**. In the field of fracture mechanics it is common to classify the displacement field of fractures or cracks into three different modes (Figure 7.6). **Mode I** is the opening (extension) mode where displacement is perpendicular to the walls of the crack. **Mode II** (sliding mode) represents slip (shear) perpendicular to the edge and **Mode III** (tearing mode) involves slip parallel to the edge of

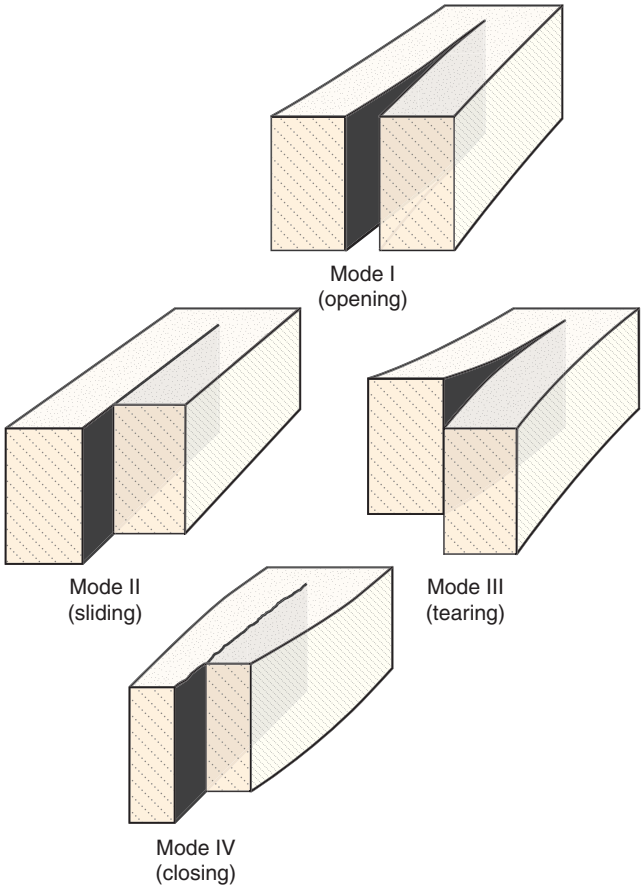

Figure 7.6 Mode I, II, III and IV fractures.

the crack. Modes II and III occur along different parts of the same shear fracture and it may therefore be confusing to talk about Mode II and Mode III cracks as individual fractures. Combinations of shear (Mode II or III) fractures and tension (Mode I) fractures are called **hybrid cracks** or fractures. Furthermore, the term **Mode IV** (closing mode) is sometimes used for contractional features such as stylolites. The mode of displacement on fractures is an important parameter, for instance when fluid flow through rocks is an issue.

Extension fractures and tensile fractures

Extension fractures ideally develop perpendicular to σ_3 and thus contain the intermediate and maximum principal stresses ($2\theta = 0°$, see Figure 4.6). In terms of strain, they develop perpendicular to the stretching direction under tensile conditions, as shown in Figure 7.5a, and parallel to the compression axis during compression tests (Figure 7.5b). Because of the small strains associated with most extension fractures, stress and strain axes more or less coincide.

Joints are the most common type of extension fracture at or near the surface of the Earth and involve very small strains. Fissures are extension fractures that are more open than joints, and are characteristic of the uppermost few hundred meters of the solid crust, where they may be up to several kilometers long (Figure 7.7).

Extension fractures are typical for deformation under low or no confining pressure, and form at low differential stress. If extension fractures form under conditions where at least one of the stress axes is tensile, then such fractures are true **tensile fractures**. Such conditions are generally found near the surface where negative values of σ_3 are more likely. They can also occur deeper in the lithosphere, where high fluid pressure reduces the effective stress (Section 7.6). Many other joints are probably related to unloading and cooling of rocks, as indicated in Section 5.4.

Shear fractures

Shear fractures show fracture-parallel slip and typically develop at 20–30° to σ_1, as seen from numerous experiments under confined compression (Figure 7.5d, e) (see Box 7.2). Such experiments also show that they commonly develop in conjugate pairs, bisected by σ_1. Shear fractures develop under temperatures and confining pressures corresponding to the upper part of the crust. They can also form near the brittle–plastic transition, where they tend to grow into wider bands or zones of cataclastic flow. Such shear factures result in strain patterns otherwise typical for plastic deformation (Figure 7.5g, h).

While extension fractures open perpendicular to σ_3, shear fractures are oblique to σ_3 by an angle that depends mostly on rock properties and state of stress.

As mentioned in the previous chapter and shown in Figure 7.8, brittle and plastic deformation show different stress–strain curves (blue versus red curves in Figure 7.8): the more ductile the deformation, the greater the amount of plastic deformation prior to fracturing. It is also interesting to note the relationship between confining pressure (depth) and strain regime (contractional or extensional) shown in Figure 7.9. The experimental data indicate that the brittle–plastic transition occurs at higher confining pressure under extension than under contraction. Temperature (Figure 7.9) and

Figure 7.7 Fissures formed in Thingvellir, Iceland, along the rift axis between the Eurasian and Laurentian plates. The fissures are open extension fractures in basalt, but the vertical displacement (right-hand side down) indicates a connection with underlying faults.

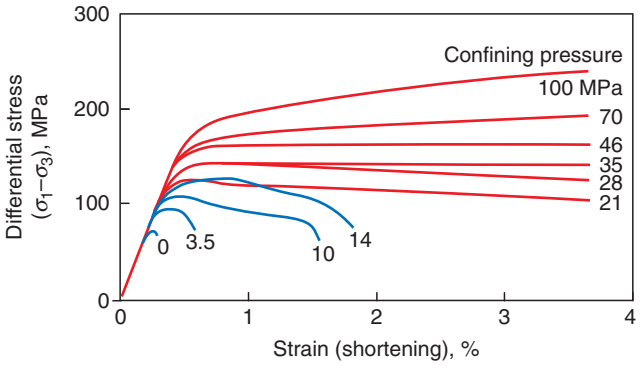

Figure 7.8 Stress–strain curves for triaxial compression of marble for a range of confining pressures. Increasing the confining pressure increases the differential stress that the rock can sustain before failure (blue curves). Above a critical confining pressure the rock retains its strength as it deforms plastically (red curves). From Paterson (1958).

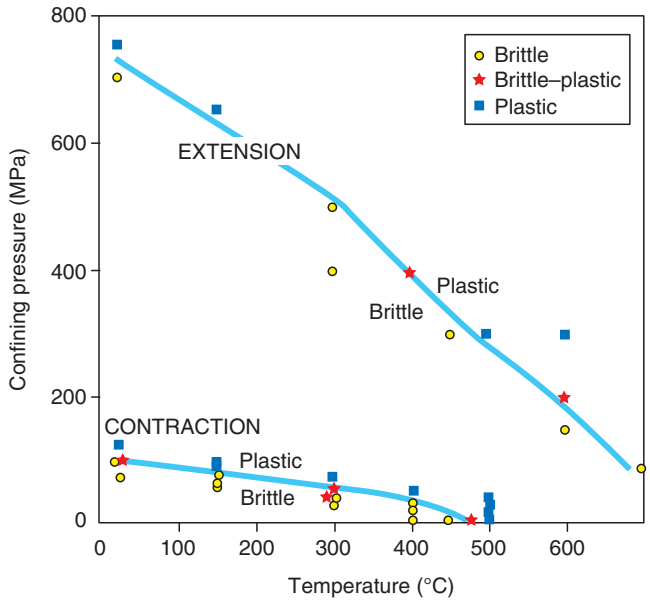

Figure 7.9 Variation of the brittle–plastic transition as a function of confining pressure and temperature for the Solenhofen limestone. From Heard (1960).

BOX 7.2 WHY SHEAR FRACTURES DO NOT FORM AT 45° TO THE LARGEST PRINCIPAL STRESS

Navier and Coulomb both showed that shear fractures do not simply form along the theoretical surfaces of maximum shear stress. Maximum resolved shear stress on a plane is obtained when the plane is oriented 45° to the maximum principal stress ($\theta = 45°$). This fact is easily extracted from the Mohr diagram, where the value for shear stress is at its maximum when $2\theta = 90°$. However, in this situation the normal stress σ_n across the plane is fairly large. Both σ_s and σ_n decrease as θ increases, but σ_n decreases faster than σ_s. The optimal balance between σ_n and σ_s depends on the angle of internal friction ϕ, and is predicted by the Coulomb criterion to be around 60° for many rock types. At this angle ($\theta = 60°$) σ_s is still large, while σ_n is considerably less. The angle depends also on the confining pressure (depth of deformation), temperature and pore fluid, and experimental data indicate that there is a wide scatter even for the same rock type and conditions.

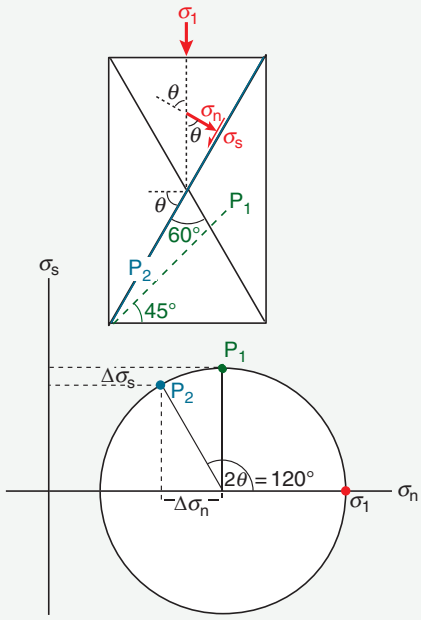

P_1 is the plane of maximum resolved shear stress ($2\theta = 90°$) and forms at 45° to σ_1. The plane P_2 oriented at 30° to σ_1 has a slightly lower shear stress (the difference is $\Delta\sigma_s$), but a much lower normal stress (by $\Delta\sigma_n$). It is therefore easier for a shear fracture to form along P_2 than along P_1.

strain rate are other important factors, as discussed in previous chapters.

7.3 Failure and fracture criteria

We learned in Chapter 6 that a rock's response to stress depends on the level of stress or amount of accumulated strain, and on factors such as anisotropy, temperature, strain rate, pore fluid and confining pressure. In the brittle regime a deforming rock accumulates elastic strain before it ruptures (fractures) at a certain critical stress level. In the brittle–plastic transition there tends to be an intermittent phase of plastic deformation prior to brittle failure, and the failure does not necessarily create an instantaneous through-going fracture, but rather a shear zone or shear band dominated by cataclastic flow. This contrasts with the plastic regime (Figure 7.5j–l) where strain is more broadly distributed and dominated by plastic deformation mechanisms.

While the main focus of Chapter 6 was on elastic–plastic deformation, we now focus on the brittle part. Key questions are *when* and *how* does a rock fracture. Let us look at the first question first. For a given rock under constant temperature and constant positive confining pressure, fracture depends on the differential stress ($\sigma_1 - \sigma_3$) as well as the mean stress ($(\sigma_1 + \sigma_3)/2$). If there is no differential stress, then the state of stress is lithostatic and there is no force pulling or pushing our rock volume in any particular direction. The only exception is the potential collapse of the porosity structure in highly porous rocks, but in order to make distinct fractures, differential stress is generally needed.

Fracture initiation requires a differential stress that exceeds the strength of the rock.

The strength of a rock depends on the confining pressure or depth of burial. In the brittle, upper part of the crust, the strength is lowest near the surface and increases downwards. This is easily explored in experiments such as the ones shown in Figure 7.8, where both confining pressure and directed axial stress are varied. We see from this figure that:

Increasing the confining pressure makes it necessary to increase the differential stress in order to fracture a rock.

In the next section we will see how this connection between confining pressure (burial depth) and differential

stress can be described by means of a simple relationship between the critical normal and shear stresses. The relationship is known as the Coulomb fracture criterion for confined compression.

The Coulomb fracture criterion

At the end of the seventeenth century, the French physicist Charles Augustin de Coulomb found a criterion that could predict the state of stress at which a given rock under compression is at the verge of failure, commonly described as being **critically stressed**. The criterion considers the critical shear stress (σ_s, or τ) and normal stress (σ_n) acting on a potential fracture at the moment of failure, and the two are related by a constant tan ϕ, where ϕ is called the angle of internal friction:

$$\sigma_s = \sigma_n \tan \phi \qquad (7.1)$$

The Coulomb fracture criterion indicates that the shear stress required to initiate a shear fracture also depends on the normal stress across the potential shear plane: the higher the normal stress, the higher the shear stress needed to generate a shear fracture. Tan ϕ is commonly called the **coefficient of internal friction** μ. For loose sand it relates to the friction between sand grains and the critical slope angles of the sand (the angle of repose, ~30°), but for solid rocks it is merely a constant that varies from 0.47 to 0.7. A value of 0.6 is often chosen for μ for general calculations.

A fracture criterion describes the critical condition at which a rock fractures.

Three centuries after Coulomb, the German engineer Otto Mohr introduced his famous circle (Section 4.7) in σ_s–σ_n-space (Mohr space), and the Coulomb criterion could conveniently be interpreted as a straight line in Mohr space, with μ representing the slope and ϕ the slope angle (note that there is also a second line representing the conjugate shear fracture on which shear stress magnitude is identical but of opposite sign).

Coulomb realized that a fracture only forms if the internal strength or cohesion C of the rock is exceeded. The complete Coulomb fracture criterion (also called the Navier–Coulomb, Mohr–Coulomb or Coulomb–Mohr fracture criterion) is therefore:

$$\sigma_s = C + \sigma_n \tan \phi = C + \sigma_n \mu \qquad (7.2)$$

The constant C represents the critical shear stress along a surface across which $\sigma_n = 0$ (Figure 7.10). C is also called the **cohesive strength**, and has its counterpart in the **critical tensile strength** T of the rock.

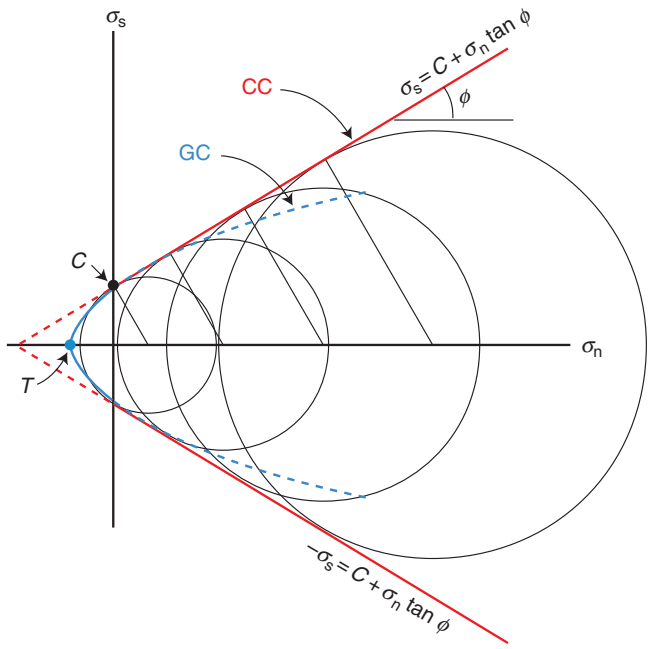

Figure 7.10 The Coulomb fracture criterion occurs as two straight lines (red) in the Mohr diagram. The circles represent examples of critical states of stress. The blue line represents the Griffith criterion for comparison. The combination of the two is sometimes used (GC in the tensile regime and CC in the compressional regime). CC, Coulomb criterion; GC, Griffith criterion; C, the cohesive strength of the rock; T, the tensile strength of the rock.

The Mohr diagram provides a convenient way of interpreting the meaning of these constants (Figure 7.10). Because Equation 7.2 is the general formula for a straight line, C represents the intersection with the vertical (σ_s) axis and T denotes the intersection with the horizontal (σ_n) axis. At point C it is clear that $\sigma_n = 0$, while at T, $\sigma_s = 0$. As an example, loose sand has no compressive or tensile strength, which means that $T = C = 0$ and the Coulomb fracture criterion reduces to Equation 7.1. The more the sand lithifies, the higher the C-value. However, lithification will change not only the C-value, but also ϕ and T. In general, C, T and ϕ vary from one rock type to another. For sand(stone), they all increase with increasing degree of lithification.

To see if a rock obeys the Coulomb fracture criterion and, if so, to determine C, T and μ for a given rock or sediment, laboratory tests are performed. A deformation rig is generally used, where the confining pressure as well as the axial load can be adjusted. The state of stress at failure is recorded and plotted in the Mohr diagram. This

can be done for many different critical states of stress (Figure 7.10 and 7.11), and for so-called Coulomb materials the line that tangents the Mohr circles represents the Coulomb fracture criterion (Equation 7.2). This line is called the **Coulomb failure envelope** for the rock.

Ideally, the point at which a Mohr circle touches the failure envelope represents the orientation of the plane of failure (remember the 2θ angle in the Mohr diagram), as well as the shear stress and normal stress on the plane at the moment of failure. Any Mohr circle that does not touch the envelope represents a stable state of stress (no fracturing possible; Figure 7.12a). The Coulomb failure envelope is always positive for brittle fracturing. This means that the higher the mean stress (or confining pressure), the higher the differential stress required for failure. In other words:

The deeper into the brittle part of the crust, the stronger the rock, and the larger the differential stress required to fracture it.

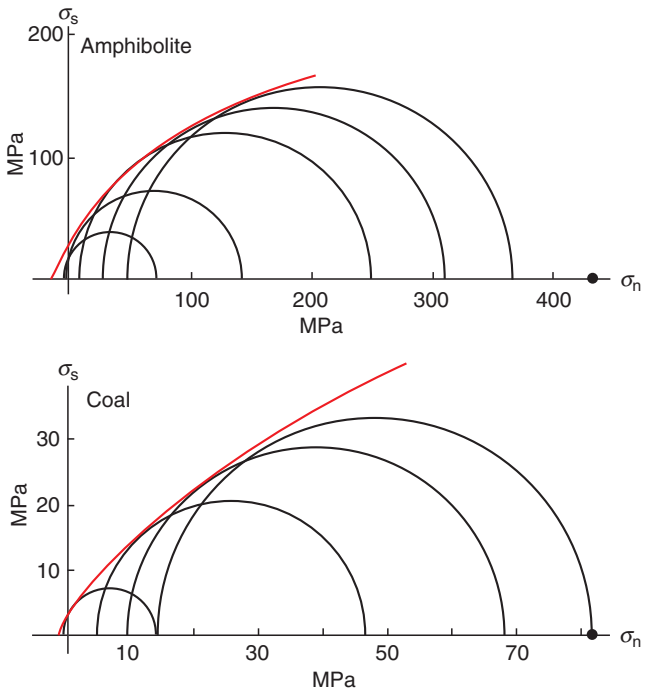

Figure 7.11 The Mohr envelope for amphibolite and coal based on triaxial tests. When the confining pressure is increased, the strength of the rock increases, and a new circle can be drawn in the figure. Note that the envelope diverges from the linear trend defined by the Coulomb criterion. From Myrvang (2001).

Note also that the effect of the intermediate principal stress (σ_2) is ignored and that the fracture plane always contains σ_2, in agreement with Anderson's theory of faulting (Figure 5.12).

The orientation of the fracture can be expressed in terms of the angle of internal friction (φ) and the orientation of the fracture (θ):

$$\phi = 45^\circ - \frac{\theta}{2} \tag{7.4}$$

or

$$\theta = 90^\circ - 2\phi \tag{7.5}$$

Most rocks have $\varphi \approx 30^\circ$ ($\mu \approx 0.6$), which means that the angle between σ_1 and the fracture, which is $90^\circ - \theta$ (see Figure 4.1), is around 30°. Thus, Andersonian normal and reverse faults dip at $\sim 60^\circ$ and 30°, respectively (Figure 7.13).

The Mohr failure envelope

The Mohr failure envelope is the envelope or curve in the Mohr diagram that describes the critical states of stress over a range of differential stress, regardless of whether it obeys the Coulomb criterion or not. The envelope, shown as a red line in Figure 7.14, separates the stable field, where the rock does not fracture, and the unstable field, which is in principle unachievable because fracture prevents such states of stress occurring.

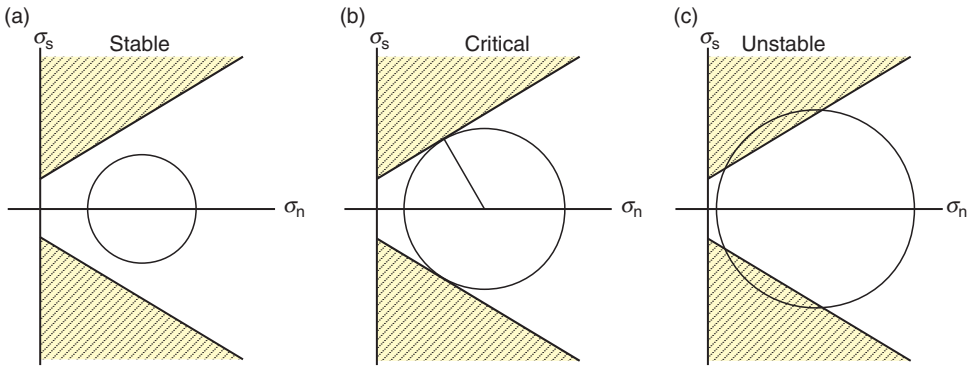

Figure 7.12 (a) Stable state of stress. (b) Critical situation, where the circle touches the envelope. This is when the rock is at the verge of failure, also called critically stressed. (c) Unstable situation where the state of stress is higher than that required for failure.

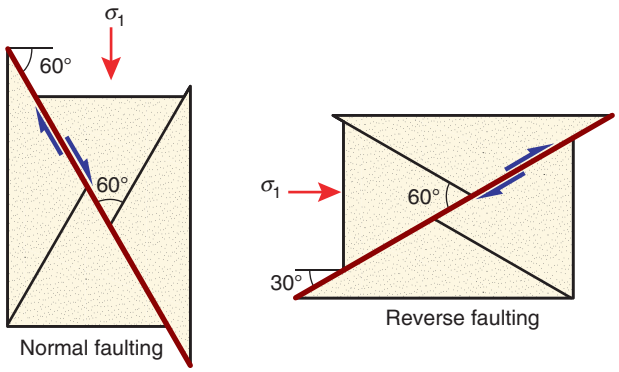

Figure 7.13 The angle between the maximum principal stress and the shear plane is commonly found to lie close to 30°. This implies that normal faults dip steeper (60°) than reverse faults (30°).

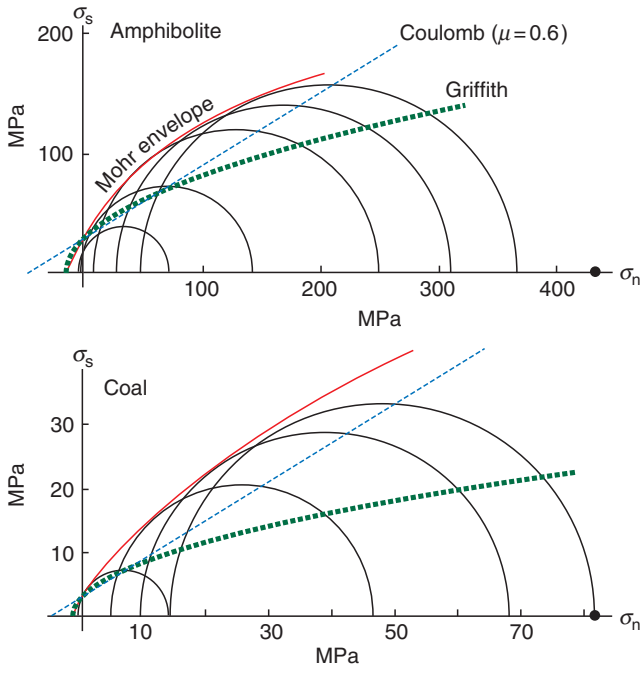

Figure 7.14 The Griffith and Coulomb fracture criteria superimposed on the experimental data presented in Figure 7.11. The criteria are placed so that they intersect the vertical axis together with the Mohr envelope. Neither of the criteria fit the data very well. The Griffith criterion works well for tensile stress (left of origin), but shows a too low slope in the entire compressional regime. The Coulomb criterion approaches the envelope for high confining pressure (right side of the diagram).

Each type of rock has its own failure envelope, and it is found experimentally by fracturing samples of the rock under different confining and differential stress. In some cases the Coulomb fracture criterion is a

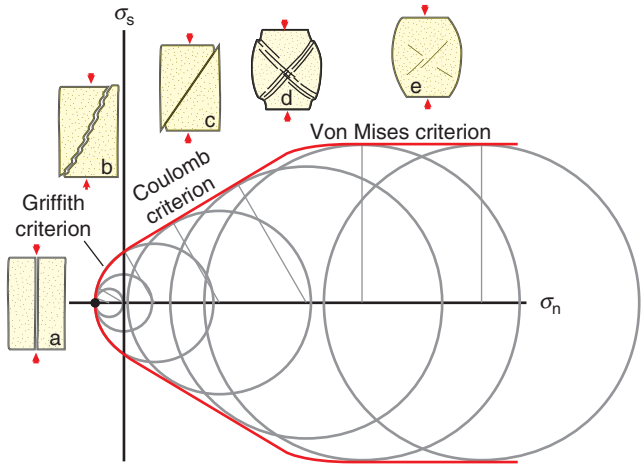

Figure 7.15 Three different fracture criteria combined in Mohr space. Different styles of fracturing are related to confining pressure: (a) Tensile fracture, (b) hybrid or mixed-mode fracture, (c) shear fracture, (d) semi-ductile shear bands, (e) plastic deformation.

reasonably good approximation for a certain stress interval, and in other cases the envelope is clearly non-linear (Figure 7.14). It is common for the envelope to flatten as the ductile regime is approached. In fact, the ductile regime can be approximated by a constant shear stress criterion (horizontal envelope), known as the **von Mises criterion** (σ = constant; Figure 7.15). A consequence of the non-linear shape of the envelope is that the angle θ between σ_1 and the failure plane decreases with increasing value of σ_3.

The tensile regime

The Coulomb criterion predicts the critical state of stress needed to create a shear fracture. Experimental data show that it does not successfully predict tensile fractures. Also, the fact that it relies on the angle of internal friction, which is physically meaningless for tensile normal stress, indicates that the Coulomb criterion is inappropriate in the tensional regime (left of origin in the Mohr diagram). Experiments suggest that the Mohr envelope in the tensile regime is shaped like a parabola. Thus, to cover the full range of stress states in the crust, it is necessary to combine different fracture criteria, such as the parabolic failure criterion for the tensile field, the Coulomb criterion for brittle fracturing in the compressive regime, and the von Mises criterion in the plastic regime (Figure 7.15).

The point where the Mohr envelope intersects the horizontal axis of the Mohr diagram represents the

critical stress at which tensile fractures start to grow and represents the **critical tensile stress** T. T is found experimentally to be lower than the cohesive strength C, and varies from rock to rock. Why does T vary so much? Griffith suggested that it is related to the shapes, sizes and distribution of microscopic flaws in the deforming sample.

Griffith's theory of fracture

Around 1920, the British aeronautical engineer Alan Arnold Griffith extended his studies of fracture to the atomic level. He noted a large difference in theoretical strength between perfectly isotropic material and the actual strength of natural rocks measured in the laboratory. Griffith based the theoretical brittle tensile strength on the energy required to break atomic bonds. The uniaxial tensile strength of flawless rock is calculated to be around 1/10 of Young's modulus. For a strong rock E could reach ~100 GPa (Table 6.1), which means a tensile strength of about 10 GPa (10 000 MPa). Experiments indicate that the tensile strength is closer to 10 MPa. Why this enormous discrepancy between theory and practice?

Griffith's answer was that natural rocks and crystals are far from perfect. Rocks contain abundant microscopic flaws, and microcracks, voids, pore space and grain boundaries are all considered as microscopic fractures in this context. For simplicity, Griffith modeled such flaws as strongly elliptical microfractures, now known as **Griffith (micro)cracks**. He considered the stress concentrations associated with these microfractures and the energy that it takes for them to grow and connect. He then obtained much more realistic (although not perfect) estimates of tensile strength.

Microscopic cracks, pores and other flaws weaken rocks.

In contrast to Coulomb, Griffith found a non-linear relationship between the principal stresses for a critically stressed rock (a rock on the verge of fracture). This relationship, which is called the **Griffith fracture criterion**, is given by the equation:

$$\sigma_s^2 + 4T\sigma_n - 4T^2 = 0 \qquad (7.6)$$

This equation can also be represented in the Mohr diagram, where it defines a parabola where the tensile strength T is the intersection with the horizontal axis. The intersection between the Griffith parabola and the vertical axis is found by setting $\sigma_n = 0$ in the equation above, which gives us $\sigma_s = 2T$. This value corresponds to C in the Mohr criterion. In other words, the **cohesive strength** of a rock is twice its tensile strength ($C = 2T$), which is in close agreement with experimental data. We can take advantage of this new information and reformulate the Coulomb fracture criterion as:

$$\sigma_s = 2T + \sigma_n\mu \qquad (7.7)$$

With this formulation it is easy to combine the Coulomb criterion for the compressional stress regime with the Griffith criterion for the tensile regime.

Griffith's important contribution is that the brittle strength of rock is controlled by randomly oriented and distributed intragranular microfractures in the rock. Microfractures with orientations close to that of maximum shear stress are then expected to grow faster than others, and will link and eventually form through-going fracture(s) in the rock.

For non-porous rocks the Griffith fracture criterion is a reasonably realistic approximation for the compressional regime as well. However, the Griffith criterion predicts that the uniaxial compressive strength should be eight times the uniaxial tensile strength (Figure 7.16), while experiments indicate that the uniaxial compressive strength of rocks is 10–50 times the uniaxial tensile strength. This discrepancy has resulted in several alternative fracture criteria. However, for porous media, such as sand and sandstone, the Coulomb criterion is quite realistic and can successfully be combined with the Griffith criterion (Figure 7.17).

7.4 Microdefects and failure

Griffith assumed that tensile fractures develop from planar microdefects or microfractures. In Griffith's model a fracture develops by a process where microfractures that are favorably oriented with respect to the external stress field grow and connect to form a through-going macrofracture. As illustrated in Figure 7.18, both tensile fractures (extension fractures) and shear fractures (faults) can form in this manner.

Observations indicate that microfractures occur at anomalously high frequencies near macroscopic fractures. This information suggests that microfractures form in a **process zone** ahead of a propagating macrofracture. In this zone microdefects expand and connect

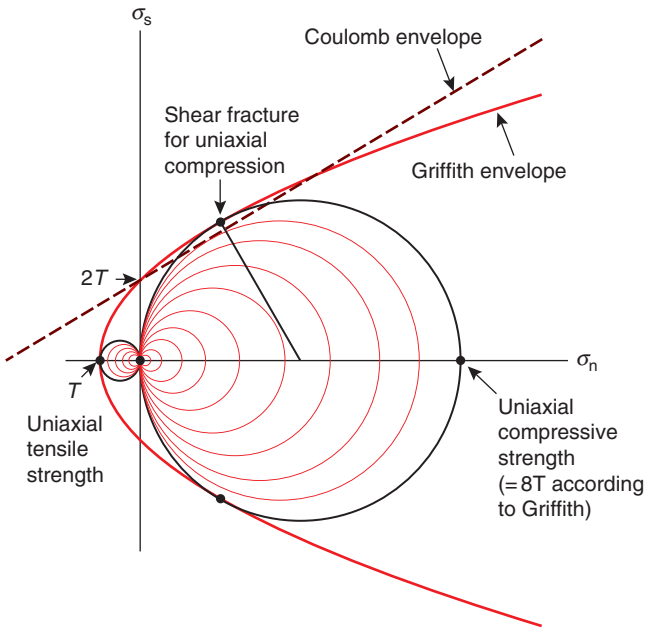

Figure 7.16 Illustration of the meaning of the terms uniaxial tensile and compressive strength in the Mohr diagram. Uniaxial means that only $\sigma_1 \neq 0$, which is obtained in a uniaxial deformation rig where the confining pressure is zero. By gradually compressing the rock sample, the uniaxial compressive strength is reached when a shear fracture first forms. By pulling the sample until a tensile fracture forms, the uniaxial tensile strength is found. Note that the uniaxial compressive strength is much larger than the tensile strength for the same rock and conditions.

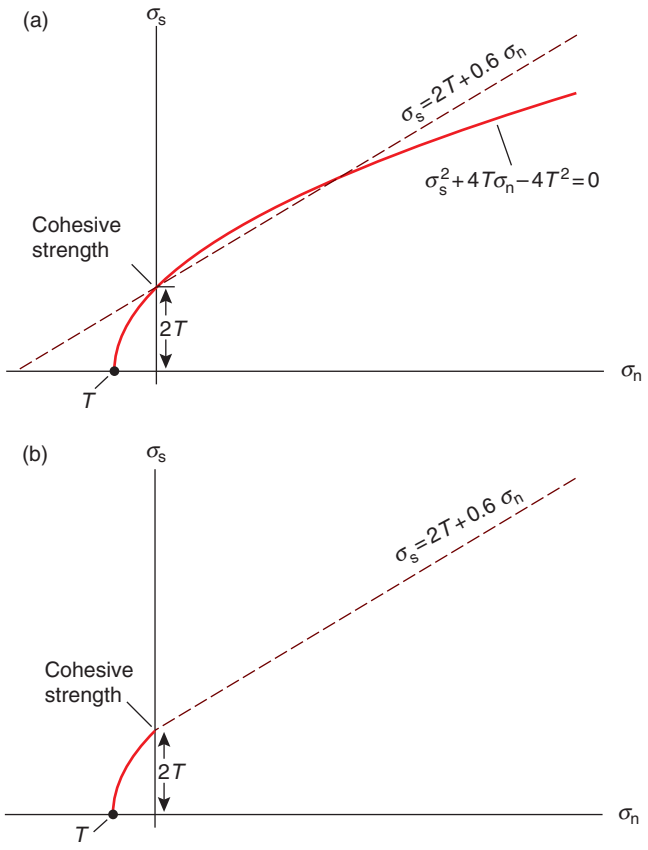

Figure 7.17 (a) Comparison of the Griffith and Coulomb fracture criteria (the coefficient of internal friction is chosen to be 0.6). (b) The combined Griffith–Coulomb criterion.

so that the macrofracture can grow. The process zone is in some ways similar to the frontal part of the damage zone that encloses a macroscopic fault, as discussed in Section 8.5. Many interesting things are going on in the process zone, such as the effect of increasing rock volume due to the growth of microfractures, which may lower the local pore pressure and temporarily strengthen the rock. But the most important aspect of microfractures is the stress concentration that occurs at their tips. This explains why they can grow into macroscopic fractures.

The Griffith criterion of fracture is based on the fact that stress is concentrated at the edges of open microfractures in an otherwise non-porous medium. This makes intuitive sense, since the stress that should have been transferred across the open fracture must "find its way" around the edges. If the microfracture is a circular pore space, then the stress concentration at the edge (around the circle) will be three times the remote stress, as illustrated in Figures 7.19 and 7.20.

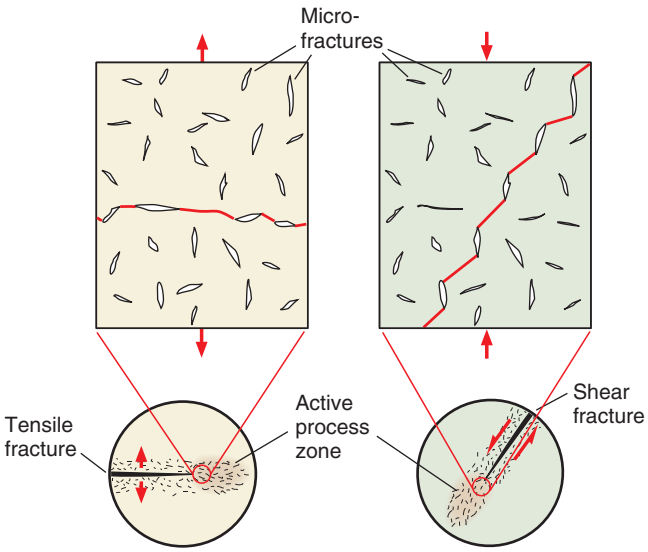

Figure 7.18 Simplified illustration of growth and propagation of extension (left) and shear fractures (right) by propagation and linkage of tensile microfractures (flaws). Propagation occurs in a process zone in front of the fracture tip. Circled figures are centimeter-scale views, while rectangular views illustrate the microscale structure.

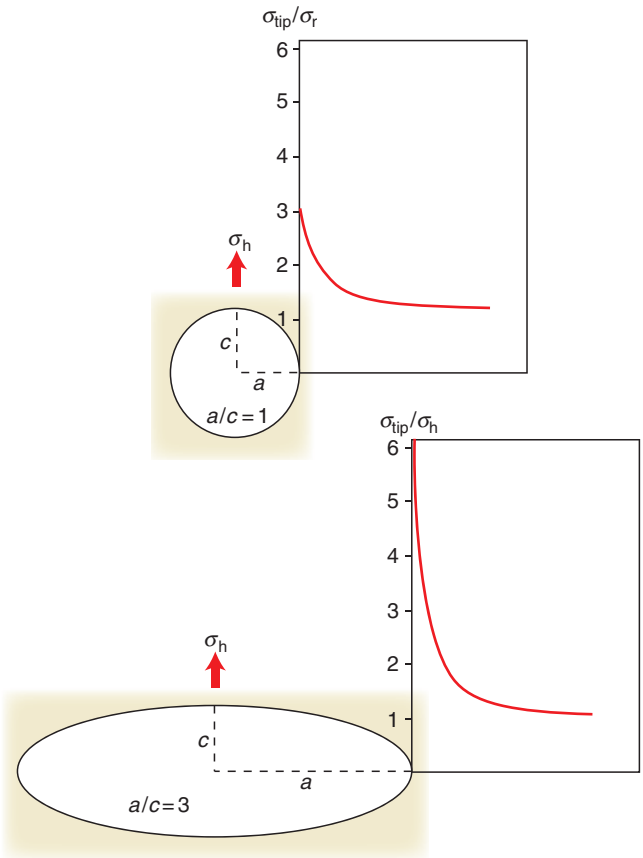

Figure 7.19 Stress concentration around a pore space or microfracture with circular and elliptic geometry in an elastic medium. Increasing the ellipticity a/c increases the stress concentration, as described in Equation 7.8. The far-field stress σ_h is tensile (negative). σ_{tip} is the stress at the circumference of the circle and at the point of maximum curvature on the ellipse (the fracture tip point). Based on Engelder (1993).

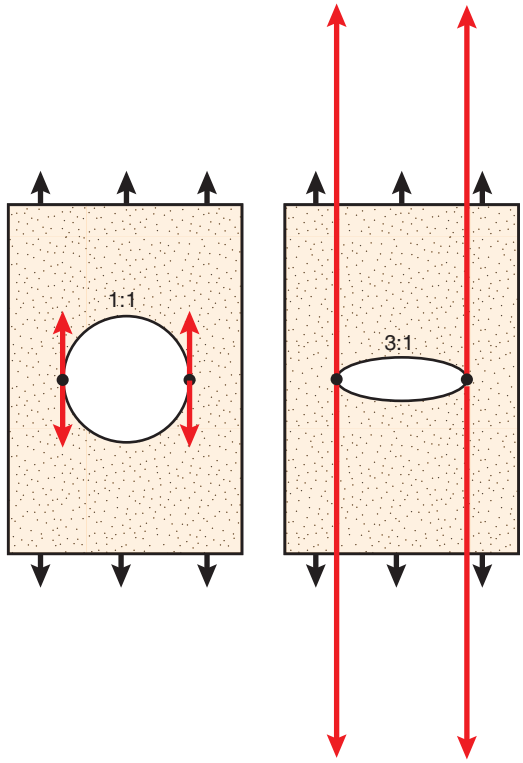

Figure 7.20 Illustration of local stress concentrations in a material with a circular and an elliptical hole. If the material is a sheet of paper it means that the paper with the elliptical hole will be easier to pull apart. Black arrows indicate the remote stress.

The stress concentration increases if the pore is elliptical and will peak at the tip-line of the ellipse. For an elliptically shaped microfracture of aspect ratio 1:3 the **local stress** at the tip is seven times the remote stress. By **remote stress**, also called **far-field stress**, we mean the stress that exists away from the local anomaly, or the state of stress if the anomaly was not there. If the ellipticity is 1:100, which is more realistic for Griffith microcracks, the local stress at the tip is 200 times the remote stress. This concentration may be sufficient to break the local atomic bonds and cause growth of the microcracks. It also implies that once the microcrack starts growing, it increases its length–width ratio, which further increases the stress concentration at its tips, and continued crack propagation is promoted.

Stress is concentrated at the tips of open microfractures in a rock, and the concentration increases with decreasing thickness/length ratio of the microfracture.

If we model the microcrack as an elliptical pore space, then the stress $-\sigma_{tip}$ at the tip of the pore can be expressed mathematically by the relationship:

$$-\sigma_{tip} = -\sigma_r(1 + (2a/c)) \qquad (7.8)$$

where σ_r is the remote stress and a/c is the ellipticity (aspect ratio of the ellipse). For a circular pore space $a/c = 1$ and $\sigma_r > 0$. The stress σ_t at the tip then becomes $\sigma_{tip} = 3\sigma_r$. The elliptical model of microfractures is of course an approximation. Fractures tend to have a sharply pointed tip zone, which promotes stress concentration even further and increases the likelihood of microfracture growth (Figure 7.21).

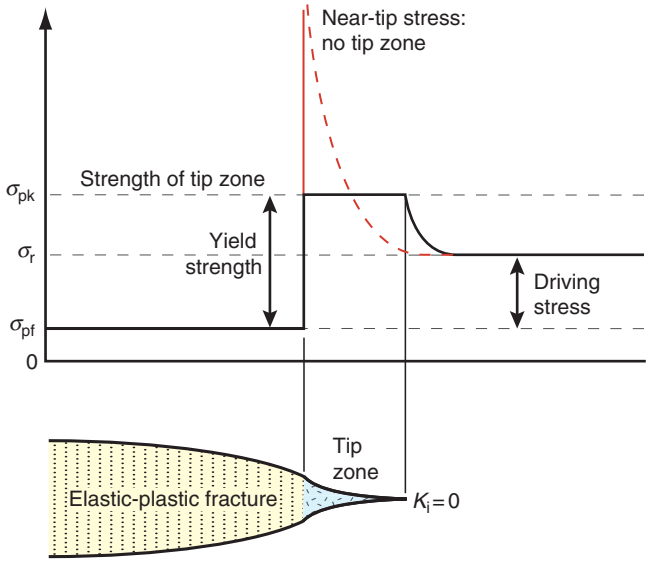

Figure 7.21 Distribution of stress (resolved on the fracture plane) near the tip of an elastic–plastic fracture. Amplified stress due to fracture wall displacements (dashed red curve) decays with distance from fracture tip to σ_r in the surrounding unfractured rock. The length s of the tip zone is defined by a constant value of yield (peak) stress σ_{pk}. The driving stress is the difference between resolved remote stress σ_r and the pore fluid pressure (or residual frictional strength σ_{pf}). The yield strength is the difference between σ_{pk} and internal boundary value σ_i. From Schultz and Fossen (2002).

These considerations suggest that it is likely for fractures to initiate from microdefects in the rock. It also explains why construction, ship and aerospace engineers are so concerned about microdefects and their shapes. Everything depends on whether or not the stress concentration at the tips of the microfractures is high enough to cause them to propagate.

Rock mechanics-oriented geologists sometimes talk about the driving force or **driving stress**. For tensile fractures modeled by means of linear elastic theory, the driving stress is the difference between remote stress resolved on the fracture plane and the internal pore-fluid pressure. Thus, for a tensile fracture to propagate, the driving stress must be large enough to exceed the resolved remote stress. Similarly, for closed shear fractures the driving stress (shear stress) must exceed the resisting forces, such as frictional resistance, for displacements to occur. The **stress intensity factor** K_i considers both the remote stress and the shape and length of the microfracture, and its critical value K_{ic} is called the **fracture toughness**. The fracture toughness can thus be considered as a material's resistance against continued growth of an existing fracture. Naturally, sedimentary rocks have lower values of K_{ic} than igneous rocks. We will not go into the details of linear elastic fracture theory in this book, but rather have a look at how temperature, fabric and sample size can affect strength.

Effects of fabric, temperature, stress geometry and sample size on strength

We have now seen how the presence of microscale heterogeneities in the form of microfractures reduces the strength of rocks. In theory, microfractures can be distributed so that the rock is macroscopically isotropic, i.e. it has the same strength in all directions. Most rocks have an anisotropy stemming from sedimentary or tectonic fabrics such as lamination, bedding, tectonic foliation, lineation and crystallographic fabric (preexisting fractures are treated separately below) and the difference in critical differential stress may vary by several hundred percent, depending on orientation. A rock with a planar anisotropy, such as a slaty cleavage, will fail either along or across the weak cleavage, depending on the orientation of the cleavage with respect to the principal stresses. In Mohr space, there will therefore be two failure envelopes, as shown in Figure 7.22. Which one is applicable depends on the orientation of the foliation.

If the foliation is oriented perpendicular or parallel to σ_1, then there is no resolved shear stress on the foliation, and the upper (blue) envelope in Figure 7.22 applies (Figure 7.22a). A shear fracture forms across the foliation at the characteristic angle of around 30° with σ_1 (i.e. $\theta \approx 60°$). Foliation-parallel extension fractures along the cleavage plane (longitudinal splitting) can develop even at low confining pressure. When the foliation is oriented closer to that typical of shear fractures in isotropic rocks, shear fractures develop along the foliation at gradually lower differential stress (Figure 7.22b, c). The orientation of the shear fracture and the strength is then controlled by the orientation of the foliation. Minimum strength is obtained where the orientation of the foliation is represented by the point where the Mohr circle touches the "along-foliation failure" envelope on Figure 7.22d. The exact angle will depend on the weakness of the foliation, which determines the slope of the lower failure curve in Figure 7.22.

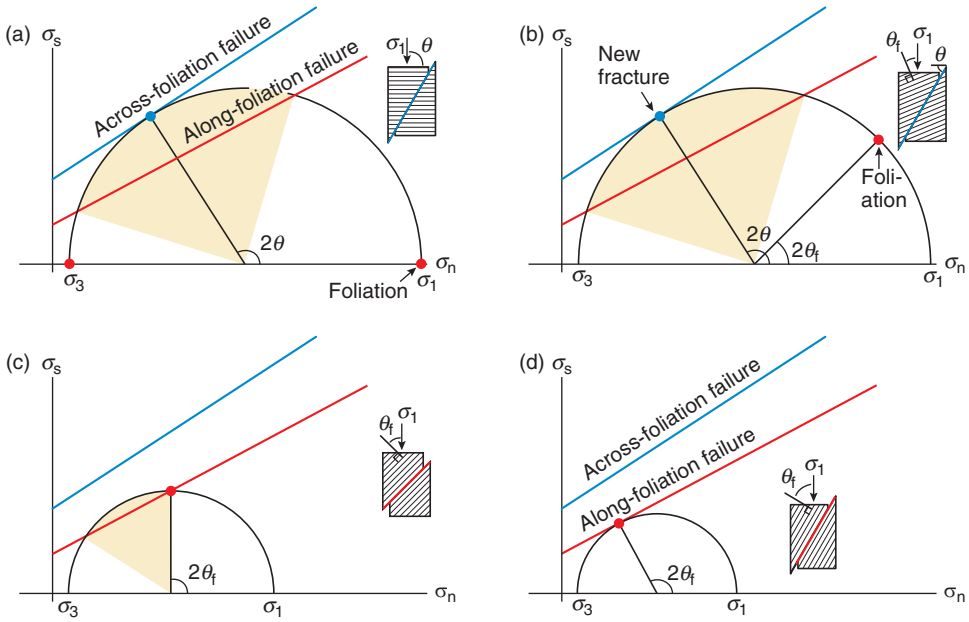

Figure 7.22 Illustration of the role of a preexisting foliation, for constant σ_3. (a) σ_1 acting perpendicular to the foliation, in which case differential stress builds up until the Mohr circle touches the upper envelope and across-foliation failure occurs. Colored sector indicates the range of orientations for along-foliation failure. (b) σ_1 at a high angle to the foliation, still too high for foliation-parallel failure (foliation still outside of the colored sector). (c) σ_1 at 45° to the foliation, causing foliation-parallel failure. Sector indicates the range of foliation orientations where along-foliation failure would occur for this particular state of stress. (d) The angle between σ_1 and the foliation that gives failure at the lowest possible differential stress. This is the weakest direction of a foliated rock.

Whether a rock fails along a weak preexisting fabric or fracture depends on the orientation of the fracture relative to the stress field.

The Mohr diagram and the failure envelopes discussed above only consider confining and differential stress and do not take into consideration σ_2. Experiments show that the influence of σ_2 is small and most pronounced when two of the stress axes are equal in size. For a vertical σ_1, the dip of the shear fracture is lowest when $\sigma_2 = \sigma_1$ and highest when $\sigma_2 = \sigma_3$. For foliated rocks where the foliation does not contain the intermediate principal stress axes, the influence of σ_2 is greater. In this case the resolved normal and shear stress on the foliation depends on all three principal stresses.

Temperature has a major influence on rheology in the plastic regime, but its influence within the brittle regime is relatively small for most common minerals. It does however control the range of the brittle regime as increasing temperature lowers the von Mises yield stress (lowers the yield point or the stress at which rock flows plastically).

An interesting laboratory observation is related to sample size: as the size of the sample increases, its strength is reduced. The reason for this somewhat surprising finding is simply that large samples contain more microfractures than small samples. Because microfractures differ in length and shape, a large sample is likely to contain some microfractures that have a shape that causes larger stress concentrations than any of those in a smaller sample of the same rock.

During a rock experiment, a large sample is likely to fracture before a smaller one.

The dependence on scale is even more pronounced at larger scales. Think of all the joints, faults and other weak structures in the crust that will be activated before the strength of the rock itself is reached. Such weak structures control the strength of the brittle crust, which means that the upper crust is not by far as strong as suggested by experimental testing of unfractured samples in the laboratory. This brings us to another important topic; the reactivation of brittle fractures by frictional sliding.

Growth and morphology of fractures

Shear fractures cannot propagate in their own plane, but rather spawn new tensile cracks (wing cracks) according

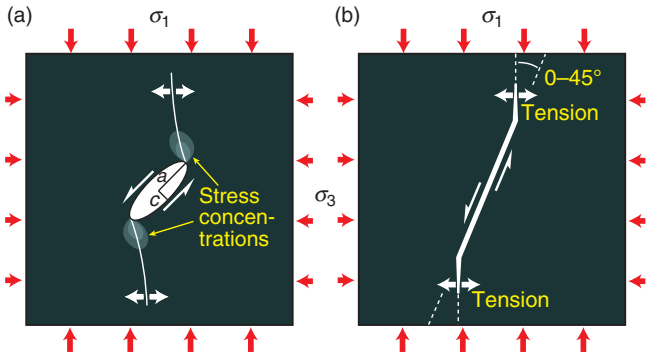

Figure 7.23 (a) Griffith crack modeled as an elliptical void. Tensile stress concentrates near the crack tips (compare with Figure 7. 20). (b) A critically stressed Griffith crack at the tip of a shear fracture. The Griffith crack is oriented between 0 and 45° with respect to σ_1, depending on the ratio σ_1/σ_3. Note that tensile stress develops near the crack tips in spite of the overall compressional stress, that crack growth is accommodated by sliding along the main crack, and that the crack grows toward parallelism with σ_1.

to Griffith's theory (Figure 7.23 and Box 7.3) or develop by activation of already existing extension fractures. In contrast, extension fractures may propagate into long structures. Ideally, an extension fracture will grow radially from a nucleation point so that at any point the propagation front (tipline) has the shape of an ellipse (Figure 7.24a, b). The rate of propagation increases after initiation, and the joint surface gets rougher until it propagates so fast that the stress readjustments or stress oscillations at the crack tip cause it to bend. In detail, the tip bifurcates and off-plane microcracks form because of high stress and/or local heterogeneities in the tip zone. The result is long, narrow planes slightly oblique to the main fracture surface named **hackles** (Figure 7.24c), and the hackles form **plumose** (featherlike) **structures**. Plumose structures reflect the propagation direction along the plume axis, as shown in Figure 7.25.

Locally the main fracture may enter an area with a different stress orientation. This would typically be a bedding interface or some other boundary between two rock types of different mechanical properties, in which case a series of twisted joints or **twist hackles** form in what is called a **fringe zone**. Twist hackles tend to be oriented **en echelon** because of the shear component on the main fracture locally imposed by the new orientation of σ_3. The twist hackles try to orient perpendicular to σ_3, hence the twisting (Figure 7.26).

Extension fractures tend to grow in pulses. Each propagation pulse tends to end with an out-of-plane propagation with a slowing down or complete arrest until

BOX 7.3 FRACTURE GROWTH AND WING CRACKS

One of the peculiarities of rock mechanics is the fact that, even though a deforming sample develops through-going shear fracture(s) that make an acute (~30°) angle to σ_1, shear fractures cannot grow in their own plane. Instead, a Mode I fracture forms parallel with σ_1. Such fractures are known as wing cracks or edge cracks. In three dimensions wing cracks (Mode I) will form along both the Mode II and Mode III edges of the main fracture.

This development is in agreement with theoretical stress considerations. But how does the shear fracture propagate from this stage? The general answer is that the Mode I wing cracks are broken by a new shear fracture – a process that keeps repeating as the main fracture grows. The result is a zone of minor fractures along and around the main shear fracture, a sort of damage zone akin to that defined for faults in Chapter 8.

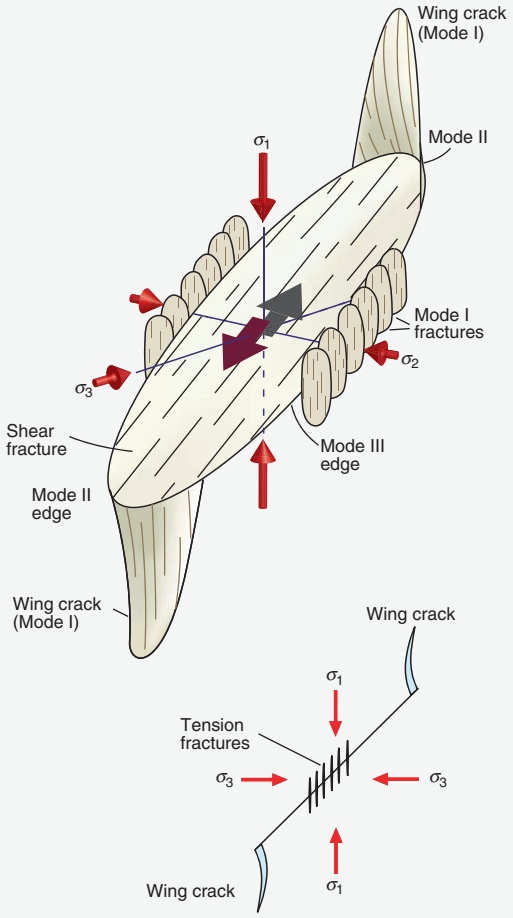

Illustration based on Scholtz (1990).

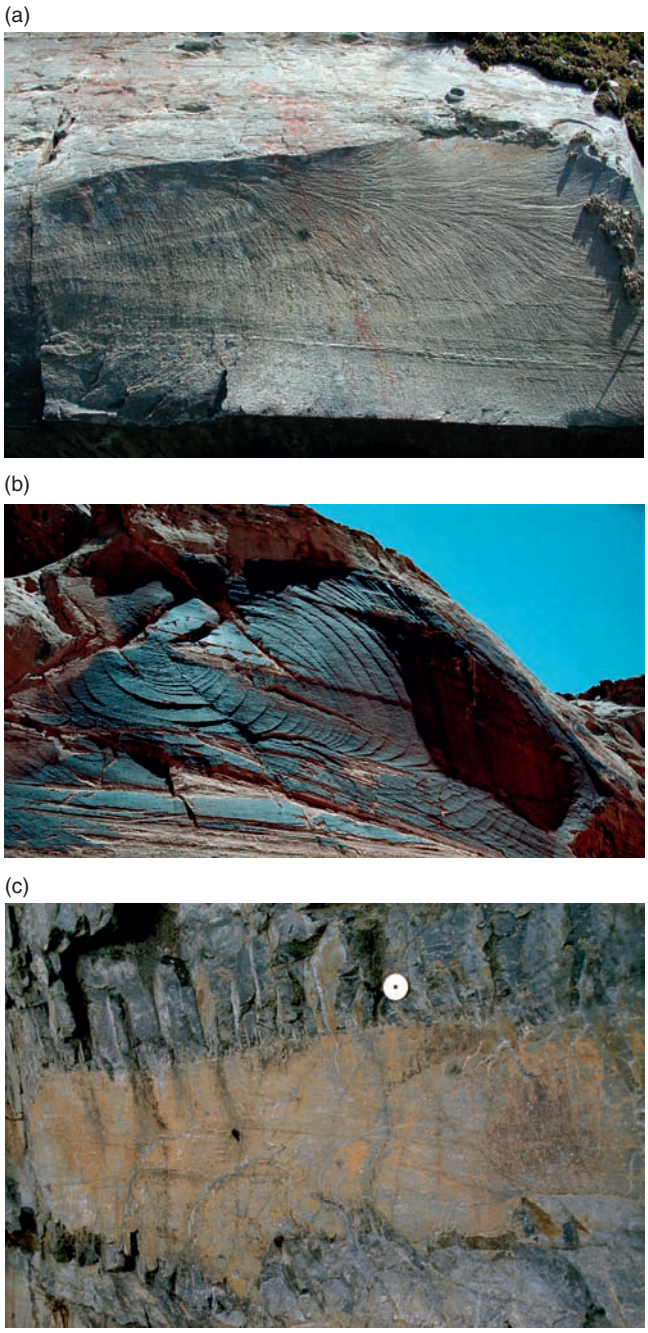

Figure 7.24 (a) Arrest lines and plumose structures in meta-greywackes from Telemark, Norway. Note the faint arrest lines oriented perpendicular to the plumose hackles. (b) Elliptically arranged arrest lines in the Navajo Sandstone, Utah. This sandstone is too coarse-grained for the plumose pattern to show up. (c) En-echelon hackle fringes (twist hackles) along a fracture in meta-rhyolite in the Caledonides of West Norway.

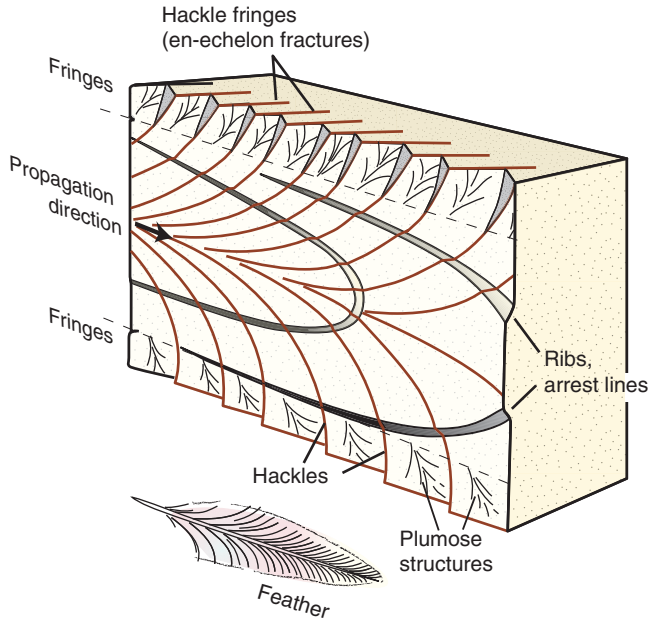

Figure 7.25 Schematic illustration of structures characteristic of joint surfaces. Based on Hodgson (1961).

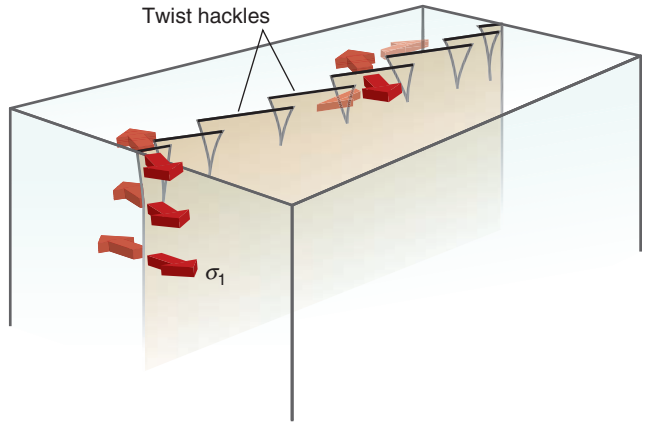

Figure 7.26 The twisting of extension fractures as they reach an interface with a mechanically different rock layer. Note the parallel twisting of σ_1 and the fractures (hackles). Compare with the hackles illustrated in Figure 7.24c.

enough energy has built up to initiate the next pulse. Ribs are thus locations of minimum propagation velocity and form parabolic (elliptic in massive rocks) irregularities sometimes referred to as **arrest lines**. Ribs are perpendicular to the plumose hackles (Figures 7.24a and 7.25) and together these structures provide unique information about the growth history of extension fractures. Plumose structures are characteristic for joints in fine-grained rocks such as siltstones, while arrest lines are also commonly seen in coarser-grained lithologies such as sandstones and granites.

7.5 Fracture termination and interaction

Studies of shear fracture terminations reveal that they sometimes split into two or more fractures with new orientations and, as indicated in Figure 7.27, a spectrum of different fracture geometries can been found. We have

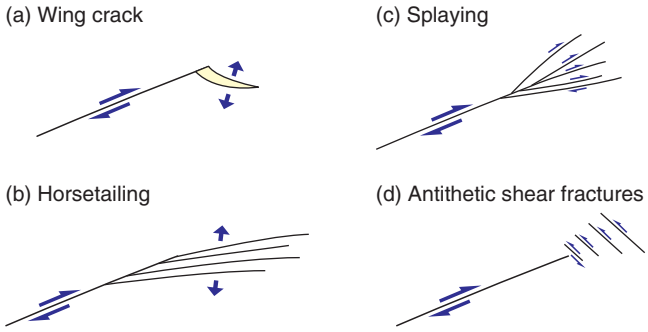

Figure 7.27 Minor fractures at the termination of shear fractures.

Figure 7.28 Horsetailing at the end of a shear fracture in gneiss.

already looked at **wing cracks**, which are tensile fractures at the end of shear fractures (Figure 7.27a). Wing cracks are represented by one or a few tensile fractures at each end of the main fracture and are associated with rapid decrease in displacement toward the tip. In other cases a whole population of minor, typically tensile fractures occur in the tip zone. These are asymmetrically arranged with respect to the main fracture and referred to as **horsetail fractures** (Figures 7.27b and 7.28). If the secondary fractures in the tip zone represent a fan-shaped splaying of the main fracture, then the commonly used term is **splay faults** (Figure 7.27c). While splay faults are synthetic with respect to the main fault, antithetic fractures may also occur in the tip zone of fractures, as shown in Figure 7.27d.

Most of these tip-zone fractures imply that the energy of the main fracture is distributed onto a number of fracture surfaces. This means that the energy on each fracture is reduced, which hampers continued fracture growth. The evolution of pronounced horsetail fractures or splay faults may thus "arrest" the main fracture and stop or at least pause further propagation of the fracture tip.

The stress field is perturbed around fractures in general and in the tip zone in particular. Thus, when the elastic strain fields around two fractures overlap, the local stress fields around each fracture will interfere and special geometries may develop. If a fracture grows toward an already existing one, the new fracture will curve as it "feels" the effect of the stress perturbation set up by the other fracture. Figure 7.29 indicates that the consequence for the resulting fracture geometry depends on the state of stress along the old fracture. If both fractures approach each other simultaneously, they will mutually affect each other, and the degree of curvature will depend on the general state of stress (Figure 7.30).

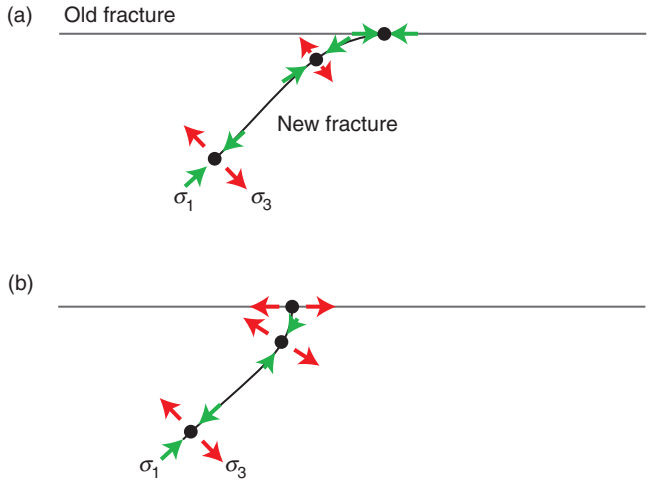

Figure 7.29 Local reorientation of fracture propagation direction in the vicinity of an existing fracture. The new fracture grows toward the preexisting one, seeking to maintain a 90° angle to σ_3. The geometry in (a) suggests that σ_1 is compressive with contraction along the preexisting fracture. If the new fracture curves against the preexisting one (b), then σ_1 and σ_3 are likely to be of similar magnitude with tension occurring along the preexisting fracture. Modified from Dyer (1988).

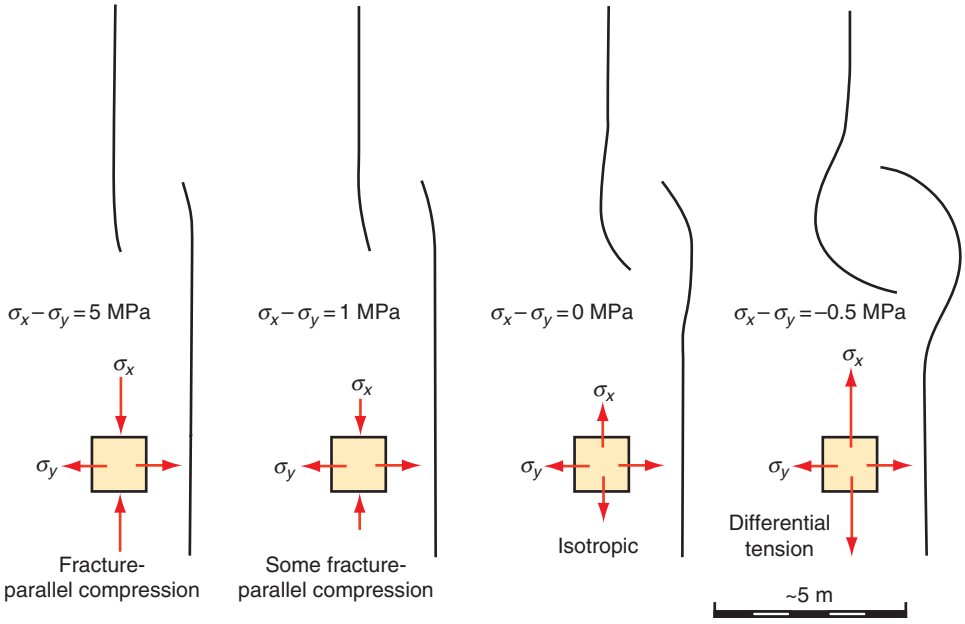

Figure 7.30 Schematic illustration of how fracture tip interaction depends on the differential stress ($\sigma_x - \sigma_y$) of the remote stress field. Based on Olsen and Pollard (1989) and Cruikshank *et al.* (1991).

7.6 Reactivation and frictional sliding

The Coulomb and Griffith fracture criteria, as formulated above, apply until the rock fails. One of the implications of this fact is that Anderson's theory of faulting, which again builds on Coulomb's theory, is only valid for infinitesimal fracture displacements. Once a fracture is formed it represents a plane of weakness. Renewed stress build-up is likely to reactivate existing fractures at a lower level of stress instead of creating a new fracture through the energy-demanding process of growth and linkage of minor flaws in the rock. Reactivation of fractures is a pre-requisite for major faults to develop. Had reactivation not happened, the crust would have been packed with short fractures with small displacements.

The orientation of a preexisting fracture and its friction are the most important parameters, in addition to the stress field itself (Figure 7.31). The orientation determines the resolved shear and normal stresses on the surface. When σ_n is oriented perpendicular to the fracture there is no shear stress on the surface, and the fracture is stable. In the general case there is a (resolved) shear stress on the fracture, and the friction constrains the reactivation potential. That local friction on the fracture is commonly referred to as the **coefficient of sliding friction** (μ_f).

The coefficient of sliding friction is simply the shear stress required to activate slip on the fracture divided by the normal stress acting across the fracture:

$$\mu_f = \frac{\sigma_s}{\sigma_n} \tag{7.9}$$

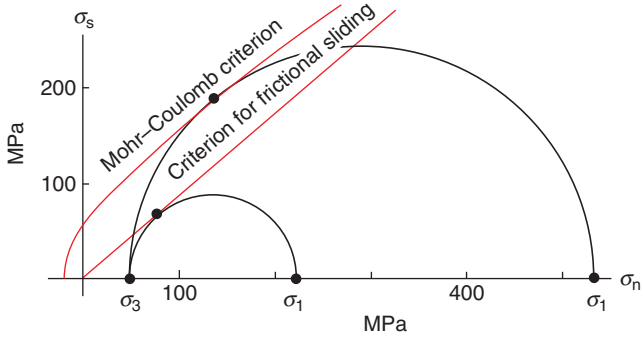

Figure 7.31 The effect of a preexisting fracture (plane of weakness), illustrated in the Mohr diagram. The criterion for reactivation (frictional sliding) is different from that of an unfractured rock of the same kind, and the differential stress required to reactivate the fracture is considerably smaller than that required to generate a new fracture in the rock. This example is based on experiments on crystalline rocks at a confining pressure of 50 MPa (*c.* 2 km depth).

In the Mohr diagram, this is a straight line (Figure 7.31), and it goes through the origin if we assume that the existing fracture has no cohesion. If the fracture has a cohesive strength (C_f) the expression becomes

$$\mu_f = \frac{\sigma_s - C_f}{\sigma_n} \tag{7.11}$$

The magnitude of C_f is usually low, and μ_f is similar for most rocks at moderate to high confining pressures. For low confining pressures the **surface roughness** of the fracture becomes important. Fault asperities resist fault slippage, and may lead to stick-slip deformation (Figure 8.34) at shallow burial depths. At deeper depths

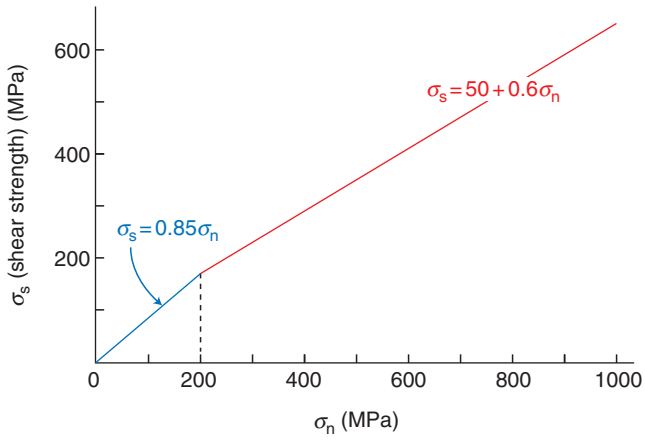

Figure 7.32 Byerlee's law is an empirical law that relates critical shear stress to normal stress. The horizontal scale is related to crustal depth (increasing to the right).

asperities play a much smaller role as far as friction is concerned. After numerous experiments, Byerlee was able to empirically define the critical shear stress at low confining pressure as

$$\sigma_s = 0.85\sigma_n \qquad (\sigma_s < 200 \text{ MPa}) \tag{7.12}$$

while the equation for higher confining pressure was found to be

$$\sigma_s = 0.5 + 0.6\sigma_n \qquad (\sigma_s > 200 \text{ MPa}) \tag{7.13}$$

These equations, shown graphically in Figure 7.32, are known as **Byerlee's law** and hold for most rocks except those that contain abundant H_2O-rich clay minerals.

Byerlee's law describes the vertical increase in critical shear stress (stress required for faulting) through the frictional upper crust.

7.7 Fluid pressure, effective stress and poroelasticity

One of the great challenges in the field of structural geology in the twentieth century was to explain how gigantic thrust nappes could be transported for hundreds of kilometers without being crushed (Box 16.2). An important part of the explanation has to do with overpressured thrust zones, i.e. the thrust fault contains fluids with anomalously high pore pressure.

This is one of several examples where fluid pressure plays an important role. We have already looked at overpressured formations in sedimentary sequences (petroleum reservoirs) in Chapter 5, where overpressure can occur if pore water in a porous and permeable formation is confined between impermeable layers. Overpressure builds up as the weight of the overburden acts on the pore pressure. An additional effect comes from the fact that water expands more quickly than rock minerals during heating. If the water cannot escape, its thermal expansion will further increase the fluid pressure in the permeable unit.

Deeper down, metamorphic reactions release water and carbon dioxide. This may also lead to overpressure if the fluid is unable to escape along fracture networks in the generally impermeable metamorphic rocks. Mineral-filled extension fractures (veins) that occur in many low-grade metamorphic rocks are probably related to the increase of fluid pressure through metamorphic fluid release. Injection of magma under pressure is also a situation where the vertical stress is balanced by fluid (magma) pressure. Finally, an increase in the fluid pressure can cause reactivation of faults and fractures.

The fluid pressure counteracts the normal stress resolved on the fracture, so that the resolved shear stress may be sufficient for reactivation.

Whether a new fracture forms or an existing one is reactivated is controlled both by the fracture orientation relative to the principal stresses and by the effective stress. **Effective stress** ($\bar{\sigma}$) is the difference between the applied or remote stress and the fluid pressure:

$$\bar{\sigma} = \sigma - p_f \tag{7.14}$$

In three dimensions the effective stress can be expressed as

$$\begin{bmatrix} \bar{\sigma}_{11} & \bar{\sigma}_{12} & \bar{\sigma}_{13} \\ \bar{\sigma}_{21} & \bar{\sigma}_{22} & \bar{\sigma}_{23} \\ \bar{\sigma}_{31} & \bar{\sigma}_{32} & \bar{\sigma}_{33} \end{bmatrix} = \begin{bmatrix} \sigma_{11} & \sigma_{12} & \sigma_{13} \\ \sigma_{21} & \sigma_{22} & \sigma_{23} \\ \sigma_{31} & \sigma_{32} & \sigma_{33} \end{bmatrix} - \begin{bmatrix} p_f & 0 & 0 \\ 0 & p_f & 0 \\ 0 & 0 & p_f \end{bmatrix}$$
$$= \begin{bmatrix} \sigma_{11} - p_f & \sigma_{12} & \sigma_{13} \\ \sigma_{21} & \sigma_{22} - p_f & \sigma_{23} \\ \sigma_{31} & \sigma_{32} & \sigma_{33} - p_f \end{bmatrix} \tag{7.15}$$

or, if the principal stresses coincide with our coordinate axes,

$$\begin{bmatrix} \bar{\sigma}_1 & 0 & 0 \\ 0 & \bar{\sigma}_2 & 0 \\ 0 & 0 & \bar{\sigma}_3 \end{bmatrix} = \begin{bmatrix} \sigma_1 - p_f & 0 & 0 \\ 0 & \sigma_2 - p_f & 0 \\ 0 & 0 & \sigma_3 - p_f \end{bmatrix} \tag{7.16}$$

Fluid pressure will weaken the rock so that deformation can occur at a differential stress that would otherwise be insufficient for failure. For porous sandstone, the pore

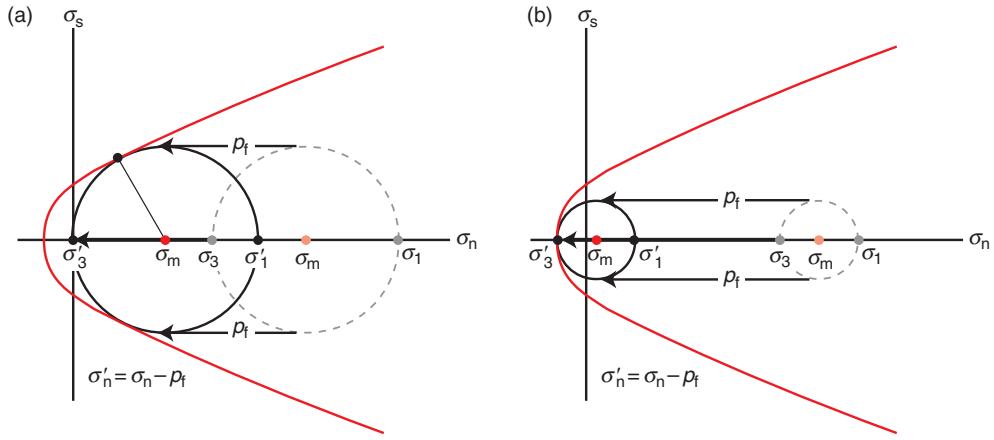

Figure 7.33 The effect of pumping up the pore fluid pressure p_f in a rock. The Mohr circle is "pushed" to the left (the mean stress is reduced) and a shear fracture will form if the fracture envelope is touched while σ_3 is still positive. A tensile fracture forms if the envelope is reached in the tensile field, as shown in (b) (low differential stress).

(fluid) pressure has the following effect on the Coulomb fracture criterion:

$$\sigma_s = C - \mu(\sigma_n - p_f) \tag{7.17}$$

An increase in pore pressure decreases the mean stress from σ_m to $\sigma_m - p_f$ while the differential stress $(\sigma_1 - \sigma_3)$ is constant (Figure 7.33).

If the effective stress is tensile (negative σ_3), i.e. if

$$\bar{\sigma}_3 = \sigma_3 - p_f < 0 \tag{7.18}$$

tensile fractures can form. In dry or hydrostatically pressured rocks tensile fractures can only be expected to form at very shallow depths (less than a few hundred meters), but fluid overpressure makes it possible to have local tensile stress even at many kilometers depth.

We can rewrite Equation 7.14 so that it becomes clearer that the total stress is the sum of the effective stress and the pore pressure:

$$\sigma = \bar{\sigma} + p_f \tag{7.19}$$

or

$$\begin{bmatrix} \sigma_{11} & \sigma_{12} & \sigma_{13} \\ \sigma_{21} & \sigma_{22} & \sigma_{23} \\ \sigma_{31} & \sigma_{32} & \sigma_{33} \end{bmatrix} = \begin{bmatrix} \bar{\sigma}_{11} & \bar{\sigma}_{12} & \bar{\sigma}_{13} \\ \bar{\sigma}_{21} & \bar{\sigma}_{22} & \bar{\sigma}_{23} \\ \bar{\sigma}_{31} & \bar{\sigma}_{32} & \bar{\sigma}_{33} \end{bmatrix} + \begin{bmatrix} p_f & 0 & 0 \\ 0 & p_f & 0 \\ 0 & 0 & p_f \end{bmatrix} \tag{7.20}$$

To illustrate this relationship, imagine a porous and permeable sandstone (Figure 7.34) that is exposed to a uniaxial-strain reference state of stress inside a container. Let us first assume that the rock is dry and that the grains exert an average stress σ_n^w against the walls of the container. This stress is not evenly distributed along the walls but concentrated at the grain–wall contact points (Figure 7.35). The grain–wall contact stress σ_n^g depends on the area across which it is distributed and can be expressed in terms of the porosity ϕ:

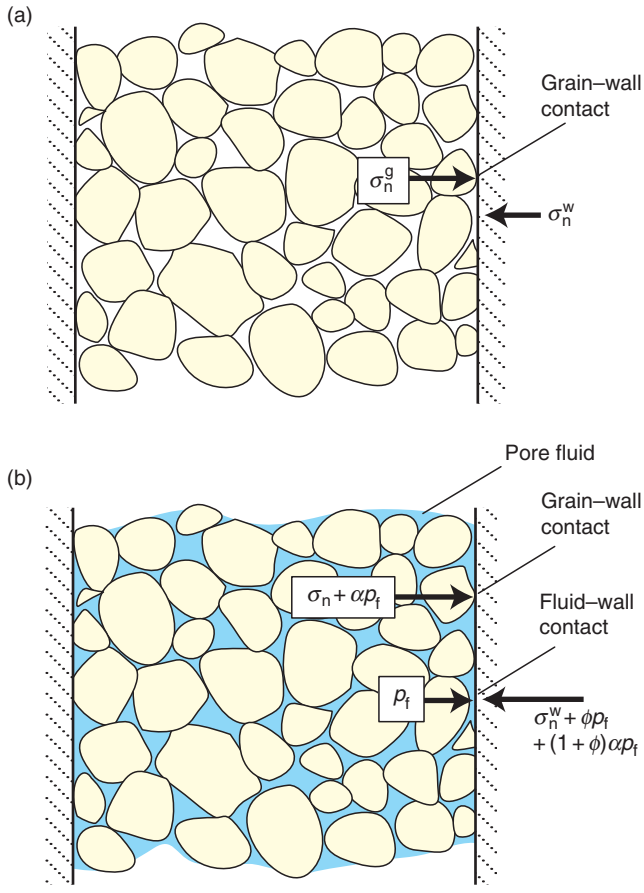

Figure 7.34 The effect of increasing the pore pressure p_f on the total stress situation in a porous rock (closed uniaxial-strain stress model). In a dry rock (a), stresses are transmitted across grain–grain or grain–wall contacts only. If pore fluid is added with a low p_f (b), then the increase in normal stress at grain–wall contacts is smaller than the increase in pore pressure because of the absorption of stress by elastic deformation in the grains. This is the poroelastic effect. Modified from Engelder (1993).

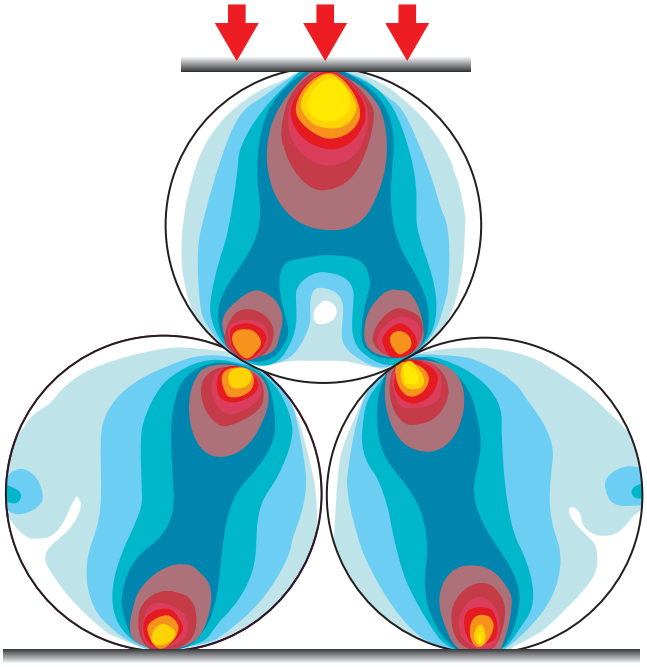

Figure 7.35 Illustration of stress concentrations (stress bridges) at grain–grain contact areas in a porous rock or sediment. Warm colors indicate high stress. Based on Gallagher *et al.* (1974).

$$\sigma_n^g = \left(\frac{1}{1-\phi}\right)\sigma_n^w \qquad (7.21)$$

We now fill the pores with fluid at some moderate pressure p_f, which causes the pressure against the walls to increase. The parts of the walls that are in contact with the fluid will "feel" the fluid pressure directly. At the grain–wall contact points the normal stress on the wall increases by a fraction of p_f, i.e. by a factor αp_f where $\alpha < 1$. The increase in stress against the wall, which we denote $\Delta\sigma_n$, will not be equal to p_f, but will be less by an amount that depends on the porosity of the sandstone:

$$\Delta\sigma_n = \phi p_f + (1-\phi)\alpha p_f \qquad (7.22)$$

The factor α is known as the Biot poroelastic parameter and characterizes the poroelastic effect. But why is the stress increase less than p_f? Because the cemented grain contacts are elastic. Thus, some of the pore fluid pressure p_f is taken up by elastic deformation.

The poroelastic effect is important when considering the state of stress in sedimentary basins. It may also contribute to the formation and propagation of fractures in porous rocks (Figure 7.36). In keeping with Griffith's theory, a flaw of some kind represents a possible nucleation point for a tensile fracture. Increasing the pore pressure by an amount Δp_f gives a new pore pressure p_f that will be identical within and outside of the flaw,

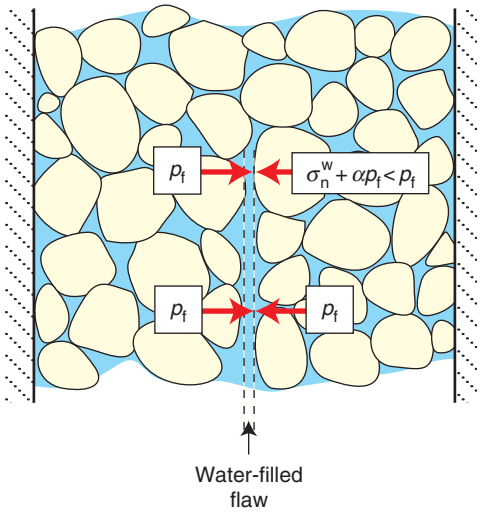

Figure 7.36 The stress situation in a flaw in a permeable porous rock. The poroelastic effect causes the stress across the grain–flaw part of the flaw walls to be less than the pore fluid pressure. Tensile stress occurs if the pore pressure is high enough.

because the rock is permeable. At the walls between the flaw and the rock, however, the poroelastic effect (Equation 7.22) comes into play. It tells us that the general increase in pore pressure causes the average normal stress at the rock sides of the flaw to increase at a lower rate than in the flaw. As the pore pressure increases, at some point the fluid pressure p_f within the flaw will exceed the average normal stress exerted by the grains on the walls of the flaw. The walls are then under tension and may further separate as the flaw grows into a larger extension fracture. The tensile stress is concentrated at the tips, and its magnitude depends on the shape of the flaw or crack according to Equation 7.8. Once the extension fracture grows, the volume of the fracture increases, the pore pressure drops, and the propagation stops or pauses until the pore pressure is restored. This kind of fracture propagation history is recorded by the formation of arrest lines (Figure 7.25).

7.8 Deformation bands and fractures in porous rocks

Rocks respond to stress in the brittle regime by forming extension fractures and shear fractures (slip surfaces). Such fractures are sharp and mechanically weak discontinuities, and thus prone to reactivation during renewed stress build-up. At least this is how non-porous and low-porosity rocks respond. In highly porous rocks and sediments, brittle deformation is expressed by related, although different, deformation structures referred to as **deformation bands**.

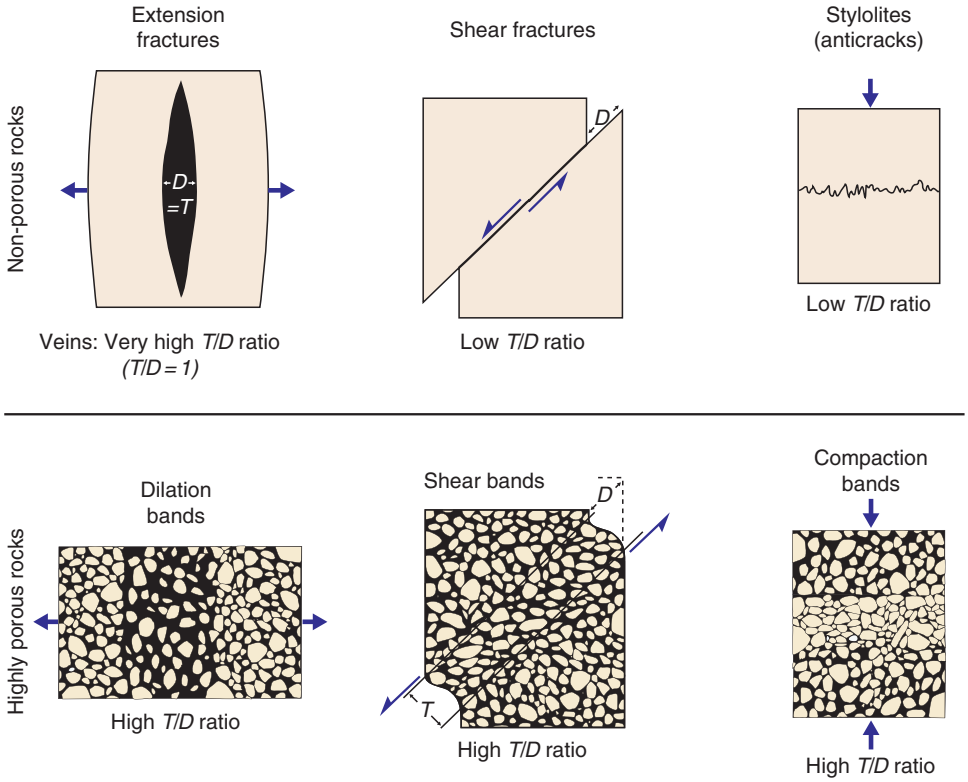

Figure 7.37 Kinematic classification of deformation bands and their relationship to fractures in low-porosity and non-porous rocks. *T*, thickness; *D*, displacement.

Figure 7.38 Cataclastic deformation band in porous Navajo Sandstone. The thickness of the band seems to vary with grain size, and the shear offset is less than 1 cm (the coin is 1.8 cm in diameter).

Deformation bands are mm-thick zones of localized compaction, shear and/or dilation in deformed porous rocks. Figure 7.37 shows how deformation bands kinematically relate to fractures in non-porous and low-porosity rocks, but there are good reasons why deformation bands should be distinguished from ordinary fractures. One is that they are thicker and at the same time exhibit smaller shear displacements than regular slip surfaces of comparable length (Figure 7.38). This has led to the term **tabular discontinuities**, as opposed to **sharp discontinuities** for fractures. Another is that, while cohesion is lost or reduced across regular fractures, most deformation bands maintain or even show increased cohesion. Furthermore, there is a strong tendency for deformation bands to represent low-permeability tabular objects in otherwise highly permeable rocks. This permeability reduction is related to collapse of pore space, as seen in the band from Sinai portrayed in Figure 7.39. In contrast, most regular fractures increase permeability, particularly in low-permeability and impermeable rocks. This distinction is particularly important to petroleum geologists and hydrogeologists concerned with fluid flow in reservoir rocks. The strain hardening that occurs during the formation of many deformation bands also makes them different from fractures, which are associated with softening.

The difference between brittle fracturing of non-porous and porous rocks lies in the fact that porous rocks have a pore volume that can be utilized during grain reorganization. The pore space allows for effective rolling and sliding of grains. Even if grains are crushed, grain fragments can be organized into nearby pore space.

The kinematic freedom associated with pore space allows the special class of structures called deformation bands to form.

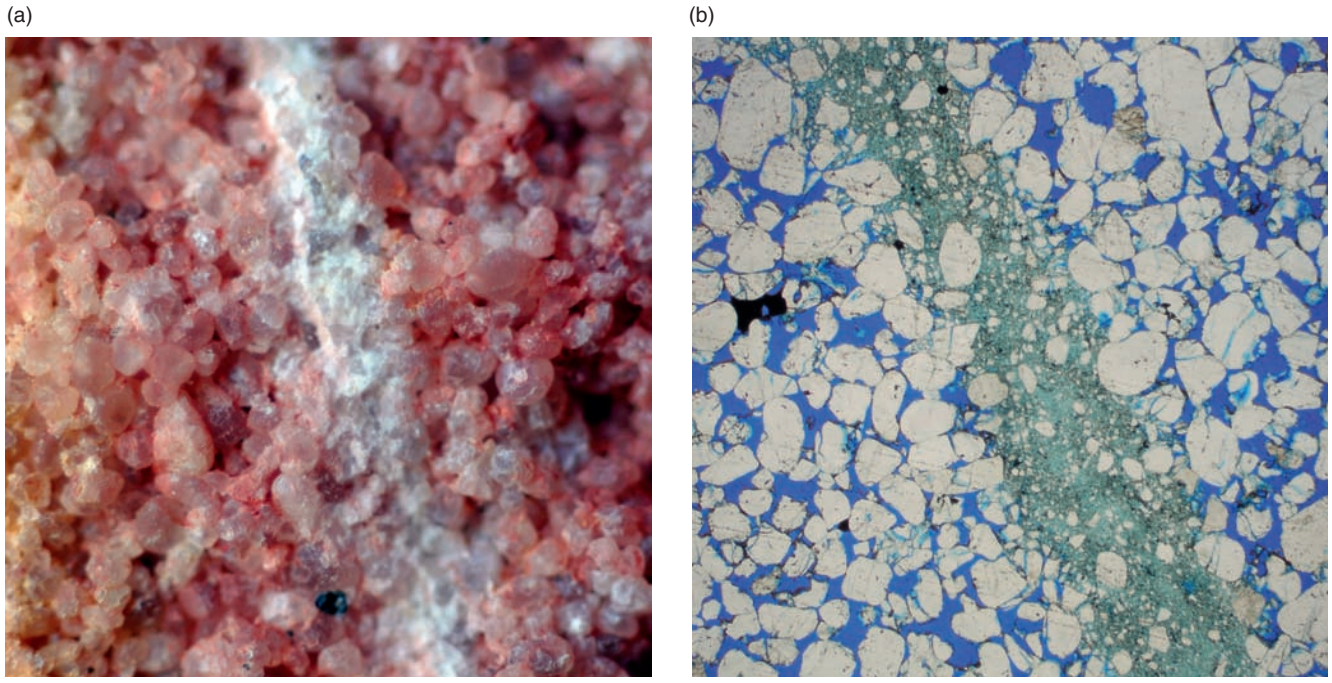

Figure 7.39 Cataclastic deformation band in outcrop (left) and thin section (right) in the Nubian Sandstone, Sinai. Note the extensive crushing of grains and reduction of porosity (pore space is blue in the thin section). Width of bands ~1 mm.

What is a deformation band?

How do deformation bands differ from regular fractures in non-porous rocks? Here are some characteristics of deformation bands:

- Deformation bands are restricted to highly porous granular media, notably porous sandstones.
- A shear deformation band is a wider zone of deformation than regular shear fractures of comparable displacement.
- Deformation bands do not develop large offsets. Even 100 m long deformation bands seldom have offsets in excess of a few centimeters, while shear fractures of the same length tend to show meter-scale displacement.
- Deformation bands occur as single structures, as clusters, or in zones associated with slip surfaces (faulted deformation bands). This is related to the way that faults form in porous rocks by faulting of deformation band zones (see Chapter 8).

Types of deformation bands

Similar to fractures, deformation bands can be classified in a kinematic framework, where **shear (deformation) bands**, **dilation bands** and **compaction bands** form the end-members (Figure 7.37). It is also of interest to identify the *mechanisms* operative during the formation of deformation bands. Deformation mechanisms depend on internal and external conditions such as mineralogy, grain size, grain shape, grain sorting, cementation, porosity, state of stress etc., and different mechanisms produce bands with different petrophysical properties. Thus, a classification of deformation bands based on deformation processes is particularly useful if permeability and fluid flow is an issue. The most important mechanisms are:

- Granular flow (grain boundary sliding and grain rotation)
- Cataclasis (grain fracturing)
- Phyllosilicate smearing
- Dissolution and cementation

Deformation bands are named after their characteristic deformation mechanism, as shown in Figure 7.40.

Disaggregation bands develop by shear-related disaggregation of grains by means of grain rolling, grain boundary sliding and breaking of grain bonding cements; the process that we called particulate or granular flow at the beginning of this chapter (Figure 7.1a). Disaggregation bands are commonly found in sand and poorly consolidated sandstones and form the "faults" produced in most

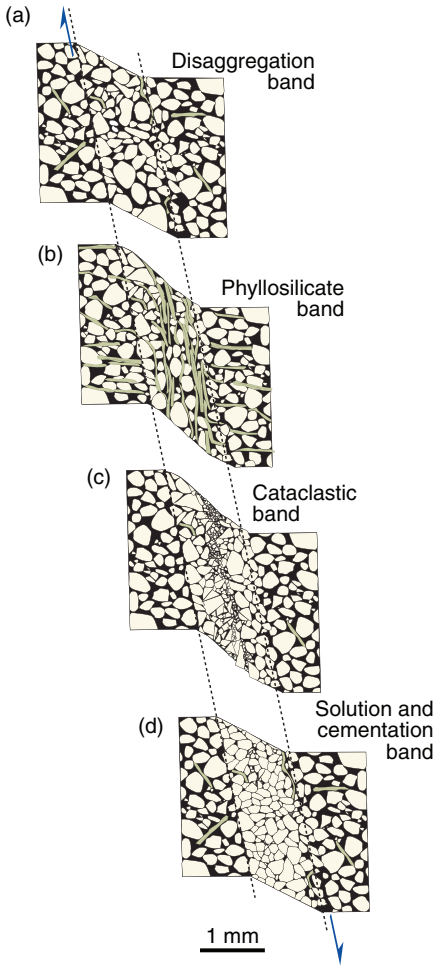

Figure 7.40 The different types of deformation bands, distinguished by dominant deformation mechanism. Modified from Fossen *et al.* (2007).

sandbox experiments. Disaggregation bands can be almost invisible in clean sandstones, but may be detected where they cross and offset laminae (Figure 7.41). Their true offsets are typically a few centimeters and their thickness varies with grain size. Fine-grained sand(stones) develop ~1 mm thick bands, whereas coarser-grained sand(stones) host single bands that may be at least 5 mm thick.

Macroscopically, disaggregation bands are ductile shear zones where sand laminae can be traced continuously through the band. Most pure and well-sorted quartz-sand deposits are already compacted to the extent that the initial stage of shearing involves some dilation (dilation bands), although continued shear-related grain reorganization may reduce the porosity at a later point.

Phyllosilicate bands (also called framework phyllosilicate bands) form in sand(stone) where the content of platy minerals exceeds about 10–15%. They can be considered as a special type of disaggregation band where platy minerals promote grain sliding. Clay minerals tend to mix with other mineral grains in the band while coarser phyllosilicate grains align to form a local fabric within the bands due to shear-induced rotation. Phyllosilicate bands are easy to detect, as the aligned phyllosilicates give the band a distinct color or fabric that may be reminiscent of phyllosilicate-rich laminae in the host rock.

If the phyllosilicate content of the rock changes across bedding or lamina interfaces, a deformation band may change from an almost invisible disaggregation band to a phyllosilicate band. Where clay is the dominant platy mineral, the band is a fine-grained, low-porosity zone that can accumulate offsets that exceed the few centimeters exhibited by other types of deformation bands. This is related to the smearing effect of the platy minerals along phyllosilicate bands that apparently counteracts any strain hardening resulting from interlocking of grains.

If the clay content of the host rock is high enough (more than ~40%), the deformation band turns into a **clay smear**. Clay smears typically show striations and classify as slip surfaces rather than deformation bands. Examples of deformation bands turning into clay smears as they leave sandstone layers are common.

Cataclastic bands form where mechanical grain breaking is significant (Figure 7.39). These are the classic deformation bands first described by Atilla Aydin from the Colorado Plateau in the western USA. He noted that many cataclastic bands consist of a central cataclastic core contained within a mantle of (usually) compacted or gently fractured grains. The core is most obvious and is characterized by grain size reduction, angular grains and significant pore space collapse (Figure 7.39). The crushing of grains results in extensive grain interlocking, which promotes strain hardening. Strain hardening may explain the small shear displacements observed on cataclastic deformation bands ($\leq$3–4 cm). Some cataclastic bands are pure compaction bands (Figure 7.41), while most are shear bands with some compaction across them.

Cataclastic bands occur most frequently in sandstones that have been deformed at depths of about 1.5–3 km, although evidence of cataclasis is also reported from deformation bands deformed at shallower depths. Comparison suggests that shallowly formed cataclastic deformation bands show less intensive cataclasis than those formed at 1.5–3 km depth.

Cementation and dissolution of quartz and other minerals may occur preferentially in deformation bands

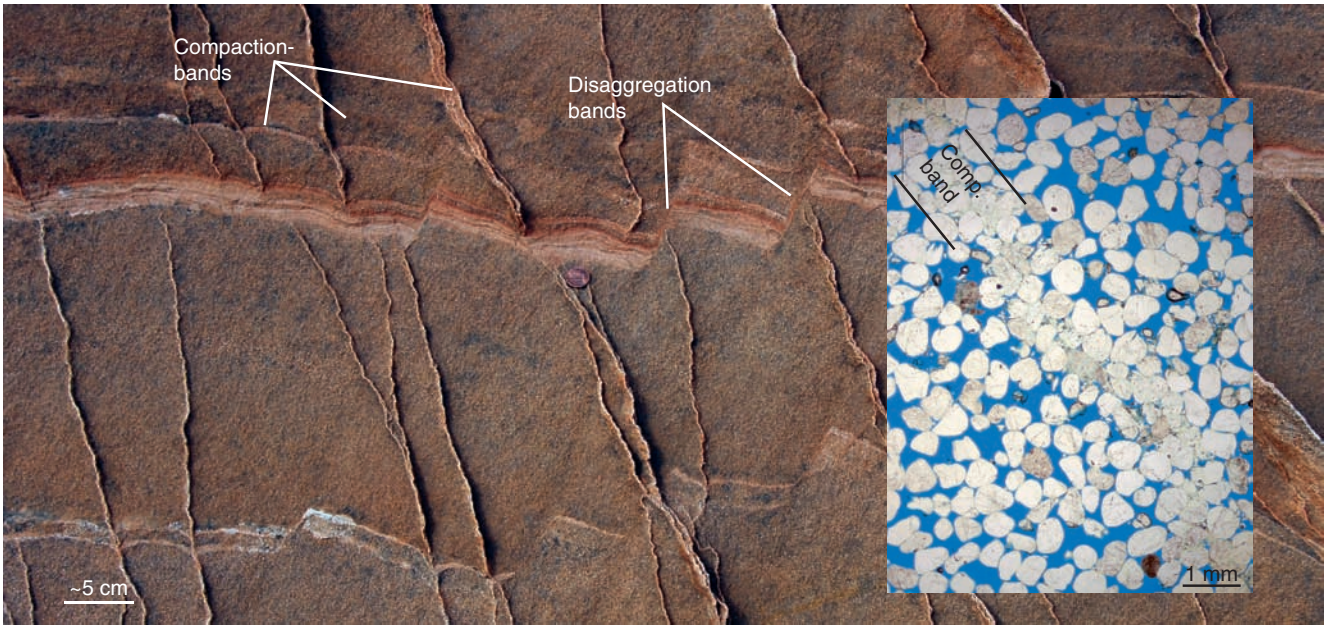

Figure 7.41 Right-dipping compaction bands overprinting left-dipping soft-sedimentary disaggregation bands (almost invisible). The sandstone is very porous except for thin layers, where compaction bands are absent. Hence, the compaction bands only formed in very high porosity sandstone. Thin section photo shows that the compaction is assisted by dissolution and some grain fracture. Navajo Sandstone, southern Utah.

where diagenetic minerals grow on the fresh surfaces formed during grain crushing and/or grain boundary sliding. Such preferential growth of quartz is generally seen in deformation bands in sandstones buried to more than 2–3 km depth (>90 °C) and can occur long after the formation of the bands.

Influence on fluid flow

Deformation bands form a common constituent of porous oil, gas and water reservoirs, where they occur as single bands, cluster zones or in fault damage zones (see next chapter). Although they are unlikely to form seals that can hold significant hydrocarbon columns over geologic time, they can influence fluid flow in some cases. Their ability to do so depends on their internal permeability structure and thickness or frequency. Clearly, the zone of cataclastic deformation bands shown in Figure 7.42 will have a far greater influence on fluid flow than the single cataclastic band shown in Figure 7.38 or 7.39.

Cataclastic deformation bands show the most significant permeability reductions.

Deformation band permeability is governed by the deformation mechanisms operative during their formation, which again depends on a number of lithological and physical factors. In general, disaggregation bands show little porosity and permeability reduction, while phyllosilicate and, particularly, cataclastic bands show permeability reductions up to several orders of magnitude. Deformation bands are thin, so the number of deformation bands (their cumulative thickness) is important when their role in a petroleum reservoir is to be evaluated.

Also important are their continuity, variation in porosity/permeability and orientation. Many show significant variations in permeability along strike and dip due to variations in amount of cataclasis, compaction or phyllosilicate smearing. Deformation bands tend to define sets with preferred orientation (Figure 7.43), for instance in damage zones, and this anisotropy can influence the fluid flow in a petroleum reservoir, for example during water injection. All of these factors make it difficult to evaluate the effect of deformation bands in reservoirs, and each reservoir must be evaluated individually according to local parameters such as time and depth of

Figure 7.42 Very dense cluster of cataclastic deformation bands in the Entrada Sandstone, Utah.

Figure 7.43 Conjugate (simultaneous and oppositely dipping) sets of cataclastic deformation bands in sandstone. Note the positive relief of the deformation bands due to grain crushing and cementation. The bands fade away downward into the more fine-grained and less-sorted unit. Entrada Sandstone, Utah.

deformation, burial and cementation history, mineralogy, sedimentary facies and more.

The influence of deformation bands on petroleum or groundwater production depends on the permeability contrast, cumulative thickness, orientations, continuity and connectivity.

What type of structure forms, where and when?

Given the various types of deformation bands and their different effects on fluid flow, it is important to understand the underlying conditions that control when and where they form. A number of factors are influential, including burial depth, tectonic environment (state of stress) and host rock properties, such as degree of lithification, mineralogy, grain size, sorting and grain shape. Some of these factors, particularly mineralogy, grain size, rounding, grain shape and sorting, are more or less constant for a given sedimentary rock layer. They may, however, vary from layer to layer, which is why rapid changes in deformation band development may be seen from one layer to the next.

Other factors, such as porosity, permeability, confining pressure, stress state and cementation, are likely to change with time. The result may be that early deformation bands are different from those formed at later stages in the same porous rock layer, for example at deeper burial depths. Hence, the sequence of deformation structures in a given rock layer reflects the physical changes that the sediment has experienced throughout its history of burial, lithification and uplift.

To illustrate a typical structural development of sedimentary rocks that go through burial and then uplift, we use the diagram from Figure 5.10 and add characteristic structures (Figure 7.44). The earliest forming deformation bands in sandstones are typically disaggregation bands or phyllosilicate bands. Such structures form at low confining pressures (shallow burial) when forces across grain contact surfaces are low and grain bindings are weak, and are therefore indicated at shallow levels in Figures 7.44 and 7.45. Many early disaggregation bands are related to local, gravity-controlled deformation such as local shale diapirism, underlying salt movement, gravitational sliding and glaciotectonics.

Cataclastic deformation bands can occur in poorly lithified layers of pure sand at shallow burial depths,

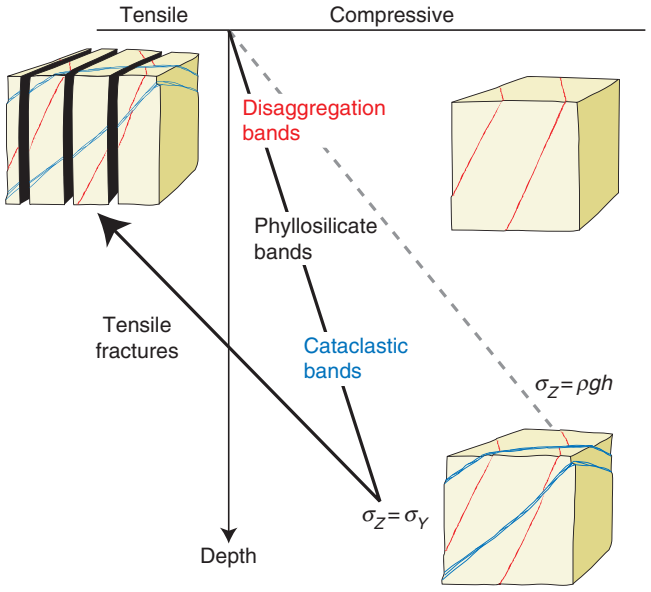

Figure 7.44 Different types of deformation bands form at different stages during burial. Extension fractures (Mode I fractures) are most likely to form during uplift. Also see Figure 5.10. From Fossen *et al.* (2007).

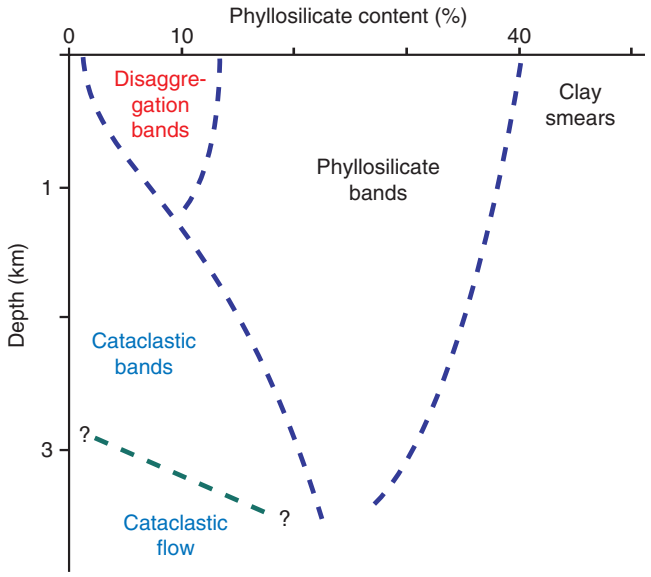

Figure 7.45 Tentative illustration of how different deformation band types relate to phyllosilicate content and depth. Many other factors influence the boundaries outlined in this diagram, and the boundaries should be considered as uncertain. From Fossen *et al.* (2007).

but are much more common in sandstones deformed at 1–3 km depth. Factors promoting shallow-burial cataclasis include small grain contact areas, i.e. good sorting and well-rounded grains, the presence of feldspar or other non-platy minerals with cleavage and lower hardness than quartz, and weak lithic fragments. Quartz, for instance, seldom develops transgranular fractures under low confining pressure, but may fracture by flaking or spalling. At deeper depths, extensive cataclasis is promoted by high grain contact stresses. Abundant examples of cataclastic deformation bands are found in the Jurassic sandstones of the Colorado Plateau, where the age relation between early disaggregation bands and later cataclastic bands is very consistent (Figure 7.44).

When a sandstone becomes cohesive and loses porosity during lithification (left side of Figure 7.44), deformation occurs by crack propagation instead of pore space collapse, and slip surfaces, joints and mineral-filled fractures form directly without any precursory formation of deformation bands. This is why late, overprinting structures are almost invariably slip surfaces, joints and mineral-filled fractures. Slip surfaces can also form by faulting of low-porosity deformation band zones at any burial depth, according to the model described in the next chapter (Section 8.5).

Joints and veins typically postdate both disaggregation bands and cataclastic bands in sandstones. The transition from deformation banding to jointing may occur as porosity is reduced, notably through quartz dissolution and precipitation. Since the effect of such diagenetically controlled strengthening may vary locally, deformation bands and joints may develop simultaneously in different parts of a sandstone layer, but the general pattern is deformation bands first, then faulted deformation bands (slip surface formation) and finally joints (tensile fractures in Figure 7.44) and perhaps faulted joints (Figure 1.4).

The latest fractures in uplifted sandstones tend to form extensive and regionally mappable joint sets generated or at least influenced by removal of overburden and cooling during regional uplift. Such joints are pronounced where sandstones have been uplifted and exposed, such as on the Colorado Plateau (Figure 1.4), but are unlikely to be developed in subsurface petroleum reservoirs unexposed to significant uplift. It therefore appears that knowing the burial/uplift history of a basin in relation to the timing of deformation events is very useful when considering the type of structures present in, say, a sandstone reservoir. Conversely, examination of the type of deformation structure present also gives information about deformation depth and other conditions at the time of deformation.

Summary

Brittle deformation tends to be extremely localized and result in structures that significantly weaken the upper crust. Separating different types of brittle structures is important because they reflect the state of stress and strain during their formation, and the different types of fractures alter rocks in different ways that affect mechanical properties, potential of reactivation and permeability structure. This has implications for engineering geoscientists, seismologists, hydrogeologists and petroleum geologists alike. The formation of fractures and deformation bands is also essential when it comes to fault formation and fault growth, which is the subject of the next chapter.There are many important points to be made from this chapter, and here are a few:

- Fractures form primarily in the brittle regime where brittle mechanisms dominate.
- Brittle deformation mechanisms are cataclasis (grain fracture), rigid grain rotation and grain translation through frictional grain boundary sliding (grain reorganization).
- Extension fractures such as joints can expand to become extensive structures, while shear fractures cannot expand as such unless small extension structures form ahead of shear fracture tips and weaken the rock. Shear fractures can then expand by coalescence of extension microfractures.
- Stress concentrates at the tip of both small and large fractures and helps them grow.
- High fluid pressure in cracks and pores also promotes fracture and fracture propagation.
- Extension fractures form perpendicular to σ_3.
- Shear fractures typically form at a 20–30° angle to σ_1.
- A fracture criterion relates the shear and normal stress that is required for a rock to fracture, i.e. the critical normal and shear stresses. The Coulomb criterion is linear, which means that there is a constant ratio between the critical shear and normal stress and is therefore represented by a straight line in Mohr space.
- The strength of undeformed rocks as measured experimentally is not representative of the brittle crust because of its many weak faults and fractures.
- A fracture's reactivation potential depends on its frictional resistance to reactivation, the fluid pressure inside the fracture, and its orientation relative to the principal stresses. The latter also determines the mode of reactivation (extension or shear).
- Both fractures and deformation bands are important in terms of permeability in deformed rocks, but generally have opposite functions: fractures increase permeability while deformation bands involve permeability reduction.

Review questions

1. What is the difference between cataclastic and granular flow?
2. What is frictional sliding?
3. What is the process zone that is located at the tip of shear fractures?

4. What is the difference between fractures and deformation bands?
5. Why do shear fractures not form at 45° to σ_1, where the resolved shear stress is at its maximum?
6. What is a wing crack and how do they form?
7. What structures can be found on joints that can reveal their growth history?
8. What does it mean that a rock is critically stressed?
9. What is a failure envelope and how is it established for a rock?
10. What is meant by the term Griffith cracks, and how do they affect rock strength and fracture propagation?
11. Why are large rock samples weaker than small samples of the same rock?
12. What is the coefficient of sliding friction and what is a representative value for this coefficient for the brittle crust?

E-MODULE

The e-learning module called *Brittle deformation* is recommended for this chapter.

FURTHER READING

Fractures and fracturing

Reches, Z. and Lockner, D. A., 1994, Nucleation and growth of faults in brittle rocks. *Journal of Geophysical Research* **99**: 18159–18172.

Scholz, C. H., 2002, *The Mechanics of Earthquakes and Faulting*. Cambridge: Cambridge University Press.

Schultz, R. A., 1996, Relative scale and the strength and deformability of rock masses. *Journal of Structural Geology* **18**: 1139–1149

Segall, P. and Pollard, D. D., 1983, Nucleation and growth of strike slip faults in granite. *Journal of Geophysical Research* **88**: 555–568.

Joints

Narr, W. and Suppe, J., 1991, Joint spacing in sedimentary rocks. *Journal of Structural Geology* **13**: 1037–1048.

Pollard, D. D. and Aydin, A., 1988, Progress in understanding jointing over the past century. *Geological Society of America Bulletin* **100**, 1181–1204.

Closing fractures

Fletcher, R. C. and Pollard, D. D., 1981, Anticrack model for pressure solution surfaces. *Geology* **9**: 419–424.

Mollema, P. N. and Antonellini, M. A., 1996, Compaction bands: a structural analog for anti-mode I cracks in aeolian sandstone. *Tectonophysics* **267**: 209–228.

Role of fluids

Hubbert, M. K. and Rubey, W. W., 1959, Role of pore fluid pressure in the mechanics of overthrust faulting. I: Mechanics of fluid-filled porous solids and its application to overthrust faulting. *Geological Society of America Bulletin* **70**: 115–205.

Deformation bands

Antonellini, M. and Aydin, A., 1994, Effect of faulting on fluid flow in porous sandstones: petrophysical properties. *American Association of Petroleum Geologists* **78**: 355–377.

Aydin, A. and Johnson, A. M., 1978, Development of faults as zones of deformation bands and as slip surfaces in sandstones. *Pure and Applied Geophysics* **116**: 931–942.

Davis, G. H., 1999, Structural geology of the Colorado Plateau Region of southern Utah. *Geological Society of America Special Paper* **342**: 1–157.

Fossen, H., Schultz, R., Shipton, Z. and Mair, K., 2007, Deformation bands in sandstone: a review. *Journal of the Geological Society, London* **164**, 755–769.

Jamison, W. R., 1989, Fault-fracture strain in Wingate Sandstone. *Journal of Structural Geology* **11**: 959–974.

Rawling, G. C. and Goodwin, L. B., 2003, Cataclasis and particulate flow in faulted, poorly lithified sediments. *Journal of Structural Geology* **25**: 317–331.

Underhill, J. R. and Woodcock, N. H., 1987, Faulting mechanisms in high-porosity sandstones: New Red Sandstone, Arran, Scotland. In *Deformation of Sediments and Sedimentary Rocks*. Special Publication **29**, London: Geological Society, pp. 91–105.

Chapter 8

Faults

Faults disturb layered rock sequences, introducing “faults” or “defects” to the primary stratigraphic framework. While representing challenges to stratigraphers and geologists mapping rocks in the field or interpreting seismic data, faults are extremely intriguing structures that have fascinated structural geologists as much as they have frustrated stratigraphers and miners. We know much more about faults today than just a few decades ago, largely because of their importance to the petroleum industry. Faults also represent challenges associated with waste repositories and tunnel operations, and active faults are closely associated with earthquakes and seismic hazards. In this chapter we will focus on fault geometry, fault anatomy and the evolution of faults and fault populations, with examples and applications relevant to the petroleum industry.

8.1 Fault terminology

While the fractures and related discontinuities covered in the previous chapter are fairly simple structures, faults are much more complex and compound features that can accommodate large amounts of strain in the upper crust. The term **fault** is used in different ways, depending on geologist and context. A simple and traditional definition states:

A fault is any surface or narrow zone with visible shear displacement along the zone.

This definition is almost identical to that of a shear fracture, and some geologist use the two terms synonymously. Sometimes geologists even refer to shear fractures with millimeter- to centimeter-scale offsets as microfaults. However, most geologists would restrict the term shear fracture to small-scale structures and reserve the term fault for more composite structures with offsets in the order of a meter or more.

The thickness of a fault is another issue. Faults are often expressed as planes and surfaces in both oral and written communication and sketches, but close examination of faults reveals that they consist of fault rock material and subsidiary brittle structures and therefore have a definable thickness. However, the thickness is usually much smaller than the offset and several orders of magnitude less than the fault length. Whether a fault should be considered as a surface or a zone largely depends on the scale of observation, objectives and need for precision.

Faults tend to be complex zones of deformation, consisting of multiple slip surfaces, subsidiary fractures and perhaps also deformation bands. This is particularly apparent when considering large faults with kilometer-scale offsets. Such faults can be considered as single faults on a map or a seismic line, but can be seen to consist of several small faults when examined in the field. In other words, the scale dependency, which haunts the descriptive structural geologist, is important. This has led most geologists to consider a fault as a volume of brittlely deformed rock that is relatively thin in one dimension:

A fault is a tabular volume of rock consisting of a central slip surface or core, formed by intense shearing, and a surrounding volume of rock that has been affected by more gentle brittle deformation spatially and genetically related to the fault.

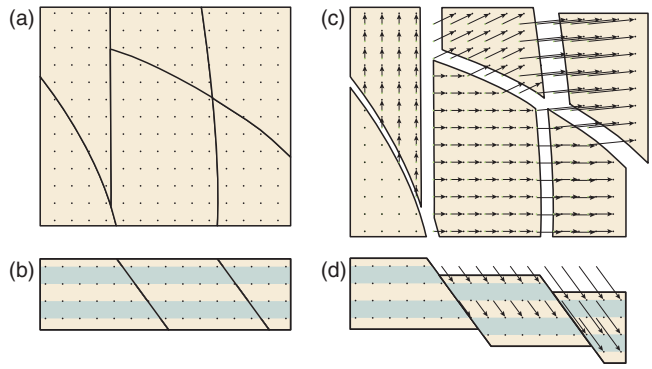

Figure 8.1 Faults appear as discontinuities on velocity or displacement field maps and profiles. The left blocks in the undeformed map (a) and profile (b) are fixed during the deformation. The result is abrupt changes in the displacement field (arrows) across faults.

The term fault may also be connected to deformation mechanisms (brittle or plastic). In a very informal sense, the term fault covers both brittle discontinuities and ductile shear zones dominated by plastic deformation. This is sometimes implied when discussing large faults on seismic or geologic sections that penetrate much or all of the crust. The term **brittle fault** (as opposed to ductile shear zone) can be used if it is important to be specific with regard to deformation mechanism. In most cases geologists implicitly restrict the term fault to slip or shear discontinuities dominated by brittle deformation mechanisms, rendering the term brittle fault redundant:

A fault is a discontinuity with wall-parallel displacement dominated by brittle deformation mechanisms.

By discontinuity we are here primarily referring to layers, i.e. faults cut off rock layers and make them discontinuous. However, faults also represent mechanical and displacement discontinuities. Figure 8.1 illustrates how the displacement field rapidly changes across faults in both map view and cross-section. A kinematic definition, particularly useful for experimental work and GPS-monitoring of active faults can therefore be added:

A fault is a discontinuity in the velocity or displacement field associated with deformation.

As mentioned in the previous chapter, faults differ from shear fractures because a simple shear fracture cannot expand in its own plane into a larger structure. In contrast, faults can grow by the creation of a complex process zone with numerous small fractures, some of

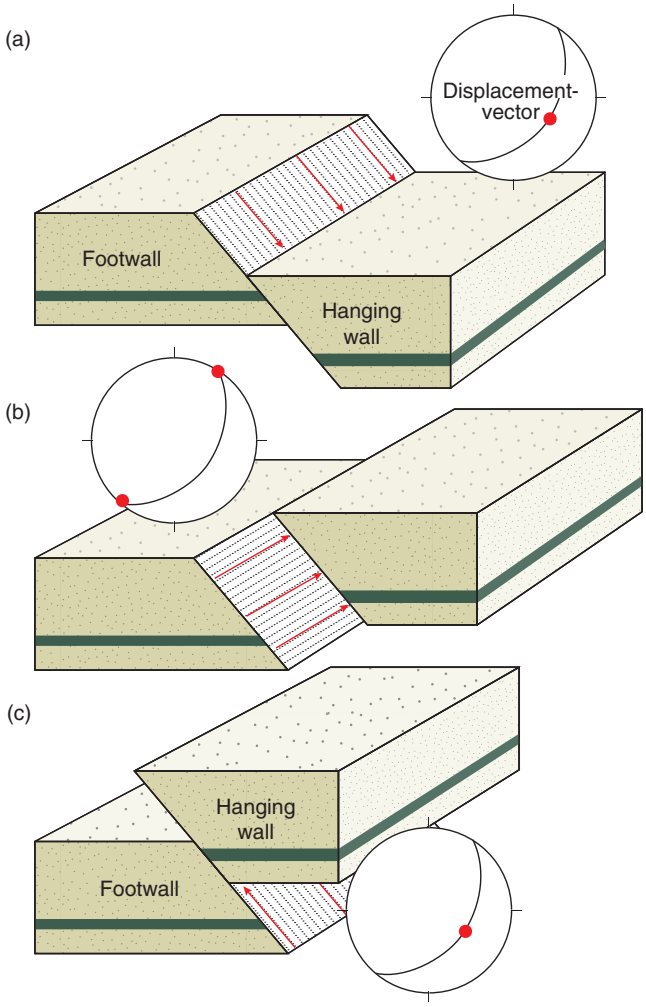

Figure 8.2 Normal (a), strike-slip (sinistral) (b) and reverse (c) faults. These are end-members of a continuous spectrum of oblique faults. The stereonets show the fault plane (great circle) and the displacement vector (red point).

which link to form the fault slip surface while the rest are abandoned.

Geometry of faults

Non-vertical faults separate the **hanging wall** from the underlying **footwall** (Figure 8.2). Where the hanging wall is lowered or downthrown relative to the footwall, the fault is a **normal fault**. The opposite case, where the hanging wall is upthrown relative to the footwall, is a **reverse fault**. If the movement is lateral, i.e. in the horizontal plane, then the fault is a **strike-slip fault**. Strike-slip faults can be sinistral (left-lateral) or dextral (right-lateral) (from the Latin words *sinister* and *dexter*, meaning left and right, respectively).

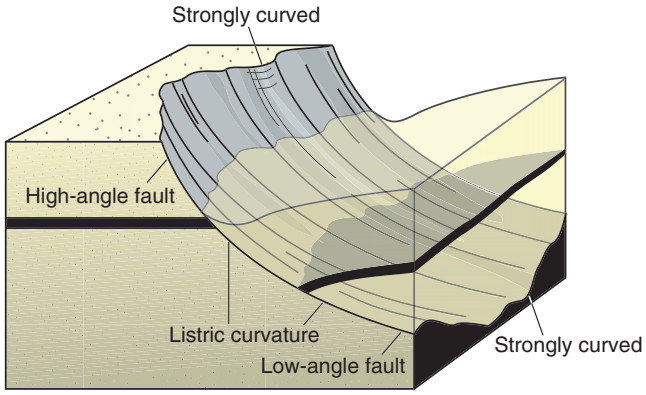

Figure 8.3 Listric normal fault showing very irregular curvature in the sections perpendicular to the slip direction. These irregularities can be thought of as large grooves or corrugations along which the hanging wall can slide.

Although some fault dip ranges are more common than others, with strike-slip faults typically occurring as steep faults and reverse faults commonly having lower dips than normal faults, the full range from vertical to horizontal faults is found in naturally deformed rocks. If the dip angle is less than 30° the fault is called a **low-angle fault**, while **steep faults** dip steeper than 60°. Low-angle reverse faults are called **thrust faults**, particularly if the movement on the fault is tens or hundreds of kilometers.

A fault that flattens downward is called a **listric fault** (Figure 8.3), while downward-steepening faults are sometimes called antilistric. The terms **ramps** and **flats**, originally from thrust fault terminology, are used for alternating steep and subhorizontal portions of any fault surface. For example, a fault that varies from steep to flat and back to steep again has a **ramp-flat-ramp geometry**.

Irregularities are particularly common in the section perpendicular to the fault slip direction. For normal and reverse faults this means curved fault traces in map view, as can be seen from the faults of the extensional oil field in Figure 8.4. Irregularities in this section cause no conflict during fault slippage as long as the axes of the irregularities coincide with the slip vector. Where irregularities also occur in the slip direction, the hanging wall and/or footwall must deform. For example, a listric normal fault typically creates a hanging-wall rollover (see Chapter 20).

A fault can have any shape perpendicular to the slip direction, but non-linearity in the slip direction generates space problems leading to hanging- or footwall strain.

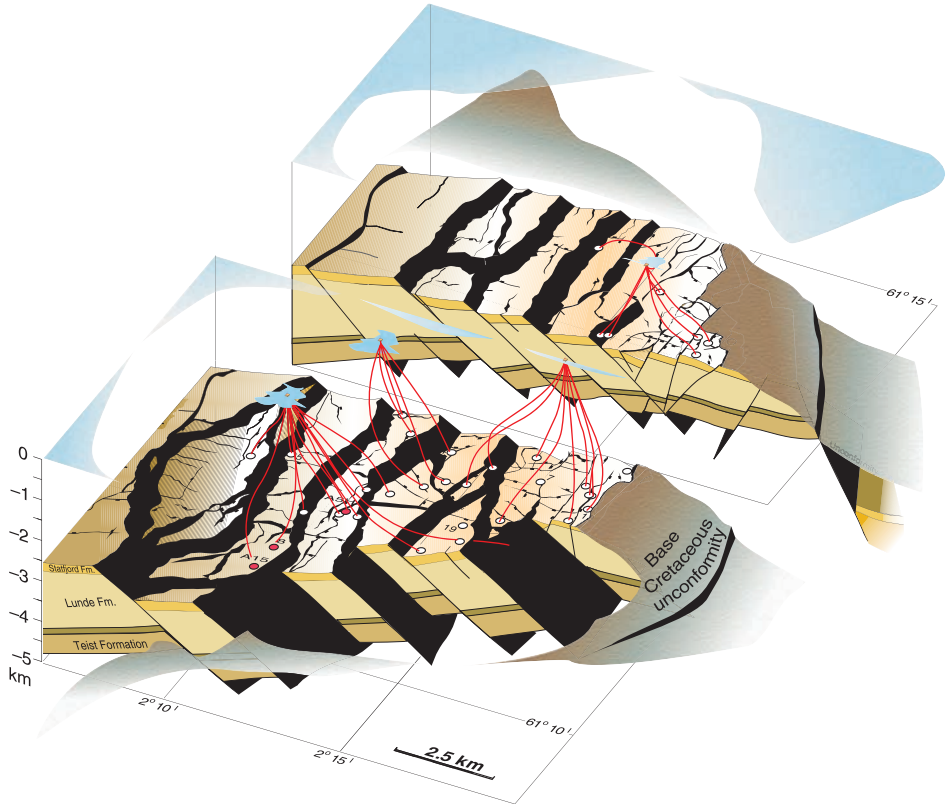

Figure 8.4 The main faults in the North Sea Gullfaks oil field show high degree of curvature in map view and straight traces in the vertical sections (main slip direction). Red lines represent some of the well paths in this field. From Fossen and Hesthammer (2000).

The term **fault zone** traditionally means a series of subparallel faults or slip surfaces close enough to each other to define a zone. The width of the zone depends on the scale of observation – it ranges from centimeters or meters in the field to the order of a kilometer or more when studying large-scale faults such as the San Andreas Fault. The term fault zone is now also used inconsistently about the central part of the fault where most or all of the original structures of the rock are obliterated, or about the core and the surrounding deformation zone associated with the fault. This somewhat confusing use is widespread in the current petroleum-related literature, so any use of the term fault zone requires clarification.

Two separate normal faults dipping toward each other create a downthrown block known as a **graben** (Figure 8.5). Normal faults dipping away from each other create an upthrown block called a **horst**. The largest faults in a faulted area, called **master faults**, are associated with minor faults that may be antithetic or synthetic. An **antithetic fault** dips toward the master fault, while a **synthetic fault** dips in the same direction as the master fault (Figure 8.5). These expressions are relative and only make sense when minor faults are related to specific larger-scale faults.

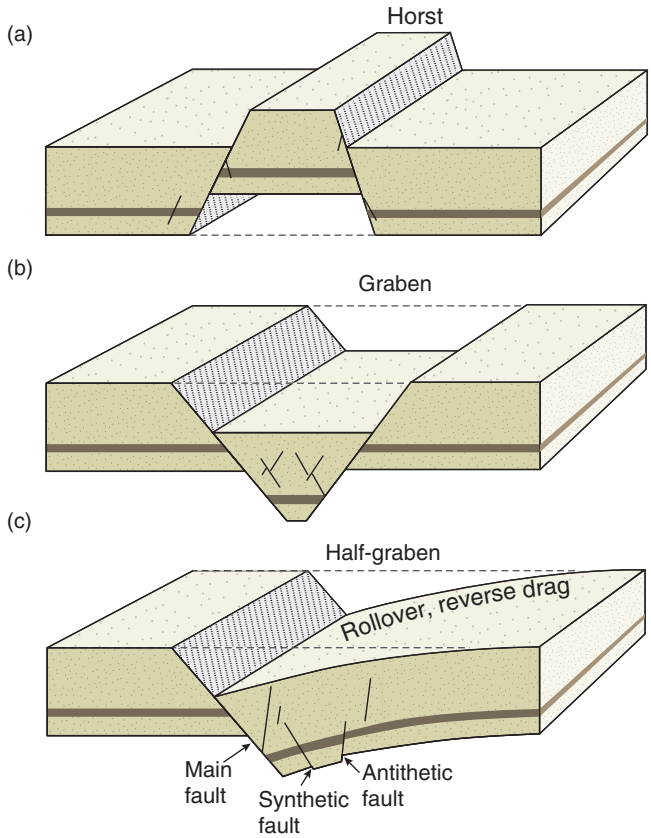

Figure 8.5 A horst (a), symmetric graben (b) and asymmetric graben (c), also known as a half-graben. Antithetic and synthetic faults are shown.

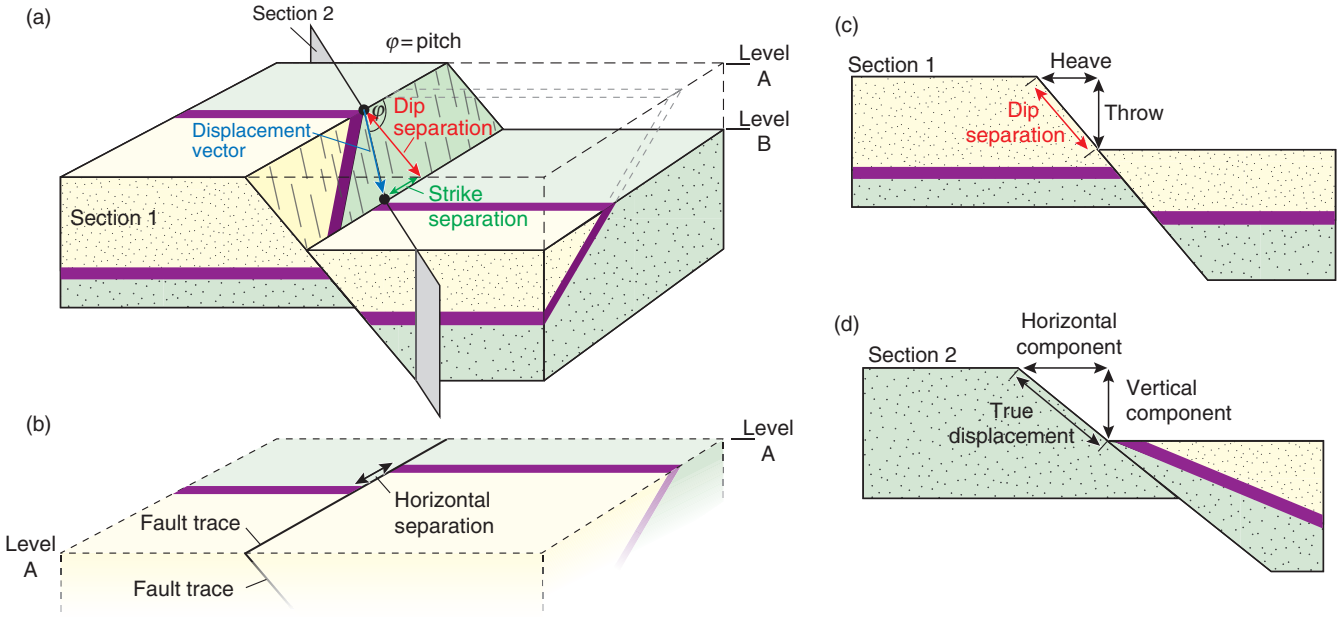

Figure 8.6 Illustration of a normal fault affecting a tilted layer. The fault is a normal fault with a dextral strike-slip component (a), but appears as a sinistral fault in map view (b, which is the horizontal section at level A). (c) and (d) show profiles perpendicular to fault strike (c) and in the (true) displacement direction (d).

Displacement, slip and separation

The vector connecting two points that were connected prior to faulting indicates the local **displacement vector** or **net slip direction** (Figure 8.6). Ideally, a strike-slip fault has a horizontal slip direction while normal and reverse faults have displacement vectors in the dip direction. In general, the total slip that we observe on most faults is the sum of several increments (earthquakes), each with its own individual displacement or slip vector. The individual slip events may have had different slip directions. We are now back to the difference between deformation *sensu stricto*, which only relates the undeformed and deformed states, and deformation *history*. In the field we could look for traces of the slip history by searching for such things as multiple striations, as discussed in the next chapter.

A series of displacement vectors over the slip surface gives us the **displacement field** or **slip field** on the surface. Striations, kinematic indicators (Chapter 9) and offset of layers provide the field geologist with information about direction, sense and amount of slip. Many faults show some deviation from true dip-slip and strike-slip displacement in the sense that the net slip vector is oblique. Such faults are called **oblique-slip faults** (Figure 8.7). The degree of obliquity is given by the **pitch** (also called **rake**), which is the angle between the strike of the slip surface and the slip vector (striation).

Unless we know the true displacement vector we may be fooled by the offset portrayed on an arbitrary section through the faulted volume, be it a seismic section or an outcrop (Figure 8.6b). The apparent displacement that is observed on a section or plane is called the (apparent) separation. **Horizontal separation** is the separation of layers observed on a horizontal exposure or map (Figure 8.6b), while the **dip separation** is that observed in a vertical section (Figure 8.6c). In a vertical section the dip separation can be decomposed into the horizontal and vertical separation. Note that this horizontal separation is different from that shown in Figure 8.6b. These two separations recorded in a vertical section are more commonly referred to as **heave** (horizontal component) and **throw** (vertical component) (Figure 8.6c). Only a section that contains the true displacement vector shows the true displacement or total slip on the fault (Figure 8.6d).

A fault that affects a layered sequence will, in three dimensions, separate each surface (stratigraphic interface) so that two **fault cutoff lines** appear (Figure 8.8). If the fault is non-vertical and the displacement vector is not parallel to the layering, then a map of the faulted surface will show an open space between the two cutoff lines. The width of the open space, which will not have any contours, is related to both the fault dip and the dip separation on the fault. Further, the opening reflects the heave (horizontal separation) seen on vertical sections across the fault (Figure 8.8).

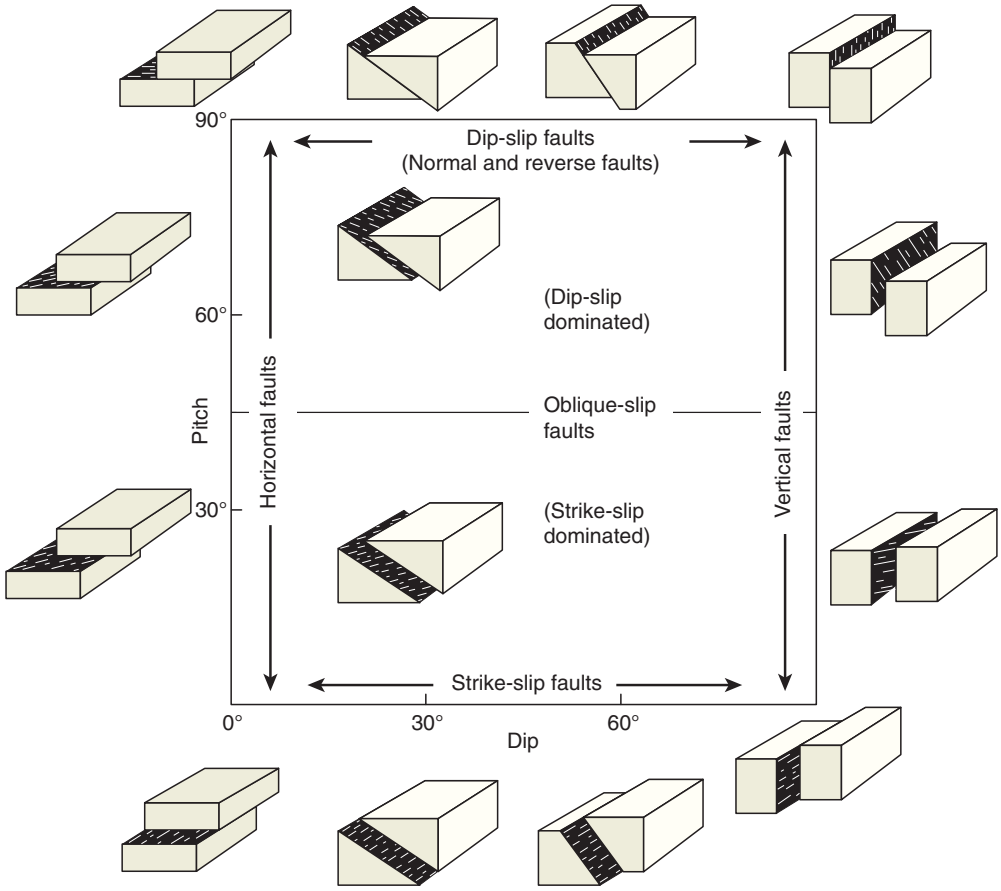

Figure 8.7 Classification of faults based on the dip of the fault plane and the pitch, which is the angle between the slip direction (displacement vector) and the strike. Based on Angelier (1994).

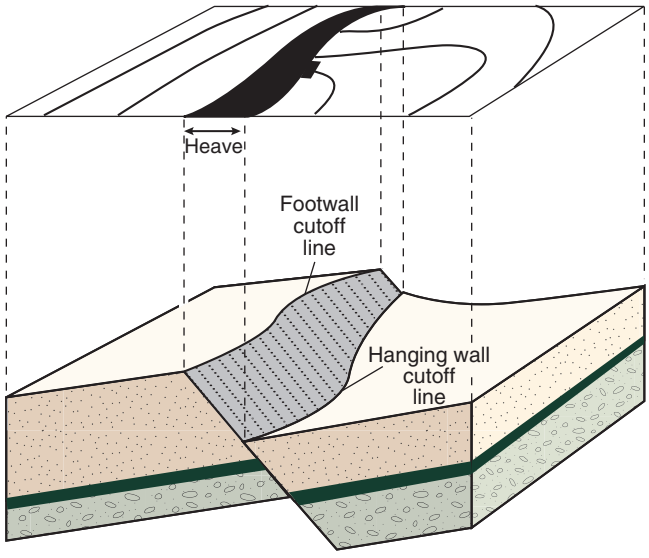

Figure 8.8 The relationship between a single fault, a mapped surface and its two fault cutoff lines. Such structure contour maps are used extensively in the oil industry where they are mainly based on seismic reflection data.

Stratigraphic separation

Drilling through a fault results in either a **repeated section** or a **missing section** at the **fault cut** (the point where the wellbore intersects the fault). For vertical wells it is simple: normal faults omit stratigraphy (Figure 8.9a), while reverse faults cause repeated stratigraphy in the well. For deviated wells where the plunge of the well bore is less than the dip of the fault, such as the well G in Figure 8.9b, stratigraphic repetition is seen across normal faults. The general term for the stratigraphic section missing or repeated in wells drilled through a fault is **stratigraphic separation**. Stratigraphic separation, which is a measure of fault displacement obtainable from wells in subsurface oil fields, is equal to the fault throw if the strata are horizontal. Most faulted strata are not horizontal, and the throw must be calculated or constructed.

8.2 Fault anatomy

Faults drawn on seismic or geologic sections are usually portrayed as single lines of even thickness. In detail,

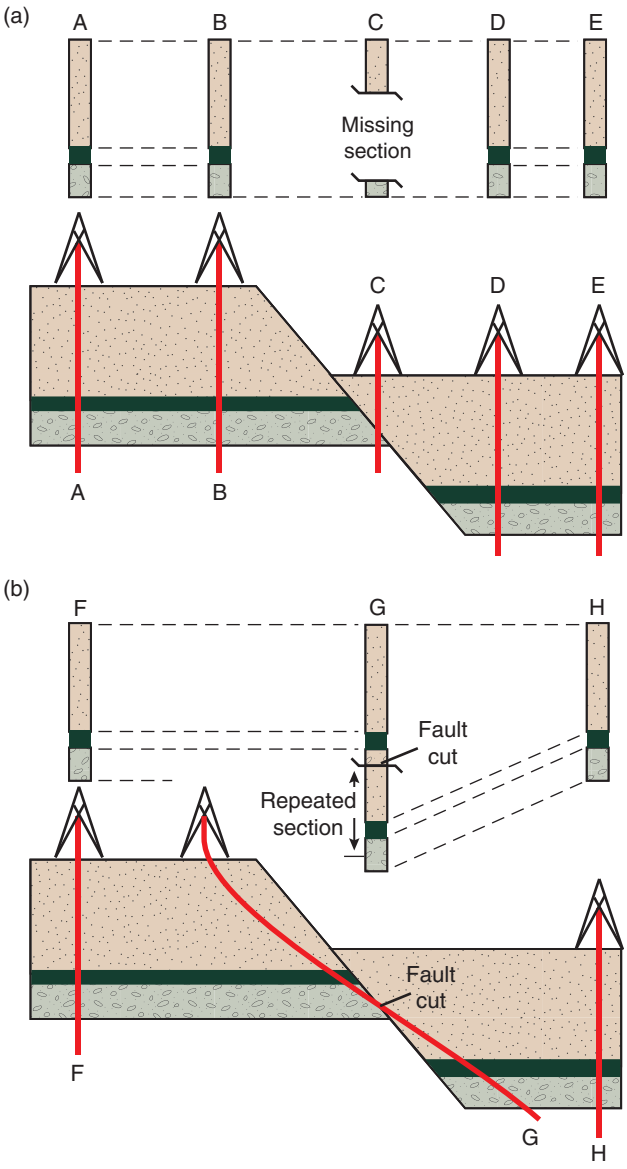

Figure 8.9 (a) Missing section in vertical wells (well C) always indicates normal faults (assuming constant stratigraphy). (b) Repeated section (normally associated with reverse faults) occurs where the normal fault is steeper than the intersecting wellbore (well G).

however, faults are rarely simple surfaces or zones of constant thickness. In fact, most faults are complex structures consisting of a number of structural elements that may be hard to predict. Because of the variations in expression along, as well as between, faults, it is not easy to come up with a simple and general description of a fault. In most cases it makes sense to distinguish between the central **fault core** or slip surface and the surrounding volume of brittlely deformed wallrock known as the **fault damage zone**, as illustrated in Figure 8.10.

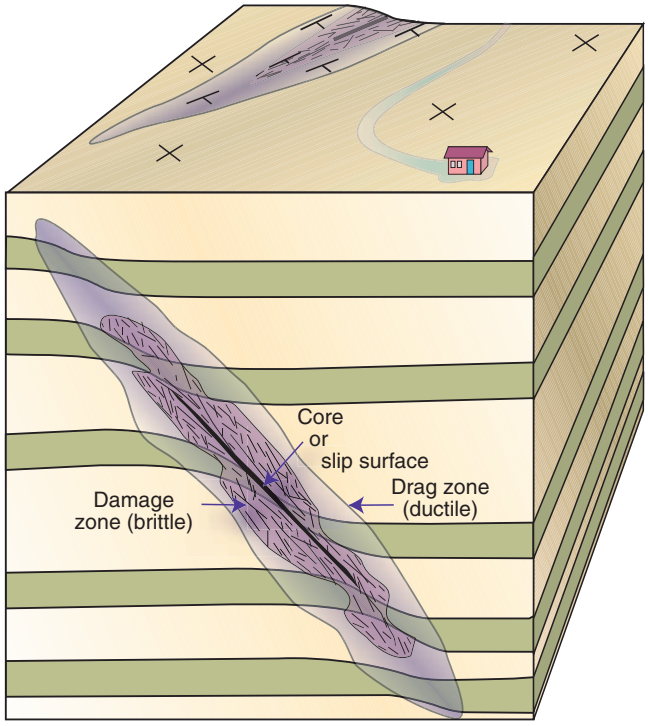

Figure 8.10 Simplified anatomy of a fault.

The fault core can vary from a simple slip surface with a less than millimeter-thick cataclastic zone through a zone of several slip surfaces to an intensely sheared zone up to several meters wide where only remnants of the primary rock structures are preserved. In crystalline rocks, the fault core can consist of practically non-cohesive **fault gouge**, where clay minerals have formed at the expense of feldspar and other primary minerals. In other cases, hard and flinty **cataclasites** constitute the fault core, particularly for faults formed in the lower part of the brittle upper crust. Various types of **breccias**, cohesive or non-cohesive, are also found in fault cores. In extreme cases, friction causes crystalline rocks to melt locally and temporarily, creating a glassy fault rock known as **pseudotachylyte**. The classification of fault rocks is shown in Box 8.1.

In soft, sedimentary rocks, fault cores typically consist of non-cohesive smeared-out layers. In some cases, soft layers such as clay and silt may be smeared out to a continuous membrane which, if continuous in three dimensions, may greatly reduce the ability of fluids to cross the fault. In general, the thickness of the fault core shows a positive increase with fault throw, although variations are great even along a single fault within the same lithology.

The damage zone is characterized by a density of brittle deformation structures that is higher than the background level. It envelops the fault core, which means

BOX 8.1 FAULT ROCKS

When fault movements alter the original rock sufficiently it is turned into a brittle fault rock. There are several types of fault rocks, depending on lithology, confining pressure (depth), temperature, fluid pressure, kinematics etc. at the time of faulting. It is useful to distinguish between different types of fault rocks, and to separate them from mylonitic rocks formed in the plastic regime. Sibson (1977) suggested a classification based on his observation that brittle fault rocks are generally non-foliated, while mylonites are well foliated. He further made a distinction between cohesive and non-cohesive fault rocks. Further subclassification was done based on the relative amounts of large clasts and fine-grained matrix. Sibson's classification is descriptive and works well if we also add that cataclastic fault rocks may show a foliation in some cases. Its relationship to microscopic deformation mechanism is also clear, since mylonites, which result from plastic deformation mechanisms, are clearly separated from cataclastic rocks in the lower part of the diagram.

Fault breccia is an unconsolidated fault rock consisting of less than 30% matrix. If the matrix-fragment ratio is higher, the rock is called a **fault gouge**. A fault gouge is thus a strongly ground-down version of the original rock, but the term is sometimes also used for strongly reworked clay or shale in the core of faults in sedimentary sequences. These unconsolidated fault rocks form in the upper part of the brittle crust. They are conduits of fluid flow in non-porous rocks, but contribute to fault sealing in faulted porous rocks.

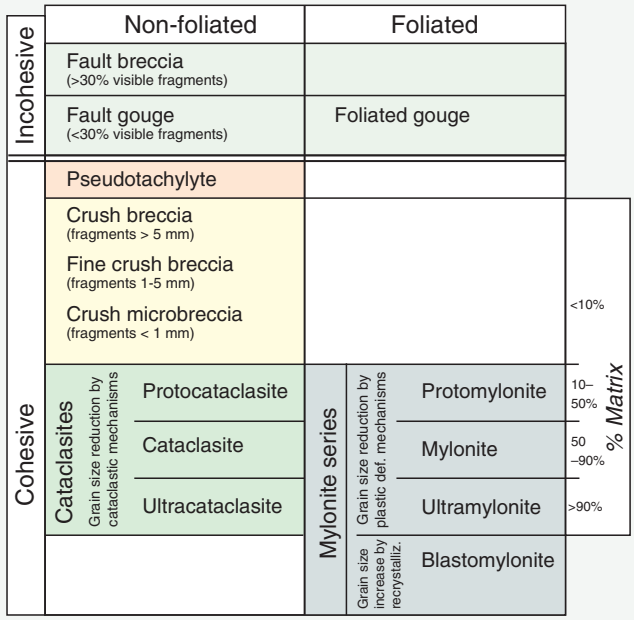

Pseudotachylyte consists of dark glass or microcrystalline, dense material. It forms by localized melting of the wall rock during frictional sliding. Pseudotachylyte can show injection veins into the sidewall, chilled margins, inclusions of the host rock and glass structures. It typically occurs as mm- to cm-wide zones that make sharp boundaries with the host rock. Pseudotachylytes form in the upper part of the crust, but can form at large crustal depths in dry parts of the lower crust.

Crush breccias are characterized by their large fragments. They all have less than 10% matrix and are cohesive and hard rocks. The fragments are glued together by cement (typically quartz or calcite) and/or by microfragments of mineral that have been crushed during faulting.

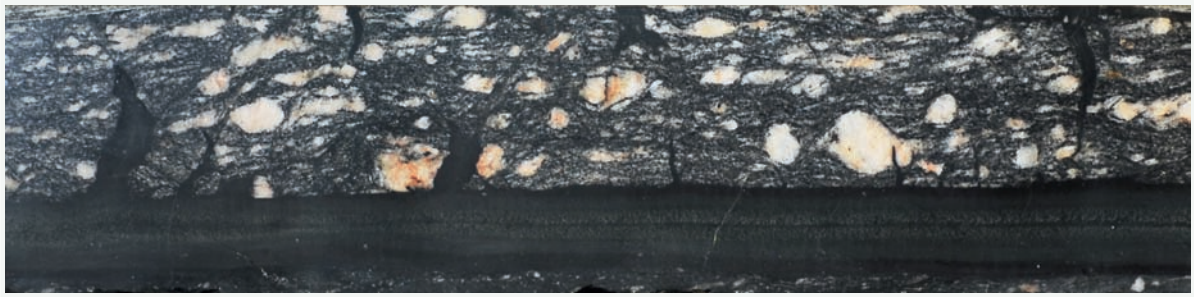

Pseudotachylyte injection veins in protomylonitic gneiss, Heimefrontfjella, Antarctica.

Continued

BOX 8.1 (CONT.)

Cataclasites are distinguished from crush breccias by their lower fragment–matrix ratio. The matrix consists of crushed and ground-down microfragments that form a cohesive and often flinty rock. It takes a certain temperature for the matrix to end up flinty, and most cataclasites are thought to form at 5 km depth or more.

Mylonites, which are not really fault rocks although loosely referred to as such by Sibson, are subdivided based on the amount of large, original grains and recrystallized matrix. Mylonites are well foliated and commonly also lineated and show abundant evidence of plastic deformation mechanisms rather than frictional sliding and grain crushing. They form at greater depths and temperatures than cataclasites and other fault rocks; above 300 °C for quartz-rich rocks. The end-member of the mylonite series, blastomylonite, is a mylonite that has recrystallized after the deformation has ceased (postkinematic recrystallization). It therefore shows equant and strain-free grains of approximately equal size under the microscope, with the mylonitic foliation still preserved in hand samples. Plastic deformation and mylonites are treated further in Chapters 10 and 15.

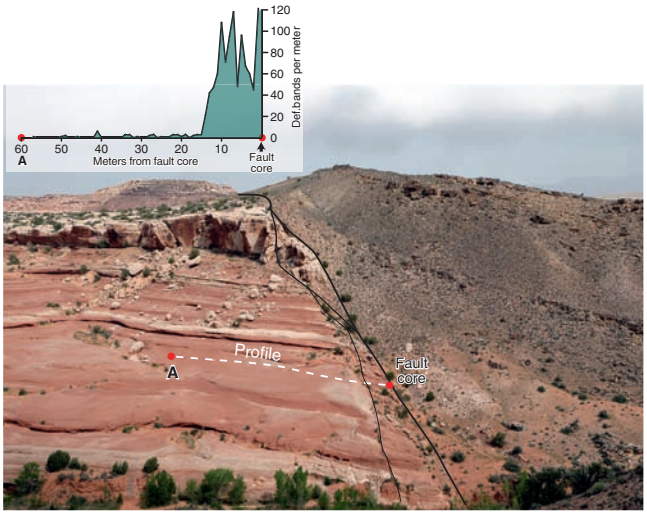

Figure 8.11 Damage zone in the footwall to a normal fault with 150–200 m throw. The footwall damage zone is characterized by a frequency diagram with data collected along the profile line. A fault lens is seen in the upper part of the fault. Entrada Sandstone near Moab, Utah.

that it is found in the tip zone as well as on each side of the core. Structures that are found in the damage zone include deformation bands, shear fractures, tensile fractures and stylolites, and Figure 8.11 shows an example of how such small-scale structures (deformation bands) only occur close to the fault core, in this case defining a footwall damage zone width of around 15 meters.

The width of the damage zone can vary from layer to layer, but, as with the fault core, there is a positive correlation between fault displacement and damage zone thickness (Figure 8.12a). Logarithmic diagrams such as shown in Figure 8.12 are widely used in fault analysis, and straight lines in such diagrams indicate a constant relation between the two plotted parameters. In particular, for data that plot along one of the straight lines in this figure, the ratio between fault displacement D and damage zone thickness DT is the same for any fault size, and the distance between adjacent lines in this figure represents one order of magnitude. Much of the data in Figure 8.12a plot around or above the line $D = \mathrm{DT}$, meaning that the fault displacement is close to or somewhat larger than the damage zone thickness, at least for faults with displacements up to 100 meters. We could use this diagram to estimate throw from damage zone width or vice versa, but the large spread of data (over two orders of magnitude) gives a highly significant uncertainty.

A similar relationship exists between fault core thickness (CT) and fault displacement (Figure 8.12b). This relationship is constrained by the straight lines $D = 1000\mathrm{CT}$ and $D = 10\mathrm{CT}$, meaning that the fault core is statistically around 1/100 of the fault displacement for faults with displacements up to 100 meters.

Layers are commonly deflected (folded) around faults, particularly in faulted sedimentary rocks. The classic term for this behavior is **drag**, which should be used

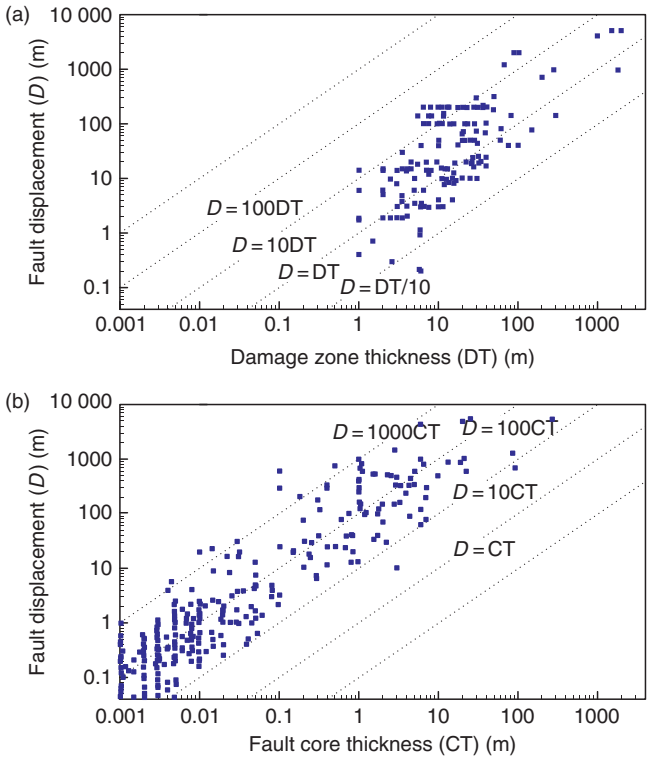

Figure 8.12 (a) Damage zone thickness (DT) (one side of the fault) plotted against displacement (D) for faults in siliciclastic sedimentary rocks. (b) Similar plot for fault core thickness (CT). Note logarithmic axes. Data from several sources.

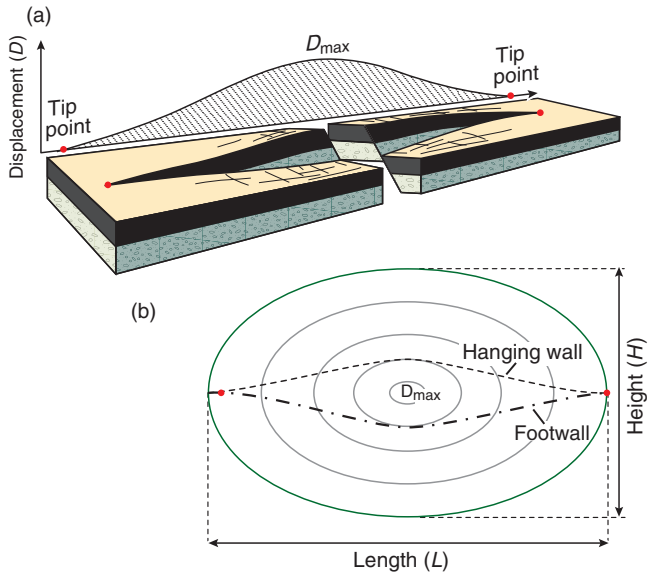

Figure 8.13 (a) Schematic illustration of an ideal, isolated fault. The displacement profile indicates maximum displacement near the center. (b) The fault plane with displacement contours. Stippled lines are the hanging-wall and footwall cutoff lines and the distance between them indicates the dip separation.

as a purely descriptive or geometric term. The drag zone can be wider or narrower than the damage zone, and can be completely absent. The distinction between the damage zone and the drag zone is that drag is an expression of ductile fault-related strain, while the damage zone is by definition restricted to brittle deformation. They are both part of the total strain zone associated with faults. In general, soft rocks develop more drag than stiff rocks.

8.3 Displacement distribution

It is sometimes possible to map displacement variations along a fault in the field in the horizontal or vertical direction. In both directions faults tend to show a maximum displacement in the central part of the fault trace, gradually decreasing toward the tips, as illustrated in Figure 8.13. The shape of the displacement profile may vary from linear to bell-shaped or elliptic. Displacement profiles are sometimes classified into those that have a well-defined central maximum (peak type) and those that have a wide, central part of fairly constant displacement (plateau type). Examples are shown in Figure 8.14.

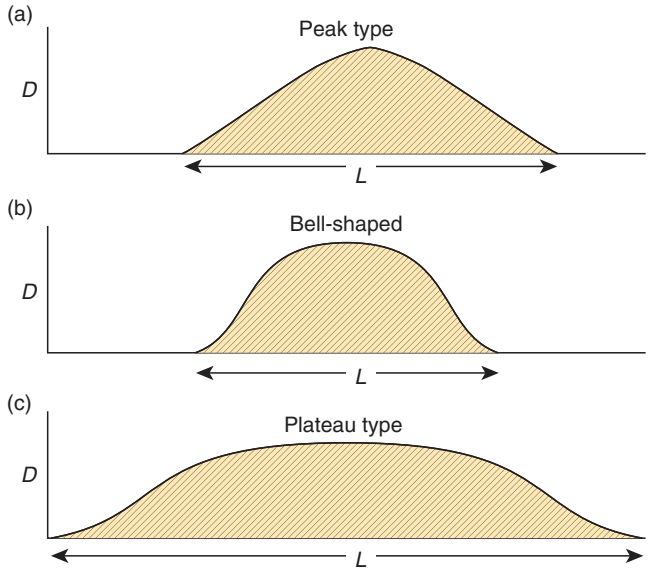

Figure 8.14 Types of displacement (D) profiles along faults.

Single faults generally show a gradual increase in displacement from the tip line toward a central point.

It may be hard to collect enough displacement data from a single fault to obtain a good picture of the

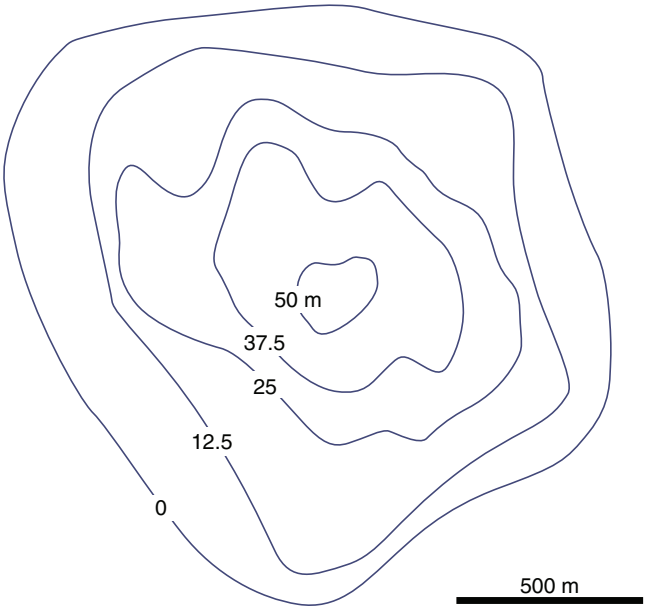

Figure 8.15 Displacement contours for a fault interpreted from high-resolution seismic data from the Gulf of Mexico. Modified from Childs *et al.* (2003).

displacement distribution on the fault surface. However, data sets from coalmines and high-quality 3-D seismic data have made it possible to contour displacement on a number of faults. Figure 8.15 is an example of such studies, and shows the general pattern that the displacement is generally greatest in the central part of a single, isolated fault, gradually decreasing toward the tip line – a conclusion that is consistent with the field observations mentioned in the previous paragraph. Hence, these observations support the idealized model shown in Figure 8.16, where an isolated fault has an elliptical tip line and elliptical displacement contours. A geometrically similar elliptical model can be applied to extension fractures, where the displacement vectors are perpendicular to the fracture. It should be emphasized that the simple elliptical fault model is meant to describe an isolated fault in an isotropic medium. In most cases fault growth is complicated by fault interaction and mechanical layering, which causes deviations from this simple model.

8.4 Identifying faults in an oil field setting

It is crucial to collect and correctly interpret information about faults in petroleum exploration and production. Here we will review some sources of data that provide key information about faults in an oil field in an extensional setting; the same principles can be applied in contractional and strike-slip regimes.

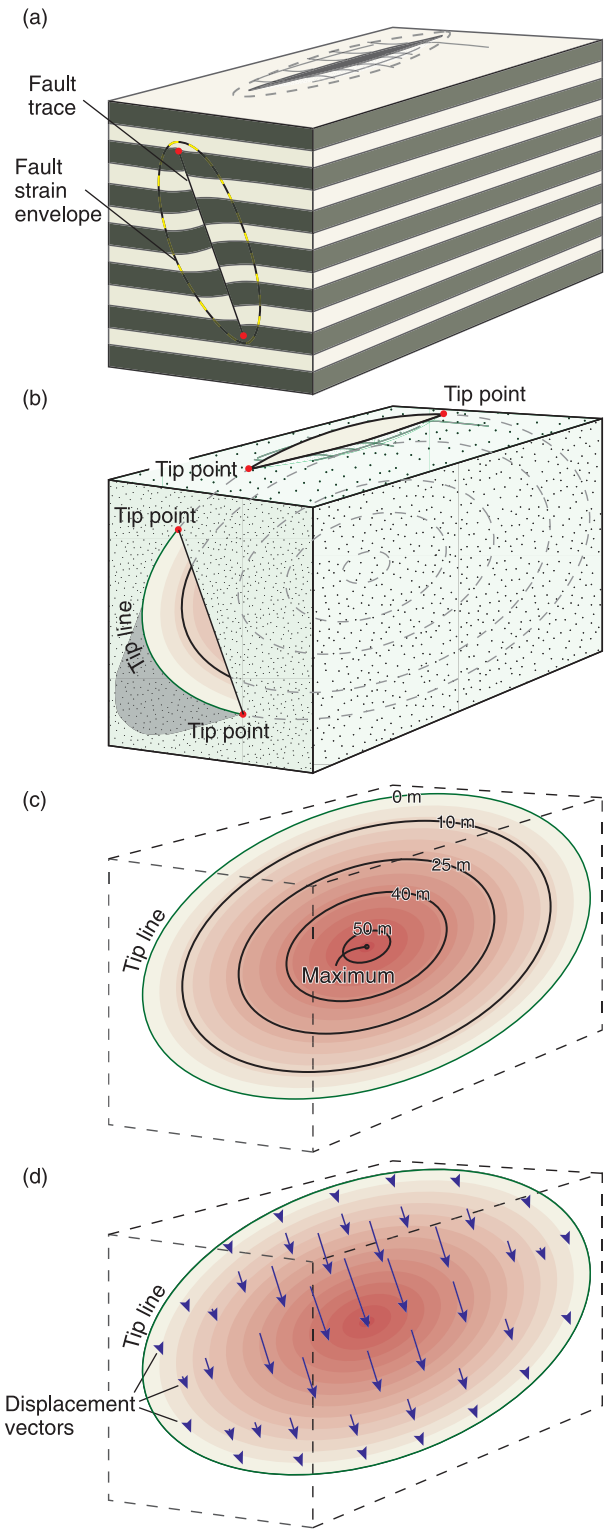

Figure 8.16 Geometric aspects of an isolated fault (elliptical fault model). (a) The fault trace is the intersection between the fault surface and an arbitrary surface (outcrop, seismic line). The endpoints of the fault trace are called tip points (b). They lie on the tip line, which is the zero-displacement line that outlines the fault (c). Displacement increases towards the center of the fault. This can be expressed in terms of displacement contours (c) or displacement vectors (d).

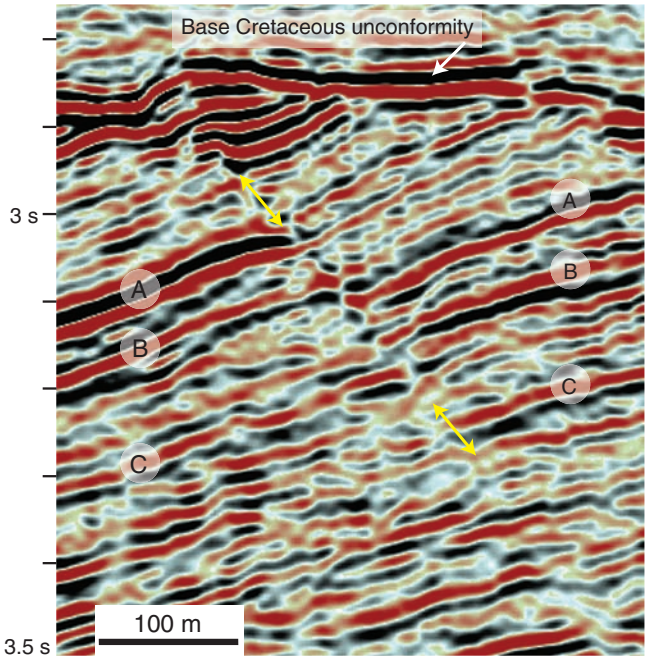

Figure 8.17 A fault imaged in seismic data (arrows). There are no clear reflections from the fault itself. The dip separation is identified by the discontinuity of reflectors (cutoffs). Three-dimensional seismic from the Visund Field, North Sea.

Seismic data

Interpretation of seismic data is the most common way of identifying and mapping faults in the subsurface. Identification of faults depends on the presence of mappable seismic reflectors. Discontinuous reflectors indicate fault locations, and the dip separation is estimated by correlation of seismic reflectors across the fault, as shown in Figure 8.17.

Seismic data have a limit in resolution that varies from data set to data set, but it is usually difficult or impossible to identify faults with throw less than 15–20 meters, even on high-quality 3-D seismic data sets. Faults that fall below seismic resolution are generally referred to as **subseismic faults**, as discussed in Box 8.2. Complications along faults, such as fault lenses and fault branching, may be difficult to resolve on seismic data alone. Where available, well information is used to constrain the seismic interpretation.

As illustrated in Figure 8.18, a 3-D data set represents a cube of data where faults and reflectors can be studied and interpreted in any direction, including horizontal sections (time slices). This allows the interpretation of the 3-D geometry of faults and fault populations.

BOX 8.2 SUBSEISMIC FAULTS

Ductile or brittle? It all depends on the scale of observation. Consider large-scale drag in the hanging wall of large normal faults. When imaged on a seismic section (or from a far distance), the layers may appear continuous and the deformation can be described as being ductile. There could still be lots of subseismic faults, because what appear to be continuous layers may be signals that are smeared out to continuous reflectors during the data processing. Two different cases are shown. In one case a series of antithetic subseismic faults affect the layers, in the other the faults are synthetic with respect to the main faults. Since the faults are too small to be imaged seismically, the two seismic images are identical, but the true small-scale dip is different in the two cases. Core data and perhaps dipmeter data will reveal the true dip. If the difference between dip determined from cores and dipmeter data is significant, then it is likely that subseismic faults occur. If the dip determined from cores is the same as the seismic dip, then the deformation is microscopic, perhaps by granular flow (typical for sediments that were poorly lithified at the time of deformation).

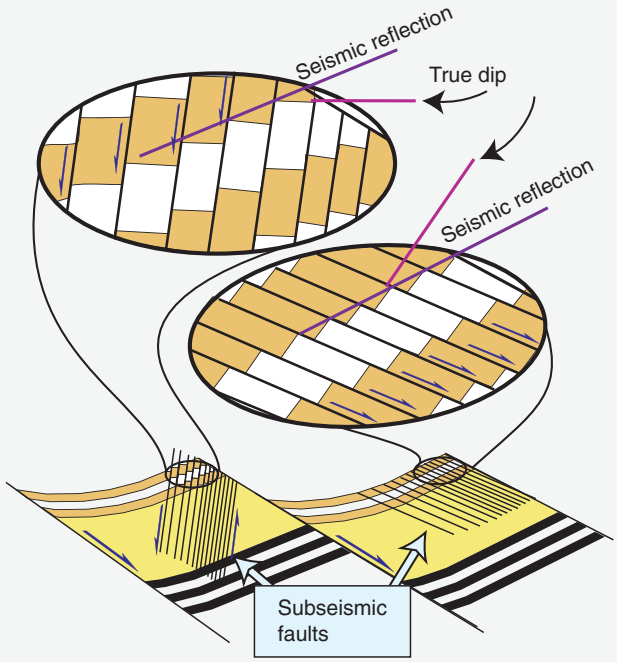

From Hesthammer and Fossen (1998).

Basin-scale faults and regional fault arrays are more commonly mapped by means of regional 2-D lines. Some 2-D lines are deep seismic lines that image the deep parts of the crust and the upper mantle (Figure 1.6). Deep seismic lines show large faults that penetrate the upper crust and sometimes the entire crust as they pass into deep shear zones.

Fault cut and well log correlation

Faults along the wellbore are typically identified by means of stratigraphic correlation. As shown in Figure 8.9, reverse and normal faults cause repetition and omission of stratigraphic sections, respectively. Knowledge of the stratigraphy from other wells in the area forms the basis for this type of fault identification.

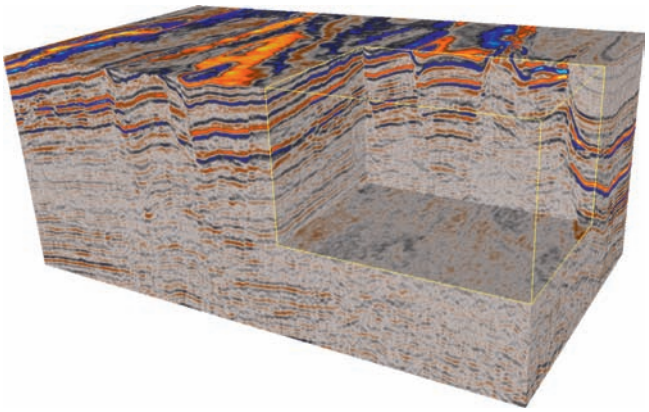

Figure 8.18 Faults as they may appear in a 3-D seismic data cube. Data from the Barents Sea.

The size of faults identifiable by this method depends on the characteristic stratigraphic markers, the number of wells, distance to other wells in the area, sedimentary facies variations and the orientation of the well. The identification of the **fault cut** (fault location in the wellbore) also depends on characteristic signatures on the well logs. Cores are generally not available, and standard logs such as gamma-ray logs, density logs, neutron logs and resistivity logs are used for stratigraphic well correlations. Figure 8.19 shows an example of how faults with as little as 6 meters of stratigraphic separation are detectable in parts of the North Sea Brent Group, where the density of wells is high. In this example the fault was confirmed by core inspection.

Dipmeter data and borehole images

Microresistivity is measured continuously along the wellbore by the three or more (usually 16) electrodes of a dipmeter tool. The responses from the different electrodes are correlated around the borehole in narrow depth intervals to fit a plane. The planes are generally bedding or lamination, but may also represent deformation bands or fractures.

Orientations (usually given by dip and dip azimuth) are plotted in dipmeter diagrams. For structural analysis, separating dip azimuth and dip into individual plots

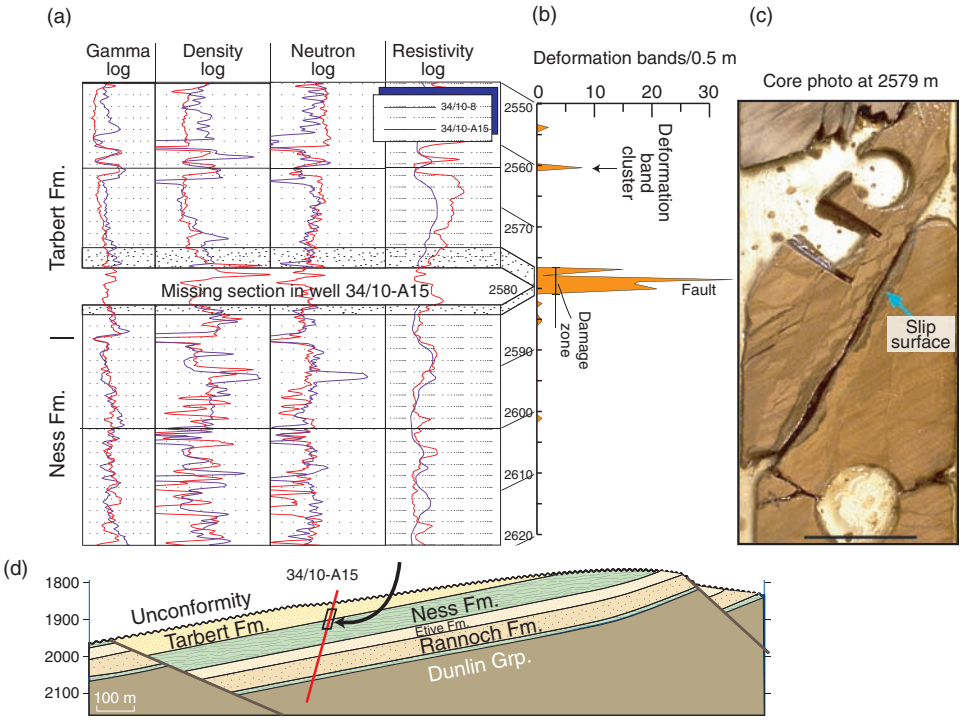

Figure 8.19 Fault separation detected by log correlation with a neighboring well. The complete log in well 8 is shown in red, and the correlation gives a missing section of ~6 m in well A15. The damage zone (orange) was estimated from core inspection to be a few meters wide. Based on Fossen and Hestshammer (2000).

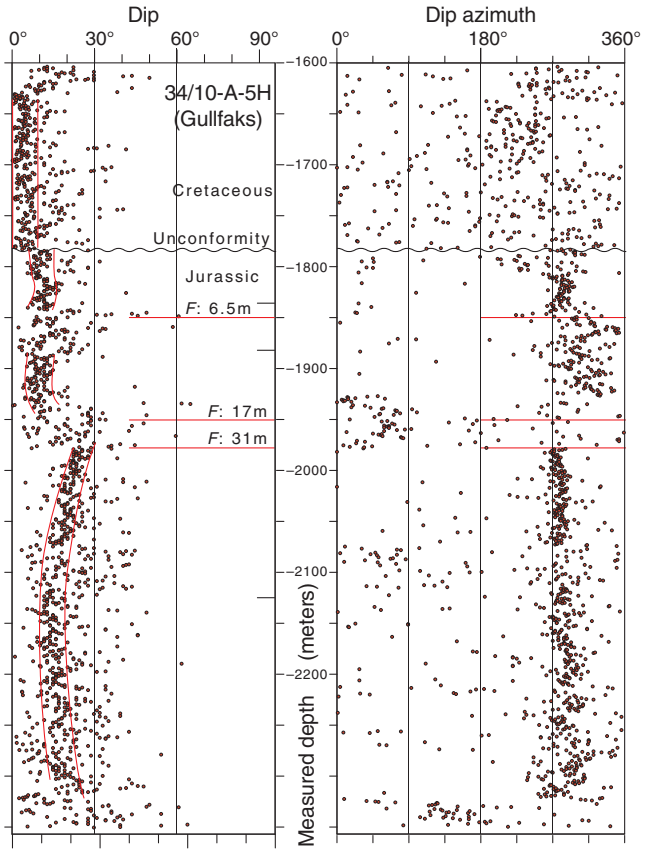

Figure 8.20 Dipmeter data from the Gullfaks Field, North Sea, where dip and dip azimuth (dip direction) are plotted against the depth measured along the wellbore. Faults identified by stratigraphic correlation (missing section) are indicated.

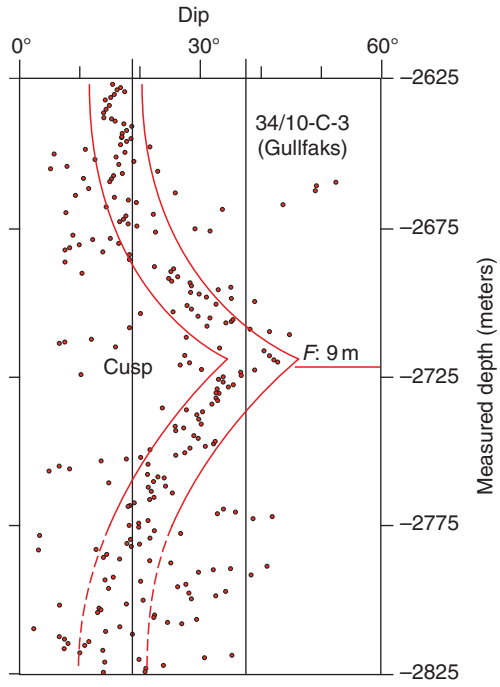

Figure 8.21 Dipmeter data (dip against depth) showing a classic cusp geometry related to drag around a minor fault. Data from the Gullfaks Field, North Sea.

and compressing the vertical scale can be advantageous, as shown in Figure 8.20. Faults can then be identified in at least three different ways. The first is represented by sudden changes in dip or dip azimuth. These occur where a fault separates two blocks in which the layering is differently oriented – a fairly common situation across many faults. An example is seen between the 17- and 31-meter faults in Figure 8.20.

Another characteristic feature is the presence of local intervals with rapid but progressive changes in dip and/or dip azimuth. Such anomalies are known as **cusps** (Figure 8.21). Cusp-shaped dip patterns indicate fault-related drag in many cases. Stratigraphic log correlation indicates a 9-meter missing section in the example shown in Figure 8.21.

The third characteristic is the appearance of anomalous orientations related to fractures or deformation bands in the damage zone or from the main slip surface itself. The high dip values at the locations of the faults in Figure 8.20 may be such examples.

It is now common to create a (almost) continuous microresistivity image of the borehole based on resistivity data from more sophisticated tools, such as the **FMI** (Formation MicroImager). This tool measures microresistivity by means of a few hundred electrodes. The result is a continuous image of the wall that is reminiscent of an actual picture of the rock. Such images are analyzed at workstations where bedding and structural features are interpreted.

Drill core information

Only a small percentage of the drilled section in a reservoir will be cored, and only rarely are faults represented in the drill core material. Drillers are reluctant to cut cores across faults because of the risk of jamming and potential pressure problems. Furthermore, some cored fault rocks may be so non-cohesive that they fall apart to form what is known as **rubble zones**. However, successfully cored faults and damage zones represent valuable information. Such samples allow for microscopic studies and permeability measurements. Furthermore, the width and nature of the damage zone, and sometimes even the fault core, can be estimated. Figure 8.22 shows an example of a core through a fault with a 6-meter missing

Figure 8.22 One-meter-long core section across a minor (6 m missing section) fault in the Gullfaks Field. Holes are from plugs sampled for permeability analysis. See also Figure 8.19.

section. The central slip surface (very thin core) and deformation bands in the damage zone are visible.

The orientation of faults and fractures in cores can be measured if the core is oriented. Usually it is not, and its orientation must then be reconstructed based on knowledge of bedding orientation from dipmeter data or seismic data. This can only be done if bedding is non-horizontal.

8.5 The birth and growth of faults

Fault formation in non-porous rocks

Faults in rocks with low or no porosity somehow grow from small shear fractures. However, this cannot happen directly from a single shear fracture, since shear fractures cannot expand in their own planes. Instead they will curve and form wing cracks or related cracks across which there is tension (Box 7.3). Experiments show that a phase of intense microfracturing occurs prior to fracture initiation or propagation. Once the density of microfractures reaches a critical level, the main fracture expands by linkage of favorably oriented microfractures. The zone of microfractures (and mesofractures) ahead of the fracture tip zone is called the **frictional breakdown zone** or the **process zone**.

For a fault to develop, a number of small shear fractures, tensile fractures and hybrid fractures must form and connect. The incipient fault surface is irregular, leading to grinding and microfracturing of the walls. A thin core of brecciated or crushed rock typically forms. During fault growth, new fractures form in the walls next to the fault core. Hence, most faults have a well-defined **core** of intense cataclastic deformation and a surrounding **damage zone** of less intense fracturing.

Fault formation and growth is a complicated process involving a frontal process zone where microfractures form and eventually connect.

Natural rocks are not isotropic, and in many cases faults form along preexisting mesoscopic weaknesses in the rock. Such weaknesses can be layer interfaces or dikes, but the structures that are most likely to be activated as faults are joints (and, of course, preexisting faults). Joints tend to be very weak planar structures with little or no cohesion. Joints may also form surfaces many tens of meters or more in length and/or height, because as extension structures they have had the freedom to expand in their own plane. Faults formed by faulting

of joints inherit some of the features of the original joints. If a fault forms by frictional sliding on a single, extensive joint, the initial fault tends to be a sharp slip surface with almost no fault core and with (almost) no damage zone. If slip accumulates, however, the fault outgrows the joint and links with other joints in the vicinity of its tip zone. The damage zone then thickens, and the fault core may grow.

Fault formation by joint reactivation requires less stress, causes less off-fault damage (narrower damage zone) and may result in a lower displacement gradient along the fault.

Fault formation in porous rocks

In highly porous rocks and sediments, fault growth follows a somewhat different path. Pore space gives the grains a unique opportunity to reorganize. If the grains in a sandstone are weakly cemented together, then the grains will reorganize by rotation and frictional grain boundary sliding (translation) during deformation. In other cases grains can also break internally. In either case, the deformation is likely to localize into narrow zones or bands to form structures known as **deformation bands**. Different types of deformation bands are discussed in the previous chapter (Section 7.8).

Field observations, as well as experimental and numerical work, show that deformation proceeds by sequential formation of new deformation bands adjacent to the initial one (Figure 8.23). This means that at some point it becomes easier to form a new band next to the existing one than to keep shearing the primary band. The result is a **deformation band zone**, and this development is commonly explained in terms of strain hardening. Strain hardening is thought to be related to the loss of porosity in the band and is most pronounced where grains are crushed (cataclastic bands). Note the difference between process zones in non-porous and highly porous rocks: The process zone in non-porous rocks weakens the host rock and increases porosity by the formation of cracks. In high-porosity rocks the deformation bands in the process zone in many cases harden the rock and reduce porosity.

Once a certain number of deformation bands have accumulated in the deformation band zone, porosity is sufficiently reduced that a slip surface can form and grow. Slip surfaces nucleate in small patches that propagate, link up, and ultimately form through-going slip surfaces. Mechanically, slip surfaces are weak structures that

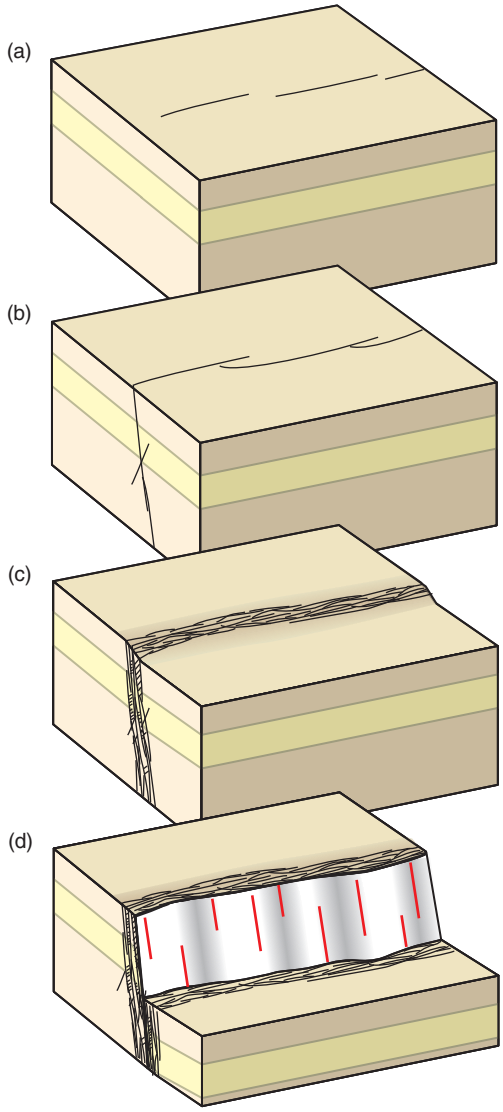

Figure 8.23 The general model for fault formation in porous sandstone, as proposed by Aydin and Johnson (1978). (a) Individual deformation bands, (b) linking of bands, (c) the formation of a deformation band zone, and (d) faulting of the zone.

relatively quickly can accumulate meters of slip or more. Through-going slip surfaces are commonly associated with a thin (millimeter-thick) zone of ultracataclasite, which may be considered as the local fault core.

Faults in highly porous rocks form in precursory deformation band zones.

The damage zone

The growth of deformation bands and/or ordinary fractures prior to the formation of a through-going slip

surface has implications for our understanding of the damage zone. The moment the slip surface (fault) forms, the enclosing zone of already existing structures will become the damage zone. Once the fault is established, the process zone in front of the fault tip moves ahead of the fault tip as the fault expands, leaving behind a zone that becomes the initial fault damage zone (Figure 8.24). In a porous rock, this zone is likely to consist of deformation bands. Because faults form in porous rocks by faulting of a deformation band zone as shown in Figure 8.23, the length of the deformation band process zone tends to be longer than the process zone seen in many non-porous rocks. This is particularly true if the deformation bands are cataclastic, in which case the process zone can be several hundred meters long.

If the structures of the damage zone form ahead of a propagating fault tip, then the damage zone should be slightly older than the associated slip surface. A consequence of this assumption would be that the width and strain of a damage zone are independent of fault displacement. Empirical data (Figure 8.12) show that this is not the case, even though the fault (slip surface) represents the weakest part of the rock and is therefore prone to reactivation without the creation of more sidewall damage. The reason is simply that faults are not perfectly planar structures, nor do they expand within a perfect plane. Faults are irregular at many scales because the rocks that they grow in are both heterogeneous and anisotropic. For example, faults may bend as they meet a different lithologic layer or as they link with other faults (Figure 8.25). Figure 8.26 shows an example of how damage may generate in the vicinity of a fault bend, in this case along with a gentle fault-bend fold.

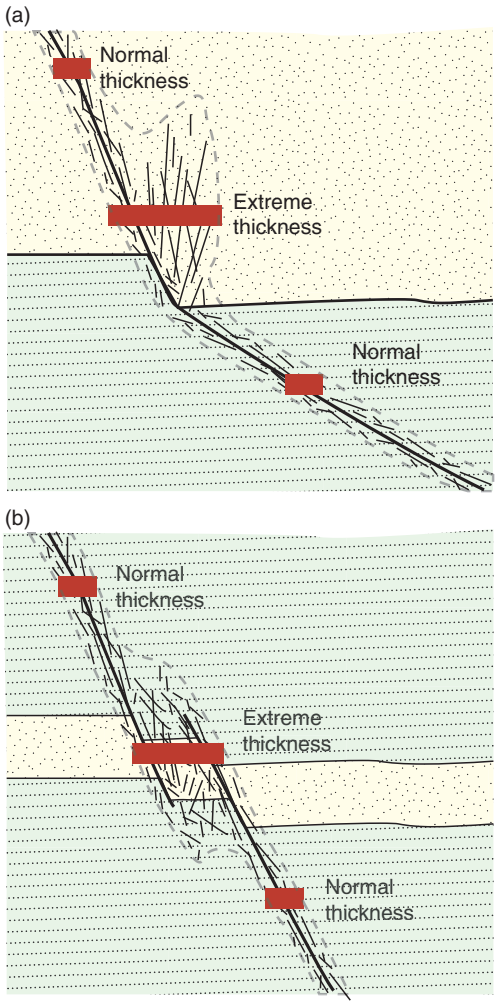

Figure 8.25 Variations in the thickness of damage zones related to (a) change in dip and (b) linkage. In these situations, minor structures are added to the damage zone until the fault cuts through the complex zone along a straighter path.

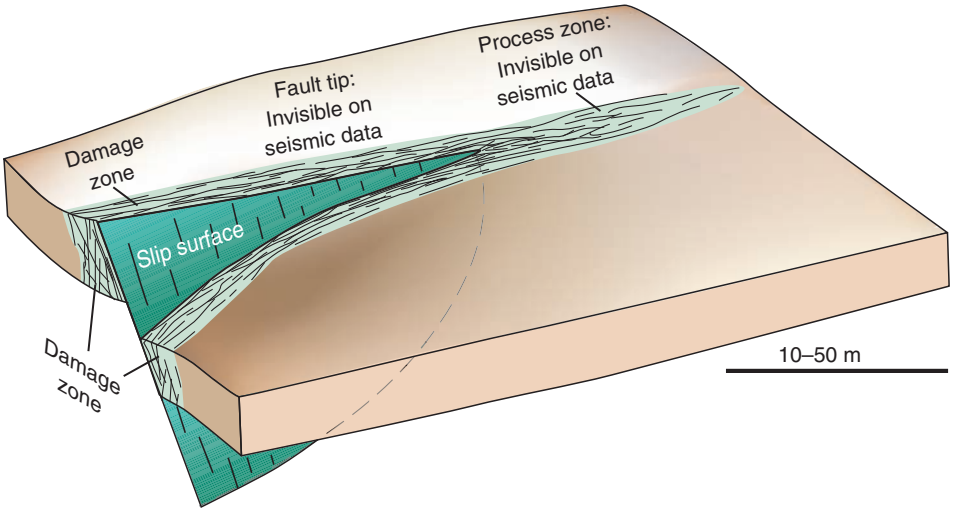

Figure 8.24 A fault is contained within a damage zone, which means that there is a (process) zone ahead of the tip where the rock is "processed" prior to fault propagation. The process zone may potentially contribute to compartmentalization of petroleum reservoirs. From Fossen *et al.* (2007).

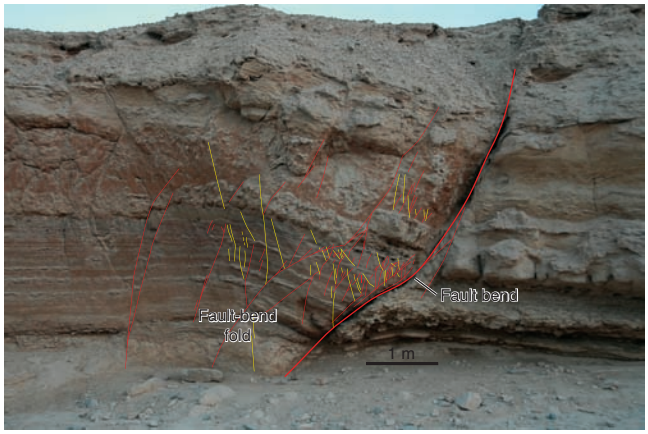

Figure 8.26 Hanging-wall rollover (fault-bend fold) related to bend in the main fault. The damage zone is unusually wide due to the complications posed by the fault bend. Synthetic and antithetic shear bands are separated by color. Matulla Formation, Wadi Matulla, Sinai. The offset of the fault exceeds the 4 m cliff height.

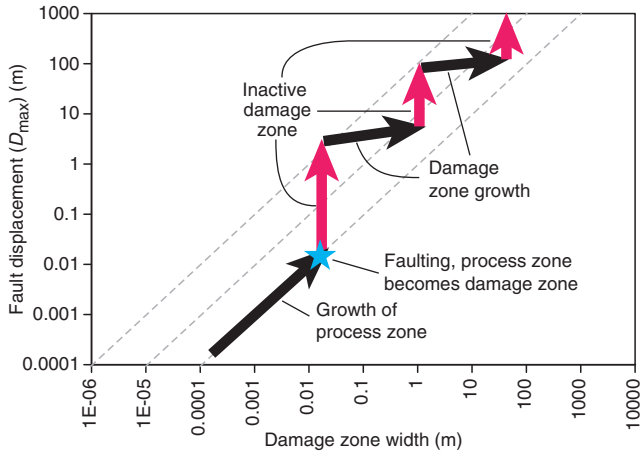

Figure 8.27 Schematic illustration of how a damage zone can grow periodically. The first stage is the growth of the process zone. Once the fault forms, the process zone becomes the damage zone and slip occurs smoothly for a while (red arrow) until complications lock the fault, which causes renewed growth of the damage zone. This repeats itself as the fault grows. The result is considerable scatter of fault data in fault displacement–damage zone width diagrams.

The structures in the damage zone form both prior to, during and after the local formation of the slip surface (fault).

If the fault is temporarily or locally planar and smooth, then there may be periods during which displacement accumulates without any deformation of the wall rocks, i.e. without any widening of the damage zone. However, at locations of fault linkage or fault bends, wall damage may also occur during fault growth, which leads to a local widening of the damage zone. Eventually, the fault may find a more planar way through zones of complications, and the damage zone becomes inactive again. Thus, the growth of damage zones may be temporal and local (Figure 8.27), contributing to the scatter seen in Figure 8.12.

The ductile drag zone

Drag is best defined as any systematic change in the orientation of layers or markers adjacent to a fault in a way that makes it clear that the change deflection is genetically related to the fault. Commonly, the term drag describes zones some meters or tens of meters wide. However, hanging-wall synclines related to normal faults in continental rift basins can extend several hundred meters into the hanging wall. Similarly, large-scale rollovers (reverse drag), up to several kilometers long on the hanging-wall side are associated with large listric faults.

Drag is folding of layers around a fault by means of brittle deformation mechanisms, directly related to the formation and/or growth of the fault.

Drag is seen in layers that are soft enough to deform ductilely in the upper, brittle part of the crust, most commonly in faulted sedimentary sequences. Although drag is commonly limited to a few-meters-wide zone along the fault (Figure 8.28), it may also be large enough to be imaged on seismic data, which in Figure 8.29 is documented by dipmeter data.

Drag can form in any tectonic regime. The kinematic requirement is that the angle between the slip vector of the fault and the layering is not too small. Because layering tends to be subhorizontal in sedimentary rocks, drag is most commonly associated with normal and reverse faults and less commonly developed along strike-slip faults. Folds also develop in subhorizontal layers along strike-slip faults (see Figure 18.10), but these are not drag folds. Thus, we may want to add another characteristic of drag folds:

The axes of drag folds make a high angle to the displacement vector of the fault.

For dip-slip faults and subhorizontal layers that means subhorizontal fold axes.

Figure 8.28 Drag of layers of siltstone and sandstone along vertical fault located along the left margin of the picture. Colorado National Monument, USA.

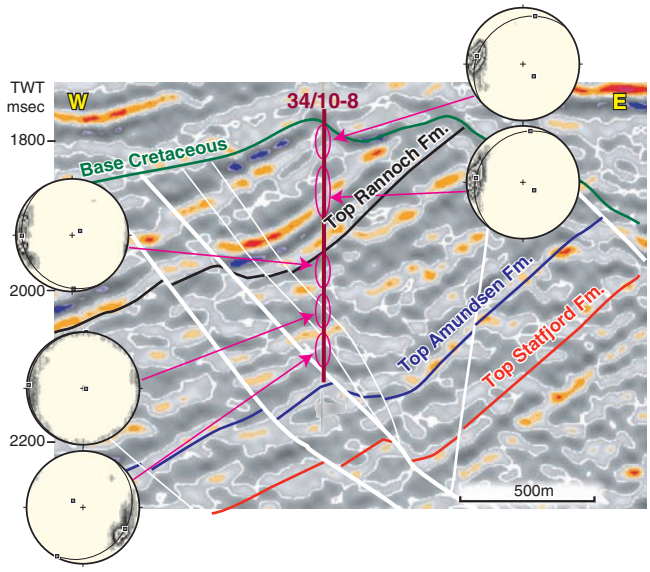

Figure 8.29 Dipmeter data collected along a vertical North Sea well. Stereonets show dip azimuth of layering in selected intervals. A change from west- to east-dipping layers is consistent with the normal drag portrayed by the seismic reflectors. Also note that the drag zone widens upward, consistent with the trishear model.

There are two geometrically different types of drag: normal drag and reverse drag. **Normal drag** is the shear zone-like geometry where layers flex toward parallelism with the fault. This is the geometry shown in Figures 8.28–32. Normal drag involves displacement, so that the total offset is the sum of the ductile normal drag and the discrete fault displacement. **Reverse drag** is used for the usually larger-scale rollover structures that occur on the hanging-wall side of listric normal faults. In this case the layers are concave in the slip direction. Both normal and reverse drag occur along faults, depending on the local fault geometry.

It was originally thought that drag was the result of friction along the fault during fault growth, but the term now includes bending of the layers prior to fault formation. The latter model seems to fit many examples of drag. This model is similar to that of damage zone development: in both cases layers are deformed in the wake of the fault tip. The difference is that drag folding is ductile down to a certain scale, commonly that of a hand sample.

The geometry of a drag fold contains information about how it formed. A drag fold in which the layers have the same geometry along the fault, with constant width of drag zone dip isogons (see Chapter 11) running parallel to the fault trace, can be modeled by simple

BOX 8.3 TRISHEAR

The trishear method, published by Eric Erslev in 1991, models the ductile deformation in a triangular fault propagation fold area in front of a propagating fault tip. The hanging-wall side of the triangle moves with a constant velocity above a fixed footwall, and the apical angle of the triangle is chosen. The triangle is symmetric with respect to the fault and the velocity vector is identical for all points located along any ray originating at the fault tip. Across the zone the velocity increases toward the hanging wall, Also, the direction of the velocity vector changes gradually from the hanging wall toward the footwall, as shown in the figure. We choose the apical angle of the trishear zone, the fault dip and amount of slip, and the propagation-to-slip ratio (P/S ratio). P/S determines how rapidly the fault tip propagates relative to the slip on the fault. $P/S = 0$ means that we fix the triangular zone to the footwall, while $P/S = 1$ fixes the zone to the hanging wall. In most cases $P/S > 1$ is realistic. Trial and error will give the geometry that most closely matches your field observations or seismically imaged structure. With a trishear program we can model the ductile deformation in front of a propagating fault tip and the resulting drag along the fault in a surprisingly realistic manner. Playing with Rich Allmendinger's freely available Fault/Fold program is recommended for understanding trishear and its parameters.

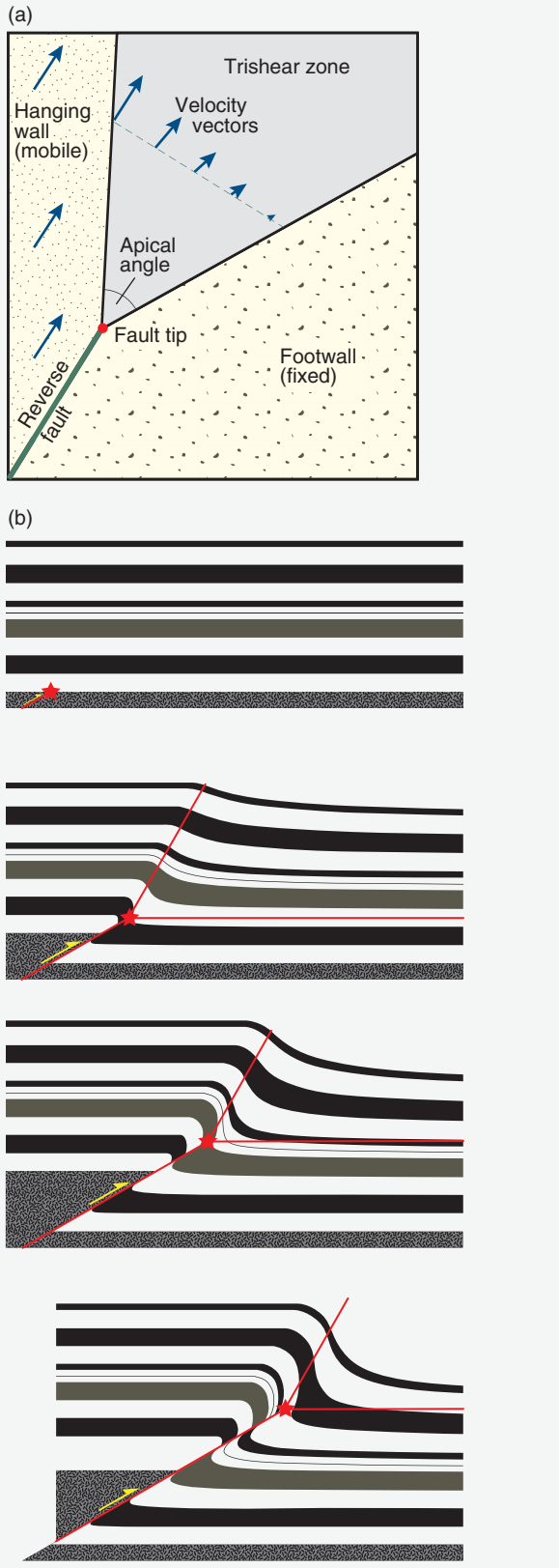

Trishear model of a reverse fault affecting an overlying sedimentary sequence. $P/S = 1.5$. Star indicates the fault tip at each stage.

shear. In this case we have a simple shear zone with a central discontinuity.

In other cases the drag zone is upward-widening, and a different kinematic model must be applied. A popular model is called **trishear**. In this model, which is more closely discussed in Box 8.3, strain is distributed in a triangular or fan-shaped zone of active deformation ahead of the fault tip (Figure 8.30). This zone moves through the rock as the fault propagates, and no further folding occurs once the fault has cut through the layers. The width of the triangular deformation zone varies from case to case, but in all cases the drag zone widens upsection. This model seems to work particularly well in places of reactivated basement faults that grow into overlying sedimentary strata. Many examples of such structures are found in the uplifts on the Colorado Plateau and in the Rocky Mountains foreland in Wyoming and Colorado, where the fold structures are commonly referred to as **forced folds**.

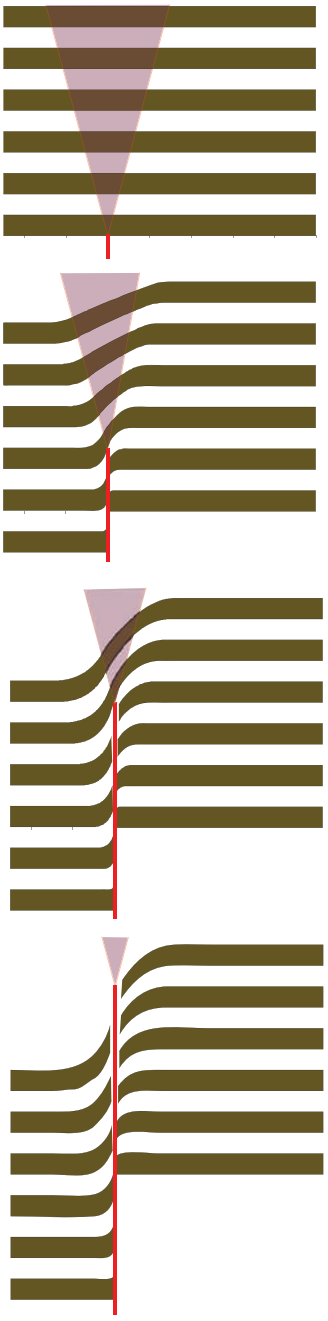

Figure 8.30 Trishear modeling of normal drag development. In this fault propagation fold model the drag zone widens upward.

Folds that form ahead of a propagating fault tip are called **fault propagation folds**. Thus, many drag folds are faulted fault propagation folds. However, drag can also form or become accentuated in the walls of an already existing fault. Just like the damage zone, fault drag can develop due to locking of the fault at fault bends, fault linkage and other complications that can increase the friction along faults. The effect of non-planar fault geometry is discussed in Chapter 20, and the development of normal drag between two overlapping fault segments is illustrated in Figure 8.31. The latter mechanism can take drag to the point where the rotated layer, which typically consists of clay or shale, forms a **smear** along the fault.

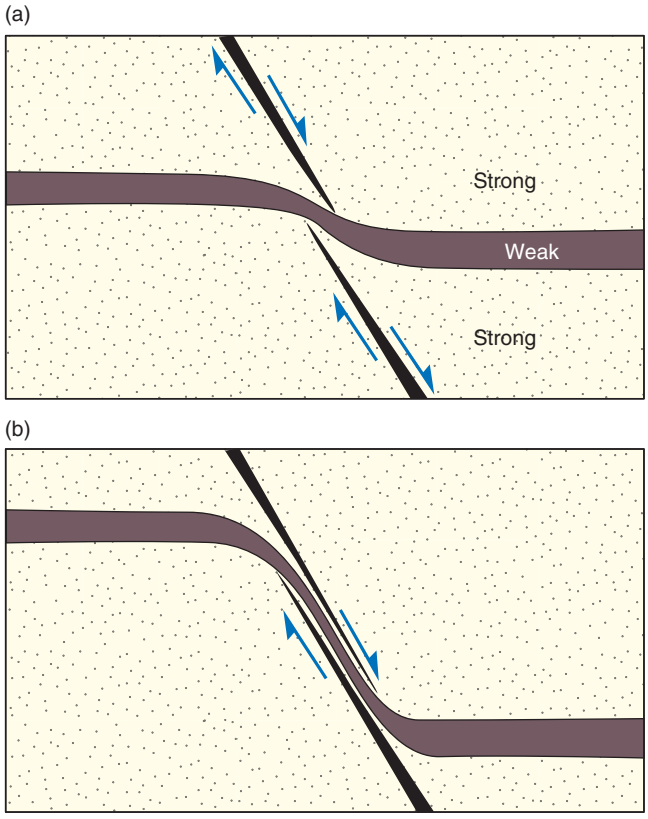

Figure 8.31 Normal dragging of mechanically weak layer (e.g. clay) between two overlapping fault segments.

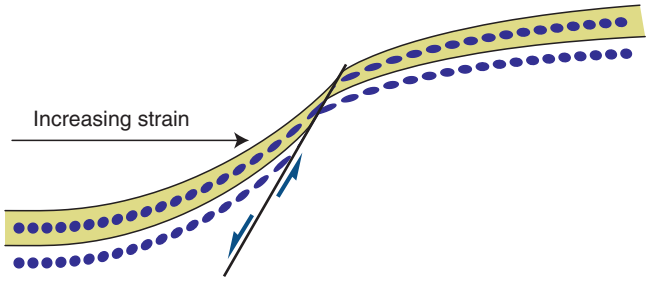

Figure 8.32 Strain ellipses portraying the relation between layer orientation and strain. Generated by means of the trishear program FaultFold. (R. Almendinger 2003).

Drag can form both ahead of the fault tip and in the walls of an active fault.

Drag, deformation mechanisms and the damage zone

Drag can occur by granular flow, particularly in poorly lithified sediments. Granular flow leaves little or no trace of the deformation except for the rotation of layering or modification of sedimentary structures. In consolidated sedimentary rocks grains may start to fracture, and the mechanism becomes distributed cataclastic flow. The mechanisms are the same as those that operate in the different deformation bands discussed in the previous chapter, but the deformation during drag folding is less localized and strain is generally lower. There is, however, a strain gradient toward the fault, as shown in Figure 8.32.

Fractures or deformation bands may occur in drag zones. In such cases the density of fractures or deformation bands increases toward the fault, as shown in Figure 8.33. The appearance of mesoscopically mappable fractures or deformation bands indicates that we are in the damage zone. Where drag folds are well developed, the drag zone tends to be wider than the damage zone, although the opposite situation also occurs.

Some faults, particularly in metamorphic rocks, show drag-like folding of the layering similar to that shown in Figure 8.28. A closer examination of many such "drag" folds reveals that they are controlled by plastic deformation mechanisms and are thus shear zones around faults that could have formed in a variety of ways, generally in the zone of brittle–plastic transition. We generally do not consider such plastic fold structures as drag folds, although the similarity can be striking.

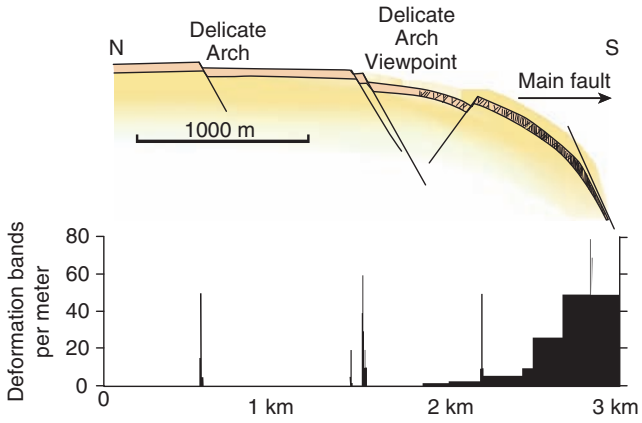

Figure 8.33 Folding of layers (rollover or reverse drag) adjacent to a major fault (not shown) accommodated by deformation band formation. Note the relationship between bed rotation and density of deformation bands. Example from Arches National Park, based on Antonellini and Aydin (1994).

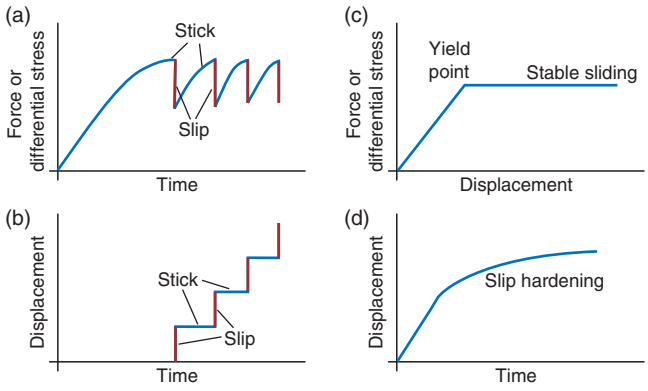

Figure 8.34 Idealized graphs illustrating the difference between stick-slip and stable sliding: (a) and (b) stick-slip graphs, (c) ideal stable sliding and (d) stable sliding with slip hardening.

Fault growth and seismicity

Once a fault surface is established it will represent a mechanically weak structure that is likely to fail again during renewed stress build-ups. Faults grow by two mechanisms. The most common one is called **stick-slip**, where slip accumulates at very sudden seismic slip events, separated by periods of no slip (Figure 8.34). Stress builds up between the slip events until it exceeds the frictional resistance of the fault. This is the model used to understand earthquakes, where each slip event causes an earthquake whose magnitude is related to the amount of energy released during the stress drop. In terms of strain, this is related to the amount of elastic strain that is released as the fault moves.

The other way for faults to accumulate slip is by **stable sliding** or **aseismic slip**. Ideally, displacement accumulates at a constant rate during stable sliding (Figure 8.34c). Some laboratory experiments show that a gradually increasing force is needed for slip to continue. This effect is called **slip hardening** (Figure 8.34d) and is related to damage of the slip surface during deformation.

Several factors control whether fault displacement accumulates gradually or by sudden slip events. Rock experiments indicate that stable sliding is more likely when the normal stress across the fault is small, which means that stable sliding is more common in the uppermost part of the brittle crust than deeper down. Low-angle faults along overpressured layers in a sedimentary sequence would also be likely to experience stable sliding even at depths of several kilometers because overpressure reduces the effective normal stress across the fault (Section 7.7).

Lithology is another important factor: porous sediments and sedimentary rocks are more likely to deform by stable sliding than are low-porosity crystalline rocks. In particular, stick-slip is favored in low-porosity quartz-rich siliceous rocks, while clay promotes stable sliding. Clay-bearing incohesive fault gouge in the fault core has some of the same effect as claystone: thick and continuous zones of clay gouge promote stable sliding. The fact that gouges (or rather slip surfaces along gouge zones) tend to represent pathways for fluid flow may add to their ability to slide in a stable fashion.

Close to the brittle–plastic transition, elevated temperatures introduce plastic deformation mechanisms that also promote stable sliding. Stick-slip deformation is of minor importance in the plastic regime, which for granitic rocks means temperatures above ~300 °C.

In summary, we could say that in the very top of the crust (upper kilometer or two), earthquakes are expected to be rare because of low normal stresses, weak and unconsolidated fault cores (gouge) and, at least in sedimentary basins, weak and porous rocks in general. Below this depth one would expect abundant seismic or stick-slip activity until the brittle–plastic transition is reached. This is exactly what earthquake data indicate, and the zone is called the **seismogenic zone** (Figure 8.35).

Typically, a single fault in the seismogenic zone shows evidence of both stick-slip and stable sliding. While seismic events may be responsible for the majority of total displacement accumulated over time, slow, **aseismic** "creep" is found to occur between **seismic** events. There

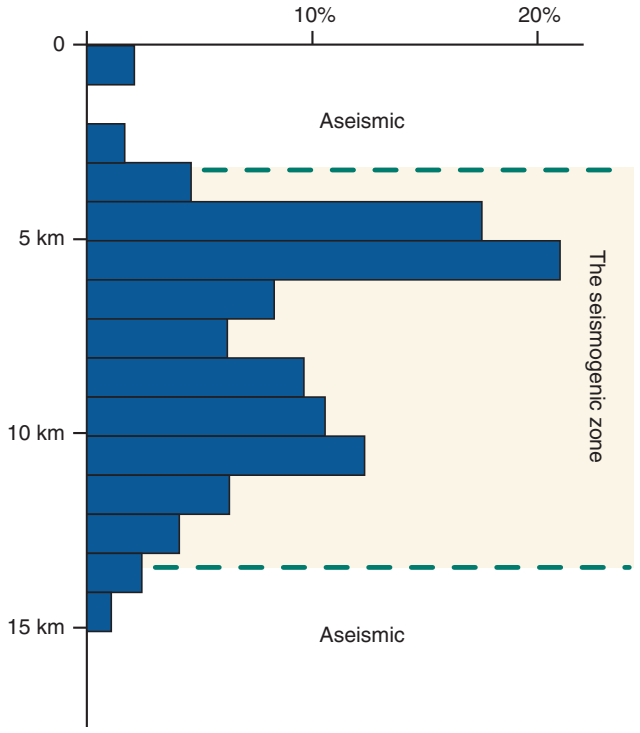

Figure 8.35 Distribution of 630 earthquakes in the crust beneath Parkfield, California. The distribution is characteristic for the continental crust away from subduction zones. Data from Marone and Scholz (1988).

is also a need for small **postseismic** adjustments that may or may not be seismic. Seismic means sudden energy release and displacement accumulations by means of earthquakes. Aseismic means gradual displacement accumulation without the generation of earthquakes.

Fault slip and displacement accumulation are commonly discussed in terms of seismicity and seismic slip behavior. It is important to realize that a single earthquake is unlikely to add more than a few meters of displacement. A quake of magnitude 6.5–6.9 that activates a 15–20 km long fault adds no more than one meter of maximum displacement to a fault. Only the largest earthquakes can generate offsets of 10–15 m. This has a very important implication:

A fault with a kilometer displacement must be the product of hundreds of earthquakes.

It is worth noting that the accumulation of such displacements would take thousands or millions of years, depending on the local displacement rate. Throw rates for faults can be found by dating sedimentary layers that are offset and measuring their displacements. Average

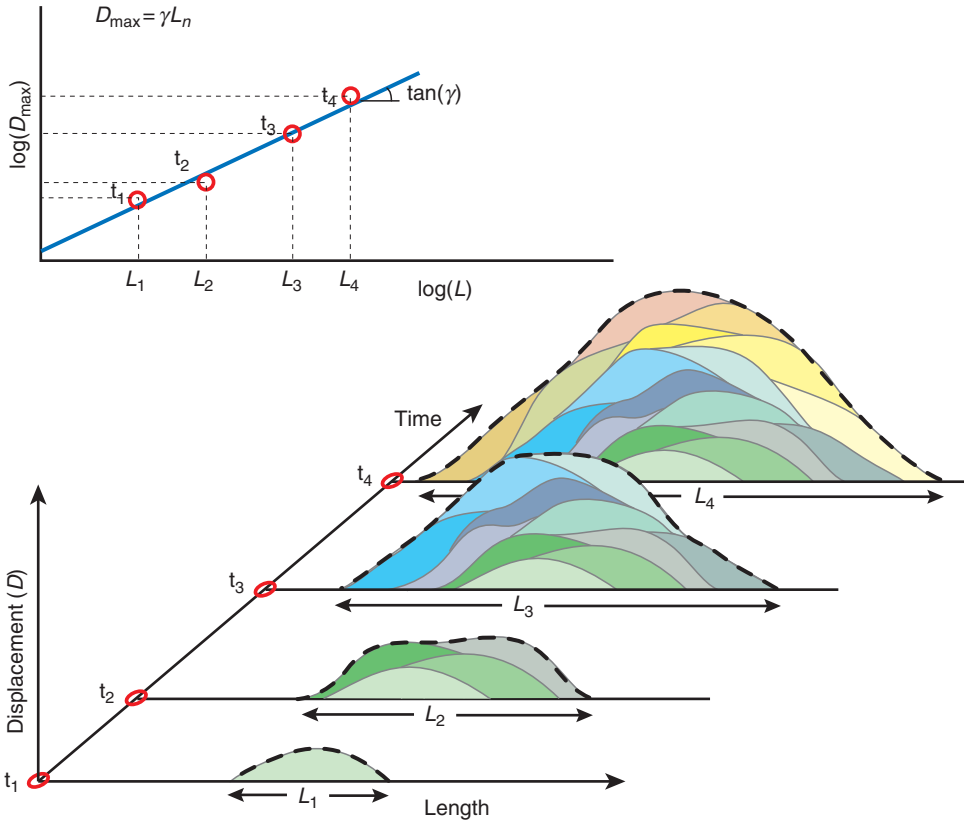

Figure 8.36 Schematic illustration of displacement accumulation through repeated slip events (earthquakes). Each event results in up to a few meters of displacement. In this model a bell-shaped cumulative displacement profile emerges which resembles that of a single slip event. The result of this model is a straight line in a logarithmic length–displacement diagram.

displacement rates of around 1–10 mm/year have been published for major faults in tectonically active areas.

Large faults tend to slip along just a limited portion of the total fault surface. The total displacement distribution for a large fault is therefore the sum of displacements contributed by individual slip events (earthquakes) (Figure 8.36). While it seems clear that single slip events produce more or less elliptical displacement contours, similar to those shown in Figure 8.15, the finite displacement distribution from a large number of slip events (earthquakes) is more difficult to predict or understand. The **characteristic earthquake model** assumes that each slip event is equal to the others in terms of slip distribution and rupture length. However, the location of the displacement maximum is shifted for each slip event. The **variable slip model** predicts that both the amount of slip and the rupture length vary from event to event, while the **uniform slip model** considers the slip at a given point to be the same in each slip event (the area varies). We will not go into the details of these models here, but simply state that displacement accumulation results in a displacement maximum near the middle of the fault, gradually tapering off toward the tips, as shown in Figure 8.13.

8.6 Growth of fault populations

Faults grow from microfractures or deformation band zones and accumulate displacement over time as deformation proceeds. Moreover, faults tend to nucleate at many different places as a region is critically stressed, for instance during rifting, and we refer to such groups of faults as **fault populations**. In general, many faults in a population soon become inactive and thus remain small. Others reach an intermediate stage before dying, while a few grow into long faults with large displacements. Hence, a fault population is always dominated by small faults, while additional long faults develop as strain accumulates.

Faults are unlikely to grow as individual structures over a long period of time. As they grow, they are likely to interfere with nearby faults. In this way two faults can join to form a single and much longer fault. Growth by linkage is a very common mechanism that creates some of the most interesting and important structures in faulted regions (Figures 8.37 and 8.38).

Fault linkage and relay structures

In a population where faults grow in length and height, faults and their surrounding stress and strain fields will

Figure 8.37 Extension fracture population along the edge of a paved road. Each of the fractures has grown from microfractures and they have reached a variety of sizes. The pavement is now more or less saturated with fractures, implying that additional strain will be accommodated by coalescence of existing fractures rather than by the nucleation of new ones.

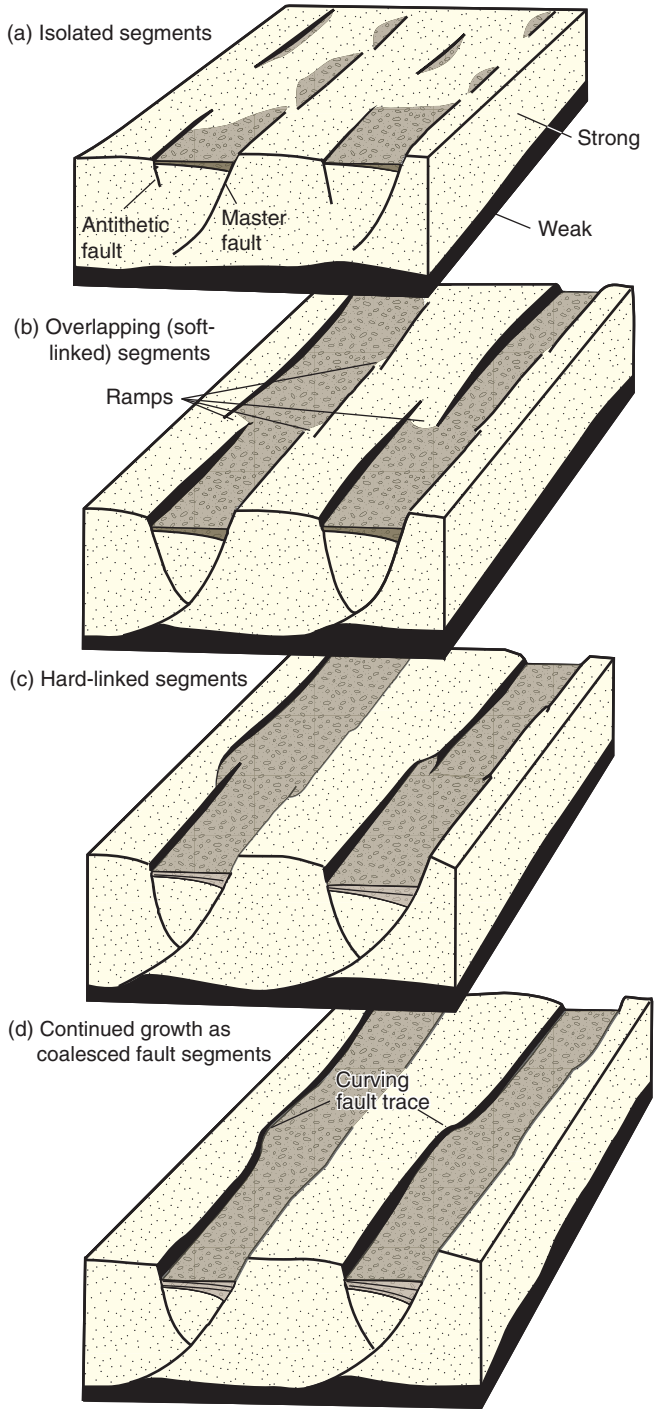

Figure 8.38 Simplified model for the development of a portion of a fault population in Canyonlands, Utah. The faults develop from isolated fractures into long faults through the formation and destruction of relay ramps. Based on Trudgill and Cartwright (1994).

locally interfere. Let us consider two faults whose tips approach each other during growth. Before the tips have reached each other (but after their strain fields have started to interfere) the faults are said to **underlap** (Figure 8.39a). Once the tips have passed each other, the faults are **overlapping** (Figure 8.39b, c). Under- and overlapping faults are said to be **soft linked** as long as they are not in direct physical contact. Eventually the faults may link up to form a **hard link** (Figure 8.39d).

Underlapping faults "feel" the presence of a neighboring fault tip in the sense that the energy required to keep the deformation going increases. The propagation rate of the fault tips in the area of underlap is thus reduced, which causes the local displacement gradient to increase. This results in asymmetric displacement profiles, where the maximum is shifted toward the overlapping tip (Figure 8.40; t_1).

This asymmetric displacement distribution becomes more pronounced as the faults overlap and the layers in

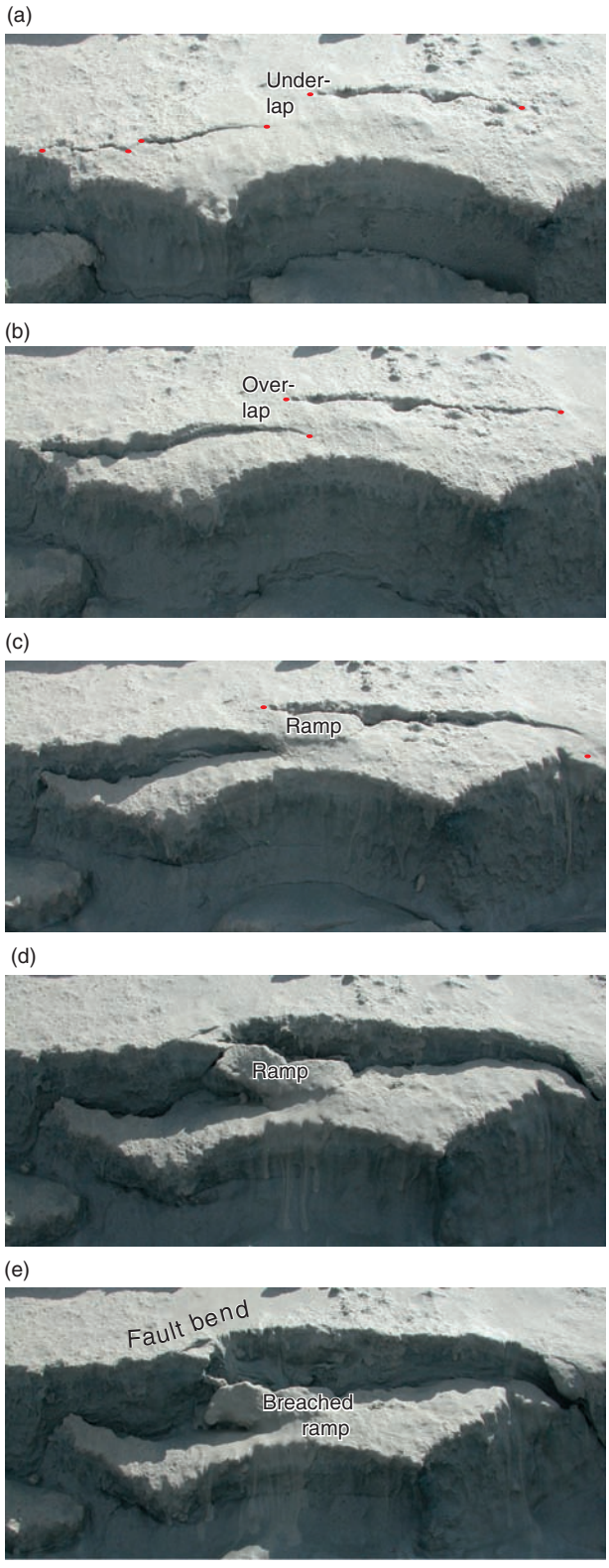

Figure 8.39 The development of curved fault systems in unconsolidated sand. Two isolated fractures (a) overlap (b, c) to form a relay ramp that eventually becomes breached (d, e). Faults were initiated by splashing water on the beach sand of a Colorado lake. The width of sand shown in each picture is *c.* 50–60 cm.

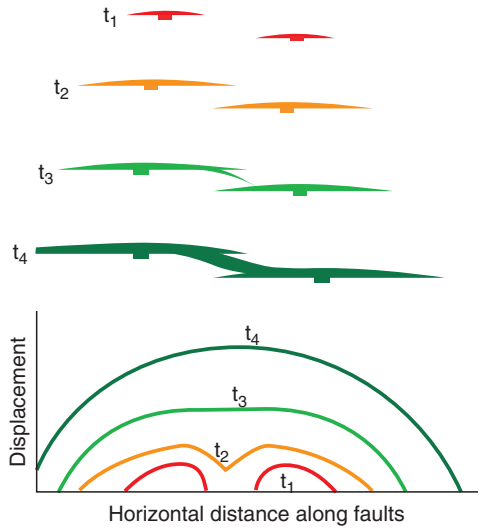

Figure 8.40 Illustration of the change in displacement along two faults that overlap and coalesce. The upper part shows the two segments in map view at four different stages of growth (t_1–t_4). The lower part shows the displacement profile at the four different stages.

the overlap zone become folded. The folding is a result of ductile displacement transfer (relay) from one fault to the other and is directly related to the high displacement gradients in the overlapping tip zones. If the fault interference occurs perpendicular to the slip direction, which for normal and reverse faults means in the horizontal direction, and if the layering is subhorizontal, then the folding is well expressed in the form of a ramp-like fold. The fold itself is called a **relay ramp** and the entire structure is known as a **relay structure** (Figures 8.39c and 8.41), and Box 8.4 explains why such structures are of particular interest to petroleum geologists.

The ramp is a fold that may contain extension fractures, shear fractures, deformation bands and/or minor faults depending on the mechanical rock properties at the time of deformation. Eventually the ramp will break to form a **breached relay ramp**. The two faults are then directly connected and associated with an abnormally wide damage zone.

Upon breaching there will be a displacement minimum at the location of the relay structure. The total displacement curve along the fault will therefore show two maxima, one on each side of the relay structure. As the deformation proceeds and the fault accumulates displacement, the displacement profile will approach that of a single fault, with a single, central maximum (Figure 8.40; t_4). However, the link is still characterized by the wide damage zone and a step in the horizontal

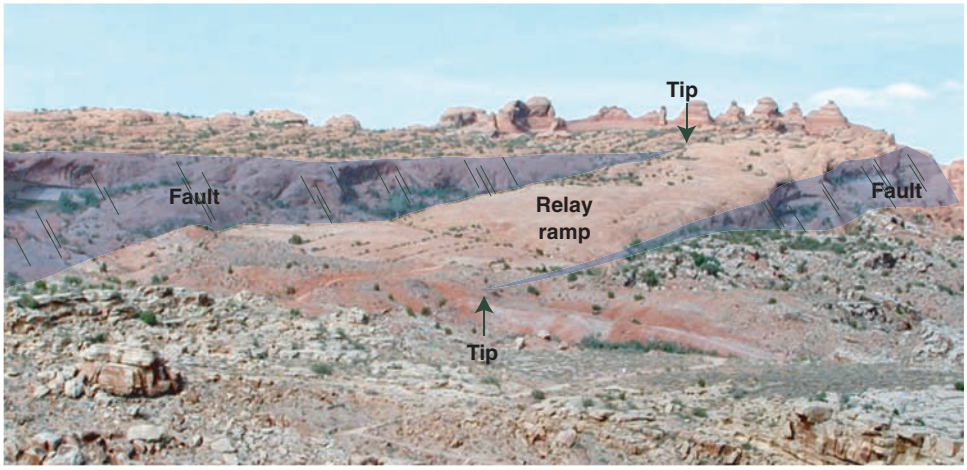

Figure 8.41 Relay ramp formed between two overlapping fault segments in Arches National Park, Utah. There is a higher density of deformation bands within the ramp than away from the ramp.

BOX 8.4 RELAY RAMPS IN PETROLEUM RESERVOIRS

Relay ramps can be important structures in a petroleum reservoir. In the context of exploration, ramps can cause communication (migration of oil) across a fault that is elsewhere sealing. During production, relay ramps may represent pathways for water, oil or gas that cause pressure communication between otherwise isolated fault blocks. Relay ramps may contain abundant subseismic structures, depending on their stage of maturity. They are generally associated with damage that could cause problems to wells placed in or near the relay structure. Both breached and intact ramps are easily interpreted as sudden bends in the fault trace. The kinks can represent the interpreter's smoothing of an intact ramp around or below seismic resolution, or a breached ramp. Unbreached and barely breached ramps may show a displacement minimum in the ramp area that may be detectable from seismic data.

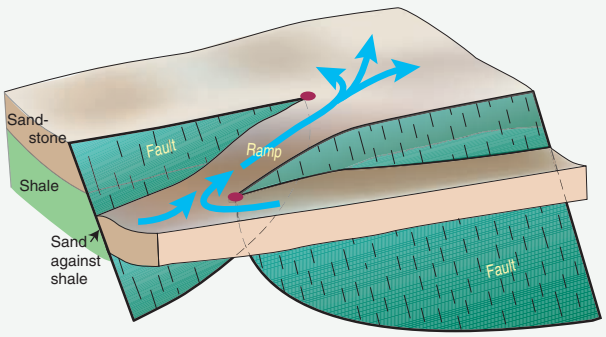

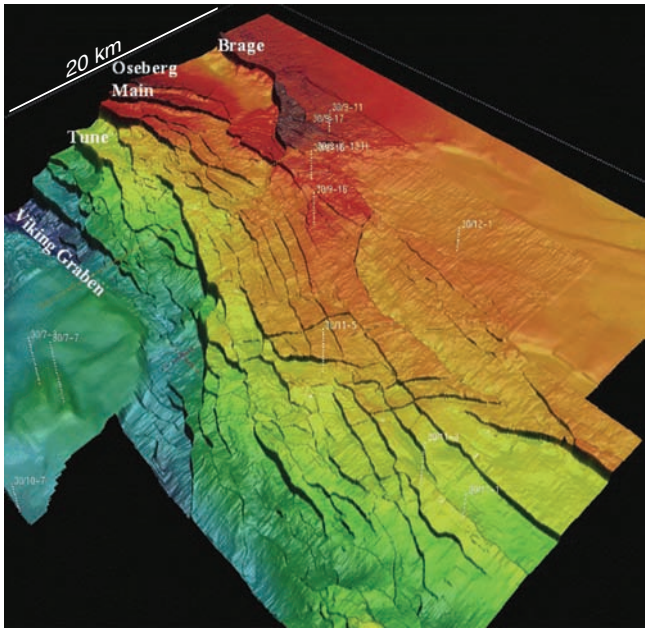

Figure 8.42 Normal fault population on the east flank of the Viking Graben, northern North Sea, illustrated at the base Cretaceous level (warm colors indicate shallow depths). The fault population shows various stages of fault linkage.

fault trace. If the mapping is based on poorly constrained outcrop information or seismic data (which always have a resolution issue), a sudden change in strike may be the only indication of a breached ramp. Such steps, seen at many locations in the seismic interpretation shown in Figure 8.42, are therefore very important as they may hint at the locations of both breached and intact relay ramps.

Bends and jogs of faults in map view are very common on many scales. Figure 8.39 shows the development of a non-planar fault in sand. The final fault geometry can

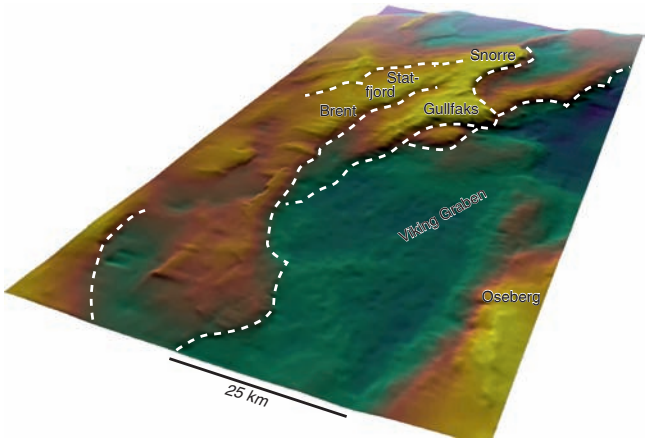

Figure 8.43 Curved fault systems (white dashed lines) in the northern North Sea basin (base Cretaceous level). Note similarities with Figures 8.39 and 8.44.

be seen to be the result of interaction between individual fault segments through the creation and breaching of relay ramps. The curved fault pattern seen in map view is very similar to that displayed by much larger faults, such as the northern North Sea faults shown in Figure 8.43 and the Wasatch Fault in Utah (Figure 8.44), so it seems likely that these large faults formed by fault linkage as portrayed in Figure 8.39. Assuming that this analogy holds, we are now able to interpret a deformation history from the geometry of a dead fault system.

It is clear that ramps come in any size and stage of development. It is also important to understand that relay ramps and overlap zones are formed and destroyed continuously during the growth of a fault population.

Fault growth by linkage involves the formation and destruction of relay structures, deviations from the ideal elliptical displacement distribution and generation of wide damage zones and fault bends at locations of linkage.

Fault linkage in the slip direction

Faults grow in the directions both normal and parallel to the slip direction and therefore interfere in both the vertical and horizontal directions (Figure 8.45). In the previous section we looked at the horizontal interaction of normal fault tips. Now we will look at the interference of normal fault tips in the vertical plane, i.e. parallel to the slip vector. Fault linkage is most commonly recognized and described in map view, but this is simply because they are easier to observe in map view. Tall vertical sections are less common than long horizontal

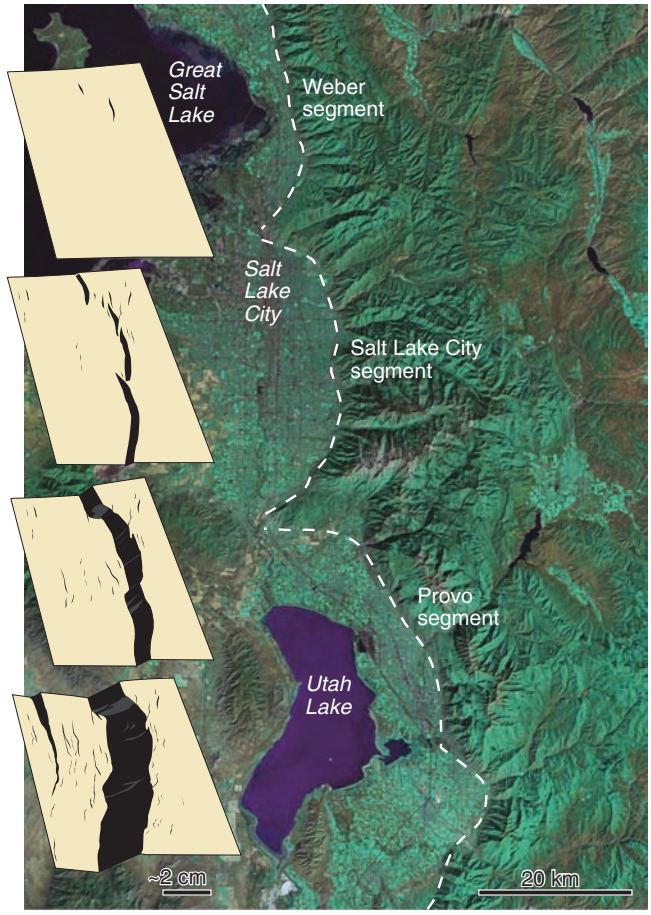

Figure 8.44 The Wasatch fault zone near Salt Lake City, Utah, crudely indicated by white dashed line. Note the curved fault geometry, indicating a history of segment linkage. Sketches of various stages of plaster extension experiment indicate how such fault zones can form.

exposures, and the continuity of good seismic reflectors in the horizontal direction makes it easier to map relays in map view than in the vertical direction. It takes a whole package of good reflectors to identify and map vertical overlap zones on seismic sections. There is therefore a good chance that vertical relay zones are underrepresented in seismic interpretations.

Faults initiate after a certain amount of strain that depends on the mechanical properties (Young's modulus, etc.). As strong rock layers start to fracture, weak rocks continue to accumulate elastic and ductile deformation. As these fractures grow into faults, they will interfere and connect. In many cases sandstones become faulted before shales. The process is similar to that occurring in map view, except that the angle between the displacement vector and the layering is different. We do not get ramps as shown in Figure 8.41, but rotation of

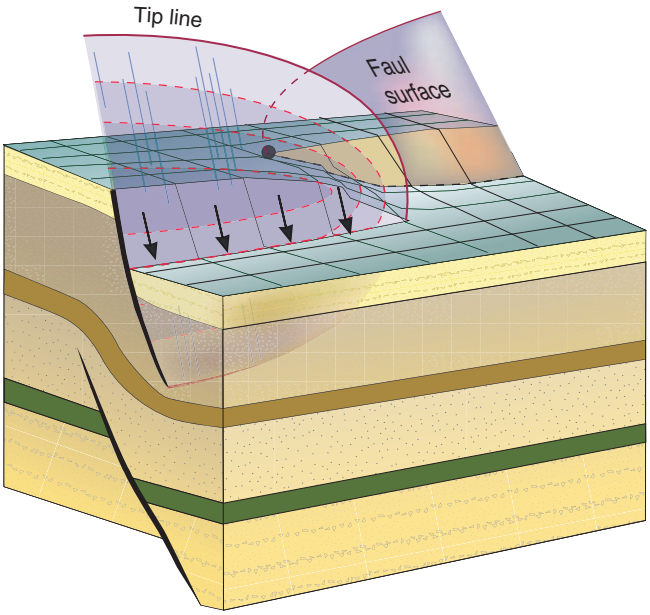

Figure 8.45 Faults interfere in both the horizontal and vertical directions as they grow. In both cases displacement is transferred from one fault to the other, and layers between the overlapping tips tend to fold into ramps or drag folds. Modified from Rykkelid and Fossen (1992).

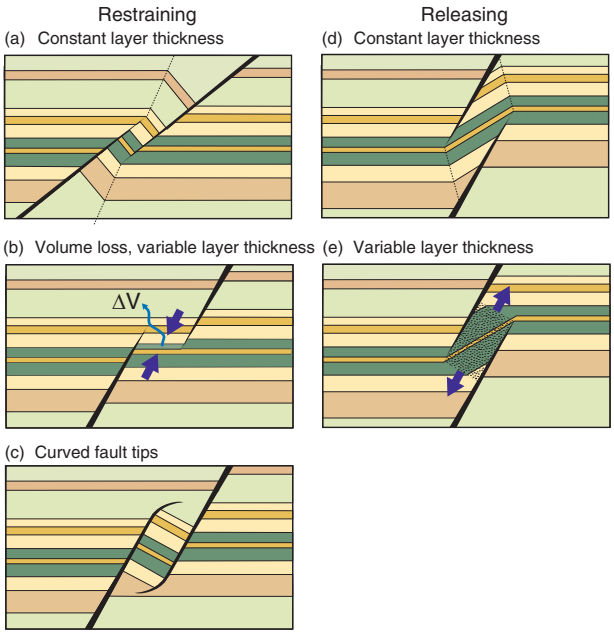

Figure 8.46 Different types of vertical overlap zones (horizontal layering). (a) Contractional or restraining type where constant layer thickness implies marked reverse drag. (b) Contraction compensated for by local dilation. (c) Restraining zone where the fault tips bend towards each other. Extensional or releasing zones with constant (d) and variable (e) layer thickness give normal drag. Based on Rykkelid and Fossen (2002).

Figure 8.47 Overlapping faults where a shale layer is caught and smeared in the overlap zone. Moab, Utah.

layers as shown in Figure 8.46. The rotation depends on fault geometry and how the faults interfere.

Restraining overlap zones (Figure 8.46a–c) are, in this connection, overlap zones with shortening in the displacement direction. In principle, volume reduction may accommodate the deformation within the zone. More commonly, however, the layers within the overlap zone rotate as shown in Figure 8.46c.

Releasing overlap zones (Figure 8.46d, e) are zones where the fault arrangement and sense of displacement cause stretching within the overlap zone. Weak layers such as shale or clay layers are rotated within releasing overlap zones. If the overlap zone is narrow, such weak layers can be smeared along the fault zone (Figures 8.31 and 8.47). Field observations show that this is a common mechanism for the formation of clay smear in sedimentary sequences, but usually on too small a scale to be detected from seismic data. Such structures may cause faults to be sealing with respect to fluid flow, which can have important implications in petroleum or groundwater reservoirs.

The role of lithology

Layering or **mechanical stratigraphy** is important as fault populations develop in layered rocks. The timing of fault formation in the different layers is one aspect, and the way that faults form (ordinary fracturing versus faulting of deformation band zones) is another. Mechanical stratigraphy simply implies that the rock consists of layers that respond mechanically differently to stress, i.e. they have different strengths and different Young's moduli (E). In simple terms, some layers, such as clay

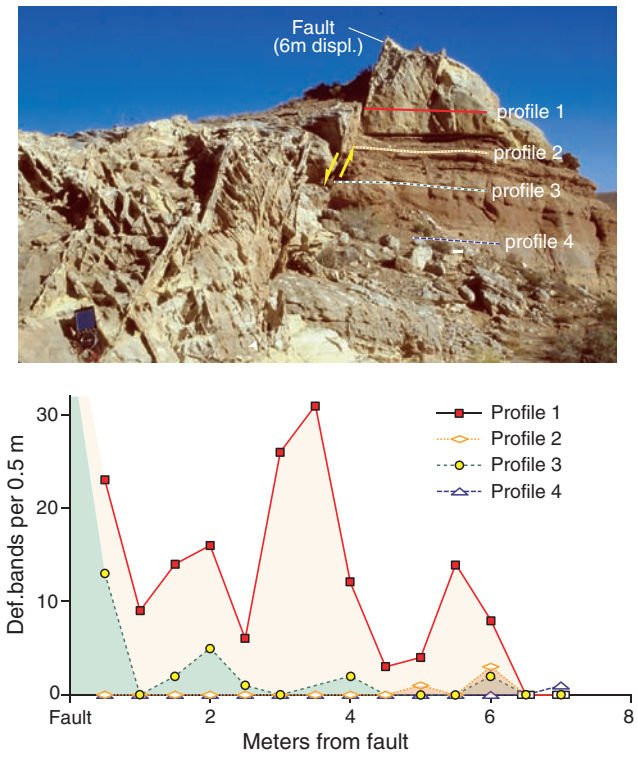

Figure 8.48 Distribution of deformation bands in the footwall to a fault with 6 m displacement. The frequency is considerably higher in the clean, highly porous sandstone (Profile 1) than in the more fine-grained layers (Profiles 2 and 3). It is also lower in the thin sandstone layer (Profile 4). San Rafael Desert, Utah.

or shale, can accommodate a considerable amount of ductile strain, while other layers, such as limestone or cemented sandstone, fracture at much lower amounts of strain. The result is that, in a layered sequence, fractures or deformation bands initiate in certain layers, while adjacent layers are unaffected or less affected by such brittle structures (Figure 8.48).

So long as the deformation band or fracture grows within a homogeneous layer, a proportionality exists between maximum displacement, length and height. This is illustrated in Figure 8.49a, where the fracture (or deformation band) has not yet (or just barely) reached the upper and lower boundaries of the layer. Once the fracture touches the layer boundaries (Figure 8.49b) it is called a **vertically constrained fracture**, and the fracture will only expand in the horizontal direction. This means that the fracture gets longer and longer while its height remains constant, i.e. its eccentricity increases. In fact, its shape is likely to become more rectangular than elliptical.

The moment a fracture is constrained, its area increases only by layer-parallel growth, and its displacement/length (D/L) ratio becomes lower than what it was during its unconstrained growth history. In simple terms, this is because displacement scales with fracture area, and since the fracture area only increases along its length, the length has to increase at a faster rate relative to displacement.

Eventually, if the fracture keeps accumulating displacement, it will break through the bounding interface and expand into the overlying/underlying layers (Figure 8.49c). The D–L relationship will then return to its original trend (Figure 8.49d). The same development is seen for deformation bands in sandstone–shale sequences. At a critical point the deformation band cluster in the sandstone is cut by a slip surface (fault) that extends into the over and/or underlying shale.

D–L relations during fault growth

The maximum displacement (D_{max}) along a fault is a function of the fault's eccentricity (ellipticity: length/height or L/H ratio) and the strength (driving stress) of the rock (Figure 7.20). L is commonly plotted against D_{max} as shown in Figure 8.50. Straight lines in such logarithmic diagrams indicate an exponential or **power-law** relation between D and L that can be expressed as

$$D_{max} = \gamma L^n$$

Faults or other discontinuities that grow such that D and L are proportional, i.e. $D_{max} = \gamma L$, define straight, diagonal lines in the logarithmic diagram with slope γ ($n = 1$). Field data seem to plot along diagonal lines, although with a considerable amount of scatter (Figure 8.50). Some structures, including joints, veins, igneous dikes, cataclastic deformation bands and compaction bands show lower slopes ($n \sim 0.5$). This may be related to their sensitivity to mechanical stratigraphy, as discussed in the previous section. Mechanical stratigraphy occurs at different scales, from meter-scale beds up to the thickness of the entire brittle crust. Hence, it is thought that the effect repeats itself to some degree at different scales, causing some of the scatter seen in Figure 8.50. Another reason for the scatter is the growth of faults by linkage, as discussed above. The relation between D and L can be of interest in several cases, for instance where the displacement is known from well information or seismic data, and the total length of the fault is to be estimated. However, the scatter of data makes predictions uncertain.

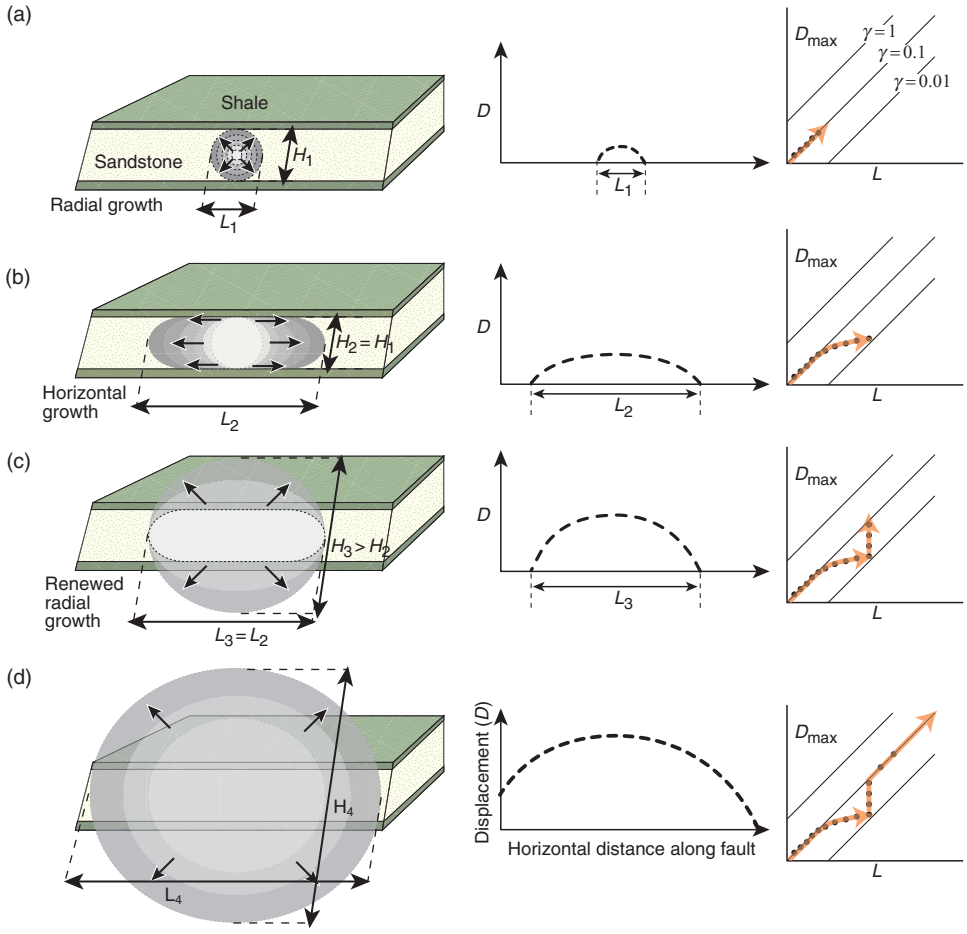

Figure 8.49 Growth of a fault in a layered sequence, with displacement profile and displacement–length evolution shown to the right (logarithmic axes). The fault nucleates in the sandstone layer (a) with a normal displacement profile and expands horizontally when hitting the upper and lower boundaries (b). A relatively long or plateau-shaped displacement profile evolves. At some point the fault breaks through the under/overlying layers (c) and starts growing in the vertical direction again. The displacement profile regains a normal shape. Such lithologic influence on fault growth causes scatter in *D*–*L* diagrams.

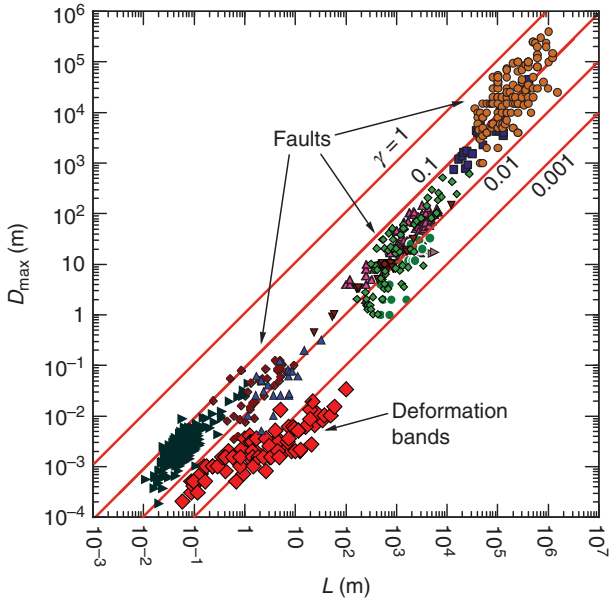

Figure 8.50 Displacement–length diagram for faults and cataclastic deformation bands. Faults from a number of localities and settings are plotted. The deformation bands show a clear deviation from the general trend in that they are longer than predicted from their displacement. Modified from Schultz and Fossen (2002).

8.7 Faults, communication and sealing properties

Faults may affect fluid flow in different ways. Faults in non-porous or low-porosity rocks are generally conduits of fluids. In particular, the fracture-filled damage zone is a good target when drilling for water in such rocks. The fault core is commonly less permeable because of its content of secondary clay minerals (fault gouge).

In highly porous rocks, faults more commonly act as baffles to fluid flow. In a petroleum reservoir setting it is important to distinguish between their effect over geologic time and their role during production. Some faults are sealing over geologic time (millions of years) and can stop and trap considerable columns of oil and gas. Other faults that are not sealing over geologic time may still baffle fluid flow during production of an oil or gas field (over days or years). The ability of faults to affect fluid flow is commonly referred to as fault **transmissibility** or **transmissivity**. Fault transmissibility is influenced by the nature of the damage zone, but is mostly controlled by the thickness and properties of the fault core.

Faults tend to increase permeability in non-porous rocks, while they commonly reduce permeability in porous rocks.

Juxtaposition

The lithological contact relations along a fault are essential when it comes to its effect on fluid flow in a porous reservoir, and several cases are shown in Figure 8.51. Where sand is completely juxtaposed against shale, the fault is sealing regardless of the properties of the fault itself. This type of seal is called a **juxtaposition seal** (1 in Figure 8.51). However, where sand is juxtaposed against sand without any clay or shale smeared between the sand (stone) beds, the transmissibility of the fault is solely controlled by the physical properties of the fault core and the fault damage zone. These properties are again controlled by the amount of smearing of fine-grained material along the fault, the fault core thickness, the deformation mechanisms within the core and in deformation bands and other structures surrounding the core. Sand–sand juxtaposition occurs when the offset is smaller than the thickness of the sand layer. Any seal resulting from brittle deformation or cementation and dissolution along the fault in this case is referred to as a **self juxtaposed seal** (2 in Figure 8.51). When the fault displacement is larger than the sand thickness, two different sand layers can be juxtaposed. If they are stratigraphically separated by a shale the shale may be smeared out to form an impermeable membrane, thereby forming a **shale smear seal** (3 in Figure 8.51).

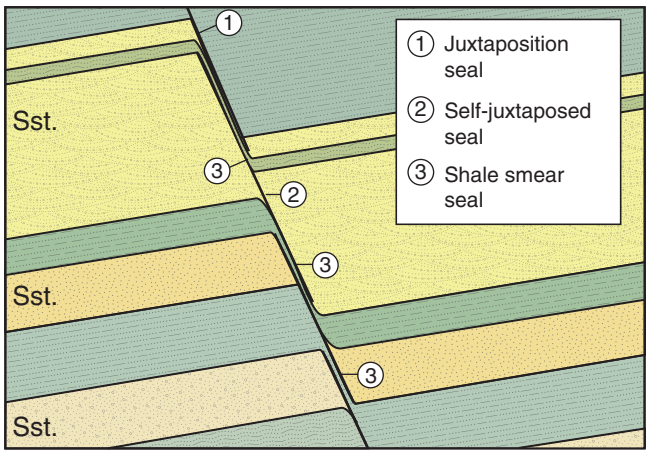

Figure 8.51 Principal sketch showing different contact relations along a fault. Yellowish layers are reservoir sandstone, while greenish layers are impermeable shale. Three principal types of seals are shown. Note that for the fault to be sealing, the membrane must be continuous also in the third direction for as far as the two sands are in contact.

Cataclasis

Cataclasis in the fault core reduces grain size and therefore reduces porosity and permeability. Cataclasis is promoted by deep (>1 km) burial depths, low phyllosilicate content, well-sorted grains and low pore-fluid pressure. Cataclasis can create a cataclasite or ultracataclasite so dense that it will stop fluid flow across the fault even if there is high-permeability sandstone on each side of the fault. Cataclasis also occurs in deformation bands in the damage zone, and the more deformation bands, the larger their effect on fault transmissibility during production. The sealing effect of cataclastic deformation bands in the damage zone is probably negligible in most cases.

Diagenetic effects

Diagenetic changes that occur after or during the faulting process can change the mechanical and petrophysical properties of the fault rock significantly in some cases. The most important change is probably caused by dissolution and precipitation of quartz, which can turn the fault rock into a non-permeable 'quartzite'. Quartz dissolution and cementation is a problem at temperatures above ~90 °C (3 km). In many basins, such as the North Sea, quartz cementation occurred much later than the faulting as the sediments were buried during post-rift subsidence. Quartz and other minerals may be preferentially deposited in faults because of the reactant surfaces that form during faulting due to the scratching and breaking of grains. In addition, fluids can easily move along faults in some cases, increasing the flux of silica-bearing fluids. Calcite cementation in faults is also fairly common, but is thought to form less continuous structures.

Clay and shale smear

The fine-grained nature of clay and shale causes them to have very small pore spaces and pore throats (connections between pores), which therefore effectively stop or hinder fluids flowing through them. Clay minerals can form secondarily along faults in almost any rock type, but in most sedimentary rocks the primary source of clay and shale is shale layers in the sedimentary sequence itself. Shale layers become incorporated into the fault core during fault movements (Figure 8.51), and the process where clay or shale is smeared out into a more or less continuous membrane is simply called **smearing**.

Figure 8.52 Minor fault in fluvial sandstone–shale layers of the Cretaceous Castlegate Formation, Salina, Utah. A centimeter-thick membrane of clay-rich material fed from shales in the hanging wall seals most of the section. Note that the uppermost part of the fault has no shale membrane, probably because of lack of shale layers at that level.

Field observations and experimental results alike show that clay and shale are likely to become smeared during faulting into a fault-core membrane separating the hanging wall and footwall. Figure 8.52 shows an example where a centimeter-thick shale membrane separates highly porous sandstones of reservoir quality. If such a membrane represents a physical barrier to fluid flow it is called a **seal**, and the fault is a **sealing fault**. A membrane must be continuous over a certain critical area of the fault to effectively seal a structure. The more clay or shale involved in a faulted sedimentary sequence, the larger the chance of smearing and sealing. A common mechanism is the smearing of clay or shale between two **vertically overlapping fault segments**, as shown in Figure 8.47. A less common mechanism is injection, where abnormally high pressures in clay layers cause **clay injection** along the fault core. **Clay abrasion**, where clay is tectonically eroded from clay-rich layers along the fault and incorporated into the fault core, is a third mechanism that contributes to clay smearing.

Smearing of clay or shale along a fault may result in sealing faults in a fluid reservoir.

The likelihood of smearing increases with increasing amount of clay, i.e. with the number of clay layers and their cumulative thickness, and decreases with increasing fault displacement. The more displacement, the higher the probability that the seal is discontinuous and the fault is leaky. If the discontinuity of the seal is local and small, it may still reduce the flow rate across the fault.

There is a need to put numbers on the clay smearing potential of faults. In the simple case where there is a single clay or shale layer and a single fault (Figure 8.53a), then the **shale smear factor** (SSF) gives the ratio between fault throw T and the thickness of the shale or clay layer (Δz):

$$\mathrm{SSF} = \frac{T}{\Delta z} \tag{8.1}$$

This puts a number to the local probability of smear, and the number will vary along the fault as displacement and perhaps also layer thickness change. For faults with offsets of tens of meters or more an SSF ≤ 4 is considered to indicate a continuous smear and thus a sealing fault, while smaller faults are less predictable. Obviously, there are other factors that influence the sealing capacity of a fault, so this method should be used with some care.

In cases where there is more than one source of clay or shale the combined contribution must be considered. This can be done at any point on the fault by summing the shale bed thicknesses of the stratigraphy that has passed that point and calculating the percentage of clay or shale in the slipped interval. Divided by the fault throw (T) we get what is known as the **shale gouge ratio** (SGR):

$$\mathrm{SGR} = \frac{\sum \Delta z}{T} \cdot 100\% \tag{8.2}$$

Alternatively, if the clay minerals are more distributed within the sequence we should use the sum of the volume fractions from all units in the interval instead of the sum of shale layer thicknesses. A high SGR-value indicates high sealing probability. There is a good chance that the

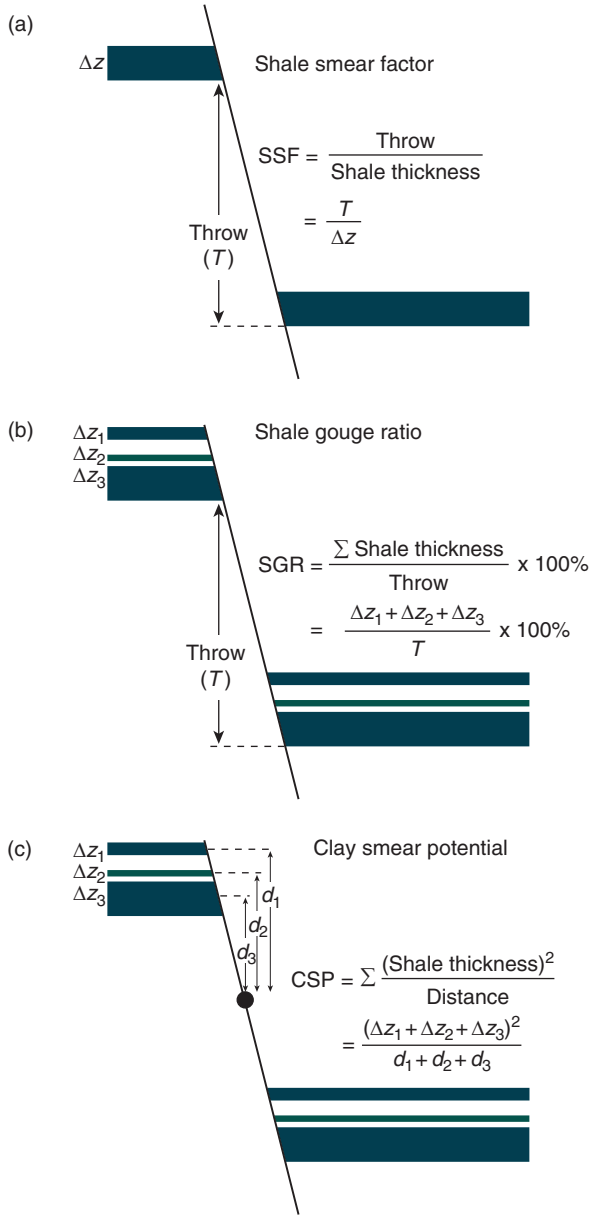

Figure 8.53 Three algorithms for estimating the likelihood of smear on a fault.

fault is sealing when the SGR-value exceeds 20%, and the probability increases with the SGR. The probability will also depend on the mechanical properties of the shale or clay layers at the time of deformation. In general, shallow burial promotes smearing while faulting at deep burial depths involves a higher risk of a leaky seal.

Clay smear can also be characterized by estimating the **clay smear potential** (CSP). CSP relates to how far a clay or shale layer can be smeared before it breaks and becomes discontinuous:

$$\mathrm{CSP} = \sum \frac{\Delta z^2}{d} \qquad (8.3)$$

where d is the distance from the source (clay) layer and Δz represents the individual thickness of each clay or shale layer.

Coal can also be smeared along faults if it is mixed with clay. However, pure coal normally behaves brittlely when faulted. Even sand can be smeared along faults when in a poorly consolidated state. Sand smearing at shallow depths may improve communication across faults, but it is rarer than shale smear.

The shale smear factor and similar algorithms help us to estimate the sealing potential of a fault, but do not catch all the complexities and variations that exist within and along natural faults.

Juxtaposition and triangle diagrams

Lithology and displacement are, as emphasized above, important factors in the estimation of the sealing properties of faults. Because both lithology and displacement vary on a fault, different portions of the fault have different sealing properties or sealing potentials. Considering a reservoir with porous reservoir sandstones interbedded with impermeable shale we can have juxtaposition seal, shale smear seal and self juxtaposed seal along the same fault, with variations occurring both across (Figure 8.51) and along stratigraphy.

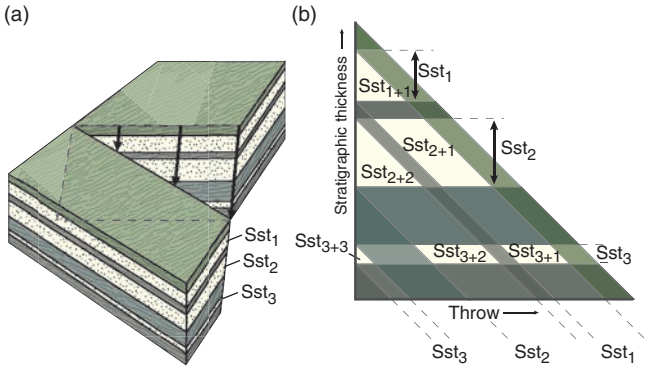

Figure 8.54 The concept of triangle diagram construction. A synthetic fault with a linearly increasing displacement is considered (a). In the block diagram the layers on the upthrown side are horizontal while they are dipping on the opposite side. This is carried over to the triangular diagram to the right (b). Because the displacement increases from zero on the left-hand side, different lithologic contact relations occur in different parts of the diagram. Areas of sand–sand and sand–clay contact can easily be found.

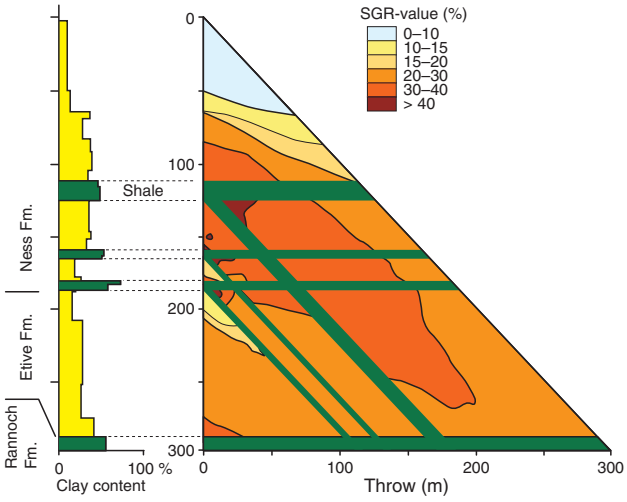

Figure 8.55 SGR-values can be added to the triangle diagram, as for this example from the North Sea Brent Group (stratigraphy shown to the left). The SGR-value is calculated for different points in the diagram and contoured. High SGR-values mean high sealing probability. Based on Høyland Kleppe (2003).

Juxtaposition as a function of stratigraphy and displacement can be visualized in a **triangle diagram** (Figure 8.54). The local stratigraphy is plotted along the vertical axis and extended parallel to the other two sides so that they gradually separate. This is in effect similar to what happens along a fault, where layer separation increases with increasing displacement. In the diagram, horizontal stratigraphic layers represent the hanging wall layers, while the dipping layers represent the footwall. Layer separation and fault displacement increase as we move to the right in the diagram, and we can read off the contact relations for any given value of fault displacement.

The different lithologies (layers) in the diagram are colored. For a sand–shale sequence different colors indicate sand–sand, sand–shale and shale–shale juxtaposition. Furthermore, for each point in the diagram one or more of the parameters SGR, SSF and CSP can be calculated and the triangular diagram can be colored to illustrate the variation in, for example, SGR (Figure 8.55).

Summary

While faults may look simple when portrayed as lines on geologic maps and interpreted seismic sections, more detailed considerations reveal that they are complicated and composite structures. Although our understanding of faults and related structures has increased significantly over the last couple of decades, much research remains to be done before we reach the point where we can predict or model their geometries and properties based on input such as tectonic regime, lithology and burial depth. Some key points and review questions from this chapter are presented here:

- Faults consist of a central core, which is a high-strain zone dominated by fault rock and slip surface(s).
- The damage zone is a low-strain zone around the core formed during the formation and evolution of the fault.
- Both the damage zone and the fault core thickness tend to increase with increasing fault displacement, but the relationship is complicated and not related to gradual widening of the two during growth.
- Faults grow from small fractures to map-scale structures by accumulating displacement from successive earthquakes.
- Faults accumulate displacement as they grow in length and height.
- Ideally, fault displacement increases from the tip line toward the centre of the fault.
- During growth, faults tend to interact and link up.
- Fault linkage is a gradual process from underlapping via overlapping to hardlinking of fault segments.
- Fault relay structures are areas of complications and involve much small-scale deformation (damage zones).
- Drag can form by faulting of a fault-propagation fold.
- The geometry of drag folds can be used to determine the sense of displacement on a fault.

- Smearing of clay or shale along faults can cause the fault to be sealing.
- A sealing fault stops fluids from flowing from the hanging wall to the footwall or vice versa.

Review questions

1. What is the difference between shear fractures and faults?
2. Why do normal faults tend to be steeper than reverse faults?
3. What is the main differences between a mylonite and a cataclasite?
4. A vertical well is drilled through a stratigraphic section twice (repeated section). What type of fault can we infer, and why can we not explain this by folding?
5. Why would the damage zone grow during faulting?
6. Would the damage zone be visible on good 3-D seismic data?
7. How can dipmeter data help identifying faults?
8. Is fault sealing good or bad in terms of petroleum exploration and production?

E-MODULE

The e-learning module called *Faults* is recommended for this chapter.

FURTHER READING

Petroleum oriented

Aydin, A., 2000, Fractures, faults, and hydrocarbon entrapment, migration, and flow. *Marine and Petroleum Geology* **17**: 797–814.

Cerveny, K., Davies, R., Dudley, G., Kaufman, P., Knipe, R. J. and Krantz, B., 2004, Reducing uncertainty with fault-seal analysis. *Oilfield Review* **16**, 38–51.

Yielding, G., Walsh, J. and Watterson, J., 1992, The prediction of small-scale faulting in reservoirs. *First Break* **10**: 449–460.

Displacement and growth rates

Barnett, J. A. M., Mortimer, J., Rippon, J. H., Walsh, J. J. and Watterson, J., 1987, Displacement geometry in the volume containing a single normal fault. *American Association of Petroleum Geologists Bulletin* **71**: 925–937.

Ferill, D. A. and Morris, A. P., 2001, Displacement gradient and deformation in normal fault systems. *Journal of Structural Geology* **23**: 619–638.

Hull, J., 1988, Thickness–displacement relationships for deformation zones. *Journal of Structural Geology* **4**: 431–435.

Morewood, N. C. and Roberts, G. P., 2002, Surface observations of active normal fault propagation: implications for growth. *Journal of the Geological Society* **159**: 263–272.

Roberts, G. P. and Michetti, A. M., 2004, Spatial and temporal variations in growth rates along active normal fault systems: an example from The Lazio–Abruzzo Apennines, central Italy. *Journal of Structural Geology* **26**: 339–376.

Walsh, J. J. and Watterson, J., 1989, Displacement gradients on fault surfaces. *Journal of Structural Geology* **11**: 307–316.

Walsh, J. J. and Watterson, J., 1991, Geometric and kinematic coherence and scale effects in normal fault systems. In A. M. Roberts, G. Yielding and B. Freeman (Eds.), *The Geometry of Normal Faults*. Special Publication **56**, London: Geological Society, pp. 193–203.

Yielding, G., Walsh, J. and Watterson, J., 1992, The prediction of small-scale faulting in reservoirs. *First Break* **10**: 449–460.

Fault geometry and linkage

Benedicto, A., Schultz, R. A. and Soliva, R., 2003, Layer thickness and the shape of faults. *Geophysical Research Letters* **30**: 2076.

Caine, J. S., Evans, J. P. and Forster, C. B., 1996, Fault zone architecture and permeability structure. *Geology* **24**: 1025–1028.

Childs, C., Watterson, J. and Walsh, J. J., 1995, Fault overlap zones within developing normal fault systems. *Journal of the Geological Society* **152**: 535–549.

Childs, C., Manzocchi, T., Walsh, J. J., Bonson, C. G., Nicol, A. and Schöpfer, P. L., 2009, A geometric model of fault zone and fault rock thickness variations. *Journal of Structural Geology* **31**: 117–127.

Peacock, D. C. P. and Sanderson, D. J., 1994, Geometry and development of relay ramps in normal fault systems. *American Association of Petroleum Geologists Bulletin* **78**: 147–165.

Damage zones

Kim, Y.-S., Peacock, D. C. P. and Sanderson, D. J., 2004, Fault damage zones. *Journal of Structural Geology* **26**: 503–517.

Shipton, Z. K. and Cowie, P., 2003, A conceptual model for the origin of fault damage zone structures in high-porosity sandstone. *Journal of Structural Geology* **25**: 333–344.

Wibberley, C. A. J., Yielding, G. and Di Toro, G., 2008, Recent advances in the understanding of fault zone internal structure: a review. In C. A. J. Wibberley, W. Kurz, J. Imber, R. E. Holdsworth and C. Collettini (Eds.), *The Internal Structure of Fault Zones: Implications for Mechanical and Fluid-Flow Properties*. Special Publication **299**, London: Geological Society, pp. 5–33.

Fault sealing and smear

Færseth, R. B., Johnsen, E. and Sperrevik, S., 2007, Methodology for risking fault seal capacity: Implications of fault zone architecture. *American Association of Petroleum Geologists Bulletin* **91**: 1231–1246.

Hesthammer, J., Bjørkum, P. A. and Watts, L. I., 2002, The effect of temperature on sealing capacity of faults in sandstone reservoirs. *American Association of Petroleum Geologists Bulletin* **86**: 1733–1751.

Knipe, R. J., 1992, Faulting processes and fault seal. In R. M. Larsen, H. Brekke, B. T. Larsen and E.Talleraas (Eds.), *Structural and Tectonic Modelling and its Application to Petroleum Geology*. NPF Special Publication, Amsterdam: Elsevier, pp. 325–342.

Manzocchi, T., Walsh, J. J. and Yielding, G., 1999, Fault transmissibility multipliers for flow simulation models. *Petroleum Geoscience* **5**: 53–63.

Fault strain

King, G. and Cisternas, A., 1991, Do little things matter? *Nature*, **351**: 350.

Marrett, R. and Allmendinger, R. W., 1992, Amount of extension on "small" faults: an example from the Viking Graben. *Geology* **20**: 47–50.

Reches, Z., 1978, Analysis of faulting in three-dimensional strain field. *Tectonophysics* **47**: 109–129.

Dipmeter data, drag and fault-propagation folding

Bengtson, C. A., 1981, Statistical curvature analysis techniques for structural interpretation of dipmeter data. *American Association of Petroleum Geologists* **65**: 312–332.

Erslev, E. A., 1991, Trishear fault-propagation folding. *Geology* **19**: 617–620.

Fault rocks

Sibson, R., 1977, Fault rocks and fault mechanisms. *Journal of the Geological Society* **133**: 191–213.

Snoke, A. W., Tullis, J. and Todd, V. R., 1998, *Fault-related Rocks: A Photographic Atlas*. Princeton: Princeton University Press.

Terminology

Peacock, D. C. P., Knipe, R. J. and Sanderson, D. J., 2000, Glossary of normal faults. *Journal of Structural Geology* **22**: 291–305.

Chapter 9

Kinematics and paleostress in the brittle regime

In the previous chapters we have indicated that a close relationship exists between stress and faulting, for example according to Anderson's tectonic stress regimes. It should therefore be possible to say something about the stress field at the time of faulting and fracturing, based on the orientation and nature of the faults and fractures. This is referred to as paleostress analysis, a field that is hampered by several assumptions. However, many paleostress analyses yield reasonable results, as can be verified by independent information. The fundamental input to paleostress analysis is kinematic observations of fault structures made in the field. Relevant structures and the fundamentals of paleostress analysis in the brittle regime are briefly presented in this chapter.

9.1 Kinematic criteria

The true finite displacement vector on a fault surface can be found directly where a point in the hanging wall can be connected to an originally neighboring point in the footwall. Such points can be faulted fold hinges or other recognizable linear structures that intersect with the fault surface.

Unfortunately, such points are rarely found. In most cases we are pleased if we can correlate layers or seismic reflectors from one side to the other. If the fault surface is exposed in the field we would use the lineation on the fault surface to estimate the orientation and length of the displacement vector. The assumption is typically made that the lineation on the fault surface represents the displacement direction. It may, however, be that the lineation only reveals the last part of the deformation history, i.e. the last slip event(s), and that lineations related to earlier slip events have been obscured or obliterated. Careful searching for multiple, overprinting lineations is therefore called for when collecting fault slip data in the field.

A lineation on a slip surface may represent only the last of several slip events, and does not have to be parallel to the finite (total) displacement vector.

In other cases it is not possible to correlate stratigraphy or marker horizons from one side of the fault to the other. We then have no information about the size of the fault (the width of the damage zone and fault core may give us a hint), and we do not even know whether the fault movement was reverse or normal, sinistral or dextral. The lineation on the fault surface is useful, but we need to look for kinematic criteria in order to determine the sense of slip. Such criteria exist, although many of them tend to be ambiguous. Hence, as many kinematic criteria as possible must be combined for kinematic fault analysis.

Mineral growth and stylolites

Fault surfaces are never perfectly planar structures, and useful kinematic structures may form where geometric irregularities occur. Where an irregularity causes local contraction, such as the contractional bend in Figure 9.1, contractional structures such as stylolites (Figure 9.2). and "cleavage" may be found. Differently oriented irregularities, such as the left bend in Figure 9.1, may cause extension and opening of voids where mineral growth takes place. A study of the relation between fault surface geometry and the occurrence of contractional

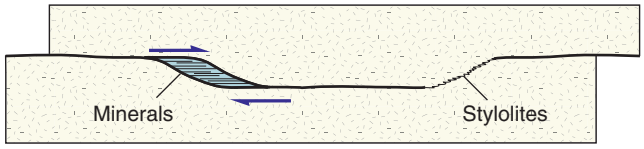

Figure 9.1 Irregularities along a fault create steps where mineral growth or shortening structures (stylolites) can form. The localization of such structures relative to the local fault geometry gives reliable information about the sense of slip.

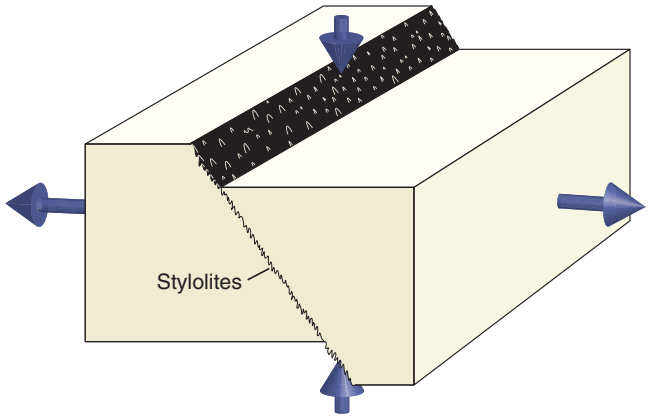

Figure 9.2 Faults with a component of shortening across the fault surface can result in pressure solution and stylolite formation in limestone and marble. Linear stylolitic structures sometimes form, called slickolites. Slickolites form a lineation that parallels the movement direction quite precisely.

versus extensional structures may reveal the sense of slip with a high degree of confidence.

Subsidiary fractures

Small fractures developed along a fault or slip surface may show geometric arrangements that carry information about the sense of slip on the fault. These small fractures have been given different names depending on their orientations and kinematics. Figure 9.3e shows these different categories of fractures in a section perpendicular to the main slip surface (M) and parallel to the slip direction. **T-fractures** are the name often used for small extension fractures in this setting. They may be open, but are more commonly mineralized with quartz or carbonates and do not show striations. The orientation of T-fractures with respect to the main or average slip surface or **M-surface** characterizes the sense of slip. T-fractures typically dip around 45° in the slip direction with respect to a horizontally oriented M-surface (Figure 9.3 a, c).

A set of shear fractures, known as **P-fractures**, is sometimes seen to dip in the opposite direction. With M still being horizontal, these make low angles to M and

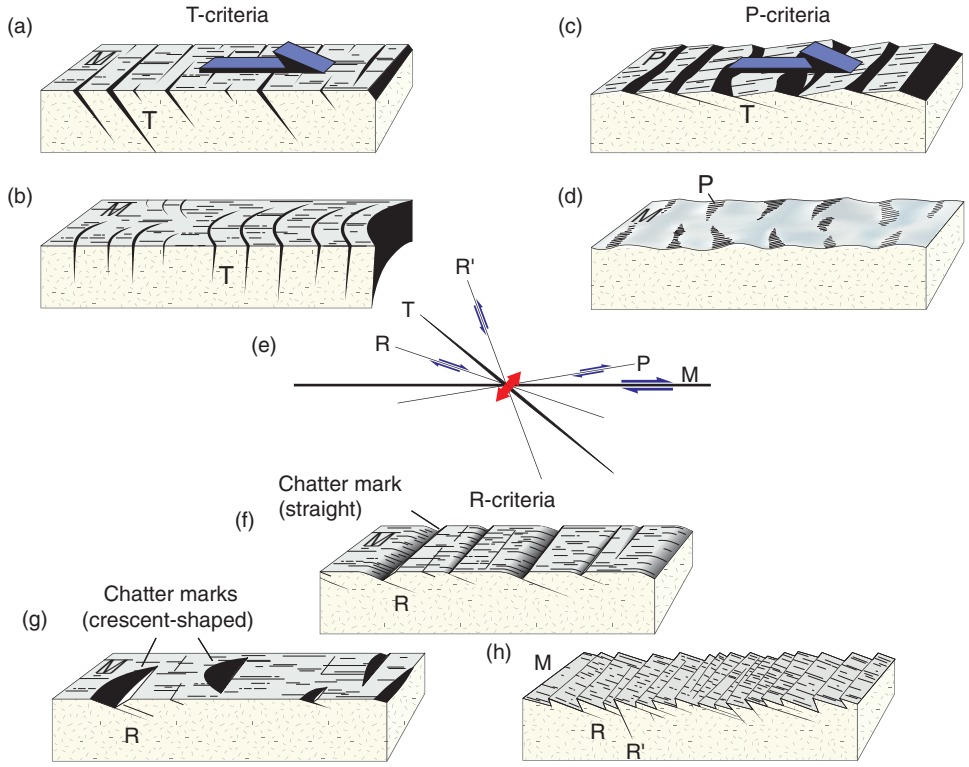

Figure 9.3 Kinematic criteria along a dextral fault with subordinate fractures or irregularities. The general nomenclature for fractures in a shear system is used (R, R′, P, T and M fractures). R, Riedel shears; P, shear fractures; T, extension fractures; M, average slip surface (fault). Identification of the type of subordinate fracture helps interpret the movement on the fault. Based on Petit (1987).

kinematically correspond to low-angle "reverse" or "thrust faults". In this setting Riedel shear fractures or **R-fractures** represent low-angle normal "faults" while **R′-fractures** correspond to antithetic reverse faults that make a high angle to M. Riedel fractures tend to be more common than R′ and P, but they all exist and their local kinematics as well as their orientation with respect to M reveal the sense of movement on the main structure. T-structures are perhaps the most reliable of these, because they are easy to distinguish from the various shear fractures.

The French geologist Jean-Pierre Petit separated the various structures that one may see along fault surfaces by T, P and R-criteria, where the letters T, P and R indicate the dominant subordinate fracture element of the structure. **T-criteria** comprise extension fractures (T) that intersect the striated fault slip surface (M). In cross-section T and M tend to form an acute angle of intersection pointing toward the slip direction, as shown in Figure 9.3a. The intersections may also occur as curved structures pointing toward the direction of slip (Figure 9.3b). Such structures resemble glacial chatter marks that form when flowing ice plucks pieces off fairly massive bedrock such as quartzite or granite.

P-criteria are dominated by P-fractures and may occur together with T-fractures (Figure 9.3c). P-surfaces may be polished and striated, and they are characterized by their low angle to M. Situations where undulations of the main slip surface create a systematic pattern with striations on the side facing the movement of the opposite wall (contractional side) and no striations on the lee (extensional) side (Figure 9.3d) can also be regarded as P-criteria.

R-criteria, which form the most commonly used type of kinematic criterion, are based on the acute angle between R and M (Figure 9.3f, g). The lines of intersection between R and M show a high (close to 90°) angle to the striae on M, and such straight (Figure 9.3f) or curved (Figure 9.3g) linear structures on the slip surface are commonly referred to as **chatter marks**. Faults with small offsets may not have developed a through-going slip or M-surface, in which case the fault may be defined by en-echelon arranged R-fractures (Figure 9.3h), and sometimes also R′-fractures. The R-fractures are then closely arranged and striations are not well developed.

Ploughing, mineral growth and slickensides

Asperities or relatively hard objects (rock fragments, pebbles or strong mineral grains) on one side of a fault surface may mechanically plough grooves or **striations**

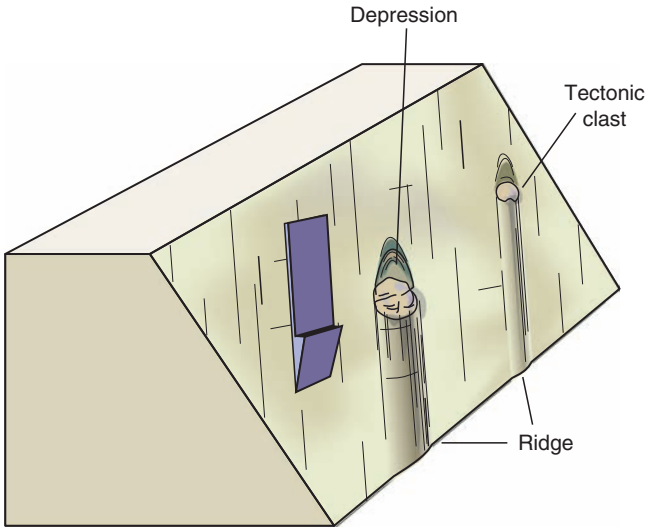

Figure 9.4 Pointed asperities or tectonic clasts sitting on fault surfaces may form depressions on the lee side and ridges on the opposite side. Such lineations are ridge-in-groove lineations.

into the opposing wall. Material in front of the object is being pushed aside, while a crescent-shaped opening occurs on the lee side, typically filled with material from the opposite wall. A ridge (or groove, depending on the point of view) is sometimes found ahead of the object, as illustrated in Figure 9.4, and such lineations are sometimes referred to as **ridge-in-groove lineations**.

The crescent-shaped opening soon evolves into a groove whose length ideally corresponds to the movement of the hard object relative to the rest of the wall. At least that's what we would like to think. But there are many examples of centimeter-scale offsets causing decimeter- or even meter-long striations. Hence, there must be other mechanisms at work than just physical carving. One explanation is that some striations are **corrugations** that did not form purely as frictional grooves. These are linear structures that formed at the initial stage of fracture growth and may be polished and striated as slip accumulates. The result may be long and well-developed striae on slip surfaces that have very small (cm- or even mm-scale) offsets. Hence, small-scale fault corrugation structures do *not* necessarily reflect the amount of slip on the surface. Striations are typically found on (but not restricted to) polished slip surfaces called **slickensides**, where the striations are known as **slickenlines**.

In addition to frictional striations, minerals may crystallize on the lee side of asperities (irregularities), thus revealing the sense of slip. When minerals crystallize as fibers, the orientation of the fibers tends to be close to the slip direction. It is commonly found that minerals precipitated on fault slip surfaces are subsequently affected by renewed slip. It is therefore common to see slickenlines developed on deformed mineral fill along fault surfaces. Lineations related to fractures are further discussed in Chapter 13.

9.2 Stress from faults

Fault observations used in paleostress analysis include the local strike and dip of the fault surface, the orientation of the lineation (usually given by its rake or pitch) and the sense of movement. When such data are collected for a fault population it is in principle possible to obtain information not only about strain but also about the orientation of the principal stresses (σ_1, σ_2 and σ_3) and their relative magnitudes (i.e. the shape of the stress ellipsoid). Paleostress methods hinge on several assumptions. The most basic is that the faults under consideration formed in the same stress field. Others are that the rocks are fairly homogeneous, that the strain is relatively low and that the structures have not rotated significantly since they initiated.

Groups of small faults from a limited area (an outcrop or a quarry) can be analyzed to reconstruct the local paleostress field.

Conjugate sets of faults

A simple case of deformation is **plane strain** expressed in terms of conjugate fault systems. As shown in Figure 9.5 for the three main tectonic regimes, a conjugate system has two sets of oppositely dipping faults where the lineations are perpendicular to the line of fault intersection. The sense of slip is complementary on the two sets, and the angle between the two sets should be constant. According to the Coulomb fracture criterion, which tells us that faults or shear fractures form at an angle to σ_1 that is controlled by the internal friction of the rock, the angle between the two sets should be consistent with the mechanical properties of the rock (and the pore fluid pressure) at the time of deformation. More importantly, conjugate sets should develop symmetrically about the principal stresses for both normal, reverse and strike-slip faults (Figure 9.5). According to the Andersonian theory of faulting (Section 5.6), the slip direction or lineation would be in the dip direction (reverse and normal faults) or in the strike direction (strike-slip faults). Hence,

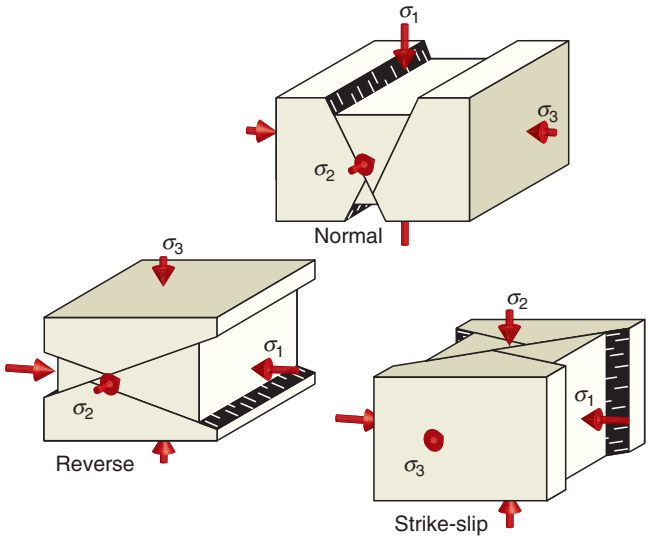

Figure 9.5 Conjugate shear fractures and their relation to stress according to Anderson's conditions for planar strain. The acute angle is bisected by σ_1 and the two fractures intersect along σ_2.

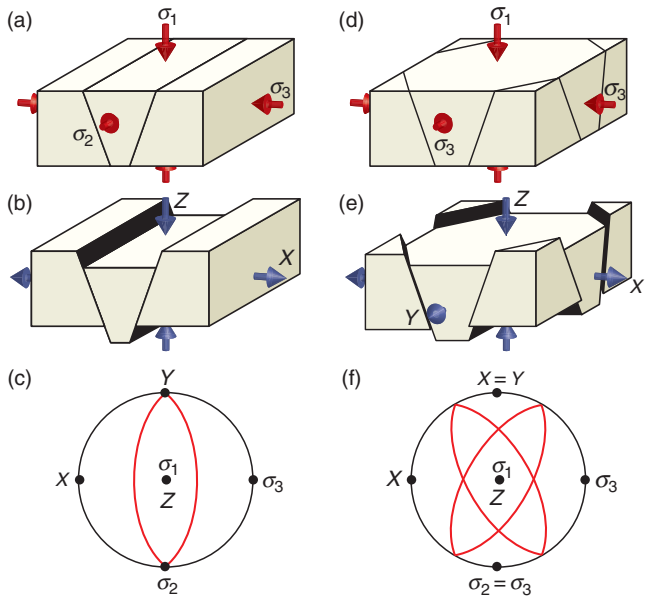

Figure 9.6 A single pair of dip-slip conjugate fault sets (a–c) form in plane strain, while multiple sets imply 3-D strain (d–f). The pattern shown in (e) is called orthorhombic from its high degree of symmetry. In these idealized cases the principal stresses (red arrows) and strains are parallel.

conjugate faults and their striations reveal the orientations of the principal stresses.

The maximum principal stress axis bisects the acute angle of conjugate faults.

In some cases we may find that the principal stresses deviate somewhat from the horizontal/vertical directions predicted by Anderson, which may indicate that the area has been tilted since the time of deformation or that the stress field was rotated or refracted through this volume of rock. As mentioned in Chapter 6, such deviations can occur near large and weak faults or joint zones.

Two conjugate sets of faults indicate plane strain (Figure 9.6a, b), and the strain axes are found by plotting the fault sets in a stereonet (Figure 9.6c). The orientation of the principal stress axes can be inferred based on the assumption of isotropic rheology, constantly oriented stress field and negligible rotation of the fault blocks. In fact, we can draw a parallel between conjugate sets observed in rock mechanics experiments and their angular relation to the principal stresses.

In other cases fault systems may contain more than two conjugate sets. A simple case is shown in Figure 9.6d, e, where two genetically related pairs of fractures coexist. This arrangement is referred to as **orthorhombic** based on its symmetry elements. Again, the strain axes are easily found from stereoplots, and the stress axes can be inferred (Figure 9.6f).

Complex fault populations

Conjugate fault sets are found in rocks that have experienced a single phase of brittle deformation. In many cases, fracture patterns show evidence of repeated activation under changing stress conditions and commonly more complicated arrangements than a simple conjugate pattern. If we have a fracture or fault population that is complex in the sense that it contains elements with a wide range of orientations, how would this fracture population respond to a new stress field?

Clearly some faults will slip while others will not. We looked at a similar example in Figure 7.22, where a weak foliation was reactivated for a certain range of orientations. Now we are looking at a population of weak elements, and we also want to know the direction and sense of slip. Prediction is not trivial, but there are some important statements that can be made.

The most obvious assumption that can be made is that faults or fractures oriented perpendicular to one of the three principal stresses will not slip. This is obvious since there is no shear component in this situation ($\sigma_s = 0$). For any other orientation $\sigma_s \neq 0$ and frictional sliding (slip) will occur if σ_s exceeds the frictional resistance against slip.

It also seems reasonable to make the assumption that slip on a surface will occur in the direction of maximum

resolved shear stress. If the largest shear stress is in the dip direction we will get normal or reverse faults. If the maximum shear stress vector is horizontal, strike-slip faulting results. Any other case results in oblique-slip movements. This assumption is known as the **Wallace–Bott hypothesis**:

Slip on a planar fracture can be assumed to occur parallel to the greatest resolved shear stress.

The hypothesis implies that the faults are planar, fault blocks are rigid, block rotations are negligible, and the faults were activated during a single phase of deformation under a uniform stress field. Clearly, these are idealized conditions. For example, intersecting faults have the potential to locally perturb the stress field. On the other hand, empirical observations and numerical modeling suggest that the deviations are relatively small in most cases, suggesting that the Wallace–Bott hypothesis is a reasonable one. Building on these simple assumptions we can measure a fault population with respect to fault orientation, lineation orientation and sense of slip, and use these data to calculate the orientation and relative size of the stress axes. The methods used for this purpose are known as **stress inversion** or **fault slip inversion techniques**.

Paleostress from fault slip inversion

While the absolute values of the principal stresses are unachievable in most cases, their relative magnitude, i.e. the shape of the stress ellipsoid, can be estimated from fault population data. For this purpose we use the stress ratio

$$\phi = (\sigma_2 - \sigma_3)/(\sigma_1 - \sigma_3) \tag{9.1}$$

where $0 \leq \phi \leq 1$. The ratio ϕ is also called R (note that R is defined as $1 - \phi$ by some authors). $\phi = 0$ for a prolate stress ellipsoid, where $\sigma_2 = \sigma_3$ (uniaxial compression). $\phi = 1$ implies that $\sigma_1 = \sigma_2$, and the stress ellipsoid is oblate (uniaxial tension). We use the ratio ϕ to express the stress tensor, which in the coordinate system defined by the principal stresses is

$$\begin{bmatrix} \sigma_1 & 0 & 0 \\ 0 & \sigma_2 & 0 \\ 0 & 0 & \sigma_3 \end{bmatrix} \tag{9.2}$$

An isotropic stress component can be added to the stress tensor, and the components can be multiplied by a constant without changing the orientation and shape of the stress ellipsoid. The stress tensor that contains information about the shape and orientation of the stress ellipsoid, but not the absolute magnitude of the principal stresses, is known as the **reduced stress tensor**. This tensor is here expressed in terms of two constants k and l, where: $k = l/(\sigma_1 - \sigma_3)$ and $l = -\sigma_3$

$$\begin{bmatrix} \sigma_1 + l & 0 & 0 \\ 0 & \sigma_2 + l & 0 \\ 0 & 0 & \sigma_3 + l \end{bmatrix} \begin{bmatrix} k & 0 & 0 \\ 0 & k & 0 \\ 0 & 0 & k \end{bmatrix} = \begin{bmatrix} 1 & 0 & 0 \\ 0 & \phi & 0 \\ 0 & 0 & 0 \end{bmatrix} \tag{9.3}$$

Adding the constant l to each principal stress is the same as adding an isotropic stress. Furthermore, multiplying the axes by the constant k means contracting or inflating the stress ellipsoid while maintaining its shape.

While the full stress tensor contains six unknowns, the reduced tensor contains only four unknowns, represented by ϕ and the orientation of the principal stresses. In other words, the reduced stress tensor gives us the orientation and shape of the stress ellipsoid. While we have discussed how stress influences slip on fractures (by causing slip in the direction of the maximum resolved shear stress), the inverse problem where the (reduced) stress tensor is calculated from slip data is more relevant to paleostress analysis.

By inversion of fault slip data we mean reconstructing the orientation and shape of the stress ellipsoid based on measured fault slip data.

Because the reduced stress tensor has four unknowns we need data from at least four different fault surfaces to find the tensor. The tensor that fits all the data is the tensor we are looking for. However, because of measuring errors, local stress deflections, rotations etc., we are searching for the tensor that best fits the fault slip data. We therefore collect data from more than four slip surfaces, usually 10–20 or more. This gives many more equations than unknowns, and a statistical model is applied that minimizes the errors.

The calculations are done by a stress inversion program, of which several are available. The results are presented in stereoplots that show the orientations of the principal stress axes, and in dimensionless Mohr diagrams that reflect the relative sizes of the principal stresses (Figure 9.7). During the calculation of the reduced stress tensor there may be remaining data that do not fit in. These may be treated separately to see if they together

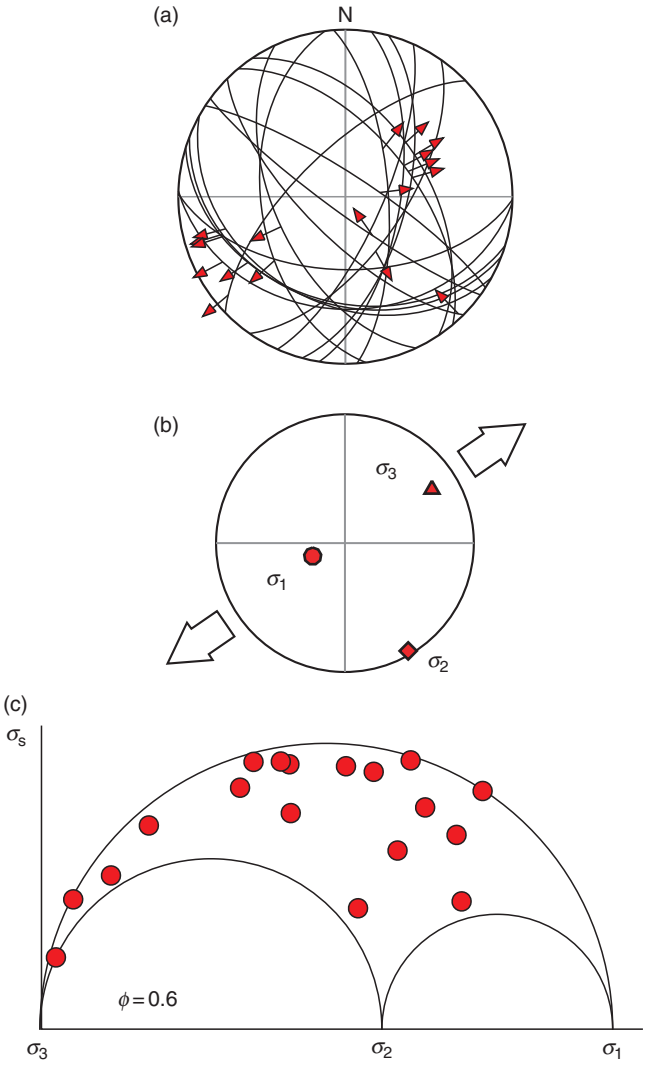

Figure 9.7 (a) Actual fault data, shown by great circles (fault surfaces) and arrows (lineations) on an equal-area lower-hemisphere plot. (b) Principal stresses found from stress inversion. (c) The data plotted in the dimensionless Mohr diagram, indicating the relative values of the principal stresses.

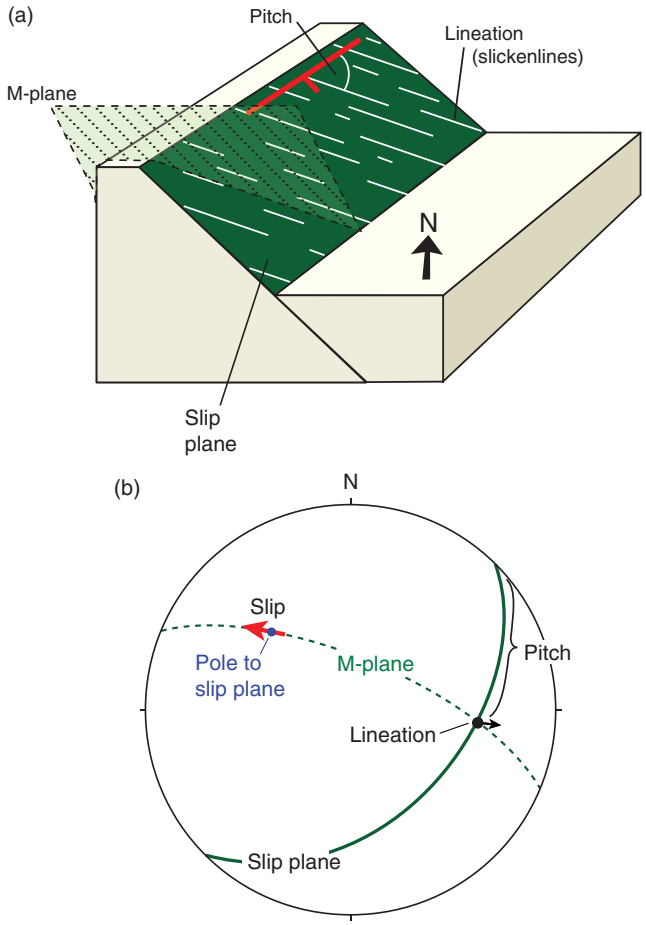

Figure 9.8 (a) Schematic illustration of pitch as measured on a fault surface. (b) The pitch plotted in a stereonet (lower hemisphere, equal area). This projection also shows how the tangent-lineation is found for a known slip plane (as shown in (a)) and its lineation (striation) by plotting a plane (the movement or M-plane) that contains the lineation and the pole to the slip plane. The tangent-lineation (red arrow) is the arrow drawn tangential to the M-plane at the pole to the slip plane. Its direction describes the movement of the footwall relative to the hanging wall; in the present case a normal movement, where the footwall moves up to the west.

define a second tensor that may relate to a separate tectonic event. A different and usually safer way to distinguish between subpopulations is to use field criteria such as cross-cutting relations and characteristic mineral phases on slip surfaces.

A geometric way of extracting stress from fault slip data is to construct **tangent-lineation diagrams**. As shown in Figure 9.8, this is done by plotting each fault plane and its lineation, the M-plane, which contains the pole to the fault plane and the lineation, and by drawing an arrow tangent to the M-plane at this pole. The direction of the arrow reflects the movement of the footwall relative to the hanging wall. When differently oriented slip surfaces are plotted, such as the example presented in Figure 9.9, the resulting pattern may reveal both the orientations and the relative magnitudes (ϕ) of the principal stress axes (Figure 9.10). Software, such as FaultKin, can be used to plot the data collected in the field, but it is important that we understand what such programs do with our data.

Clearly, many data points from faults with a variety of orientations are required to obtain a good result. An example is shown in Figure 9.9, and it is clear from this plot that the distribution of data is not consistent enough to constrain the relative stress magnitudes – a relatively

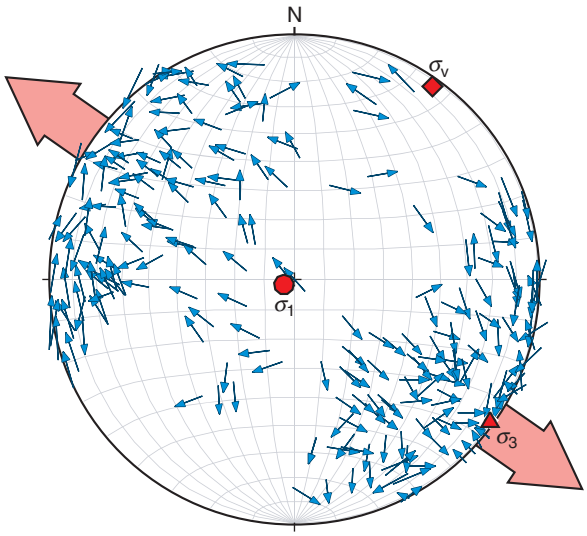

Figure 9.9 Tangent-lineation diagram for fault data from basement gneisses west of Bergen, Norway. σ_1 can be defined, but the ϕ-value, which in principle is found by comparing with the next figure, is more difficult to define in this case. This is quite common and is partly due to limited variation in fault orientations.

common situation when working with real data sets, especially data sets from polyphasally deformed rocks.

Paleostress analyses need to be treated with care for several reasons. One is the fact that they heavily depend on our ability to identify fault populations formed under a stress field that was constant during the history of faulting. Another is that the stress field needs to be uniform within the locality under investigation. We know that fault interaction, as well as any mechanical layering, tends to perturb the stress field, so this assumption is likely to be an approximation only. Outputs from paleostress analyses have to be interpreted in the light of these facts and additional locality-specific circumstances.

9.3 A kinematic approach to fault slip data

The paleostress method based on inversion of fault slip data relates stress and slip through the Wallace–Bott hypothesis and relies on assumptions that clearly oversimplify the actual situation in the crust. For this reason, some of us prefer a purely kinematic approach where strain or strain rate rather than stress are treated.

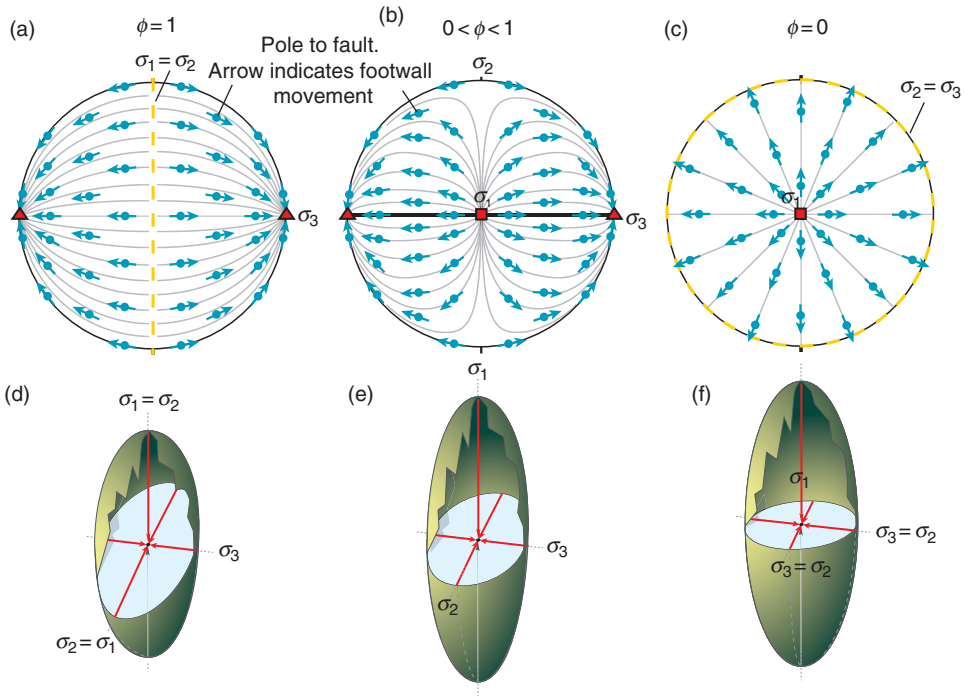

Figure 9.10 (a–c) Stereographic projection of poles to faults (points). Arrows indicate footwall versus hanging wall movements. The pattern emerges by considering faults with different orientations, and the assumption is made that the movement is parallel to the direction of maximum shear stress on each surface. The pattern depends on the ratio between the principal stresses, expressed by ϕ. By plotting field data in these diagrams one can obtain an estimate for the orientation of the principal stresses and ϕ. The geometry of the strain ellipsoid is shown (d–f). Based on Twiss and Moores (2007).

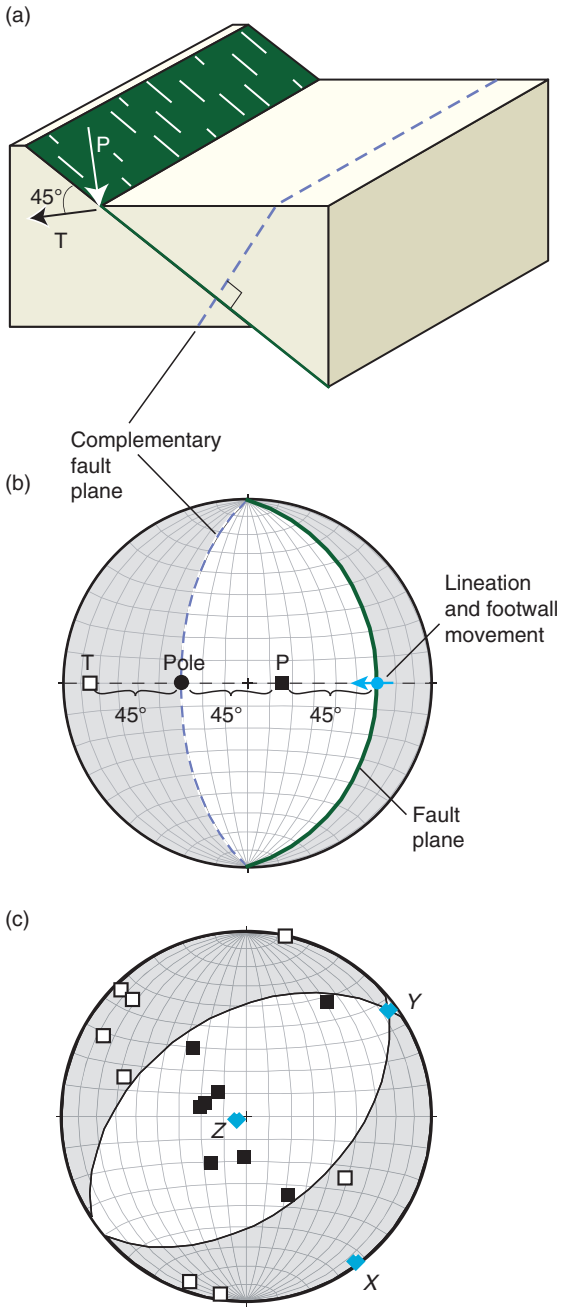

Figure 9.11 Kinematic analysis of fault data. (a) A simple normal fault. (b) Plot of the fault, the lineation and the sense of movement. The complementary shear plane oriented 90° to the fault is shown. The T- and P-axes bisect these two planes. (c) Data from 16 faults with different orientations. Each of the faults is plotted as illustrated in (b). Ideally, the P- and T-axes will plot within two sectors separated by two mutually orthogonal planes. If they do not, then the conditions are not fulfilled; they may for example have formed in two different stress fields. The few data are a minimum, but indicate a NW–SE stretching and vertical shortening, i.e. an extensional regime.

Graphically the kinematic method consists of plotting the fault planes and corresponding slip-related lineations in a stereoplot, as shown in Figure 9.11. Based on the orientation and sense of slip, P- and T-axes are found for each fault plane, somewhat similar to focal mechanism solutions treated in Box 9.1. These axes are symmetry axes of the contractional and extensional quadrants. They are perpendicular to each other and are contained in the plane that is perpendicular to the fault plane. The fault plane also contains the lineation (slip direction). Furthermore, P and T make 45° to the fault plane (Figure 9.11). The position of T and P depends on the sense of fault movement (normal, reverse, sinistral or dextral).

A pair of P- and T-axes is found for each fault in the population. For fault populations with a distribution in fault orientations we end up with a distribution of P- and T-axes. Ideally, they can be separated by two orthogonal surfaces, which are fitted to the plot. *Y* (the intermediate strain axis) is represented by the line of intersection between the planes, while *Z* and *X* are located in the middle of the P- and T-fields, respectively (Figure 9.11c). This gives the orientation of the paleostrain axes – the magnitude can only be approached by adding information about displacement and area of each fault included in the analysis. The kinematic method is quickly done by means of a computer program, and in most cases it can be shown that the strain axes found by this method are very similar to the stress axes found by inversion of slip data as described in the previous section. The kinematic method also relies on a uniform strain field and on a correct grouping of slip information generated during different phases of deformation.

9.4 Contractional and extensional structures

While analyses of fault slip data are concerned with shear fractures and faults, contractional and extensional structures are also useful for stress or strain rate considerations. Contractional structures, also known as anticracks, are found as solution seams or stylolites in some (mostly) brittlely deformed rocks. In general, such structures represent small strains with little or no rotation. A close connection between stress and strain axes can therefore be assumed. The same is the case with low-strain extension structures such as veins and joints.

BOX 9.1 FOCAL MECHANISMS AND STRESS

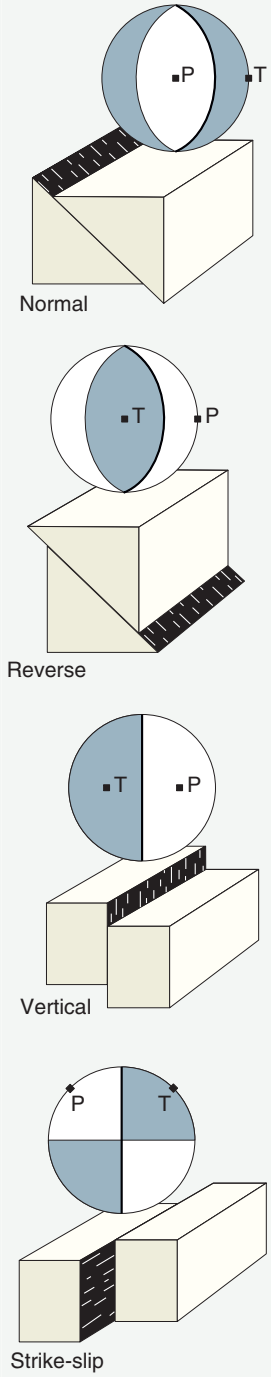

A so-called **fault-plane solution** is found by mapping the distribution of P- or S-waves around the hypocenter of an earthquake. The actual fault plane and its complementary, orthogonal theoretical shear plane (together called nodal planes) are plotted as stereographic projections based on the principle that the sense of slip (normal, reverse etc.) on a fault controls the distribution of seismic waves. The nodal planes are found by using observations of the first P-wave movement at various seismic stations and deciding whether they are compressive or tensile. The planes are plotted as stereographic projections, and the result is the well-known "beach-ball"-style projections shown to the left. Information about the first arrival (compressive P or tensile T) from several seismologic observatories is used to constrain the orientations of the nodal planes and their senses of movement, known as the focal mechanism. The quadrants are separated by the fault plane and the complementary nodal plane, and the P- and T-axes are plotted in the middle of the quadrants. As shown to the left, different "beach balls" indicate different **focal mechanisms** or sense of fault movement.

Which of the two nodal planes actually represents the fault plane is unknown from seismic data alone, unless aftershock analysis is involved. Only the P- and T-axes are known. P and T are *not* identical to σ_1 and σ_3, although this assumption was commonly made previously. With a crust full of weak structures, many quakes must be expected to result from reactivation of preexisting fractures. There is therefore no precise relationship between fault orientation and the stress field. However, we know that σ_1 must lie in the P-field, and σ_3 in the T-field. Thus, observations from multiple earthquakes on variously oriented faults give a distribution of data that increases our chances of a good estimate of the stress axes. In principle we can use stress inversion to estimate the principal stresses from such data.

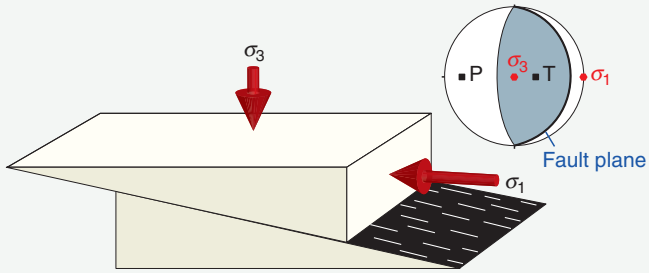

Example where the principal stresses and the P- and T-axes are not identical. A low-angle thrust fault is activated with a vertical σ_3 and a horizontal σ_1. Since P and T always bisect the nodal planes the principal stresses and the P- and T-axes will only coincide if the fault is oriented at 45° to σ_1.

Paleostress indicators must record small strains that do not involve much rotation to ensure that strain and stress axes can be correlated.

While contractional structures tend to form perpendicular to σ_1, extensional fractures form perpendicular or at least at a high angle to σ_3. This makes joints and veins the structures that give the quickest and simplest connection

between stress and strain. The combination of contraction and extension structures is particularly valuable, and when they occur in faulted rocks these structures can be used in or compared to the results of stress-inversion methods.

Non-rotated joints, veins and dikes are structures that immediately define the orientation of σ_3 at the time of initiation.

A related kinematic method involves the reconstruction of walls displaced during dike intrusion. Magma overpressure during intrusion may cause fracturing of the surrounding rock, into which magma flows to form dikes. In the presence of a significant tectonic stress, the fractures and thus the dikes are oriented perpendicular to σ_3. In most cases, however, the rock contains preexisting fractures that will be filled with magma.

Fractures with an orientation perpendicular to σ_3 will preferentially open perpendicular to the walls, but if we

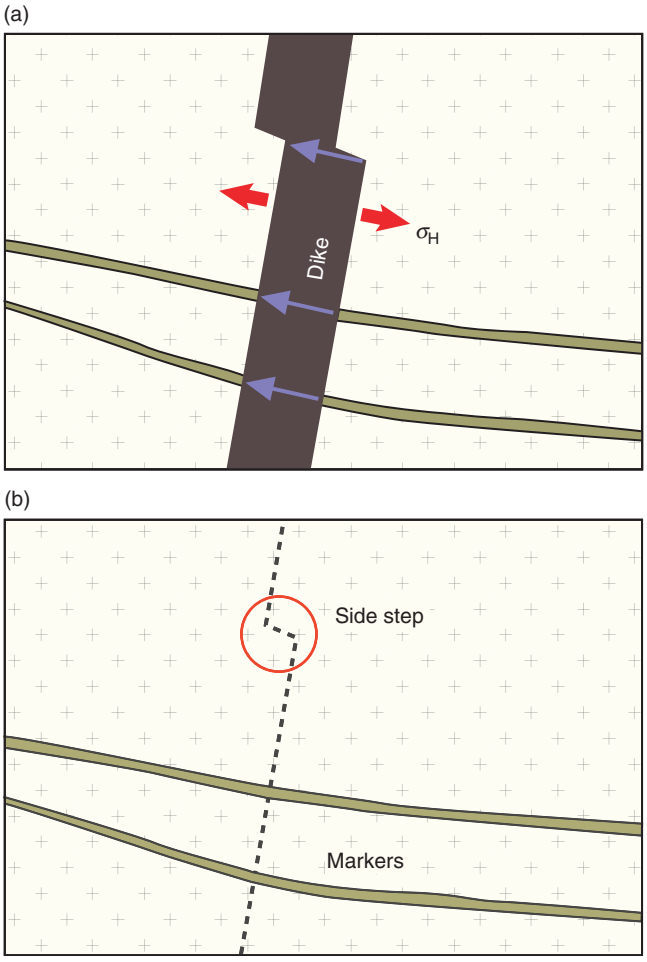

Figure 9.12 Reconstruction of a horizontal section (a) to the situation prior to dike intrusion (b). Arrows can be drawn between points that once were neighbors to find displacement vectors. For small strains these vectors approximate σ_H. From Fossen (1998).

Figure 9.13 Left-stepping dike intrusion, well suited for stress determination. The corners were connected prior to the intrusion, and the extension direction, which can be assumed to be close to the minimum principal stress, is found by connecting the corners. Permian dike along the shoulder of the North Sea rift system.

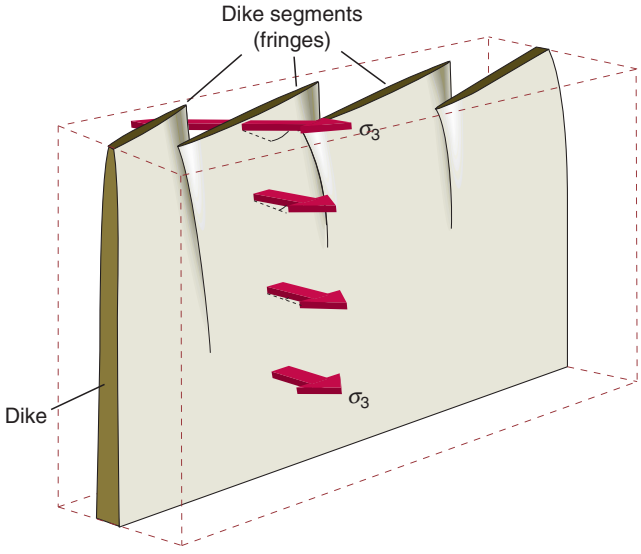

Figure 9.14 En-echelon dike system that is connected at depth – one of Anderson's popular interpretations published in 1951. Anderson interpreted this phenomenon as the result of an upward rotation of σ_3 towards the surface during magma intrusion.

want to find the orientation of σ_3 we have to look for points on each side of the dike that once were adjacent to each other. Such points can be corners where dikes step sideways (Figure 9.12), in which case displacement vectors can be constructed by connecting separated corners, as shown in Figure 9.13. Structures that were separated by dikes can also be used, such as veins, older dikes, fold hinges and steeply dipping layers. In these cases we observe strain (the local extension direction), but because of the small displacements usually involved it is reasonable to correlate the horizontal extension direction with σ_H. Assuming that the vertical stress is a principal stress axis we can further assume that $\sigma_H = \sigma_3$. It is the local stress that is found, and it is not uncommon to find that dikes rotate in the vertical direction into a fringe-like geometry such as shown in Figure 9.14. Such geometries indicate that the σ_H changes direction in the vertical direction, similar to fringe zones around fractures (Figure 7.26).

Summary

We have looked briefly at ways to determine sense of slip on faults and to use this and other brittle structures to get information about paleostress. In all cases, we should be aware of the fact that stress can only be deduced from strain patterns and never observed directly. Some assumption must always be made to go from strain to stress. It is therefore wise to take precautions when extracting paleostress information from deformed rocks.

Paleostress and the paleostress method are not treated in much detail in this chapter, so the interested reader is encouraged to explore the literature listed after these key points and review questions:

- Several kinematic criteria can help determine the sense of displacement on a slip surface. We should be able to make a sketch of the most important ones.
- Joints and veins are extension structures that initiate perpendicular to the smallest stress axis, and are therefore useful paleostress indicators.
- Conjugate faults are another useful set of structures that allows for a quick estimate of the stress field.
- Inversion of slip data gives the orientation of the principal stresses and the shape of the stress ellipsoid.
- Complex fault slip datasets may contain slip surfaces formed under two or more stress fields that must be separated to obtain useful results.

Review questions

1. Why must we be careful when interpreting lineations as displacement indicators?
2. What are the premises for successful paleostress analysis?
3. What is meant by the expression "slip inversion"?
4. What are conjugate faults, and what stress information do they give?
5. What does the Wallace–Bott hypothesis postulate?
6. What is the reduced stress tensor?

E-MODULE

The section called *Brittle structures* in the *Kinematic indicators* e-learning module is recommended for this chapter.

FURTHER READING

General

Anderson, E. M., 1951, *The Dynamics of Faulting*. Edinburgh: Oliver & Boyd.

Sense of slip

Petit, J.-P., 1987, Criteria for the sense of movement on fault surfaces in brittle rocks. *Journal of Structural Geology* **9**: 597–608.

Stress and strain from fault populations

Angelier, J., 1994, Fault slip analysis and palaeostress reconstruction. In P. L. Hancock (Ed.), *Continental Deformation*. Oxford: Pergamon Press, pp. 53–100.

Cashman, P. H. and Ellis, M. A., 1994, Fault interaction may generate multiple slip vectors on a single fault surface. *Geology* **22**: 1123–1126.

Etchecopar, A., Vasseur, G. and Daignieres, M., 1981, An inverse problem in microtectonics for the determination of stress tensors from fault striation analysis. *Journal of Structural Geology* **3**: 51–65.

Lisle, R. J., Orfie, T. O., Arlegui, L., Liesa, C. and Srivastava, D. C., 2006, Favoured states of palaeostress in the Earth's crust: evidence from fault-slip data. *Journal of Structural Geology* **28**: 1051–1066.

Marrett, R. and Allmendinger, R. W., 1990. Kinematic analysis of fault-slip data. *Journal of Structural Geology* **12**: 973–986.

Stress from extension and contraction structures

Dunne, W. M. and Hancock, P. L., 1994, Paleostress analysis of small-scale brittle structures. In P. L. Hancock (Ed.), *Continental Deformation*. Oxford: Pergamon Press, pp. 101–120.

Fry, N., 2001, Stress space: striated faults, deformation twins, and their constraints on paleostress. *Journal of Structural Geology* **23**: 1–9.

Jolly, R. J. H. and Sanderson, D. J., 1995, Variation in the form and distribution of dykes in the Mull swarm, Scotland. *Journal of Structural Geology* **17**: 1543–1557.

The relationship between stress and strain

Marrett, R. and Peacock, D. C. P., 1999, Strain and stress. *Journal of Structural Geology* **21**: 1057–1063.

Twiss, R. J. and Unruh, J. R., 1998, Analysis of fault slip inversions: do they constrain stress or strain rate? *Journal of Geophysical Research* **103** (B6): 12,205–12,222.

Watterson, J., 1999, The future of failure: stress or strain? *Journal of Structural Geology* **21**: 939–948.

Chapter 10

Deformation at the microscale

In most of this book we study structures observable in thin sections, outcrops, maps and satellite photos. However, it is very useful and interesting to also take a closer look at the processes and mechanisms that take place from the grain scale down to that of atoms. This is a range that is more difficult to approach, especially the atomic scale, but a basic understanding is important and forms a foundation for a good understanding of mesoscale structures. The most important distinction is between brittle and plastic deformation mechanisms. Brittle deformation is sudden and violent: atomic lattices are forcefully torn apart and the lattice structure is forever damaged and weakened. Mechanisms in the plastic regime are more complicated and sluggish. Several factors influence the atomic-scale response of a crystal to stress, but temperature is the single most important factor: high temperature promotes plastic deformation mechanisms and microstructures. In this chapter we will briefly review brittle deformation mechanisms before focusing on the fundamentals of microscale plastic deformation of rocks and crystals.

10.1 Deformation mechanisms and microstructures

When strain accumulates in a deforming rock, certain **deformation processes** occur at the microscale that allow the rock to change its internal structure, shape or volume. The processes involved may vary – we have already looked at brittle processes in Chapter 7, and in the plastic regime there are other and different processes (Table 10.1). If these microscale processes lead to a change in shape or volume of a rock we call them **deformation mechanisms**:

Strain is accommodated through the activation of one or more microscale deformation mechanisms.

Most of the structures that reveal the type of mechanism at work are microscopic, and we therefore call them **microstructures**. They range in size from the atomic scale to the scale of grain aggregates. **Intracrystalline** deformation occurs within individual mineral grains. The smallest deformation structures of this kind actually occur on the atomic scale and can only be studied with the aid of the electron microscope. Larger-scale intracrystalline microstructures can be studied under the optical microscope, and encompass features such as grain fracturing, deformation twinning and (plastic) deformation bands.

When deformation mechanisms produce microstructures that affect more than one grain, such as grain boundary sliding or fracturing of mineral aggregates, we have **intercrystalline** deformation. Intercrystalline deformation is particularly common during brittle deformation.

The two expressions deformation mechanisms and deformation processes are closely related and are often used interchangeably. However, it is sometimes useful to distinguish between the two. Some define deformation mechanisms as processes that lead to strain. There are other microscopic changes that can occur that do not lead to strain, even though they may still be related to deformation. These are still deformation processes, and include rotation recrystallization, grain boundary migration (explained later in this chapter) and, in some cases, rigid rotation. Furthermore, two or more processes can combine to form a (composite) deformation mechanism. Note that the term deformation process is also used in a more general sense in other fields of structural geology.

Table 10.1 An overview of deformation processes in the brittle and plastic regimes.

BRITTLE DEFORMATION	Fracturing	
	Frictional sliding	
BRITTLE FLOW	Granular flow	Frictional sliding Rolling
	Cataclastic flow	Grain fracturing
PLASTIC FLOW	Diffusion	Wet diffusion Grain-boundary diffusion Volume diffusion
	Crystal plasticity	Twinning Dislocation creep

10.2 Brittle versus plastic deformation mechanisms

Brittle mechanisms dominate the upper crust while plastic mechanisms are increasingly common as pressure and, particularly, temperature increase with depth. However, brittle mechanisms can occur in deep parts of the lithosphere, and plastic mechanisms do occur at or near the surface in some cases. The reason is that not only temperature and pressure control deformation mechanisms, but also the rheology of the deforming mineral(s), availability of fluids and strain rate. While brittle deformation mechanisms can completely dominate deformation of a granitic rock in the upper crust, the transition from completely brittle to perfectly crystal-plastic deformation is gradual. There is a wide range in physical conditions or crustal depths where brittle and plastic mechanisms coexist. For a granitic rock, for example, quartz and feldspar respond differently to stress, particularly for the 300–500 °C window. Because most rocks consist of more than one mineral, and different minerals have different brittle–plastic transition windows, the brittle–plastic transition may be a kilometer-thick transition zone even for a single rock type. We therefore find that brittle and plastic deformation mechanisms commonly coexist in the same sample even when deformed at a constant depth during a single phase of deformation.

The controlling deformation mechanism determines whether the deformation belongs to the brittle or plastic regime.

Brittle deformation in an overall plastic setting is mostly restricted to intergranular fracturing. This is again

related to the different ways different minerals respond to stress. Fracturing of a stiff mineral, such as garnet or feldspar, in a matrix of quartz is a typical example. The fractures are restricted to the garnet or feldspar grains, while plastic deformation mechanisms make quartz flow plastically.

10.3 Brittle deformation mechanisms

The characteristic feature of brittle deformation is fracturing and frictional sliding. As pointed out in Section 7.1, a distinction is drawn between **intergranular fracturing**, **intragranular fracturing**, **frictional sliding** on fractures and grain boundaries, and **grain rotation**. The combination of these deformation mechanisms is called **cataclastic flow**. Note that intragranular and intracrystalline are equivalent expressions, except that intragranular is used for granular media such as sand and sandstone, while intracrystalline is used about crystalline rocks where the porosity is (almost) zero.

The deformation mechanisms at very shallow depths are different for porous sediments and (almost) nonporous, crystalline rocks. Deformation of an unconsolidated sand or weakly consolidated sandstone buried at less than ~1 km depth is governed by two mechanisms: **grain rolling** (grain rotation) and **frictional grain boundary sliding**. The process involving these mechanisms is referred to by either of the equivalent terms **particulate flow** and **granular flow**. This is intergranular deformation in the sense that there is no permanent internal deformation of the grains.

Granular flow characterizes the deformation of highly porous sediments deforming in a shearing mode or in response to vertical loading (compaction). This is explored in a field of research known as **soil mechanics**, relevant to slope stability issues and other soil-oriented engineering problems. If the stresses across grain contacts become high enough, grains in a highly porous sediment or sedimentary rock will fracture. The fractures are confined to individual grains and are therefore intragranular microfractures. Under certain circumstances (low pore pressure and small grain contact areas) microfractures may form close to the surface, commonly by chipping off small flakes of the grains. This type of microfracturing is referred to as **spalling** or **flaking** (Figure 10.1). At higher confining pressures, corresponding to depths in excess of ~1 km, fractures split the grains into more evenly sized parts, and this mechanism is sometimes described as **transgranular fracturing**. Some use the term transgranular as a substitute for intergranular, i.e. about fractures that cut across *several* grains,

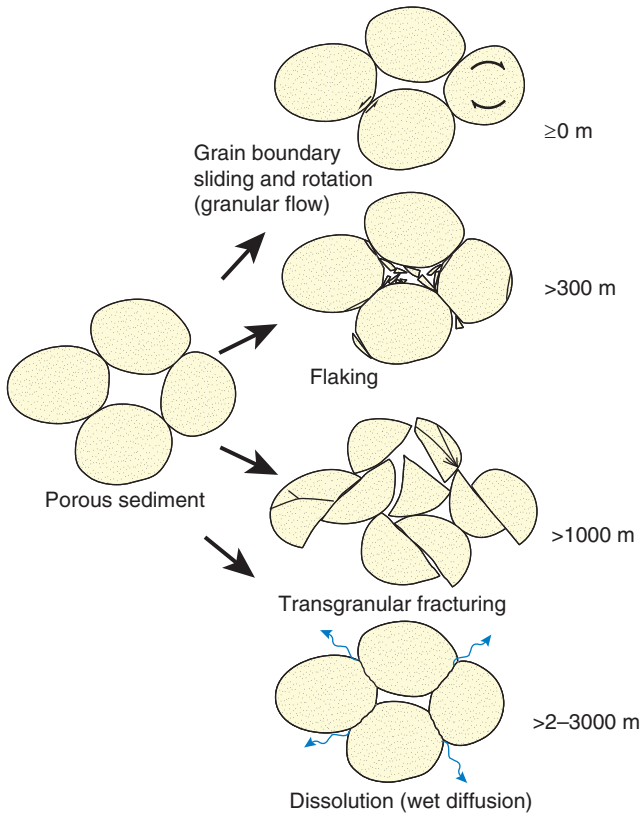

Figure 10.1 Deformation mechanisms operative at shallow depths. Very approximate depths are indicated.

so some care should be exercised when using these terms. Once fractured, the grains reorganize themselves by frictional sliding and rotation, leading to porosity reduction.

Grains in non-porous or low-porosity rocks develop fractures that may already be intergranular at the initial stages of deformation. As more and more fractures form, frictional sliding along these fractures together with rotation of grains may be widespread enough that we can characterize the deformation by the term cataclastic flow. From this point on the rock becomes crushed into a gouge, breccia or cataclasite (Box 8.1). In general, cataclasis in low-porosity rocks involves dilation and increased permeability as fractures form and open. Incohesive gouge and breccia dominate the uppermost few kilometers of the crust, while cohesive breccia and cataclasite are more common from roughly 3–5 to 10–12 km depth. In the rest of this chapter we will look at crystal-plastic deformation mechanisms.

10.4 Mechanical twinning

Stress can result in mechanical bending or kinking of the crystal lattice of some minerals, even at very low temperatures. Plagioclase feldspar and calcite (Figure 10.2)

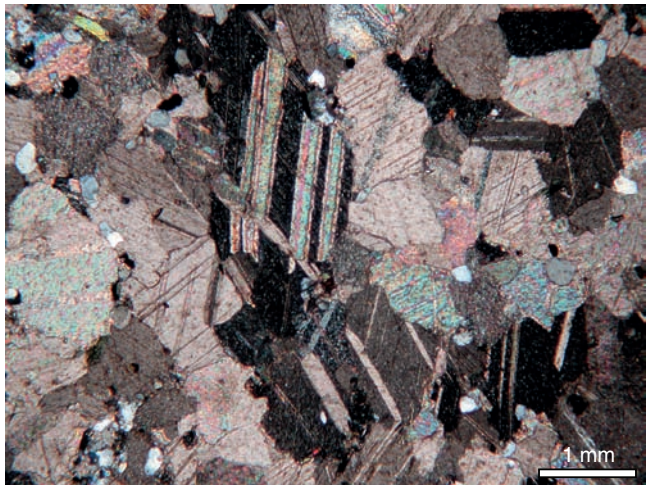

Figure 10.2 Deformation twins in an aggregate of calcite crystals.

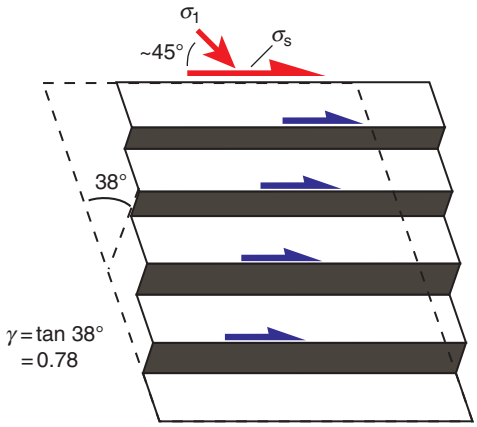

Figure 10.3 Deformation (glide) twins in a calcite crystal. Stress is ideally at 45° to the shear (glide) plane. Dark lamellae have been sheared (simple shear).

are common examples. These intracrystalline kink structures are expressions of strain and are also known as **deformation twins** and the process as **mechanical twinning**. Mechanical twinning does not involve breaking of the crystal lattice, and is therefore considered a plastic deformation mechanism. The structures must be distinguished from twins formed during crystal growth (growth twins) and cooling (transformation twins). Because deformation twins are found in only a few of our common minerals, they are easily distinguished. One useful criterion is that mechanical twins tend to taper out to form an interfingering pattern.

Calcite commonly shows a type of deformation twin formed by **twin gliding**. Twin gliding involves simple shear along the twin plane, as illustrated in Figure 10.3. The kinked and unkinked parts are mirror images of one another about this plane. Calcite twin gliding occurs at a shear stress just above a critical value of ~10 MPa for so-called e-twins (the most common of several calcite twin systems) – a value that seems to be more or less independent of normal stress, temperature and strain rate. This means that calcite can deform by twinning at any level in the crust, even at the surface (and by hand for demonstration purpose), as long as the critical stress is reached. Low-temperature (<200 °C) calcite twins are typically thinner and straighter than those formed at higher temperatures.

The ideal orientation for a deformation twin plane is where the shear stress is at its peak, which we know from Chapter 2 to be at 45° to σ_1. This relationship between the orientation of well-developed twins and σ_1 can be used to estimate stress. Optical *c*-axes for the twinned portions of calcite crystals can be found using a universal stage or goniometer. Then the statistically determined orientation of the *c*-axis from a number of observations in the same thin section gives the approximate orientation of σ_1. A simple method is shown in Figure 10.4. More sophisticated methods also exist.

Mechanical twinning accumulates small shear strains and elongations of just a few percent. The amount of shear strain associated with a single kink in the crystal lattice is restricted to a fixed angle (38° for calcite), the angle that turns the twin plane into a mirror plane. The shear strain in the twinned portion of a crystal is $\tan(38°) = 0.78$. Depending on how much of the crystal

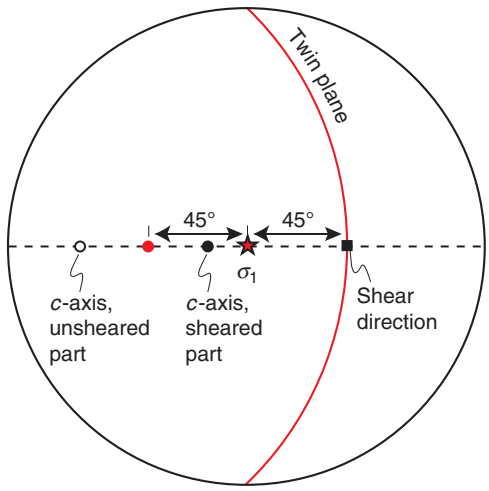

Figure 10.4 Finding the orientation of σ_1 from the measured orientation of the twin plane and *c*-axes of twinned and untwinned lamellae. The two *c*-axes lie on a great circle that also contains σ_1 and the pole to the twin plane (red). Ideally the angle between them should be 45°. When several grains are plotted, the orientation of σ_1 can be found statistically.

is twinned, the total shear strain accommodated by the grain is around half of this value.

Mechanical twinning of calcite is a low-strain and low-temperature plastic deformation mechanism that stores information about the stress field at the time of deformation.

When a twin has formed, further strain is accommodated by the formation of new twins. In aggregates of twinned calcite grains the different grains will be sheared according to their crystallographic orientation. Those favorably oriented relative to the *X*-axis of the strain ellipse are more sheared than other grains. Hence, the orientation of the strain ellipse can also be found. The classic textbook example of how patterns of stress or small strain can be mapped over large regions is the study done on calcite twinning in the carbonates of the Appalachian foreland region. Stress attributed to the Alleghany orogeny in the Appalachian Mountains can be mapped almost 100 km into the North American continent from the actual thrust front on the east coast. However, calcite twinning also has applications on a small scale, for example in the mapping of stress and strain associated with folded layers.

10.5 Crystal defects

The atomic lattice of any mineral grain, deformed or not, contains a significant number of defects. This means that the crystal has energy stored in the lattice. The more defects, the higher the stored energy.

There are two main types of defects. Some are known as **point defects**, represented by either vacancies or, less importantly, impurities in the form of extra atoms in the lattice (Figure 10.5). The point defect of interest to us is the one represented by a missing atom. Movement of vacancies is called **diffusion** (Figures 10.6 and 10.7).

The other type of defect is **line defects**, generally referred to as **dislocations**. A dislocation is a mobile line defect that contributes to intracrystalline deformation by a mechanism called **slip**. Slip implies movement of a dislocation front within a plane. A slip plane is usually the plane in a crystal that has the highest density of atoms. There are also some called **plane defects**, which include structures such as grain boundaries, subgrain boundaries and twin planes. These defects are discussed in Section 10.6.

When a crystal is deformed by plastic deformation, the dislocation density increases. Deformation adds energy to the crystal, and a high density of defects implies that

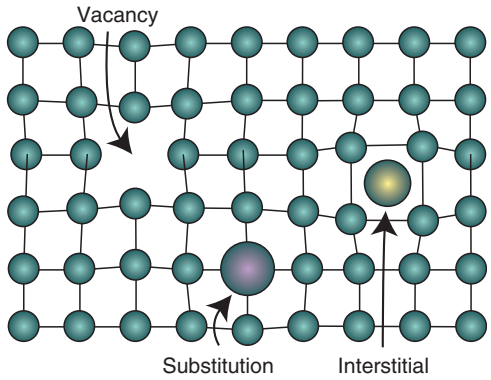

Figure 10.5 Point defects in a crystal lattice include vacancies (holes), substitutional impurities, and interstitial impurities. Vacancies represent the most important point defect in crystal-plastic flow.

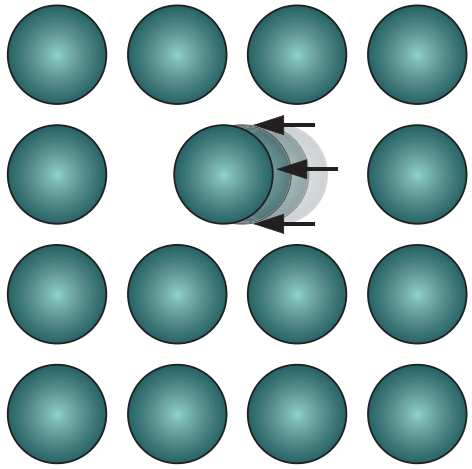

Figure 10.6 Migration of vacancies through an atomic lattice is called diffusion. A hole moves as it is replaced by a neighboring atom.

the crystal is in a high-energy state. A low-energy state is more stable, and there is thus a thermodynamic drive to reduce the number of crystal defects. Both the building up of defects such as dislocations and the reduction of them occur by the movement of defects within the atomic lattice. Such movements are not "painless". It takes energy to move dislocations around, and the movement will occur in the crystallographic plane or direction where dislocation movements involve the least energy.

Diffusion creep

Migration of vacancies in crystallographic lattices (Figure 10.6) is called **diffusion mass transfer**, usually referred to simply as **diffusion** or **diffusion creep**. Diffusion of vacancies through crystals is known as **volume diffusion** or **Nabarro–Herring creep** (Figure 10.7). The rate is not

BOX 10.1 HOW MANY?

In an undeformed natural crystal the dislocation density is around $10^6/cm^2$. In a deformed grain the density is several orders of magnitude higher (an order of magnitude more means 10 times as many).

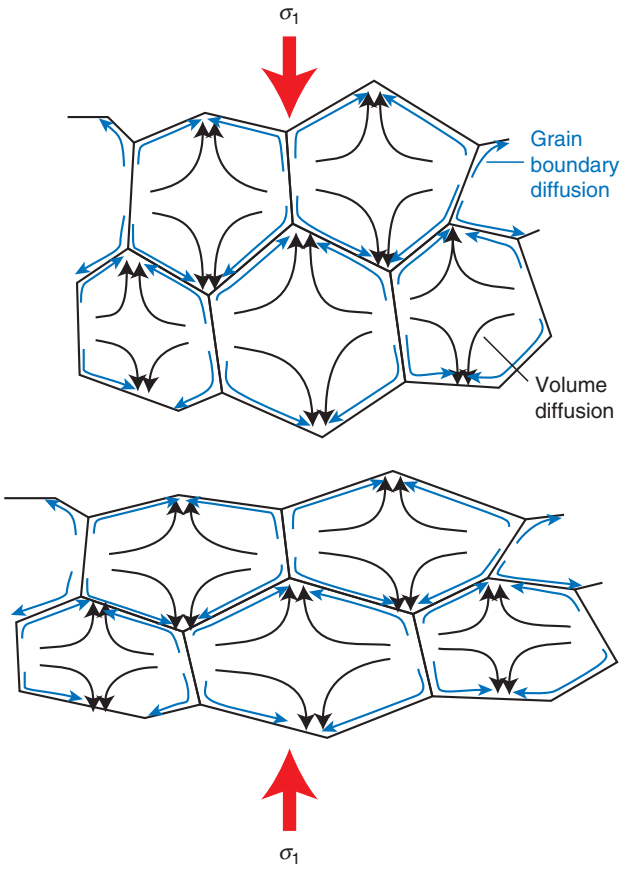

Figure 10.7 Diffusion in a mineral can occur within grains by means of volume diffusion, or along grain boundaries by means of grain boundary diffusion. In both cases vacancies move toward high-stress sites so that the minerals accumulate strain over time.

BOX 10.2 DEFORMATION MECHANISM MAPS

The different deformation mechanisms that are operative in a deforming mineral under various physical conditions can be expressed by means of a deformation mechanism map. Stress–temperature maps have been constructed, and the diagrams (maps) are contoured for a range of strain rates. Deformation mechanism maps show the range for which each deformation mechanism dominates. They are partly based on experimental data that have been extrapolated into geologically realistic strain rates and temperatures, and partly on theoretical considerations. The example shown here is for quartz. Realistic natural strain rates are indicated in yellow (10^{-12}–10^{-15} s^{-1}). Note that this and similar maps are hampered by many uncertainties and limited data availability.

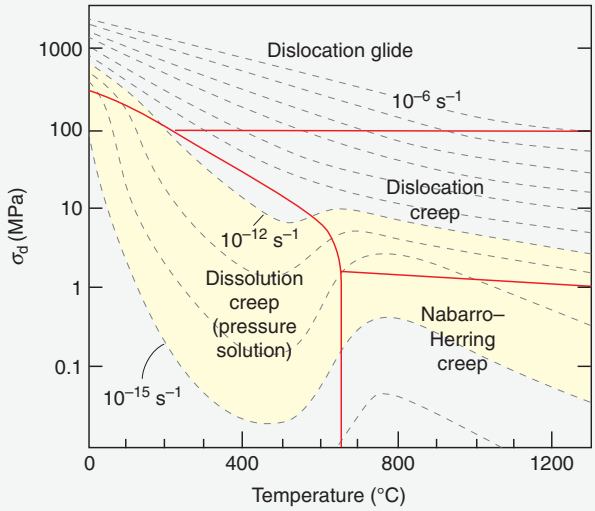

From Rutter (1976).

overly high, perhaps a few centimeters per million years. However, at some point vacancies will reach a grain boundary and disappear. Because vacancies migrate towards sites of maximum stress the crystals acquire a shape fabric or strain. During this process the crystal will gain regularity and turn into a more perfect crystal. Volume diffusion requires a lot of energy, so the migration rate is highly temperature dependent: high temperatures give high vibrations in the lattice, which increases the rate. For this reason, volume diffusion is important only in the lower part of the crust and in the mantle.

In other cases, migration of vacancies occurs preferentially along grain boundaries. This type of diffusion is known as **grain boundary diffusion** or **Coble creep**. Coble creep is a bit less energy demanding than Nabarro–Herring creep, and is more important in the deformation of the plastic crust. In both types of diffusion, mineral grains change shape, and over time this change adds to mesoscopic strain that can be seen in a hand sample or in outcrop. It is interesting to note that

the grain size is important, particularly for Nabarro–Herring creep: the smaller the grains, the higher the strain rate.

Pressure solution (or dissolution) is another important diffusion process. It bears similarities to Coble creep, and geometrically and mathematically it can be treated in the same way. However, in the case of pressure solution, diffusion occurs along a thin film of fluid along grain boundaries. A better name for pressure solution is therefore **wet diffusion**. Wet diffusion can occur at very low (even diagenetic) temperatures. During such diffusion the mineral is dissolved and the ions are carried with the fluid to be precipitated some other place. This mechanism is chemically controlled but also strongly affected by stress. Dissolution is significantly quicker where stress is high, particularly at surfaces oriented perpendicular to σ_1, while precipitation is favored on surfaces at high angles to σ_3. In porous rocks, wet diffusion at grain contacts is promoted by the stress concentrations there (Figure 7.36).

Precipitation can also occur far away in a different part of the rock or in a completely different rock layer or unit. Rocks exposed to wet diffusion experience a volume reduction. Wet diffusion is the main mechanism in what is known as **chemical compaction**, for example of sand that is undergoing lithification. Quartz sand(stone) experiences wet solution at temperatures above ~90 °C (Figure 10.8). The mechanism reduces the pore space in sandstones and not only makes the sandstone stronger and more cohesive, but also reduces porosity and permeability in clastic reservoir rocks. Wet diffusion is also common in limestones, where pressure solution seams known as **stylolites** form.

Volume diffusion: vacancies move through crystals (temperature and stress controlled).

Grain boundary diffusion: vacancies move along grain boundaries (temperature and stress controlled).

Pressure solution: ions move in fluid films and pore fluid (chemically and stress controlled).

Grain boundary sliding accommodated by dry or wet diffusion can occur at high temperatures when diffusion is quick enough to modify the shapes of the grains as they slide along each other. In contrast to frictional sliding in the brittle regime, diffusion-accommodated sliding along the grain boundaries is frictionless and no voids open during the deformation. This deformation mechanism, which is characterized by relatively rapid strain rates at low differential stress, occurs in fine-grained rocks in the mantle and lower crust, typically after a phase of grain-size reduction by dynamic recrystallization (dislocation creep).

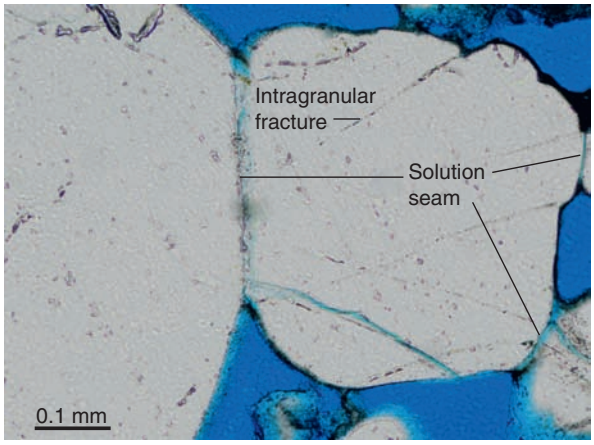

Figure 10.8 Pressure solution at grain contacts in Nubian Sandstone (Sinai). Also note intragranular fractures.

Small grain sizes favor diffusion because of short distances to grain boundaries (short diffusion paths).

Rocks deformed by diffusion-driven grain boundary sliding are always fine-grained and can accommodate large strains without developing any preferred grain shape fabric. The type of deformation process sometimes referred to as **superplastic creep** or **superplasticity** is dominated by grain boundary sliding and fine grain size.

Dislocations and dislocation creep

A dislocation is a mobile line defect that contributes to intracrystalline deformation by a mechanism called **slip**. Slip implies movement of a dislocation front within a **slip plane**, as shown in Figure 10.9, and should not be confused with frictional slip associated with brittle deformation and fault slippage. Slip planes are relatively weak crystallographic directions controlled by the atomic structure, and are usually the plane(s) in a crystal that have the highest density of atoms. Minerals have one or more such directions that can be variably activated, depending on temperature and state of stress. Both the amount of differential stress and the orientation of the stress field is of importance, as the critically resolved shear stress on any given slip system must be high enough for the system to be activated.

Mica has only one slip plane, while quartz has as many as four. One of the slip planes in quartz is in the basal plane (normal to the crystallographic *c*-axis) and is activated at low metamorphic grade (300–400 °C). The activation of basal slip for quartz produces a strong preferred orientation

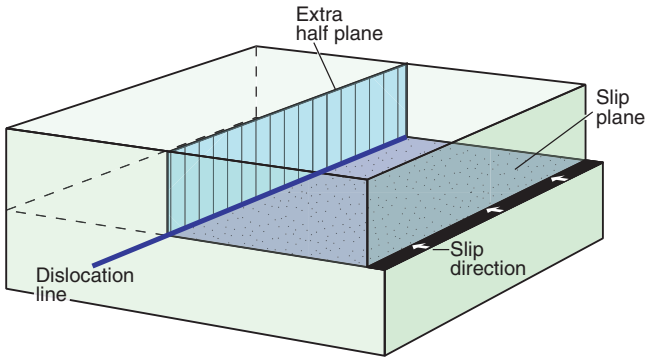

Figure 10.9 Block diagram representing the concept of dislocation line, slip plane, extra half plane and slip direction for an edge dislocation. Compare with the next two figures. Based on Hobbs *et al.* (1976).

of quartz *c*-axes that when measured optically (the *c*-axis and optical axis of quartz are coincident) can reflect the deformation mechanism as well as the kinematic framework of the deformation. For high shear strains, the quartz *c*-axes are oriented at a high angle to the foliation.

Dislocations are too small to be seen under the optical microscope, but can be identified by means of the transmission electron microscope (TEM) (Figure 10.10a and b). Studies of dislocations have shown that there are two different types of dislocations. The simplest one is the **edge dislocation**, which is the edge of an extra half-plane in the crystal lattice (Fig. 10.11a). The edge dislocation is the line drawn in Figure 10.11a, and it moves in the horizontal plane, which is the slip plane. The dislocation line or end of the extra half-space is thus perpendicular to its slip direction.

The other type is the **screw dislocation**, where the dislocation line is oriented parallel to the slip direction. The slip plane is vertical in Figure 10.11b. Screw dislocations are a bit like tearing a piece of paper. The motions of these two types of dislocations through a crystal are therefore somewhat different, and they may join forces to make composite dislocations that contain elements of both kinds.

The formation, motion and destruction of dislocations in a crystal are all contained in the term **dislocation creep**. Only a small volume around the line defect is being deformed at any time during dislocation creep. The process by which edge dislocations move is called **dislocation glide** and is shown in Figure 10.12. Eventually the dislocation has slipped through the crystal, and the offset is complete. This is different from brittle microfracturing, where the entire grain is cut almost instantaneously.

Dislocation creep allows the deformation to take place at much lower differential stress than that required for

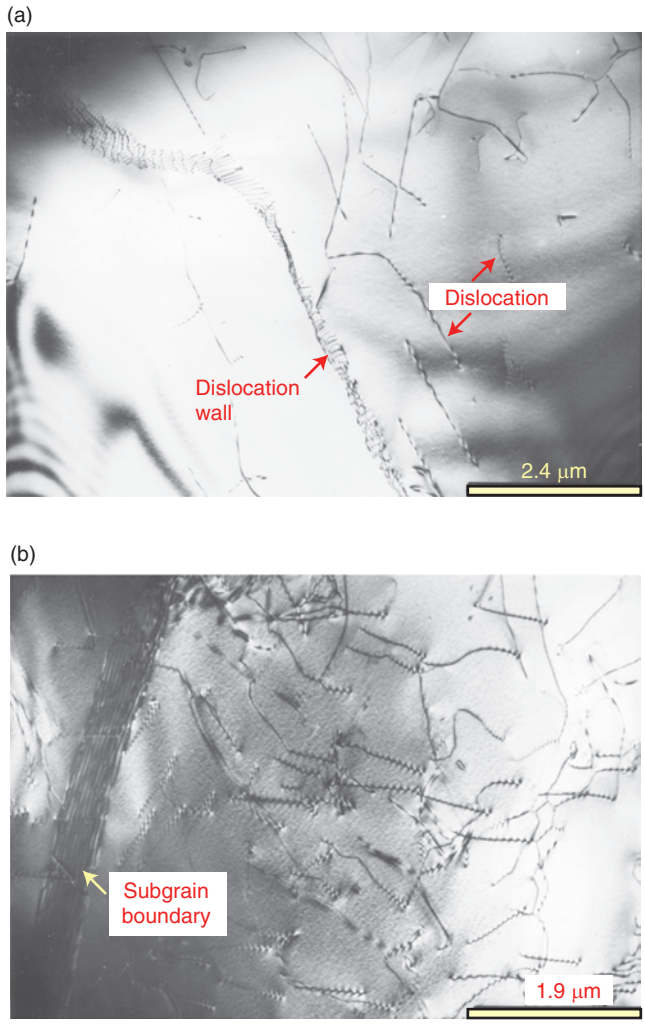

Figure 10.10 Electron microscope (TEM) photo of dislocations in deformed quartz from a deformed conglomerate in the Swedish Caledonides (Lisle, 1984). (a) Low-density area where several dislocations have free terminations. A dislocation wall is seen. (b) Somewhat higher dislocation density. The thick zone to the left is a subgrain boundary. Dislocation creep was an important mechanism in this case, together with some grain boundary sliding and pressure solution. The dislocation density indicates a deviatoric stress of 30–60 MPa. Photo: Martyn Drury.

brittle fracturing. This is why rocks do not fracture if dislocation creep is active, and the reason why the strength of the crust decreases downward as we enter the brittle–plastic transition (Box 10.3).

There is another difference between brittle fracturing and deformation by dislocation movement, namely that dislocations leave no trace:

Dislocation movements do not damage or weaken the mineral.

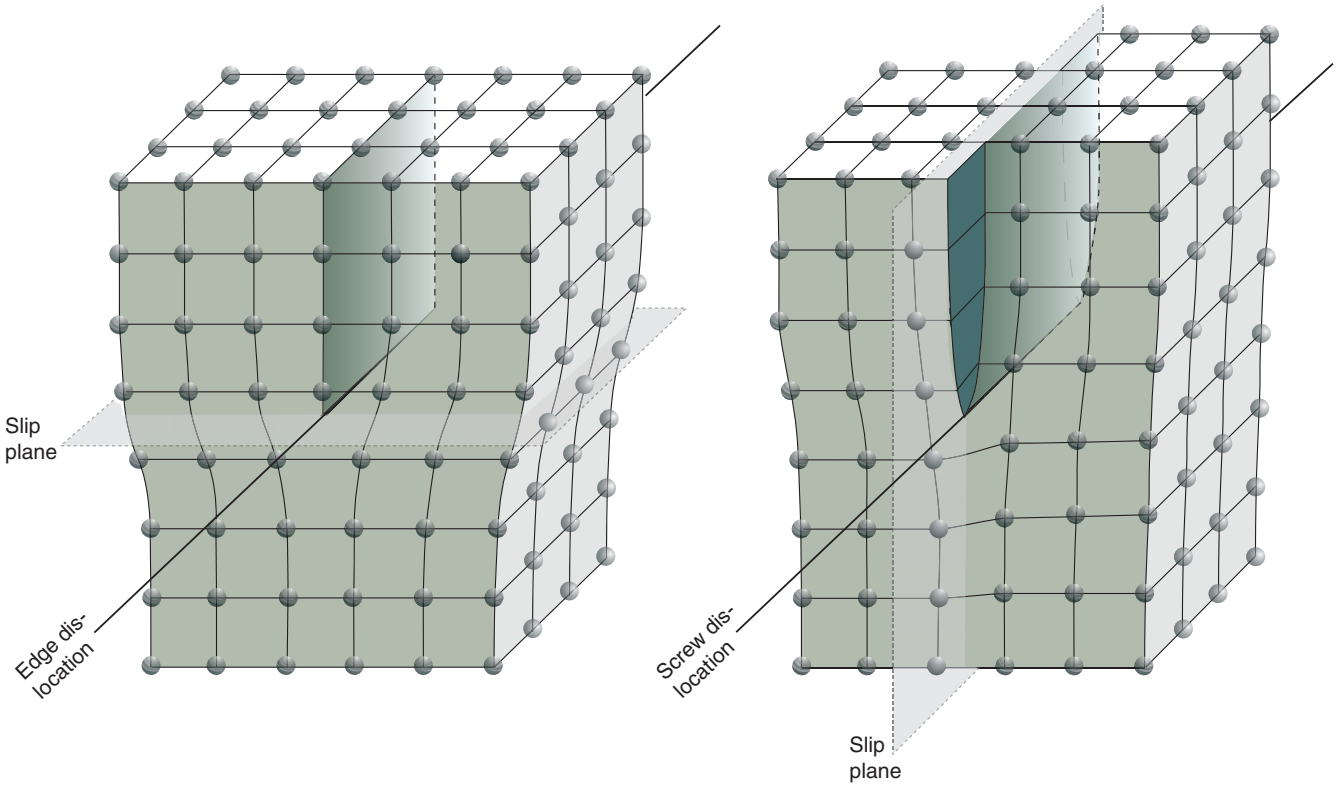

Figure 10.11 The two types of dislocations. An edge dislocation (left) occurs where an extra half-space of atoms interrupts the lattice, while a screw dislocation (right) involves twisting of the lattice.

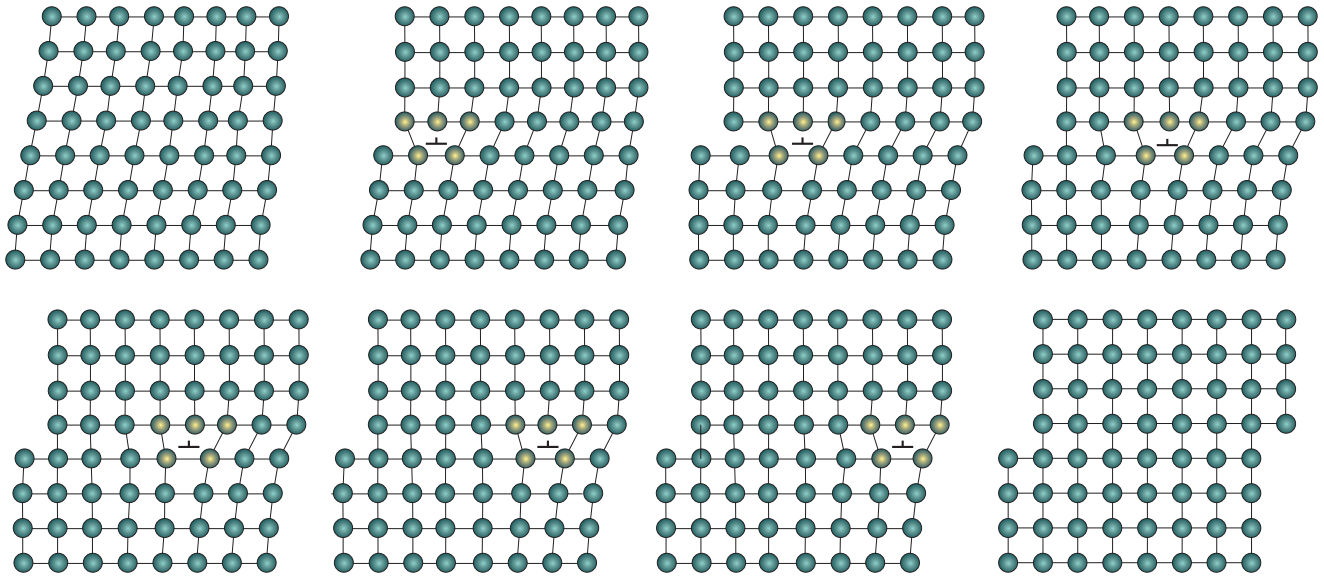

Figure 10.12 Formation and movement of an edge dislocation through a crystal lattice. The process can be compared to the way a caterpillar moves, as only bonds along the dislocation line (which is perpendicular to the page) are broken at the same time. Thus, the energy that it takes to move the dislocation is kept at a low level. Instantaneous fracturing of the whole crystal would require much higher energy.

Once the dislocation has slipped through the crystal, the crystal is completely healed with respect to this particular imperfection. The imperfection is gone and no weakness is introduced, which there would be where fracturing has occurred. Hence, dislocation movements do not reduce the internal strength of crystals.

When a crystal is strained, the dislocation density increases. We therefore refer to this energy as **strain**

BOX 10.3 FLOW LAWS

Flow laws are useful for estimating the strength of the lithosphere. Flow laws and experimental data indicate that the crust becomes weaker as pressure and temperature increase within the plastic regime. At the same time we know that there is a temperature limit for plastic deformation. At lower temperatures frictional gliding controls the crustal strength, meaning that the upper crustal strength is controlled by how much stress it takes to form or reactivate a fracture. This regime is governed by Byerlee's law from Chapter 7. We therefore have to combine Byerlee's law and flow laws to obtain a realistic model for the strength of the entire crust. The point of intersection between Byerlee's law and the appropriate plastic flow law indicates the brittle–plastic transition (see also Figure 6.18). In reality, this intersection is not sharp, but a gradual transition.

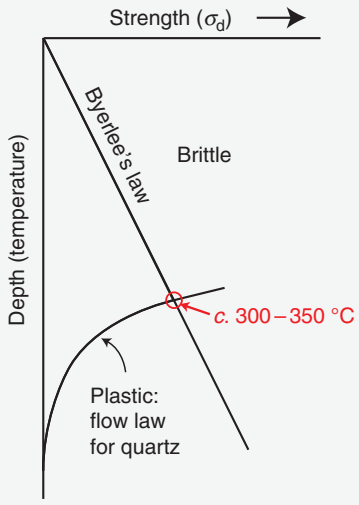

energy. We could also say that differential stress creates new dislocations at the grain boundaries, and these dislocations will move through the crystal. Hence differential stress adds energy to the crystal:

A high density of defects implies that the crystal is in a high-energy state.

A low-energy state is more stable, and there is thus a thermodynamic drive to reduce the number of crystal defects. Slip of defects through the atomic lattice requires energy. The movement therefore occurs in the crystallographic plane and direction where dislocation movements require the least energy.

Gliding or slipping dislocations may encounter interstitials, substitutions or other dislocations on their way through the crystal. If the dislocation has too little energy to bypass the obstacles it will get stuck. **Dislocation pile-ups** form where multiple dislocations entangle and accumulate. Bypassing obstacles requires dislocations to change slip planes by a process called **cross-slip**. This may be possible for screw dislocations, but edge dislocations "jump" to another slip plane by the process known as **climb**. Climb and cross-slip require energy, which in this context means temperature. As a rule of thumb, climb and cross-slip occur for temperatures in excess of 300 °C for quartz and 500 °C for feldspar. Below these temperatures it is hard to move dislocations, and we quickly leave crystal-plasticity and enter the frictional or brittle regime. In general:

Dislocation glide is most important where temperature is too low for volume diffusion and it is not wet enough for wet diffusion to occur.

Flow laws

Dislocation movement depends not only on temperature (T), but also on differential stress (σ_d) and the activation energy (E^*) involved. These three variables can be related to the strain rate (σ_d) by means of a flow law. This law, which is a constitutive equation because it relates stress to strain rate, also depends on the deformation mechanism.

Flow laws relate stress to strain rate and depend on the dominating deformation mechanism, which again depends on the mineral and temperature.

For dislocation glide, i.e. where temperature is too low for dislocations to climb over lattice obstacles, the flow law is:

$$\dot{e} = A \exp(\sigma_d) \exp(-E^*/RT) \qquad (10.1)$$

where A is an empirically determined material constant, R is the gas constant and T is the temperature in K. For higher temperatures, where dislocation creep dominates, the law becomes:

$$\dot{e} = A(\sigma_d)^n \exp(-E^*/RT) \qquad (10.2)$$

Note that stress is the main variable in this formula. Differential stress is raised to the nth power and dislocation creep, where dislocations can both glide and climb,

is therefore called **power-law creep**. Typical values of n lie between 3 and 5 for power-law creep. This is the most widely used flow law, applicable to many crustal and even mantle-level settings.

When temperature is really high (or grain size is very small), the flow law for diffusion is applied:

$$\dot{e} = A(\sigma_d) \exp(-E^*/RT) \qquad (10.3)$$

This formula is identical to the one for dislocation creep (Equation 10.2), with $n = 1$. This points to the linear relation between strain rate and stress, typical for perfectly (Newtonian) viscous deformation.

10.6 From the atomic scale to microstructures

Atomic-scale deformation structures such as dislocations can only be studied by means of electron microscopy at 10 000–100 000 times magnification. However, the effects of these structures and related mechanisms can be seen under the optical microscope. They are referred to as **microstructures** and carry information about temperature, state of stress and rheological properties at the time of deformation. Microstructures and microtextures such as recovery and recrystallization can be seen under the optical microscope. However, keep in mind that the controlling mechanisms are the atomic-scale ones discussed above.

Recovery

Processes such as dislocation creep reduce the internal energy of a mineral grain by moving dislocations to the grain boundary or collecting them in zones within the grain. Dislocations can organize themselves into what are known as **dislocation walls** (Figures 10.10 and 10.13). Such walls are visible in thin sections if they contain sufficient dislocations. What makes them visible is the change in their crystallographic orientation across the walls. For minerals such as quartz, the two sides of the wall show slightly different extinction angles. Thus, **undulose extinction** is characteristic of dislocation walls in mineral grains. Elongated grain-internal zones with slightly different extinction, as shown in Figure 10.14, are known in the (older) literature as **deformation bands**. Such deformation bands have nothing to do with mesoscopic deformation bands in deformed sandstones (Chapter 7), and unless the meaning is clear from the context, the name should be reserved for tabular strain discontinuities in porous rocks. Where dislocations migrate further and arrange themselves into more well-defined networks that outline small patches with few or no dislocations, we have a process called **subgrain formation**. Subgrains are polygonal patches of a mineral grain that are slightly (usually less than 5°) misoriented with respect to their neighbors or host grain. Subgrain formation (Figures 10.15 and 10.16) is an advanced stage in the process called **recovery**, where deformed grains can reduce their stored energy by the removal or rearrangement of dislocations.

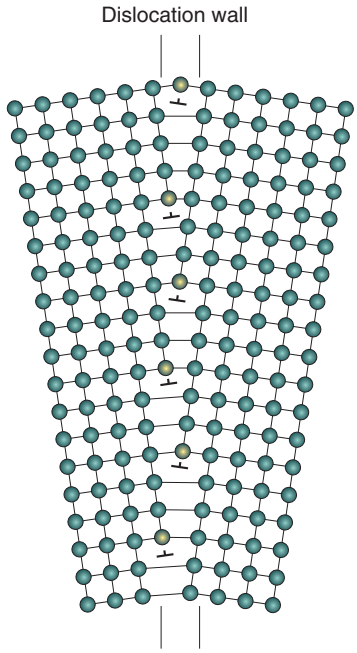

Figure 10.13 Simple dislocation wall composed of edge dislocations. Dislocation walls separate parts of a crystal with slightly different lattice orientation, such as the boundary between neighboring subgrains.

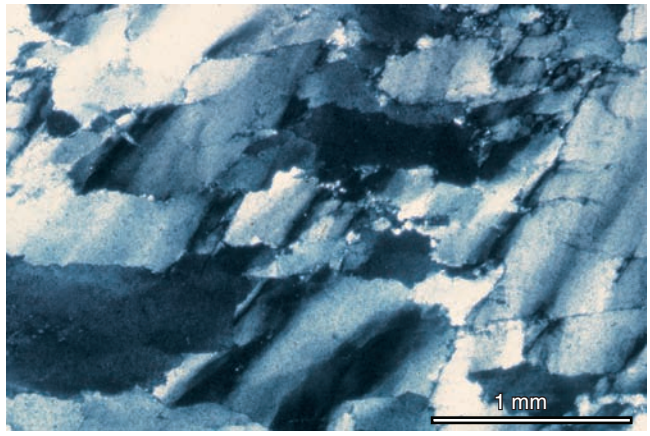

Figure 10.14 Deformation bands in quartz crystals, characterized by undulose extinction. Quartz pebble in the deformed conglomerate shown in Box 3.1.

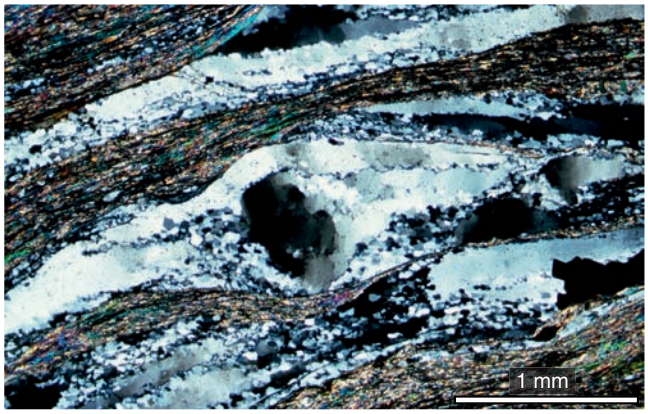

Figure 10.15 Subgrains and deformation bands in quartz. A large grain is breaking down, forming a core of relict quartz with a mantle of subgrains and new grains (core–mantle structure). Quartz band in sheared phyllite, Scandinavian Caledonides.

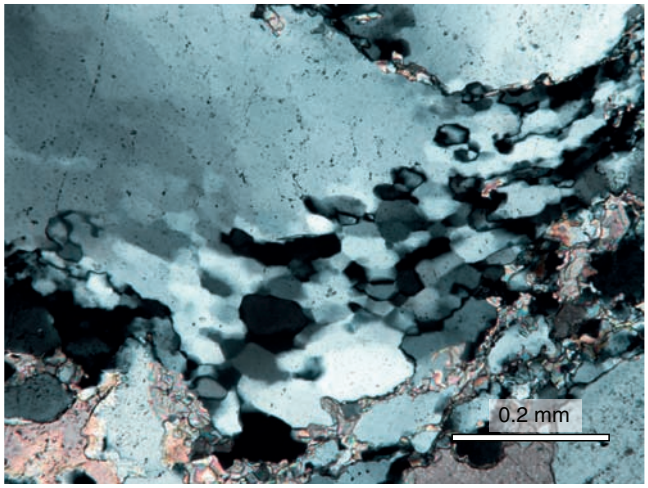

Figure 10.16 Gradual evolution of subgrains at the tail of a larger quartz grain. Note faint shadows of subgrains as they rotate out of alignment with the host grain. Heimefrontfjella, Antarctica.

Recovery comprises all processes that move, cancel out and order dislocations into walls that separate portions of the original grain with slightly different crystallographic orientations.

Recrystallization

If recovery continues so that the dislocations still present in subgrains are removed and the grains become strain-free with little or no undulose extinction, then the mineral has recrystallized (Figure 10.17). This type of recrystallization, where subgrains rotate until they classify as a separate

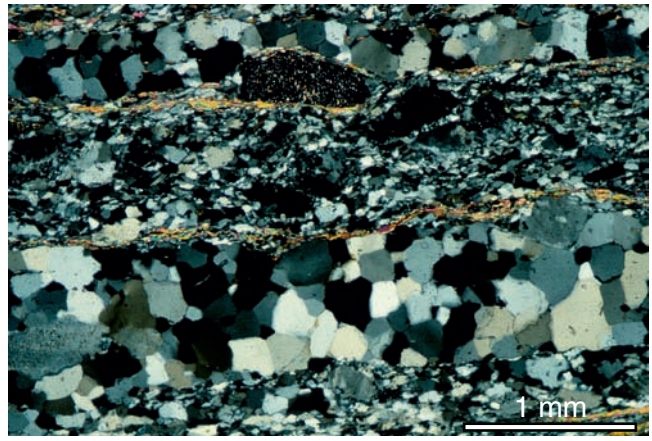

Figure 10.17 Recrystallized quartz bands in metarhyolite. Note the even size and strain-free nature of the recrystallized grains. Grain boundaries are more irregular than what would be expected for static recrystallization, and are therefore interpreted as dynamic.

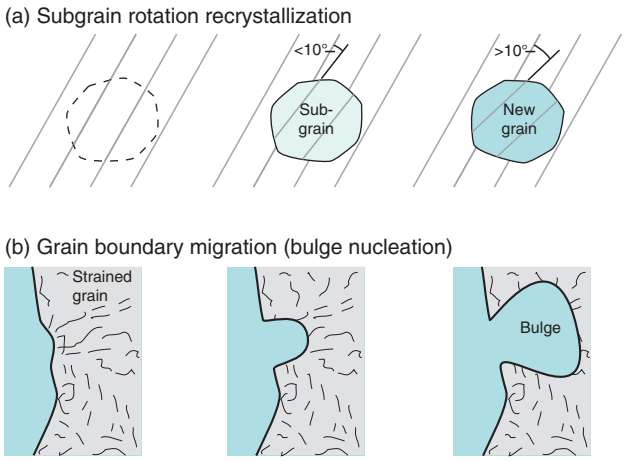

Figure 10.18 (a) Illustration of recrystallization by means of subgrain rotation. (b) Bulging, resulting from migration of a grain boundary into a more strained grain (with more dislocations).

grain (by definition more than 10° relative to neighboring grains) is known as **subgrain rotation recrystallization** (Figure 10.18a). Subgrain rotation requires that dislocations are free to move and climb relatively freely, a process favored by elevated temperatures and known as climb-accommodated dislocation creep.

Minerals can also recrystallize by the migration of grain boundaries, a process known as **grain boundary migration** or **migration recrystallization**. In general, grain boundary migration is driven by differences in strain energy, and grains with high dislocation density have higher energy than a neighboring strain-free (dislocation-free) grain. Along the boundary between two grains there will be a slight movement of atoms

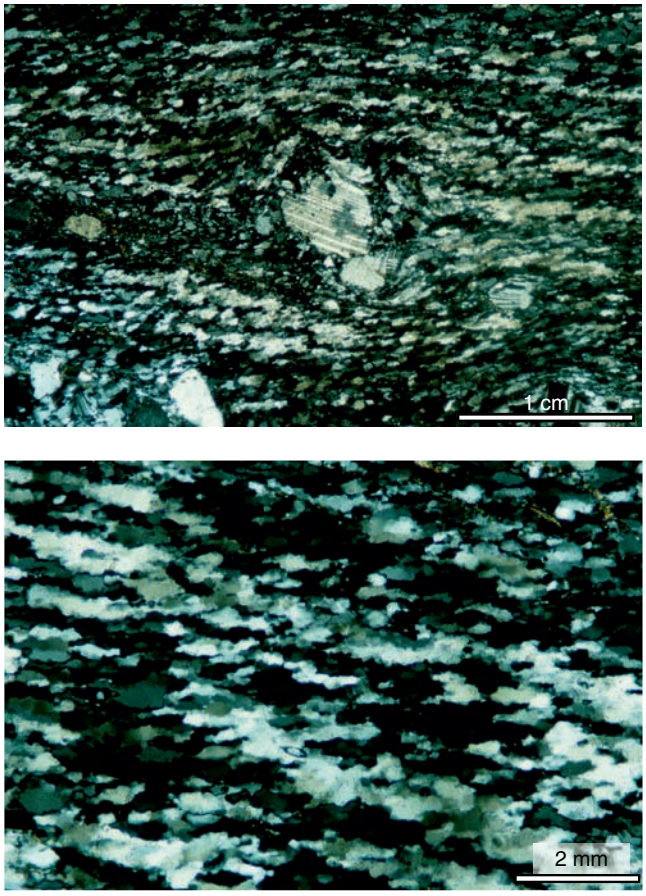

Figure 10.19 Dynamic recrystallization in a greenschist-facies shear zone. The new grains are oblique to the main foliation because they have only experienced the last part of the non-coaxial deformation. The middle grain in (a) is a feldspar porphyroclast. (b) is a close-up view of part of (a).

in the more strained grain to fit the lattice of the strain-free grain. In this sense the grain boundary migrates into the grain with high dislocation density. One variant of this process, illustrated in Figure 10.18b, is referred to as **bulging**. Nucleation of new strain-free grains that expand in a strained grain is also described. Both types of boundary migration are stimulated by temperature and differences in dislocation density.

In many cases recrystallization in the crust is seen to be a combination of grain boundary migration and subgrain rotation. Recrystallized grains tend to be bigger than related subgrains and in many cases the grain boundaries are straighter.

Recrystallization is the process whereby strained and dislocation-rich grains are replaced by unstrained grains with few or no dislocations.

Recrystallization that occurs as the rock is being deformed (under differential stress) is referred to as **dynamic recrystallization** (Figure 10.19). Rocks can also recrystallize after the deformation has come to a halt. This process is called **static recrystallization** or **annealing**. Static recrystallization tends to produce larger and more equant grains, typically forming a polygonal pattern. Grains that undergo dynamic recrystallization are continuously recrystallizing under the influence of tectonic stress. New dislocations will form in the grains, seen under the microscope as undulatory extinction. In addition, dynamically recrystallized grains will soon become strained with a preferred orientation that depends on the sense of shear. There is always competition between continuous deformation by crystal-plastic deformation mechanisms and temperature-stimulated recovery by recrystallization during dynamic recrystallization. The higher the temperature, the faster the recrystallization.

Dislocation accumulation is counteracted by recrystallization, which involves formation or migration of grain boundaries.

One of the characteristics of recrystallized rocks is the **pinning** effect of non-recrystallizing minerals, such as small mica grains in quartzite or quartz-rich mylonites. Such minerals hinder grain boundary migration and cause the recrystallized rock to have an uneven or smaller grain size.

Stress and grain size

Recrystallization is driven by differences in dislocation density across grain boundaries, which again depend on differential stress. This implies that the dislocation density in a deformed rock can tell us something about the differential stress at the time of deformation. Hence, the size of subgrains and dynamically recrystallized grains is related to the differential stress during deformation.

Using grain size to estimate paleostress in dynamically recrystallized rocks is a tool referred to as a **paleopiezometer** ("piezo" is derived from the Greek word for pressure). In general, the average grain size goes down with increasing differential stress and strain rate. The temperature is also of interest: low temperature implies higher stress and, according to Figure 10.20, a smaller grain size. This is consistent with the general

observation that greenschist facies mylonites have lower grain size than amphibolite facies mylonites. Estimated stress values from naturally deformed rocks lie between a few MPa for high-temperature mylonites and up to ~100 MPa for low-temperature mylonites (i.e. mylonites formed close to the brittle–plastic transition).

The method is based on the assumption that the deformation is stable. In this context this means that the average grain size is constant for subgrains and recrystallized grains, independent of the duration of the deformation. As reflected by the different curves in Figure 10.20, there is considerable uncertainty involved in using this method. There is uncertainty in defining the average grain size, different types of recrystallization mechanisms may give different stress–grain size relations, and the influence of fluids should be accounted for. Static (postkinematic) growth of minerals that interfere with dynamic recrystallization textures is yet another source of error. Nevertheless, this is the only way of quantifying stress in the middle and lower crust that we know of today.

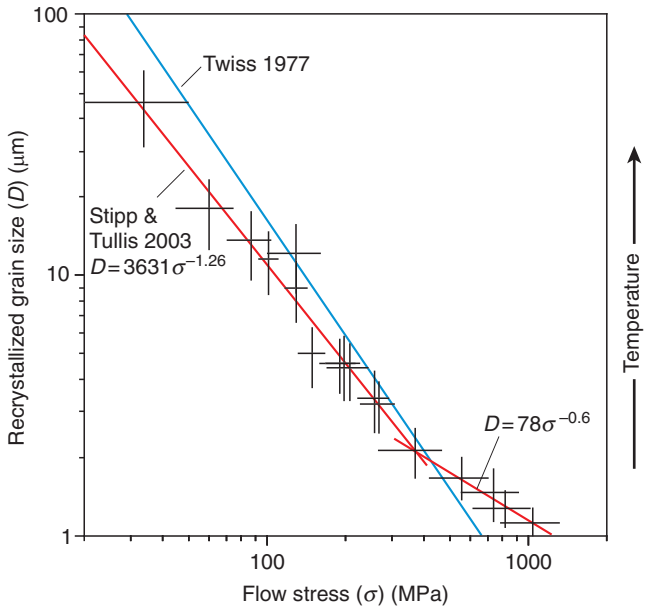

Figure 10.20 Grain size plotted against differential stress for quartz. Experimentally derived data by Stipp and Tullis (2003) are shown together with the two curves that best fit their data. A theoretically estimated curve (Twiss 1977) is shown for comparison.

Summary

Plastic deformation at the microscale is the foundation for all plastic deformation structures that can be observed in hand samples, outcrops, maps, profiles etc. Folds, plastic shear zones, mylonite zones and similar structures are all results of dislocation creep and diffusion. Keep this in mind as we move on to look at such structures in the next chapters. First go through these summary points and make sure you can address the review questions below:

- Brittle deformation mechanisms involve frictional sliding and breaking of crystal lattice and atomic bonds. Plastic deformation is healing and produces or leaves no flaws.
- Plastic deformation can occur by twinning, different types of diffusion and dislocation creep.
- Minerals can recrystallize during deformation (synkinematic or dynamic recrystallization) or after deformation (postkinematic or static recrystallization).
- Dynamic recrystallization competes against dislocation formation and straining of grains.
- The stress required to drive dislocation motion decreases with increasing temperature.
- The size of recrystallized grains is related to differential stress, and can to some extent be used to estimate paleostress.
- Recrystallization occurs by concentration of dislocations along existing or new grain boundaries so that dislocation-free domains (new grains) emerge.
- Undulatory extinction in quartz indicates the presence of dislocations (strain).

Review questions

1. What is the difference between a slip plane in a plastically deforming crystal and a slip plane associated with brittle faulting?
2. What are the main principal differences between brittle and plastic deformation?
3. Why is intracrystalline fracturing so common in brittle deformation of highly porous rocks?
4. Name two plastic deformation mechanisms that can operate at shallow crustal depths.
5. What is meant by the term dislocation creep and how does it differ from diffusion?
6. What deformation mechanism is particularly active in fine-grained rocks at high temperatures (in the lower crust and the mantle)?
7. What information can we get from dynamically deformed quartz that disappears during static recrystallization?
8. What is the difference between recrystallization by subgrain rotation and grain boundary migration?

E-MODULE

The e-learning module called *Plastic deformation* is recommended for this chapter.

FURTHER READING

General

de Meer, S., Drury, M., Bresser, J. H. P. and Pennock, G. M., 2002, Current issues and new developments in deformation mechanisms, rheology and tectonics. In S. de Meer, M. R. Drury, J. H. P. de Bresser and G. M. Pennock (Eds.), *Deformation Mechanisms, Rheology and Tectonics: Current Status and Future Developments.* Special Publication **200**, London: Geological Society, pp. 1–27.

Karato, S.-I., 2008, *Deformation of Earth Materials: An Introduction to the Rheology of Solid Earth.* Cambridge: Cambridge University Press.

Knipe, R. J., 1989, Deformation mechanisms: recognition from natural tectonites. *Journal of Structural Geology* **11**: 127–146.

Passchier, C. W. and Trouw, R. A. J., 2006, *Microtectonics.* Berlin: Springer Verlag.

Dislocation creep

Hirth, G. and Tullis, J., 1992, Dislocation creep regimes in quartz aggregates. *Journal of Structural Geology* **14**: 145–159.

Flow laws

Carter, N. L. and Tsenn, M. C., 1987, Flow properties of continental lithosphere. *Tectonophysics* **136**: 27—63.

Schmid, S. M., 1982, Microfabric studies as indicators of deformation mechanisms and flow laws operative in mountain building. In K. J. Hsü (Ed.), *Mountain Building Processes.* London: Academic Press, pp. 95–110.

Grain size piezometers

Shimizu, I., 2007, Theories and applicability of grain size piezometers: the role of dynamic recrystallization mechanisms. *Journal of Structural Geology* **30**: 899–917.

Stipp, M. and Tullis, J., 2003, The recrystallized grain size piezometer for quartz. *Journal of Geophysical Research* **30**: doi:10:1029/2003GL018444.

Pictures of structures

Snoke, A. W., Tullis, J. and Todd, V. R., 1998, *Fault-related Rocks: A Photographic Atlas.* Princeton: Princeton University Press.

Chapter 11

Folds and folding

Folds are eye-catching and visually attractive structures that can form in practically any rock type, tectonic setting and depth. For these reasons they have been recognized, admired and explored since long before geology became a science (Leonardo da Vinci discussed them some 500 years ago, and Nicholas Steno in 1669). Our understanding of folds and folding has changed over time, and the fundament of what is today called modern fold theory was more or less consolidated in the 1950s and 1960s. Folds, whether observed on the micro-, meso- or macroscale, are clearly some of our most important windows into local and regional deformation histories of the past. Their geometry and expression carry important information about the type of deformation, kinematics and tectonics of an area. Besides, they can be of great economic importance, both as oil traps and in the search for and exploitation of ores and other mineral resources. In this chapter we will first look at the geometric aspects of folds and then pay attention to the processes and mechanisms at work during folding of rock layers.

11.1 Geometric description

It is fascinating to watch folds form and develop in the laboratory, and we can learn much about folds and folding by performing controlled physical experiments and numerical simulations. However, modeling must always be rooted in observations of naturally folded rocks, so geometric analysis of folds formed in different settings and rock types is fundamental. Geometric analysis is important not only in order to understand how various types of folds form, but also when considering such things as hydrocarbon traps and folded ores in the subsurface. There is a wealth of descriptive expressions in use, because folds come in all shapes and sizes. Hence we will start this chapter by going through the basic jargon related to folds and fold geometry.

Shape and orientation

Folds are best studied in sections perpendicular to the folded layering, or perpendicular to what is defined as the axial surface, as shown in Figure 11.1. Unless indicated, we will assume that this is the section of observation in this chapter. In general, folds are made up of a **hinge** that connects two usually differently oriented **limbs**. The hinge may be sharp and abrupt, but more commonly the curvature of the hinge is gradual, and a **hinge zone** is defined. A spectrum of hinge shapes exists, from the pointed hinges of **kink bands** and **chevron folds** (sharp and angular folds) to the well-rounded hinges of **concentric folds** (Figure 11.2). Classification of folds relative to hinge curvature is referred to as **bluntness**.

The shape of folds can also be compared to mathematical functions, in which case we can apply terms such as **amplitude** and **wavelength**. Folds do not necessarily show the regularity of mathematical functions as we know

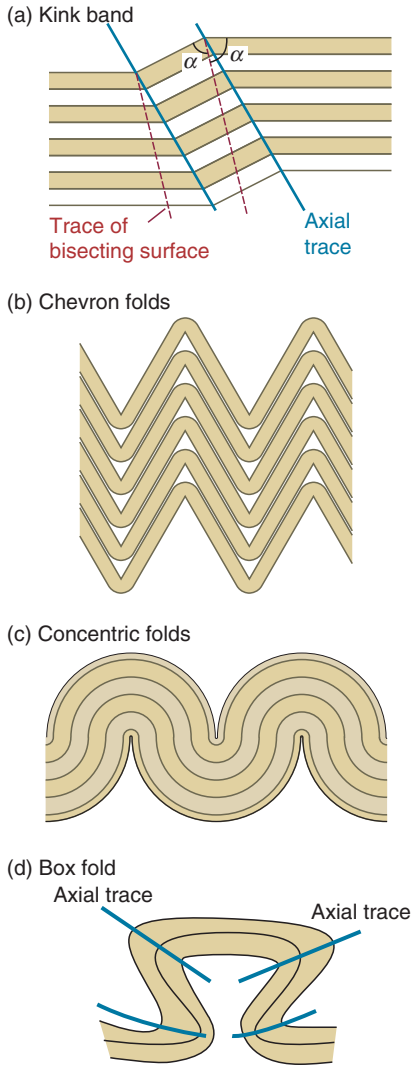

Figure 11.2 (a) Kink band, where the bisecting surface, i.e. the surface dividing the interlimb angle in two, is different from the axial surface. (b) Chevron folds (harmonic). (c) Concentric folds, where the arcs are circular. (d) Box folds, showing two sets of axial surfaces.

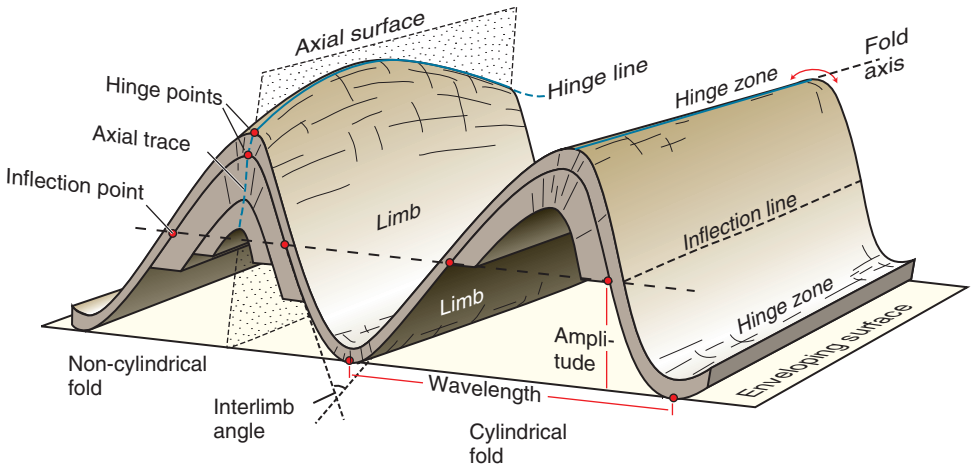

Figure 11.1 Geometric aspects of folds.

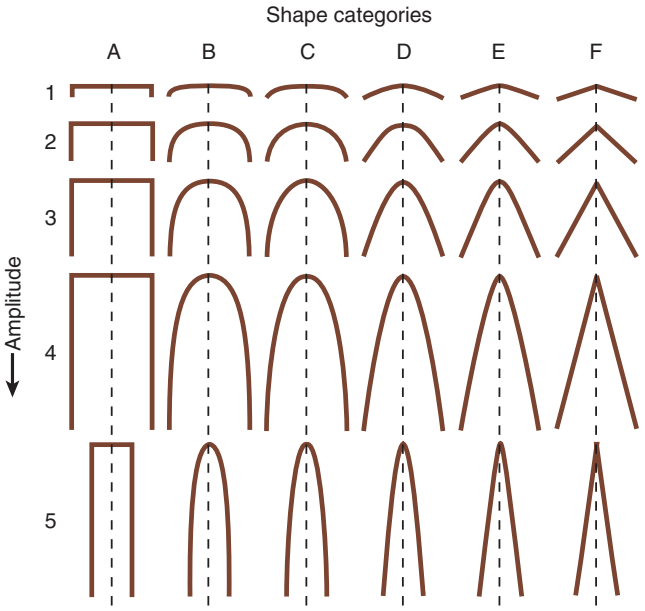

Figure 11.3 Fold classification based on shape. From Hudleston (1973).

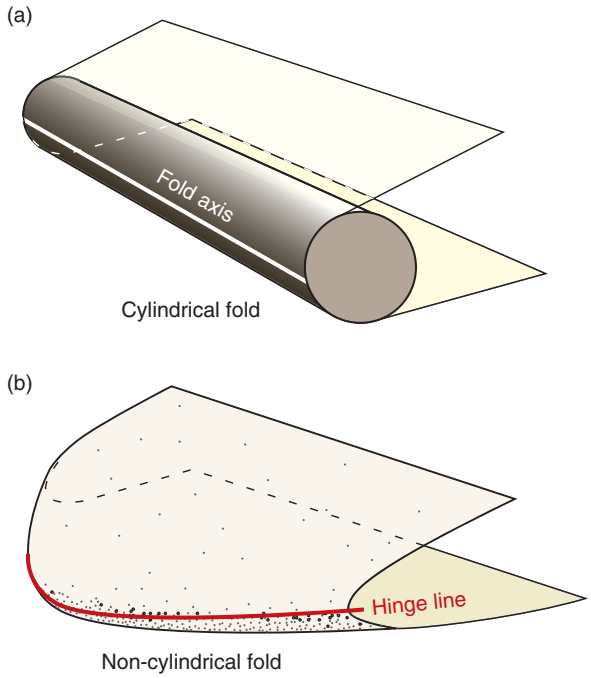

Figure 11.4 Cylindrical and non-cylindrical fold geometries.

them from classes of elementary algebra. Nevertheless, simple harmonic analysis (Fourier transformation) has been applied in the description of fold shape, where a mathematical function is fitted to a given folded surface. The form of the Fourier transformation useful to geologists is

$$f(x) = b_1 \sin x + b_3 \sin 3x + b_5 \sin 5x \ldots \qquad (11.1)$$

This series converges rapidly, so it is sufficient to consider only the first coefficients, b_1 and b_3, in the description of natural folds. Based on this method, Peter Hudleston prepared the visual classification system for fold shape shown in Figure 11.3.

In multilayered rocks, folds may be repeated with similar shape in the direction of the axial trace, as seen in Figure 11.2a–c. Such folds are called **harmonic**. If the folds differ in wavelength and shape along the axial trace or die out in this direction they are said to be **disharmonic**.

The point of maximum curvature of a folded layer is located in the center of the hinge zone and is called the **hinge point** (Figure 11.1). Hinge points are connected in three dimensions by a **hinge line**. The hinge line is commonly found to be curved, but where it appears as a straight line it is called the **fold axis**.

This takes us to an important element of fold geometry called **cylindricity**. Folds with straight hinge lines are **cylindrical**. A cylindrical fold can be viewed as a partly unwrapped cylinder where the axis of the cylinder defines the fold axis (Figure 11.4a). At some scale all folds are non-cylindrical, since they have to start and end somewhere, or transfer strain to neighboring folds (Box 11.1), but the degree of cylindricity varies from fold to fold. Hence, a portion of a fold may appear cylindrical as observed at outcrop (Figure 11.5), even though some curvature of the axis must exist on a larger scale.

Cylindricity has important implications that can be taken advantage of. The most important one is that the poles to a cylindrically folded layer define a great circle, and the pole (π-axis) to that great circle defines the fold axis (Figure 11.6a). When great circles are plotted instead of poles, the great circles to a cylindrically folded layer will cross at a common point representing the fold axis, in this case referred to as the β-axis (Figure 11.6b). This method can be very useful when mapping folded layers in the field, but it also works for other cylindrical structures, such as corrugated fault surfaces.

Another convenient property of cylindrical folds is that they can be projected linearly, for example from the surface to a profile. Cylindricity is therefore commonly assumed when projecting mapped structures in an area onto cross-sections, particularly in the early 1900 mapping of the Alps by Swiss geologists such as Emile Argand and Albert Heim. Since the validity of such projections relies on the actual cylindricity of the projected structures, the uncertainty increases with projection distance.

The **axial surface**, or **axial plane** when approximately planar, connects the hinge lines of two or more folded surfaces. The **axial trace** of a fold is the line of intersection

BOX 11.1 FOLD OVERLAP STRUCTURES

Individual folds can overlap and interfere. Just like faults, they initiate as small structures and interact through the formation of overlap or relay structures. Fold overlap structures were first mapped in thrust and fold belts, particularly in the Canadian Rocky Mountains, and many of the fundamental principles of fault overlap structures come from the study of fold populations. Fold overlaps are zones where strain is transferred from one fold to another. Rapid changes in fold amplitude characterize fold overlap structures.

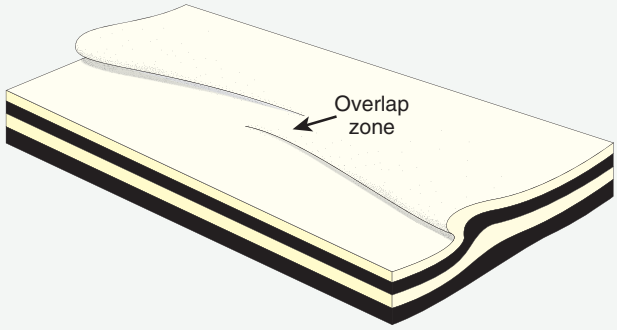

of the axial surface with the surface of observation, typically the surface of an outcrop or a geologic section. The axial trace connects hinge points on this surface. Note that the axial surface does not necessarily bisect the limbs (Figure 11.2a). It is also possible to have two sets of axial surfaces developed, which is the case with so-called **box folds**, which are also called **conjugate folds** from the characteristic conjugate sets of axial surfaces (Figure 11.2d). In other cases, folds show axial surfaces with variable orientations, and such folds are called **polyclinal**.

The orientation of a fold is described by the orientation of its axial surface and hinge line. These two parameters can be plotted against each other, as done in Figure 11.7, and names have been assigned to different fold orientations. Commonly used terms are **upright** folds (vertical axial plane and horizontal hinge line) and **recumbent** folds (horizontal axial plane and hinge line).

Most of the folds shown in Figure 11.7 are **antiforms**. An antiform is a structure where the limbs dip down and away from the hinge zone, whereas a **synform** is the opposite, trough-like shape (Figure 11.8b, c). Where a stratigraphy is given, an antiform is called an **anticline** where the rock layers get younger away from the axial surface of the fold (Figures 11.8e and 1.6). Similarly, a

Figure 11.5 Cylindrically folded granitic dike in amphibolite.

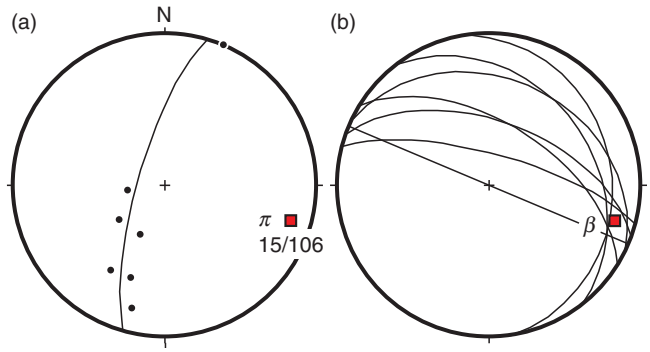

Figure 11.6 Measurements of bedding around a folded conglomerate layer. (a) Poles to bedding plot along a great circle. The pole to this great circle (π-axis = 15/106) represents the fold axis. (b) The same data plotted as great circles. For a perfectly cylindrical fold the great circles should intersect at the point (β-axis = 15/106) representing the fold axis. Data from the fold shown in Box 3.2.

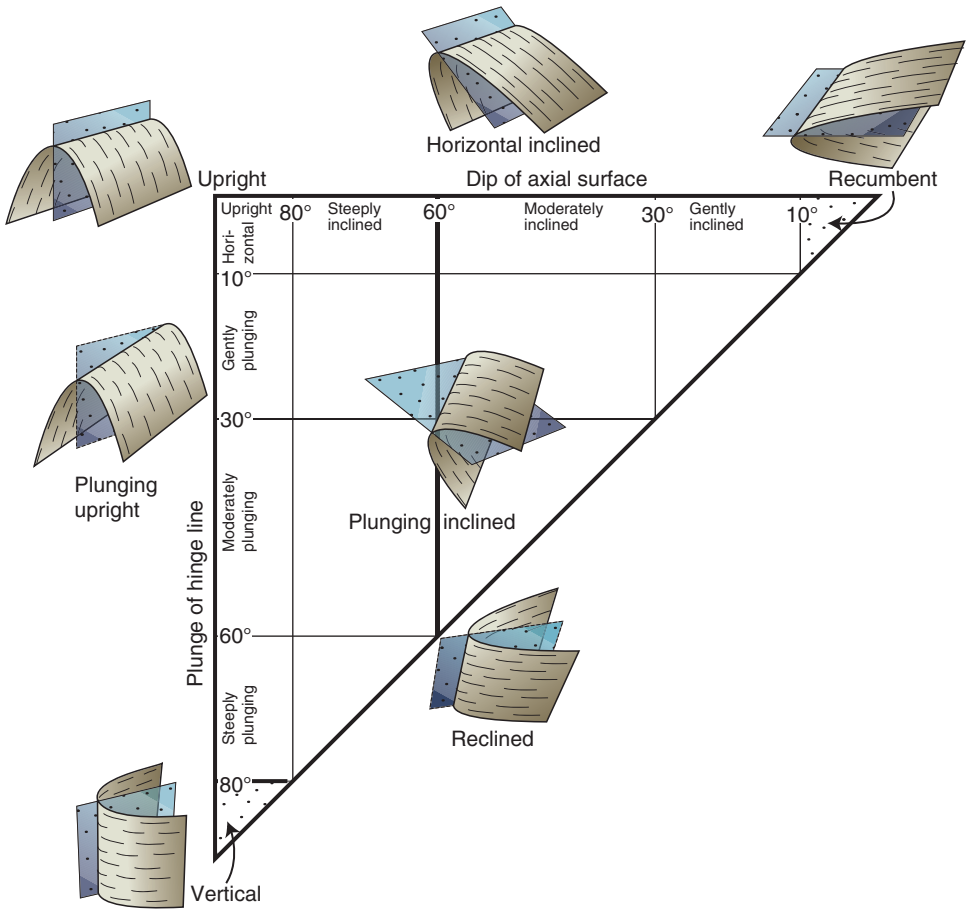

Figure 11.7 Classification of folds based on the orientation of the hinge line and the axial surface. Based on Fleuty (1964).

syncline is a trough-shaped fold where layers get younger toward the axial surface (Figure 11.8d). Returning to Figure 11.7, we can have upright or plunging synforms as well as antiforms. We can even have recumbent synclines and anticlines, because their definitions are related to stratigraphy and younging direction. However, the terms recumbent and vertical antiforms and synforms have no meaning.

Imagine a tight to isoclinal recumbent fold being refolded during a later tectonic phase. We now have a set of secondary synforms and antiforms. The younging direction across their respective axial surfaces will depend on whether we are on the inverted or upright limb of the recumbent fold, as shown in Figure 11.8h. We now need two new terms, synformal anticline and antiformal syncline, to separate the two cases (Figure 11.8f, g). A **synformal anticline** is an anticline because the strata get younger away from its axial surface. At the same time, it has the shape of a synform, i.e. it is synformal. Similarly, an **antiformal syncline** is a syncline because of the stratigraphic younging direction, but it has the shape of an antiform. Technically, a synformal anticline is the same as an anticline turned upside down, and an antiformal syncline looks like an inverted syncline. Confused? Remember that these terms only apply when mapping in polyfolded stratigraphic layers, typically in orogenic belts.

As already stated, most folds are non-cylindrical to some extent. A non-cylindrical upright antiform is sometimes said to be **doubly plunging**. Large doubly plunging antiforms can form attractive traps of oil and gas – in fact they form some of the world's largest hydrocarbon traps. When the non-cylindricity is pronounced, the antiform turns into a **dome**, which is similar to a cereal bowl turned upside-down (or Yosemite's Half Dome made whole). Domes are classic hydrocarbon traps, for example above salt structures, and geoscientists commonly talk about such traps as having a **four-way dip closure**. Correspondingly, a strongly non-cylindrical synform is in fold terminology called a **basin** (the cereal bowl right-way up).

A **monoclinal fold** is a sub-cylindrical fold with only one inclined limb (Figure 11.8a). Monoclinal folds (or just monoclines for short) are commonly found as map-scale structures related to reactivation of, or differential compaction across, underlying faults or salt structures (Figure 1.6).

In addition to orientation and stratigraphic relations, folds are commonly described or classified according to **tightness**. Tightness is characterized by the opening or

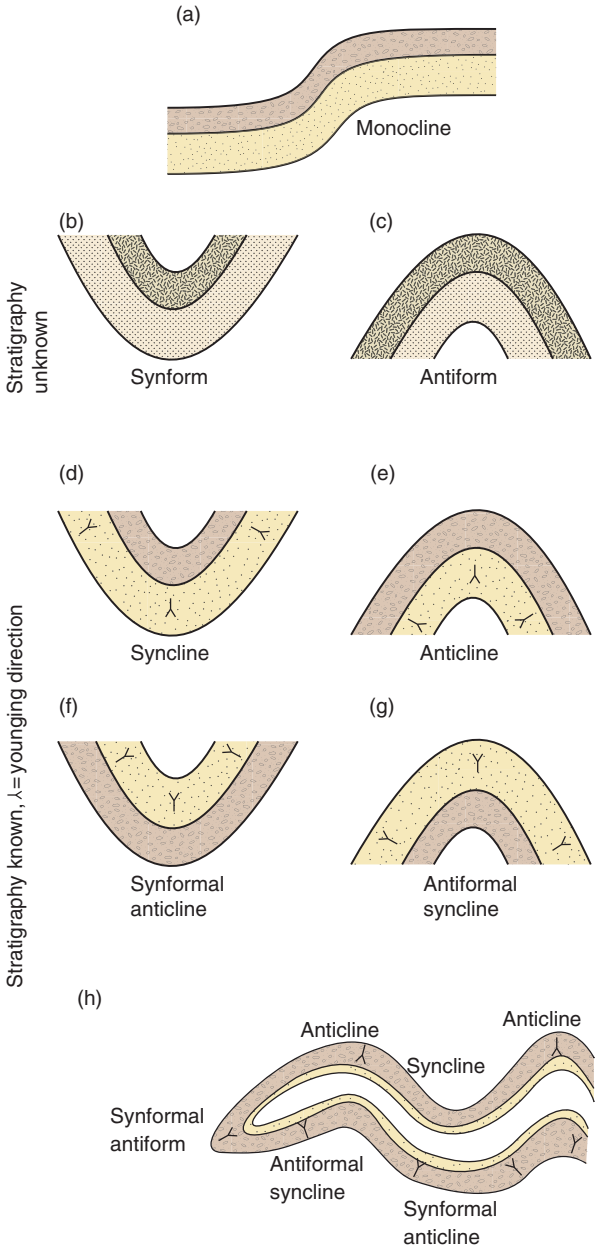

Figure 11.8 Basic fold shapes. The bottom figure illustrates how various types of syn- and antiforms may occur in a refolded fold.

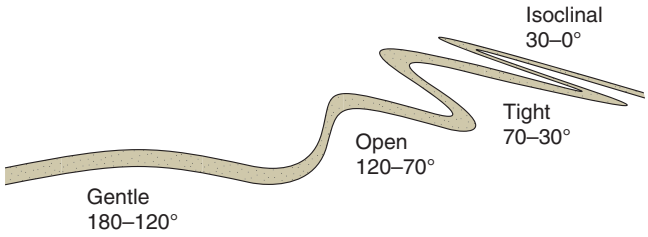

Figure 11.9 Fold classification based on interlimb angle.

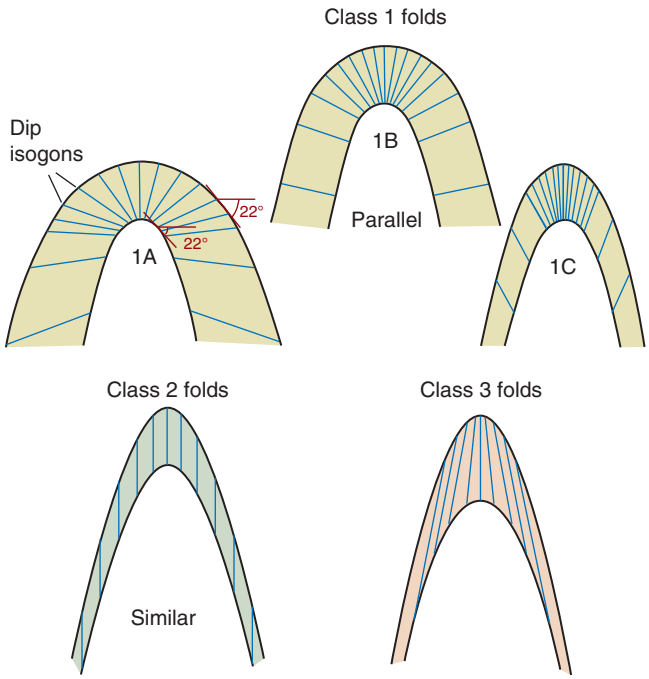

Figure 11.10 Ramsay's (1967) classification based on dip isogons. Dip isogons are lines connecting points of identical dip for vertically oriented folds.

interlimb angle, which is the angle enclosed by its two limbs. Based on this angle, folds are separated into gentle, open, tight and isoclinal (Figure 11.9). Tightness generally reflects the amount of strain involved during the folding.

Folds usually come in groups or systems, and although folds may be quite non-systematic, neighboring folds tend to show a common style, especially where they occur in rows or trains. In these cases they can, akin to mathematical functions, be described in terms of wavelength, amplitude, inflection point and a reference surface called the **enveloping surface**. The enveloping surface is the surface tangent to individual hinges along a folded layer, as shown in Figure 11.1. Note that the enveloping surface does not generally connect the hinge lines, although it does so for symmetric folds.

Dip isogons

Some folds have layers that maintain their thickness through the fold, while others show thickened limbs or hinges. These, and related features, were explored by the British geologist John Ramsay, who classified folds geometrically by means of **dip isogons**. By orienting the fold so that its axial trace becomes vertical, lines or dip isogons can be drawn between points of equal dip on the outer and inner boundaries of a folded layer. Dip isogons portray the difference between the two boundaries and thus the changes in layer thickness. Based on dip isogons, folds can be classified into the three main types shown in Figure 11.10:

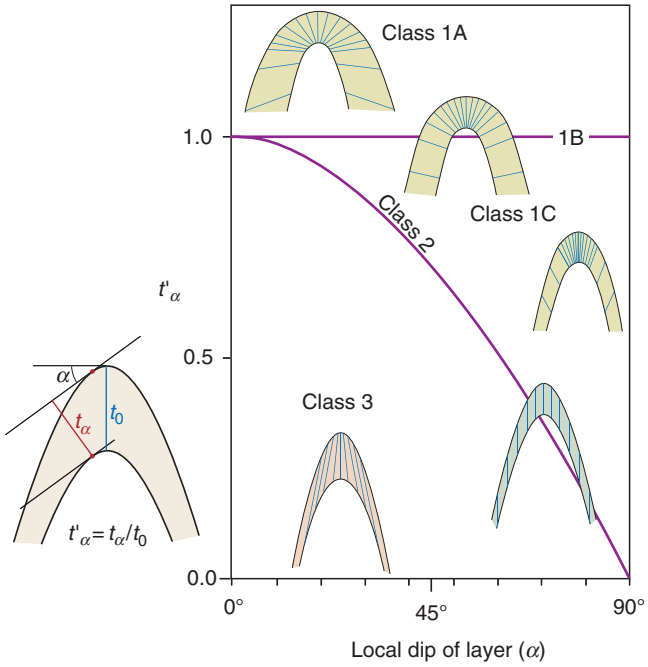

Figure 11.11 Fold classes plotted in a diagram where normalized layer thickness is plotted against dip of the folded surface. t'_α is the local layer thickness divided by the layer thickness in the limb, according to Ramsay (1967).

Class 1: Dip isogons converge toward the inner arc, which is tighter than the outer arc.

Class 2 (**similar folds**, also called **shear folds**): Dip isogons parallel the axial trace. The shapes of the inner and outer arcs are identical.

Class 3: Dip isogons diverge toward the inner arc, which is more open than the outer arc.

Class 1 folds are further subdivided into classes 1A, 1B and 1C. 1A folds are characterized by thinned hinge zones, while 1B folds, also called **parallel folds** and, if circle-shaped, **concentric folds** (Figure 11.2c), have constant layer thickness. Class 1C folds have slightly thinned limbs. Class 2 and, particularly, Class 3 folds have even thinner limbs and more thickened hinges. Among these classes, Class 1B (parallel) and 2 (similar) geometries stand out because they are easy to construct and easy to identify in the field.

One way of plotting folds according to the dip isogon classification is shown in Figure 11.11, where folds are considered as upright structures (vertical axial planes), so that the dip of the limb (α) increases in each direction from 0° at the hinge point. The vertical parameter in this figure, t'_α, is the normalized version of the orthogonal thickness, which is denoted t_α in Figure 11.11. This is the thickness measured orthogonal to the layer at one of the two corresponding points of equal dip on each arc (red points in Figure 11.11). For a Class 1B fold $t'_\alpha = t_\alpha$ regardless of the location on the folded layer, and each fold limb will plot along the horizontal $t'_\alpha = 1$ line. Hence, plotting measurements from a single folded layer will give a series of points that define two lines (one for each side of the hinge point) in Figure 11.11.

Symmetry and order

Folds can be symmetric or asymmetric in cross-section. A fold is perfectly symmetric if, when looking at a cross-section perpendicular to the axial surface, the two sides of the axial trace are mirror images of one another. This implies that the two limbs are of equal length. The chevron folds and concentric folds shown in Figure 11.2 are examples of symmetric folds.

If we extend this concept to three dimensions, the axial plane becomes a mirror plane, and the most symmetric folds that we can think of have two other mirror planes perpendicular to the axial plane. This is the requirement of **orthorhombic** symmetry. For symmetric folds the bisecting surface coincides with the axial plane. Hence, the kink band shown in Figure 11.2a is not symmetric. In fact, this is how we distinguish between kink bands and chevron folds: chevron folds are symmetric while kink bands have one long and one short limb. This leaves us with one symmetry (mirror) plane only, the one perpendicular to the axial surface, and the symmetry is said to be **monoclinic**.

Symmetric folds are sometimes called **M-folds**, while asymmetric folds are referred to as **S-folds** and **Z-folds**, as shown in Figure 11.12. Distinguishing between S- and Z-folds may be confusing to some of us, but Z-folds have short limbs that appear to have been rotated clockwise with respect to their long limbs. Z-folds thus mimic the letter Z when considering the short limb and its two adjacent long limbs. S-folds imply a counter-clockwise rotation, and resemble the letter S (this has nothing to do with the difference in angularity between S and Z). Interestingly, S-folds become Z-folds when viewed from the opposite direction. Plunging folds are usually evaluated when looking down-plunge, while viewing direction must be specified for folds with horizontal axes.

Fold systems consisting of folds with a consistent asymmetry are said to have a **vergence**. The vergence can be specified, and the vergence direction is given by the sense of displacement of the upper limb relative to the lower one (Figure 11.13). We can also relate it to the clockwise rotation of the inclined short limb in Figure 11.13, where a clockwise rotation implies a right-directed vergence.

Fold vergence is important in structural analysis in several ways. Large folds tend to have smaller folds occurring

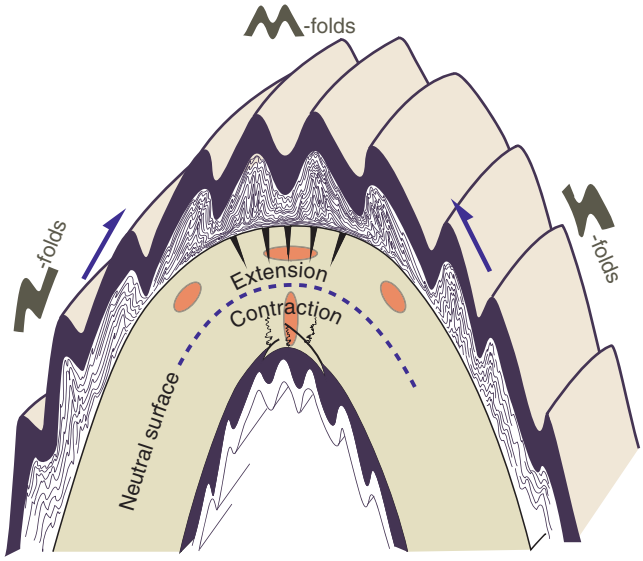

Figure 11.12 Z-, M- and S-folds may be related to lower-order folds, in which case they provide information about the geometry of the large-scale fold.

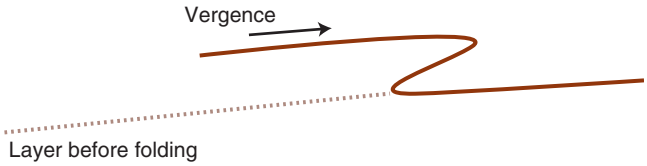

Figure 11.13 The concept of fold vergence. This fold is right-verging and a Z-fold according to the clockwise rotation of the short limb.

in their limbs and hinge zones, as shown in Figure 11.12. The largest folds are called the first-order folds, while smaller associated folds are second- and higher-order folds. The latter are also called **parasitic folds**. First-order folds can be of any size, but where they are map scale we are likely to observe only second- or higher-order folds in outcrops. If a fold system represents parasitic (second-order) folds on a first-order synformal or antiformal structure, then their asymmetry or vergence indicates their position on the large-scale structure. As shown in Figure 11.12, parasitic folds have a vergence directed toward the hinge zone. This relationship between parasitic and lower-order folds can be extremely useful for mapping out fold structures that are too large to be observed in individual outcrops.

The vergence of asymmetric fold trains in shear zones is generally unrelated to lower-order folds and can give information about the sense of shear of the zone. Such kinematic analysis requires that the section of observation contains the shear vector and should be used together with independent kinematic indicators (see Chapter 15).

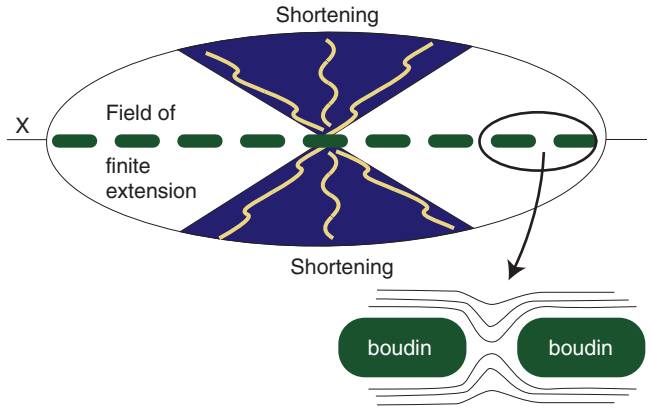

Figure 11.14 Fold vergence in relation to the strain ellipsoid for coaxial deformation, Note that folds can also occur between boudins in the field of finite extension.

The (a)symmetry of folds may also reflect strain and the orientation of the strain ellipse. In general, layers that are parallel to ISA_3 (the fastest shortening direction, see Chapter 2) will develop symmetric folds. For coaxial strain this is straightforward (Figure 11.14), but for simple shear and other non-coaxial deformations things get somewhat more complicated, since layers rotate through the position of ISA_3 during the deformation.

Fold asymmetry may relate to position on a lower-order fold, sense of shear or orientation of the folded layer relative to the strain ellipse.

11.2 Folding: mechanisms and processes

Every geologist mapping or describing folds in the field probably has the same question in mind: how did these structures actually form? As geologists we tend to look for a simple history or mechanism that can explain our observations reasonably well. Folding is no exception, and there are different approaches and process-related terms. One approach is to consider the way force or stress acts on a layered rock, which leads to the three-fold classification and terminology shown in Figure 11.15. Other terms are related to how the layer(s) react to force and stress, for instance whether layers fold by layer-parallel shearing, orthogonal flexure or some other mechanism that is controlled by rock rheology. Still other classes of folding, such as kinking and chevron folding, are related to fold geometry. For this reason, several different fold mechanisms are defined, and many of them overlap in definition. This is why terms such as buckling, kink

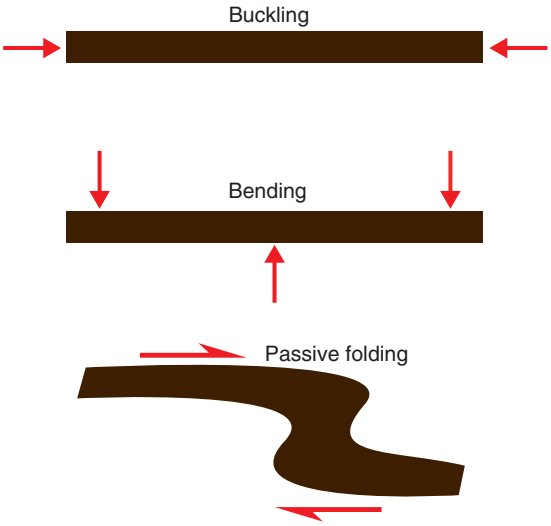

Figure 11.15 The relation between how force is applied and fold mechanisms.

folding and bending can be confusing when discussed in terms of mechanisms such as flexural slip and simple shear. In summary, we are dealing with differences in orientation of stress axes relative to the layering, kinematics, and mechanical and rheological properties, and thus mechanisms that emphasize different aspects of folding.

The most important distinction between the ways folds form probably lies in whether the layering responds actively or passively to the imposed strain field. We will start out by considering **active folding** (buckling), where the competence or viscosity contrast between the folding layer and its host rock is important. We will then look at **passive folding**, where layers are simply passive markers with no rheological influence, and then consider **bending**, where forces are applied across the layering (Figure 11.15). The following sections will then discuss models known as **flexural folding** mechanisms (flexural slip, flexural shear and orthogonal flexure), which can contribute to both active folding and bending. Finally, we will discuss **kinking** and the formation of **chevron folds**.

Active folding or buckling (Class 1B folds)

Active folding or **buckling** is a fold process that can initiate when a layer is shortened parallel to the layering, as shown schematically in Figure 11.16. Folds such as the ones seen in Figure 11.17 appear to have formed in response to layer-parallel shortening. A contrast in viscosity is required for buckling to occur, with the folding layer being more competent than the host rock (matrix). The result of buckling is rounded folds, typically parallel and with more or less sinusoidal shape.

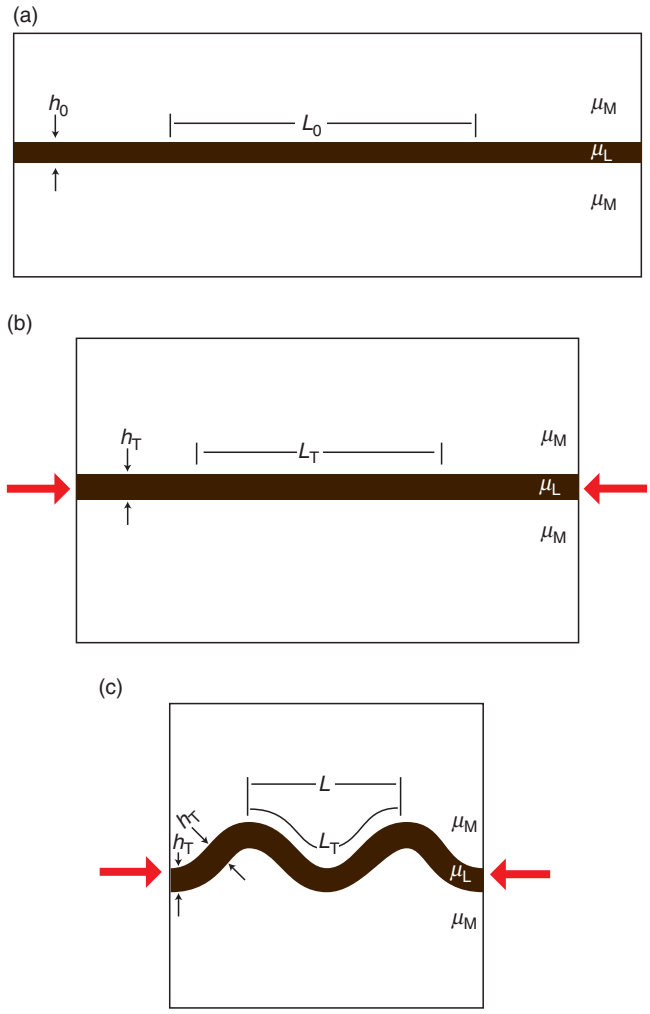

Figure 11.16 Buckling of a single layer. L_0 is the original length that is changed into L_T after initial shortening (a, b) while μ_L and μ_M are layer and matrix viscosities, respectively. h_0 is the original layer thickness (a), which increases to h_T during the initial thickening phase (b). L is the wavelength while L_T is the arc length. Based on Hudleston (1986).

Figure 11.17 Two folded layers of different thickness. The upper and thinner one shows a smaller dominant wavelength than the lower one.

Buckling occurs when a competent layer in a less competent matrix is shortened parallel to the length of the layer.

If an isotropic rock layer has perfectly planar and parallel boundaries and is perfectly parallel with a constantly oriented σ_1 or ISA_1, then it will shorten without folding even though there is a significant viscosity contrast between the layer and the host rock. However, if there are small irregularities on the layer interfaces, then these irregularities can grow to form buckle folds with a size and shape that depend on the thickness of the folded layer and its viscosity contrast with its surroundings.

Buckling or active folding implies that there is layer parallel shortening and a viscosity contrast involved, and also irregularities on which folds can nucleate.

Buckling of single, competent layers in a less competent matrix (Figure 11.16) is relatively easy to study in the laboratory and has also been explored numerically. Single-layer folds formed by buckling have the following characteristics:

- The fold wavelength–thickness ratio (L/h) is constant for each folded layer if the material is mechanically homogeneous and if they were deformed under the same physical conditions. Such folds are often called **periodic folds**. If the layer thickness varies, then the wavelength is changed accordingly (Figure 11.17).
- The effect of the folding disappears rapidly (about the distance corresponding to one wavelength) away from the folded layer.
- The folds in the competent layer approximate Class 1B folds (constant layer thickness). If there are two or more folded competent layers then the incompetent layers in between are folded into Class 1A and Class 3 folds (Figure 11.18). Cusp (pointed) hinges point to the more competent layers.
- The outer part of the competent layer is stretched while the inner part is shortened. The two parts are typically separated by a **neutral surface** (Figure 11.19). Note that layer-parallel shortening, which always takes place prior to folding, can reduce or eliminate the outer extensional zone.
- The normal to the axial surface or axial cleavage indicates the direction of maximum shortening (Z).

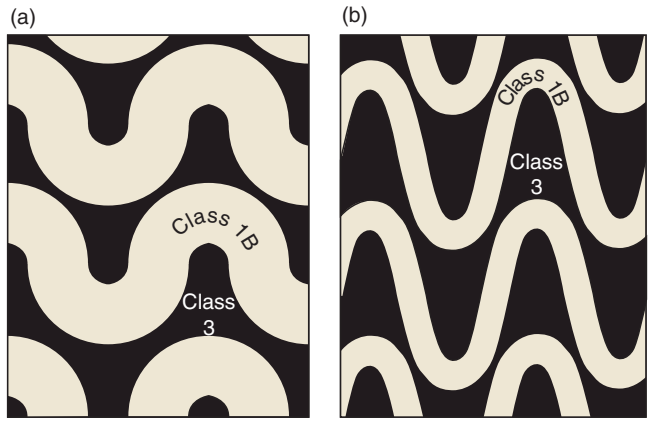

Figure 11.18 Alternating Class 1B and 3 folds are commonly seen in folded layers. Competent layers exhibit Class 1B geometry.

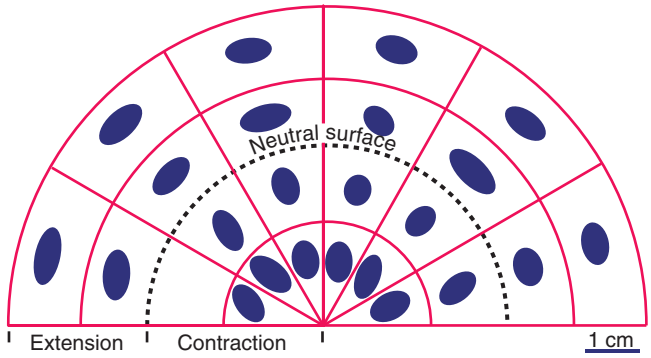

Figure 11.19 Strain distribution in the hinge zone of a folded limestone layer in shale. Outer-arc stretching is separated from inner-arc shortening by a neutral surface. From Hudleston and Holst (1984).

If the layers are Newtonian viscous, and disregarding any layer-parallel shortening, then the relation between wavelength and thickness is given by

$$L_d/h = 2\pi(\mu_L/6\mu_M)^{1/3} \qquad (11.2)$$

μ_L and μ_M are the viscosities of the competent layer and the matrix, respectively, while L_d is the dominant wavelength and h the layer thickness. Experiments and theory show that homogeneous shortening (T) occurs initially, together with the growth of irregularities into very gentle and long-amplitude fold structures. When the most accentuated folds achieve opening angles around 160–150°, the role of layer-parallel shortening decays. From that point on the folds grow without any significant increase in layer thickness. Equation 11.2 can be expanded to include layer-parallel thickening:

$$L_{dT}/h_T = 2\pi(\mu_L/6\mu_M(T+1)T^2)^{1/3} \qquad (11.3)$$

L_{dT} is here the revised expression of the dominant wavelength, while h_T is the thickness when layer-parallel shortening (thickening) is taken into account. The factor T is identical to the strain ratio X/Z, or $(1 + e_1)/(1 + e_3)$.

The viscosity contrast $\mu_L/6\mu_M$ can be estimated (formulas not shown here) by measuring the average length of the folded layer over one wavelength and h_T for a fold population. In addition, the layer-parallel shortening T in the competent layers must be estimated.

Buckling has been modeled under the assumption of linear or Newtonian viscosity (Equation 6.23). It is likely that most rocks show non-linear rheological behavior during plastic deformation, which has consequences for the buckling process. A power-law rheology is then assumed (Equation 6.24), where the exponent $n > 1$. The higher the n-exponent, the quicker the fold growth and the less the layer parallel shortening T. Many natural folds show low T-values, and, together with low L/h ratios ($L/h < 10$), this indicates a non-linear rheology. However, the differences between the results from viscous and power-law rheology models are not great.

Buckle folds are most easily recognized as single competent layers, but can also occur where several competent layers occur in parallel. L_d/h is significantly less for multilayer than for single layer buckling. Where two thin layers are close they will behave more like a single layer whose thickness is the sum of the two thin layers, as seen from the experimental results shown in Figure 11.20. Where we have alternating thick and thin layers, the thin layers will start to develop folds first (Figure 11.21a, b). At some point the thick layers will start to fold (with longer wavelength) and take control over the further development. The result is relatively large folds controlled by thick layers together with small, second-order folds formed earlier in the process (Figure 11.21c). An example of multilayer folding where the wavelength is controlled by a package of layers is shown in Figure 11.22.

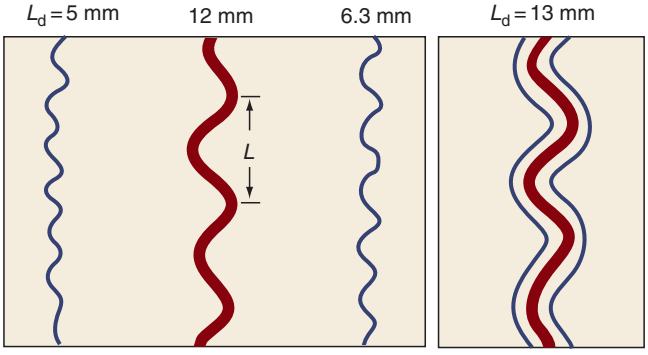

Figure 11.20 Folding of multilayered rocks. Far-apart layers act as individual layers (left). The closer they get, the more they behave as a single layer with thickness larger than that of the thickest of the individual layers. Based on experiments by Currie *et al.* (1962).

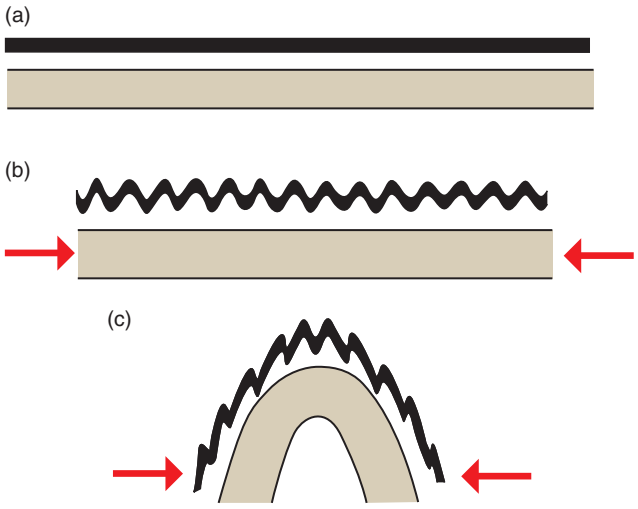

Figure 11.21 Illustration of how folding initiates in thin layers. Once the thicker layer starts to fold, the smaller folds in the thin layer become parasitic and asymmetric due to flexural flow.

Several mechanisms can be involved during buckling. The simplest ones can collectively be termed **flexural folding** and are separated into orthogonal flexure, flexural slip and flexural flow. In addition there is always the possibility of having volume change, particularly in the hinge zone. We will briefly review these idealized models after a look at two other models of folding known as passive folding and bending.

Passive folding (Class 2 folds)

Passive folding is typical for rocks where passive flow occurs, i.e. where the layering exerts no mechanical influence on the folding. In these cases the layering only serves as a visual expression of strain with no mechanical or competence contrast to neighboring layers. Such layers are called **passive layers**. Perfectly passive folds produced by simple shear are Class 2 (similar) folds, and passive folds that are associated with simple shear, or at least a significant component of simple shear, are called **shear folds** (Figure 11.23a).

Passive folds generated by simple shearing are perfectly similar folds.

Passive folds of perfect Class 2 geometry can easily be generated by differentially shearing a card deck. Drawing lines perpendicular to the cards prior to shearing helps visualize the fold. However, the formation of passive folds is not restricted to simple shear. Passive folds can form in

Figure 11.22 Buckled multilayers. Note how the largest folds affect the entire layer package.

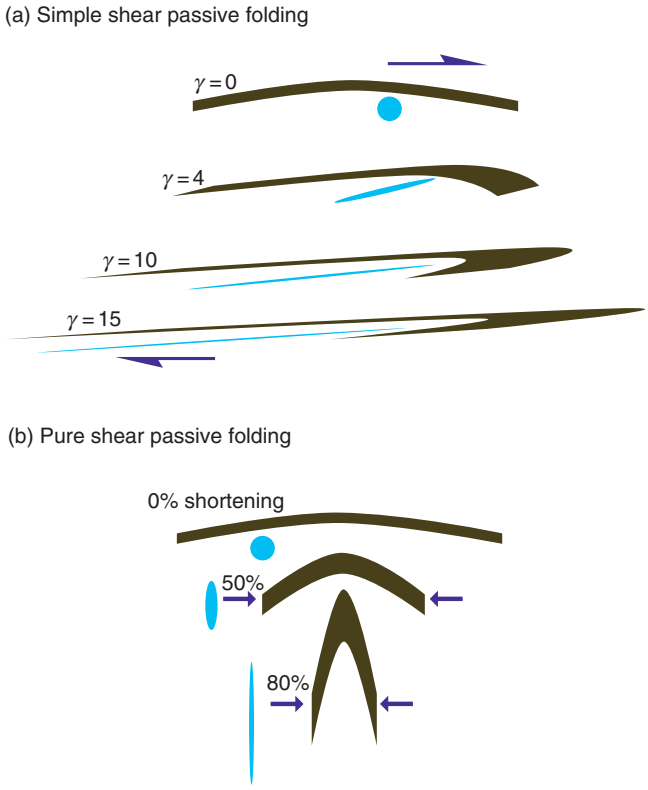

Figure 11.23 Formation of Class 2 folds by (a) simple shearing and (b) pure shearing of a gently curved layer. No viscosity contrast is involved, meaning that the folds can be regarded as passive.

response to any kind of ductile strain, for instance subsimple shear, transpression (Chapter 18) and even coaxial strain (Figure 11.23b). Hence simple shear is only one of an infinite spectrum of kinematic models that can produce passive folds.

Passive folding produces harmonic folds where the layering plays no mechanical role and therefore no influence on the fold shape.

Examples of passive folding are found where passive layers enter shear zones or otherwise are affected by heterogeneous strain. Drag folds along faults (Chapter 8) are examples typical for the brittle regime, although many layered sequences contain beds of quite different mechanical properties so that slip occurs between layers (see flexural slip below). Passive folds are frequently found in mylonite zones, particularly in monomineralic rocks such as quartzite (Figure 11.24), marble and salt.

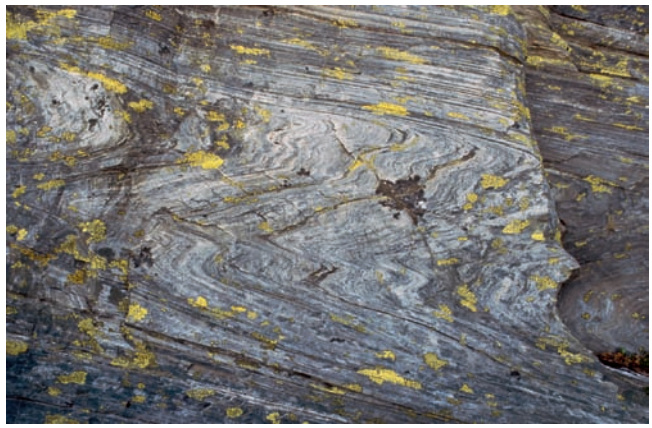

Figure 11.24 Passive harmonic folding of quartzite in a Caledonian mylonite zone. The similar geometry of this Z-fold and its setting in a Caledonian shear zone indicate that it is a shear fold.

Bending

Bending occurs when forces act across layers at a high angle (Figure 11.25), unlike buckle folds where the main force acts parallel to a layer. This is also the case for passive folding, and the two are closely related. However, bending

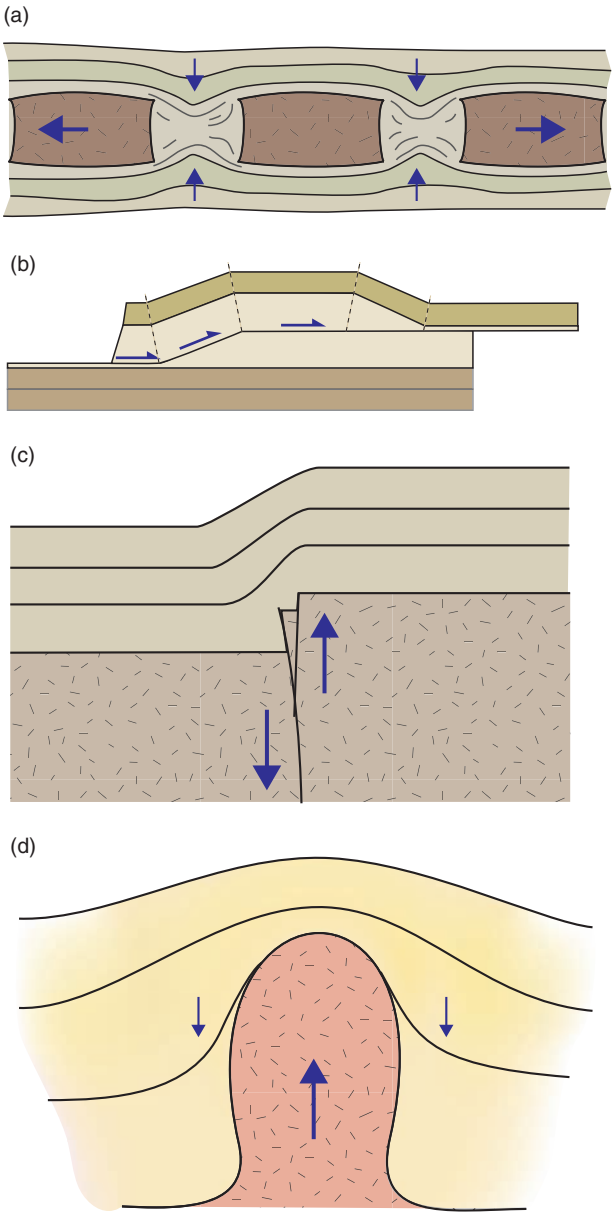

Figure 11.25 Examples of bending in various settings and scales: (a) between boudins; (b) above thrust ramps; (c) above reactivated faults; and (d) above shallow intrusions or salt diapirs.

is generally thought of as something that is more directly forced upon the layers by geometries and kinematics of the bounding rock units. Several aspects of bending have been studied in great detail by engineers because of its importance in the field of construction engineering, such as in horizontal beams supported by vertical pillars.

Bending occurs when forces act across layers, and may involve more than one mechanism.

Classic geologic results of bending are the **forced folds** created in sedimentary layers blanketing faulted rigid basement blocks (Figure 11.25c). The displacement is forced upon the sediments by fault movement on a preexisting basement fault, and the sediments are soft enough to respond by monoclinal folding until at some critical point they rupture and the fault starts propagating up-section. Such structures are particularly well exposed in the Colorado Plateau–Rocky Mountains area, where numerous Laramide-related uplifts have created such structures.

Bending as such is a boundary condition- or external load-related model, not a strain model, particularly not when a free surface is involved such as during forced folding mentioned above (Figure 11.25c). In other words, there are many ways that folding and strain can accumulate internally in a fold during bending.

An obvious response to bending is deformation by simple shear, in which case we are back to passive folding. The simple shear passive folding model may work if we have a wide fault zone underneath the fold or if the fold is very narrow. In most cases the fold widens upward, telling us that we have to modify the simple shear model. In this case trishear comes in handy. Trishear distributes shear in a triangular zone ahead of a propagating fold, and seems to work very well for several mapped examples.

Still, trishear cannot explain all features seen in many forced folds. Field studies show evidence of bedding-parallel slip or shear. This is manifested by striations on weak bedding-parallel surfaces or by bedding-parallel deformation bands. We will discuss this mechanism below as flexural slip. Also the related flexural mechanism described below as orthogonal flexure can result from bending loads.

There are many other examples of bending. One is **fault-bend folds**, for instance where thrust sheets are passively bent as they move over a ramp structure (Figure 11.25b) (see Chapter 16). Such folds are commonly modeled as kink folds, again related to flexural slip. They may also be modeled by means of simple shear, which is commonly done for fault-bend folds formed above non-planar (e.g. listric) faults (see Chapter 20).

Differential compaction, where a sedimentary sequence compacts more in one area than in another due to different degrees of compaction of the underlying layers, is also a type of bending. This is common across the crests of major fault blocks in postrift-sequences in sedimentary basins, but can also occur along salt diapirs (19.5a) and shallow intrusions. Folds formed by differential compaction are gentle.

Forceful intrusion of magma or salt can also bend roof layers, as shown in 19.21. Again the strain accumulation mechanism may vary, with flexural slip being a common constituent.

Figure 11.26 Passive folding of layers between boudins.

In the plastic regime, bending is less common because of the high ductility of all or most parts of the deforming rocks. However, bending is frequently associated with rigid **boudins** (Figure 11.25a and 11.26).

Flexural slip and flexural flow (Class 1B)

Flexural slip implies slip along layer interfaces or very thin layers during folding (Figure 11.27). It is one of three kinematic models of folding (the others being flexural flow and orthogonal flexure) that maintains bed thickness and thus produces Class 1B or parallel folds. Simple flexural slip experiments can be performed simply by folding double sandwiches with jelly. The sandwich maintains its thickness even though slip occurs between the pieces of bread, until the fold becomes too tight. It is a prerequisite for flexural slip that the deforming medium is layered or has a strong mechanical anisotropy.

In nature, the anisotropy could be mica-rich thin layers in a quartzite or mylonite, or thin shale layers between thicker sandstone or limestone beds in sedimentary rocks. Flexural slip can occur in the middle crust where plastic deformation mechanisms would be involved, but is perhaps more common where sedimentary strata are folded in the upper crustal brittle regime. In the latter case, bedding surfaces act like faults, and slickenlines (red lines in Figure 11.27a) will sometimes develop on slipping surfaces.

Maximum slip occurs at the inflection points and dies out toward the hinge line, where it is zero. The sense of slip is opposite on each limb, and the slip is consistent relative to the hinges, where sense of slip changes. Relative slip on the convex side of a flexural slip fold is always toward the fold hinge, whereas on the concave side slip is opposite.

Slickenlines on folded weak layers and constant bed thickness reveal flexural slip.

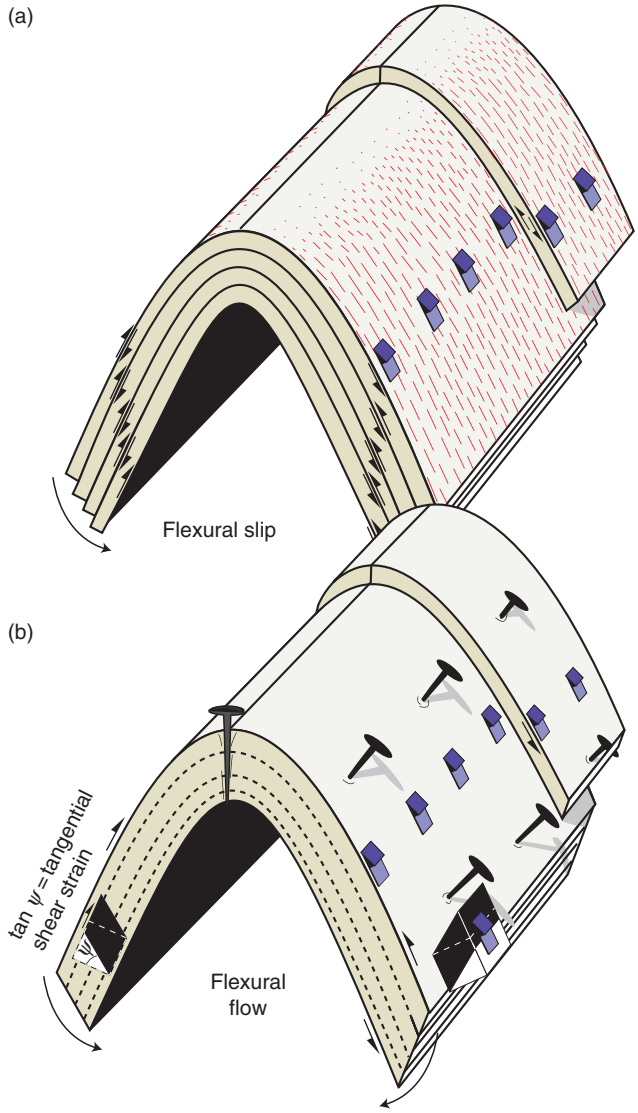

Figure 11.27 (a) Flexural slip, showing opposite sense of slip on each limb, decreasing towards the hinge zone. (b) Flexural flow, where fold limbs are being sheared. Ideally, layer thickness is preserved in both models.

In cases where strain is more evenly distributed in the limbs in the form of shear strain, as is more commonly the case in the plastic regime, flexural slip turns into the closely related mechanism called **flexural shear** or **flexural flow**. Flexural flow experiments are conveniently done by bending a soft paperback book or a deck of cards (remember to draw circles for strain markers). During this process slip occurs between individual paper sheets. If we put strain markers on our paperback, we would see that strain is zero in the hinge zone and increasing down the limbs. This is so because the shear strain is directly related to the orientation (rotation) of the layers, as shown in Figure 11.27b: the higher the rotation, the higher the shear strain.